University of Bath

UNIVERSITY OF BATH

PHD

Some problems in hydraulic circuit design

Yang, Huayong

Award date:
1987

Awarding institution:
University of Bath

Link to publication

SOME PROBLEMS IN HYDRAULIC CIRCUIT DESIGN

Submitted by

HUAYONG YANG

for the degree of Ph D
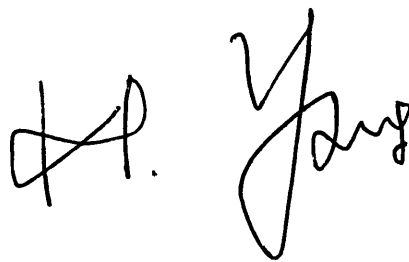
of the University of Bath

1987

COPYRIGHT

UMI Number: U005053

UMI®

Dissertation Publishing

ProQuest®

SUMMARY

This thesis considers a possibility of savings in size, cost and energy supply in many hydraulic circuits by introducing unboosted closed or partially closed hydraulic circuits in the place of the normal open circuit designs. The thesis firstly examines the physical behaviour of the circuits considered in detail, and supports this by a careful theoretical analysis using digital simulation. It shows how simulation can be used to give accurate analysis of system performance in conditions where normal deductive or mathematical techniques would fail. In order to provide a comprehensive understanding of the circuit designs proposed, they are applied to a small boat hydrostatic drive propeller system. It goes on to investigate the system behaviour with careful computer simulations both of the system dynamics and of the thermodynamics of the system considered. Finally, it provides a theoretical approach to thermal transient analysis in fluid power systems with a fundamental consideration some of the basic thermodynamic processes including heat transfer from the pipe walls. The results of simulation and experimental fluid and pipe wall temperatures have shown that radiation effects under room temperature region are far more significant than previously thought.

ACKNOWLEGEMENTS

CONTENTS

LIST OF FIGURES

Transient Flowrate from the Open Ended Pipe

NOTATION

Chapter 3

A	cross-sectional pipe area
A_o	opening area of orifice
B	fluid bulk modulus
C	compressibility of liquid
C_c	coefficient of contraction
C_d	coefficient of discharge
d	pipe diameter
D	pump displacement
g	gravitational acceleration
h	fluid height in the open ended pipe
J	effective inertia of electric motor
k	energy loss coefficient
K_1	damping torque coefficient due to eddy currents
K_e	constant of electric motor torque/speed
K_l	constant of pump leakage flow/pressure
L	pipe length
L_1	fluid jet length
m	mass of fluid in the open ended pipe
m	mass of fluid jet at orifice downstream
P_1	pump inlet pressure
P_2	return line pressure
P_3	pump delivery pressure
P_c	pressure at vena contracta
P_f	friction pressure of pipe
Q	flowrate
Q_3	upstream flowrate of orifice
Q_5	downstream flowrate of orifice
Q_{pin}	pump inlet flowrate
Q_{pout}	pump delivery flowrate
S	slip loss of electric motor
T_e	developed torque of electric motor

T_f	pressure dependent torque loss
T_L	load torque of electric motor
T_p	net torque of pump
T_{th}	theoretical torque of pump
T_v	speed dependent torque loss
v	fluid velocity in open ended pipe
v_1	upstream fluid velocity of orifice
v_4	downstream fluid velocity of orifice
v_{3c}	fluid velocity at the vena contracta
v_c	fluid velocity at the vena contracta
V	volume of oil

DIMENSIONLESS GROUPS

Re	Reynolds number

GREEK SYMBOLS

μ	dynamic viscosity
ν	kinematic viscosity
ω	angular working speed of electric motor
ω_s	maximum angular speed of electric motor
ρ	fluid density
lamda	friction factor

Chapter 4

A	area of pipe across section
A_a	area of orifice A
A_b	area of orifice B
A_t	area of tank base
C_i	coefficient of pressure loss at tank inlet
C_o	coefficient of pressure loss at tank outlet
d	pipe diameter
g	gravitational acceleration
G	coefficient of the first order lag
H	fluid height in the tank

K_{13}	pressure loss coefficient of pipe junction
K_{23}	pressure loss coefficient of pipe junction
l	pipe length
m	fluid mass in the pipe
Q_a	flowrate to tank
Q_b	flowrate to pump entry
Q_i	tank inlet flowrate
Q_o	tank outlet flowrate
Q_r	return line flowrate
Q_t	flowrate from tank
P_1	suction pressure
p_b	pressure at the pipe bottom
P_e	effective mean pressure
P_f	friction pressure loss
p_i	tank inlet pressure
p_{is}	tank inlet static pressure
P_o	tank outlet pressure
p_{os}	tank outlet static pressure
p_r	return line pressure
P_s	static pressure
P_t	pressure at the pipe top to tank
v	fluid velocity in pipe
ρ	fluid density
μ	fluid viscosity
λ	friction factor
ϕ	coefficient of area ratio

Chapter 5

C_e	constant speed/torque gradient coefficient
D	diameter of propeller
J	effective inertia of propeller/motor
J_e	effective inertia of engine/pump
K_t	propeller torque coefficient
R_e	ratio of gear box between motor and propeller
T_e	torque supplied from engine
T_h	torque required by pump

T_m	hydraulic torque supplied from motor
T_p	propeller load torque
ρ	density of fluid surrounding to the propeller
ω	angular shaft speed
ω_g	governor set shaft speed
ω_m	angular speed of motor shaft
ω_p	angular speed of propeller shaft

Chapter 6

A_1	inside surface area of pipe
A_1	tank base area
A_2	outside surface area of pipe
A_2	one side of fluid vertical area in the tank
A_3	another side of fluid vertical area in the tank
A_m	logarithmic mean surface area of pipe
B	fluid bulk modulus
C	velocity
C_{pf}	fluid specific heat
C_{pp}	pipe wall specific heat
d	pipe diameter
E	internal energy
g	gravitational acceleration
h	enthalpy
h_a	heat transfer coefficient by natural convection
h_{av}	heat transfer coefficient by natural convection for tank vertical plate
h_{ap}	heat transfer coefficient by natural convection for tank horizontal plate at bottom
h_f	heat transfer coefficient by forced convection
H	heat flow
H_1	rate of heat flow transferred from fluid to pipe wall by forced convection
H_2	rate of heat flow transferred from pipe wall to atmosphere by natural convection
k	thermal conductivity of pipe wall material
L	length of pipe section

m	mass flowrate
m_1	inlet mass flowrate at port 1 of pipe junction
m_2	inlet mass flowrate at port 2 of pipe junction
m_3	outlet mass flowrate at port 3 of pipe junction
M_f	fluid mass in the system
M_p	mass of wall material
Q	heat flow
R_1	pipe inside radius
R_2	pipe outside radius
T_1	wall temperature at internal pipe surface
T_1	fluid temperature at port 1 of pipe junction
T_2	wall temperature at external pipe surface
T_2	fluid temperature at port 2 of pipe junction
T_a	constant surrounding atmospheric temperature
T_f	fluid temperature
T_{wp}	outside tank bottom wall temperature
T_{wv}	outside tank vertical wall temperature
U	molecular energy
W	rate of power loss converted into heat energy
x	thickness of tank wall
Z	height above reference level

DIMENSIONLESS GROUPS

Nu	Nusselt number
Re	Reynolds number

GREEK SYMBOLS

ϵ	emissivity
θ	temperature difference (relative to wall)
μ	dynamic viscosity
ρ	density
σ	Stefan-Boltzman constant; surface tension

CHAPTER 1

INTRODUCTION

1.1 This thesis considers the possibility of using open suction pumps in closed hydraulic transmission circuits, thus reducing the necessity for suction lines of large diameter, and large reservoirs. It considers such systems, both experimentally and by simulation, from the stand point of pump suction pressure, dynamic performance and also temperature rise.

1.2   Conventional Types of Hydraulic Circuit Designs   Many hydraulic systems appear complicated, but their basic circuit designs are quite simple. Existing system designs can be classed as open or closed hydraulic circuits. A simplified hydraulic system with an open circuit without filtration or cooling is shown in Fig. 1.1. In this, the system flow returns to a reservoir. Normally, a large reservoir is required to meet the varying volume demands of a particular system and allow air bubbles to escape. The reservoir also allows some contaminants to settle out of fluid and acts as a reservoir for heat during periods of high heat generation in the system. The full flow demand of the pump is supplied through a suction pipeline, which has to be of a large diameter in order to prevent cavitation at the pump inlet. A simple example of a closed circuit is shown in Fig. 1.2. In this, a boost pump with sufficient capacity is employed to make up the flow variation due to leakage and compressibility and to prevent cavitation in the pump suction line under transient conditions. It may be necessary to provide a cooler to cope with the energy losses in the pump, motor and associated equipment.

1.3   Pressure for Improving Performance of Hydraulic Systems   Although the hydraulic industry has been firmly established over the years, hydraulic transmission is under constant pressure to improve its performance to face up to the

challenges from mechanical and electrical transmissions. This pressure has increased greatly in the last two decades, mainly due to the rapid developments in electrical engineering. A new generation of electric motor has been developed which has a far wider range of speed and torque output to suit the load conditions. The competitive features of the transmission systems have been examined from points of view which include the system reliability, efficiency, capacity and cost. It is therefore necessary to increase pressures, speeds, capacity, transient response with high reliability and low noise, if the hydraulic industry is to maintain its position.

In many hydraulic system applications, the need to reduce the size and energy requirements are important, particularly when used in mobile equipments. For example, Fig. 1.3 illustrates an open hydraulic system used for lowering and raising the nose wheel of an aircraft landing gear. In this case, the size of the hydraulic reservoir could be vital when considering the feasibility of a particular system design. Another example illustrated in Fig. 1.4 shows a closed hydraulic transmission system applying a two-man operated submarine for the control of the steering and stabilizing systems, bow thrusters, grappling hooks, net winches and anchor windlasses. In such an environment, any possible reduction in the system energy requirement and size would be of particular advantage. In both of the above cases, since the hydraulic reservoir in the open hydraulic system requires a large space and the energy consuming boost pump in the closed hydraulic system demands an additional driving power, neither the traditional open hydraulic system nor the closed hydraulic system may be the best design choice under such special working conditions.

Numerous attempts have been made over years to improve the performance of the traditional system designs. For instance, Volvo supply a boost unit for use in the closed hydraulic systems as shown in Fig. 1.5. In this, the feed section includes an injector to which the return flow from the hydraulic motor is taken. About 10 percent of the return flow is drained off before it reaches the injector. This hydraulic fluid and the fluid draining from the pump and motor is taken to the reservoir through a filter and also a cooler if necessary. The usual boost pump is replaced by this injector unit to circulate fluid in the main loop for cooling and filtration and to maintain a certain surplus pressure in the low pressure section of the system. The performance of this unit is not quoted in the Volvo literature but it does seem to form a bridge between the boosted system in practical use and the systems proposed in this thesis.

1.4 **The Systems Investigated** The systems investigated in this thesis are a combination of closed and open systems. In one version, the return line is directly connected to the pump inlet and the reservoir is placed at the position above the pump as shown in Fig. 1.6. The supply from the reservoir need only be sized to take leakage to drains, and if actuators are used, sufficient flow to make up deficiencies during actuator extensions.

In Fig. 1.7 the simple system of Fig. 1.6 has been modified to allow a proportion of the flow to return to the reservoir and the remainder direct to the pump inlet. This system allows interchange of oil from the main loop into the reservoir and allows air bubbles to escape the air-liquid interface. It also allows for the fluid in the reservoir to be used to store thermal energy and improve energy dissipation. The flow and return lines to the reservoir can be of smaller diameter than those in a conventional open system. Filtration can be carried out in either the main loop, or in the lines to and from the reservoir. Filters can be of smaller capacity than in an open system, since the flows required are much lower. This materially reduces the cost of system.

Although these modifications to the systems in Fig. 1.6 and 1.7 seem simple they have not, to author's knowledge, been used extensively in hydraulic practice, partly because designers are wary of of cavitation problems, the problems of elimination of air and the problems of obtaining thermal equilibrium. In this thesis it was decided to investigate the use of the above two systems and to determine their suitabilities for use in practical hydraulic systems. These two suggested systems have been examined by means of both practical test rigs and simulations using a digital computer. The simulation work has been carried out using the computer simulation package HASP developed at University of Bath. In this way, a better understanding of the theoretical aspects of the unboosted and partially closed hydraulic systems have been obtained so that such systems could be incorporated into a large variety of hydraulic systems.

1.5 **Plan and Scope of the thesis** The work in this thesis has been divided into six main parts. The simulation package, HASP is discussed in the first part. In the second part the package is used to investigate the fundamental performance of an unboosted closed hydraulic system. The simulation used previously developed

mathematical models for some components but necessitated the development of mathematical models for several other components within the system. The theoretical analysis based upon mathematical and computer simulation modelling has been supported by an extensive test programme. This programme has been carried out on a simple test rig, which is constructed under the principle of unboosted closed hydraulic circuit design.

Considerable attention has been given to digital computer modelling by using HASP as an aid to the investigation of the hydraulic circuit design proposed and its application. A large part of this thesis is given to the descriptions of the new HASP models developed. These model descriptions are followed closely to the standard form of documentation developed for HASP models in University of Bath. These model descriptions for model library are included in the Appendix II in order not to distract the attention of the reader from the main theme of the thesis.

In the third part, the attention is given to a partially closed hydraulic circuit design as shown in Fig. 1.7. Again computer simulation work has been justified by experimental results. Further consideration is given to the comparison of the system pressure performance with that of conventional system designs.

The fourth part of the thesis deals with a problem connected with linking component models which occurred in modelling the suction pipe junction. A linear interpolation method has been used to solve both algebraic and differential equations in a single model.

The fifth part considers a application of the partially closed circuit design to a hydrostatic drive boat propeller system. A test rig with the capability of performing open, unboosted and partially closed hydraulic systems for driving a boat propeller has been built in the Fluid Power laboratory in University of Bath. The system was then simulated using HASP. This entailed the development of a computer model for a propeller and transient performance of the whole system during initial start up of the propeller have been examined.

Finally, the sixth part is concerned with theoretical approaches to simulate

- 4 -

temperature distributions in hydraulic systems. The consideration is also given to the implementation of the theoretical approaches developed into the computer HASP software in order to model temperatures in other complex hydraulic systems. The temperature analysis of the partially closed hydrostatically driven boat propeller system has been given in order to provide a comprehensive understanding of thermodynamic processes during a hydraulic system operation. The results of the temperature simulation of the system have been justified by the experimental results which were obtained from the hydraulic drive boat propeller test rig mentioned above.
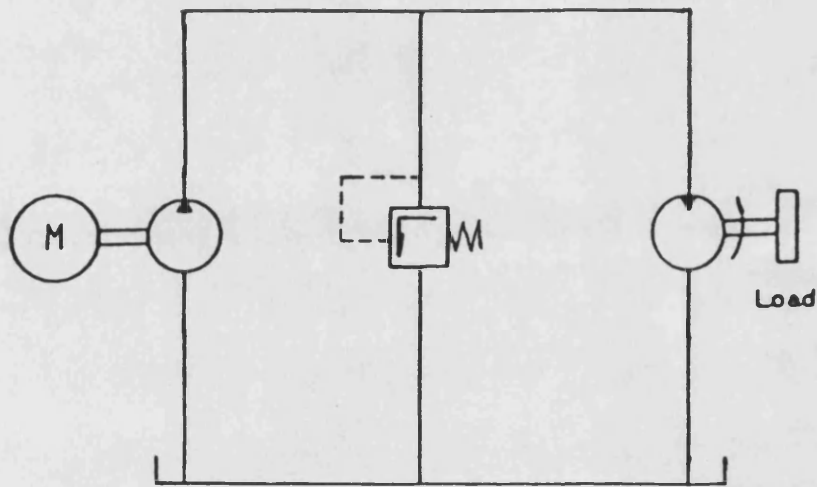
Fig. 1.1   A Typical Open Hydraulic System

Fig. 1.2   A Typical CLosed Hydraulic System
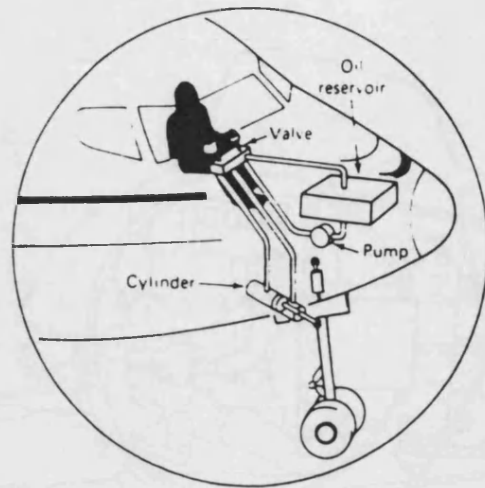
Fig. 1.3 An Application of an Open Hydraulic System to an Aircraft Landing Gear
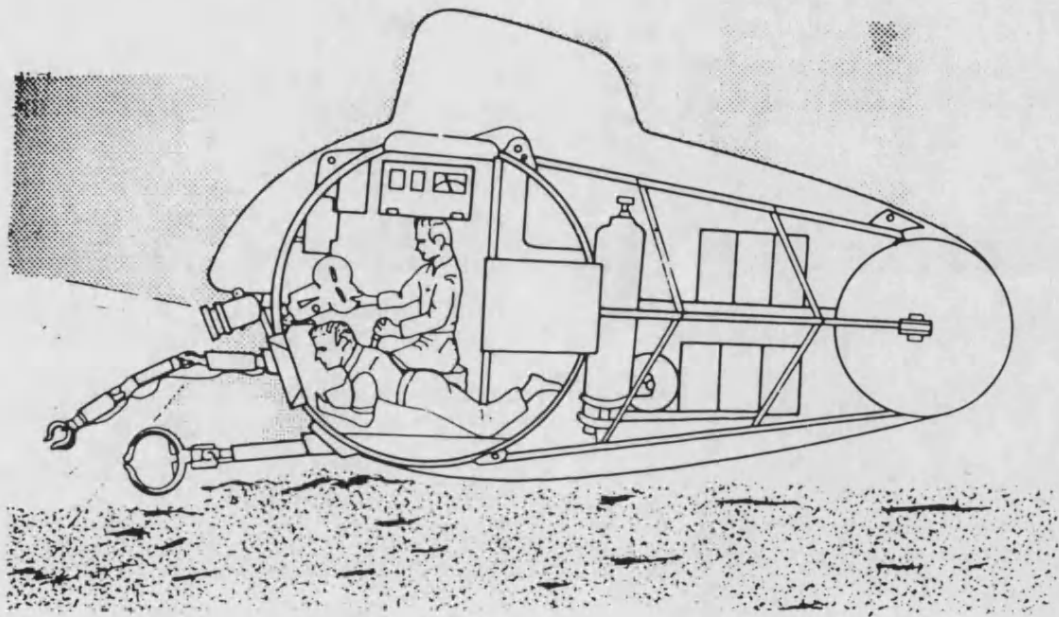
Fig. 1.4   An Application of a Closed Hydraulic System to an Undersea
Submarine

1 Pump
2 Motor
3 Feed section
4 Cooler

5 Filter
6 Pressure relief valve
7 Full-flow filter
   (when needed)
8 Hydraulic fluid tank
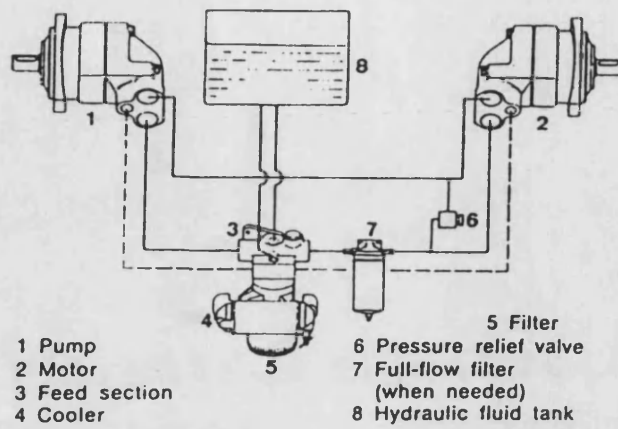
Connecting diagram
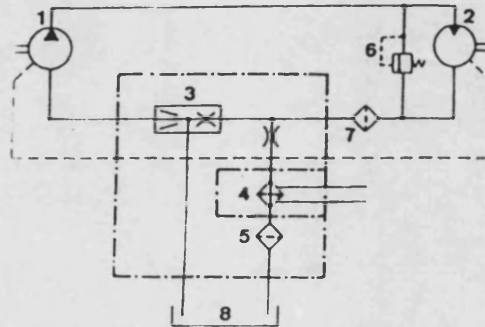
Fig. 1.5   The Volvo Injector Unit

Fig. 1.6   An   Unboosted   Closed Hydraulic System

Pump Entry Line

Interconnecting Line

Suction Line

Return Line to Reservoir

Load
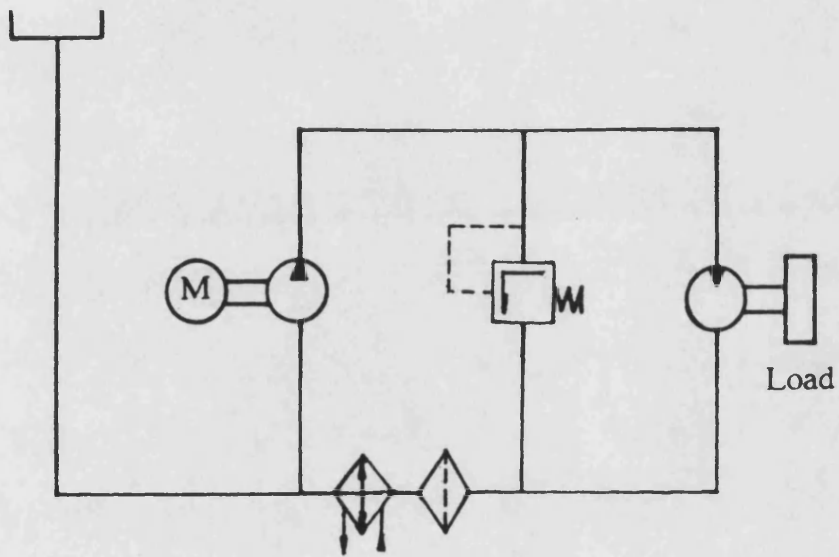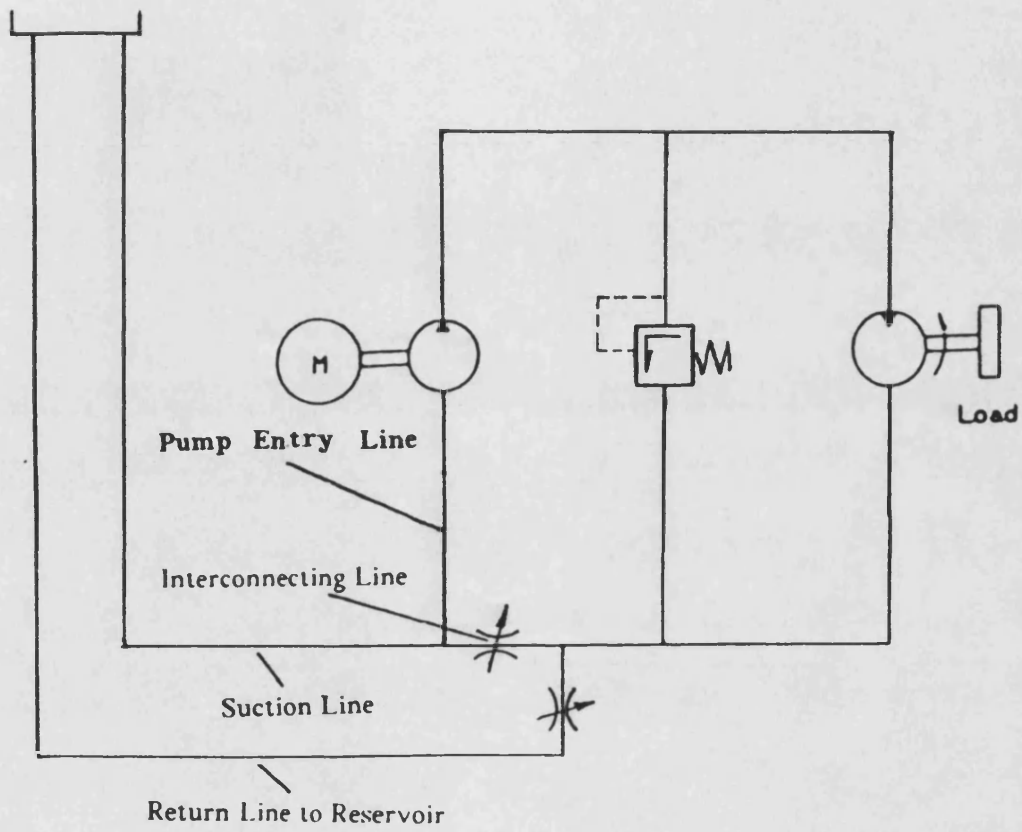
Fig. 1.7   The Proposed Partially Closed Hydraulic System

CHAPTER 2

PREDICTION FOR PERFORMANCE OF FLUID POWER SYSTEMS
USING HASP

Introduction

2.1 The Hydraulic Automatic Simulation Package (HASP) developed at the Fluid Power Centre of the University of Bath is used to simulate transient and steady state behaviour of hydraulic system and component. It has also been extended to account for the interactions between mechanical-hydraulic and electro-hydraulic devices. The fundamental aims of the package are:

1). to provide a computational tool which can be used by an industrial engineer or researcher with little or no knowledge of computer systems;

2). to provide a library of models for majority types of hydraulic components;

3). to provide a facility which allows changes in component parameters or in circuit configuration to be carried out without further need for programming;

4). to allow simple numerical and graphical examination of the behaviour of selected circuit parameters.

To satisfy these aims, the package automatically generates a simulation program for the hydraulic circuit or component under investigation. The program may be used at either the design stage, where the design of a proposed hydraulic system is investigated or else for a system already in operation.

Some details of HASP package have been in Ref. (2.1), (2.2), (2.3) and (2.4). A brief introduction to the package is given in this chapter since the simulation work described in this thesis has been carried out using the facilities available in the package. Moreover, the mathematical models, which will be discussed in this thesis for some components used in the unboosted and partially closed hydraulic systems and also for hydraulic system temperature analysis, have been used to set up corresponding HASP models to analyse the transient behaviours of the systems proposed. In this way, the component model library of the package has been extended.

Structure of HASP

2.2   Fig. 2.1 diagrammatically shows the main structures of HASP. In order to use the program, user is required to construct a type of a power bond diagram of the hydraulic circuit. This diagram represents how individual models of the system components are connected together in the hydraulic circuit to be simulated. It is then used to supply the computer with the information required to produce a simulation program defining the hydraulic circuit.

2.3   The component models in HASP exist in the form of individual subroutines in a component model library. These models can be connected together to define the hydraulic circuit configurations in a simple way so that the modifications of circuit can be easily carried out. The program which automatically links these individual component models is called a 'Program Generator'. The main purpose of the program generator is to provide subroutines which link existing component models to form a complete simulation program. The process of producing a simulation program for a hydraulic circuit is named as 'program generation'. The data required by the program generator to perform the program generation is termed 'Circuit Data'. The data consists of four character model names in the boxes together with the link ordering and signal numbers. It is also necessary to specify a model which is used more than once in a given circuit.

2.4 In order to determine the calling sequence of the component models in a simulation, the program generator checks the validity of the component data details supplied from the user by reference to a special file called COMPON.DAT. This file contains:

> 1). the number of links used in each model and the specification
>   of the information on a link as input or output;

> 2). the order of physical variables in the model calculation
>   subroutine argument list;

> 3). the arguments of state variables which are required for the
>   calling of the model calculation subroutines;

> 4). the number of data items supplied by the user to a input
>   subroutine.

If any information in the circuit data supplied is invalid, an error message will be given by the computer to help the user in making the appropriate corrections. If the circuit data are correct, the program generator will write a source file of main segments which is necessary to compile and link to the appropriate model subroutines to form the simulation program.

2.5 Once the procedure is completed satisfactorily, the program generator initially produces the main control segments (AUX) for the simulation. It automatically selects the relevant model subroutines from the component model library, and also links these with the integrator and the output control segment to produce the complete simulation program. The output control segment enables the simulation results to be stored and retried for graphical display or as a printout. The program generation need only be repeated when changes are required in the circuit configuration. Finally, a standard integrator employing Gear's method (Ref. 2.5) to solve stiff differential equations is included to complete the automatic building of the simulation program. One part of the simulation program is called the 'input stage' which allows the user to supply the dimensions and input parametric data of each model before the simulation starts. Hence, the simulation program is run interactively, the user responding to questions posed by the computer. When the program is first run, all the dimensions and parametric data must be supplied into

each model in turn. The simulation time and printing interval for the output data are also necessitated to be specified. The simulations of the same circuit can be carried out by the user reading the parametric data from disc and changing the selected items.

The User's Viewpoint

2.6 To demonstrate how the package may be employed to simulate the dynamic behaviour of a hydraulic system, a simple open loop hydrostatic transmission system is considered in Fig. 2.2. In this, a pump driven by a prime mover, an electric motor, supplies fluid to a hydraulic motor which drives a load. A relief valve is incorporated in the circuit to limit the maximum system pressure. The first step the user is required to take is to select appropriate component models by referring to the model library section. The computer power bond diagram of the circuit in terms of component models is shown in Fig. 2.3, the interconnecting links being numbered arbitrarily. The user must convert this diagram into a table of information (circuit data). The data corresponding to Fig. 2.3 acceptable to the program generator are given below:

```
09
TK0001      01
PU0001      01 02 03
PM0001      03
PI0501      02 04 05
PC0101      04 06
TK0002      06
MO0001      05 07 08
LR0001      08
TK0003      07
```

The first line indicates the number of component models in the circuit. The remainder of the lines give the component model names and define the link ordering between them. In each line, the four character mnemonic for the component model is followed by two digital number which indicate multiple occurrence of the same model, and the remainder of numbers relate to the external links. The program

generator initially checks the validity of the data supplied. When it is satisfied, a number of files are written and the program generation stops, so the simulation program is now ready for use.

There are two types of information can be transferred on the model external links. The first type is the link representing a one way transfer of information. The variable being transferred is called a 'free' variable due to its independence of other information which may exist on that link. The second type is the link representing a two way transfer of information. In such a case, one of items must be a state variable which is the result of the integration. Models calculating algebraic variables must be called first since their output forms the input to models producing state variables. When a practical circuit is simulated, it is likely that models will have a combination of these two link types. Hence, attention must be given to ensure that all input information to a model has been calculated either by adjacent models or by the integrator before inserting that model in the call list. The program generator continually goes through the user defined component list for a model where this criterion is met. If the generator finds there are still models to be included in the call list but none available due to two algebraic variables appearing on the same link, an error message will be shown on the terminal stating that an implicit relationship between the model exists. A certain amount of attention will be given in Chapter 4 and Appendix I to develop two alternative approaches as to avoid this type of implicit relationship on the model linking.

Mathematical Modelling

2.7   The mathematical representation of a component is to some extent shaped by the method of integration employed. For instance, in the pipe line modelling, the transient pressure change is affected by the compressibility of fluid and also fluid inertia and pipe friction terms. A complete dynamic model leads to the use of the distributed parameter method (Ref. 2.6 and 2.7). For most practical cases, the effects of compressibility only are significant, except in the case of extremely long pipelines. Hence the lumped parameter method can be used to analyse the transient response of fluid pipelines. For most hydraulic systems, this form of modelling provides an excellent representation of the true system dynamic behaviour. For this

reason, the present version of HASP does not attempt to represent distributed parameter phenomena using partial differential equations, but uses ordinary differential equations to describe dynamic behaviour of hydraulic components. For example, for the simulation of the open loop hydrostatic transmission system shown in Fig. 2.3, the following relations exist in the component models.

Pump Model   The input parameters calculated in the adjacent models to the pump model PU00 are:

1) the pump rotating speed ω_p which is defined by
    the prime mover model PM00 and given as the flow on
    link 3;

2) the pump inlet pressure P_1 which is defined by
    the tank model TK00 and given as the effort on link 1;

3) the pump inlet pressure P_2 which is defined by
    the tank model PI05 and given as the effort on link 2.

The pump model calculates its inlet and outlet flowrates, Q_1 and Q_2. The pump outlet flowrate is obtained from

$$Q_2 = Q_{th} - Q_{si} - Q_c$$
$$= \omega_p D_p - C_{si} \frac{(p_2 - p_1)}{\mu} - \frac{p_2 - p_1}{B} \omega_p D_p \qquad \ldots\ldots (2.1)$$

In the above equation, Q_{th} is the theoretical flowrate, Q_{si} the internal slip loss, Q_c the compressibility loss, B the fluid bulk modulus, D_p the displacement of the pump and C_{si} the internal slip loss coefficient. Similarly, the pump inlet flowrate is given by

$$Q_1 = Q_{th} - Q_{si} \qquad \ldots\ldots (2.2)$$

Motor Model   Similarly, the motor inlet and outlet pressures, P_5 and P_7, and also the motor shaft speed ω_m are calculated in the motor adjacent models. The motor model MO00 gives the inlet and outlet flowrates, Q_5 and Q_7, and also the torque required to drive the load. The motor outlet flowrate is defined from

$$Q_7 = Q_{th} - Q_{si} + Q_c$$

$$= \omega_m D_m - C_{si} \frac{(p_s - p_7)}{\mu} + \frac{p_s - p_7}{B} \omega_m D_m \qquad \dots \dots (2.3)$$

and the inlet flowrate is given by

$$Q_s = Q_{th} - Q_{si} \qquad \dots \dots (2.4)$$

The torque delivered by a motor is calculated from:

$$T_m = T_{th} + T_v + T_f \qquad \dots \dots (2.5)$$

where T_v is the speed dependent torque loss and T_f the pressure dependent torque loss. The details for the coefficient calculations for the pump and motor models of PU00 and M000 are well documented in the HASP model write up (Ref. 2.8), similar information is shown in Appendix II for the descriptions of the pump and motor models PUAH and MOAH.

Relief Valve Model   The flowrate through the relief valve is calculated in the simple relief valve model PC01 on the basis of the relation

$$Q_4 = K(p_4 - p_6) \qquad \dots \dots (2.6)$$

Pipe Model   As mentioned before, the only fluid compressibility effect is considered in the pipe model PI05, the pressure in the pipe linking the pump, motor and relief valve is given from

$$\frac{dp}{dt} = \frac{B}{V}(Q_2 - Q_4 - Q_5) \qquad \dots \dots (2.7)$$

This pressure value appears as state variables in the form of the effort on link 2, 4 and 5.

Load Model This model calculates the shaft speed of the motor on the basis of the following relation

$$\frac{d\,\omega_m}{dt} = \frac{T_m - f\,\omega_m}{J} \qquad\qquad \ldots\ldots(2.8)$$

In the above, T_m is given by the motor model and the coefficient f is determined by the characteristics of the load.

Using the above models, simulations can be carried out to investigate the transient and steady state behaviours of the open loop hydrostatic transmission system shown in Fig. 2.2. The simulations can also be used in the design stage to aid the designer to select the parameters of the components in the system.

2.8 Accuracy of Simulation The simulations using HASP have been found over the years to be as accurate as the data input permits. The errors due to digital integration appear to be generally insignificant. when simulations are performed for the systems existing in a laboratory, the results can be as accurate as the experimental techniques available to check them. However, the focus is what is required in the way of input data in order to perform simulations and it is here that the greatest inaccuracies are found. In the simulations, the commonest difficulty is the identification of the load and its corresponding duty cycle. Without appropriate experimental tests on an actual machine being simulated during a series of duty cycle, it is almost impossible to obtain the information with any accuracy.

Some of component characteristics can be obtained from manufacturers. But these can be too optimistic, particularly when the components are running at regions away from the design point. In many cases, very little information is available concerning the dynamic characteristics of the component investigated. In these cases simulation can be of significant assistance to determine the component characteristic values which are usually far too time consuming to do by hand calculation. In most cases, a careful analytical approach is essential to develop new component models. Indeed, the simulation results, which are obtained by adding a new component model into a simulation circuit, are needed to correlate with corresponding

experimental results. Attention is often necessary to amend some of input parameters to take into account degradation due to wear or other causes. Further studies may be carried out to extend the applicability of the newly developed model. The procedure for the development and verification of new HASP models will be demonstrated in the following chapters.
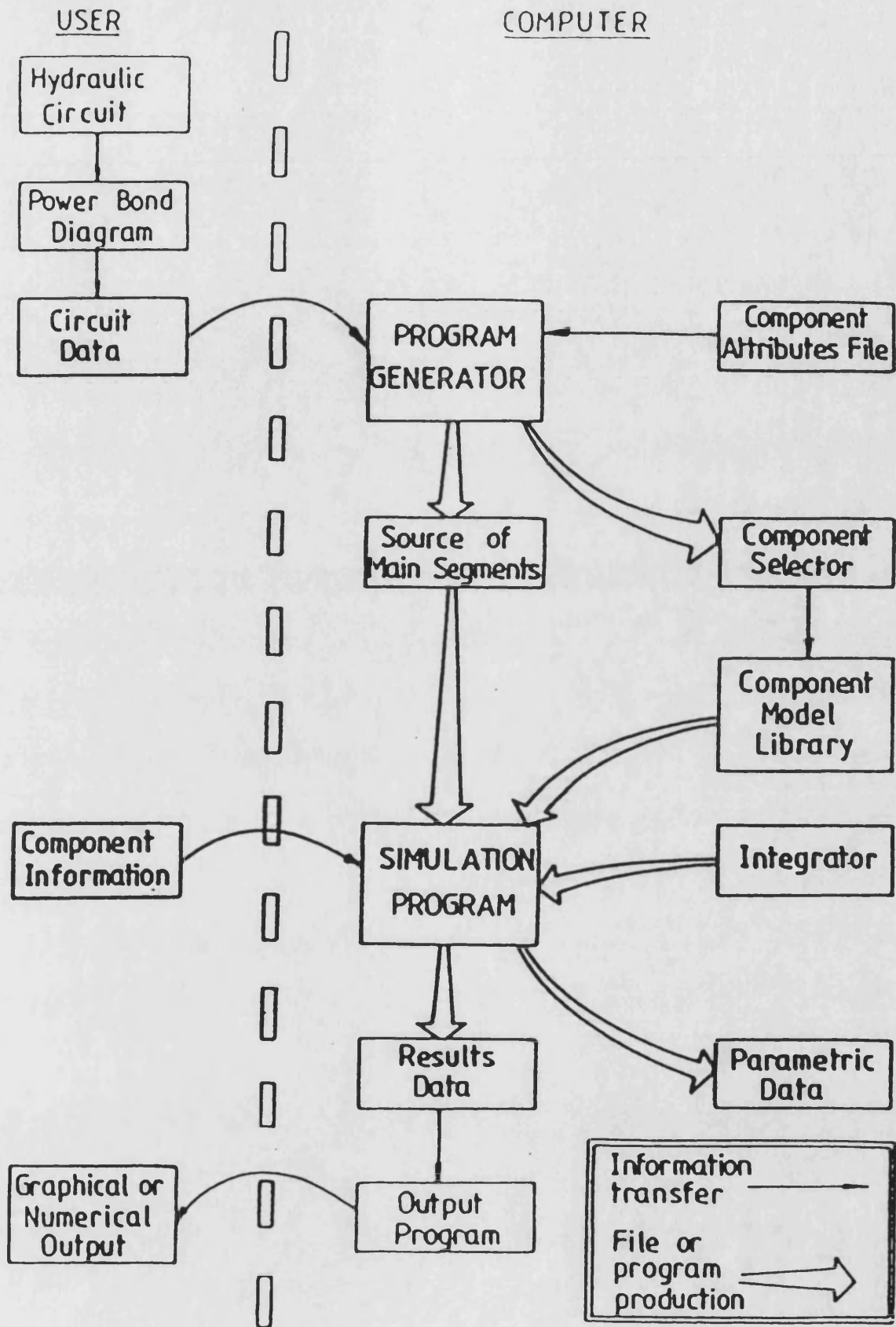
Fig. 2.1   General Structure of HASP
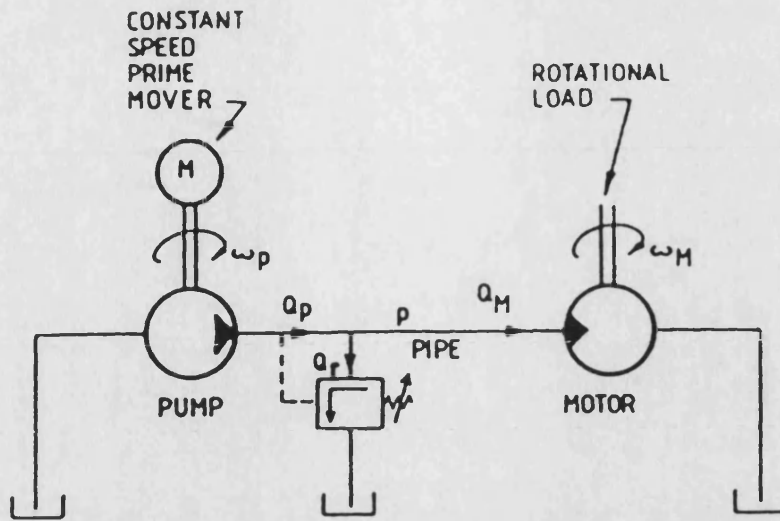
Fig. 2.2 Simple Open Loop Hydrostatic Transmission System
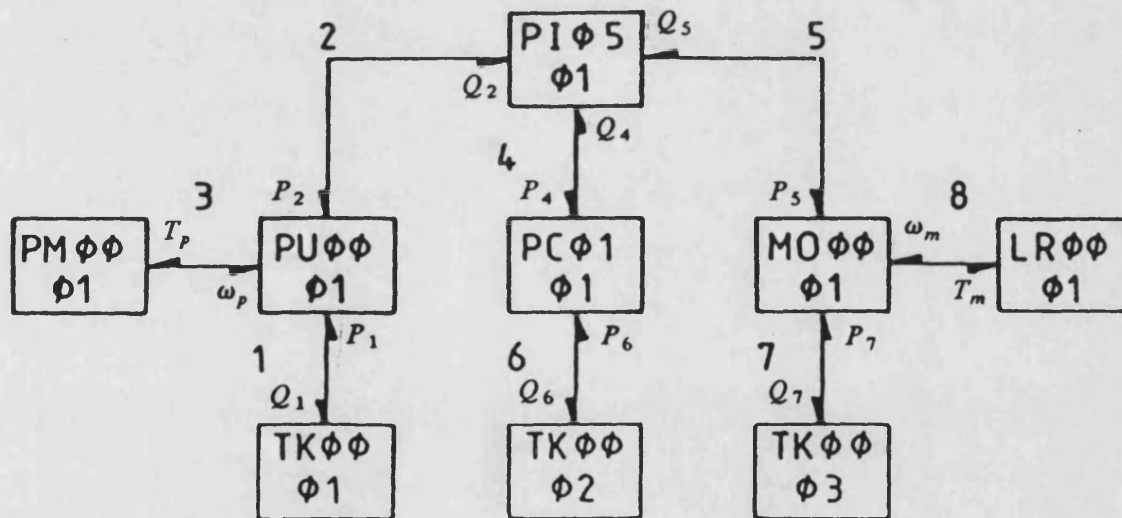
Fig. 2.3 HASP Linking Diagram Corresponding to the Open
Loop Hydrostatic Transmission System

CHAPTER 3

FUNDAMENTAL STUDY OF AN UNBOOSTED CLOSED HYDRAULIC CIRCUIT

Introduction

3.1 The object of this chapter is to establish the fundamental understanding of the characteristics of an unboosted closed loop hydraulic circuit. An unboosted closed loop hydraulic circuit design can originate either from the removal of the boosted pump in the closed loop circuit or from the change in the piping arrangement of an open loop hydraulic circuit to give a reduction in the tank size. The work here is mainly concentrated on the theoretical and experimental analysis of the transient system performance with particular reference to the transient system discharge pressure and suction pressure. The theoretical analysis is involved with using HASP mathematical models for some system components and the development of other mathematical models for other components within the system in order to form a complete system equations to describe the dynamic behaviour of the system. The mathematical models developed are programmed in the form of HASP computer models for numerical simulation of the system transients. The theoretical analysis of the computer simulation is compared with the experimental measurements obtained from an extensive test programme on a simplified circuit test rig.

3.2 Simplified Circuit for Fundamental Investigation   The performance of the system can be investigated in a simple test system. The theoretical approach used for the simple system can be extended to cover more complex systems. Even the most complex of hydraulic systems may be considered to be constructed from just four basic elements. These are pumps, pipelines, control valves and loading components. Hence, a simplified system which leads to a pump-pipe-loading valve

system has been considered as shown in Fig. 3.1.

In this system, an electric motor being used is one of two usual prime movers (another is a diesel engine) to provide energy source. A gear pump without external drain is driven by the electric motor. An orifice restrictor simulates the usual loading component (ie. hydraulic motor or actuator), together with a by pass through a manually operated directional control valve. The system is loaded by closing this valve. A cooler is incorporated in the return line to dissipate the heat generated and a filter is placed before the cooler to keep the contamination at an acceptable level. Since no external flow leakage in the system, an extreme case is tested in which the reservoir is completely removed from the system and the suction line held vertically above the pump inlet, with its top end open to atmosphere. Therefore, the flow variations due to the compressibility effects are made up by the flow from the open ended pipe under a pressure head.

3.3 In this work, wave propagation effects have been ignored because the pipe lengths are relatively short and therefore the approaches of the distributed parameter technique have been considered unnecessary. In the system considered in Fig. 3.1, the simulation of the system behaviour can be carried out using HASP models to represent most of the system components. However, some of component models including the suction open ended pipe are not readily available in the model library of the package, hence some new models are required to be developed. The mathematical modelling of each of the components involved will be firstly discussed.

3.4 Electric Motor In many hydraulic transmission systems, an induction electric motor is the energy source. An induction motor operates under dynamic conditions when the speed changes from one steady value to another. A change in speed will result from a change in the voltage applied to the motor or from a change in load conditions when the machine is operating under the stable conditions. The case which is considered here is not a change in the supply voltage but in the pump load conditions. Such machines operate at a speed steadly less than synchronous and to a first approximate line 'slip' is proportional to the torque supplied during steady operation. The slip will change when the applied voltage changes or when the load torque changes.

The torque-speed curve for an induction motor is shown in Fig. 3.2, in which T_1, T_2 and ω_1, ω_2 are the torques and shaft speeds under two specific working conditions. In general, the motor is working below the torque value of T_{max} stable region. In this region, the slip S is defined by

$$S = \frac{\omega_s - \omega}{\omega_s} \qquad \qquad \ldots \ldots (3.1)$$

It is noted that under normal operating conditions the change in the

speed is relatively small. The torque is assumed to be a linear function of speed up to the load T_L, so the developed torque at ω can be described as

$$T_e = K_e(\omega_s - \omega) \qquad \qquad \ldots\ldots (3.2)$$

where

$$K_e = \tan\alpha = \frac{T_2 - T_1}{\omega_1 - \omega_2} \qquad \qquad \ldots\ldots (3.3)$$

can be obtained experimentally for a specific practical system.

In the general equation for torque, the dynamic electrically developed torque with the motor on load for induction motor can be evaluated as follows

$$T_e = T_L + J\frac{d\omega}{dt} + K_1\omega \qquad \qquad \ldots\ldots (3.4)$$

where J is the effective inertia and K_1 is the damping torque due to eddy currents. Substituting Equation (3.2) to (3.4) and re-arranging enables the dynamic speed to express from

$$\frac{d\omega}{dt} = \frac{K_e\omega_s - (K_e + K_1)\omega - T_L}{J} \qquad \qquad \ldots\ldots (3.5)$$

Equation (3.5) can be numerically integrated if the initial conditions are known. A HASP model of the induction electric motor, incorporated equations (3.2), (3.3) and (3.5), is given in Appendix II and has been allotted the name PM2H.

3.5 **Internal Drained Gear Pump**   Since an external gear pump with an internal drain pathway is used in the system, the pump delivery flowrate Q_{pout} is defined by

Q_{pout} = theoretical flow - internal leakage flow - compressibility flow

$$Q_{pout} = \omega D - K_l(p_3 - p_1) - \frac{p_3 - p_1}{B}\omega D \qquad \dots\dots(3.6)$$

The pump inlet flowrate Q_{pin} is expressed from

Q_{pin} = theoretical flow - internal leakage flow

ie.

$$Q_{pin} = \omega D - K_l(p_3 - p_1)$$

The torque required to drive a pump is calculated from:

$$T_p = T_{th} + T_v + T_f \qquad \dots\dots(3.7)$$

where T_{th} = $(p_3 - p_1)D$ is the theoretical torque. $T_{i}v$ is the speed dependent torque loss and T_f the pressure dependent torque loss. The pump torque T_p is the load torque of the electric motor T_L.

3.6 Fluid Lines

A great deal of research effort has been put into the study of the pressure ripple phenomenon in pipelines (Ref. 3.1 and 3.2). Following electrical transmission line technique a hydraulic line between two cross sections is characterised by a four-terminal network with pressure and flow the interacting variables. On the basis of this, a method of distributed parameters was developed to analyse the effects of compressibility and compliance of pipeline under unsteady flow in fast response hydraulic systems as well represented in (Ref. 3.3 and 3.4). For most practical purposes, except in the case of extremely long pipelines, the effects of fluid compressibility only are significant. So the constant lumped approach can be applied to describe the fluid transient behaviour in the pipelines of the system.

- 19 -

The following assumptions are made during the study of the pipelines:

(1).   The temperature variation is very small during the transient
       conditions so that the fluid viscosity may be considered to
       be constant.

(2).   The pipe friction has been neglected because the
       pipe lengths are short.

Let L designate the distance between two cross-section along the pipe, B the effective Bulk Modulus and A the cross-sectional area. When fluid inertia and pipe friction terms are neglected, the derivation of average pressure at a pipe cross section will be only denoted by $p(t)$, as shown in Fig. 3.3. The relationship of the flowrates at the two cross sections of the line is given by

$$Q_i = Q_{ii} + \frac{AL}{B} \frac{dp}{dt} \qquad\qquad \ldots\ldots (3.8)$$

In the above argument the effect of fluid inertia has not been taken into account. In one of the pipes, it is considered to be very important. This is the open ended pipe, and it is modelled separately as given in Section 3.12. For most pipes HASP model PI05 has been used. This model not only takes into account compressibility but also models the effects of air release and cavitation.

3.7   Orifice Restrictor   It is generally assumed that orifices follow closely their steady state characteristics during transient operation. However, this assumption of steady behaviour may lead to errors in predicting transient flow conditions under certain circumstances. In order to evaluate the transient behaviour of orifice, a differential equation relating the flow through and the pressure drop across an orifice was derived.

I. Flow Characteristics of Orifice

As the results have been shown in Ref. (3.5), the flow through a sharp edged orifice initially separates at the sharp entrance edge, except at very low Reynolds numbers (Re less than about 10), or at conditions where compressibility effects are significant. Downstream of this, the flow may either remain separated right through the orifice or may reattach to the wall of the orifice. The orifice thickness/diameter ratio, t/d, at which the flow changes from one condition to the other will be influenced by flow parameters such as Reynolds number and by geometrical parameters. In common with most separation phenomena there is likely to be a range of values of t/d over which condition may occur with a discontinuity in the pressure loss coefficient when the change over takes place.

3.8   The Effects of Orifice thickness/Diameter Ratio   The characteristics of the flow through an orifice depend on whether the jet which is formed downstream of the orifice entry remains separated or whether it reattaches to the orifice wall. The influence of t/d on the separation and reattachment of the flow has been investigated by Ward Smith (Ref. 3.6). Various incompressible flow regimes have been identified and the corresponding flow patterns are shown in Fig. 3.4 to Fig. 3.8 which have been taken from Ref. (3.6).

In the fully separated flow regime (over a range of small t/d) shown in Fig. 3.4 and Fig. 3.5, the flow remains separated from the surface of the orifice. As t/d is increased, the jet tends to spread to touch the inner wall of the orifice and this is known as the marginally-separated flow regime as shown in Fig. 3.6. With further increase in t/d, the jet reattaches to the orifice and immediately separates again as shown in Fig. 3.7. This is the marginally-reattached flow regime. In the fully-reattached flow regime (t/d large) shown in Fig. 3.8, the flow separates from the orifice entry and, for the high Reynolds numbers under consideration, reattaches in the form of a turbulent boundary layer. The two intermediate stages of marginally-separated and marginally-reattached flow in Fig. 3.7 and Fig. 3.8 represent an uncertain regime where, for a given value of t/d, either reattached or separated flow can occur. Two main types of flow have therefore been identified: separated and reattached flow.

Free Jet Flow   In the limiting case of zero wall thickness ($\frac{t}{d} \to 0$), as in the case of sharp edged orifice, the flow separates away from the surface of the orifice to

form a discrete jet, which contracts to a minimum cross-sectional area known as the vena contracta, with a separated flow region, as shown in Fig. 3.4. The separating streamline is well defined between the orifice entry and the vena contracta, in which region the flow has the characteristics of a laminar free shear layer as it is subject to a pressure gradient. Downstream from the vena contracta, transition takes place and the distinct identities of the jet and separated flow are rapidly lost due to turbulent mixing in a region dominated by a adverse pressure gradient. Flow is entrained into the edge of the jet in the mixing region, thereby giving rise to a circulatory motion within the separated region. Since the continuity condition must be satisfied within the separated region an amount of fluid, equal to that previously entrained, is returned to the separated flow in the region where the jet boundary finally attaches to the duct wall. It is suggested in Ref. (3.7) that the axial static pressure gradient associated with the frictional flow in a straight pipe is strictly not recovered for about 30D downstream of the component although a distance of 6D may usually be assumed with no significant loss in accuracy.

Fully Reattached Flow   The case at the other extreme (i.e. large t/d) is considered next and Fig. 3.8 shows how the flow appears. The flow separates cleanly from the surface at the orifice entry to form a free shear layer. For the high Reynolds numbers under consideration, transition takes place within the shear layer and reattachment in the form of a turbulent boundary layer follows. Between the free shear layer and the internal boundary of the orifice, a separation bubble is formed. The experimental results given in Ref. (3.8) suggest that the length of this separation bubble is about 0.8D. Downstream from the reattachment point, the turbulent boundary layer develops and eventually separates at the downstream face of the orifice. The exit condition is simply that of flow with a developing velocity profile through a sudden enlargement, for which recovery of the flow is achieved about 4 duct diameters downstream from the enlargement plane suggested by Hall and Orme (Ref. 3.9).

II.   Pressure Drop Characteristics

3.9   Definition of Pressure Loss   Fig. 3.9 taken from Ref. (3.7) shows a typical experimental static pressure distribution along the axis of a duct containing an

orifice plate. The static pressure drop is defined by

$$p_s = (p_{m1} - \Delta p_{s1}) - (p_{m4} + \Delta p_{s4}) = p_1 - p_4 \qquad \ldots\ldots (3.9)$$

where p_{m1} and p_{m4} are static pressures measured in the system at station 1 and 4 respectively and p_1 and p_4 are static pressures at the same points but corrected for pipe friction losses up to the entry and beyond the exit of the orifice. Δp_{s1} and Δp_{s4} are the friction losses in the straight pipes upstream and downstream of the orifices. The total pressure loss, Δp_t, is defined similarly. Station 1 and 4 are strictly taken to be in region of fully developed flow but provided that the velocity profile is symmetrical and not far removed from that appropriate to fully developed flow, no significant effect of inlet velocity profile is found.

3.10 Analysis of the Pressure Drop Characteristics
The flow models which have been described in Section 3.8 will now be analysed. The analysis will be aimed at determining the broad features influencing the flow, and the simplifications consistent with this end will be introduced.

In Fig. 3.4 to 3.8, station 1 corresponds to conditions in the duct upstream of the orifice, station 2 corresponds to the upstream face of the orifice, station 3 corresponds to the vena contracta, station 4 to recovery downstream and station 5 corresponds to the downstream face of the orifice.

In what follows it is assumed in Ref. (3.10) that:

1). the flow is incompressible;

2). at the vena contracta, a separated region and a free jet can be identified;

3). the length of fluid jet is a time independent factor and for the sharp edged orifice this length is usually assumed as 6 times duct diameters;

4). the properties of the flow at station 1 and 4 and of the jet at station 3 may be adequately described by one-dimensional flow relations;

5).   the flow in the jet is isentropic between station 1 and station 3;

6).   the contribution of the shear stress at the duct wall to the momentum balance can be ignored;

7).   the contribution to the momentum balance of the separated flow at station 3 is negligible; (It implies that the net momentum flux of the velocities moving upstream and those moving downstream in the separation region is small compared with the momentum flux in the jet. and follows from a consideration of the continuity condition in the separated region.)

8).   the mean static pressures of the separated flow and of the jet at station 3 are equal.

Free Jet and Fully Separated Flow   Incorporating the assumptions outline above, the following equations may be written down for both free jet and fully separated flow:

The Bernoulli equation applied to the jet between the plane 1-1 and 3-3 is

$$p_1 + \frac{1}{2}\rho v_1^2 = p_3 + \frac{1}{2}\rho v_{3c}^2 + \frac{1}{2}k\,\rho v_{3c}^2 \qquad\qquad \ldots\ldots (3.10)$$

where k is the energy loss coefficient reforced to the dynamic pressure at the vena contracta.

Continuity of flow in the jet is represented by the relations under incompressible conditions

$$v_1 = \phi C_c v_{3c} = v_4 \qquad\qquad \ldots\ldots (3.11)$$

where C_c is coefficient of contraction and

$$\phi = \frac{A_o}{A}$$

(A_o is the opening area of orifice and A pipe cross sectional area).

The above two equations can be solved to obtain steady state fluid velocity at vena contracta

$$v_c = \frac{1}{(1 + \phi^2 C_c^2 + k)^{\frac{1}{2}}} (\frac{2\Delta p_c}{\rho})^{\frac{1}{2}} \qquad \dots \dots (3.12)$$

The flowrate through orifice can be expressed from

$$Q = v_c A_o = C_v C_c A_o (\frac{2\Delta p_c}{\rho})^{\frac{1}{2}} = C_d A_o (\frac{2\Delta p_c}{\rho})^{\frac{1}{2}} \qquad \dots \dots (3.13)$$

For fluid power system in which orifices are used as flow restrictors, $(\frac{d}{D})^2$ is usually below 0.1. Under the conditions when Reynolds Number is large, the coefficient of contraction C_c is given in (Ref. 3.11) between 0.61 to 0.63, then velocity coefficient is between 0.97 to 0.98, therefore the discharge coefficient is between 0.60 to 0.61.

When cavitation occurs at the downstream of orifice, the local pressure of $p_c = p_v$, the vapour pressure. The vapour pressure of mineral oils are much lower than that of water, typically 4.5 $\times 10^{-5}$ mbar at 20° C and increases with temperature such as 6 $\times 10^{-4}$ mbar at 40° C. For practical purposes it can be taken as absolute zero pressure at room temperature. If the pressure $p_c = p_v = 0$, then the flow will be limited by the vapour cavities and the air release. In this case, the flow equation becomes

$$Q_{max} = C_d A_o (\frac{2\Delta p_c}{\rho})^{\frac{1}{2}} = C_d A_o (\frac{2p_1}{\rho})^{\frac{1}{2}} \qquad \ldots \ldots (3.14)$$

The Reynolds number has its effects on the flow pattern and also the discharge coefficient C_d. The experiments have been performanced to investigate these effects using glass or perspex models (Ref. 3.12). The following phenomena have been observed. At very low values of Reynolds number Re (less than about 10) based on orifice diameter and mean velocity in the orifice, the flow remains attached to the orifice. When Re = 150, the flow starts to separate from the surface at the orifice entry to form slow vetox and a jet at downstream of the orifice. As Re = 250, outer edge of jet becomes unstable due to the shearing effects of the outer layers. As the Reynolds number increases, jet flow fully contracts and outside a lot of vetox exist but jet itself is stable. The above theory applies when the Reynolds number is greater than 1000. W. Wuest (3.12) studied fluid condition for sharp edged orifice under low Reynolds Number conditions, he recommended the following relations for the discharge coefficient calculations

$$C_d = \begin{cases} 0.2\sqrt{Re} & \text{If smooth entrance} \\ 0.157\sqrt{Re} & \text{If sharp edged entrance} \end{cases} \qquad \ldots \ldots (3.15)$$

The above relations can be only applied to the conditions in which the Reynolds number is smaller than 200 and the orifice diameter is much smaller than in line pipe diameter.

Dynamic Behaviour of in Line Sharp Edged Orifice When a step change in pressure drop across the orifice occurs, the flow is accelerated due to the formation of the jet at the downstream of the orifice. In most orifice employed in fluid power systems the upstream velocity of approach effects is much smaller than that of the fluid jet at the downstream and hence the effects of fluid acceleration at the upstream are negligible. In such cases, when a lumped parameter method is used, the fluid mass of jet being accelerating can be assumed as constant, the momentum balance between stations 3 and 4 is proposed to be expressed by

$$(p_3 - p_4)A_o = \rho Q (v_4 - v_{3c}) + \frac{d(mv_{3c})}{dt} \qquad \dots \dots (3.16)$$

In the equation above, the fluid mass of jet m has arbitrarily been assumed to be of conical shape and all accelerating at the velocity v_3

$$m = \rho \frac{(C_c A_o + A)}{2} L_1 \qquad \dots \dots (3.17)$$

where L_1 is the distance between station 3 and 4 as shown in Fig. 3.10.

Now, substituting Equation (3.17) into Equation (3.16) we have

$$p_3 - p_4 = \rho(\phi C_c - 1)v_{3c}^2 + \frac{\rho L_1}{2A_o}(C_c A_o + A)\frac{dv_{3c}}{dt} \qquad \dots \dots (3.18)$$

If we take

$$L = \frac{L_1}{2A_o}(C_c A_o + A) = \frac{L_1}{2}(C_c + \frac{1}{\phi C_c}) \qquad \dots \dots (3.19)$$

in above equation, L_1 is a time independent factor of fluid jet length and has been assumed to be 6 times downstream duct diameter (6D) for the in line sharp edged orifice. This assumption is based upon the experimental results reported in Ref. (3.6) and (3.7). In the case where the downstream of orifice is a large reservoir, fluid jet emerges with fluid in the reservoir. Zalmanzon and Semikova (Ref. 3.13) have discussed the pressure distribution within the conical shape fluid jet in detail and a number of empirical equations have been proposed to study the pressure along the jet axis. But such a case will not be considered in this thesis, since we are more interested in the dynamic behaviour of in line orifice restrictor. Hence from Equation (3.19), Equation (3.18) becomes

$$p_3 - p_4 = \rho(\phi C_c - 1)v_{3c}^2 + \frac{\rho L}{A_o}\frac{dQ}{dt} \qquad \dots\dots(3.20)$$

Combining Equation (3.10), (3.11) and (3.20) gives the following recommended relationship for the dynamic characteristics of the sharp edged orifice

$$p_1 - p_4 = \frac{\rho}{2C_d^2 A_o^2}Q^2 + \frac{\rho L}{A_o}\frac{dQ}{dt} \qquad \dots\dots(3.21)$$

In the above equation, L is the equivalent length of fluid jet at downstream of the orifice and is defined in Equation (3.19). This equation needs computer solution, and using this equation a dynamic orifice HASP model OR2H has been developed to simulate transient behaviour of orifice loading valve in the system considered. The detailed description of OR2H in the HASP model writing up format is included in Appendix II.

3.11 Cooler and Filter
When flow passes through the cooler and cooler, both flow fluctuation and pressure surge reduce in amplitude and frequency due to the large fluid capacity. The effects of the cooler and filter on the system flowrate and pressure are similar to that of a surge tank. Hence, the cooler can be considered as an equivalent capacity pipeline between two fixed orifice restrictors as shown in Fig. 3.11. In this way, the flow restrictions can be lumped to the entrance of the filter and the exit of the cooler, the filter and cooler have been simulated by two orifices, to give their pressure drops, and a pipe, to simulate their combined compliance.

3.12 Open Ended Pipe
In the system being investigated as shown in Fig. 3.1, when the directional control valve is closed , the flowrate through the valve, Q_4, reduces to zero. Meanwhile, the pump delivery pressure p_3 rises to a higher value which is determined by the orifice loading valve.

One of the consequences of the increment of p_3 is the occurrence of

compressibility in the high pressure line of the system. As a result, the pump spontaneously takes flow from the open ended pipe at the rate of Q_1 to make up the compressibility loss. Hence the column of the flow in the open ended pipe is accelerated, and oscillates towards a new stationary condition. Correspondingly, when the directional control valve is unloaded, the acceleration will be in the opposite direction.

Applying momentum theory for the flow in the open ended pipe

inertia force + friction force + static fluid force =
transient fluid force at the bottom of the pipe

ie.

$$\frac{d\,(mv\,)}{dt} + p_f\,A + A\,\rho gh = p_1 A \qquad\qquad \ldots\ldots(3.22)$$

In the above equation, the pressure loss to friction is defined by the flow conditions as

$$p_f = \begin{cases} \dfrac{32\mu h v}{d_1} & \textit{Laminar Condition } \mathrm{Re} \leqslant 2000 \\[2mm] \lambda\dfrac{l\rho v^2}{d} & \textit{Turbulent Condition } \mathrm{Re} > 2000 \end{cases}$$

$$\ldots\ldots(3.23)$$

For the smooth circular pipes under turbulent condition, the friction factor λ can be obtained from the empirical relations proposed by Blasius (Ref. 3.14) and Nikuradse. These relations can be written down as

$$\lambda = \begin{cases} \dfrac{0.3164}{Re^{0.25}} & 10^4 < Re < 10^5 \\[2mm] 0.0032 + \dfrac{0.221}{Re^{0.237}} & 10^5 < Re < 3\times10^6 \end{cases}$$

$$\dots \dots (3.24)$$

In Equation (3.22), m = ρAh, and

$$\frac{d(mv)}{dt} = m\frac{dv}{dt} + v\frac{dm}{dt} \qquad \dots \dots (3.25)$$

where for any flow in the pipe changes in the volume, oil density and mass with time are related according to the following equation

$$\frac{dm}{dt} = \rho\frac{dV}{dt} + V\frac{d\rho}{dt} = \rho A\frac{dh}{dt} + Ah\frac{d\rho}{dt} \qquad \dots \dots (3.26)$$

Substitute Equation (3.25) and (3.26) into (3.22), then re-arrange as

$$\rho h\frac{dv}{dt} + \rho v\frac{dh}{dt} + vh\frac{d\rho}{dt} + p_f + \rho gh = p_1 \qquad \dots \dots (3.27)$$

The variation of the density of mineral oil in the open ended pipe is not considered to be sufficiently significant to include in the theoretical analysis. If the column of the flow in the open ended pipe is assumed to move as a whole, the fluid velocity in the pipe is expressed from v = $\dfrac{dh}{dt}$. Hence, Equation (3.27) becomes

$$p_1 = \rho h\frac{dv}{dt} + \rho v^2 + p_f + \rho gh \qquad \dots \dots (3.28)$$

As can be observed, there are considerable difficulties in any attempt to solve this equation as being a non-homogeneous differential equation. However, a clearer view can be obtained by putting the time derivation on the left hand side

- 30 -

$$\frac{dv}{dt} = \frac{p_1 - p_f}{\rho h} - \frac{v^2}{h} - g \qquad \qquad \dots \dots (3.29)$$

If the initial conditions are given, this equations can be used to calculate v by applying the numerical integration techniques which are widely used in computer simulation. A corresponding model has been developed incorporating this equation and allotted the mnemonic PIOH.

3.13 Fluid Expansion in the Downstream of Pressure Valve

It is a general accepted assumption in any theoretical analysis of the flow conditions of pressure control valve that the fluid density is a constant both in the inlet and outlet pipelines. This assumption was based on the fact that a very small change in fluid density was found with a large variation of the fluid working pressure. It is applicable in the theoretical modelling to the majority of the hydraulic systems. However, this assumption of constant fluid density can lead to errors in predicting the system characteristics of the recirculatory system being investigated. Therefore, the changes in the fluid density across the orifice can not be ignored in this special case. This small but significant difference between the orifice inlet and outlet flowrates due to fluid expansion should be considered. This can be taken into account in the orifice model in the following manner.

At constant temperature the variation of fluid density with pressure is usually expressed in terms of a compressibility defined as

$$C = -\frac{1}{v} \left(\frac{\partial v}{\partial p} \right) \qquad \qquad \dots \dots (3.30)$$

where $v = \dfrac{1}{\rho}$ = specific volume or its reciprocal, the Bulk Modulus, B. In general, C is a point function varying for a given liquid with both pressure and temperature. Over pressure regions where the variation of specific volume with pressure is small and nearly linear (Ref. 3.15), either of two essentially equivalent equations may be used

- 31 -

$$\rho = \rho_o \left[1 + C(p - p_o) \right] \qquad \dots \dots (3.31)$$

or

$$\rho = \frac{\rho_o}{1 + C(p - p_o)} \qquad \dots \dots (3.32)$$

where ρ_o = density at pressure p_o (usually atmospheric pressure)

ρ = density at pressure p.

Equation (3.31) and (3.32) are often used even where the variation of specific volume (or density) is not linear, C being interpreted as an average value effective over the range of pressure p_o to p. Other more complex methods for prediction of liquid densities are available in the literature.

For applying the above equation and the flow continuity equation for the orifice valve in the system, the relationship between the orifice inlet and outlet flowrates can be found

$$Q_3 = \left[1 - C(p_3 - p_2) \right] Q_s \qquad \dots \dots (3.33)$$

or

$$Q_3 = (1 - \frac{p_3 - p_2}{B}) Q_s \qquad \dots \dots (3.34)$$

This equation has been also incorporated in the orifice model OR2H to account the fluid expansion effects.

In general, for all the pressure control valves, we have

$$Q_{in} = (1 - \frac{\Delta p}{B})Q_{out} \qquad\qquad \ldots\ldots (3.35)$$

where Q_{in} = valve inlet flowrate,

Q_{out} = valve outlet flowrate,

Δp = pressure drop across the valve,

B   = effective bulk modulus of fluid and pipe.

The above equation is recommended for use to account for the variation of flowrate through a pressure control valve due to the variation of fluid density with pressure in any a hydraulic system.

3.14 Experimental Test Rig and Measurements In order to justify the proposed theoretical analysis, a considerable number of tests were undertaken to investigate experimentally the transient behaviour of the unboosted closed system proposed. The experimental rig used in this investigation is shown diagrammatically in Fig. 3.12. The rig utilised an external gear pump without external drain, 25.4 mm bore flexible hydraulic hoses, a relief valve acting as a safety valve, a manually operated directional control valve and a sharp edged orifice loading valve. A cooler is used in the return line to dissipate the heat generated and a filter is incorporated before the cooler to keep the contamination at an acceptable level. Since no external flow leakage in the system, an extreme case is tested in which the reservoir is completely removed from the system and the suction line held vertically above the pump inlet, with its top end open to atmosphere. Dynamic pressures were measured by using three   transducers at positions shown. The transient pressures were recorded by an Ultra-Violet recorder (Oscillograph 3006/DL) which connected with the transducers. A turbine flowmeter with a digital counter (type TSA 6646/6) measured the full flow through the system and a thermometer attached on the outlet of the pump body to monitor the system working temperature. The technical data for each component of the system are listed in Table 3.1.

3.15 Experimental Test Procedure The pump was run at a constant speed of 1500 rev/min to deliver a flowrate at 84 l/min. The restrictor was adjusted to give a mean system pressure of 100 bar. The tests were carried out in the following sequences: first the pump was started with the direction control valve (DCV) opening, run steady for a minute or two, then the DCV was closed rapidly by hand to load the pump to 100 bar. The system normally ran 5 minutes under load, next it was unloaded by opening the DCV, then ran for one more minute, finally the electric motor was switched off to stop it. This is the worst case test procedure.

3.16 Experimental Pressure Transients Following closely the above test procedure, an extensive test programme was taken to investigate experimentally the system transient and steady state performances. A considerable   number of

tests were perform   to monitor the system transient conditions, particularly the pressure transients occurring in the system pipelines. A typical set of pressure transient recordings in the system from these tests are presented as follows.

Following the closure of the directional control valve for loading the system, the pump delivery pressure increased to its previous setting value of 100 bar as shown in Fig. 3.13. An noticeable feature of the test result is the occurrence of a dip during the pressure rise period. The other consequence of the loading the system is the transient variation of the return line pressure as shown in Fig. 3.14. Similarly, a transient variation was found in the system suction pressure in Fig. 3.15. These pressure transients are determined by many complicated factors as suggested in the above mathematical modelling section. It is impossible to draw any convincing conclusions just from the examinations of the test results. Fortunately, the theoretical analysis proposed in the above Sections can be used to analyse the system test results and the effects of each individual acting factor on the pressure transients by implementing them into the digital computer HASP software.

3.17   Long Term Effects   Using the same test rig, steady state tests of the system have been carried out to investigate the long term effects of the proposed unboosted closed system. Five repeated 7 hour tests were taken, analysis of the test results are given as follows.

As soon as the directional control valve is closed to load the pump, the pump delivery flowrate of 84 l/min passes through the orifice load valve and the pressure drop across the orifice is considerable (98 bar). In order to achieve this value of pressure drop across the orifice, the valve opening area must be very small (about 15.76 mm^2 or 4.48 mm in opening diameter). As a result, fluid velocity at the orifice plate is as high as (89 m/sec) and the fluid velocity at the orifice vena contracta is even higher. In this condition, the local dynamic fluid pressure at the orifice downstream is high and the local static pressure reduces below the atmospheric pressure. Consequently, the dissolved air in oil gradually comes out of solution to form visible air bubbles. This continuous air release phenomenon during the loading of the test rig can be observed through the   plastic hose in the downstream of the orifice load valve. Meanwhile, when the mixed air-liquid flow passes into the high pressure region, the air bubbles tend to go back to the solution,

specially in the system high pressure line. But air dissolves slowly in liquids, moreover, the fluid velocity in the pipelines is relatively high (2.75 m/sec), and it is impossible for air bubbles to escape completely from the pipelines just through the open ended pipe. As a consequence, free air bubbles can be observed in the system pipelines even after a long period of the pump loading, in addition some air bubbles may accumulate inside of the cooler and filter. The fluid height in the open-ended pipe and the pressures in the system would be affected by the processes of the air release and air dissolution.

Fig. 3.16 shows the fluid height variation in the open ended pipe during the system 7 hour loading. As can be seen, the fluid height is 1 m under   steady state unloading conditions at which the pressure p_3 at the pump delivery line is 7 bar. Once the pump is loaded to 100 bar, the flow in the open ended pipe is taken by the pump to compensate the fluid compressibility loss in the high pressure line. Hence, the fluid height in the open ended pipe falls to 0.95 m within one minute. Next the fluid height recovers to 1.1 m in 5 minutes because air release at the downstream of the orifice load valve is predominant factor during this first period of the system loading. In the following 4 hours, the fluid height gradually rises to 1.17 m and maintains the same level for the rest of 3 hours. This demonstrates the equilibrium of the air release at the orifice downstream, air dissolution in the high pressure line and the air escapement from the open ended pipe has been gradually established.

This gradual equilibrium process would also affect the pump delivery pressure p_3 and the return line pressure p_2 as can be seen in Fig. 3.17 and 3.18. In Fig. 3.17, the high pressure p_3 increases to 100 bar in 0.2 second of the directional control valve operation. After one second the system loading, p_3 falls from 100 bar to 97 bar in 5 minutes. This is because the rapid increase of the air proportion in the system flow results in the reduction of the pressure loss across the orifice restrictor. The reduction rate of p_3 is determined by the reduction rate of the increasing rate of the air proportion and the reduction of the return line pressure p_2. Meantime, for the exactly same reason of the air release, the reduction of p_2 has resulted due to the reduction of flow restrictions along the return pipeline and the filter and cooler. In other words, the reduction in the flowrate in the return line due to the rise of air proportion in the oil has resulted the reduction of p_2 from 2 bar to 1.4 bar within 5 minutes of the system loading. In the next 2 hours of the system loading, the high pressure gradually reduces towards a stationary value of 95 bar while the return line pressure decreases to the steady value of 1.32 bar. Again, these gradual

reductions of the pressures indicate the establishment of the process for air release, dissolution and escapement.

The pump suction pressure does not change under steady conditions during the system loading. This is because the fluid height change is too small to be monitored by the instrumentation in terms of bar.

Another important feature of the steady state test results is the temperature rise during the system running. In the pump loading period, the pressure loss across the orifice load valve is the main resource of the power loss converted into heat. The oil temperature in the system increases due to this energy conversion. The system temperature was monitored at the pump outlet by a thermo-couple and the result is shown in Fig. 3.19. In this, the temperature increases from the room temperature of 15° C to 30° C after 30 minutes loading the pump. After this transient temperature period, the temperature gradually rises 4° C in the following 6 hours towards the steady state conditions. The fluid temperature at the downstream of the orifice is expected to be higher than the rest of the system due to the occurrence of the energy conversion in this part of the system. In order to maintain the system fluid temperature at an acceptable level, a cooler was incorporated in the return line to dissipate the system power loss. The full examination of temperature behaviour in a hydraulic system will be given in Chapter 6.

From the above analysis of the test results, it can be seen that the variation of the steady state test rig performance has been caused by the way of system loading rather than due to the nature of the unboosted closed system proposed. It can be said that the circuit design proposed has not any long term effects on the performance of a practical hydraulic system where the circuit design proposed is incorporated.

3.18   In order to investigate the validity of the system theoretical analysis, the mathematical equations being established have been converted to equivalent HASP computer models so that the computer simulation of the system behaviour can be obtained to compare with the experimental transient pressure recordings. The majority of computer models in HASP can be used to cover most of hydraulic systems simulations. However, these models are not wholly applicable to the study of this special system considered. Based upon the mathematical modelling established, three new HASP models, PM2H, OR2H and PI0H, have been developed. Using these models together with other models available in HASP, the system simulation block diagram can be constructed.

3.19   **Simulation Block Diagram**   Fig. 3.20 gives the complete system block diagram for simulation. In the diagram, PM2H is a dynamic electric motor model with speed droop characteristics. This electric motor model drives a hydraulic gear pump model PU0H without external drain. This pump model takes into account of compressibility flow loss and viscous and pressure dependent torque losses. OR2H is a sharp edged orifice dynamic model which considers the effects of the fluid jet at downstream of the orifice and the fluid density variation across the orifice due to fluid expansion at the orifice downstream. OR2H acts in the system as a loading orifice restrictor. PI0H is a vertical open ended pipe model which takes the effects fluid momentum and pipe friction into account. The model of a two way two position directional control valve, DC1C, has also been modified to consider the difference between the inlet and outlet flowrates across the valve due to expansion. This model is used together with a duty cycle model DEDT which simulates the sudden change in the operating position of the valve. The rest computer models are the standard HASP models, they are the frictionless pipe model PI05 and orifice model OR3Z. The cooler was represented by a pipe model between two orifice models so that the computational simulation time has been led to comparatively short. The only acceptable input to the program generator for the system block diagram is given in Table 3.2.

3.20   Fluid Properties in the Simulation   The fluid properties in the simulation basis are given in Table 3.3. The oil temperature of 20° C in the table was the experimental temperature reading during the transient tests. The simulations for analying the experimental pressure transients have been carried out under the assumption that the change in oil temperature during the transient tests is insignificant to the test results. The data of fluid properties in the table are calculated on the basis of fluid temperature and oil type in the fluid property section model FLPROP of HASP. These data are very close with those which might be otherwise obtained from fluid property-temperature charts available in the literature.

3.21   Simulation Data for Electric Motor Model   The simulation data for electric motor model PM2H is listed in Table 3.4. The initial motor synchronous speed of 1500 rev/min has been obtained from the experimental measurements for the motor shaft speed. The effective inertia of electric motor and pump is calculated from the geometrical data obtained on the test rig. The two speed/torque coefficients K_e and K_1 can be estimated from the experimental measurements of two load conditions of the motor.

3.22   Simulation Data for the Pump Model   The input data for the gear pump model of PU0H without external drain is given in Table 3.5. The pump displacement value is from the data of pump used on the test rig. The coefficients for calculation pump slip and torque losses were obtained from the suggested values in HASP pump and motor unit model HUJT, which was developed based upon the intensive investigation carried out by McCandlish and Dorey (Ref. 3.16).

3.23   Simulation Data for Pipe Models   The simulation data for the high pressure line model PI05(01) is given in Table 3.6. In practice, this part of the high pressure line consists a length of flexible hydraulic hose and a length of rigid pipes. The pipe internal diameter and total length can be measured from the test rig. For simplicity, if this part of pipeline is represented just by an equivalent length of hydraulic hose, the effective fluid/pipe Bulk Modules can be calculated in the standard HASP pipe model PI05 in which four different common used pipe

materials are available to be chosen to calculate the bulk modulus. The bulk modulus calculation is based upon the generally accepted assumptions that the pressure of air saturation in oil is zero and the proportion of dissolved air in normal hydraulic oil is 10 %. The details of the fluid/pipe bulk modulus calculation in PI05 is given in (Ref. 2.8).

The result of fluid/pipe effective bulk modulus given by PI05 with the measured 9 mm thickness of hydraulic hose is 10261 bar as shown in the table. The initial fluid pressure 7 bar in this part of the pipeline was obtained from the practical measurement.

be
The same procedure can/applied to the simulation data acquisition for the return pipeline. The detail of simulation values for the return line pipe is listed in Table 3.10. Table 3.12 gives the simulation input data of pipe model PI05(3) to simulate the large flow volume in the cooler and filter. The rigid pipe of the suction line is simulated by pipe model PI05(4) whose simulation input data is listed in Table 6.14. The fluid/pipe effective bulk modulus of 18361 bar was calculated in model PI05 after inputing the measured thickness of the steel pipe. The pure fluid bulk modulus value in HASP is taken as 18400 bar.

3.24 **Simulation Data for the Orifice Loading Valve**   The simulation data for the orifice loading valve model OR2H is provided in Table 3.7, the equivalent length of the fluid jet at downstream of orifice is calculated using the relation in Equation (3.19) in which the coefficient ϕ was calculated according to the orifice steady state conditions. The data of the orifice steady state flowrate and pressure drop are obtained on the basis of the experimental conditions. The value of bulk modulus is taken as the same as the effective bulk modulus in the return line.

3.25 **Simulation Data for the Open Ended Pipe**   The input simulation data for the vertical open ended pipe is given in Table 3.15. The geometrical pipe sizes and fluid height were measured from the test rig. The initial flowrate is zero before the system is loaded.

3.26   Simulation Data for the Directional Control Valve   The simulation data provided in Table 3.8 presents the pressure drop across the directional control valve at its initial open position before it is selected to load up the orifice valve. The speed of change the valve position is very difficult to measure, if the value of 10 ms is assumed in the duty cycle model DEDT as shown in Table 3.9 the simulation will be carried out to justify this speed. Under such conditions, computer simulations have been carried out. The loading is identical with the experimental tests.

3.27 Under the conditions defined above, the simulation was performanced to predict the pressure transients which were generated by the rapid operation of the directional control valve in the system. A typical set of the simulation results are compared with corresponding experimental measurements under the loading of the system and the comparisons are shown in Fig. 3.21.

3.28   Analysis of the High Pressure Transients

The Effects of the Directional Control Valve Closure Time   Fig. 3.22 shows the flowrate as simulated through the directional control valve with a range of the valve closure time under the loading condition. The corresponding result in Fig. . 3.21e is one specific case where the valve closure time was taken as 10 ms for the practical system performance simulation.

As this flowrate rapidly reduces, the flowrate through the orifice load valve rises respectively. In Fig. 3.23 a number of the simulation flowrates through the orifice, Q_3, are plotted to demonstrate the main trends of the valve closure time effects. The non-linear shape of Q_3 show the effects of fluid compressibility. The same effects on the pipe line pressure p_3 are shown in Fig. 3.24.

The Effects of Fluid Compressibility   The compressibility term is associated with fluid volume of the high pressure line. If the length of the high pressure line L_3 increases, the system compliance increases. As a consequence, a relatively slow rise of Q_3 and p_3 is found. Fig. 3.25 and Fig. 3.26 are plots of Q_3 and p_3 with increasing the value of L_3 due to the influence of the compressibility is clearly shown.

The Effects of Orifice Dynamics   As discussed previously the fluid jet acceleration of a sharp edged orifice plays a major role in the dynamic response. For a sharp edged orifice incorporated in the system to act as a load valve, this jet effect

becomes of considerable importance to the system transient behaviour. Fig. 3.27 represents the simulation result of p_3 under a condition of varying the length of the high pressure line. As can be seen, when the length of the high pressure line L_3 is reduced to a small value, the compressibility loss effects can be eliminated. Then the system high pressure p_3 is determined by the orifice dynamics and the valve closure time. The overshot part of p_3 shows the transient fluid jet acceleration effects.

The Effects of the Pump Transient Shaft Speed   Fig. 3.21a shows a comparison between the calculated and measured results of the pump shaft speed at the instant of loading the pump. The variation of ω indicates the inertia effects of the rotating parts of the motor/pump including a stiffness coupling. Any increase in the load of the hydraulic system will result in a small reduction in the shaft speed. In the result, the peak to peak variation of ω is about 4% and the steady value reduces 2% after the pump is loaded from 7 bar to 100 bar. The validity of the computer model PM2H is confirmed by a close agreement between the simulation and experimental results.

The variations in the pump delivery flowrate Q_p in Fig. 3.21b correspond with the variation of the shaft speed ω. The reduction in the steady value of Q_p is caused by the pump shaft speed reduction, the increasing in the internal leakage and the compressibility loss inside the pump body. The effects of the variation in Q_p on p_3 shows in Fig. 3.28 with only a consideration of the influences of the shaft speed and the rapid closure of the directional control valve.

Analysis of Pressure Transient   A comparison between the predicted and experimental results of the system high pressure p_3 is made in Fig. 3.21c. The result is a combination of these acting factors described above. The dip in the curve of p_3 is found to be the combination of the two principal factors: compressibility and orifice dynamics. Fig. 3.29 plots the results of p_3 with 1 m and 5 m high pressure pipelines. It is clear that, if the pipelength increases, the compressibility term will be more predominant so that p_3 is a first order response curve. On the other extreme, the orifice dynamic response will become more significant such that an overshoot will occur on the curve of p_3.

From the above analysis it can be said that the valve closure speed, the fluid compressibility in the high pressure line and the fluid jet effects in the dynamic response of a sharp edged orifice are the most important factors in determining the

system high pressure transient.

3.29   Analysis of Transients in the Return Line

The Effects of the Valve Operating Speed   Fig. 3.30 shows the relations between the pressure transient in the return line and the valve operating time. From the results, it is clear that when the valve closing speed is fast, the peak of pressure transient becomes high. This is due to the effect of increasing in the fluid compressibility loss of the high pressure line.

The Effects of Fluid Compressibility   From a range of the return line pressure predictions using different return line lengths, it was found that the return line pressure p_2 is insensitive to the return line pipelength. In other words, the fluid compressibility in the return line is insignificant. However, the effects of fluid compressibility in the high pressure line would be expected to affect the return line pressure p_2, when loading valve is rapidly operated. When it was closed slowly, no variation in the return line pressure was recorded in experiments.

The Effects of Orifice Dynamics   The acceleration of the fluid jet at the outlet of a sharp edged orifice also affects the transient pressure. Fig. 3.31 shows a comparison between the predicted and experimental results of the return line transient pressure p_2 without the consideration of this fluid jet effects of the orifice. A good correlation of the experimental result is achieved in Fig. 3.21f, when the fluid jet effects of the orifice load valve are taken into account in the model OR2H.

The Effects of the Suction Line Dynamic Transients   For the system recirculatory construction, not only the dynamics in the high pressure line have influences on the return line dynamics but also the suction line dynamics through the pipeline can affect the return line transients. For instance, any change in the transient flowrate in the open ended pipe will result in a corresponding change in the return line flowrate Q_2 so that the transient pressure p_2 changes respectively.

Analysis of Return Line Flow and Pressure Transients   In the simulation result of the return line flowrate Q_2 in Fig. 3.21g, the flowrate decreases at the beginning of the valve closure. This is due to less flow being available from the high pressure line. At the point of the valve closure, Q_4 rapidly reduces to zero while Q_3 rises relatively slowly due to the occurrence of the compressibility in the high pressure line. As Q_3 increases, the gross tendency of Q_2 recovers to the original value. During the recovering of Q_2, some oscillations are superimposed on Q_2. This oscillation of Q_2 has been found to be generated by the transient compensating flow from the open ended pipe. This variation of Q_2 greatly affects the transient p_2. In the return line, when the total input flowrate $(Q_3 + Q_4)$ is greater than the output flowrate Q_2, the return line pressure p_2 increases. As the value of the transient flowrate difference reverses (ie. $Q_3 + Q_4 - Q_2 < 0$), the return line pressure p_2 will decrease.

Mixed results have been achieved in the quantitative comparison in Fig. 3.21f. On the one hand, for t < 60 ms, the predicted result of p_2 is close to the experimental measurement, and the deduction that the jet effects are very significant to the sharp edged orifice dynamic response is well reflected by the experimental result. On the other hand, the peak values of practical p_2 for t > 60 ms is rather lower than those of the prediction. It must be recognised, however, that some input data in the open ended pipe model PIOH were not accurate for representing precise realistic values, partly for the estimation of the actual fluid proportion being accelerated in the open ended pipe. In addition, the capacity volume of the cooler and filter in the simulation is difficult to be represented accurately.

In the analysis of the return line transient, it has been found that the speed of the valve closure, the fluid jet effects in the orifice transient response, the dynamics of the high pressure and the suction lines are the most critical factors in determining the system return line pressure transient. By considering these factors in the computer simulation, a moderate agreement between the experimental measurement and the theoretical prediction of the return line pressure transient have been achieved.

3.30   Analysis of the Suction Line Transients   In the system proposed, the occurrence of fluid compressibility in the high pressure line makes a transient reduction in the return line flowrate Q_2 so that a transient difference between the transient return line flowrate Q_2 and the pump demanding inlet flowrate Q_{pin} occurs

as can be observed in Fig. 3.21h and 3.21l. This transient difference has to be compensated by the pump taking the flow from the open ended pipe. Consequently, the column of flow in the pipe is being accelerated to generate the variation in the pressure transient p_1 at the bottom of the pipe as shown in Fig. 3.21i. It has been seen that the fluid compressibilities in the system pipelines and the dynamics of the open ended pipe, the transients in the return line are the factors influencing the pump suction condition. The details in analysis of each individual effect and the synthesis of their output as the transient pressure p_1 are given below.

The Effects of the Dynamics of the High Pressure and the Return Lines   In this recirculatory system, both the dynamics of the high pressure and the return lines are significant in determining the pump suction pressure. It is clear that fluid compressibility in the high pressure line is predominant as numerically comparing with the compressibilities of the return and the suction lines. For this reason, it has been found from a range of simulation results that the closure speed of the directional control valve as well as the length of the high pressure line is a very important factor in determining the flowrate from the open ended pipe, Q_1. Fig. 3.32 and 3.33 show an example of their effects on Q_1.

The Effects of the Open Ended Pipe   Under steady state, it is clear that the pipe pressure head gives the pump inlet pressure. In the transient conditions, the results of the experiment and simulation have shown that this pressure head is still playing a major role. Fig. 3.34 shows this key factor of the initial fluid height in determining the transient pump suction pressure p_1. This   suggests   that the shorter open ended pipe is, the lower transient variation of the pump suction pressure.

Analysis of Pressure Transient in the Suction Line   The transient pump inlet pressure p_1 is depended very much on the flow conditions. When the transient total input flowrate to the pipeline is greater than its output flowrate, the fluid pressure p_1 increases. When this reverses p_1 will decrease.

At the instant of loading the pump, the pump inlet demanding flowrate Q_{pin} only changes slightly due to the variation in the pump shaft speed and a small increment of the pump internal leakage. Simultaneously, there is a transient drop in the transient Q_2 in because of the effects of fluid compressibility in the high

pressure line. It is shown in Fig. 3.21j that a time requirement is necessary for the fluid column in the open ended pipe to be accelerated to the rate of Q_1. As a consequence, the transient suction line input flowrate is lower than the pump demanding flowrate so that the pump inlet pressure p_1 reduces below the atmospheric value, as shown in Fig. 3.21i. It is clear that the variation of Q_1 is a predominant factor in affecting the variation of p_1.

The other consequence of the rapid increase in Q_1 is the generation of a flow variation on the return line flowrate Q_2, a small variation superimposed on Q_2 occurs as shown in Fig. 3.21g and 3.21h. The difference between the transient downstream and upstream flowrates of the cooler and filter shows their damping effects due to the large volume.

In the correlation of suction line pressure p_1 in Fig. 3.21i, the predicted result of p_1 has a broad agreement in the below atmospheric region and the variation phase with the experimental result but its peak values are rather higher (for the first peak value about 0.7 bar compared with 0.5 bar) than the experimental ones. A possible explanation is that there is an inaccuracy in determining the actual fluid proportion being accelerated in the open ended pipe. Nevertheless, from a range of the calculated and measured results, it is reasonable to conclude that the closure speed of the system directional control valve, the height of the fluid column with its dynamics in the open ended pipe and fluid compressibility in the system high pressure line are the most critical factors in determining the transient suction pressure.

3.31 Simulation Fluid Height in the Open Ended Pipe   The fluid height in the open ended pipe has been predicted in Fig. 3.21k. It is clear that the transient height variation is associated with the fluctuation of flowrate in the open ended pipe. After the pump is loaded from 7 bar to 100 bar, the steady drop in the fluid height was predicted to 5 cm in a 25.4 mm (1' in) bore of the pipeline and this value was well reflected by the experimental observation. This fluid height drop is used to compensate the amount of the flow (about 25 ml) being compressed in the system high pressure line under the working conditions.

As has been discussed, it is necessary in the theoretical modelling of a hydraulic system to consider the difference between the inlet and outlet flowrates across a pressure control valve due to the variation of fluid density gradient under

the different pressure conditions. If this term is ignored as in the conventional theoretical modelling, it may make no difference in the predicted results for the majority types of the hydraulic systems, since a tank model is usually used in the simulation and the small fluid variation in the tank will not be shown in the simulation result. But it would lead to a non-realistic prediction in an attempt for modelling this special recirculatory hydraulic system with unboosted closed loop design.

If the variation of fluid density in the system have not been taken into account, the steady state flowrate in the open ended pipe will not be zero as shown in Fig. 3.35. This means a flow is constantly demanded from the open ended pipe to compensate for the pump compressibility loss. Although this flowrate is small, if the simulation is run for 10 seconds, however, the fluid height in the open ended pipe would gradually drop as shown in Fig. 3.36a. This prediction does not agree with the practical results. Good agreement was obtained between theory and experiment as shown in Fig. 3.36b, when the variation of fluid expansion was included in the orifice model OR2H.

3.32 Simulation and Experimental the Pressure Transients When the Pump is Unloaded
A similar approach has been undertaken to verify the analysis for the system under unloading conditions. The simulation data were essentially the same to those in Table 3.3 - 3.15 except the pipe and orifice model initial conditions which are listed in Table 3.16 to 3.19. A typical set of results was represented in Fig. 3.37. It is apparent that the procedure of the above analysis are wholly applicable to interpret the system transients under the unloading conditions. Only a brief representation of the results are given below.

As would be expected, the high pressure line pressure p_3 drops following the opening of the directional control valve. It is clear that the valve opening speed and the fluid expansion play a major role in determining the transient shape of p_3. The opening time was assumed to be within 40 ms for the simulation, the agreement between the calculated and measured pressure transient shown in Fig. 3.37c confirms its validity.

The effects of fluid expansion on the flowrate through the directional control

valve is shown in Fig. 3.37e. The transient input flowrate for the return line is greater than its output, as a result the return line pressure rises rapidly to the first peak value of 11 bar, then oscillates towards a stationary value as shown in Fig. 3.37f. It has been found that the return line pressure transient is greatly affected by the valve opening speed and the expansion of the compressed flow from the high pressure line. The pipelengths of the system high pressure and the return lines are also important factors in determining the pressure transient. A moderate agreement has been achieved between the predicted and the practical values. The difference in the lower pressure region is suggested to be caused by the inaccurate modelling of the cooler and filter dynamics.

In the system suction line, the predominant factor was found to be the fluid expansion effects showing on the return line flowrate Q_2. This fluid expansion is depended very much on the valve opening speed and the high pressure pipelength. Besides the open ended pipe dynamics and the suction line pipelength are also determining factors for the pump suction conditions. A good agreement of the calculated and measured values of the suction line pressure has been achieved by considering these acting factors in Fig. 3.37i.

From the examination of the system transient behaviour, it can be concluded that the system transient characteristics are mainly governed by the operating speed of the directional control valve and the dynamics of the system pipelines. In addition, the dynamic response of the sharp edged orifice plays a important role in the system transients at the loading of the pump.

3.33   **High Frequency Pressure Ripples**   Experimental measurements of the pressure transients have revealed a high frequency pressure ripples which was created by the flow ripple due to the pump geometrical flow variations.

A typical example in Fig. 3.38 shows that the ripple magnitude of pressure fluctuations is very sensitive to mean inlet pressure. The peak to peak value of ripple pressure fluctuations is 0.1 bar when the inlet mean pressure at 0.04 bar. As the pressure in the suction line was reduced to below atmospheric value at -0.3 bar, the pressure fluctuations are suppressed and become quite small and unstable

because of the occurrence of air release. Increasing the mean pressure to 1 bar increased the ripple amplitude considerably to 0.35 bar. This large change is due to the change in the pump inlet flow ripple with mean pressure. Although this does not usually show as a reduction of volumetric efficiency, it is important to recognise that its presence makes the conditions at the suction port of a pump extremely complex. Edge and Freitas (Ref. 3.17 and 3.18) have studied the behaviour of this suction pressure ripple in detail, following the plane wave theory applied to hydraulics by Bowns and McCandlish (Ref. 3.19).

No.	Component Name	Technical parameters	Data	Unit
1	electric motor	maximum speed at 15 kw	1500	rev/min
2	gear pump with internal drain	theoretical displacement maximum pressure	57.3 172	cm^3/rev bar
3	high pressure pipeline	1" rigid pipe + 1" hydraulic hose	1 2.6	m m
4	sharp edged loading orifice	maximum flowrate	100	L/min
5	return line	1" hydraulic hose	4.3	m
6	suction line	1" hydraulic hose	1.5	m
7	open ended pipe	1" plastic pipe	2	m
8	2 way 2 position manually directional operated control valve	maximum flowrate maximum pressure	110 210	L/min bar
9	cooler	maximum flowrate maximum heat dissipation volumetric size	111 30 10	L/min kw Litres

Table 3.1   Technical Data of Components on Test Rig

Component Number	Model Name	Model Number	Link Position				
1	PM2H	1	1		15		
2	PUOH	1	2		3		1
3	PIO5	1	3		4		5
4	OR2H	1	4		6		
5	DC1C	1	5		7		8
6	DEDT	1	8				
7	PIO5	2	6		7		9
8	OR3Z	1	9		10		
9	PIO5	3	10		11		
10	OR3Z	2	11		12		
11	PIO5	4	2		12		13
12	PIOH	1	13		14		

Table 3.2 Model Linking Input Data for Program Generation

Fluid Properties Section Model FLPROP			
No.	Parameters	Data	Unit
1	oil temperature	20	deg. C
2	oil type	BP HLP 32	
3	fluid density	870	$\dfrac{kg}{m^3}$
4	fluid Bulk Modulus	18400	bar
5	fluid kinematic viscosity	74.56	cSt
6	fluid absolute viscosity	64.87	cP

Table 3.3   parametric Data Used in Simulation for Fluid Properties

Component No. 1: Electric Motor Model PM2H (No. 1)			
No.	Input Parameters	Data	Unit
1	motor synchronous speed	1500	rev/min
2	effective pump/motor inertia	0.5	kg.m^2
3	motor torque/speed slip	19.6	Nm/(rev/min)
4	damping torque coefficient	0.01	Nm/(rev/min)
5	initial motor speed	1500	rev/min

Table 3.4   parametric Data Used in Simulation for Electric Motor

Component No. 2: Hydraulic Pump Model PU0H (No. 1)			
No.	Input Parameters	Data	Unit
1	maximum pump displacement	0.0573	L/rev
2	fraction of full displacement	1	
3	slip loss coefficient	1.4×10^{-8}	
4	torque loss coefficient	2	
5	viscous friction coefficient	0.8	
6	clearance volume	0	

Table 3.5   parametric Data Used in Simulation for Hydraulic Pump

Component No. 3: Frictionless Pipe Model PI05 (No. 1)			
No.	Input Parameters	Data	Unit
1	pipe internal diameter	25.4	mm
2	pipe length	3.6	m
3	pipe volume	1.824	Litres
4	fluid/pipe Bulk Modulus	10261	bar
5	air saturation pressure	0	bar
6	proportion of dissolved air	0.1	
7	initial pressure	7	bar

Table 3.6   parametric Data Used in Simulation for High Pressure Pipeline

Component No. 4: Orifice Restrictor Load Valve Model OR2H (No. 1)			
No.	Input Parameters	Data	Unit
1	steady state flowrate	1.4	L/sec
2	corresponding pressure drop	98	bar
3	equivalent fluid jet length	0.54	m
4	initial flowrate	0.1	L/sec
5	fluid Bulk Modulus	10261	bar

Table 3.7   parametric Data Used in Simulation for Orifice
            Loading Valve

Component No. 5: 2 Way 2 Position DCV Model DC1C (No. 1)			
No.	Input Parameters	Input Data	Unit
1	restriction constant	0.626	
2	linear region limit	0.01	bar

Table 3.8   parametric Data Used in Simulation for 2 Way 2 Position
Directional Control Valve

Component No. 6: Movement of DCV Model DEDT (No. 1)			
Stage	Spool Displacement	Time (second)	Valve Position
1	0	0	open
2	1	0.01	close
3	1	1	close

Table 3.9   parametric Data Used in Simulation for Different Time
Relate Slip of Directional Control Valve

Component No. 7: Frictionless Pipe Model PI05 (No. 2)			
No.	Input Parameters	Data	Unit
1	pipe internal diameter	25.4	mm
2	pipe length	4.3	m
3	pipe volume	1.013	Litres
4	fluid/pipe Bulk Modulus	10261	bar
5	air saturation pressure	0	bar
6	proportion of dissolved air	0.1	
7	initial pressure	2	bar

Table 3.10   parametric Data Used in Simulation for Return Pipeline Before Cooler

Component No. 8: Orifice Restrictor Model OR3Z (No. 1)			
No.	Input Parameters	Data	Unit
1	steady state flowrate	1.4	L/sec
2	corresponding pressure drop	1	bar

Table 3.11   parametric Data Used in Simulation for Pressure Drop at Filter Entrance

Component No. 9:	Frictionless Pipe Model PI05 (No. 3)		
No.	Input Parameters	Data	Unit
1	pipe internal diameter	25.4	mm
2	pipe length	20	m
3	pipe volume	10.13	Litres
4	fluid/pipe Bulk Modulus	15437	bar
5	air saturation pressure	0	bar
6	proportion of dissolved air	0.1	
7	initial pressure	1	bar

Table 3.12   parametric Data Used in Simulation for Cooler and Filter

Component No. 10:	Orifice Restrictor Model OR3Z (No. 2)		
No.	Input Parameters	Data	Unit
1	steady state flowrate	1.4	L/sec
2	corresponding pressure drop	0.9	bar

**Table 3.13   parametric Data Used in Simulation for Pressure Drop
at Cooler Exit**

Component No. 11: Frictionless Pipe Model PI05 (No. 4)			
No.	Input Parameters	Data	Unit
1	pipe internal diameter	25.4	mm
2	pipe length	1.5	m
3	pipe volume	0.76	Litres
4	fluid/pipe Bulk Modulus	18361	bar
5	air saturation pressure	0	bar
6	proportion of dissolved air	0.1	
7	initial pressure	0.1	bar

Table 3.14   parametric Data Used in Simulation for Suction Pipeline

Component No. 12: Open Ended Pipe Model PI0H (No. 1)			
No.	Input Parameters	Data	Unit
1	pipe internal diameter	25.4	mm
2	initial fluid height	1	m
3	initial fluid velocity	0	m/sec

Table 3.15   parametric Data Used in Simulation for Open Ended Pipe

Component No. 1: Electric Motor Model PM2H (No. 1)			
No.	Input Parameters	Data	Unit
1	motor synchronous speed	1500	rev/min
2	effective pump/motor inertia	0.5	$kg.m^2$
3	motor torque/speed slip	19.6	Nm/(rev/min)
4	damping torque coefficient	0.01	Nm/(rev/min)
5	initial motor speed	1470	rev/min

Table 3.16   parametric Data Used in Simulation for Electric Motor During Unloading System

Component No. 3: Frictionless Pipe Model PI05 (No. 1)			
No.	Input Parameters	Data	Unit
1	pipe internal diameter	25.4	mm
2	pipe length	3.6	m
3	pipe volume	1.824	Litres
4	fluid/pipe Bulk Modulus	10261	bar
5	air saturation pressure	0	bar
6	proportion of dissolved air	0.1	
7	initial pressure	100	bar

Table 3.17   parametric Data Used in Simulation for High Pressure Pipeline During Unloading System

Component No. 4: Orifice Restrictor Load Valve Model OR2H (No. 1)			
No.	Input Parameters	Data	Unit
1	steady state flowrate	1.4	L/sec
2	corresponding pressure drop	98	bar
3	equivalent fluid jet length	0.54	m
4	initial flowrate	1.4	L/sec
5	fluid Bulk Modulus	10261	bar

Table 3.18   parametric Data Used in Simulation for Orifice
Loading Valve During Unloading System

Component No. 6: Movement of DCV Model DEDT (No. 1)			
Stage	Spool Displacement	Time (second)	Valve Position
1	1	0	close
2	0	0.01	open
3	0	1	open

Table 3.19   parametric Data Used in Simulation for Different Time Relate
Slip of Directional Control Valve During Unloading System

Vertical Open Ended Pipe
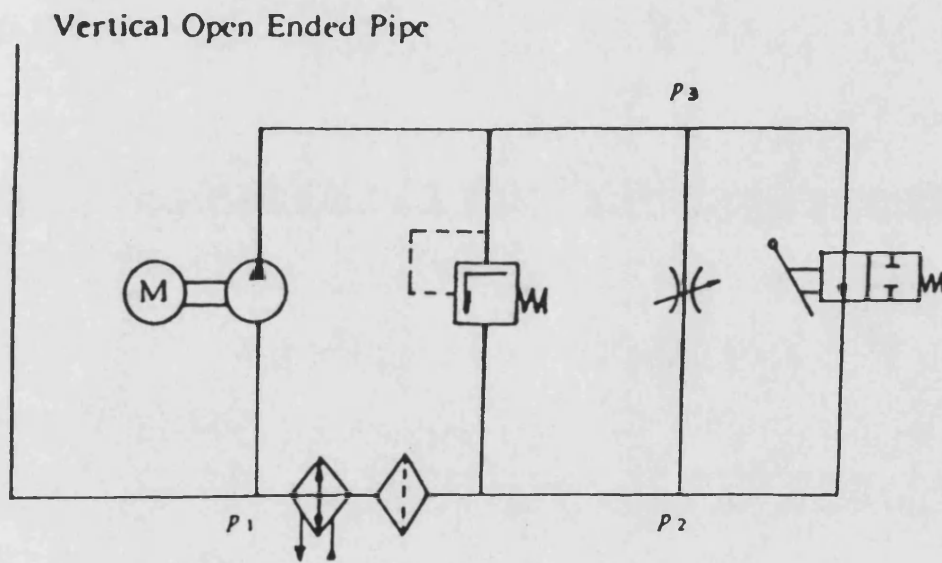
Fig. 3.1   An Unboosted Closed System Investigated
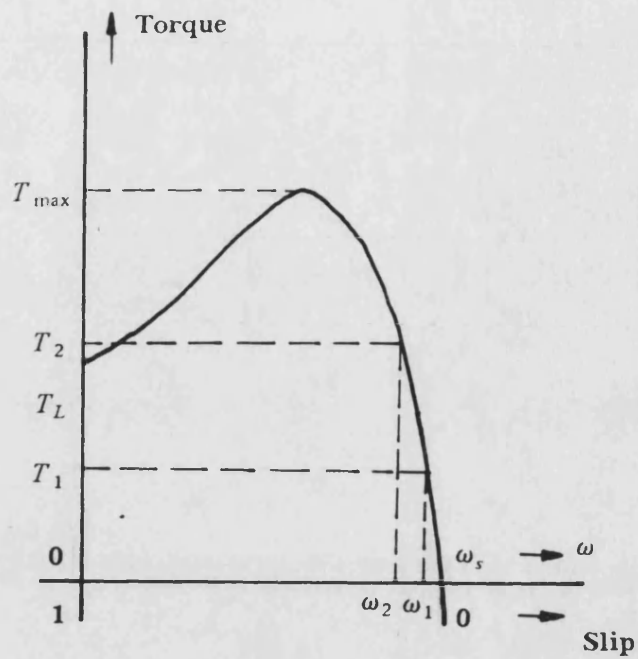
Fig. 3.2   Electric Motor Torque-Speed Curve
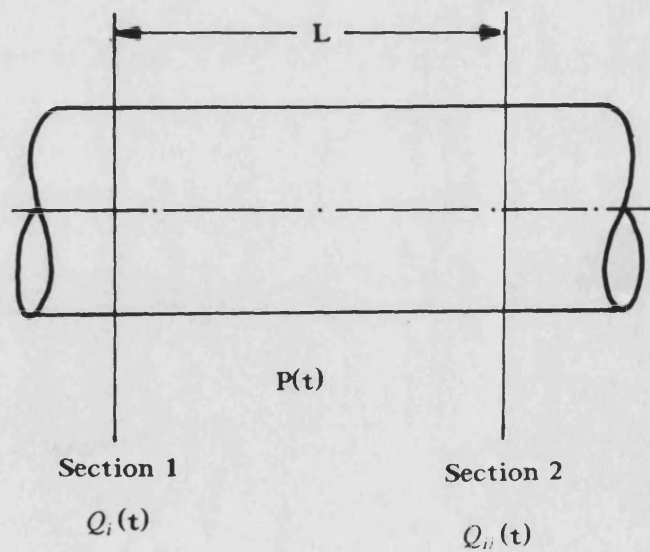
Uniform Pipe of Constant Cross Sectional Area A

Fig. 3.3   Pipe Schematic
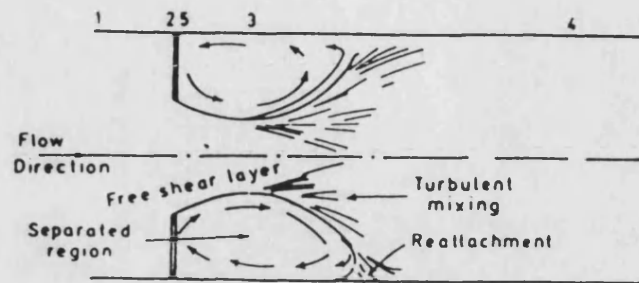
Fig. 3.4   Free Jet Flow
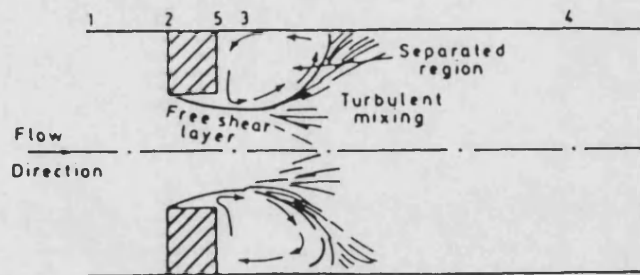
Fig. 3.5   Fully Separated Flow
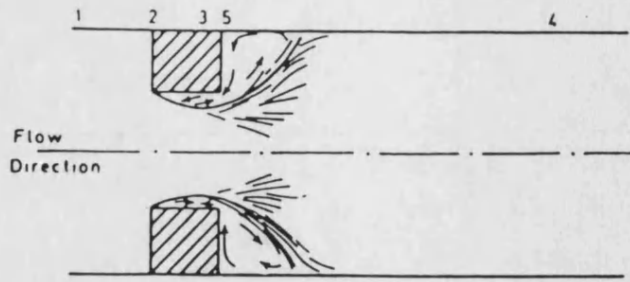
Fig. 3.6   Marginally Separated Flow
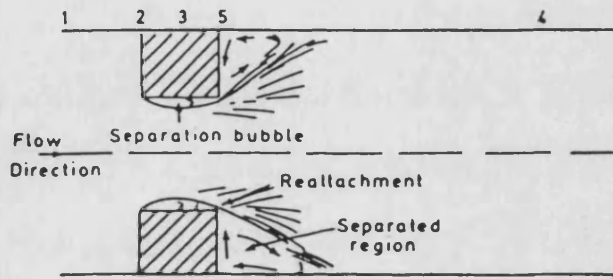
Fig. 3.7   Marginally Reattached Flow
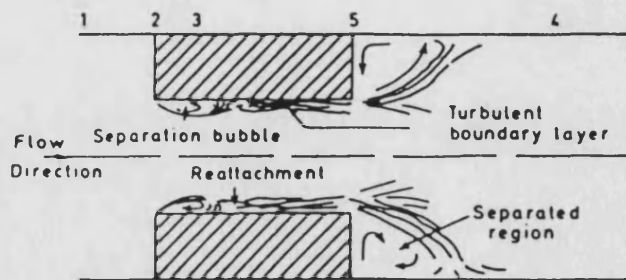
Fig. 3.8   Fully Reattached Flow
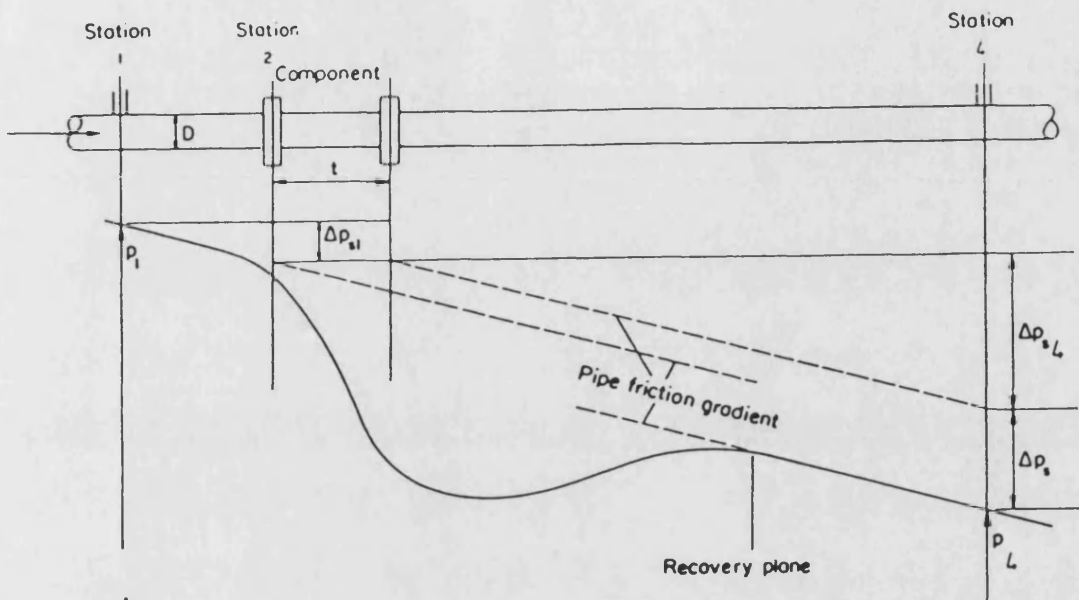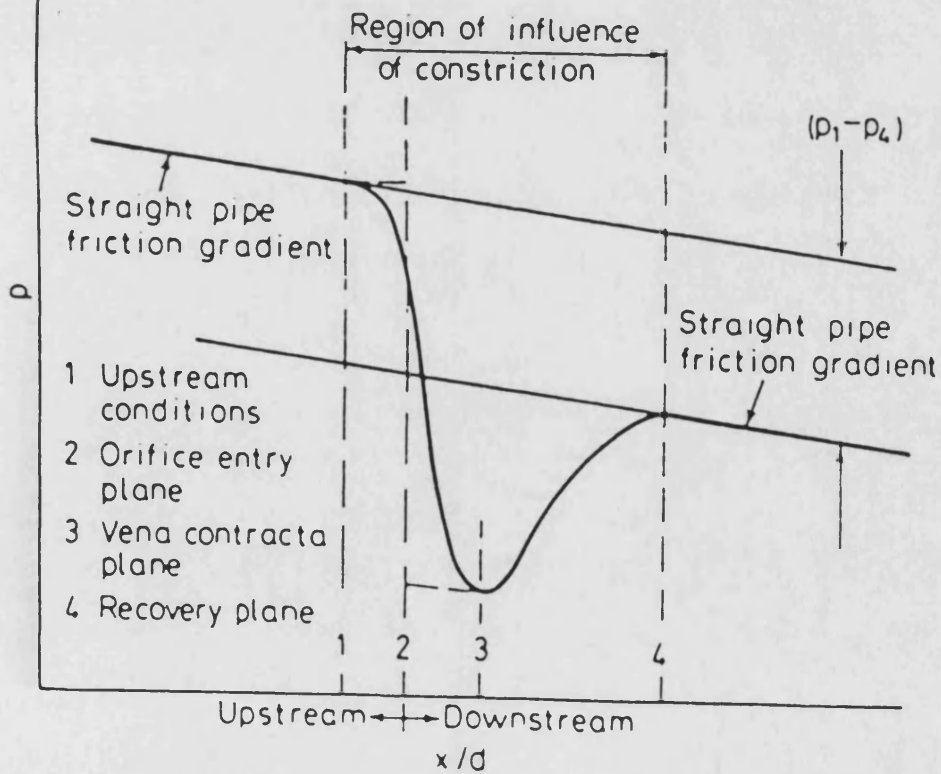
Fig. 3.9 *Static pressure distribution along a pipeline containing an orifice plate. Note. $(p_1 - p_4)$ is the pressure drop across the orifice plate corrected for the straight pipe friction gradient*
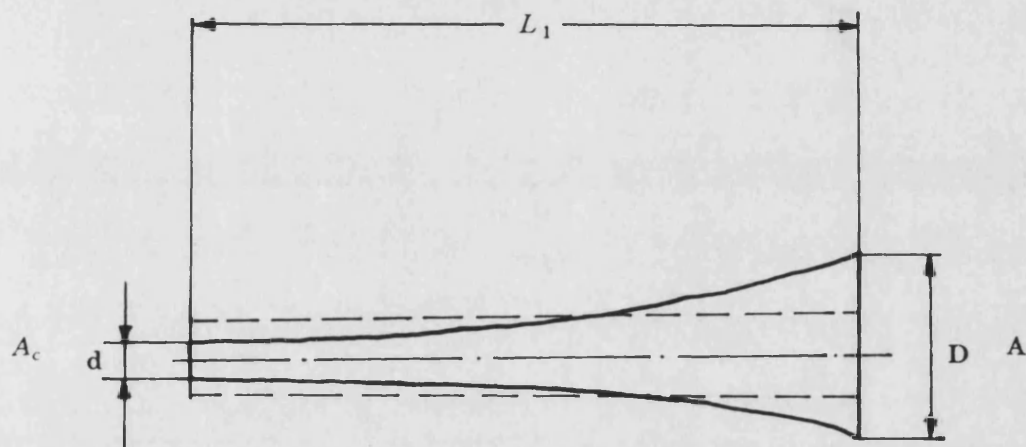
Mean Area: $\dfrac{(C_c A_c + A)}{2}$

Jet Mass Accelerated: $m = \dfrac{\rho(C_c A_c + A)}{2}$

Jet Length for Sharp Edged Orifice: $L_1 = 6D$

Fig. 3.10   Transient Fluid Jet being Accelerated at the Downstream of the Orifice
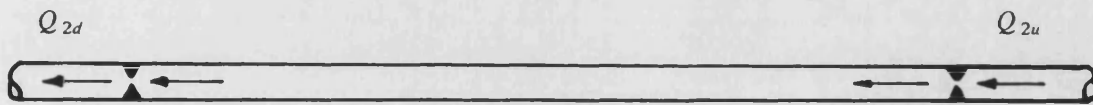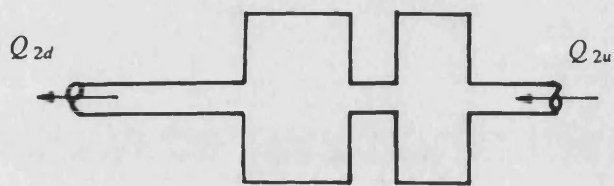
Fig. 3.11   Using Pipe Volume and Orifice Model to Represent Capacities
of the Cooler and Filter
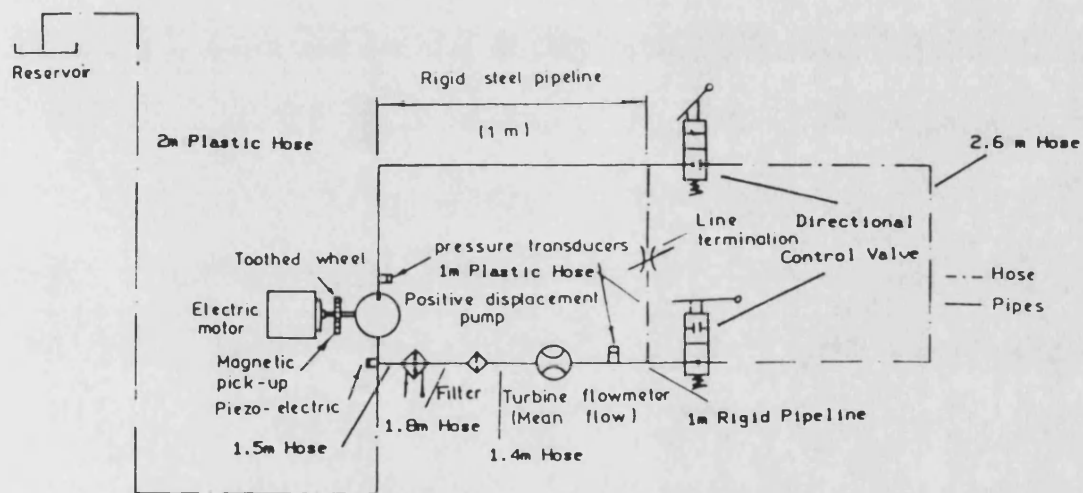
Fig. 3.12   Experimental Test Rig of Unboosted Closed System
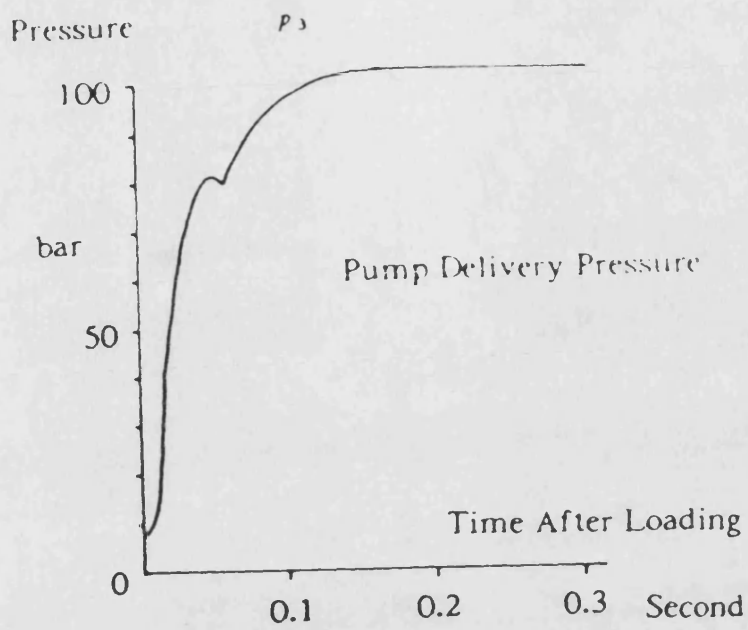
Fig. 3.13   Experimental Transient Pump Delivery Pressure in the Unboosted Closed System
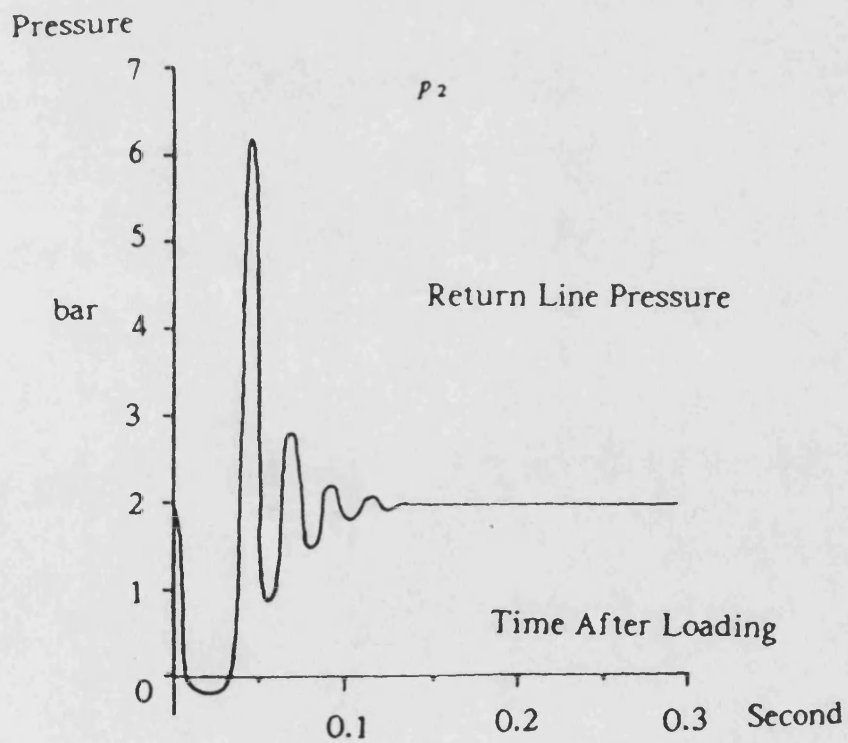
Fig. 3.14   Experimental Transient Return Line Pressure in the Unboosted Closed System
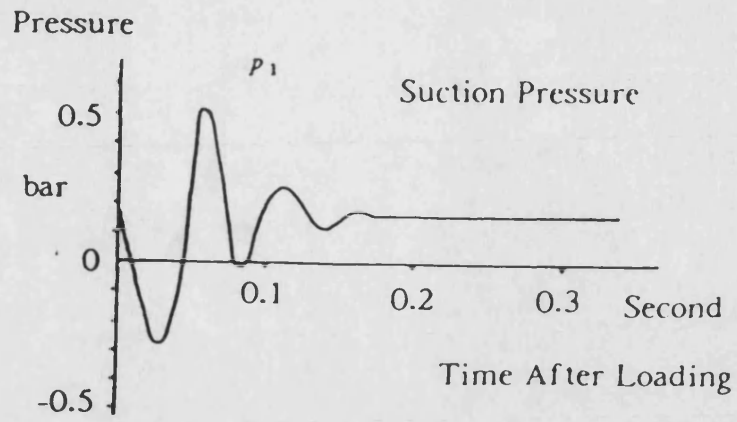
Fig. 3.15   **Experimental Transient Suction Pressure in the Unboosted Closed System**
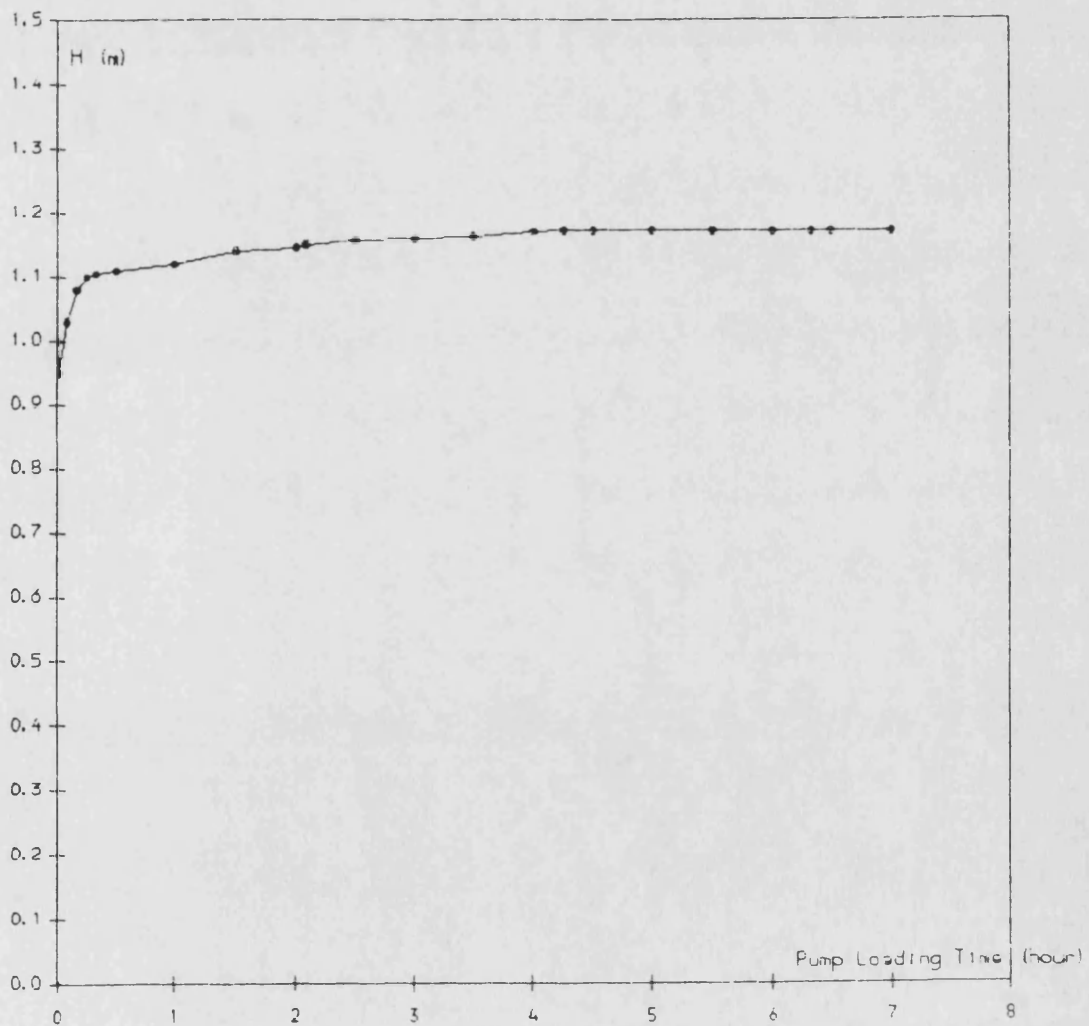
Fig. 3.16   **Experimental Recording of the Fluid Height in the Open-Ended Pipe of the Unboosted Closed System**
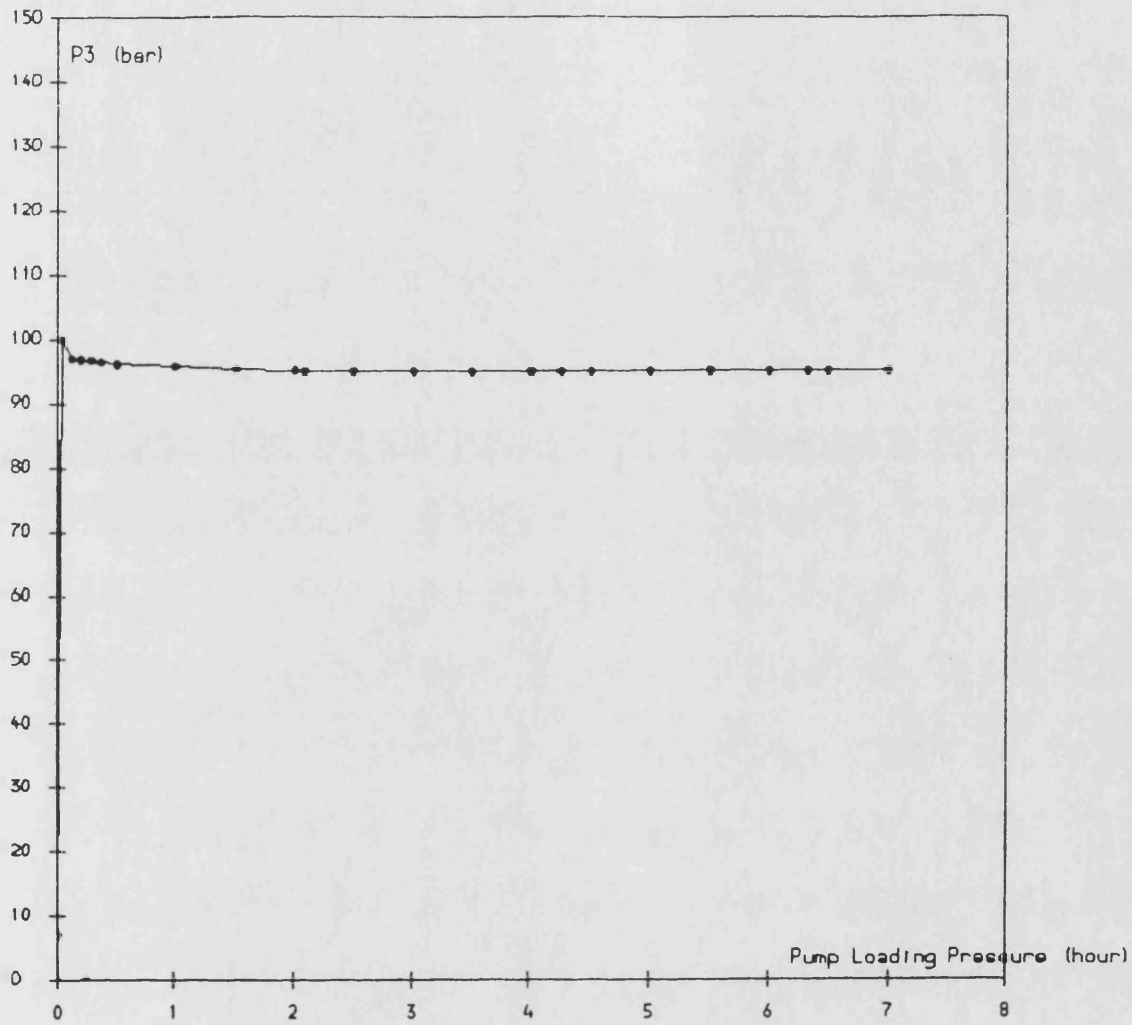
Fig. 3.17   **Steady State Pump Delivery Pressure in the Unboosted Closed System**
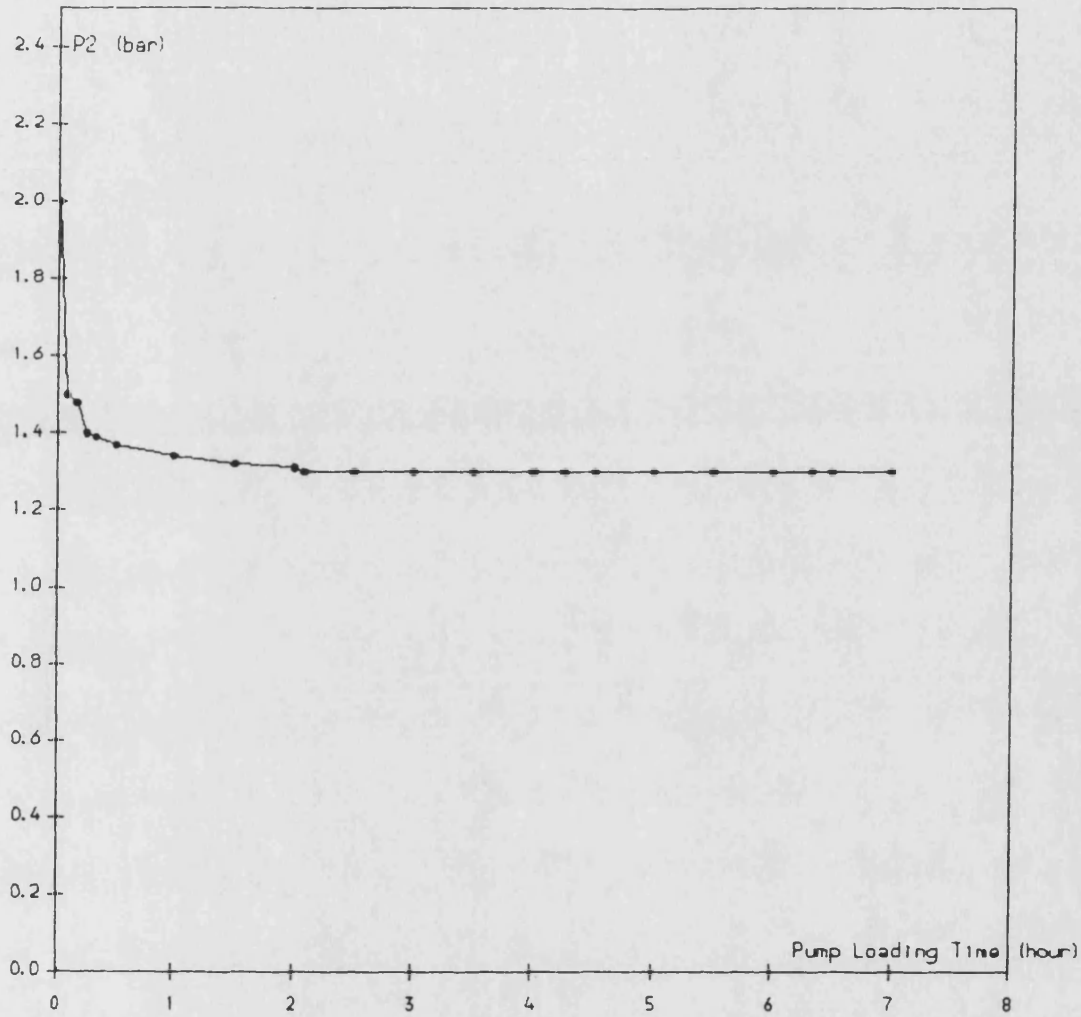
Fig. 3.18   **Steady State Return Line Pressure in the Unboosted System**
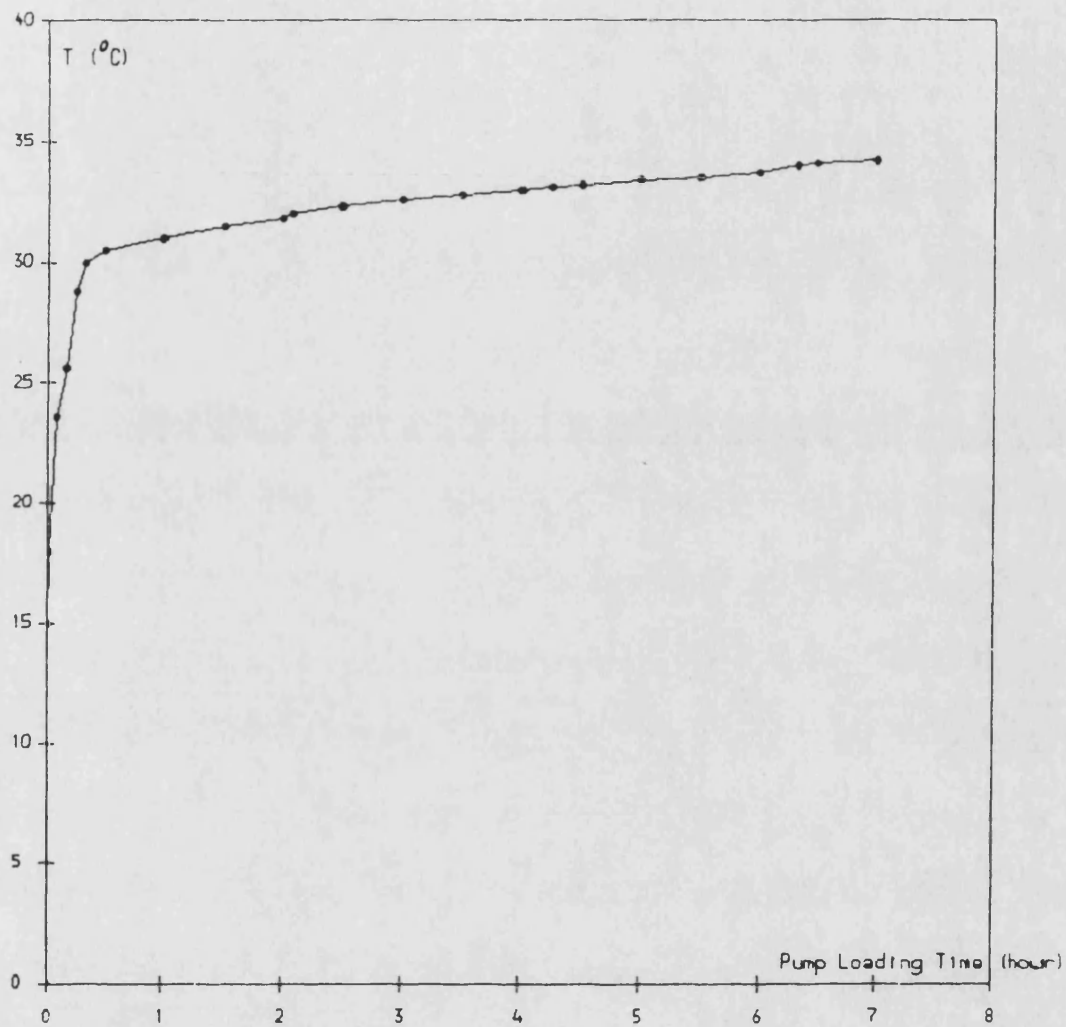
Fig. 3.19 Temperature Recording at the Pump Outlet in the Unboosted System

Fig. 3.20   Block Diagram for the Simulation of the Unboosted Closed
              Hydraulic System

k. Fluid Height in the Open-Ended Pipe

j. Transient Flowrate from the Open-Ended Pipe

i. Transient Suction Pressure

a. Pump Shaft Speed

b. Pump Delivery Flowrate

c. Transient Pump Delivery Pressure

L. Pump Inlet Flowrate

d. Flowrate through Orifice Loading Valve

e. Flowrate through Directional Control Valve

h. Return Line Flowrate at Downstream of the Cooler

g. Return Line Flowrate at Upstream of the Filter

f. Transient Return Line Pressure

Fig. 3.21   Transient Characteristics of Unboosted Closed System
During the System Loading

L/s

Q_4

1

DCV Flowrate

Increase of Operating Time b

0

1   2   3   X10^{-1} SECONDS
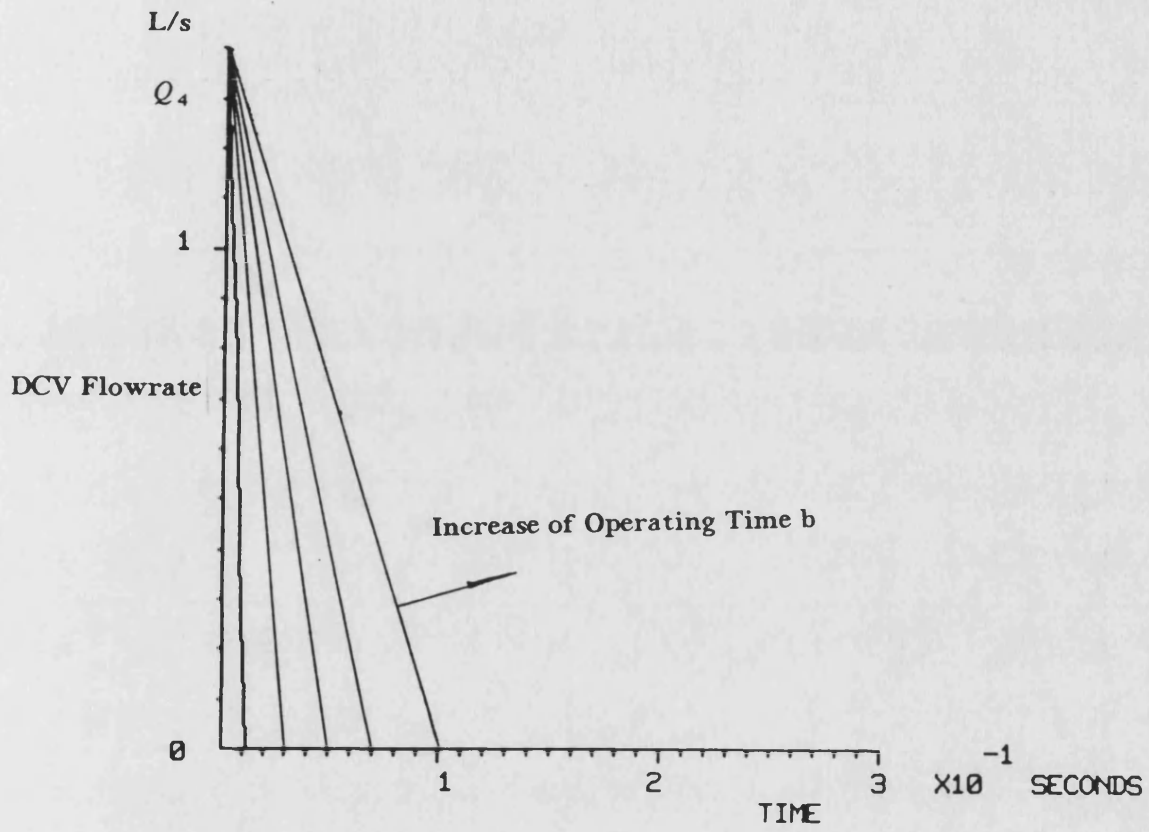
TIME

Fig. 3.22   The Effects of the Directional Control Valve (DCV) Operating
Time on Flowrate through DCV
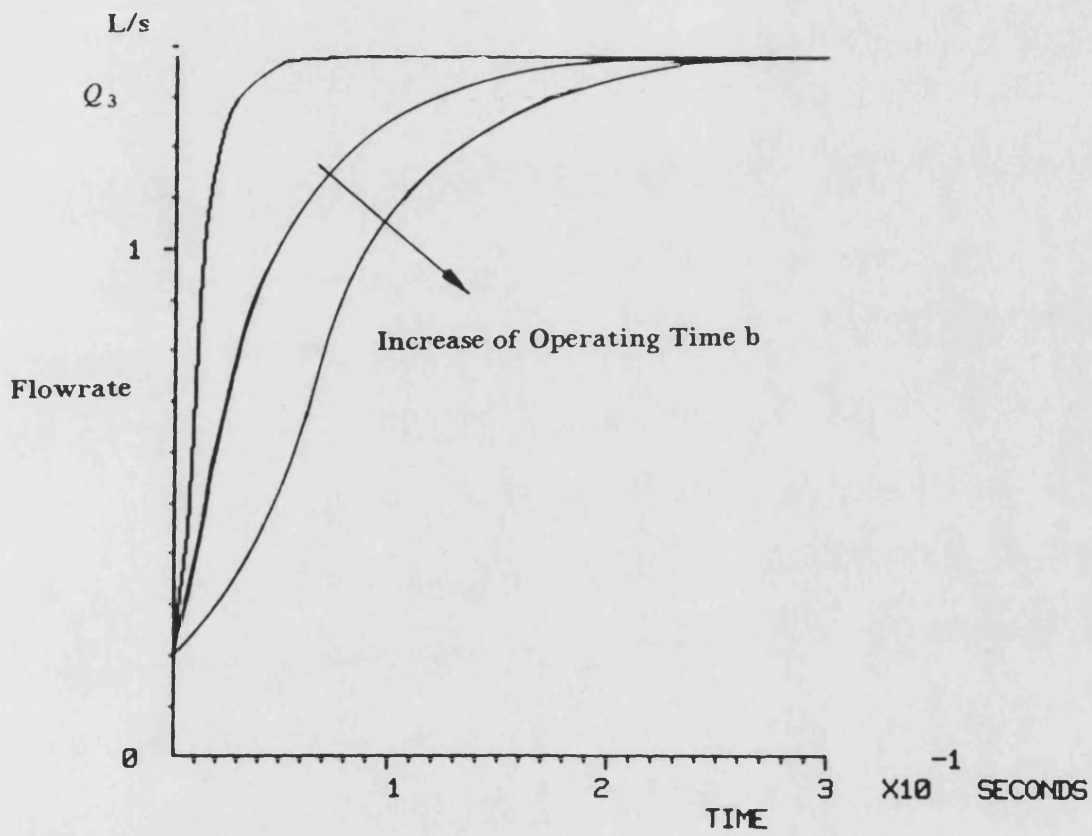
Fig. 3.23   The Effects of the Directional Control Valve (DCV) Operating Time on Flowrate through the Orifice Loading Valve
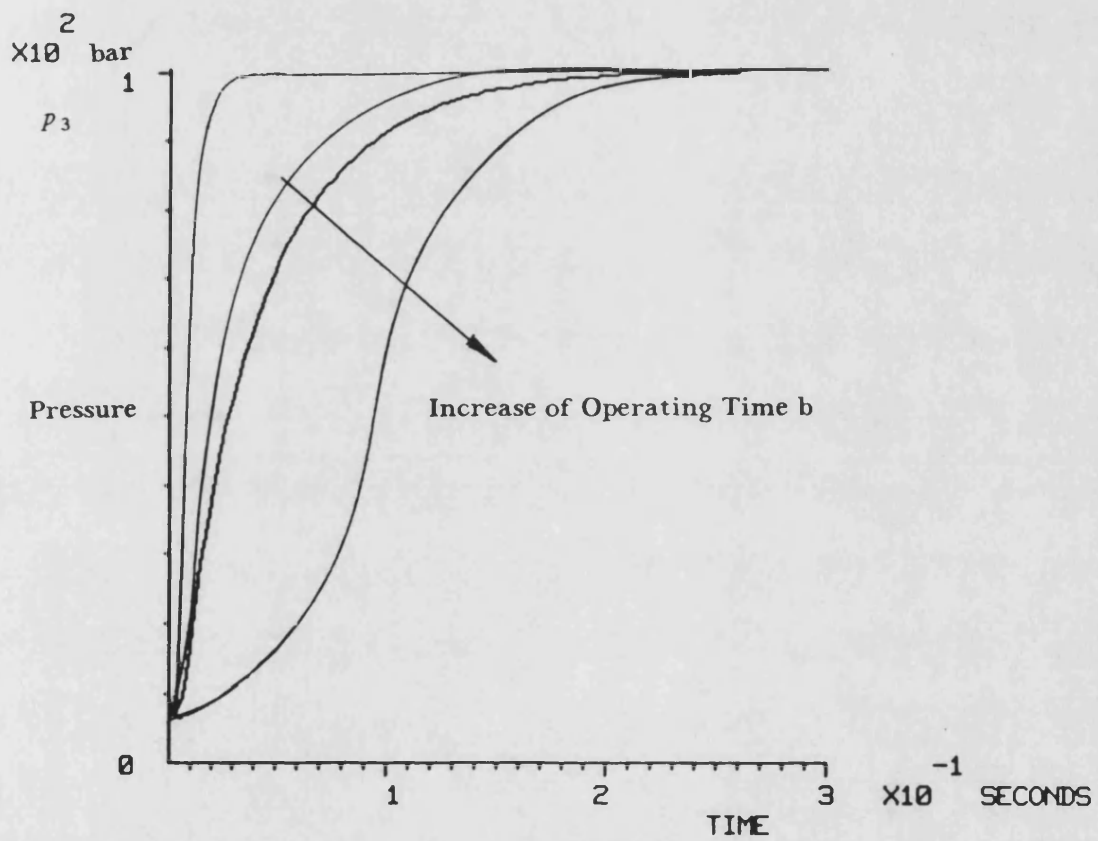
Fig. 3.24   The Effects of the Directional Control Valve (DCV) Operating
Time on the Transient Pump Delivery Pressure

DCV Operating Time b = 10 ms
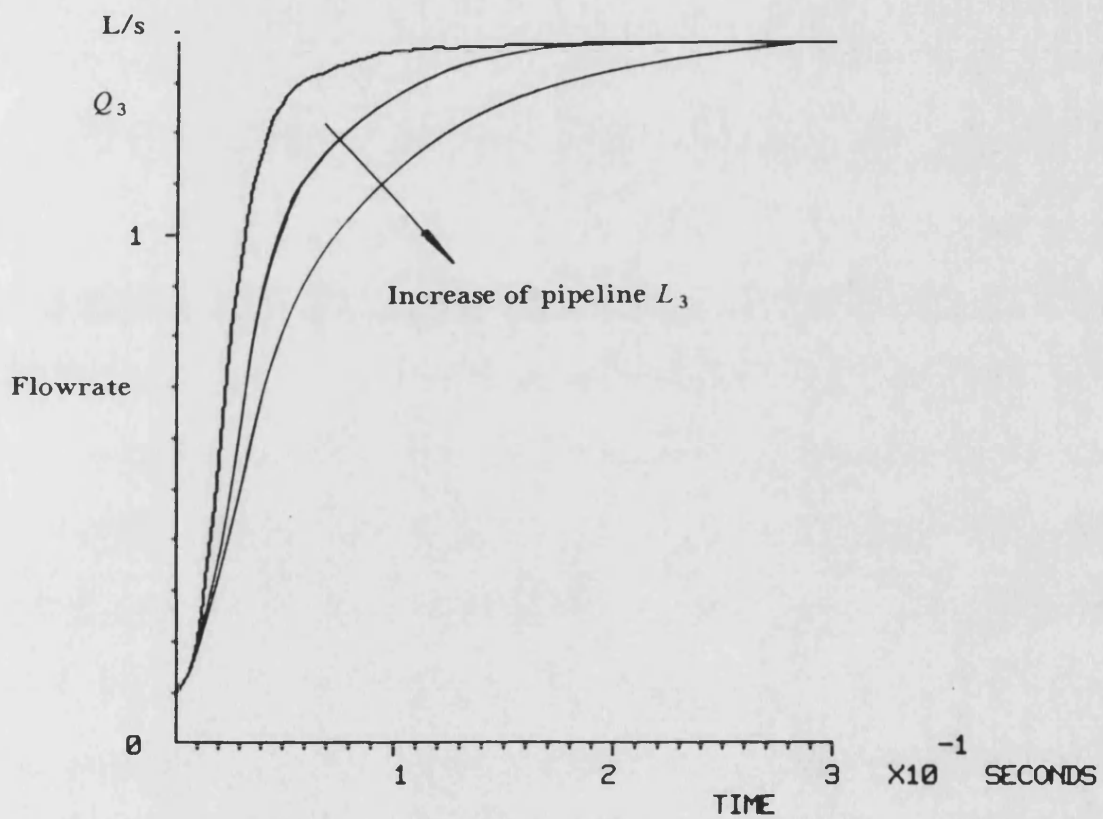
Fig. 3.25   The Effects of the Length of the High Pressure Line on the Flowrate through the Orifice Loading valve Q_3

DCV Operating Time b = 10 ms

Increase of pipeline L_3
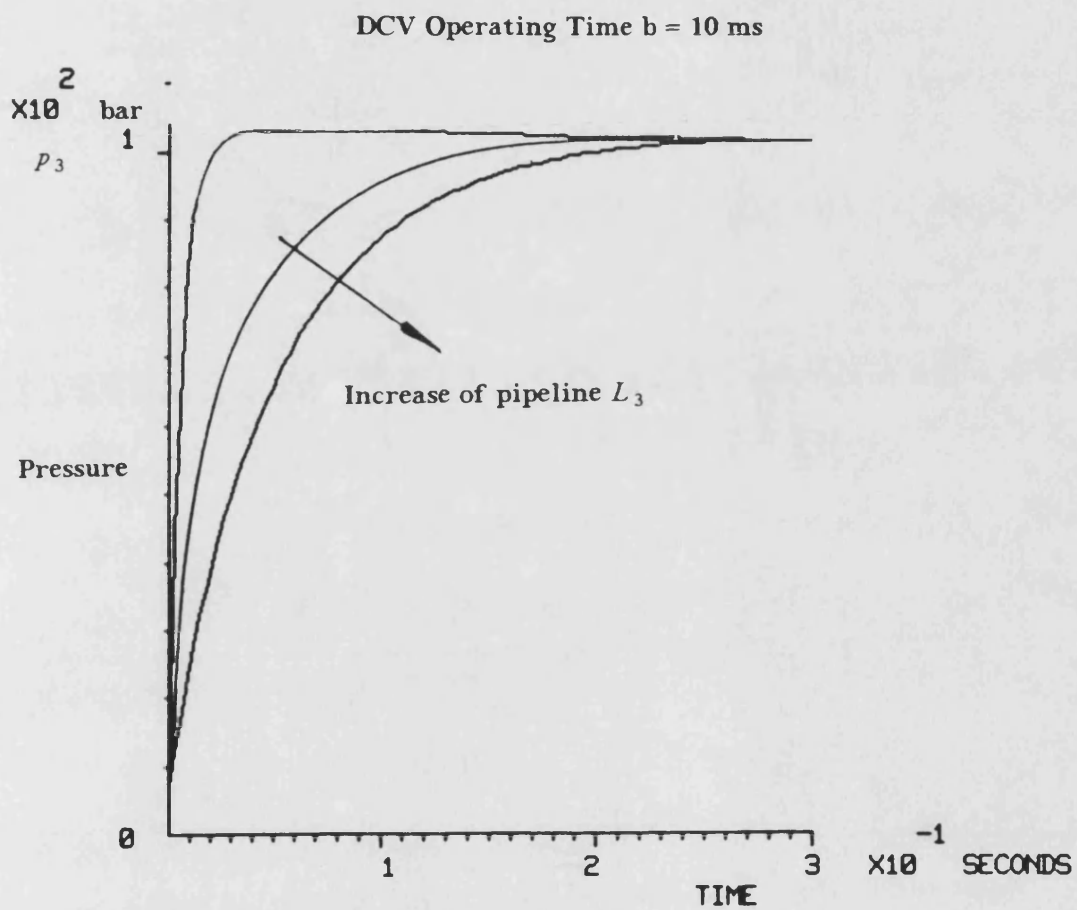
Fig. 3.26 The Effects of the Length of the High Pressure Line on the Transient Pump Delivery Pressure
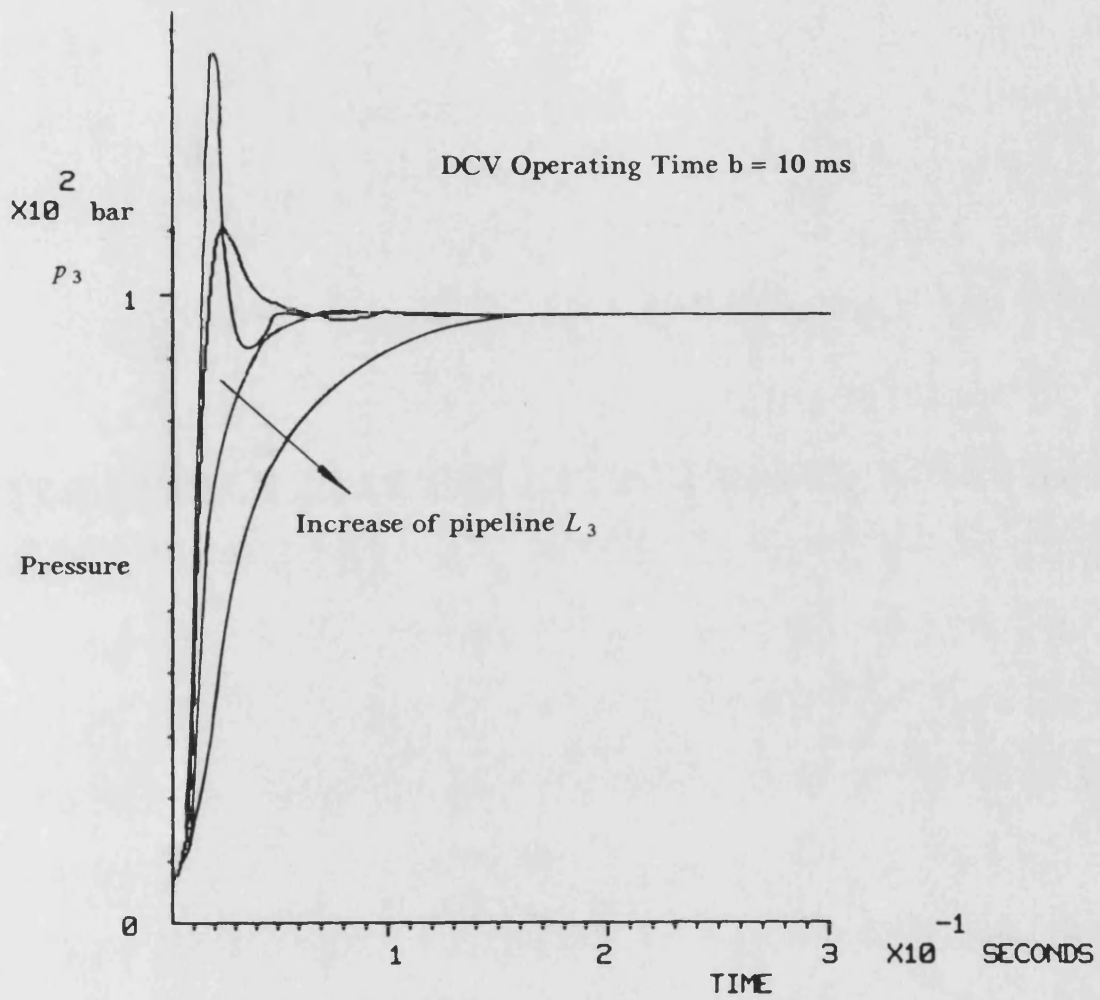
Fig. 3.27   The Transient Fluid Jet Inertia Effects on the
Transient Pump Delivery Pressure

DCV Operating Time b = 10 ms
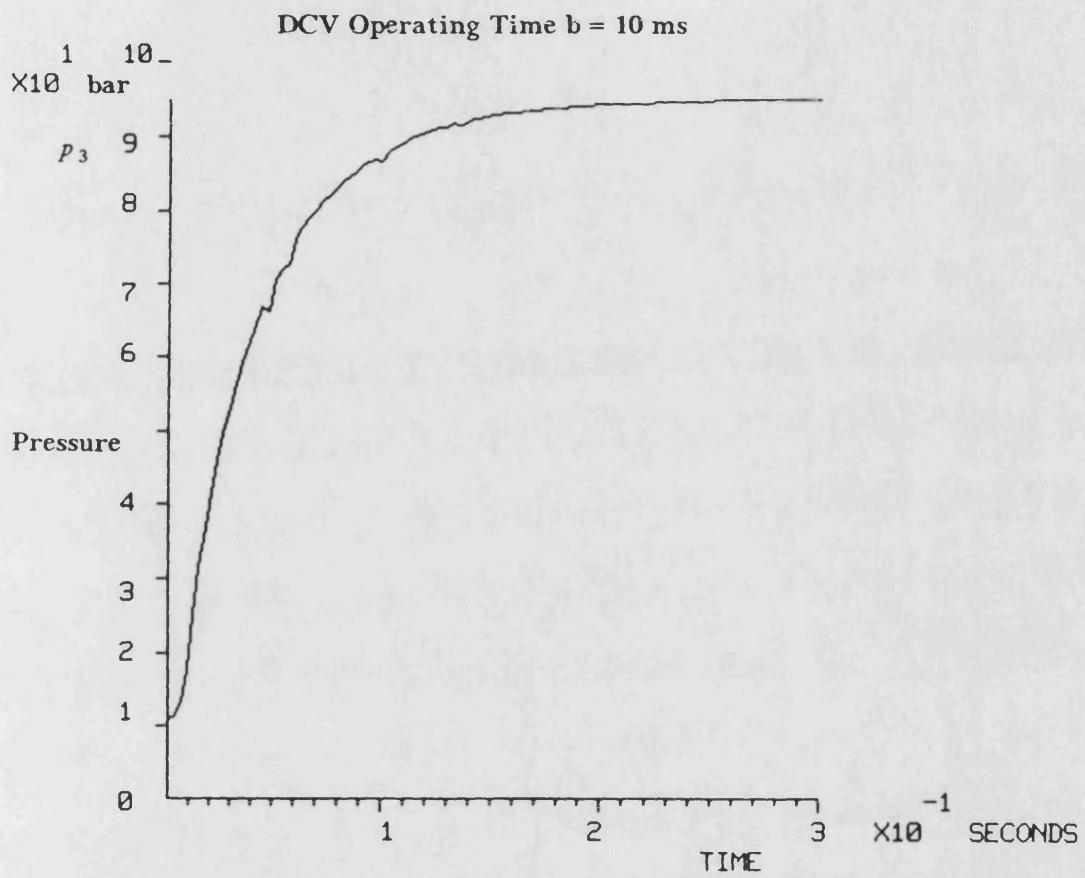
Fig. 3.28   The Effects of the Variation of the Pump Shaft Speed on the
Transient Pump Delivery Pressure
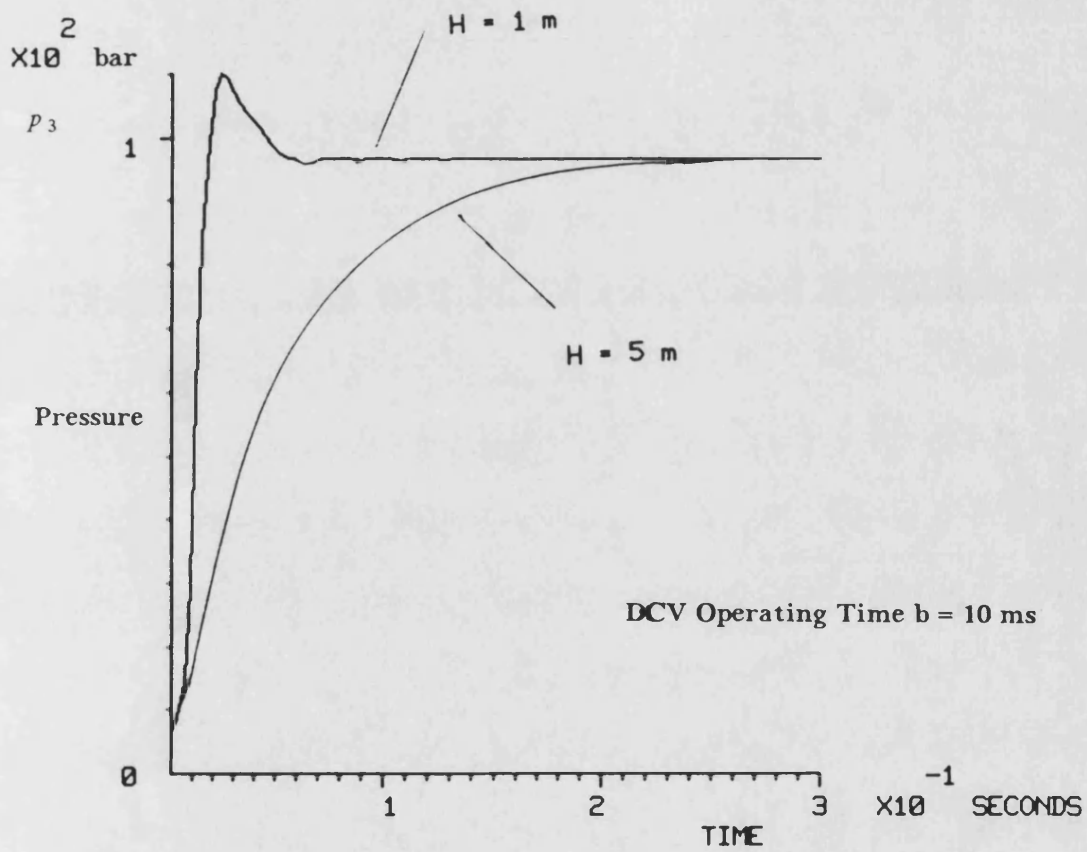
Fig. 3.29   The Simulated Transient Pump Delivery Pressures with the Change of the High Pressure Pipe Length
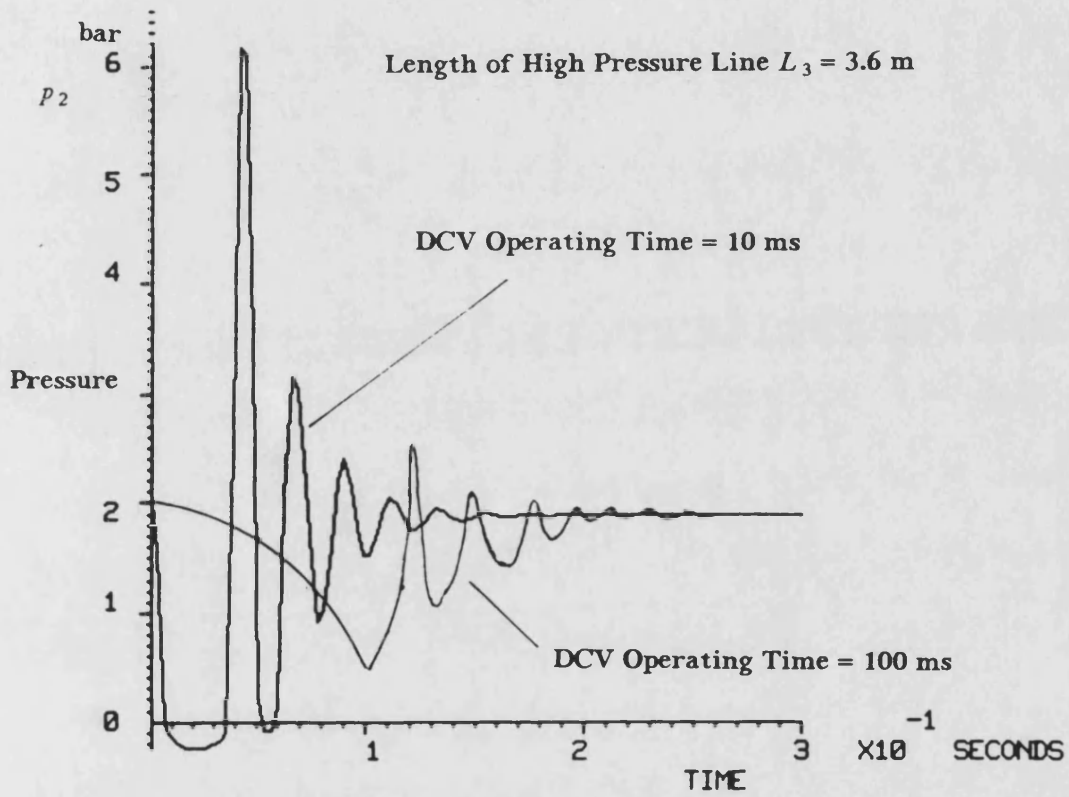
Fig. 3.30 The Effects of the Directional Control Valve (DCV) Operating Time on the Return Line Pressure
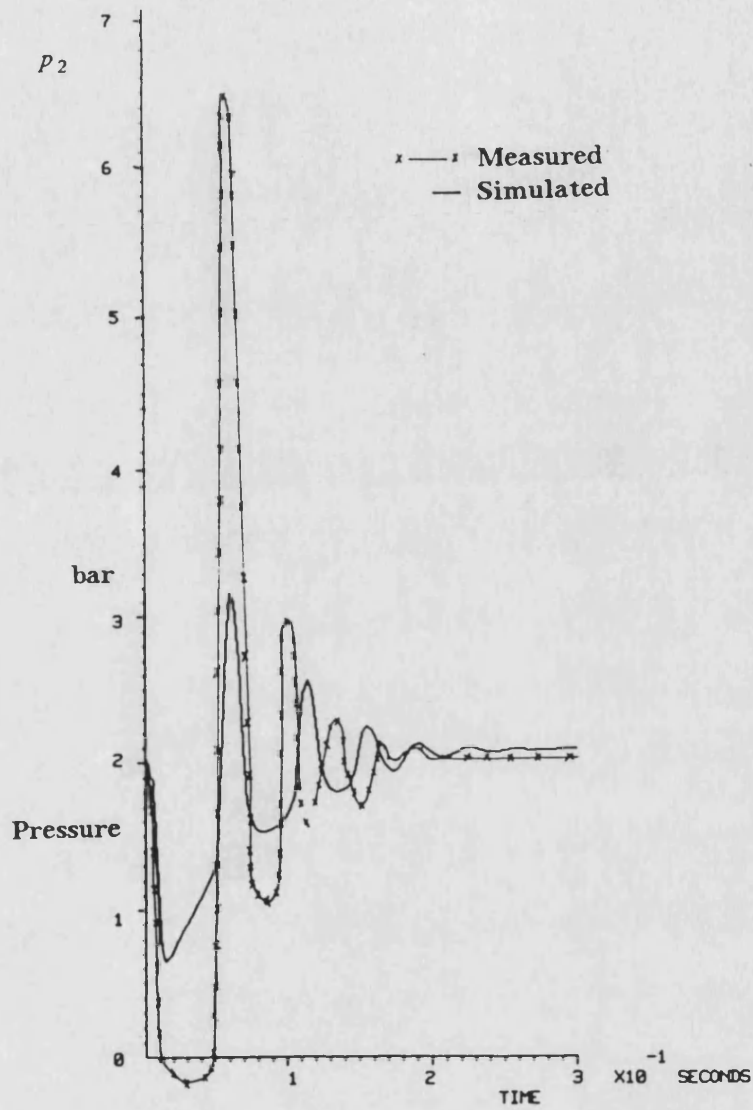
Fig. 3.31   A Comparison of Measured and Simulated Return Line Pressures
without the Consideration of Fluid Jet Effects
at the Orifice Downstream
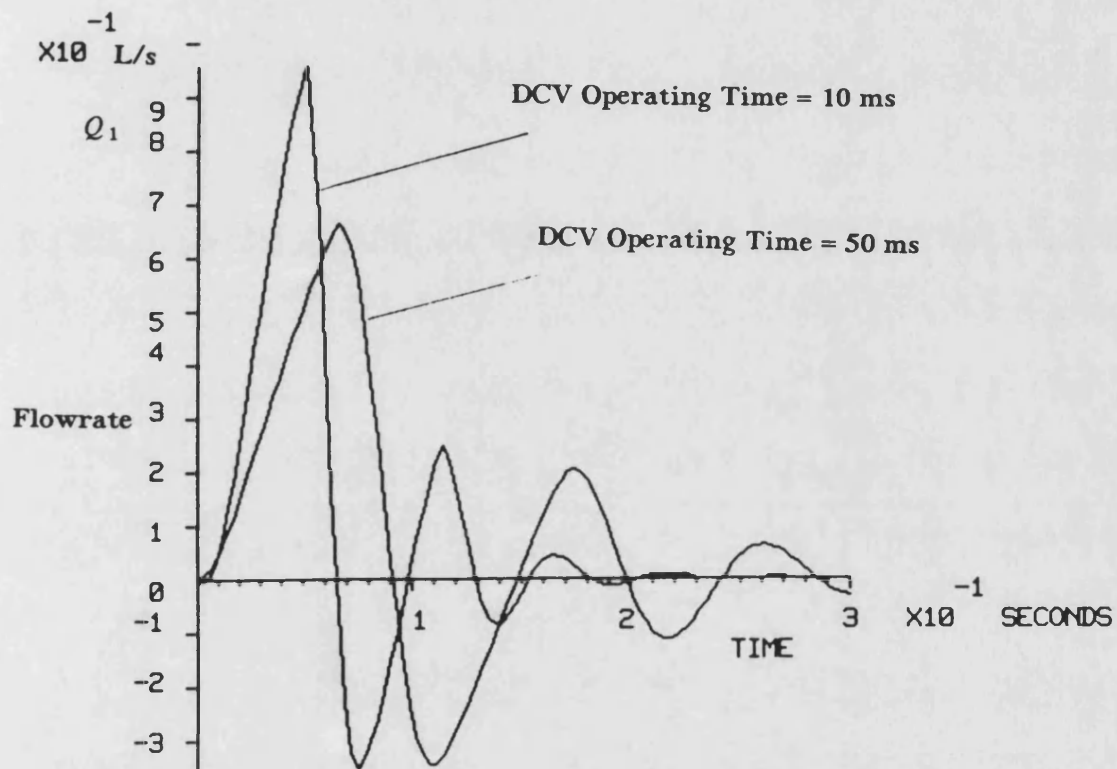
Fig. 3.32 The Effects of the Directional Control Valve (DCV) Operating Time on Transient Flowrate from the Open Ended Pipe
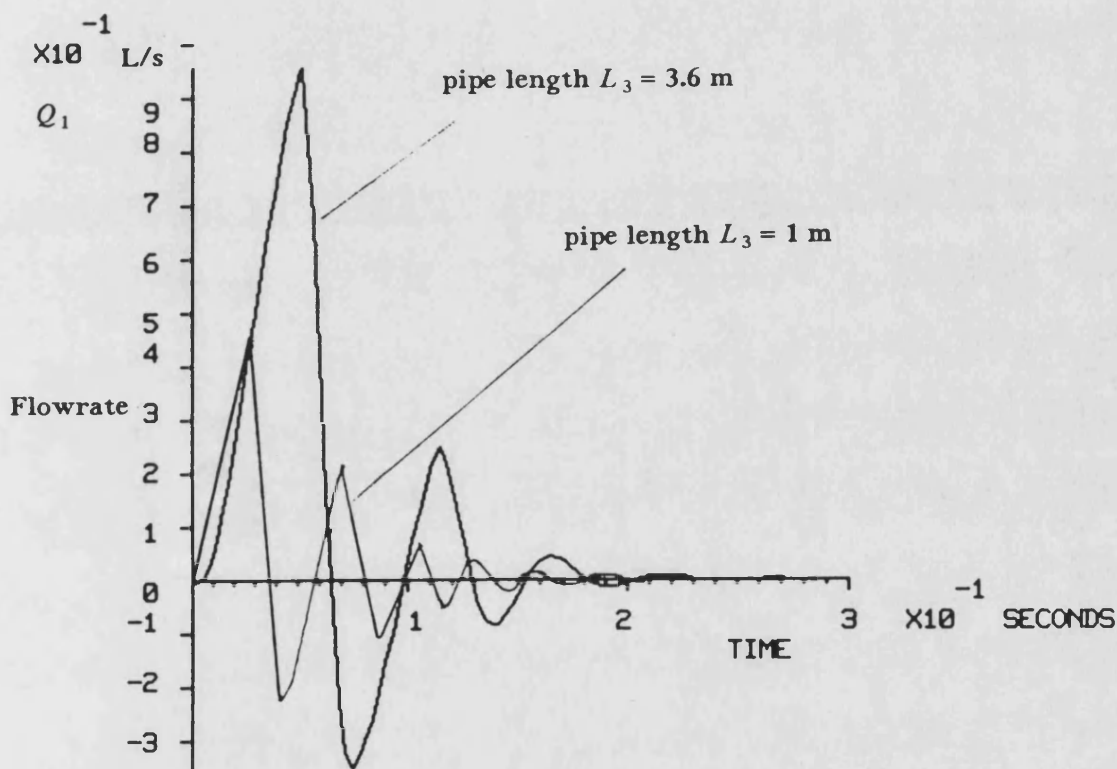
Fig. 3.33   The Effects of the Length of High Pressure Line on the
Transient Flowrate from the Open Ended Pipe
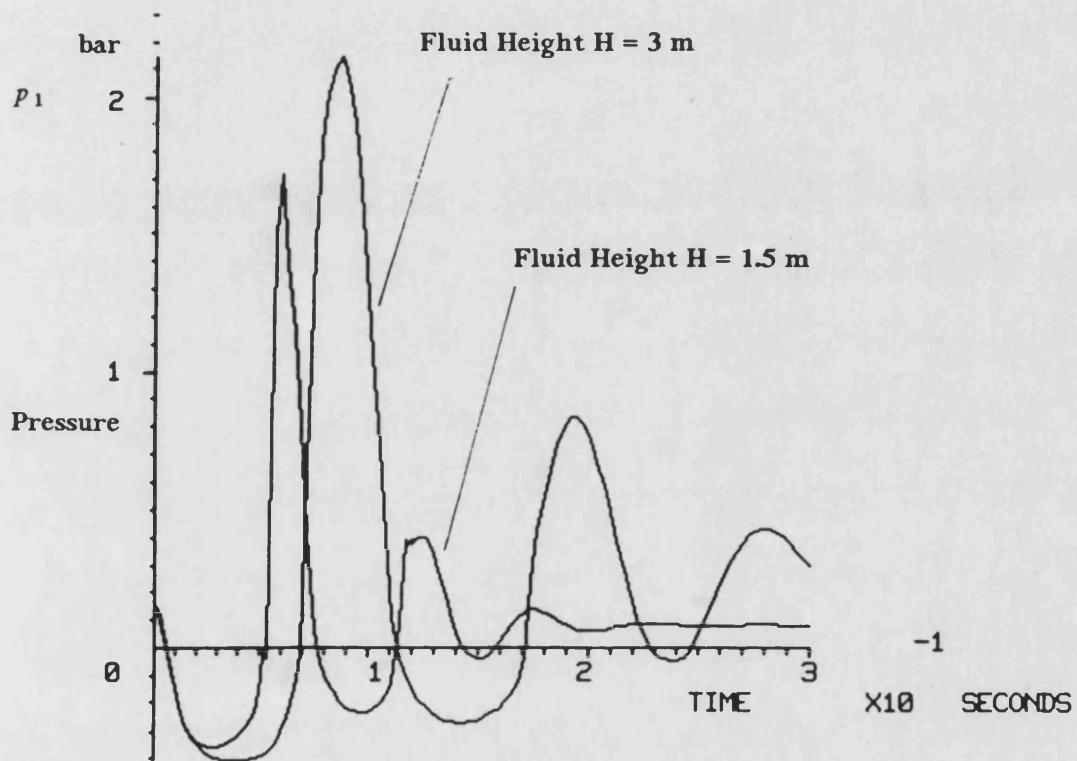
Fig. 3.34   The Effects of the Fluid Height in the Open Ended Pipe
on the Transient Suction Pressure at the Instant of
the System Loading
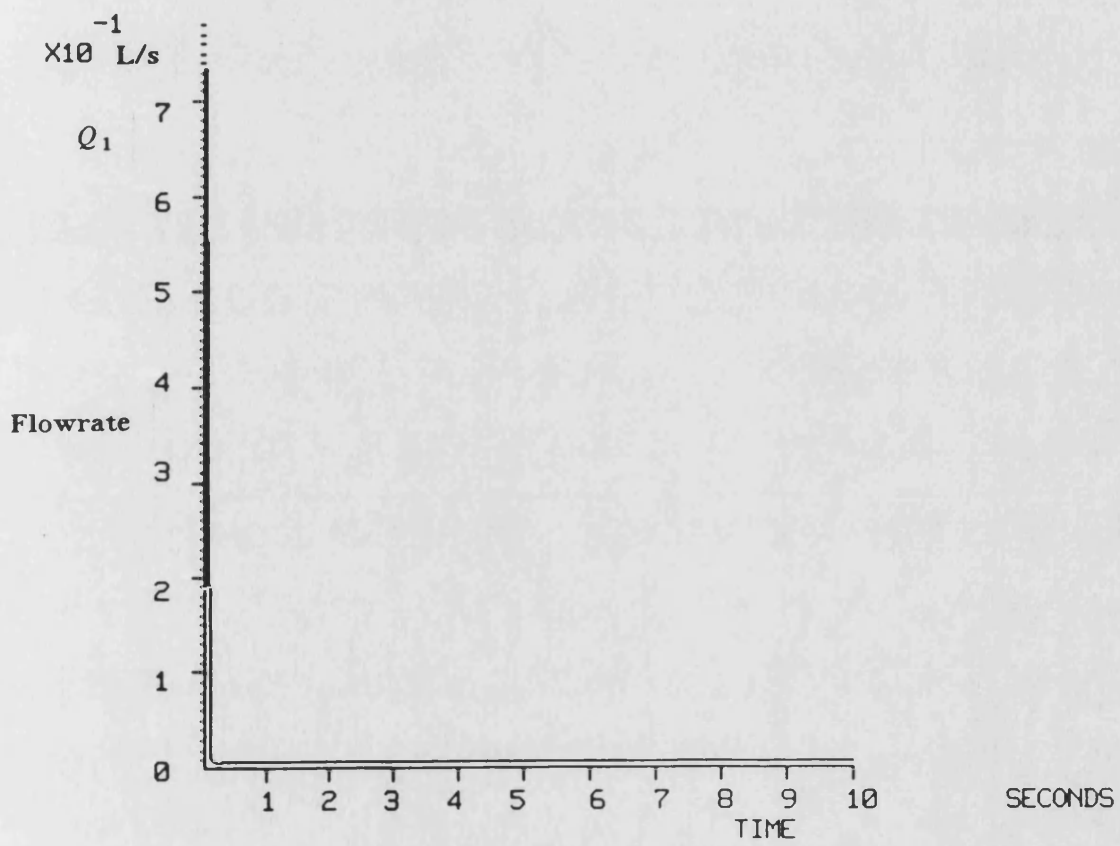
Fig. 3.35   The Simulated Flowrate from the Open Ended Pipe without
Consideration of the Fluid Expansion across the Orifice
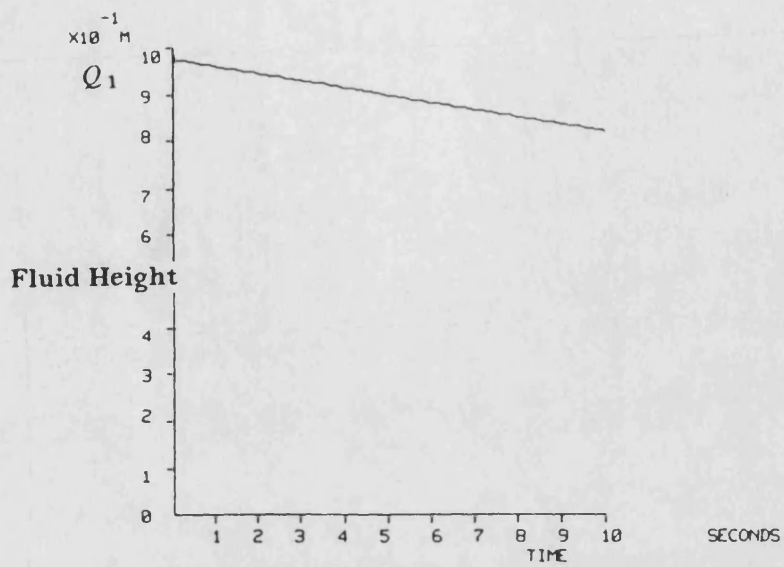
a.   The Simulated Fluid Height without Taking
Fluid Expansion into Account
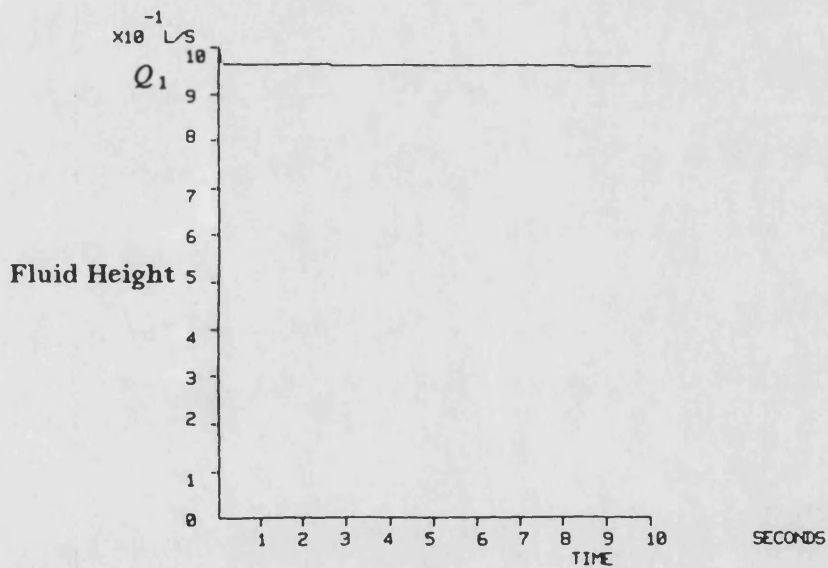
b.   The Simulated Fluid Height with Consideration of
Fluid Expansion

Fig. 3.36   The Effects of Fluid Expansion on the Fluid Height
in the Open Ended Pipe

k. Fluid Height in the Open-Ended Pipe

L. Pump Inlet Flowrate

b. Pump Delivery Flowrate

c. Transient Pump Delivery Pressure

j. Transient Flowrate from the Open-Ended Pipe

a. Pump Shaft Speed

d. Flowrate through Orifice Loading Valve

e. Flowrate through Directional Control Valve

i. Transient Suction Pressure

h. Return Line Flowrate at Downstream of the Cooler

g. Return Line Flowrate at Upstream of the Filter

f. Transient Return Line Pressure

Fig. 3.37   Transient Characteristics of Unboosted Closed System
During the Unloading of the System

FIG 3.37 cont'd
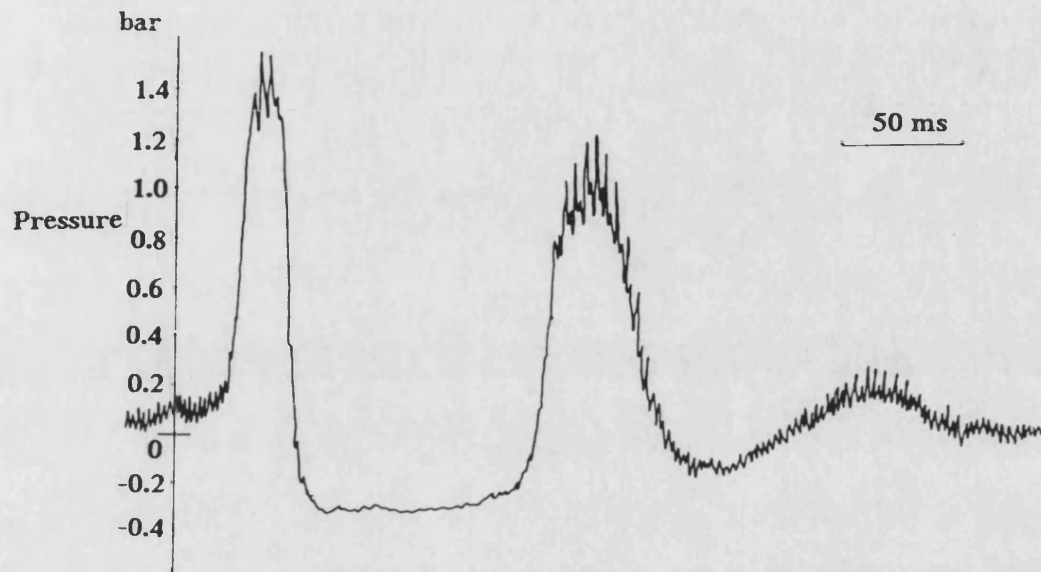
Fig. 3.38   Pressure Ripples Superimposed on the Pump Inlet
Pressure When the System is Unloaded

CHAPTER 4

INVESTIGATION INTO A PARTIALLY CLOSED HYDRAULIC SYSTEM

Introduction

4.1 Fundamental investigations on an unboosted closed hydraulic system has been carried out in Chapter 3, the test results have shown the practical feasibility and advantages of the unboosted closed system, but some difficulties have also been revealed. One difficulty is that the reduction of the reservoir size has adversely affected the mechanism of air release and heat dissipation of the system investigated. Another is that the removal of the boost pump from a closed system will result in a greater likelihood of oil degradation.

4.2 A modification on the unboosted closed hydraulic system has resulted an introduction to the partially closed hydraulic system as shown in Fig. 4.1. In this partially closed system, a controlled proportion flow returns to the reservoir and the rest flow returns direct to the pump entry line. Such a system allows interchange of oil from the main loop into the reservoir and also allows air bubbles to be released from the fluid surface of the reservoir. The fluid in the reservoir of the system can be used to store thermal energy and so the ability of the system energy dissipation can be improved. The return line to the reservoir and the suction line can be of smaller diameter than those in a conventional open hydraulic system. The pump entry line can be of shorter length to improve the pump suction conditions. Filtration and cooling can be carried out in either the main loop, or in the return line to the reservoir. Filters can be of smaller capacity than in an open system.

4.3 In this chapter, pressure and flow characteristics of the partially closed hydraulic system have been theoretically predicted and analysed. The theoretical analysis involves the establishment of mathematical equations to describe the transient pressure characteristics of a reservoir and a Y-junction suction pipeline. These mathematical equations have been implemented into HASP to set up the corresponding models by employing a computational 'false transient' technique and a 'linear interpolation method' for solving implicit relationship on model linking. As a result, the system pressure and flow performances have been theoretically predicted using HASP. The theoretical work is supported by an experimental programme in which a large number of tests have been conducted on a partially closed hydraulic test rig to analyse the system transient performance. Hence, the feasibilities and advantages of the partially closed hydraulic system have been reported.

4.4 The dynamic models for the majority of components used in the simple partially closed hydraulic system shown in Fig. 4.1 can be found in HASP models and the models developed in Chapter 3. However, transient behaviour of some of components in the system, such as the level in the reservoir, the vertical return pipe to the reservoir and the suction pipe junction, need to be examined to study the system transient performance.

4.5   Reservoir Model   In most systems, the reservoir is considered as a flow supply source at a constant pressure. In the system investigated, where a reservoir with a small volume is enlarged, at the instant of loading, there is a transient difference between the pump suction and return line flowrates so that the variation of fluid height in the reservoir could significantly affect the pressure at entry to the suction line from the reservoir. In such a case, a static reservoir model can lead errors in predicting transient suction pressure. It is generally assumed that the static pressure is the same as the mean total pressure so that the pressure at reservoir entry is the same as to the pressure at exit as shown in Fig. 4.2. The transient pressure at the reservoir inlet and outlet may be expressed by the change in fluid height, ie.

$$\frac{dp}{dt} = \rho g \frac{Q_o - Q_i}{A_t} \qquad \qquad \ldots \ldots (4.1)$$

where Q_o and Q_i are the reservoir inlet and outlet flowrates and A_t is the area of the reservoir. The above equation has been used to set up a HASP 'dynamic' reservoir model TK2H as given in Appendix II. This model can be also used to determine a suitable design of reservoir to obtain the suction conditions required in the system proposed.

In practice, however, the effective mean total pressure p_e, at a pipe across-section, is defined by

$$p_e = p_s + \frac{1}{2}\rho v^2 \qquad\qquad \dots\dots(4.2)$$

In the above equation, p_s is the piezometric pressure and v the mean velocity at a cross-section of the pipe. If the difference between the mean total pressure and the static pressure is taken into account, the Bernoulli Equation will be applied to express the static pressure at the reservoir inlet and outlet as indicated in Fig. 4.3, ie.

$$p_i = \rho g H - \frac{\rho}{2A^2}(1 + C_i)Q_i^2 \qquad\qquad \dots\dots(4.3)$$

where p_i is the pressure at suction pipe entrance. Similarly, the pressure in the reservoir outlet can be obtained by

$$p_o = \rho g H - \frac{\rho}{2A^2}(1 + C_o)Q_o^2 \qquad\qquad \dots\dots(4.4)$$

where C_i and C_o are the pressure loss coefficients at the reservoir entrance and exit and A is the pipe across-sectional area. In each of above two equations, the transient fluid level in the reservoir can be obtained from

$$\frac{dH}{dt} = \frac{Q_o - Q_i}{A_t} \qquad\qquad \dots\dots(4.5)$$

When the above three equations are used to develop a HASP reservoir model to calculate the pressures on the basis of flowrates, considerable difficulties will appear on model linking. This is because the model input flowrates are usually given by orifice algebraic equations and the output pressures are also expressed from algebraic equations (4.3) and (4.4).

4.6 Implicit Relationship of Model Linking

This type of problem in numerical system simulation is known as an implicit relationship for model linking.

This implicit relationship results from the attempt to solve two set of algebraic equations simultaneously within two adjacent models. The difficulties are due to the problem of data transfer between two models by means of model linking because the rule of model linking requires at least one state variable (or a variable resolved by a differential equation) to appear on each link. the usual solution for the implicit relationship in model linking is to combine the two models into a single model. In some cases, when several algebraic models have to be combined into a large model, a large amount of user defined input data will be required, and the combination coding work in the development of model could be very tedious and time consuming.

4.7 False Transient Technique An alternative approach to the model combination is to use the 'false transient technique'. The principle of this technique is to create an artificial first order differential equation.

For instance, the standard form of a first order equation like

$$Q_i = (1 + \tau_s)Q_o \qquad\qquad \dots\dots(4.6)$$

can be re-written as

$$\frac{dQ_o}{dt} = \frac{1}{\tau}(Q_i - Q_o) \qquad\qquad \dots\dots(4.7)$$

where τ is the time constant. Any algebraic equation may be re-written in a form of the differential equation which can be used together with other differential equations in a computer model to describe a component dynamic response. Such a group of equations can be then solved simultaneously by normal numerical analysis.

When the false transient technique is applied, the pressures in inlet and outlet of reservoir in Equation (4.3) and (4.4) can be obtained by solving the following equations, ie.

$$\frac{dp_i}{dt} = G(p_{is} - p_i) \qquad\qquad \ldots\ldots(4.8)$$

and

$$\frac{dp_o}{dt} = G(p_{os} - p_o) \qquad\qquad \ldots\ldots(4.9)$$

where p_{is} and p_{os} are defined by the original Equations (4.3) and (4.4). In the above two equations, G is a reciprocal of the time constant. When the value of G is big enough, a close result of p_i and p_{is} can be obtained as a graphic example shown in Fig. 4.4. It is noticed that a time delay, which is the production of the false transient equation, is shown in the numerical simulation result. However, if G is too big, a stiffness problem in the system numerical system would occur and a rather long computational time will be required. An empirical value of G is recommended above 1000 without loosing significant accuracy. On the basis of false transient technique, a dynamic reservoir model TKSH incorporated Equations (4.3), (4.4), (4.5), (4.8) and (4.9) has been developed and the detailed description of TKSH is given in Appendix II.

4.8   Modelling of the Return Line to Reservoir   It is a usual assumption in HASP pipe modelling that fluid inertia and pipe friction are negligible so that only the fluid compressibility is considered. This assumption is applicable for the theoretical modelling of the majority of the hydraulic pipe lines under the normal pressure conditions.

Under certain circumstances, however, this assumption may lead to errors in predicting transient pipe conditions. For example, the assumption is not suitable when simulating the transient conditions of the two vertical return and suction pipes in the system being investigated in Fig. 4.5. This is because the fluid acceleration and pipe friction in the pipes are more predominant than the fluid compressibility under the small pressure change which occurs at the instant of loading the system. The equation describing the fluid forces on the vertical return line pipe may be written as

- 56 -

inertia force + friction force − static pressure head =

difference in pressure force across return pipe

ie.

$$\frac{d\,(mv\,)}{dt} + p_f\,A\ -\ A\,\rho g h\ =\ (p_b\ -\ p_t\,)A \qquad \ldots\ldots (4.10)$$

In the above equation, the pressure loss due to friction is defined by the flow conditions as

$$p_f = \begin{cases} \dfrac{32\mu l\,v}{d_1} & \text{Laminar Condition Re} \leqslant 2000 \\[2mm] \lambda\dfrac{l\,\rho v^2}{d} & \text{Turbulent Condition Re} > 2000 \end{cases} \qquad \ldots\ldots (4.11)$$

The determination of friction factor λ under different condition for circular pipes has been given in Section 2.13.

In Equation (4.10), m = ρAh=constant, and Q_i = Av. Following closely the derivation given in Section 2.13, Equation (4.10) becomes

$$\frac{dQ_i}{dt}\ =\ \frac{A}{\rho h}(p_b\ -\ p_t\ -\ p_f\ )+\ Ag \qquad \ldots\ldots (4.12)$$

If the initial conditions are given, this equation can be used to calculate Q_i by applying numerical integration techniques. The above equation has been adapted into a HASP vertical return pipeline model PI3H whose details are given in Appendix II. A similar equation can be used to predict the transient flowrate in the vertical suction pipeline as given in a suction pipe junction model PITH below.

4.9 Modelling Pressure Losses in a Three-Leg Junction for Combining

Flows   Because there is a continuous flow in the suction pipe, it is necessary to

consider the flow-pressure condition at the junction between the suction and return lines and the pump entry line. Consider the flow at a Y-junction suction pipe as given in Fig. 4.6. The flow in legs 1, 2 and 3 is assumed to be one dimensional and incompressible in the vicinity of the junction. Under such conditions, the pressure distribution is shown schematically in Fig. 4.7. This is taken from sketch (i) of Ref. (4.1) and is based on experimental observations but is essentially illustrative. The diagram shows the variation of the effective mean total pressure, p_e, at a cross-section through the separate legs of the components. The static pressure loss across a pair of inlet and outlet legs can be estimated by applying the Bernoulli Equation

$$p_1 + \frac{1}{2}\rho v_1^2 = p_3 + \frac{1}{2}\rho v_3^2 + \Delta p_{13} \qquad \ldots\ldots (4.13)$$

where Δp_{13} is loss in total pressure between section 1 and 3. There are two loss coefficients which it is convenient to define for combining flow. Referring to Fig. 4.7 there are

$$K_{13} = \frac{\Delta p_{13}}{\frac{1}{2}\rho v_3^2} \qquad \ldots\ldots (4.14)$$

and

$$K_{23} = \frac{\Delta p_{23}}{\frac{1}{2}\rho v_3^2} \qquad \ldots\ldots (4.15)$$

On combining equation (4.13) and (4.15) there results

$$p_1 + \frac{1}{2}\rho v_1^2 = p_3 + \frac{1}{2}\rho(1 + K_{13})v_3^2 \qquad \ldots\ldots (4.16)$$

Now if these pipes are equal area, the above equation can be written as

$$\frac{\rho}{2A^2}(1 + K_{13})Q_3^2 - \frac{\rho}{2A^2}Q_1^2 - (p_1 - p_3) = 0 \qquad \dots\dots(4.17)$$

On the base of Equation (4.15) and (4.17), the static pressure loss across a pair of inlet and outlet legs 2 and 3 can be similarly estimated from

$$\frac{\rho}{2A^2}(1 + K_{23})Q_3^2 - \frac{\rho}{2A^2}Q_2^2 - (p_2 - p_3) = 0 \qquad \dots\dots(4.18)$$

If the effects of Reynolds Number on the pressure loss coefficients are assumed to be not important, then K_{13} can be given a specific value. Fig. 4.8 referred from Ref. (4.1) given pressure loss coefficients. In the similar way, K_{23} can be given a specific value.

At the Y-Junction on the test rig as shown in Fig. 4.6, the continuity condition must be satisfied. For incompressible flow in the vicinity of the junction, we may write

$$Q_3 = Q_1 + Q_2 \qquad \dots\dots(4.19)$$

If the effects of fluid inertia and pipe friction are assumed not to be important in the legs 2 and 3 of the Y-junction and only fluid compressibility is taken into account, then these two lengths of the pipe can be represented by two standard HASP pipe models of PIO5.

In the vertical suction pipe, however, at the instant of loading the system, a transient reduction in the return line flowrate occurs due to the effect of fluid compressibility in the high pressure line. As a consequence, a transient increment in the flowrate of the suction pipe, Q_1, is demanded to compensate this fluid compressibility loss so that the column of flow in the vertical suction pipe has been accelerated. In this case, the effects of fluid momentum and pipe friction have been taken into account as in order to obtain a realistic prediction of the pipe transient conditions. If compressibility is also taken into account, the pipe would have to be treated in a distributed parameter basis, leading to great complicational problems.

However, the rates of pressure change are low and compressibility effects have therefore been deemed to be insignificant.

Consider the fluid momentum and pipe friction in the vertical suction pipe. A similar derivation to Equation (4.12), there yields

$$\frac{dQ_t}{dt} = \frac{A}{\rho L_1}(p_t - p_1) - \frac{32\nu}{d^2}Q_0 + Ag \qquad \ldots \ldots (4.20)$$

where p_f is given in Equation (4.13).

Again, if an attempt is made to convert the above four equations (4.18) to (4.20) into a single HASP model, a typical implicit relationship will occur on the model linking because no any state variable would appear on the external link as illustrated in Fig. 4.9. The false transient technique discussed in Section 4.7 is not applicable for the solution of these four equations due to a long computational time would result . The usual way of combining these equations with the other three models of a reservoir and two pipe models PIO5 would be tedious and time consuming. Fortunately, a new approach to resolve this type of the implicit problem for solving both algebraic and differential equations in a single HASP model has been lately developed and given in Appendix I. Consequently, these four equations have been converted into a single HASP pipe junction model FPTH whose detailed description is given in Appendix II.

4.10   Flowrates in the Return and Suction Lines   In the return line of the partially closed hydraulic system in Fig. 4.10, the proportion of return line flowrate returning to the reservoir is controlled by the ratio of opening areas of two orifice diameters, A_a/A_b. Because the pressure losses in the orifices is designed to be small, momentum effects have not been taken into account. The steady value of flowrate through orifice B, Q_b, can be obtained from the simple orifice equation

$$Q_b = C_d A_b \frac{2}{\rho} (p_r - p_1)^{\frac{1}{2}} \qquad\qquad \dots\dots(4.21)$$

Similarly, the steady flowrate directly returning to tank Q_a can be calculated from

$$Q_a = C_d A_a \frac{2}{\rho} (p_r - p_t)^{\frac{1}{2}} \qquad\qquad \dots\dots(4.22)$$

Standard pipe orifice models PI05 and OR3Z have been used. At steady state conditions, the inlet flow of the return line must be equal to the outlet flow, then

$$Q_r = Q_a + Q_b \qquad\qquad \dots\dots(4.23)$$

4.11 **System Block Diagram** In order to examine the system transient performance, it is necessary to consider dynamic characteristics of each component involved. These consist of the electric motor, the pump, the pipe lines, the directional control valve, the loading orifice restrictor and the reservoir. These components may be simulated by use of HASP standard models as well as the models developed in Section 4.8, 4.9 and 4.10. The simulation block diagram of the system investigated as shown in Fig. 4.11.

In the diagram, a electric motor model PM2H is identical to that used in Chapter 3 to simulate the dynamic response of the motor speed. Similarly, the gear pump model PU0H, the frictionless pipe model PI05, the dynamic orifice loading valve model OR2H, the two way two position directional control valve model DC1C together with the duty cycle model DEDT are used in the conditions identical with those described in Chapter 3. The dynamic pipe model of PI3H can be used to simulate the effects of fluid acceleration in the vertical return line to the reservoir. As a consequence, a dummy standard pipe model PI05 with a short pipe length is used to match the model linking requirement between PI3H and the orifice model OR00. The dynamic reservoir model TKSH and the suction pipe junction model PITH are used to simulate the dynamic behaviours in a hydraulic reservoir and a suction pipe junction.

The test rig was modified to investigate experimentally the performances of the partially closed hydraulic system and the simulation was carried out using as input data the salient parameters of the modified system.

Experimental Investigation

4.12 Experimental Test Rig and Measurements The experimental test rig was modified as in Fig. 4.12. When the directional control valve is closed, the full pump flow was passed through an adjustable orifice restrictor which was set under those conditions to give a pump delivery pressure of 100 bar. Two orifices were incorporated in the return line to control the flowrates to the reservoir through orifice A and to the pump entry line through orifice B.

The dynamic and steady state pressures in the various parts of the system pipelines were monitored by four pressure transducers at the positions shown. Details of technical data for each component and measuring instruments are listed in Table 4.1.

4.13 Experimental Test Procedure The tests were carried out in the following sequence: first the pump was started with the directional control valves (DCV) open, ran steady for a minute or two, then the DCV was closed rapidly by hand to load the pump to 100 bar. The system ran 3 minutes under load, next it was unloaded by opening of the DCV which had been closed and after one more minute of steady running the electric motor was switched off. The procedure was then repeated by changing the size of orifice in the return line.

4.14 Experimental High Pressure Transient The detailed analysis of the system transients in the high pressure and return lines have been given in Section 2.24 and 2.25. Here a brief summary is given below. The transient high pressure is determined by the following factors:

   1). the closure speed of the directional control valve;

   2). the fluid compressibility in the high pressure pipe;

   3). dynamics of the orifice loading valve.

A typical recording of the transient pressure in the high pressure line is given in Fig. 4.13.

4.15   Experimental Pressure Transients in the Return and Suction Lines

After the rapid closure of the directional control valve, the fluid compressibility in the high pressure line and dynamics of the orifice loading valve cause pressure variations in the return line. Fig. 4.14a and 4.14b show the pressures upstream of the filter and downstream of the cooler for the same case. The damping effects due to the compliance of the cooler and filter housing can be discerned.

Fig. 4.15 shows the pressure at the pump entry line during the same test. This transient variation of the suction pressure is generated by a proportion of the transient reduction in the return line flowrate passing orifice B, Q_b. The acceleration of constant fluid mass in the vertical suction pipe is different to the variable fluid mass acceleration in the vertical open ended pipe in the transient tests of the unboosted closed system discussed in Chapter 3. Hence the high frequency spike exhibited in the return line pressures does not appear. In addition, the static suction pressure value is determined by the fluid head in the vertical suction pipe and in the reservoir. This static suction pressure is also subject to the dynamic pressure, suction line pipe friction and the pressure loss across the suction and pump entry lines at the suction pipe junction. The individual effect of each factor on the suction transient pressure is not easy to understand from physical deduction but can be seen in Section 4.20 and 4.21 to be represented in the computer simulation.

4.16   Comparison of Performances of Circuit Designs   The test rig can be also used to examine the performance of a conventional open system design. When orifice B is closed with fully opening of orifice A in Fig. 4.12, the system becomes a conventional open hydraulic system. Since all the system flow returns directly to the reservoir, the transient variation of the return line flowrate at the system loading will be absorbed by the large fluid volume in the reservoir. Hence, no transient variation has been found in the suction pressure recordings of the open system. However, the value of the system suction pressure was recorded as a constant value of -0.2 bar (gauge) in the experimental result. This low static suction

pressure in the open system results from the increase in the dynamic suction pressure head and pipe friction. As a result of this low suction pressure (below the normally atmospheric pressure), air bubbles release at the pump entry and cavitation occurs. Hence the pump delivers the mixed air-liquid flow into the high pressure line. Consequently, the experimental recordings of the pump delivery pressure as one example shown in Fig. 4.16 are actually lower than before in spite of the fact that delivery line loading conditions had not been changed. Meanwhile a loud noise was generated by the pump as another consequence of the air-liquid flow in the system. The suction pressure may be increased in a practical open hydraulic system by introducing a significant increase in the suction pipe diameter so as to avoid the possibility of air release.

On another case, when orifice A in Fig. 4.12 is closed with fully open of orifice B, the rig becomes an unboosted closed loop system. The previous test result has shown a higher static suction pressure which is determined by the fluid head in the open ended pipe, but a greater variation of transient suction pressure was also resulted due to the bigger transient reduction in the return flow caused by fluid compressibility and orifice dynamics. Moreover, the system may have difficulties in air release, heat dissipation and a great likelihood of oil degradation. Therefore, the partially closed hydraulic circuit design is recommended in future applications.

4.17 Effects of Orifice Size on the Suction Pressure   The experimental recording of the suction pressure in the open system has shown the influence of the flowrate returning to the reservoir on the suction pressure. The proportion of this flowrate is controlled by the two return orifices A and B. The following relations may be derived from Equation (4.21), (4.22) and (4.23) to analyse the experimental results. From these equations, the return line flowrate Q_r in Fig. 4.10 can be expressed by

$$Q_r = \left| \frac{A_a}{A_b} (\frac{P_r - P_t}{P_r - P_1})^{\frac{1}{2}} + 1 \right| Q_b \qquad \ldots\ldots(4.24)$$

Or

$$Q_r = \left| \frac{A_b}{A_a} \left(\frac{p_r - p_1}{p_r - p_t} \right)^{\frac{1}{2}} + 1 \right| Q_a$$

...... (4.25)

These relations show that the proportion of the system flow going to reservoir is also determined by the ratio of the pressure loss across the two orifices. Fig. 4.17 shows the effects of changing the two orifice sizes on the suction pressure in the partially closed system. The results have shown that when these orifice sizes are chosen to increase the static suction pressure an increase in oscillatory behaviour in suction pressure also result at the instant of the system loading. In general, from consideration of the system long term performance, a better choice for the system static suction pressure is more important than the better selection of the transient suction pressure. Further consideration is also necessitated to select a sufficient proportion of the return flow going to reservoir to free air from the air-liquid mixed flow in the system. When the partially closed circuit design is put into a practical application, approximately 10 - 15 % return flow is recommended for returning to reservoir for optimal system performance. This optimal proportion of return flow was obtained on the basis of a number of experimental results.

4.18   Simulation Data Acquisitions   The simulation parameters were obtained from the test rig described in Section 4.12. The details of user defined parameters of each model are listed in Table 4.2 - 4.21. The determination for the data in Table 4.2 - 4.13 are identical with those used in Chapter 3. In input data of 5.54 mm for orifice A diameter listed in Table 4.14, this value was obtained from the experimental test condition and the fluid discharge coefficient has been taken as the recommended value of 0.69 in the HASP standard orifice model OR00. In the simulation data for the dummy pipe model [PI05(5)] is given in Table 4.15, the pipe size has been kept in the same value as that of the vertical return pipe, the length of this pipe is taken as 0.1 m so as to avoid the possible occurrence of the computational stiffness problem but without any significant loss in accuracy of the calculated results.

The geometrical values of the vertical return line to the reservoir given in Table 4.16 are the measured results from the test rig. The initial flowrate in the pipe is estimated according to the measured initial pressure conditions before the system loading. The simulation data in Table 4.17 for the reservoir based on the data obtained on the test rig. The coefficient of the first order lag is the artificial constant used in the false transient technique. In the similar way, the input for the pipe junction in Table 4.18 are originated from the experimental test rig and the initial test conditions. The data in Table 4.19 are obtained from the test rig and used to simulate the effects of interconnecting pipe between the orifice B and the pipe junction. Again the simulation value of 14.2 mm for the diameter of orifice B in Table 4.20 are acquired from the experimental initial pressure conditions and the size of the sharp edged orifice used in the experiments. The simulation data in Table 4.21 for the pump entry line are based on the data obtained from the test rig.

Under such conditions, simulations were carried out to predict the system transient characteristics. A comparison was made between calculated and measured pressure transients, which were generated by the rapid operation of the directional control valve in the system. The analysis will mainly concentrate on the suction pressure transient. Attention will be also given to examine the effects of the suction pipe junction and the vertical suction pipe length on the suction pressure.

4.19 Analysis of Transients in Return line Downstream of Cooler

Simulations have been carried out with different combination of orifice size. When the directional control valve is selected to load the system in 10 ms, the simulation results of the transients, in the high pressure line and the return line upstream of the filter, are identical to the experimental measurements. Fig. 4.18 show the simulated transients in the return line downstream of the cooler.

Fig. 4.18a shows the transient variation of the flowrate from the cooler, Q_r, which is caused by the dynamics of the orifice loading valve and the fluid compressibility in the high pressure line as discussed previously. Fig. 4.18b shows the simultaneous variation of the simulated transient pressure at the downstream of the cooler. As this pressure is in the region below the atmospheric value, the direction of flowrate to the reservoir Q_a reverses in Fig. 4.18c. As a consequence, a small variation was generated and superposed on the return line flowrate Q_r and the pressure p_r as they recover to the steady values. The transient reduction in the flowrate through orifice B, Q_b, was shown in Fig. 4.18d.

4.20 The Effects of Suction Pipe Junction on the Suction Pressure

As discussed previously in Section 4.9, the difference between the effective mean total pressure and the static pressure as well as the pressure losses across the pairs of the pipe junction components has been taken into account in the theoretical predictions of the system transient performance. The importance of these factors can be seen from consideration of Fig. 4.19 and 4.20. In Fig. 4.19 the effect was omitted, in Fig. 4.20 it was included, with good agreement between theory and experiment.

4.21 The Effects of Suction Pipe Length on the Suction Pressure

As discussed previously, the effects of the fluid inertia in the vertical suction pipe is more significant than fluid compressibility under a small pressure change in the low pressure region at the instant of loading the system. For this reason, the pipe length of the suction line, which determines the fluid mass being accelerated, would be expected to affect the transient suction pressure. In addition, the pipe length also determines the pressure loss along the pipe due to the pipe friction. The effects of this suction pipe length on the simulation results for the suction pressure are shown in Fig. 4.21. As can be seen, the shorter the length, the lower the transient

variation.

No.	Component Name	Technical parameters	Data	Unit
1	electric motor	maximum speed at 15 kw	1500	rev/min
2	gear pump with internal drain	theoretical displacement maximum pressure	57.3 172	cm^3/rev bar
3	high pressure pipeline	1" rigid pipe + 1" hydraulic hose	1 2.6	m m
4	sharp edged loading orifice	maximum flowrate	100	L/min
5	return line	1" hydraulic hose	4.3	m
6	suction line	1" hydraulic hose	1.5	m
7	open ended pipe	1" plastic pipe	2	m
8	2 way 2 position manually directional operated control valve	maximum flowrate maximum pressure	110 210	L/min bar
9	cooler	maximum flowrate maximum heat dissipation volumetric size	111 30 10	L/min kw Litres
10	return line orifice A	maximum flowrate maximum pressure	100 50	L/min bar
11	return line orifice B	maximum flowrate maximum pressure	100 50	L/min bar

Table 4.1   Technical Data of Components on Test Rig

Fluid Properties Section Model FLPROP			
No.	Parameters	Data	Unit
1	oil temperature	20	deg. C
2	oil type	BP HLP 32	
3	fluid density	870	$\frac{kg}{m^3}$
4	fluid Bulk Modulus	18400	bar
5	fluid kinematic viscosity	74.56	cSt
6	fluid absolute viscosity	64.87	cP

Table 4.2   parametric Data Used in Simulation for Fluid Properties

Component No. 1:	Electric Motor Model PM2H (No. 1)		
No.	Input Parameters	Data	Unit
1	motor speed	1500	rev/min
2	effective pump/motor inertia	0.5	$kg.m^2$
3	motor torque/speed slip	19.6	Nm/(rev/min)
4	damping torque coefficient	0.01	Nm/(rev/min)
5	initial motor speed	1500	rev/min

Table 4.3   parametric Data Used in Simulation for Electric Motor

Component No. 2:	Hydraulic Pump Model PU0H (No. 1)		
No.	Input Parameters	Data	Unit
1	maximum pump displacement	0.0573	L/rev
2	fraction of full displacement	1	
3	slip loss coefficiency	1.4×10^{-8}	
4	torque loss coefficiency	2	
5	viscous friction coefficiency	0.8	
6	clearance volume	0	

Table 4.4   parametric Data Used in Simulation for Hydraulic Pump

Component No. 3:	Frictionless Pipe Model PI05 (No. 1)		
No.	Input Parameters	Data	Unit
1	pipe internal diameter	25.4	mm
2	pipe length	3.6	m
3	pipe volume	1.824	Litres
4	fluid/pipe Bulk Modulus	10261	bar
5	air saturation pressure	0	bar
6	proportion of dissolved air	0.1	
7	initial pressure	7	bar

Table 4.5   parametric Data Used in Simulation for High Pressure Pipeline

Component No. 4:	Orifice Restrictor Load Valve Model OR2H (No. 1)		
No.	Input Parameters	Data	Unit
1	steady state flowrate	1.4	L/sec
2	corresponding pressure drop	98	bar
3	equivalent fluid jet length	0.54	m
4	initial flowrate	0.1	L/sec
5	fluid Bulk Modulus	10261	bar

Table 4.6   parametric Data Used in Simulation for Orifice
            Loading Valve

Component No. 5:	2 Way 2 Position DCV Model DC1C (No. 1)		
No.	Input Parameters	Input Data	Unit
1	restriction constant	0.626	
2	linear region limit	0.01	bar

Table 4.7   parametric Data Used in Simulation for 2 Way 2 Position Directional Control Valve

Component No. 6:	Movement of DCV Model DEDT (No. 1)		
Stage	Spool Displacement	Time (second)	Valve Position
1	0	0	open
2	1	0.01	close
3	1	1	close

Table 4.8   parametric Data Used in Simulation for Different Time Relate Slip of Directional Control Valve

Component No. 7: Frictionless Pipe Model PI05 (No. 2)			
No.	Input Parameters	Data	Unit
1	pipe internal diameter	25.4	mm
2	pipe length	4.3	m
3	pipe volume	1.013	Litres
4	fluid/pipe Bulk Modulus	10261	bar
5	air saturation pressure	0	bar
6	proportion of dissolved air	0.1	
7	initial pressure	2	bar

Table 4.9 parametric Data Used in Simulation for Return Pipeline Before Cooler

Component No. 8: Orifice Restrictor Model OR00 (No. 1)			
No.	Input Parameters	Data	Unit
1	steady state flowrate	1.4	L/sec
2	corresponding pressure drop	1	bar

Table 4.10 parametric Data Used in Simulation for Pressure Drop at Filter Entrance

Component No. 9: Frictionless Pipe Model PI05 (No. 3)			
No.	Input Parameters	Data	Unit
1	pipe internal diameter	25.4	mm
2	pipe length	20	m
3	pipe volume	10.13	Litres
4	fluid/pipe Bulk Modulus	15437	bar
5	air saturation pressure	0	bar
6	proportion of dissolved air	0.1	
7	initial pressure	1	bar

Table 4.11   parametric Data Used in Simulation for Cooler

Component No. 10: Orifice Restrictor Model OR00 (No. 2)			
No.	Input Parameters	Data	Unit
1	steady state flowrate	1.4	L/sec
2	corresponding pressure drop	0.9	bar

Table 4.12   parametric Data Used in Simulation for Pressure Drop
            at Cooler Exit

Component No. 11: Frictionless Pipe Model PI05 (No. 4)			
No.	Input Parameters	Data	Unit
1	pipe internal diameter	25.4	mm
2	pipe length	0.5	m
3	pipe volume	0.76	Litres
4	fluid/pipe Bulk Modulus	10261	bar
5	air saturation pressure	0	bar
6	proportion of dissolved air	0.1	
7	initial pressure	0.1	bar

Table 4.13   parametric Data Used in Simulation for Return Line
Pipe at Downstream of Cooler

Component No. 12: Orifice Restrictor Model OR00 (No. 3)			
No.	Input Parameters	Data	Unit
1	orifice diameter	5.54	mm
2	sharp edged orifice discharge coefficient	0.69	
3	laminar boundary in bar	0.1	bar

Table 4.14   parametric Data Used in Simulation for Orifice
A in Return Line to Reservoir

Component No. 13:	Frictionless Pipe Model PI05 (No. 5)		
No.	Input Parameters	Data	Unit
1	pipe internal diameter	25.4	mm
2	pipe length	0.1	m
3	pipe volume	0.50661	Litres
4	fluid/pipe Bulk Modulus	10261	bar
5	air saturation pressure	0	bar
6	proportion of dissolved air	0.1	
7	initial pressure	0.2	bar

Table 4.15   parametric Data Used in Simulation for the Dummy Pipe Model for Model Linking

Component No. 14:	Vertical Pipe Model PI3H (No. 1)		
No.	Input Parameters	Data	Unit
1	pipe internal diameter	25.4	mm
2	pipe length	2	m
3	initial pipe outlet flowrate	0.3	L/s

Table 4.16   parametric Data Used in Simulation for Return Line to Reservoir

Component No. 15:	4 Link Dynamic Tank Model TKSH (No. 1)		
No.	Input Parameters	Data	Unit
1	length of tank base	1	m
2	width of tank base	0.1	m
3	diameter of extending pipe	25.4	mm
4	initial fluid height in tank	0.1	m
5	initial pressure at entry	0.1	bar
6	coefficient of first order lag	1000	

Table 4.17   parametric Data Used in Simulation for Reservoir

Component No. 16:	Vertical Pipe Junction Model PITH (No. 1)		
No.	Input Parameters	Data	Unit
1	pipe internal diameter	25.4	mm
2	pipe length	2	m
3	initial vertical pipe inlet flowrate	0.3	L/s
4	fluid/pipe Bulk Modulus	10261	bar
5	initial vertical pipe outlet pressure	0.02	bar

**Table 4.18   parametric Data Used in Simulation for Vertical Suction
Pipe and Pipe Junction Model**

Component No. 17: Frictionless Pipe Model PI05 (No. 6)			
No.	Input Parameters	Data	Unit
1	pipe internal diameter	25.4	mm
2	pipe length	1.5	m
3	pipe volume	0.5067	Litres
4	fluid/pipe Bulk Modulus	10261	bar
5	air saturation pressure	0	bar
6	proportion of dissolved air	0.1	
7	initial pressure	0.02	bar

Table 4.19   parametric Data Used in Simulation for
Interconnecting Flow Pipeline

Component No. 18: Orifice Restrictor Model OR00 (No. 4)			
No.	Input Parameters	Data	Unit
1	orifice diameter	14.2	mm
2	sharp edged orifice discharge coefficient	0.69	
3	laminar boundary in bar	0.1	bar

Table 4.20   parametric Data Used in Simulation for Orifice
B in Interconnecting Pipeline

Component No. 19: Frictionless Pipe Model PI05 (No. 7)			
No.	Input Parameters	Data	Unit
1	pipe internal diameter	25.4	mm
2	pipe length	0.5	m
3	pipe volume	0.25335	Litres
4	fluid/pipe Bulk Modulus	18361	bar
5	air saturation pressure	0	bar
6	proportion of dissolved air	0.1	
7	initial pressure	0.01	bar

Table 4.21   parametric Data Used in Simulation for Pump Entry Line
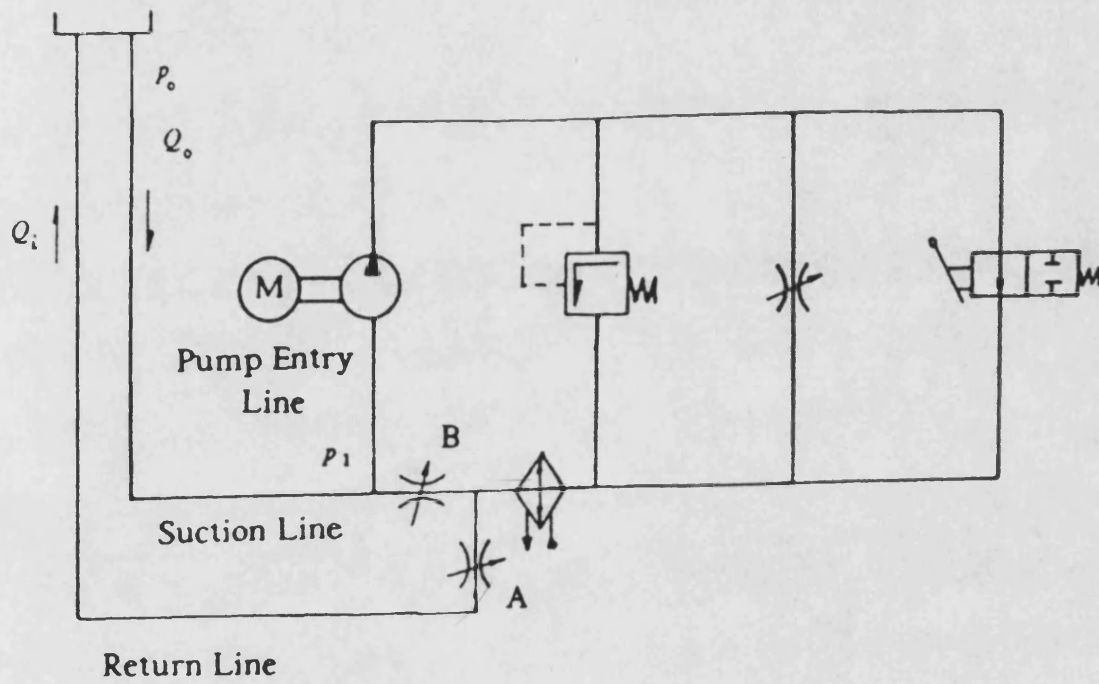
Fig. 4.1   A Partially Closed Hydraulic System
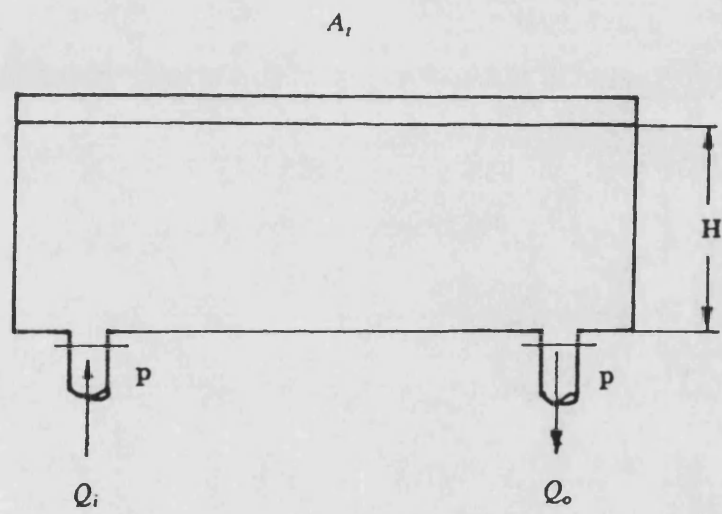
Fig. 4.2   Transient Flow Condition of A Hydraulic Reservoir
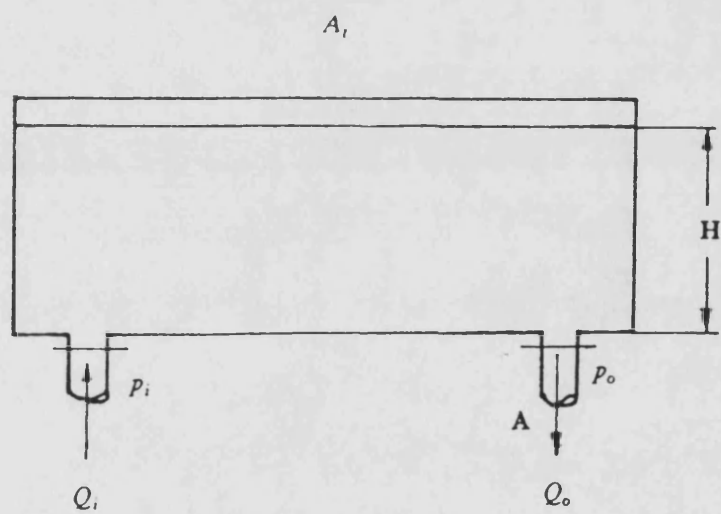
Fig. 4.3   Transient Pressure and Flow Conditions of A Hydraulic Reservoir
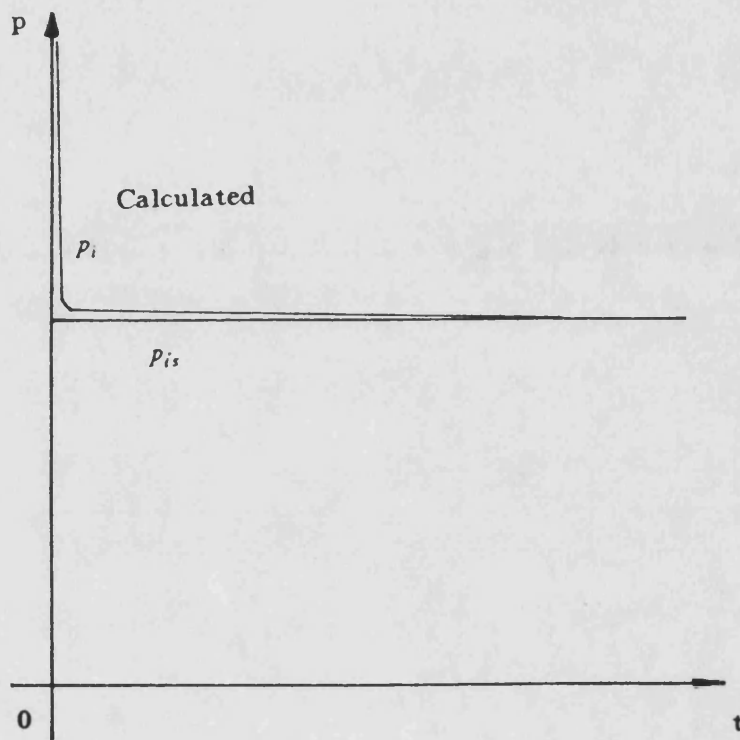
Fig. 4.4   The Computational Result of the False Transient Method
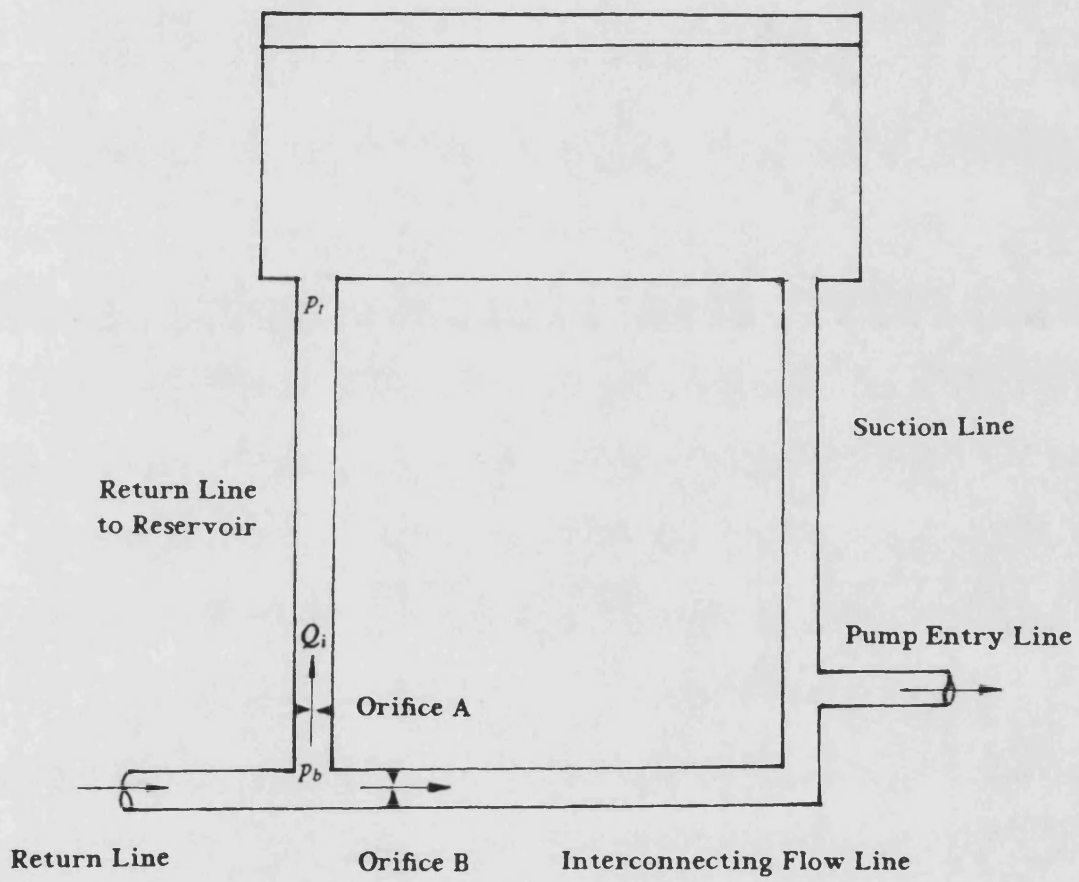
Fig. 4.5   Vertical Pipes of the Flow Lines to and from Reservoir
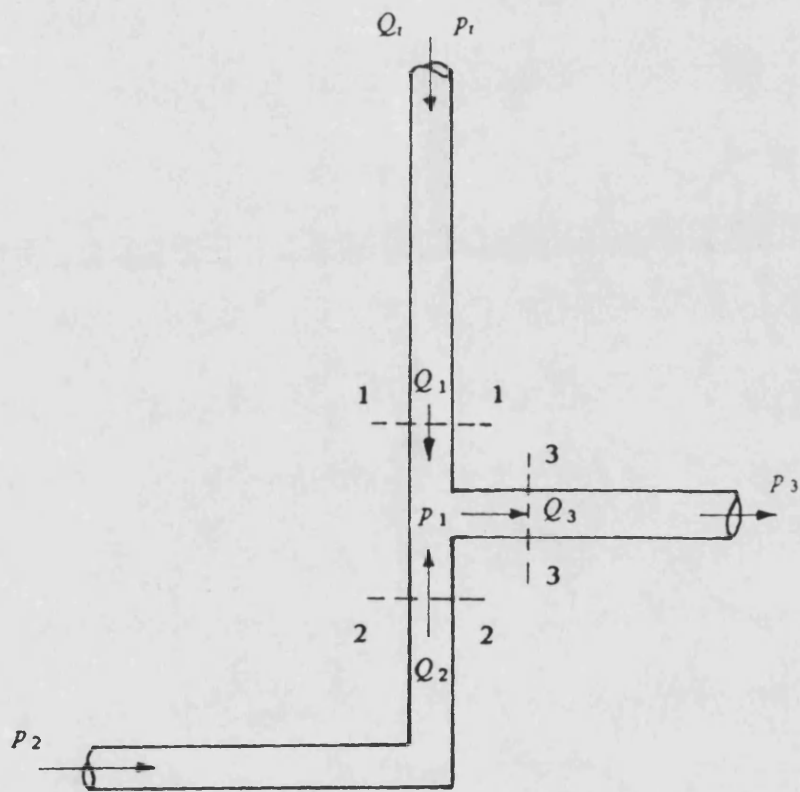
Fig. 4.6   A Suction Pipe Y-Junction
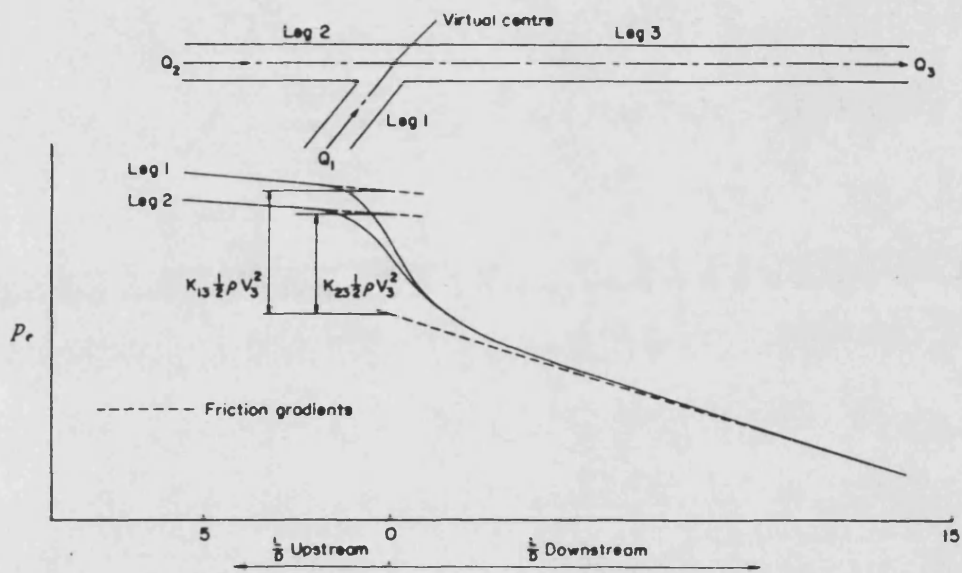
Fig. 4.7   The Variation of Total Pressure in the Vicinity of a Junction
            Taken from Sketch (i) of Ref. (4.1)
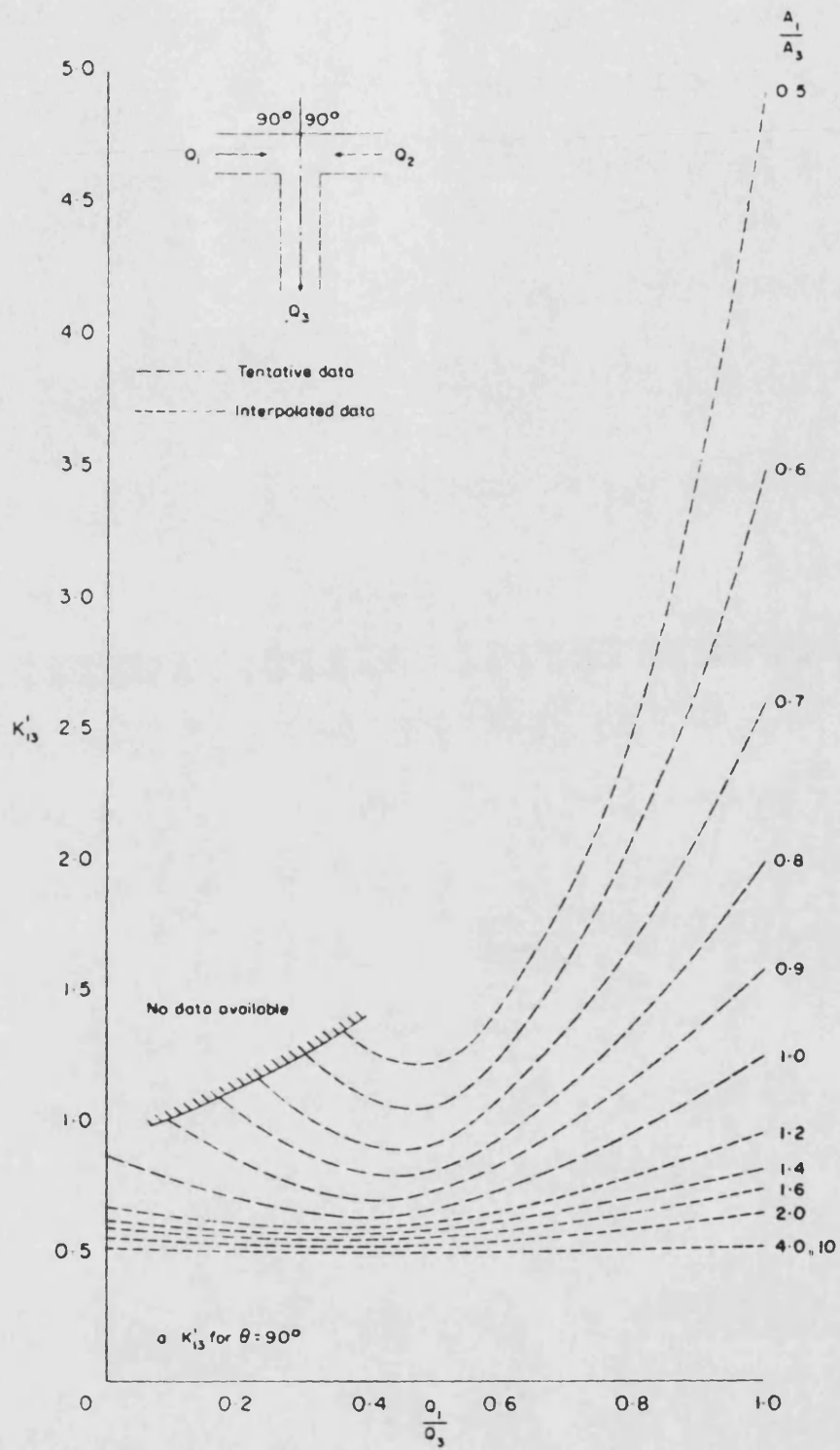
Fig. 4.8 K_{13} for Combining Y-Junctions with Sharp Corners
             Taken from Fig. 1 of Ref. (4.1)
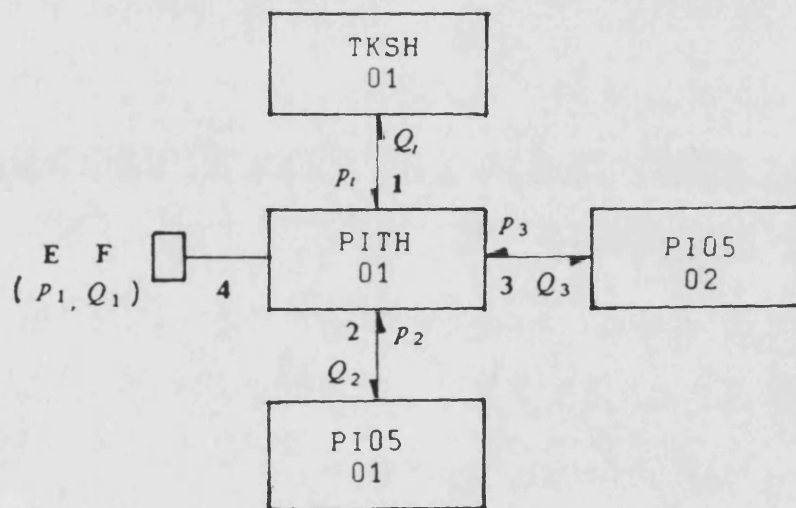
Fig. 4.9   The Linking for Junction Pipe Model
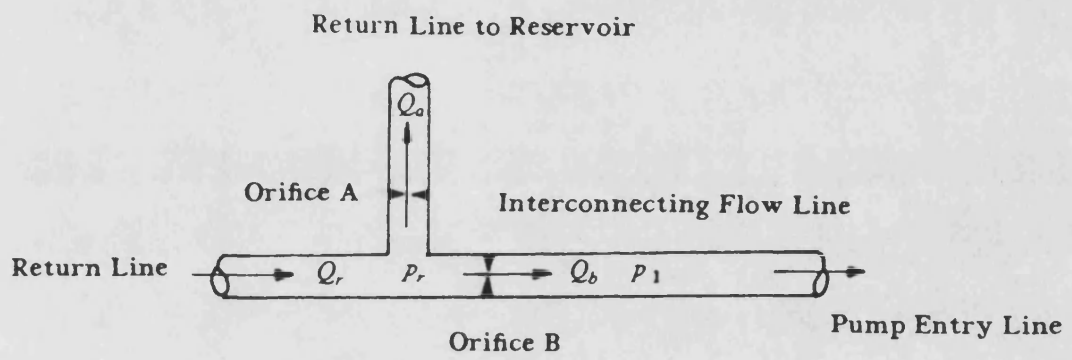
Fig. 4.10   Flow Line Connections in the Return Line
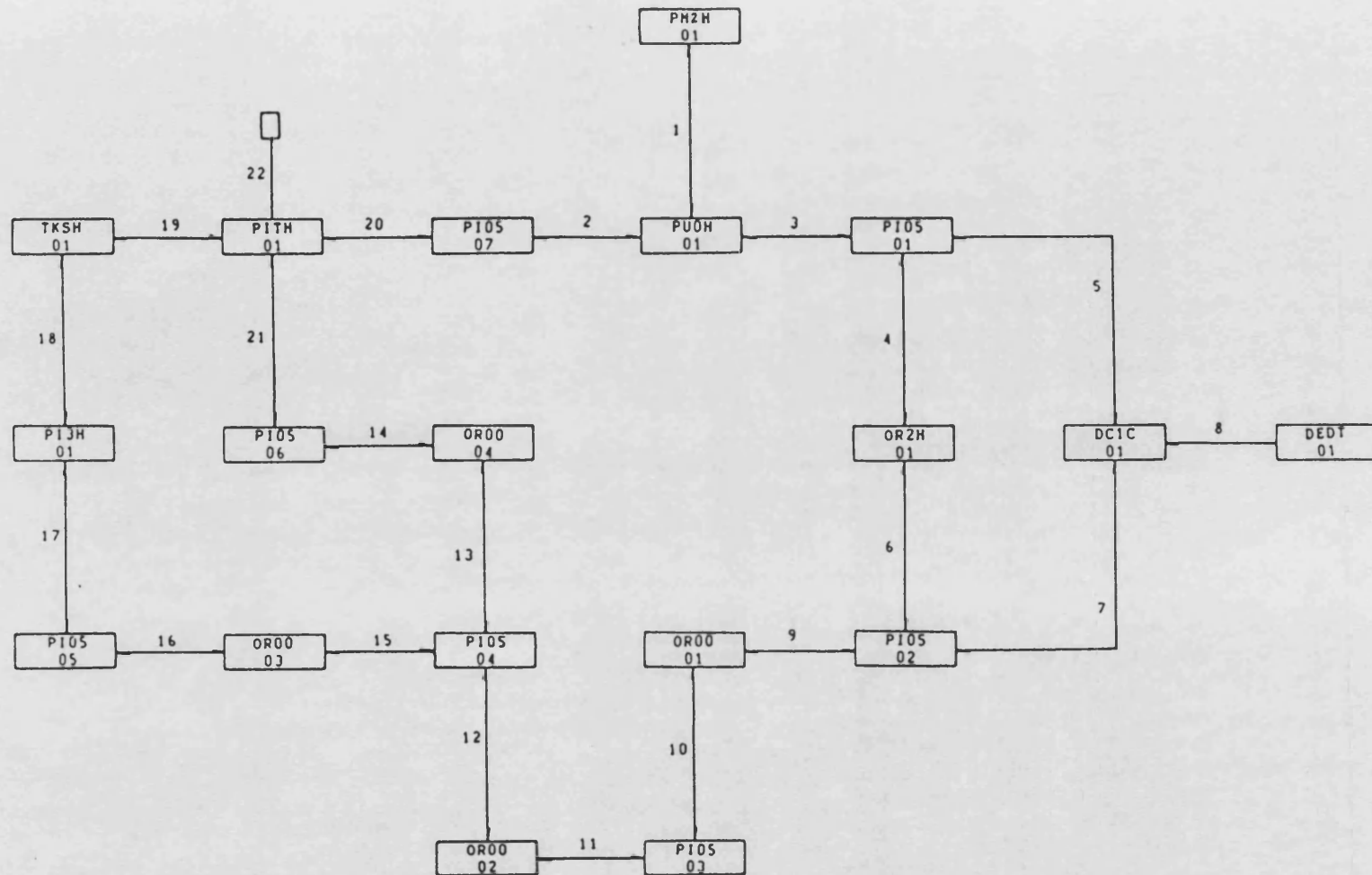
Fig. 4.11   Block Diagram for the Simulation of the Partially Closed
Hydraulic System
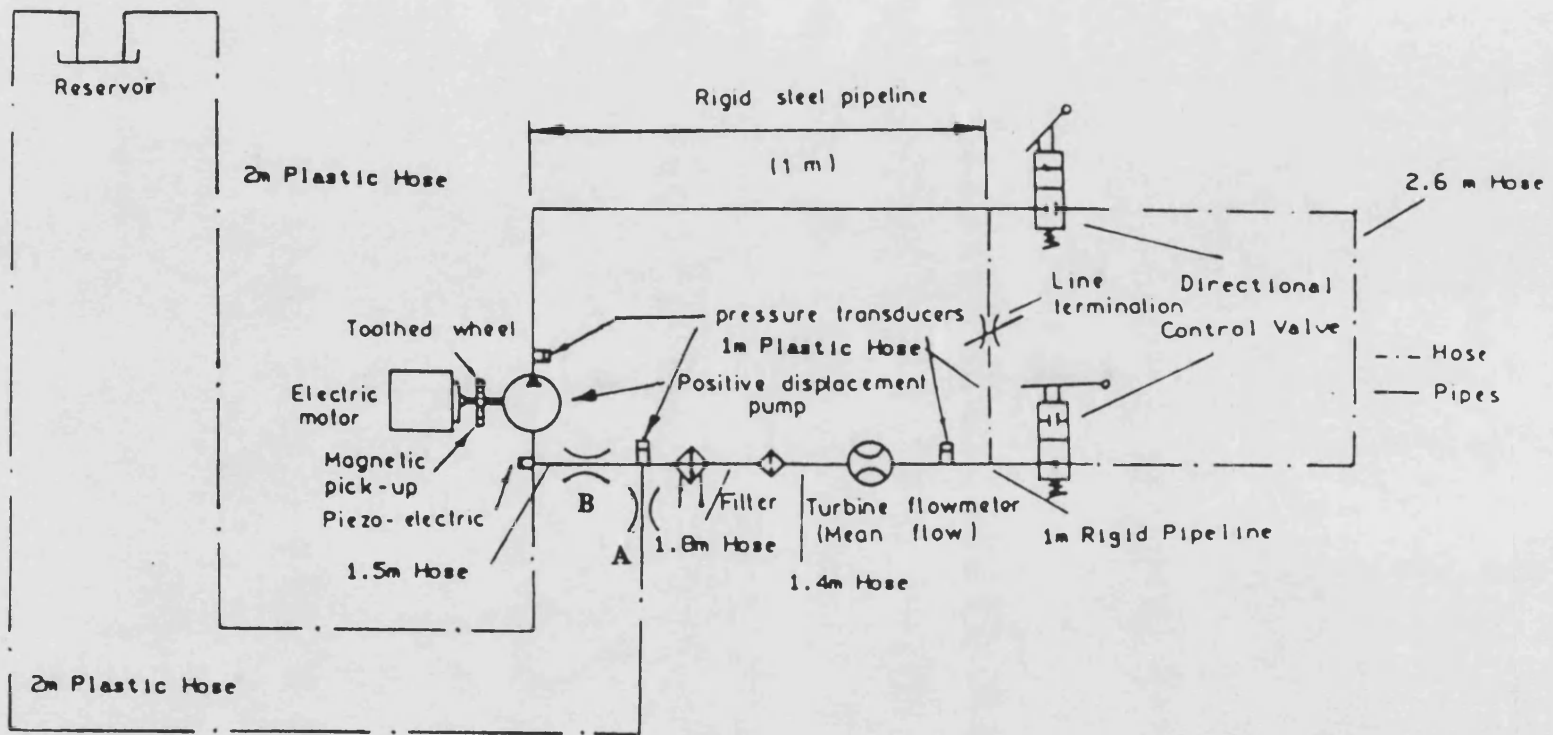
Fig. 4.12   A Partially Closed Hydraulic System Test Rig
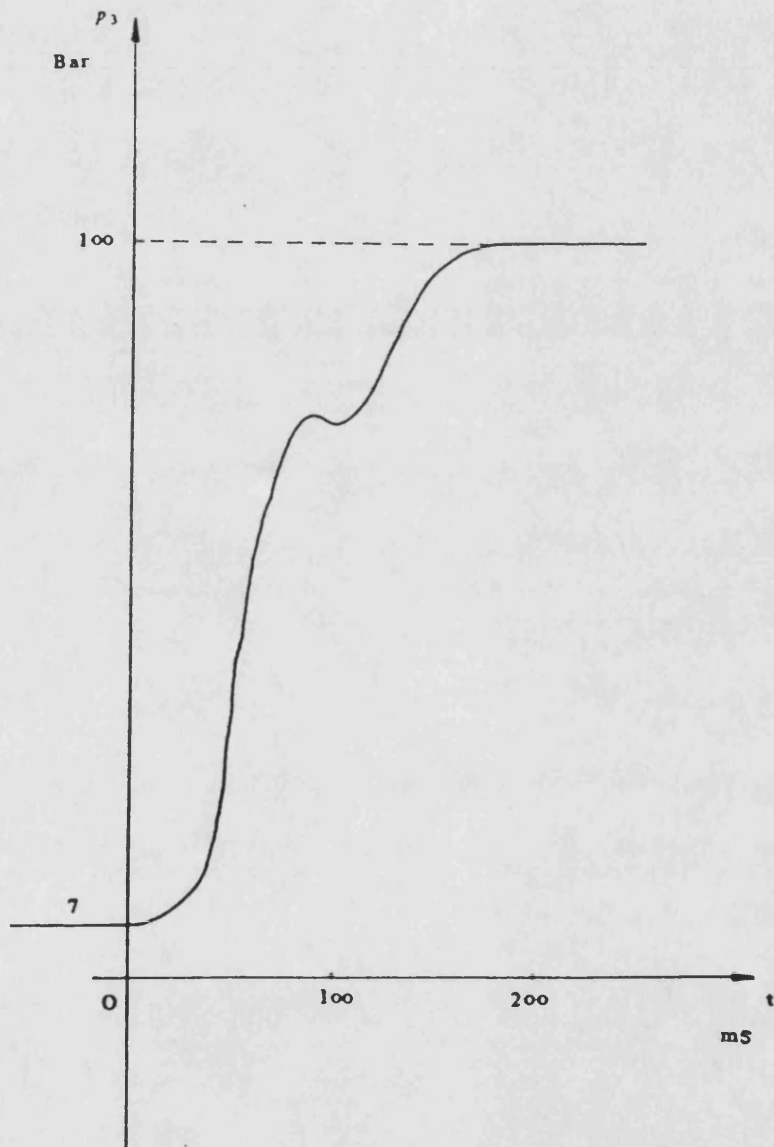
Fig. 4.13   Experimental High Pressure Transient in the Partially
             Closed Hydraulic System Test Rig
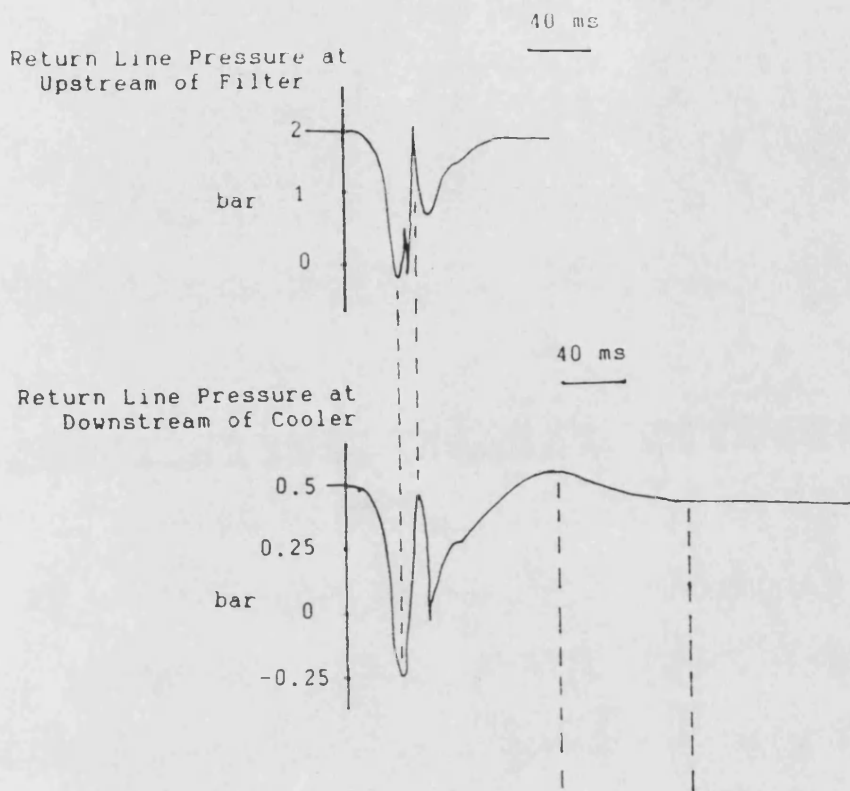
Fig. 4.14 Experimental Return Line Pressure Transient in the Partially Closed Hydraulic System Test Rig
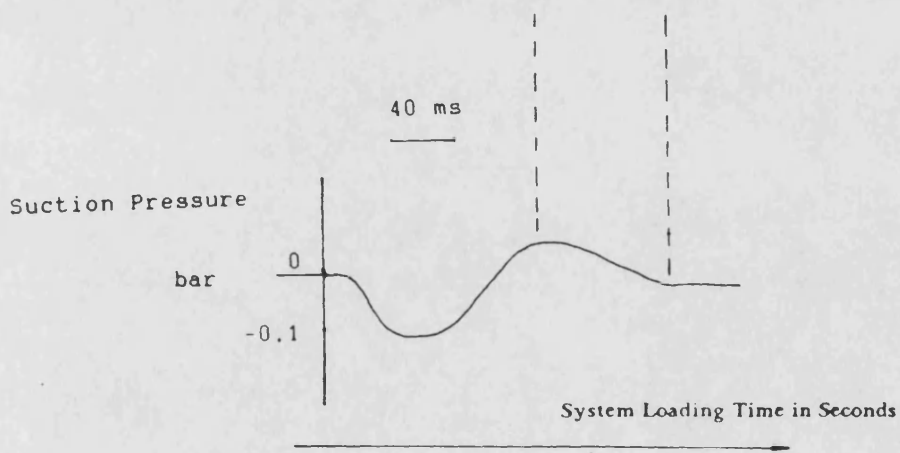
Fig. 4.15 Experimental Suction Pressure Transient in the Partially Closed Hydraulic System Test Rig
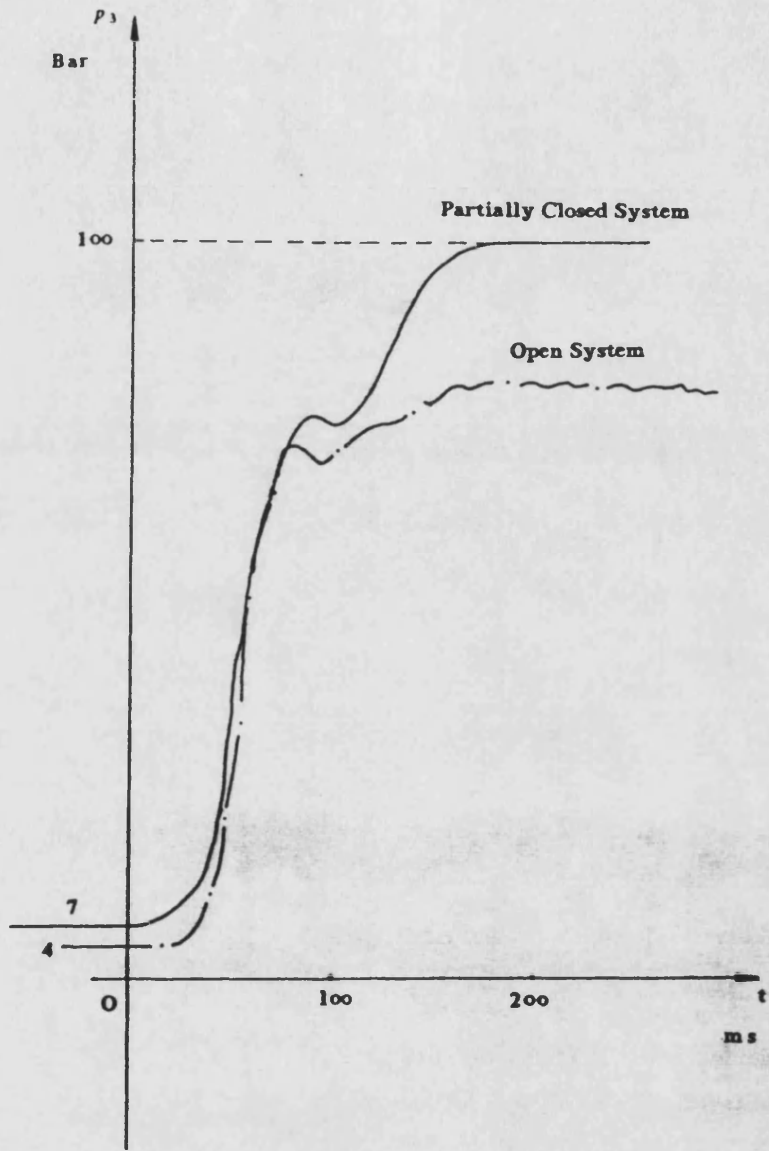
Fig. 4.16   Comparison of High Pressure Transient in the Open Hydraulic
System with That of the Partially Closed System
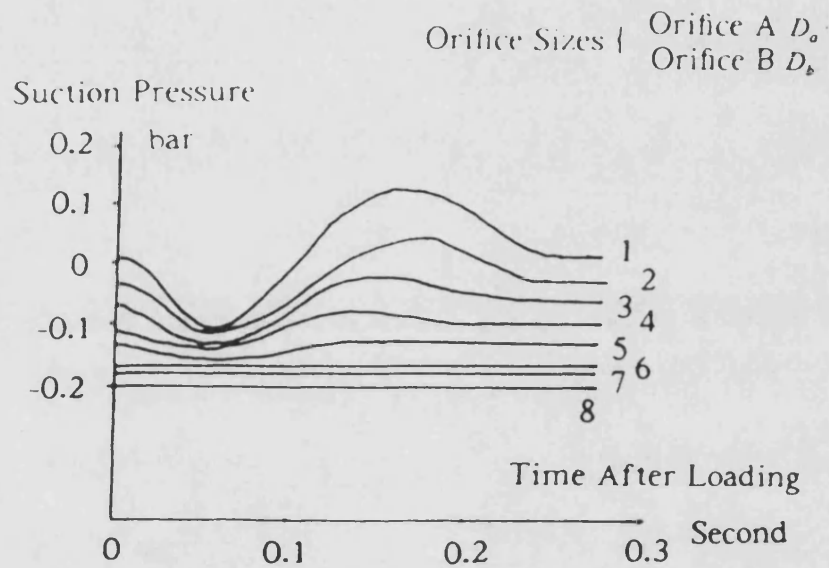
Orifice Sizes { Orifice A D_a
                Orifice B D_b

Suction Pressure

1 { D_a = 0   mm
    D_b = 25.4 mm

2 { D_a = 5.54 mm
    D_b = 11   mm

3 { D_a = 7.8 mm
    D_b = 11.6 mm

4 { D_a = 14.2 mm
    D_b = 11.6 mm

5 { D_a = 11.6 mm
    D_b = 10.6 mm

6 { D_a = 10.6 mm
    D_b = 7.8 mm

7 { D_a = 12.6 mm
    D_b = 7.8 mm

8 { D_a = 25.4 mm
    D_b = 0   mm

**Fig. 4.17   The Effects of the Sizes of Orifice A and B on the Experimental
Suction Pressure Transient**

c. Transient Flowrate to Reservoir

a. Transient Return Line Flowrate

b. Return Line Pressure Transient

d. Transient Flowrate Through Orifice B
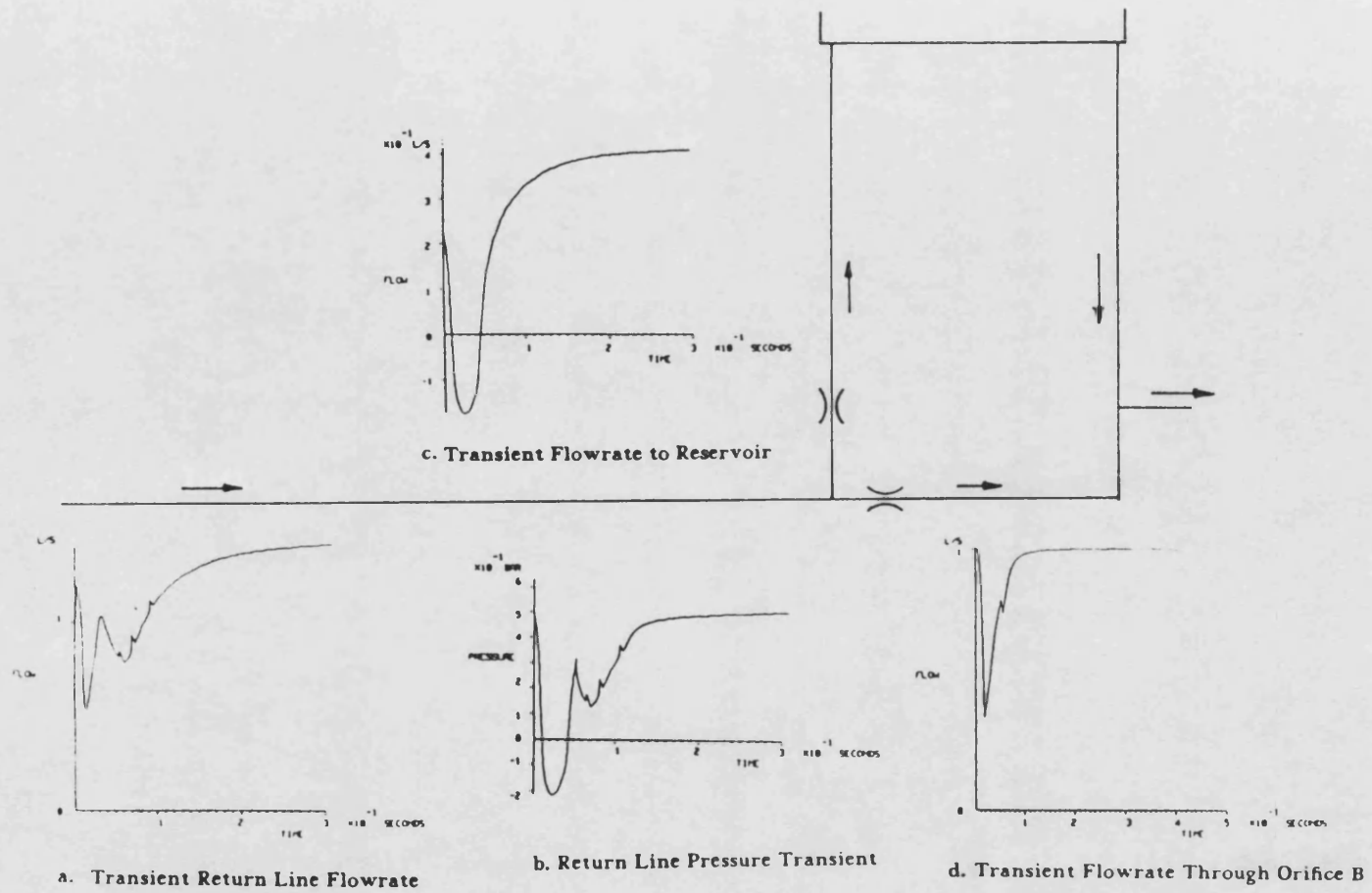
Fig. 4.18   A Typical Set of the System Transient Simulation Results
in the Return Line When the Pump is Loaded
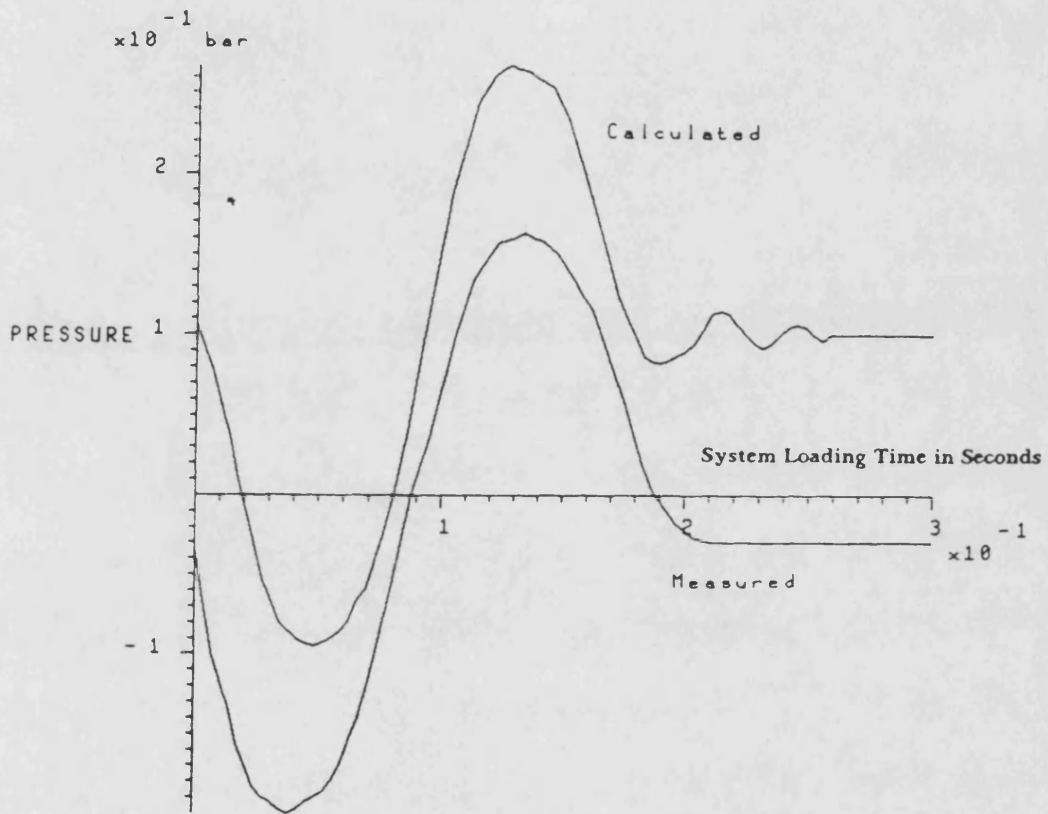
Fig. 4.19   Comparison of Simulation and Experimental Suction Pressure
                 Transients Without Consideration of Pipe Junction Effects
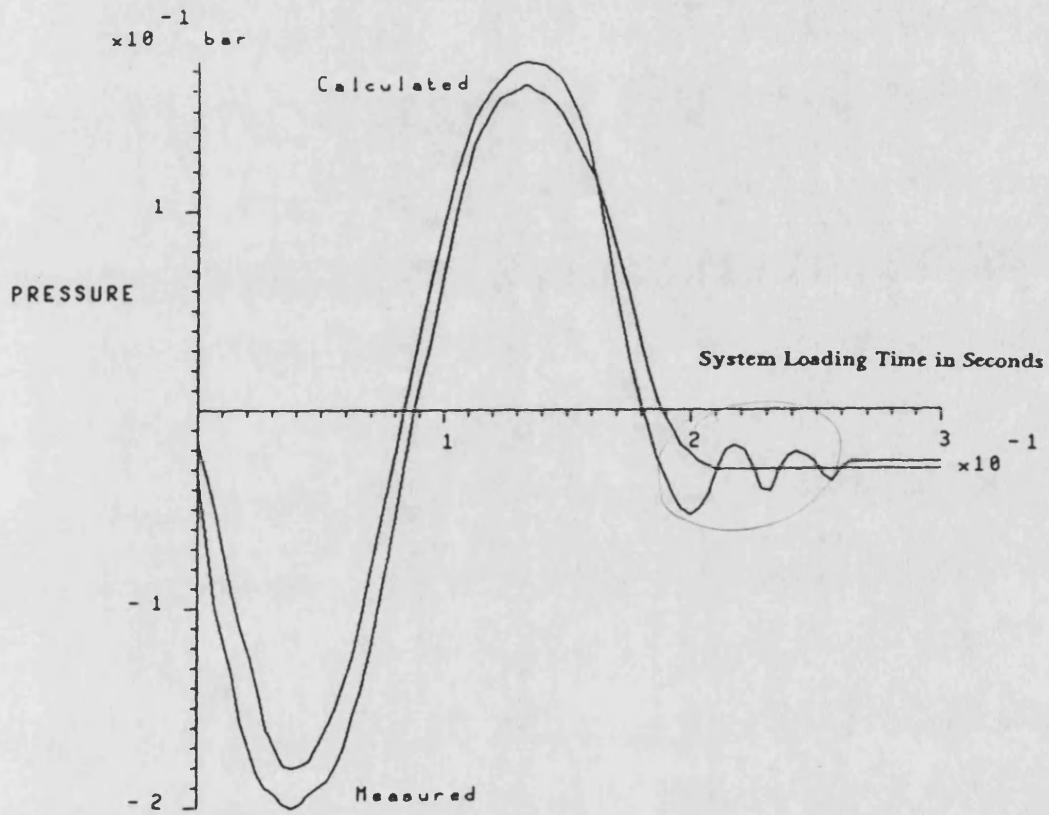
Fig. 4.20   Comparison of Simulation and Experimental Suction Pressure
Transients With   Consideration of Pipe Junction Effects
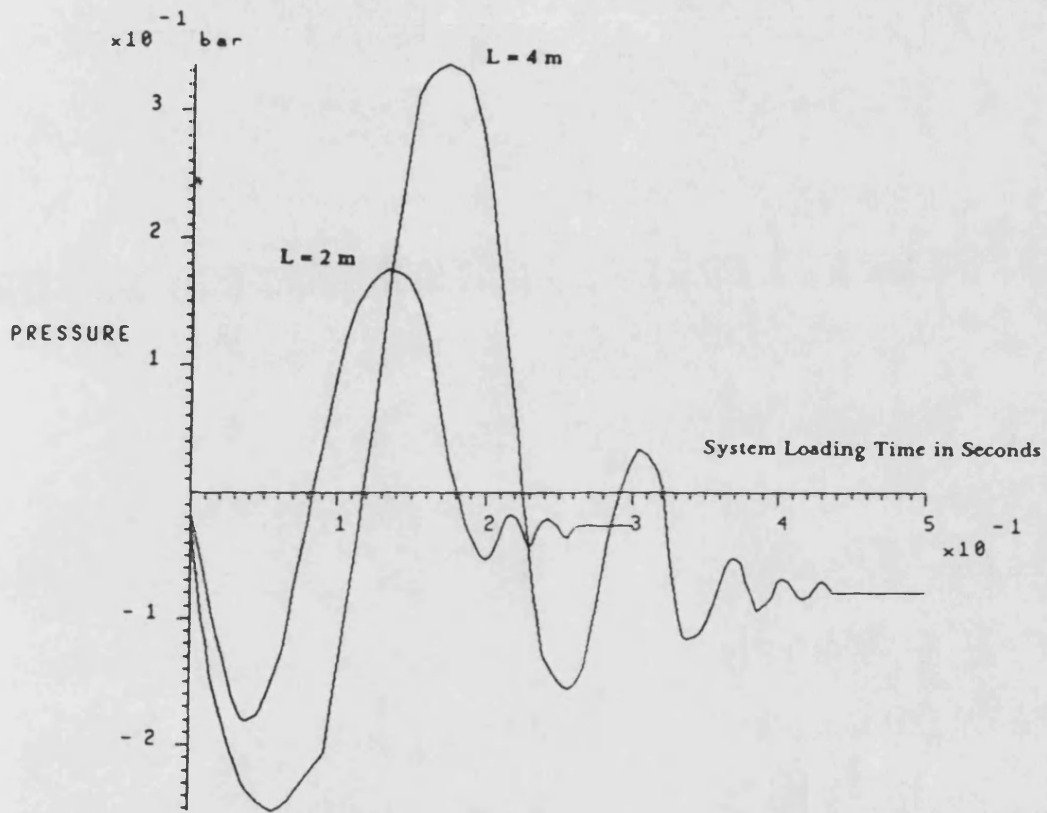
Fig. 4.21   The Effects of the Length of the Flow Line from Reservoir on
              Suction Pressure Transient

CHAPTER 5

A PARTIALLY CLOSED HYDROSTATIC DRIVE BOAT PROPELLER SYSTEM

Introduction

5.1   A Suggested Circuit Design Application   The fundamental features of the suggested unboosted and partially closed circuit designs for fluid power systems have been investigated in Chapter 3 and 4. Extensive test work and theoretical analysis of the systems proposed have been carried out and also the feasibility and advantages of the systems have been reported. A practical application will now be investigated.

5.2   Design Features of Hydrostatic Drive Boat Propeller System   For the drive of propellers in ships and barges, it is normal to find a mechanical drive shaft between the engine and the propeller with a gear box if necessary. In boats, one of the problems is the power transfer from an engine, fitted with vibration isolating mounts to a fixed propeller. Another problem is the sitting of an engine, in line, with the propeller, in a place which might otherwise be used for passenger accommodation. This offers an opening for hydrostatic drive system as shown in Fig. 5.1. The boat is driven by an engine which supplies power to a hydraulic pump. The pump is connected through the piping system to a hydraulic motor, directly coupled to the boat driving propeller.

In this type of hydraulic drive, the varying thrust required from the propeller can be achieved by changing the speed of the engine. A further advantage of this type of the system design arises from the possibility that some other hydraulic devices may be mounted on aboard by sharing the same engine. For

instance, small hydraulic winches may be useful, and such a hydraulic winch mounted in a trailer may reduce the work of landing a boat and pulling it into the water.

5.3   Advantages of the Application of the Partially Closed Circuit Design

Under this special working environment, the demands to reduce the size of the hydraulic transmission system are very critical. This is an ideal place to apply the partially closed hydraulic circuit design. With the suggested system design incorporated in the hydrostatic drive propeller system as shown in Fig. 5.2, the size of the reservoir can be reduced considerably compared with the conventional open hydraulic circuit and the suction pipe size can be also reduced. In addition, the system cost can be reduced with comparison to the closed hydraulic circuit due to the removal of its boost pump. The filter, if necessary, could be placed in the return line to reservoir for which a smaller size of filter can be chosen, thus further reduction in the system cost is resulted. Since the decision whether a cooler is needed in such a system is particular of importance, an intensive investigation of the system temperature changes during the operation will be given in the next chapter .

5.4   In this chapter, the system performance has been theoretically predicted and examined. The theoretical work is supported by an experimental programme in which tests on the transient and steady state pressures are reported. The computer software HASP has been used for the theoretical study and some component models have been developed as a result.

5.5   In order to examine the system performance, it is necessary to consider the steady state and dynamic characteristics of each of the component involved. The system shown in Fig. 5.2 consists of a pump, pipelines, a directional control valve, a relief valve, a motor and a propeller. Mathematical models were available in HASP to simulate the majority above components, but some models like the engine and the propeller are necessary to be developed.

5.6   A _Simplified Engine Model_   A variety of engine models have been developed over years by Bowns (Ref. 5.1), Hargreaves (Ref. 5.2) and Huckvale (Ref. 5.3). These models deal with complex engines and give a whole range of details of the engine dynamic and steady state performance. These models generally require a large number of inputs, which include throttle position, atmospheric conditions, fuel quality and load speed. Since only a simple single cylinder 4 stroke spark-ignited petrol engine is used on the test rig, the detailed mechanical and thermodynamic characteristics of engine models are outside the scope of this thesis. The attention in this chapter has been drawn to develop a simplified engine model which determines the dynamic acceleration of engine speed as a function of the torque condition and the effective engine inertia. Such a model has been set up in HASP on the basis of work given in Ref. (5.3).

The following assumptions have been made in constructing the engine model:

1). all rotary components coupled to the engine and pump may be
     lumped into an effective inertia:

2). the output torque from the engine can be represented by a
     D.C. level, ie. torque ripple effects are ignored:

3). thermal effects are neglected:

4). all the dynamic characteristics of the engine internal components
     such as fuel injection system and turbocharger are unimportant

compared with the overall engine characteristics, so the engine will meet all changes in load conditions instantaneously.

These assumptions are only applied in dynamic modelling of the engine performance. This means that under both dynamic and steady state conditions, the torque produced by a governed engine T_e will only be a function of the difference between the governor set speed ω_g and the actual engine working speed ω, which means

$$T_e = F(\omega_g - \omega) \qquad \ldots\ldots (5.1)$$

A constant speed/torque gradient coefficient may be introduced and defined as C_e, which gives the relation

$$T_e = \frac{\omega_g - \omega}{C_e} \qquad \ldots\ldots (5.2)$$

For the above equation to be general, C_e must not change over the operating range of the engine. This is to assume that the fuel metering valve, which has linear flow-displacement characteristics independent of cylinder pressure and the torque produced, is proportional to the amount of fuel introduced per stroke. The above equation indicates that an unlimited amount of torque can be produced, so the boundary restriction must be introduced to validate the equation working range. In practice, the restriction placed on the engine is generally defined by the maximum fuel torque curve and minimum brake-torque curve. The typical curves of an actual engine are shown in Fig. 5.3. The brake-torque curve is the effective loading characteristics of the driven engine. These two curves can be correlated by introducing the coefficients of two third order polynomial equations:

$$T_{max} = T_u + C_{u1}\omega + C_{u2}\omega^2 + C_{u3}\omega^3 \qquad \ldots\ldots (5.3)$$

and

$$T_{brake} = T_d + C_{d\,1}\omega + C_{d\,2}\omega^2 + C_{d\,3}\omega^3 \qquad \dots\dots(5.4)$$

where T_u is the maximum torque at zero speed, T_d the minimum braking torque at zero speed, and correspondingly $C_{u\,1,2,3}$ are the maximum torque coefficients, $C_{d\,1,2,3}$ the minimum torque coefficients. Hence, the torque calculated in Equation (5.2) passes outside one or other of the two limiting curves, the torque is set equal to the limiting value, ie.: for all ω

$$T_{brake} \leqslant T_e \leqslant T_{max} \qquad \dots\dots(5.5)$$

The engines used in boats use some form of governor to regulate the output speed so that the boat speed can be easily changed. The torque produced by the engine T_e, after overcoming internal losses at some instant in time, not only drives the hydraulic pump but also accelerates and decelerates the effective engine inertia. If the total effective engine inertia is denoted by J_e, T_h the torque required by the hydraulic pump, then the engine acceleration can be found from

$$\frac{d\omega}{dt} = \frac{T_e - T_h}{J_e} \qquad \dots\dots(5.6)$$

The equations discussed above have been used to write a HASP engine model called PM3H which is described in Appendix II.

5.7   Analysis of Propeller Characteristics   A number of methods to analyse the dynamic characteristics of a propeller have been well established in the literature of 'Fluid Mechanics'. One of common used methods is the non-dimensional analysis of propeller coefficients. An excellent presentation about this method has been given by Streeter (Ref. 5.4) and Duncan, Thom & Young (Ref. 5.5). In order to develop a HASP propeller load model, a brief summary for theoretical analysis of propeller characteristics is given as follows.

The propeller is a device for obtaining a propulsive thrust from a rotating shaft, the case being studied is that a propeller is mounted on the boat and rotates in

the fluid medium surrounding it. A screw propeller consists of a number of equal blades which are evenly distributed on a circular disk as shown in Fig. 5.4. The blades are mounted on the propeller hub which is carried out by the driving shaft. The diameter D of propeller is defined as the diameter of the propeller disk which is the circle through the tips of the blades.

In the words of Duncan, Thom & Young (Ref. 5.5):

If the propeller rotates steadily making n revolutions in unit time, while the constant speed of advance of the propeller relative to the undisturbed fluid is V and the propulsive thrust provided by the screw in the direction of motion may be denoted by F and T the torque required to maintain the rotation of the screw, then the useful work done in unit time is FV while the energy supplied is $2\pi nT$. Consequently the efficiency of the propeller is

$$\eta = \frac{FV}{2\pi nT} \qquad \qquad \ldots \ldots (5.7)$$

where all the quantities are measured in consistent units.

When the propeller screw is engaged with a fixed 'nut' of corresponding form it will advance a distance equal to the pitch P_i in each revolution and the rate of advance would be

$$V' = nP_i \qquad \qquad \ldots \ldots (5.8)$$

The excess of V' over V is called the slip and the ratio of the slip to V' is called slip ratio s. Then the slip ratio can be given from

$$s = \frac{(V' - V)}{V} = 1 - \frac{V}{nP_i} \qquad \qquad \ldots \ldots (5.9)$$

and this is often quoted as a percentage. The pitch P_i of the propeller is that of the driving faces of the blades and the pitch-diameter ratio is

$$\phi = \frac{P_i}{D} \qquad\qquad \ldots\ldots(5.10)$$

From the above equation, we have

$$s = 1 - \frac{J}{\phi} \qquad\qquad \ldots\ldots(5.11)$$

where

$$J = \frac{V}{nD} \qquad\qquad \ldots\ldots(5.12)$$

and is called the advance ratio. It is noted that s and J are non-dimensional quantities. For similar screw propellers ϕ is constant and Equation (5.11) shows that the slip ratio s is then determined by J alone.

If J is constant, from the above equation $nD = \frac{V}{J}$, the corresponding velocities will be proportional to V, then the corresponding pressures will be proportional to V while corresponding force will be proportional to $\rho V^2 D^2$. In particular, the thrust F will be proportional to $\rho V^2 D^2$ and the non-dimensional thrust coefficient accordingly is

$$F_c = \frac{F}{\rho V^2 D^2} \qquad\qquad \ldots\ldots(5.13)$$

But $V = JnD$ so the above equation produces

$$J^2 F_c = \frac{F}{\rho n^2 D^4} = C_f = K_f \qquad\qquad \ldots\ldots(5.14)$$

which is another non-dimensional thrust coefficient. When all the conditions for similarity are satisfied, the corresponding moments will be proportional to $\rho V^2 D^3$. Hence the non-dimensional torque coefficient can be derived from

$$T_c = \frac{T}{\rho V^2 D^3} \qquad \ldots \ldots (5.15)$$

while

$$J^2 T_c = \frac{T}{\rho n^2 D^5} = C_t = K_t \qquad \ldots \ldots (5.16)$$

is also non-dimensional.

As an alternative to these torque coefficients the power coefficient may be adopted as

$$C_p = \frac{P}{\rho n^3 D^5} \qquad \ldots \ldots (5.17)$$

where P is the power absorbed. Since

$$P = 2\pi n T \qquad \ldots \ldots (5.18)$$

it follows from Equation (5.16) and (5.17) that

$$C_p = 2\pi K_t \qquad \ldots \ldots (5.19)$$

Also the efficiency of the screw is

$$\eta = \frac{FV}{P} = \frac{\rho n^2 D^4 C_f V}{\rho n^3 D^5 C_p} = \frac{C_f}{C_p}(\frac{V}{nD}) = \frac{J C_f}{C_p} = \frac{J}{2\pi}(\frac{K_f}{K_t}) \ldots \ldots (5.20)$$

Thus the efficiency can be calculated at once when the values of C_f and C_p corresponding to the selected value of the advance ratio J are known.

Some non-dimensional characteristics taken from Ref. (5.4) are plotted in Fig. 5.5 and are computed from the actual characteristics of a marine propeller with 9 ft diameter, four blades, pitch ratio = 0.9. It is noted that the propeller efficiency rises gradually with J until the maximum is reached and thereafter falls rather rapidly.

5.8   A Propeller Load Model   When a propeller has been designed and selected to work on a boat, the load conditions of the propeller can be analysed by using non-dimensional propeller coefficients analysis. For example, in the partially closed hydrostatic drive propeller system being investigated, the propeller is driven by the hydraulic motor. The torque provided by the hydraulic motor is the torque which not only drives the propeller load but also accelerates or decelerates the inertia consisted of propeller, motor, shaft and gear box. Thus the motor speed acceleration is given by

$$\frac{d\omega_m}{dt} = \frac{T_m - \dfrac{T_p}{R_e}}{J} \qquad\qquad \dots\dots (5.21)$$

where R_e is the ratio of the gearbox, T_m the hydraulic torque provided by the motor, J the combined effective inertia of the propeller and motor, and the propeller load torque T_p can be calculated from Equation (5.16) as

$$T_p = K_t \rho \frac{\omega_p^2}{4\pi^2} D^5 \qquad\qquad \dots\dots (5.22)$$

where the propeller speed $\omega_p = 2\pi n_p$ is noted. The angular speed of the propeller can be found as $\omega_p = \dfrac{\omega_m}{R_e}$. As shown in the propeller coefficients analysis, the non-dimensional torque coefficient K_t is a function of the advance rate $J = \dfrac{V}{ND}$. It depends also on the design of propeller and the interaction of the propeller hull.

A HASP propeller load model LROH has been set up, using the above two equations and standard propeller curves (like those in Fig. 5.5) obtained from the literature. When this model is applied to a particular system simulation, however,

- 78 -

coefficient values have to be supplied by the user because of the particular propeller shape. For instance, when the model LR0H is used in the simulation for the partially closed hydrostatic drive propeller system, the torque coefficient K_t has to be amended because of the fact that in the test rig the propeller is not attached to a boat and hence the propeller does not make any advance movement. The adjustment can be made by measuring the hydraulic torque applied to the motor at one particular operating condition, allowing for motor and gearbox friction and then adjusting the coefficient K_t on a proportional basis. The details of LR0H is given in Appendix II.

5.9   In order to justify the proposal of the partially closed hydrostatic drive boat
propeller system, an extensive test programme was undertaken to investigate
experimentally the suggested system performances. A test rig of the partially
closed hydrostatic drive boat propeller system was designed and constructed in the
Laboratory of the Fluid Power Centre in University of Bath to meet the
requirements of the test programme.

5.10   Selection of Main Test Rig Components   Fig. 5.2 shows the main
components required for a partially closed hydrostatic drive boat propeller system.
These are an energy supply engine, a hydraulic pump, pipelines, a hydraulic
directional control valve, a relief valve, a small hydraulic reservoir, a hydraulic
motor coupled with a marine propeller through a gear box with the ratio of 3.5:1.

The selection of a gear pump without external drain, which has a fixed
displacement of 5 cm^3/rev, was made to provide an unit most suitable for test work
rather than for any particular boat hydraulic system application. A gear motor
with an external drain was selected to demonstrate the partially closed circuit
design is capable of coping with oil circulation in the system due to component
external flow leakage. The main criterion for the choice of the pump or the motor
was that they should be capable of easy mounting and mechanically as simple as
possible. The choice was finally made of an Oleodinamica Ozzano GMM external
gear pump and a motor with displacement of 5 cm^3/rev. The pump was to be
driven in line by a Clinton petrol engine with maximum power supply of 1 kw.

The choice of a four way three position at tandem central position of the
direction control valve was made to allow the reverse of the propeller movement
and to unload the pump at the valve central position. All the pipes in the system
were chosen as flexible hydraulic hoses to allow the flexibility of arranging
installations for the hydraulic transmission system components, and also to mount
the propeller and the engine at the convenient operating positions. The minimum
diameter of the system hydraulic hoses was chosen as 9.53 mm ($\frac{3}{8}$ inch) internal

bore in the system return line to limit a maximum fluid speed below 3.5 m/sec when the pump was driven at nominal speed of 2300 rev/min under the unloading conditions. A single stage relief valve was selected to limit the maximum system pressure and so this relief valve acts as a safety valve. The diameter of a marine propeller was chosen as 230 mm to load the hydraulic motor.

5.11   Test Rig Hydraulic Circuit Structure   It is essential that the boat hydraulic transmission driven propeller system should have as small as possible for the requirements of the power supply and also the installation space. This offers a chance to apply the partially closed hydrostatic drive boat propeller system. With incorporating the partially closed circuit design as shown in Fig. 5.2, the choice was made to use a small hydraulic reservoir with size of 19 cm X 25 cm X 25 cm (wide X length X high), which has capacity of 12 litres but only filled with 5 litres mineral oil. As a comparison, under the same condition, if the engine is driven at a nominal speed of 2000 rpm, the reservoir size in a conventional open system is normally chosen as 5 or 6 times of the system flowrate. This means that a 50 or 60 litres reservoir has to be used in an open system. Two adjustable orifice restrictors were placed in the system return line at the position A, B as illustrated to control the proportion of flow going back to reservoir. With this arrangement in the return line, the release of air bubbles in the oil and the limit of fluid temperature can be carried out. Moreover, by the control of the opening areas of these two orifices, the test rig can be used to compare the performances of open loop with those of the two suggested unboosted and partially closed hydraulic systems.

5.12   Test Rig Layout   The test rig of the partially closed hydrostatic drive boat propeller system is diagrammatically shown in Fig. 5.6.

In the test rig, one 1 kw Clinton single cylinder four stroke spark-ignition engine is placed on the floor and coupled together with the chosen gear pump without external drain. The pump outlet flange with a 9 inch long half inch bore mild steel pipe is connected by a 1 m long half inch of diameter single wired hydraulic hose to the pressure port of a 4 way 3 position at tandem centre position of the directional control valve, which is placed on the top of the hydraulic reservoir at the height of 1.1 m for the convenient position of operation. The A port

of the directional control valve is connected to the one side of hydraulic motor by a 1.15 m long half inch of diameter single wired hydraulic hose, while B port of the valve is linked with the other side of the hydraulic motor by a 1.9 m long half inch of diameter single wired hydraulic hose.

The hydraulic motor is fixed on a steel frame 30 centmeters above a water pool and 1.5 m away from the place of the reservoir. The actual position of each system component, such as the engine, the reservoir, the directional control valve and the motor, can be located according to the requirement of the space arrangement in a practical hydrostatic drive boat propeller system. This feature of flexible sitting of each system component can be advantageous for some applications like on fishing boats where the sitting of components are of particular importance. The propeller is connected to the hydraulic motor by a shaft and placed in a pool under 0.5 m deep water to provide a load condition similar to a boat. The location of the propeller in the pool illustrated by a sketch in Fig. 5.8.

The T port (to the return line) of the directional control valve is connected with a 2.9 m long single wired hydraulic hose with 9.53 mm ($\frac{3}{8}$ inch) diameter size. This return line hose is joined with a rigid pipe network. The pipe network together with two orifice restrictors forms the return line to reservoir and the suction and pump entry lines as shown in Fig. 5.9. The return line to reservoir is a 1.2 m long single wired flexible hydraulic hose (half inch in diameter). The suction line is a 0.5 m long half inch of diameter single wired hydraulic hose which is connected down to a suction pipe junction at position shown. The small diameter size of the suction line is noticed. In the same condition, in order to restrict the suction fluid velocity within 0.5 m/s to avoid the occurrence of air release, the pipe diameter size must be at least one inch in an open system. A detail listing of technical data for the test rig is given in Table 5.1.

5.13 **Instrumentation and Measuring Equipment**   To measure the dynamic pressure changes in the system pipelines, it was necessary to equip the test rig with electrical pressure transducers. Hence, the pressures at the various parts of the system were monitored by five   transducers mounted at the positions shown in Fig. 5.6. These transducers were driven by a carrier amplifier integral with a demodulator unit. The acquisition of digital response data for the pressure

signals were recorded using galvanometers recording on ultra-violet paper.

In addition to the electronic instrumentation for dynamic measurements, the steady state pressure values were measured by three in line pressure gauges. The shaft speeds of the of pump and motor were measured using a high quality non-contacting digital hand tachometer with LED display. The flowrate in the system was monitored by a displacement flow meter incorporated in the return line of the system.

5.14 **Experimental Test Procedure**   The engine was started in an unloaded condition with the direction control valve at the tandem central position. Then the position of the direction control valve was selected to load the hydraulic motor. The hydraulic system was run for one minute under load for transient tests and for two hours for steady state tests. Subsequently, the motor was unloaded by operating the direction control valve, then run for one more minute, and finally the engine was cut off by setting its governor to the stop position.

5.15 **Analysis of the Experimental Results**   A partially closed hydrostatic driven boat propeller system can be obtained by setting the opening size of the orifice A and B in Fig. 5.2 to allow approximate 10 percent of the return line flowrate return to the reservoir. Following closely the above test procedure, a large number of tests were taken to investigate experimentally the system transient pressure performance. The recordings of the high and suction pressure transients occurring in the system in the transient tests are analysed as follows. The detailed analysis of the high pressure transient will be given in the later simulation results discussion.

In the transient test for this system, when the working position of the directional control valve is rapidly selected to supply flow to the hydraulic motor, the pump delivery pressure rises to drive the propeller load as shown in the recording of transient pressure in Fig. 5.10. A noticeable dynamic feature of the system is the high pressure transient overshot. In the result shown, the pump delivery pressure from the unloading condition of 5 bar increases to the peak value

- 83 -

of 25 bar at 30 ms after loading and then decreases from 25 bar to 22 bar between 30 ms to 50 ms, next the high pressure gradually reduces between 50 ms to 300 ms (0.3 second) from 22 bar toward the stationary value of 21 bar. This high pressure transient is affected by many factors which include fluid compressibility, the operating speed of the directional control valve, the relief valve setting pressure and the dynamic speed of the propeller. It is considerably difficult just from the examination of test results to analyse the effects of each individual factor on the pressure transient. In addition, some of factors like operating speed of the directional control valve and the relief valve setting pressure are difficult to be determined experimentally. The computer simulation studies have been carried out to make the analysis feasible as given in Section 5.28.

This rapid rise in the pump delivery pressure produced a similar increase in applied shaft torque of engine/pump. The engine responses to this torque increase by a droop in the shaft speed from 2300 rev/min under unloaded condition to an average value of 1880 rev/min. Meanwhile, the average shaft speed of the motor was 1740 rev/min. The difference in the speeds of the pump and motor under the load can be used to calculate the external leakage flow of the motor in the system. In the next 10 minutes of the system loading, the pressure fell to 21 bar and then remained constant during the remainder of the 2 hours test as shown in Fig. 5.11. This small fall off in pressure was due to the reduction of friction loss in the hydraulic motor as the oil heated up and also the reduction in friction in the right angled gear box in the drive to the propeller. In the same period, the engine speed gradually recovered to 1900 rev/min as dictated by the governor characteristics, and consequently the motor-speed increased to 1750 rev/min. The rise in engine speed affects the fall in pressure so that eventually equilibrium conditions are achieved.

At the instant of the system loading by a fast operation of the directional control valve, fluid is compressed in the high pressure line, so a transient reduction in the return line flowrate is resulted. A small proportion of the transient reduction in the return flow goes into the reservoir and is absorbed by the reservoir large volume of the flow. The remainder of the transient reduction in the return flow passes through orifice B to the suction pipe junction. Consequently, the pump takes more flow from the reservoir to compensate for this transient flow reduction, thus transient acceleration of flow in the suction line occurs. This fluid acceleration generates a transient time delay to compensate the transient reduction of the

flowrate in the interconnecting flow line. Hence a transient reduction in the inlet flowrate of the pump entry line is produced at the initial stage of the system loading. Meanwhile, at the instant of the system loading, a transient reduction in the outlet flowrate of the pump entry line is caused by the engine speed droop due to the load increase. But a difference exits between the transient variations of the inlet and outlet flowrates of the pump entry line. Thus, a transient reduction is generated in the suction pressure at the pipe junction as one specific case shown in the experimental measurement in Fig. 5.12.

As can be seen, the suction pressure from initial value of 0.05 bar fell below atmospheric pressure between 23.2 ms to 94.7 ms (the minimum value was - 0.122 bar of gauge pressure at 57.4 ms), next it recovered towards the stationary value of 0.05 bar around 120 ms after loading and remained at this same value for the rest two hours of the system loading. The static suction pressure is determined by the factors which include

1) the fluid head in the vertical suction pipe and in the reservoir;

2) the dynamic pressure head in the suction line;

3) the pressure loss due to the pipe friction of the suction pipe;

4) the cross port pressure loss between the suction and pump entry lines at the pipe junction.

The pressure losses due to 3) and 4) are determined by the fluid velocity in the suction line. This fluid velocity is given by the return flowrate to reservoir through orifice A. Moreover, the transient suction pressure is affected by many factors which include

1) the transient reduction in the return line flowrate to the pump entry line;

2) the transient flowrate required by the pump;

3) the effects of fluid inertia in the vertical suction pipe.

The pressure losses across the directional control valve and the pipe friction in the high pressure line were recorded to be 2.5 bar. The transient pressure recording at the motor inlet is the essentially same but 2.5 bar lower than that of the pump outlet in Fig. 5.10. The steady state pressure loss in the return line was also found to be 2.5 bar which includes the pipe friction and the cross port pressure loss of the directional control valve. The steady state pressure at the outlet of the pump was measured to be 5 bar before the hydraulic motor was loaded.

5.16   Comparison of the Different System Performances   The test rig can be also used to examine the performance of a conventional open system design. When orifice B at position shown in Fig. 5.2 is closed with fully opening of orifice A, the system becomes a conventional open circuit hydraulic system. Since all the system flow returns directly to the reservoir, the transient reduction in the return line flow due to fluid compressibility in the high pressure line is absorbed by the large volume of the flow in the reservoir. Hence, a constant pressure value of - 0.2 bar (gauge) was recorded in the experimental suction pressure of the open system. This static suction pressure is rather lower than that of the partially closed system. This is because the suction line of the partially closed system becomes the pump entry line of the open system, so the rise of fluid velocity in the line has resulted the pressure losses caused by the pipe junction and pipe friction. Since this suction pressure is below the normal atmospheric pressure, air release occurs at the pump entry line so a large amount of air-liquid mixed flow could be observed in the reservoir. As a result, the pump delivered less flow to the high pressure line, and the shaft speed of motor decreased to 1180 rev/min. Hence, the recorded pump delivery pressure of 14 bar is lower than that of the partially closed system (21 bar at steady state). So the torque applied on the engine reduced, consequently the engine was run at the shaft speed of 1975 rev/min. Another consequence of the low suction pressure is a loud noise generated by the pump. The low suction pressure may be increased in a practical open hydraulic system if the diameter of the suction pipe and the reservoir size are significantly increased to avoid the occurrence of air release in the pump entry line.

On another case, when orifice A in Fig. 5.2 is closed with fully open of orifice B, the rig becomes an unboosted closed loop system. The high pressure transient is

essential the same to that shown in Fig. 5.10 of the partially closed system but a bigger variation is shown in the suction pressure in Fig. 5.13. This is because no flow returns to the reservoir in the unboosted closed system so all the transient reduction in the return line flowrate goes to the system suction line and hence a greater transient flowrate is required to take from the reservoir to compensate the transient flow reduction. In addition, the system difficulties in air release, heat dissipation and great likelihood of oil degradation have also been resulted. Therefore, the partially closed hydraulic circuit is the most suitable design to be applied on the hydrostatic drive boat propeller systems. As similar to the situation discussed in the above chapter, when this system design is put into a particular practical application, 10 - 15 % return line flow is recommended to return to the reservoir to obtain an optimal performance of the system.

5.17   In order to obtain full   understanding of the transient characteristics of the system experimental performance, the simulation studies for the partially closed hydrostatic drive boat propeller system have been carried out. Two lately developed engine and propeller models of PM3H and LR0H are used together with a hydraulic gear motor model MOAH, which is modified from an existing HASP pump-motor unit for the suitabliity of this special case of the system simulation and is documented in Appendix II, to construct the system simulation block diagram as shown in Fig. 5.14.

5.18   System Simulation Block Diagram   In the diagram, the engine model PM3H with the speed droop characteristics is used to simulate dynamic behaviour of the engine used on the test rig. The model PU0H is used to represent the system hydraulic gear pump without external drain line. The four way three position directional control valve can be simplified in the way illustrated in Fig. 5.15, where the valve is simulated correspondingly by two orifice restrictor models OR00 with a two way two position direction control valve model DC1C acting as a bypass valve. The model DC1C has its position changed by a duty cycle model DEDT to represent a rapid change in the operating position of the directional control valve. The model LR0H is used to simulate the dynamic hydraulic motor speed and also the propeller load putting on the motor shaft. The hydraulic motor on the test rig with an external drain line is simulated by the model MOAH. The inertia effects in the majority of pipelines in the system have been ignored and the pressure losses due to pipe friction are lumped into orifice models. So the frictionless pipe HASP model PI05 is used to simulate most of the system pipelines. The return line to reservoir is simulated by a vertical pipe model PI3H with a fixed level of fluid height so as to consider the effects of fluid inertia and pipe friction. In order to meet the demand of model linking between PI3H and OR00 as required by HASP programme generator, a   dummy pipe model of PI05 with 0.05 m length is used between these two models. The variation of the fluid level in the reservoir could be significant to affect the transient suction pressure, so the reservoir is modelled by the dynamic reservoir model TKSH. The horizontal pipelines of the interconnecting flow line and the pump entry line are simply represented by two PI05 pipe models. But the flow and pressure conditions are rather complex around the suction Y-junction. This offers a

chance to apply the vertical suction pipe and Y-junction model PITH, which has been developed in Chapter 4 to incorporate with the linear interpolation computer method for solving a group of algebraic equations together with a differential equation as a full discussion given in Appendix I. The only accepted input data of model link ordering for programme generator of HASP to define the circuit details of simulation is given in Table 5.2.

The simulation input data for each model have been determined based upon the parameters of each component on the experimental test rig. Some computer input data has been obtained and justified according to the test measurements. The details of user input data for the models used in the simulation of the system loading are given as follows.

5.19   Fluid Properties Data in the Simulation   The input data of fluid properties in the simulation is given in Table 5.3. The oil temperature of 15° C in the. table was obtained from the fact that the transient experimental results presented in Section 5.15 were obtained from the tests under the condition of 15° C fluid temperature. The computer simulations for the system transient tests have been carried out under the assumption that the change in oil temperature during the transient tests is insignificant to the test results. The data of fluid properties given in the table are the results calculated on the basis of fluid temperature and oil type by the HASP fluid property section model FLPROP. These data are very close with those which might be otherwise obtained from fluid property-temperature charts available in the literature.

5.20   Input Data for the Engine Model   The simulation data for engine model PM3H is listed in Table 5.4. The engine initial speed of 2300 rev/min has been obtained from the experimental measurements for the system tests. The engine speed/torque gradient coefficient can be estimated from the experimental measurements of two load conditions of the engine. The governor set speed was measured when the engine entirely is separated from the test rig under the unloading condition.

5.21 Input Data for the Pump and Motor Models   The simulation data for the gear pump model PUOH is given in Table 5.5. The data for calculating pump internal slip loss was obtained from the suggested values in HASP pump and motor unit motor HUJT which was developed based upon the intensive investigation carried out by McCandlish and Dorey (Ref. 3.16). The same way has been applied to determine the simulation input data for the hydraulic gear motor with drain line. The simulation data of the motor shown in Table 5.9 is essentially same to the hydraulic pump except one coefficient is added to define external slip loss coefficient.

5.22 Input Data for High Pressure Pipeline Models The simulation data for the first part of high pressure line model PI05(01) is given in Table 5.6. In practice, this part of the high pressure line consists a length of flexible hydraulic hose and two lengths of rigid pipes. The pipe internal diameter and total length has been measured from the test rig. The sum of these two rigid pipe lengths is less than 20 % of total pipelength. For simplicity, if the part of pipeline is represented just by an equivalent length of hydraulic hose, the effective fluid/pipe Bulk Modules can be calculated in the standard HASP pipe model PI05 in which four different common used pipe materials are available to be chosen to calculate the bulk modulus. The bulk modulus calculation is based upon the generally accepted assumptions that the pressure of air saturation in oil is zero and the proportion of dissolved air in normal hydraulic oil is 10 %. The details of the fluid/pipe bulk modulus calculation in PI05 is given in (Ref. 2.8).

The result of fluid/pipe effective bulk modulus given by PI05 with the measured 8.5 mm thickness of hydraulic hose is 11261 bar as shown in the table. The initial fluid pressure 5 bar in this part of the pipeline was obtained from the practical measurement. Fluid pressure loss in the part of the pipe due to pipe friction is lumped into the local pressure loss of the directional control valve and defined by the orifice model.

The same procedure was applied to the simulation data acquisition for the second part of the high pressure pipeline between the outlet of the directional control valve and the inlet of the hydraulic motor. The rigid pipe in this part of line is about 24 % of total length of 1.53 m. The detail of simulation values for the second part of the high pressure pipeline is listed in Table 5.8. Table 5.7 gives the simulation input data of orifice model OR00 to simulate the steady state flowrate across the directional control valve in the high pressure line and the corresponding

pressure drop which is lumped together the pressure losses within two parts of the high pressure pipelines due to the pipe friction. One input parameter of the laminar boundary in OR00 is to consider the fluid density difference at the upstream and downstream of the orifice.

5.23   Input Data for the Propeller Model   The simulation data for the propeller is given in Table 5.10. The effective inertia of the propeller/motor was estimated from the practical geometrical parameters of the rotatory parts of propeller/motor. The diameter of propeller 230 mm and the ratio of 3.5 of the gearbox between the propeller and motor were measured from the test rig. The initial propeller angular velocity is zero before the hydraulic motor is loaded. The propeller was driven under water, so the density for the propeller surrounding fluid is given as 1000 kg/m^3. The non-dimensional torque coefficient K_t for a stationery propeller can be obtained from the data provided in Fig. 5.5 as 0.125. If the effects the physical shape of this particular propeller used on the test rig are taken into account, the value of K_t, 0.125, has been justified as 0.101 according to Equation (5.16) and the measurements of the motor shaft speed and the hydraulic torque applied on the motor at one particular system operating condition.

5.24   Input Data for Return line and Orifice Models   The simulation data provided in Table 5.11 presents the first part of the return line pipe before the directional control valve at the outlet of the hydraulic motor. The data acquisition is the same with in that for the inlet pipeline of the motor as in Table 5.8. The pressure losses in the return line and across the directional control valve are lumped into the simulation data of a orifice model OR00 in Table 5.12. The determination of simulation data for the return pipeline after the directional control valve was the essentially same as for the previous pipelines as listed in Table 5.13. The only difference is the fluid/pipe bulk modulus which was resulted from a different pipe thickness. Since the opening sizes of the two return orifices were set to give 10 % return flow to reservoir, the defined flowrates through these two orifices are given in the input simulation data for the orifice models in Table 5.14 and 5.15.

5.25 Input Data for Interconnecting, Suction and Pump Entry Lines, Pipe

Junction and Reservoir Models   The rigid pipes in the interconnecting and pump entry lines are simulated by two pipe models PI05(05) and PI05(06) whose simulation input data are listed in Table 5.16 and 5.17. The fluid/pipe effective bulk modulus of 18351 bar was calculated in the pipe PI05 model by the input of the measured steel pipe thickness.

The input simulation data for the return line to reservoir is given in Table 5.18 while the data for the suction line and pipe junction is listed in Table 5.19. The geometrical sizes for both pipe models were measured from the test rig. The initial pressure at the bottom of the vertical suction pipe before the system is loaded was obtained according to the test result in Fig. 5.13 of 0.05 bar. The fluid/pipe effective bulk modulus in PITH(01) was calculated according to the input of the pipe material and thickness. The input simulation data for the dummy pipe model PI05(07) is given in Table 7.24, the pipe diameter is taken as the same size of the vertical return pipe to reservoir in Table 5.18 but its length is defined as 0.05 m to obtain a relatively short computational time.

The simulation data for the dynamic reservoir model TKSH are listed in Table 5.20. The initial pressures at the entrance and exit of the reservoir are based upon the fluid height of 10 cm in the reservoir. The value of the first order lag coefficient is chosen to obtain a fast computational time without loss significant accuracy in the calculation.

5.26   Input Data for the Directional Control and Relief Valve Models   The simulation data provided in Table 5.21 presents the pressure drop across the directional control valve at its central position before it is selected to load up the hydraulic motor. The speed of change the valve position is very difficult to measure, if the value of 20 ms is assumed in the duty cycle model DEDT(01) as shown in Table 5.22, the simulation will be carried out to justify this speed. The behaviour of the single stage relief valve is simulated by a steady state model PC01(01) which simulation data is given in Table 5.23. Under such conditions, computer simulations have been carried out. The loading is identical with the partially closed hydrostatic drive boat propeller system in the experimental tests.

5.27   Analysis of the Motor Speed and High Pressure Transient   At the
initial stage of loading, the directional control valve is rapidly operated to supply
flow into the inlet pipe of the hydraulic motor. The transient pressure in the high
presure line is determined by fluid compressibility, which is expressed in the terms
of fluid volume, bulk modulus and the sum of the pipe inlet and outlet flowrates.
Hence, the directional control valve operating speed, which determines the transient
flowrate at the pipe inlet, and also the dynamic motor shaft speed, which plays an
important part in determining the pipe transient outlet flowrate supplied to the
motor, are the influential parameters in determining the system transient high
pressure. The increasing rate of the transient pipe inlet flowrate is generally greater
than that of the outlet flowrate due to the inertia effects of the motor/propeller on
the motor dynamic speed. As a result, the transient high pressure increases to a
higher value and then reduces towards the steady value required by the propeller
load condition. The transient overshoot of the experimental high pressure in Fig. 5.10
is a result of the transient difference between the increasing rates of the inlet and
outlet flowrates of the second part of the high pressure line.

The influence of each individual factor on the system high pressure can be
examined from a range of the simulations by varying each corresponding input
simulation data. When the directional control valve is rapidly operated to supply
flow to the hydraulic motor, the shaft speed of the hydraulic motor simultaneously
increases. Hence, the transient motor speed would be affected by the directional
control valve operating time as shown in the simulation results in Fig. 5.16. The
effects of the non-dimensional torque coefficient K_t on the motor shaft speed are
shown in the simulation results in Fig. 5.17. The simulated steady value of the
motor speed with $K_t = 0.101$ agrees with the measured motor shaft speed. When
the size of propeller is changed, the motor speed would be affected. Some typical
simulation predictions of the motor speeds in Fig. 5.18 show the effects of the
propeller diameter on the motor speed. Similarly, the propeller speed would be
affected as shown in the simulated propeller speeds in Fig. 5.19. These results are
identical to the results in Fig. 5.18 except the fact that the motor speed is 3.5 times
as the propeller speed due to the ratio of the gearbox between the motor and
propeller.

When the combined inertia of the motor/propeller increases, the rate of the motor speed increase reduces as shown in the calculated motor speeds in Fig. 5.20. Consequently, the transient high pressure will be affected as shown in Fig. 5.21, since the transient high pressure is mainly determined by the sum of the transient inlet and outlet flowrates of the high pressure line. When the rate of the motor speed increase is small in response to the flowrate supplied to the motor inlet pipeline, the transient high pressure of the system will increase above the cracking pressure of the relief valve. Thereafter, the motor speed increases to match the flowrate supplied to the motor, the flow condition in the high pressure line will settle down so the system high pressure will reduce towards the steady value required by the propeller load conditions. Hence, a transient overshot would be generated on the system working pressure. This transient overshot of high pressure can be a problem to meet the stable requirement of the system transient high pressure. If the setting pressure of the relief valve is lower than the propeller load condition required, the system high pressure will be given by the relief valve setting pressure at which some proportional flow returns to the return line. Thus, no overshoot will occur on the transient high pressure but the propeller speed will be lower than otherwise it could be achieved. Hence, the potential of the system will not be fully used and adversely the power loss caused by the relief flow will be converted into heat flow which increases the level of fluid temperature in the system. In some cases, when the propeller speed responses fast to the increase of the motor inlet flowrate due to a small effective inertia of the motor/propeller or a small size of the propeller diameter, no overshot will result in the transient high pressure. In a certain range of the rate of the propeller speed increase, the system high pressure will initially rise above the normal system working pressure, as the pressure increases towards the setting pressure of the relief valve, the motor speed increases above the value at which the high pressure will begin to fall back before it gets to the setting pressure of the relief valve.

Using the simulation results, a suitable value for the setting pressure of the relief valve can be determined. Moreover, a reasonable close correlation has been found between the simulated and recorded results of the transient high pressures as shown in Fig. 5.22. The difference between the simulation and experimental high pressure results after the transient overshot was due to the fall off of the motor torque as the oil is heated up and also due to the reduction in gear box losses for the same reason.

In order to obtain a satisfactory performance of the partially closed hydrostatic drive boat propeller system, in the system design stage, the computer simulations can be used to optimise the transient system load conditions together with parameters of the system components.

5.28   Engine Speed   For a consequence of rapid rise in the system high pressure, the torque required from the engine will correspondingly increase. The engine responds to this change in torque by reducing its shaft speed. The reduction value of the engine speed is determined by the speed-torque gradient coefficient as discussed in Equation (5.2) and shown in the simulation results in Fig. 5.23. With the engine model input simulation data defined in Table 5.4, which was based upon the experimental engine shaft speed and high pressure measurements, the simulation result in Fig. 5.24 shows the engine speed droop as the result of the load change. This engine speed change after the system loading agrees with the steady state experimental measurements. The transient pump delivery and inlet flowrates are affected by this droop in the engine speed and hence the transient high and suction pressures of the system will be indirectly affected.

5.29   Suction Pressure at the Pipe Junction   The reasons for the transient reduction in the suction pressure are discussed in Section 5.15 and also the acting parameters in determining the suction pressure of the partially closed hydraulic system have been identified. For the simulation data defined, a favourable agreement has been shown between the simulation and experimental transient suction pressures as shown in Fig. 5.25.

Up to this stage, the computer simulations have been used to analyse the experimental results. The comparisons of the simulated and experimental results have shown that the accuracy of the simulation is at an accepted level. It can be said now with confidence that the computer models developed can be used to investigate the performance of the other more complex partially closed hydrostatic drive boat propeller system.

5.30 Further Considerations in the Application of the Partially Closed System

Since the usual means of the hydraulic cooling (water cooler) is not applicable here due to the limitation of energy supply and space, the system ability of heat dissipation is the key factor to decide the feasibility of a particular system design. For the partially closed hydrostatic drive boat propeller system proposed, the system power loss has a limited number of sources, which include the power losses generated from the motor and pump internal leakages and the pressure drops across the directional control valve and due to the pipe friction. The fluid temperature in the system loop will be increased due to the heat flow converted from the power losses. Normally, the maximum fluid temperature in the system is limited below 60° C to maintain a stable system working pressure. In this suggested partially closed system, the maximum fluid temperature can be controlled by optimising a small proportion of system flow returning to the reservoir. If the heat dissipation of the system is not sufficiently high enough to meet the demand of the limited fluid temperature, a possible way to reduce the maximum fluid temperature may be achieved by putting the system pipelines (usually hydraulic hoses) into water.

In the above examination of the performance of the partially closed hydrostatic drive propeller system, the fall off in pressure due to heating was not predicted as oil viscosity was assumed to remain constant. Therefore, the investigations for the performance of the partially closed hydrostatic drive boat propeller system will not have been completed unless an intensive study for the system thermodynamic processes have been carried out.

No.	Component Name	Technical parameters	Data	Unit
1	Clinton single cylinder 4 stroke spark-ignited engine	rated speed rated power inertia	2300 1 0.01	rev/min kw $kg.m^2$
2	Oleodinamica ozzano GMM gear pump with internal drain	displacement maximum pressure	5 100	cc/rev bar
3	High pressure pipeline before DCV	$\frac{1}{2}$ inch hydraulic hose	1	m
4	4 way 3 position directional control valve	maximum flowrate maximum pressure	25 63	L/min bar
5	High pressure pipeline after DCV	$\frac{1}{2}$ inch hydraulic hose	1.15	m
6	Oleodinamica ozzano GMM gear motor with external drain	displacement maximum pressure	5 100	cc/min bar
7	Propeller	diameter inertia	230 0.006	mm $kg.m^2$
8	Return line before DCV	$\frac{1}{2}$ inch hydraulic hose	1.9	m
9	Return line after DCV	$\frac{3}{8}$ inch hydraulic hose	2.9	m
10	Orifice B in interconnecting line	maximum flowrate	20	L/min
11	Orifice B in flow line to tank	maximum flowrate	20	L/min
12	Iron tank size b x L x H	0.19 m x 0.25 m x 0.25 m	12	litres
13	Return line to tank	$\frac{1}{2}$ inch hydraulic hose	1.2	m
14	Suction line	$\frac{1}{2}$ inch rigid steel pipe	0.5	m
15	Single stage relief valve	maximum pressure maximum flowrate	100 15	bar L/min

Table 5.1   Technical Data of main Components on Test Rig

Comp. No.	Model Name	Model No.	Link Position			
1	PM3H	1	1			
2	PUOH	1	2	3	1	
3	PI05	1	3	4	25	21
4	OR00	1	4	5		
5	PI05	2	5	6		
6	MOAH	1	6	7	14	20
7	LR0H	1	14	23	24	
8	PI05	3	7	8		
9	OR00	2	8	9		
10	PI05	4	9	10	15	26
11	OR00	3	10	11		
12	OR00	4	15	16		
13	PI05	5	11	12		
14	PI05	6	13	2		
15	PI05	7	16	17		
16	PI3H	1	17	18		
17	PITH	1	12	19	13	
18	TKSH	1	18	19	20	22
19	DC1C	1	25	26	27	
20	DEDT	1	27			
21	PC01	1	21	22		

Table 5.2   Model Linking Input Data for Program Generation

Fluid Properties Section Model FLPROP			
No.	Parameters	Data	Unit
1	oil temperature	15	deg. C
2	oil type	BP-HLP 32	
3	fluid density	872.5	$\frac{kg}{m^3}$
4	fluid Bulk Modulus	18400	bar
5	fluid kinematic viscosity	94.50	cSt
6	fluid absolute viscosity	82.45	cP

Table 5.3   parametric Data Used in Simulation for Fluid Properties

Component No. 1: Speed Droop Engine Model PM3H (No. 1)			
No.	Input Parameters	Data	Unit
1	initial engine speed	2300	rev/min
2	speed/torque gradient	91	(rev/min)/Nm
3	governor set speed	2400	rev/min
4	engine inertia	0.008	$kg.m^2$

Table 5.4   parametric Data Used in Simulation for Engine

Component No. 2: Hydraulic Pump Model PU0H (No. 1)			
No.	Input Parameters	Data	Unit
1	maximum pump displacement	5	ml/rev
2	fraction of full displacement	1	
3	slip loss coefficiency	1.4×10^{-8}	
4	torque loss coefficiency	2	
5	viscous friction coefficiency	0.8	
6	clearance volume	0	

Table 5.5   parametric Data Used in Simulation for Hydraulic Pump

Component No. 3: Frictionless Pipe Model PI05 (No. 1)			
No.	Input Parameters	Data	Unit
1	pipe internal diameter	12.7	mm
2	pipe length	1.32	m
3	pipe volume	0.1672	Litres
4	fluid/pipe Bulk Modulus	11261	bar
5	air saturation pressure	0	bar
6	proportion of dissolved air	0.1	
7	initial pressure	2.5	bar

Table 5.6   parametric Data Used in Simulation for High Pressure
Pipeline Before Directional Control Valve

Component No. 4: Orifice Restrictor Model OR00 (No. 1)			
No.	Input Parameters	Data	Unit
1	steady state flowrate	0.145	L/sec
2	corresponding pressure drop	2.5	bar
3	laminar boundary in bar	0.1	bar

Table 5.7   parametric Data Used in Simulation for Orifice Restrictor
to Represent Pressure Loss Across Directional
Control Valve in High Pressure Line

Component No. 5: Frictionless Pipe Model PI05 (No. 2)			
No.	Input Parameters	Data	Unit
1	pipe internal diameter	12.7	mm
2	pipe length	1.53	m
3	pipe volume	0.1938	Litres
4	fluid/pipe Bulk Modulus	11261	bar
5	air saturation pressure	0	bar
6	proportion of dissolved air	0.1	
7	initial pressure	0	bar

Table 5.8   parametric Data Used in Simulation for High Pressure
Pipeline After Directional Control Valve

Component No. 6: Hydraulic Motor Model MOAH (No. 1)			
Stage	Spool Displacement	Time (second)	Valve Position
1	maximum motor displacement	5	cc/rev
2	slip loss coefficiency at low speed	2.91×10^{-9}	
3	low speed at which slip is quoted	1000	rev/min
4	slip loss coefficiency at high speed	3.76×10^{-9}	
5	high speed at which slip is quoted	2500	rev/min
6	fraction of slip loss coefficient for drain leakage	0.08	
7	speed dependent torque loss coefficient	3×10^5	
8	pressure dependent torque loss coefficient at low speed condition	0.029	
9	pressure dependent torque loss coefficient at high speed condition	0.043	
10	reference viscosity in centipoise at which volumetric efficiency is quoted	94	cSt

Table 5.9   parametric Data Used in Simulation for Hydraulic Motor

Component No. 7: Propeller Load Model LR0H (No. 1)			
No.	Input Parameters	Data	Unit
1	effective inertia of propeller	0.008	$kg.m^2$
2	non-dimensional torque coefficient	0.101	
3	diameter of propeller	230	mm
4	initial angular velocity	0	rev/min
5	density of fluid surrounding propeller	1000	kg/m^3
6	ratio of gearbox between motor and propeller	3.5	

Table 5.10   parametric Data Used in Simulation for Propeller Load

Component No. 8: Frictionless Pipe Model PI05 (No. 3)			
No.	Input Parameters	Data	Unit
1	pipe internal diameter	12.7	mm
2	pipe length	2.257	m
3	pipe volume	0.28591	Litres
4	fluid/pipe Bulk Modulus	11261	bar
5	air saturation pressure	0	bar
6	proportion of dissolved air	0.1	
7	initial pressure	0	bar

Table 5.11   parametric Data Used in Simulation for the First Part
Return Line Before Directional Control Valve

Component No. 9:	Orifice Restrictor Model OR00 (No. 2)		
No.	Input Parameters	Data	Unit
1	steady state flowrate	0.145	L/sec
2	corresponding pressure drop	2	bar
3	laminar boundary in bar	0.1	bar

Table 5.12 parametric Data Used in Simulation for Orifice Restrictor to Represent Pressure Loss Across Directional Control Valve in Return Line

Component No. 10:	Frictionless Pipe Model PI05 (No. 4)		
No.	Input Parameters	Data	Unit
1	pipe internal diameter	9.5	mm
2	pipe length	2.9	m
3	pipe volume	0.2066	Litres
4	fluid/pipe Bulk Modulus	13116	bar
5	air saturation pressure	0	bar
6	proportion of dissolved air	0.1	
7	initial pressure	0.5	bar

Table 5.13 parametric Data Used in Simulation for Return Pipeline After Directional Control Valve

Component No. 11:	Orifice Restrictor Model OR00 (No. 3)		
No.	Input Parameters	Data	Unit
1	steady state flowrate	0.1305	L/sec
2	corresponding pressure drop	0.45	bar
3	laminar boundary in bar	0.1	bar

Table 5.14   parametric Data Used in Simulation for Orifice B
in Interconnecting Pipeline

Component No. 12:	Orifice Restrictor Model OR00 (No. 4)		
No.	Input Parameters	Data	Unit
1	steady state flowrate	0.0145	L/sec
2	corresponding pressure drop	0.4	bar
3	laminar boundary in bar	0.1	bar

Table 5.15   parametric Data Used in Simulation for Orifice A
in Return Line to Reservoir

Component No. 13:	Frictionless Pipe Model PI05 (No. 5)		
No.	Input Parameters	Data	Unit
1	pipe internal diameter	12.7	mm
2	pipe length	0.15	m
3	pipe volume	0.0285	Litres
4	fluid/pipe Bulk Modulus	18361	bar
5	air saturation pressure	0	bar
6	proportion of dissolved air	0.1	
7	initial pressure	0.07	bar

Table 5.16   parametric Data Used in Simulation for
Interconnecting Flow Pipeline

Component No. 14:	Frictionless Pipe Model PI05 (No. 6)		
No.	Input Parameters	Data	Unit
1	pipe internal diameter	12.7	mm
2	pipe length	0.05	m
3	pipe volume	0.0095	Litres
4	fluid/pipe Bulk Modulus	18361	bar
5	air saturation pressure	0	bar
6	proportion of dissolved air	0.1	
7	initial pressure	0.05	bar

Table 5.17   parametric Data Used in Simulation for Pump
Entry Line

Component No. 15:	Vertical Return Pipe Model PI3H (No. 1)		
No.	Input Parameters	Data	Unit
1	pipe internal diameter	12.7	mm
2	pipe length	1	m
3	initial pipe outlet flowrate	0.0145	L/s

Table 5.18   parametric Data Used in Simulation for Return Line
to Reservoir

Component No. 16:	Suction Pipe & Pipe Junction Model PITH (No. 1)		
No.	Input Parameters	Data	Unit
1	pipe internal diameter	12.7	mm
2	pipe length	1	m
3	initial suction pipe inlet flowrate	0.0145	L/s
4	fluid/pipe Bulk Modulus	11261	bar
5	initial suction pipe outlet pressure	0.05	bar

Table 5.19   parametric Data Used in Simulation for Vertical Suction
Pipe and Pipe Junction Model

Component No. 17:	4 Link Dynamic Tank Model TKSH (No. 1)		
No.	Input Parameters	Data	Unit
1	length of tank base	0.25	m
2	width of tank base	0.19	m
3	diameter of extending pipe	12.7	mm
4	initial fluid height in tank	0.1	m
5	initial pressure at entry	0.01	bar
6	coefficient of first order lag	1000	

Table 5.20   parametric Data Used in Simulation for Reservoir

Component No. 18:	2 Way 2 Position DCV Model DC1C (No. 1)		
No.	Input Parameters	Input Data	Unit
1	defined flowrate	0.145	L/min
2	corresponding pressure drop	5	bar
3	linear region limit	0.001	bar

Table 5.21   parametric Data Used in Simulation for 2 Way 2 Position Directional Control Valve

Component No. 19: Movement of DCV Model DEDT (No. 1)			
Stage	Spool Displacement	Time (second)	Valve Position
1	0	0	open
2	1	0.02	close
3	1	1	close

Table 5.22   parametric Data Used in Simulation for Different Time
Relate Slip of Directional Control Valve

Component No. 20: Relief Valve Model PC01 (No. 1)			
No.	Input Parameters	Data	Unit
1	Relief Valve Cracking Pressure	40	bar
2	Relief Valve Constant	0.05	(L/sec)/bar

Table 5.23   parametric Data Used in Simulation for a Single
Stage Relief Valve

Component No. 21:	Frictionless Pipe Model PI05 (No. 7)		
No.	Input Parameters	Data	Unit
1	pipe internal diameter	12.7	mm
2	pipe length	0.05	m
3	pipe volume	0.0095	Litres
4	fluid/pipe Bulk Modulus	18361	bar
5	air saturation pressure	0	bar
6	proportion of dissolved air	0.1	
7	initial pressure	0.1	bar

Table 5.24   parametric Data Used in Simulation for the Dummy Pipe
Model for Model Linking

Engine

Fixed Displacement
Pump

Fixed Displacement
Motor

Hydraulic Connecting
Pipelines
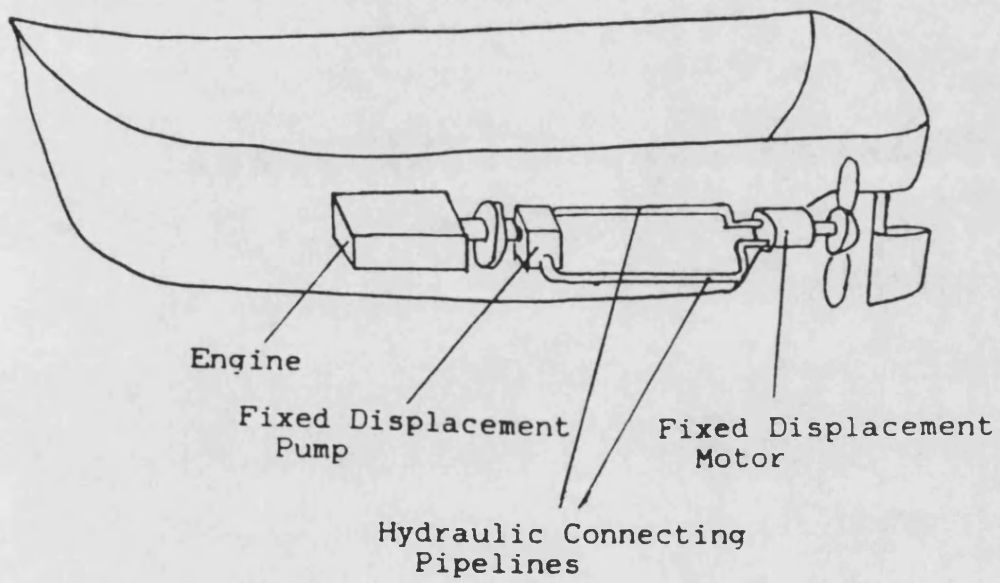
Fig. 5.1   A Hydrostatically Driven Propeller System

Fig. 5.2   A Partially Closed Hydrostatically Driven Propeller System

$\omega_{GOV} = 2400$

ω_E ENGINE SPEED rev/min

2400
2000
1600
1200
800
400

$$T_E = \frac{\omega_{GOV} - \omega_E}{G_E}$$

200   400   600   800
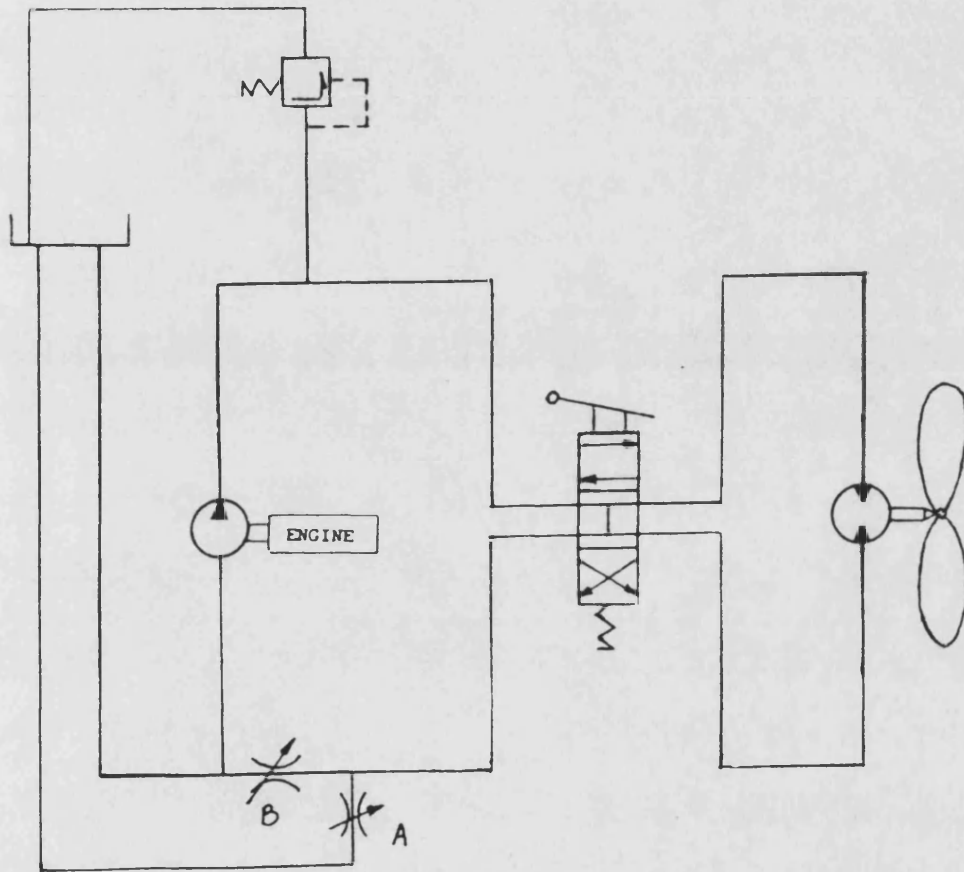
T_E ENGINE TORQUE - Nm
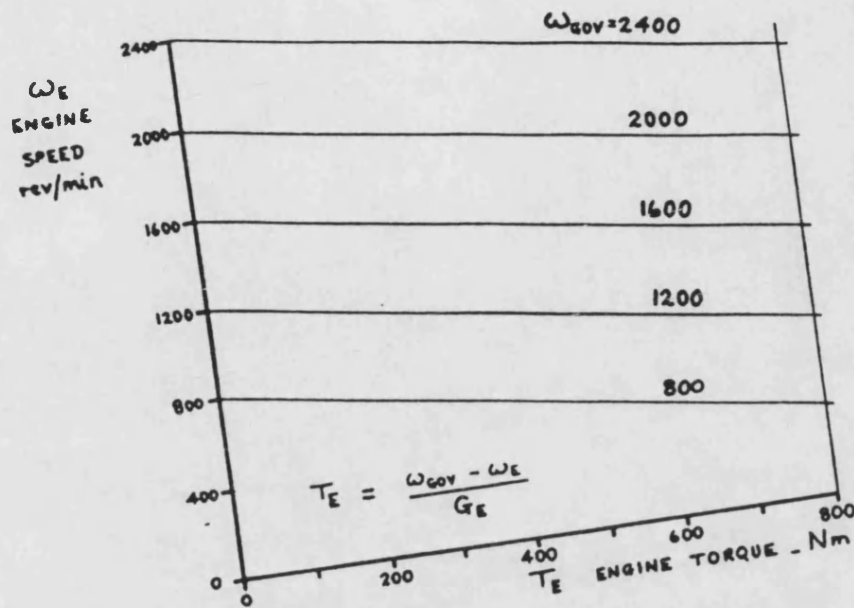
A. ENGINE LOAD DROOP CHARACTERISTICS

maximum torque curve

ENGINE TORQUE Nm

800
700
600
500
400
300
200
100
0
-100

idling speed

maximum speed

800   1200   1600   2000   2400

ENGINE SPEED - rev/min

brake torque curve
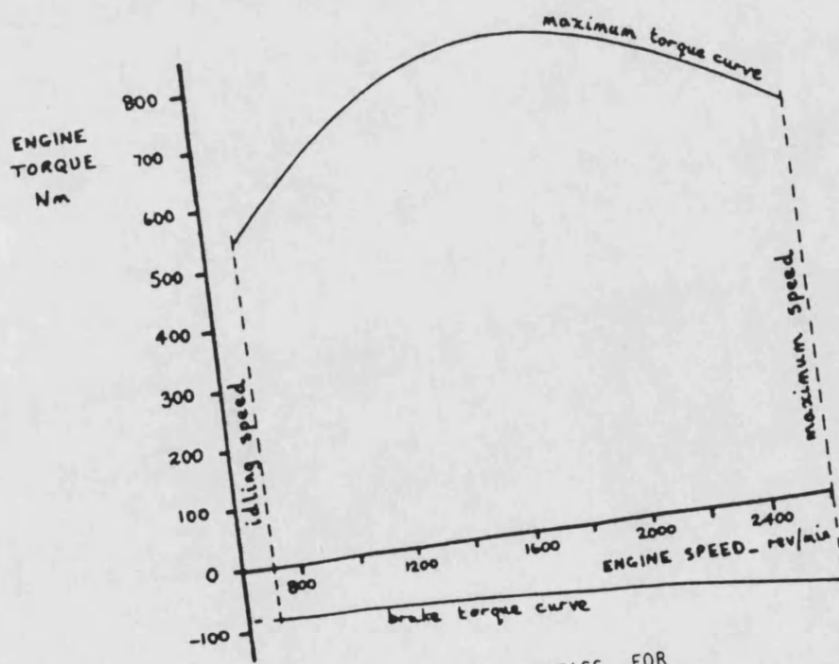
B : TORQUE CHARACTERISTICS FOR A PERKINS V8 DIESEL ENGINE

Fig. 5.3   Speed-Torque Characteristics of a Practical Engine
(Taken from Ref. 5.3)
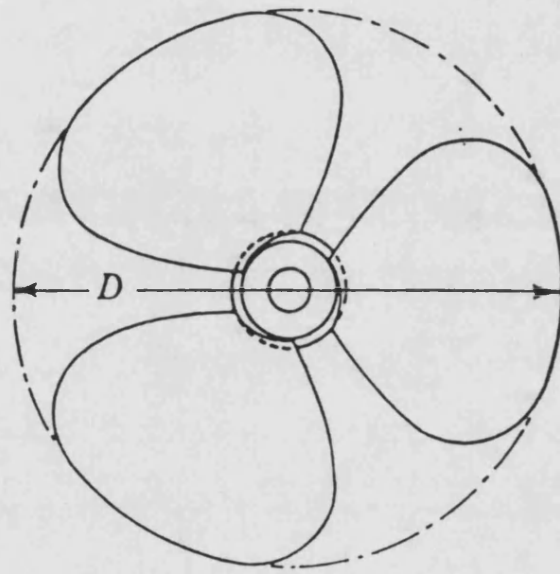
Fig. 5.4   A Screw Propeller With Equal Blades Evenly Distributed

$$K_t = \frac{T}{\rho n^2 D^5}$$

$$K_f = \frac{F}{\rho n^2 D^4}$$

$$C_P = \frac{P}{\rho n^3 D^5}$$

η

$\times 10^{-1} = K_f$; efficiency; C_P $\times 10^{-2} \cdot K_t$

V/nD
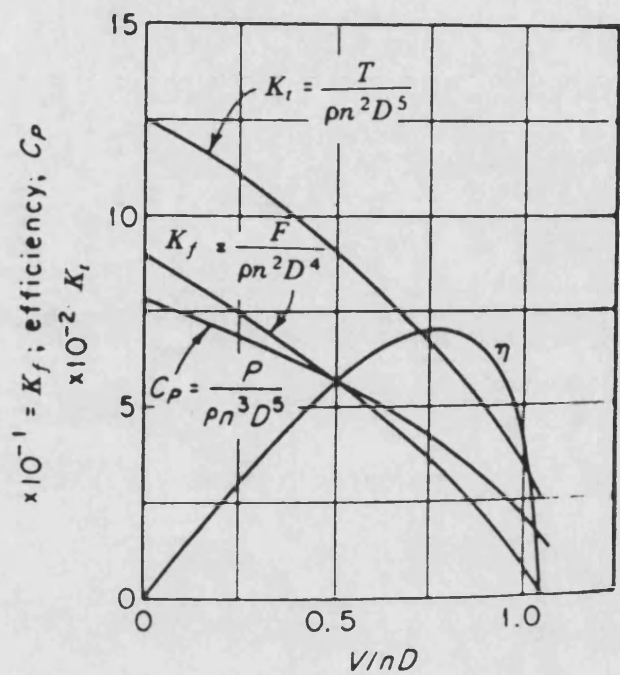
Fig. 5.5   The Standard Characteristic Curves for a Marine Propeller Taken from Ref. (5.4)
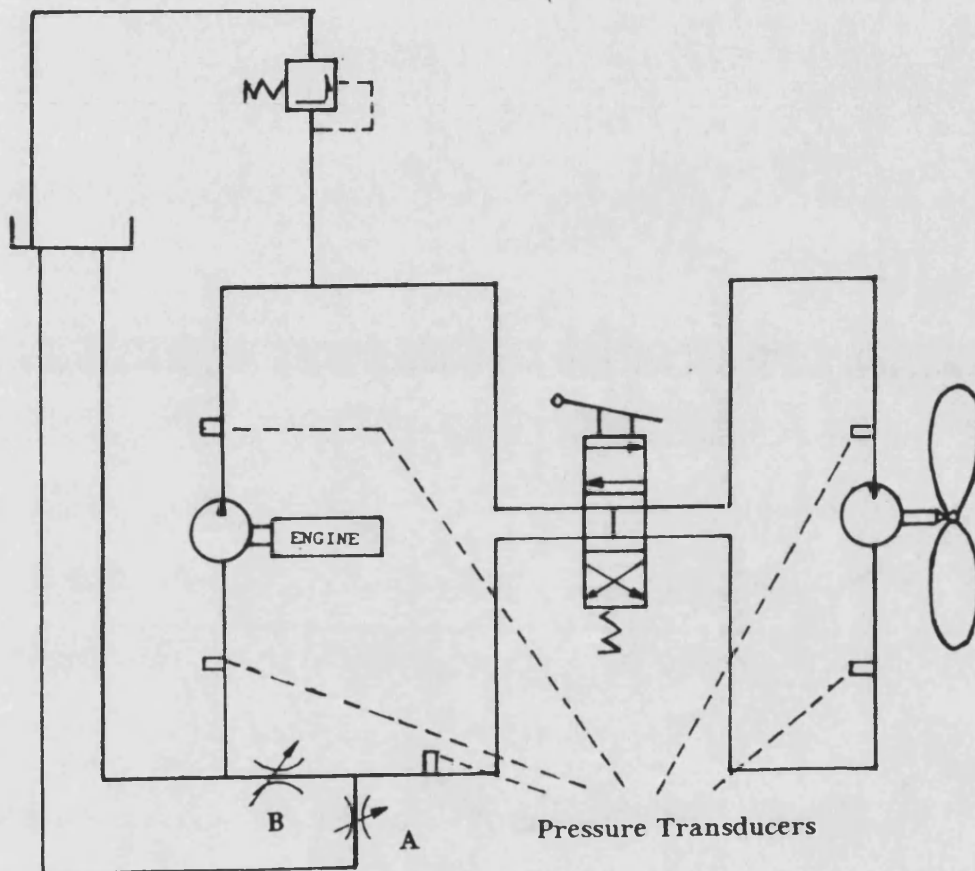
Fig. 5.6   A Partially Closed Hydrostatic Drive Boat Propeller Test Rig

Fig. 5.8   The Location of the Propeller Inside A Water Pool

Return Line
to Reservoir

Suction Line

Orifice A

Pump Entry Line

Return Line

Orifice B

Interconnecting Flow Line
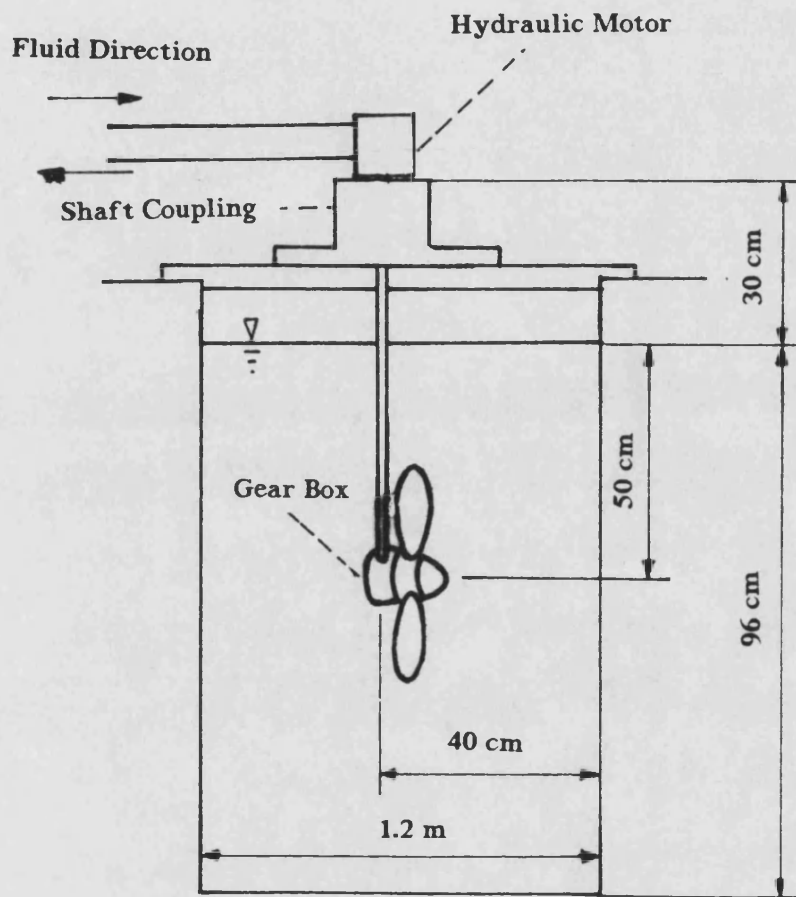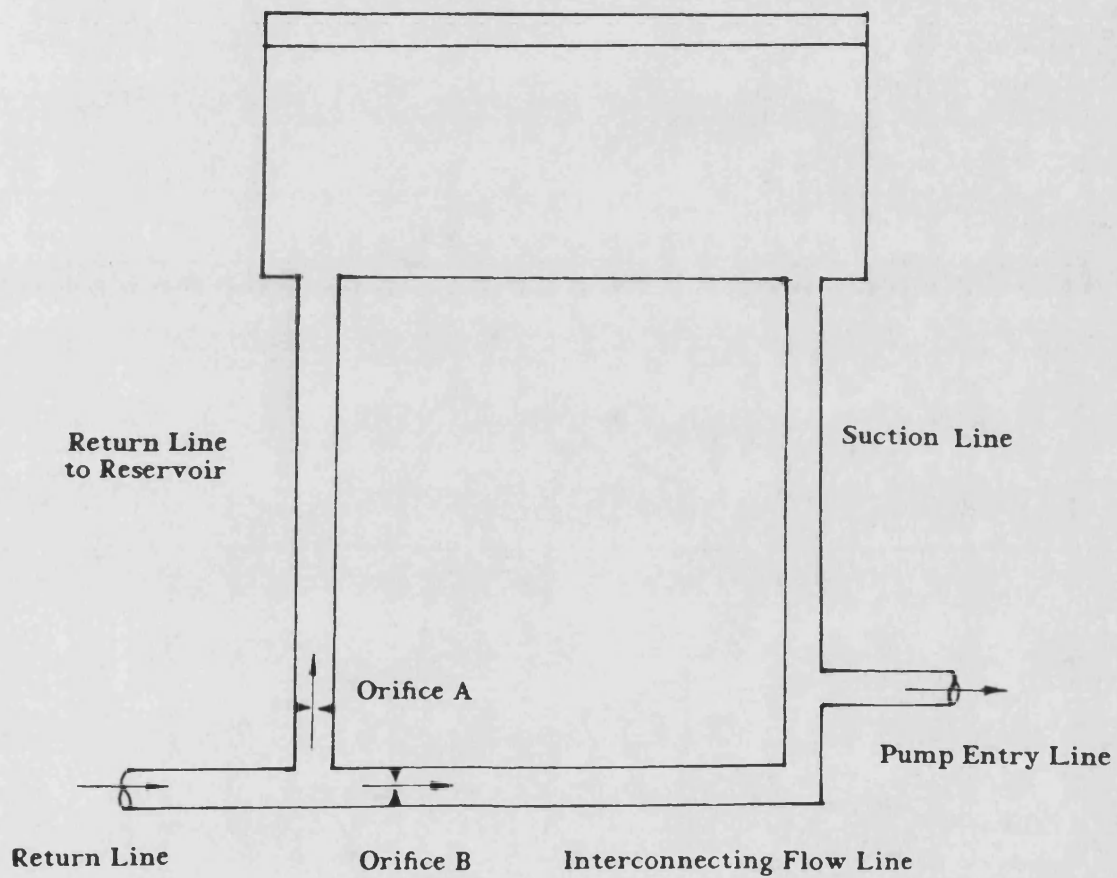
Fig. 5.9   Detailed Arrangement of the Return Pipeline on the Test Rig
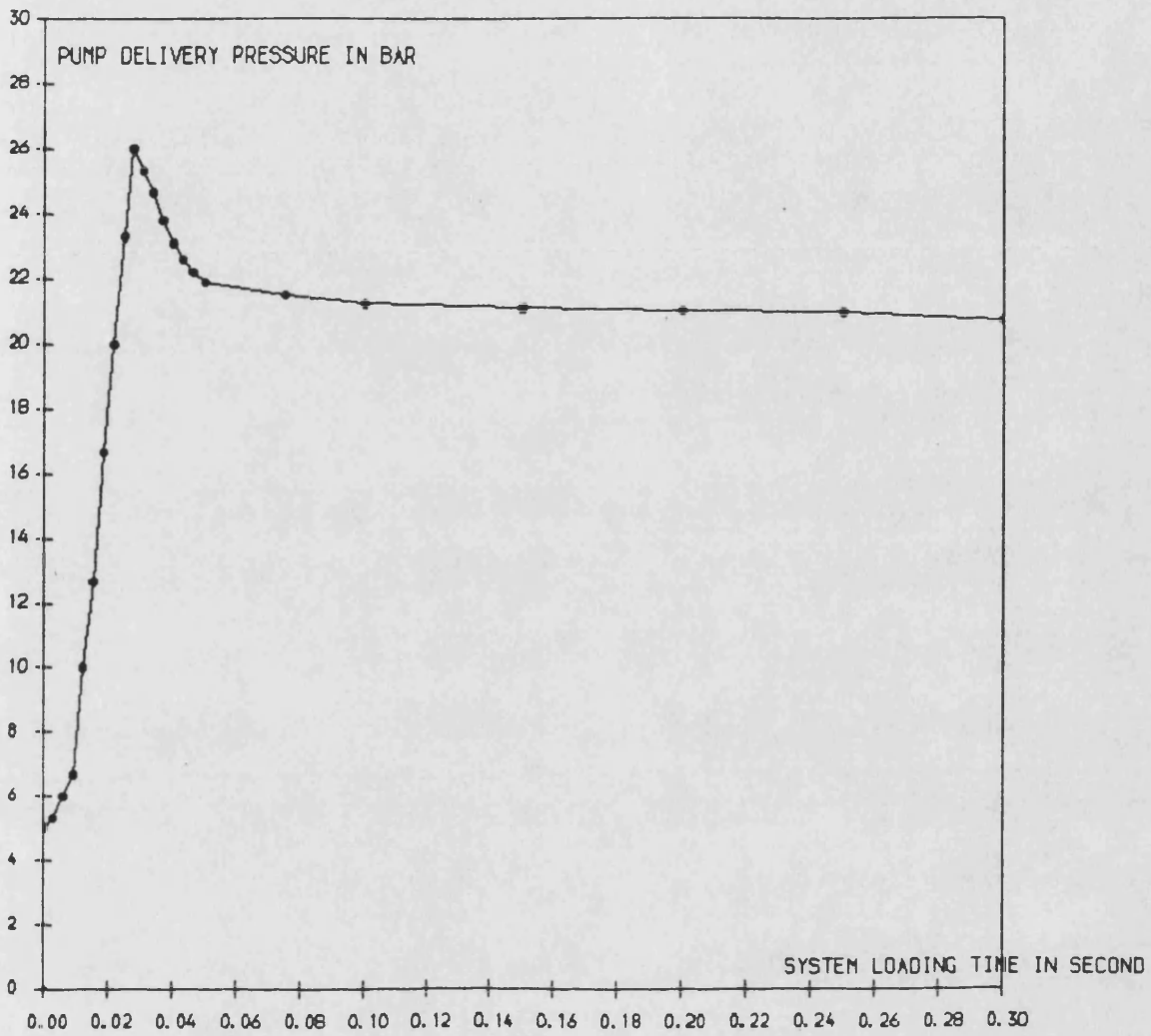
Fig. 5.10   Experimental High Pressure Transient in the Partially
Closed Hydrostatic Drive Propeller Test Rig
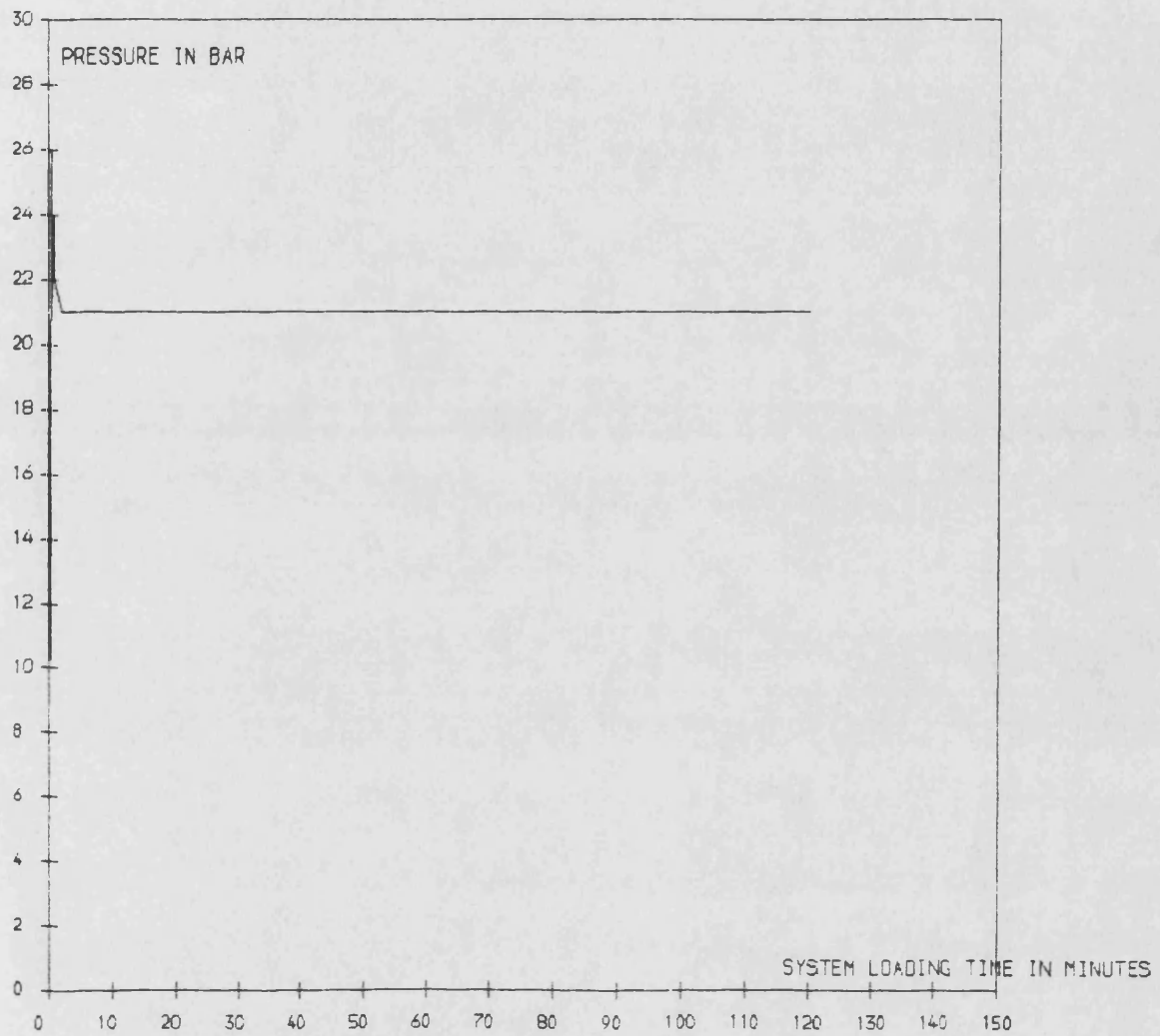
Fig. 5.11   Experimental High Pressure in the Partially
Closed Hydrostatic Drive Propeller Test Rig
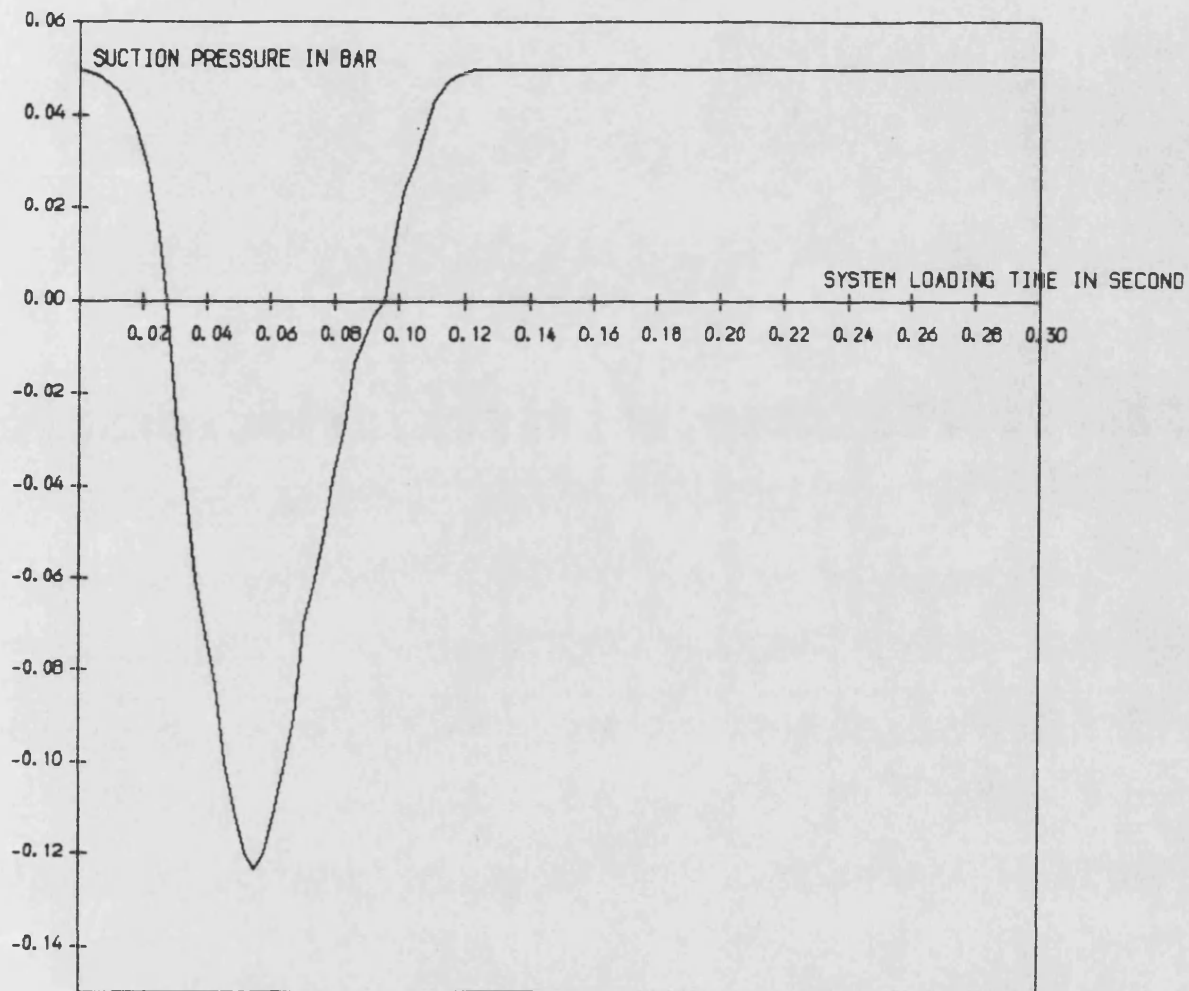
Fig. 5.12 Experimental Suction Pressure Transient in the Partially Closed Hydrostatic Drive Propeller Test Rig
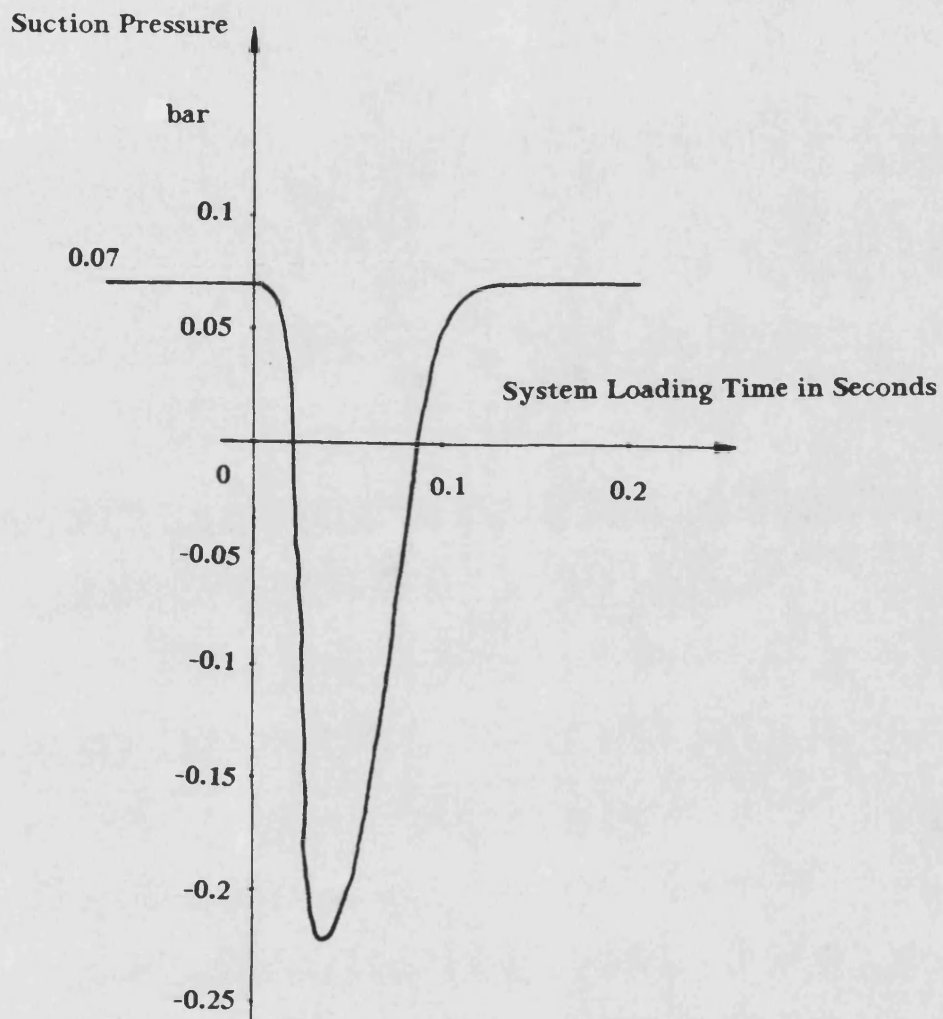
Fig. 5.13   Experimental Suction Pressure Transient in the Unboosted
Closed Hydrostatic Drive Boat Propeller Test Rig
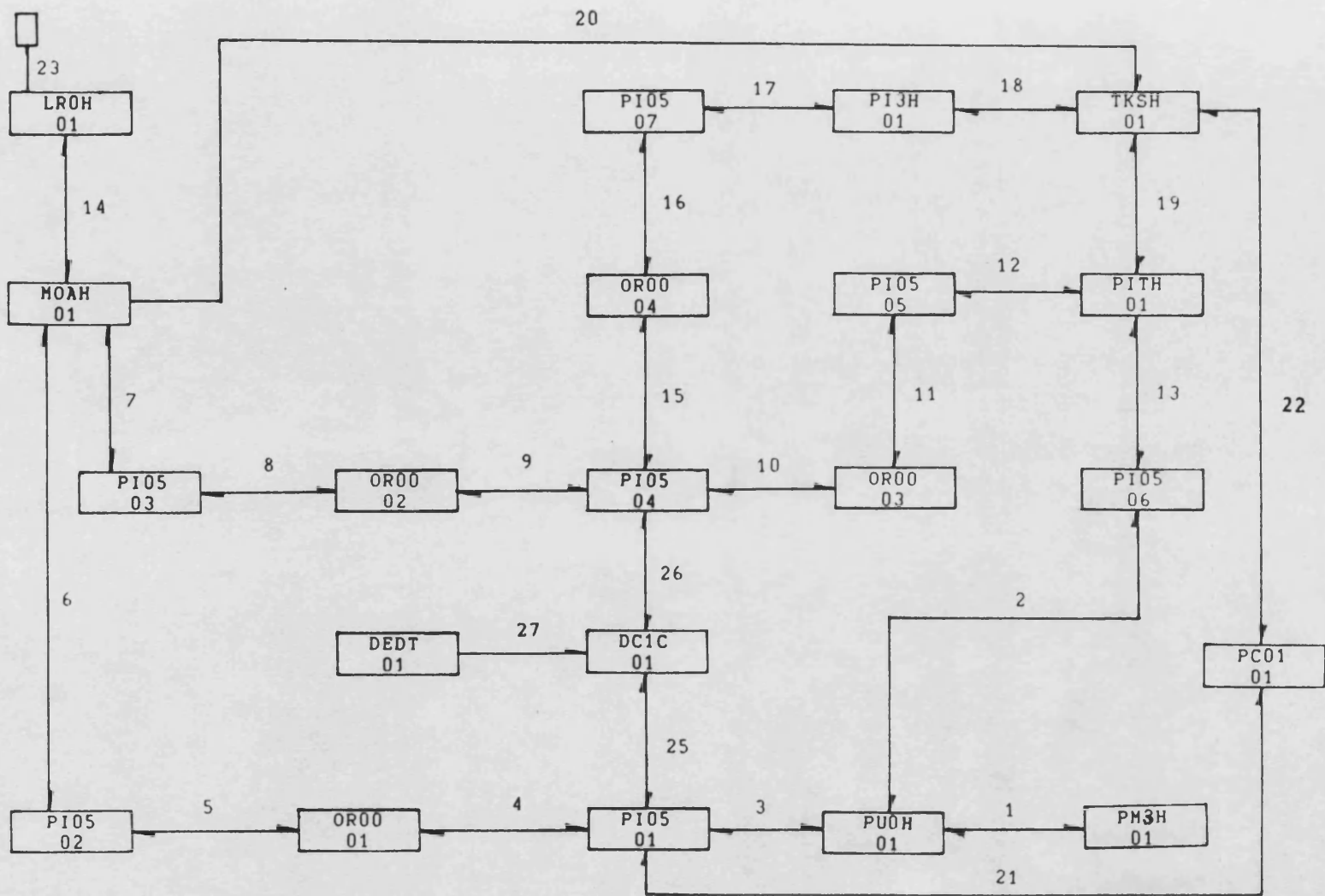
Fig. 5.14   Block Diagram for the Simulation of the Partially Closed
Hydrostatic Drive Boat Propeller System
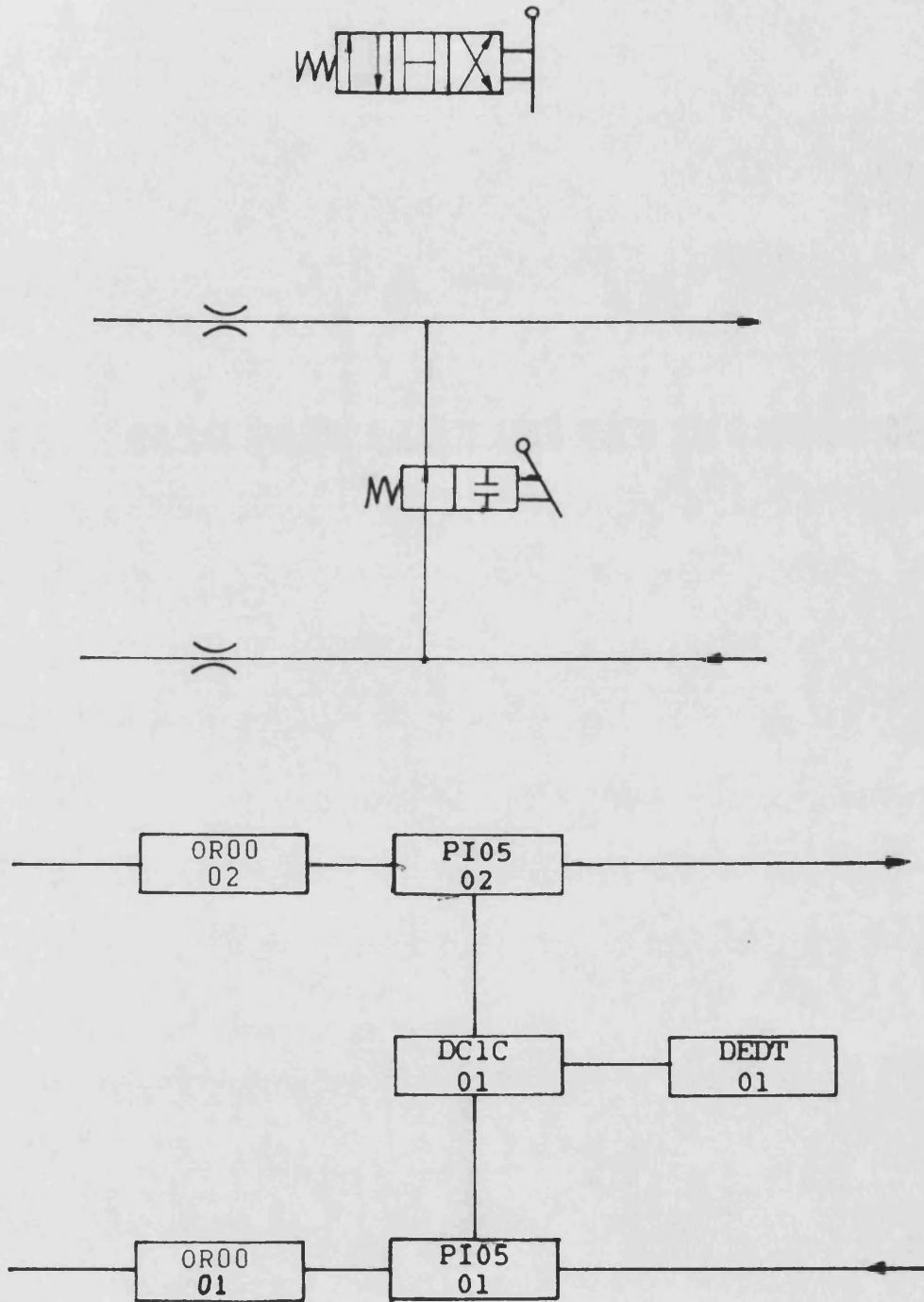
Fig. 5.15   A Simplified Way to Simulate a Directional Control Valve

$\times 10^3$ rev/min

Directional Control Valve Operation Time:

0.01 second
0.02 second
0.03 second
0.04 second

1

ANGULAR SPEED

1   2   3 $\times 10^{-1}$

System Loading Time in Seconds
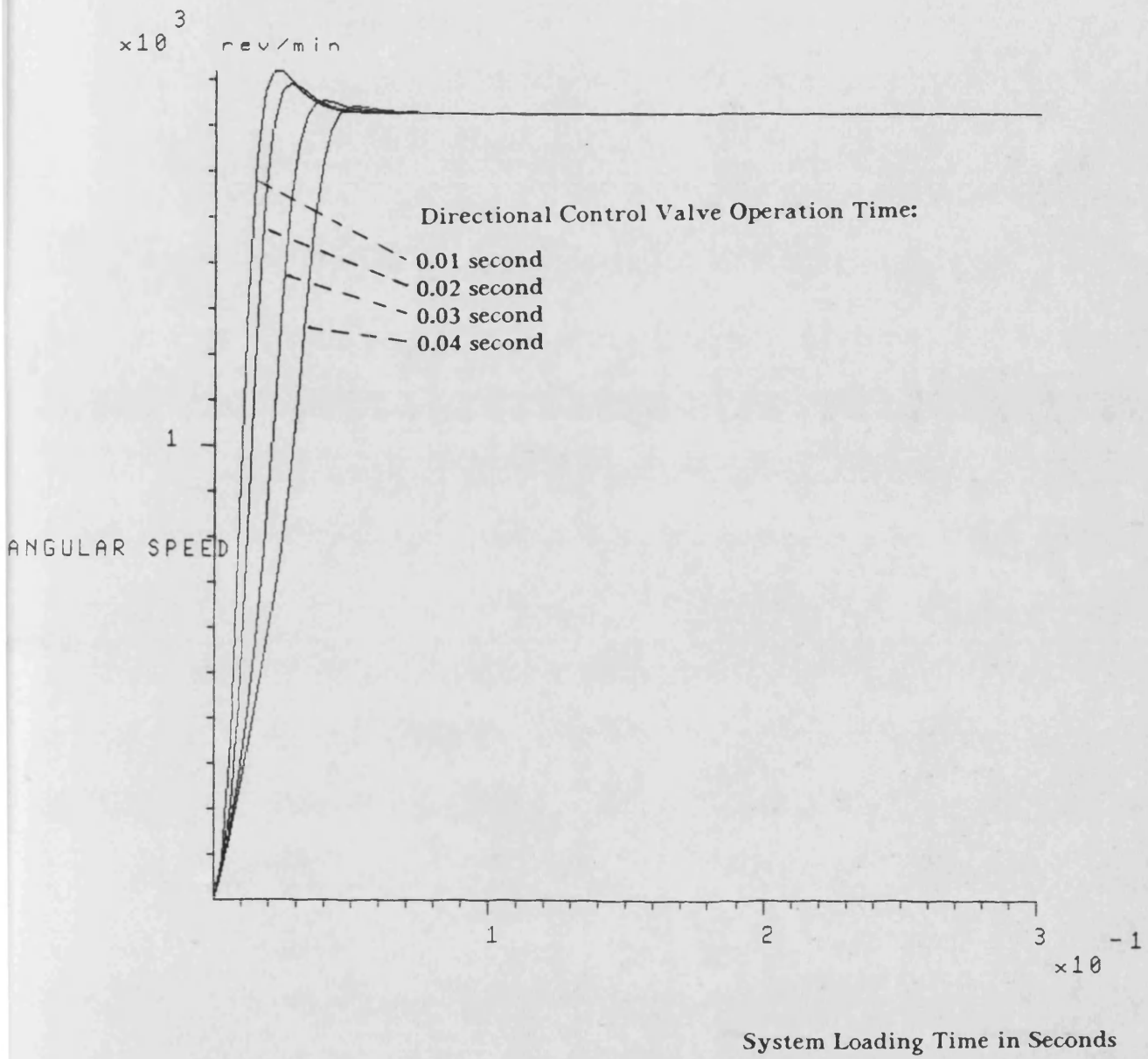
Fig. 5.16   The Effects of the Directional Control Valve Operating Time
on the Motor Speed

Non-dimensional Torque Coefficient:

$\times 10^3$ rev/min

2

$K_t = 0.05$

$K_t = 0.111$

$K_t = 0.2$

$K_t = 0.3$

1

ANGULAR SPEED

1   2   3 -1
                                                  $\times 10$

System Loading Time in Seconds
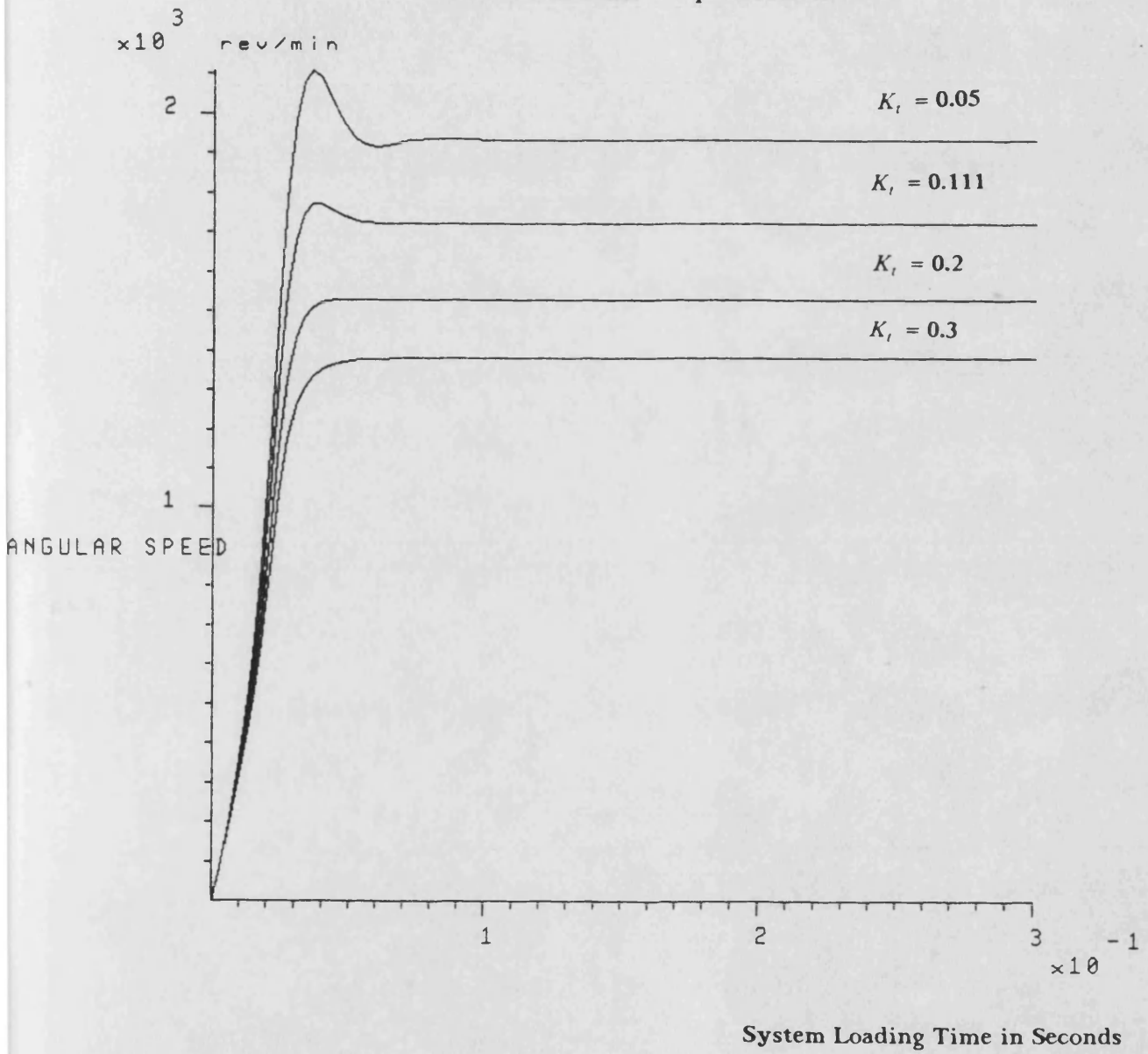
Fig. 5.17   The Effects of the Non-dimensional Torque Coefficient on
             the Motor Speed
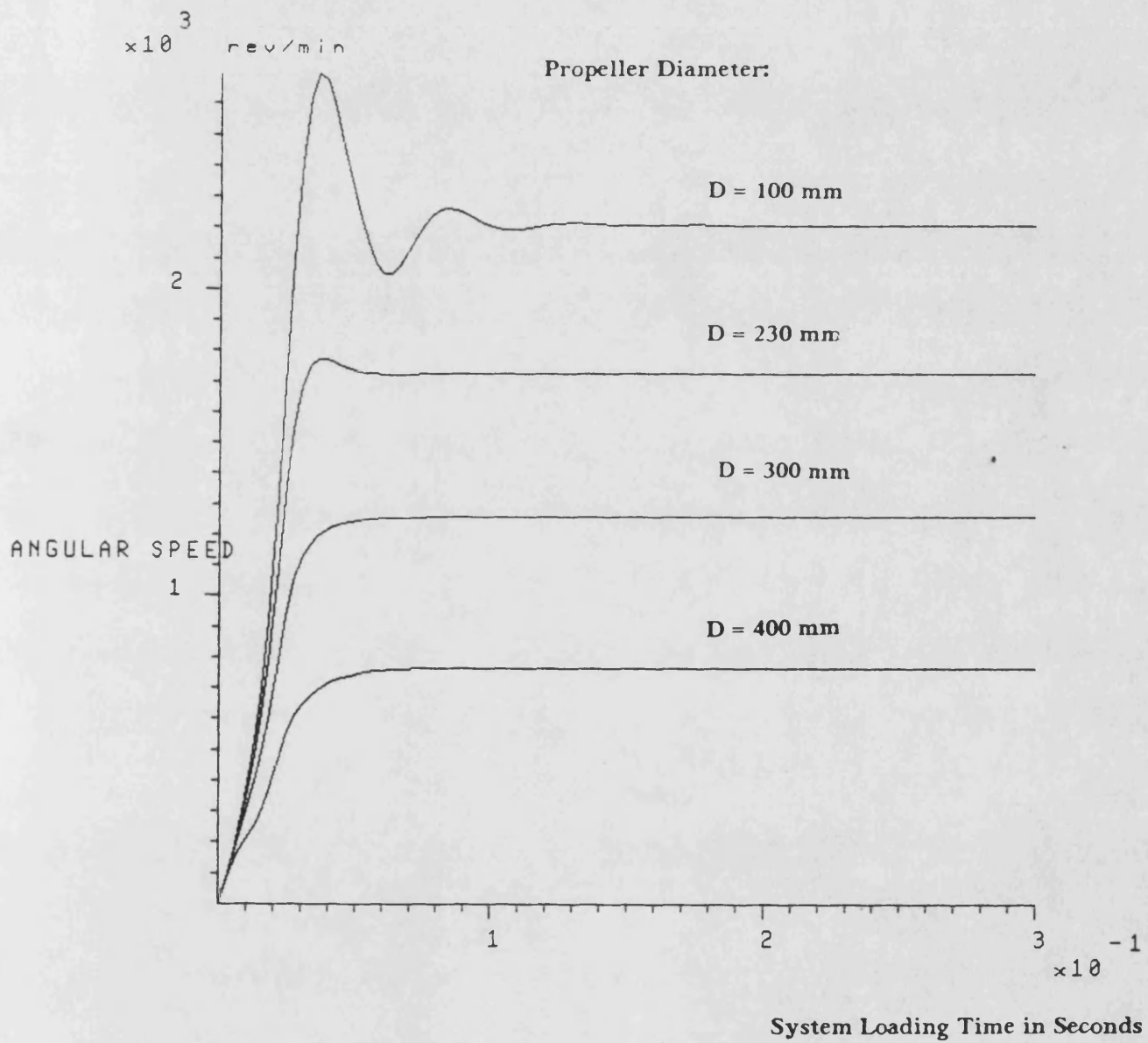
Fig. 5.18   The Effects of the Propeller Diameter on the Motor Speed
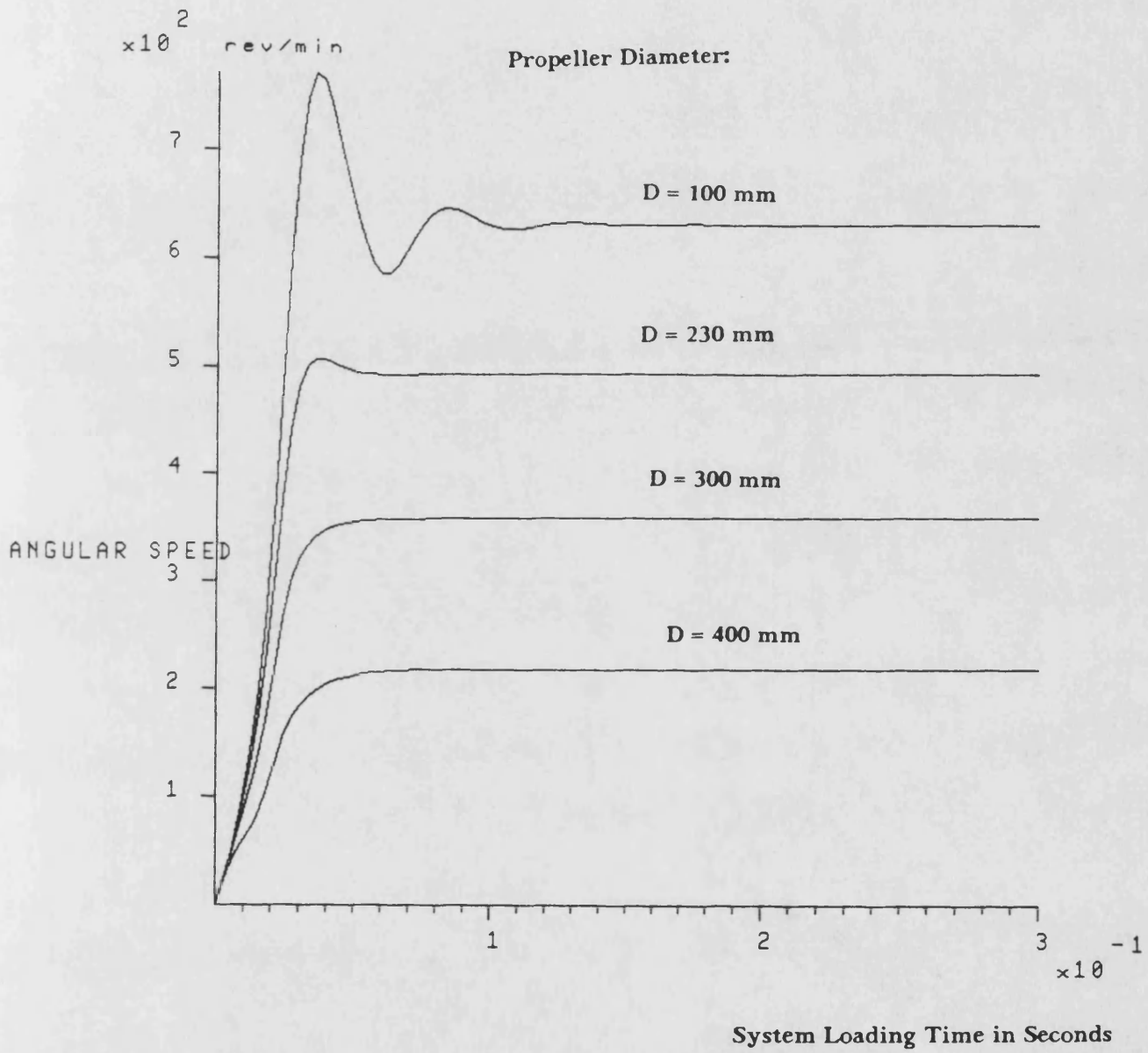
Fig. 5.19   The Effects of the Propeller Diameter on the Propeller Speed
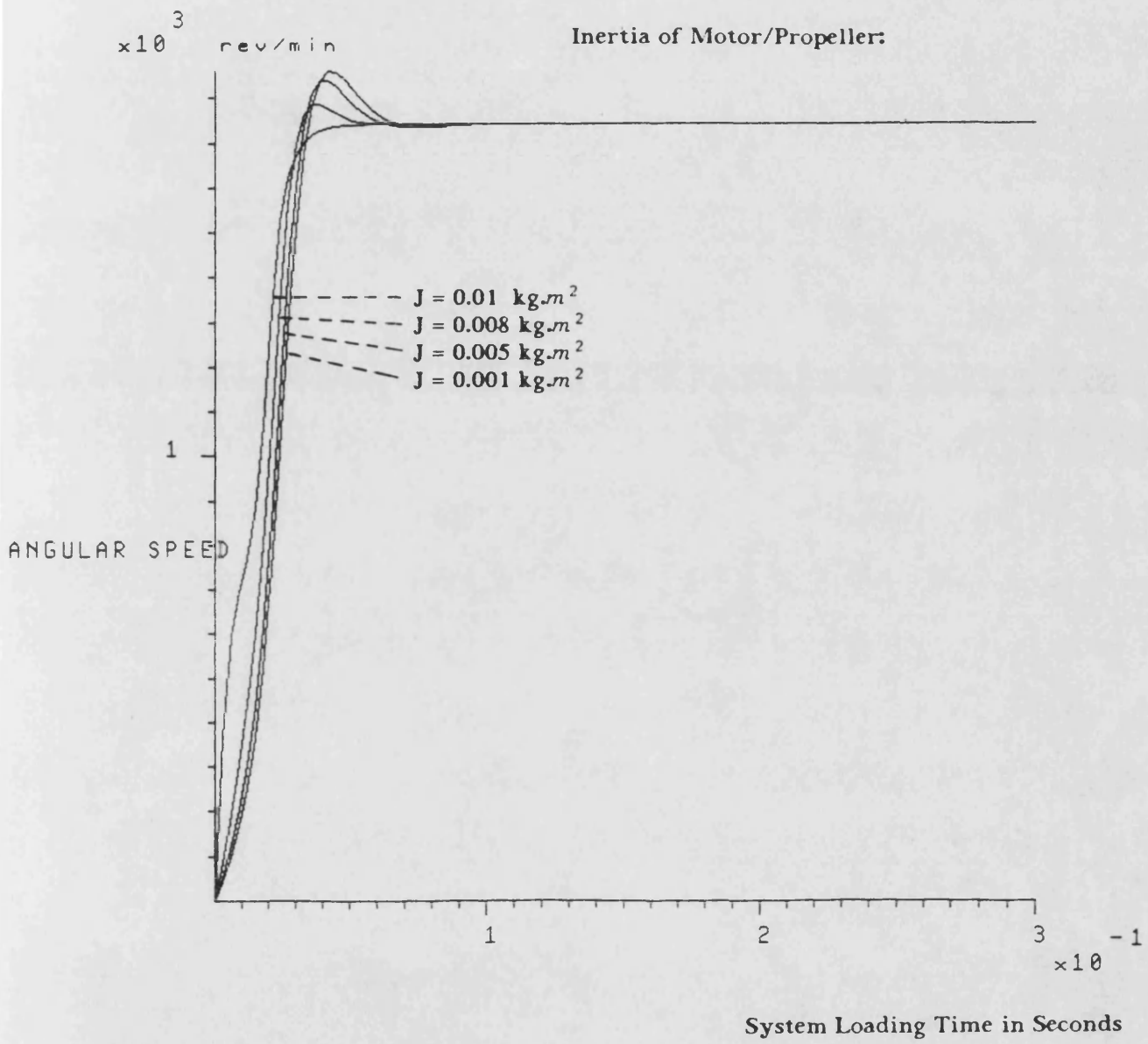
Fig. 5.20   The Effects of the Combined Inertia of the Motor/Propeller
on the Transient Motor Speed
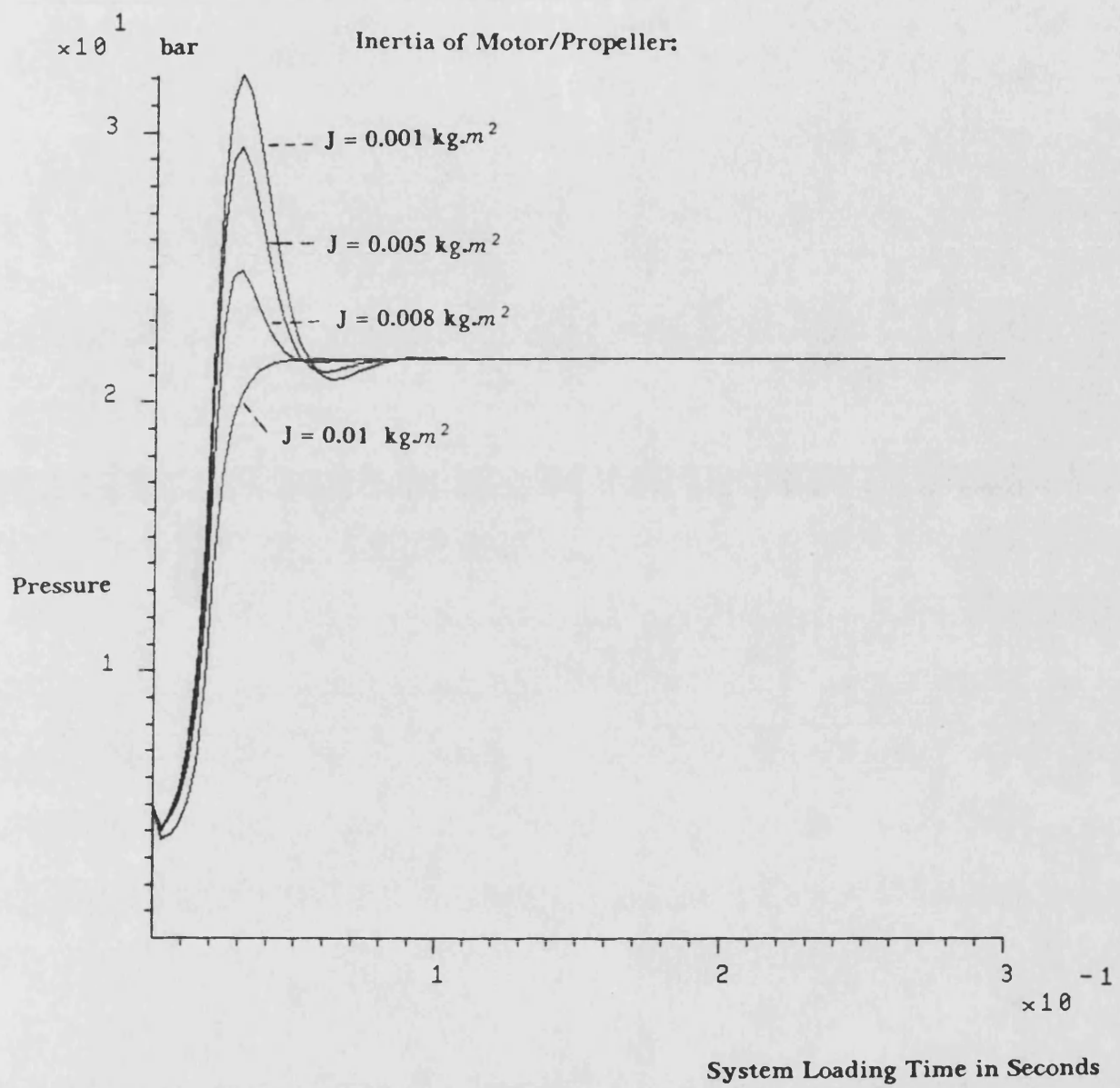
Fig. 5.21   The Effects of the Transient Motor Speed on the High Pressure
               Transients in the Partially Closed Hydrostatic Drive Boat
               Propeller System
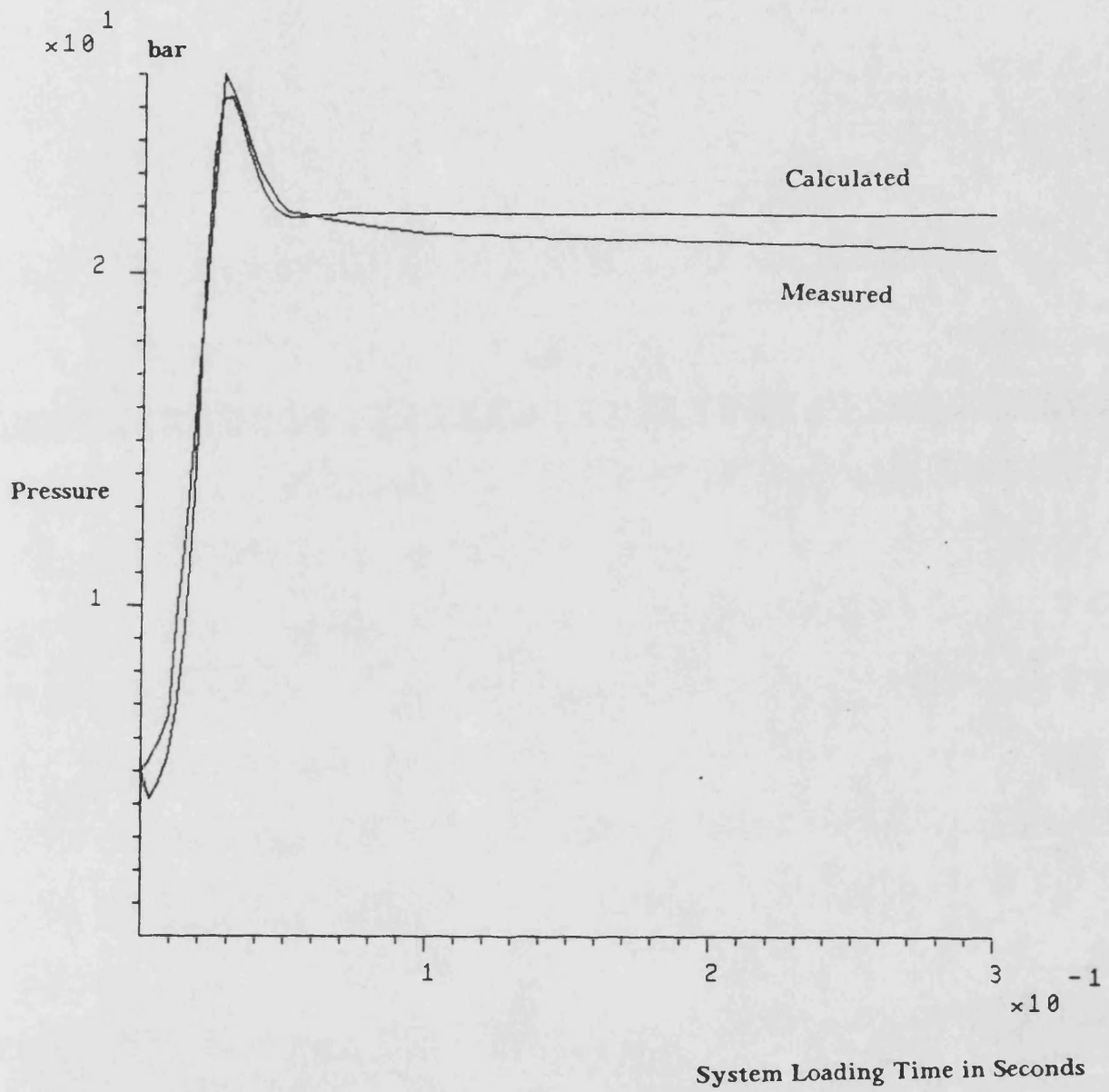
Fig. 5.22   Comparison of the Calculated and Experimental High Pressure
            Transients

$\times 10^3$ rev/min

Speed - Torque Coefficient:

$C_e = 30$

$C_e = 60$

$C_e = 90$

$C_e = 120$

2

ANGULAR SPEED

1

1   2   3 -1 $\times 10$

System Loading Time in Seconds
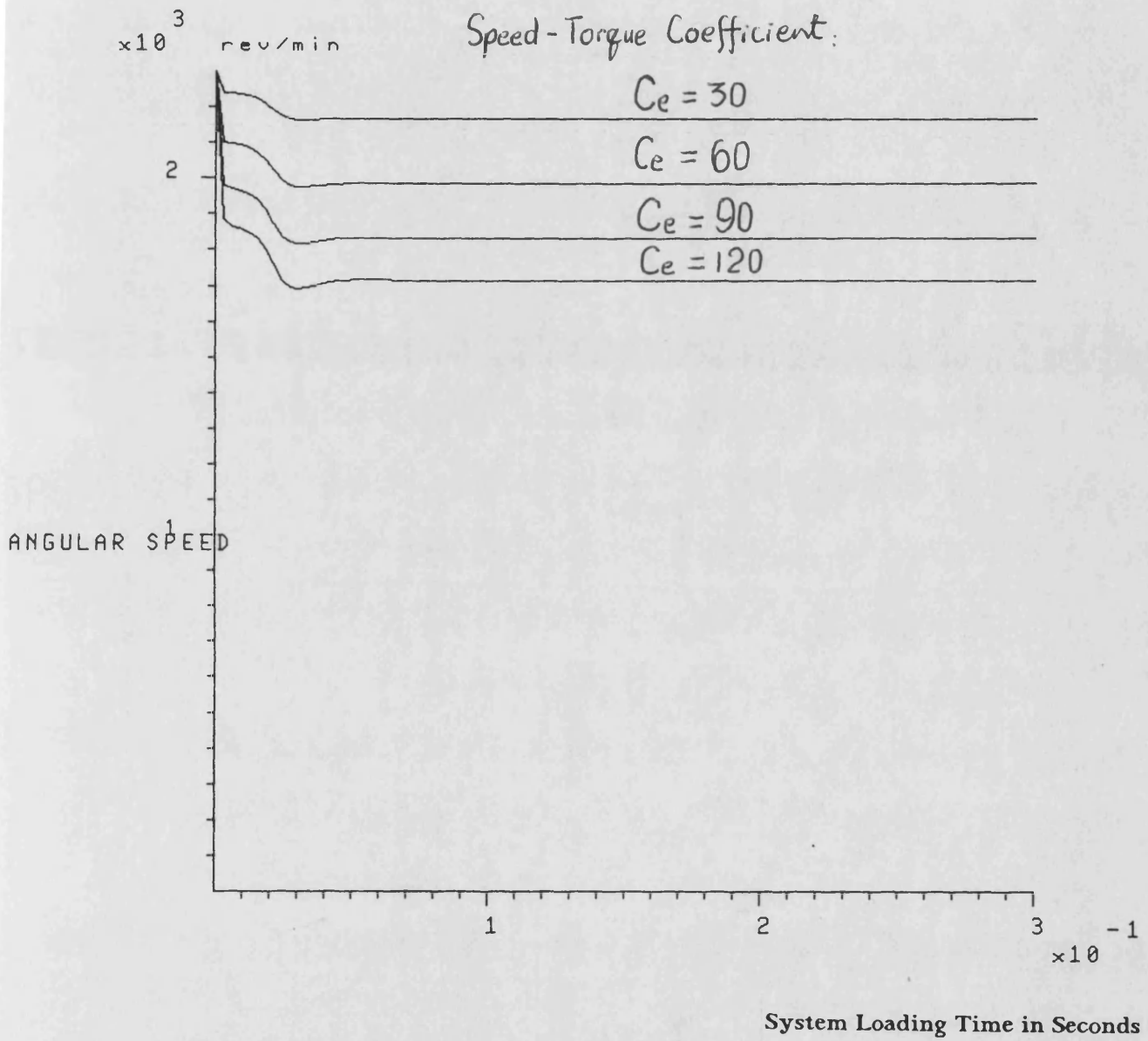
Fig. 5.23   The Effects of the Engine Speed-Torque Gradient Coefficient on the Shaft Engine Speed
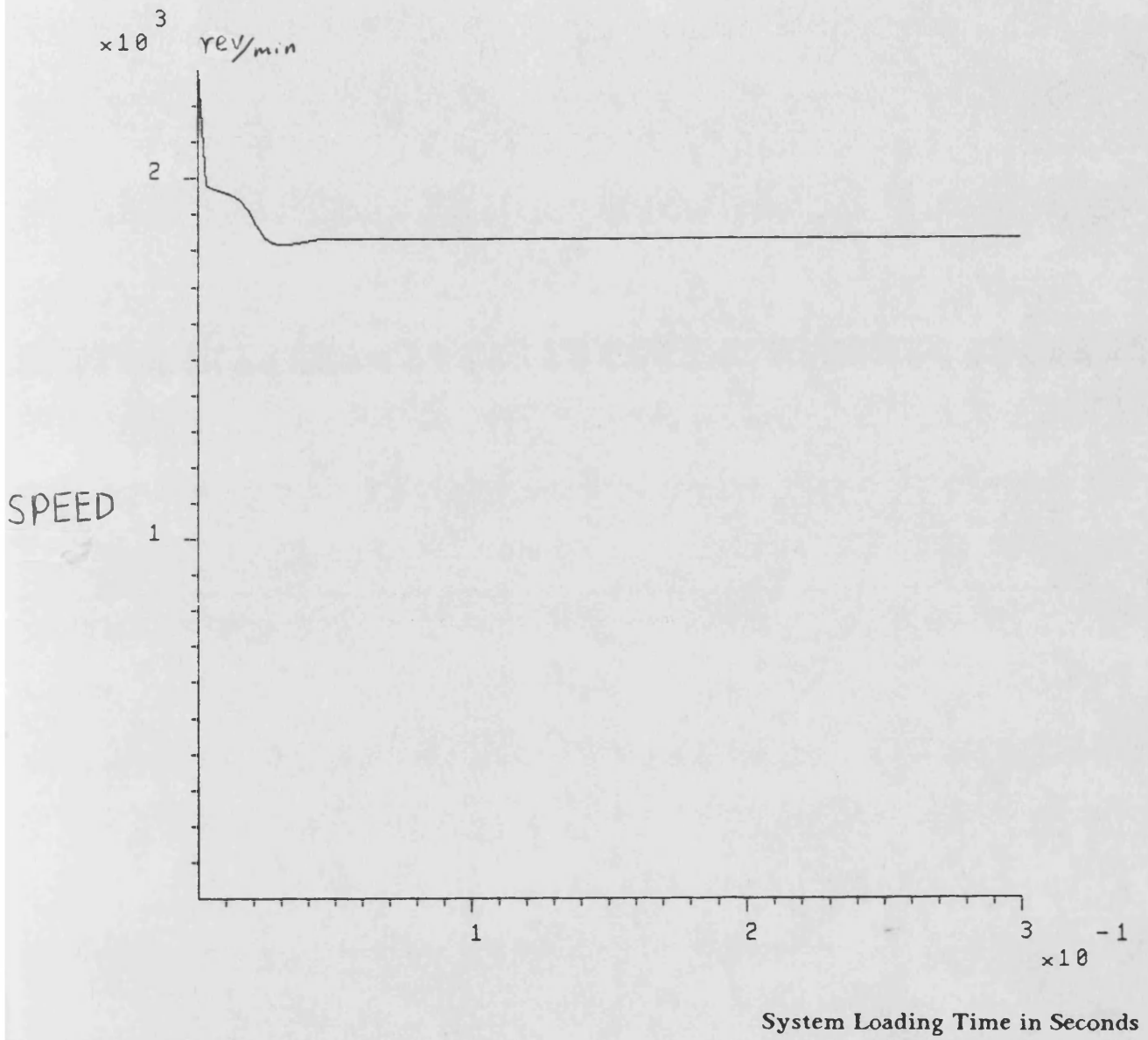
Fig. 5.24   The Effects of the Engine Speed-Torque Gradient Coefficient on the Shaft Engine Speed
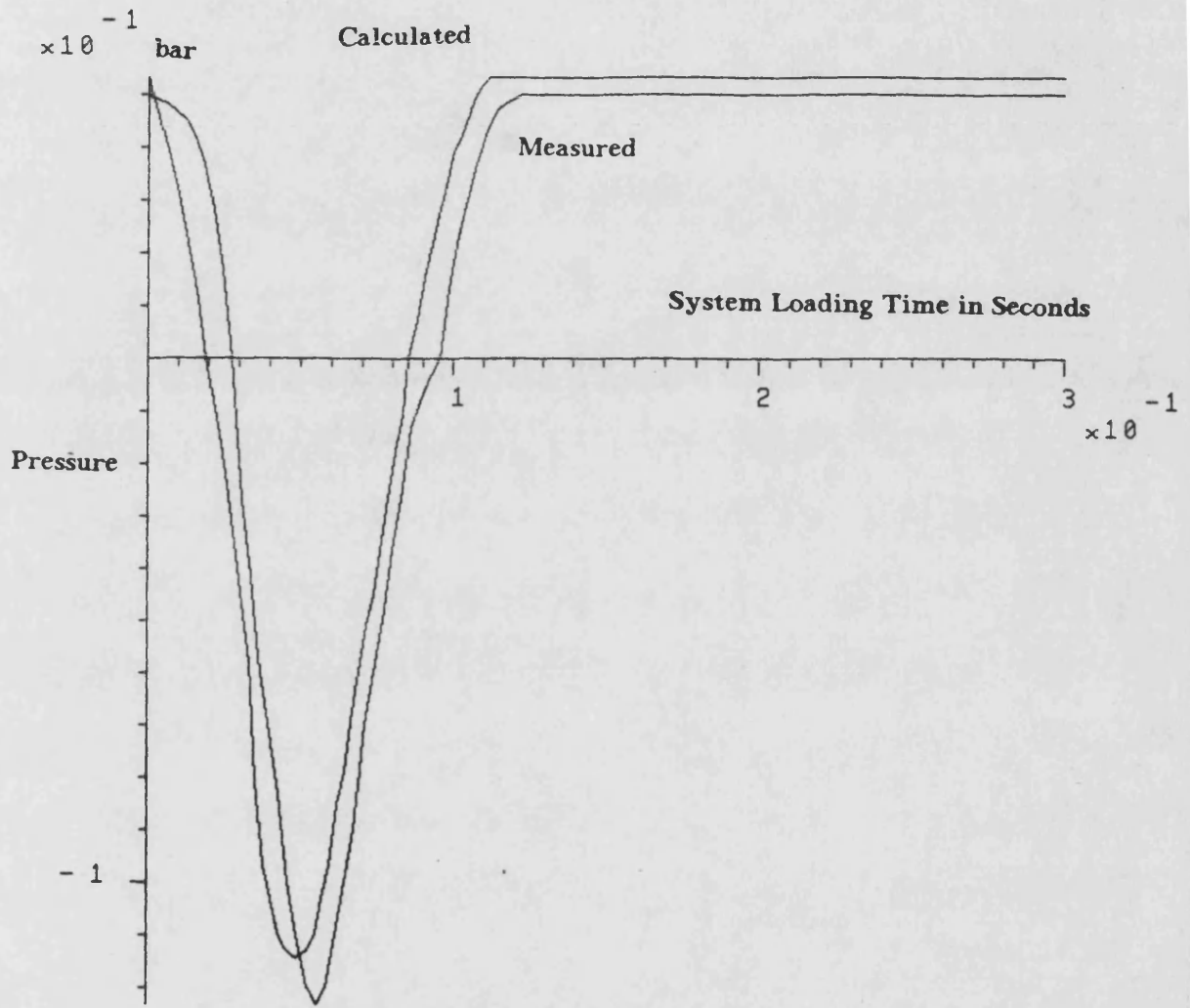
Fig. 5.25   Comparison of Simulation and Experimental Suction Pressure
            Transients

CHAPTER 6

TEMPERATURE ANALYSIS IN HYDRAULIC SYSTEMS

Introduction

6.1   The work in this chapter suggests three theoretical approaches each involving a different degree of accuracy to simulate the temperature distribution in hydraulic systems and their applications to analyse the temperature distribution in a hydrostatic drive propeller system. Principally this work is concerned with establishing theoretical approaches for temperature analysis from a fundamental consideration of major thermodynamic processes under unsteady state conditions in a hydraulic system, but consideration is also given to the implementation of the theoretical approaches developed in the HASP software package with the aim of allowing the modelling of temperature in other more complex hydraulic systems. In order to provide a comprehensive understanding of thermodynamic processes in the hydraulic systems, the approaches are applied to analyse the temperature performance in a hydrostatic drive propeller system. It includes experimental work to correlate the simulations with the values found in practice. Power dissipation inevitably occurs in any a hydraulic system due to inefficiencies of the system components and the losses of pressure and torque. The power losses will be converted into heat energy which causes the variations of the system temperatures. In a practical hydraulic system, the fluid temperature differs from the wall temperatures of the pipes in the loop due to the heat flow transferred to the loop surroundings during the system operation.

6.2   **Previous Work**   Thermal transients in a hydraulic system are a fundamental aspect of system performance and generally are concerned with thermodynamic processes which are associated with the power losses converted into

heat and also heat flow transfer and losses during the system operation. Most conventional studies for temperature change in the hydraulic systems deal with steady state conditions like those given in Ref. (6.1) and (6.2), in which heat flows continuously at a uniform rate and unsteady processes are ignored due to their complexities. The transient temperatures in the hydraulic systems have been studied by Buckingham (Ref. 6.3) and Tomlinson (Ref. 6.4) but both researchers did not consider heat transfer effects, even those associated with coolers.

The following assumptions were usually made in the previous studies:

(1).   both the system inside and outside pipe wall temperature
        is the same as the fluid temperature;

(2).   the heat generated by the pressure losses due to pipe
        friction is neglected.

Assumptions (2) is acceptable if the accuracy of the theoretical prediction is not critical. However, assumption (1) implies that the heat transfer process in which the rate of heat transferred by conduction and convection through the system pipe walls has been ignored. This assumption may lead to errors in predicting fluid temperature in a practical hydraulic system.

6.3   **Suggested Approaches**   1) In order to give an appropriate theoretical representation to the temperatures in a hydraulic system at any instant in time, one simple approach for temperature analysis is proposed in this thesis to consider a system (such as the unboosted closed hydraulic system) as a closed thermal system with an uniform fluid and pipe wall temperatures. In this approach the difference between the fluid and pipe wall temperatures has been taken into account so that the transient difference in the heat flows transferred from fluid to the pipe wall and from the pipe wall to the system surrounding atmosphere can be estimated to predict transient behaviour of outside pipe wall temperature. This theoretical approach has been improved to include the differences in pipe wall temperatures at the various parts of the system pipelines due to different pipe wall materials.

2) On the basis of the simple approach, a further study has been carried out

to consider a hydraulic system as two distinct temperature regions. In such an approach, the system main loop is considered as an open thermal system where an uniform temperature is assumed to represent the loop fluid temperature, while the reservoir is another open thermal system. Hence, the fluid energy exchanges between the loop and the reservoir can be investigated and the theoretical fluid temperatures in the loop and reservoir can be predicted separately.

3) In a practical hydraulic system, the differences exist between fluid temperatures of the system pipelines in the main loop due to the difference in heat generation in the different parts of the system. A more accurate approach for analysis of the thermodynamic processes in a hydraulic system has been suggested in this thesis. The principle of the analytic approach proposed is to consider the hydraulic system loop as a series of open thermal systems with a constant fluid temperature in each section of the system so that the difference between fluid temperatures in the loop of the system can be estimated.

6.4 An appropriate theoretical derivation for thermodynamic analysis in a hydraulic system is not immediately available in the literature. A certain degree of confusion   existed among previous hydraulic thermal transient analysts. Some of intermediate equations in the conventional thermodynamic theories have been misquoted and used as widely applied laws. In order to establish the suggested approaches, it is necessary to give a brief summary of some fundamental thermodynamic concepts. On the basis of this, the theory of the First Law Applied to an open thermal system has been used to derive a group of equations to analyse basic thermodynamic processes associated with an open pipe section of hydraulic systems. This set of equations can be then applied to construct the proposed approaches for temperature analysis in hydraulic systems.

Fundamentals of the Suggested Approaches for Thermodynamic
Analysis in a Hydraulic System

6.5 Closed and Open Thermal Systems   The First Law of Thermodynamics is
generally applied to a closed thermal system where no mass flow crosses the
boundary. However, in many engineering applications it is difficult to separate a
mass of the working substance and treat it as a closed thermal system. In such
systems, we are concerned with a fixed region or volume in space which has
material flowing through it. Such a system is defined as an open thermal system.
Gillespie and Coe. (Ref. 6.5) suggested that it is possible to regard the continuous-
flow process as a series of non-flow processes undergone by an imaginary closed
system. This concept is widely accepted and illustrated in Fig. 6.1. The boundary of
the closed system includes the fluid contained in the open system at any instant,
plus a portion of the fluid entering and leaving the system. The features of the open
system should be noted:

(1).   the boundary of the open system need not have a physical
       form any more than the boundary of the closed system but
       may be drawn in any convenient position;

(2).   there are two separate concepts of mass to be considered:

       (a).   the mass or masses crossing the open system
              boundary;

       (b).   the mass within the open system boundary at any
              instant of time.

In this way, continuous flow may be regarded as a succession of these non-
flow processes, carried out for every element of fluid entering the open system.
Hence it now becomes possible to apply the energy equation which has been
developed from a study of closed system. The study of the First Law applied to a
flow process is well documented by Wallace and Linning (Ref. 6.6) and by Look
and Sau-er (Ref. 6.7).

6.6 The First Law Applied to An Open System

A review of the general concepts give below, after which they will be applied to a length of pipe as a component of a hydraulic system. Fig. 6.2 shows an open system filled with any fluid (compressible or incompressible). The thermodynamic and mechanical states of the element of fluid mass δM_1, which is about to enter the open system, may be assumed to be known. The random molecular energy is U_1, and if the element is moving with a velocity C_1 at a height Z_1 above the reference level, the inlet flow energy of the mass δM_1 is

$$\Delta E_{in} = U_1 + (KE)_{in} + (PE)_{in} \qquad \ldots \ldots (6.1)$$

.

where U_1 = internal energy

$(KE)_{in} = \dfrac{1}{2}\delta M_1 C_1^2$ = kinetic energy

$(PE)_{in} = \delta M_1 g Z_1$ = potential energy

If the element is small enough for the thermodynamic properties to be uniform within it, the above equation becomes

$$\delta E_{in} = \delta M_1 (u_1 + \frac{1}{2}C_1^2 + gZ_1) \qquad \ldots \ldots (6.2)$$

The mass element entering δM_1 will perform flow work on the system, the work done on the flow element is given by $\delta W_{flow} = p_1 \delta V$, where δV_1 is the volume of the element of fluid about to enter the system. Using the definition of the specific volume, ie. $v_1 = \dfrac{\delta V_1}{\delta M_1}$, the constitutes work done by the imaginary fluid element on the system given by

$$(W_{(flow)})_{in} = \delta M_1 (p_1 v_1) \qquad \ldots \ldots (6.3)$$

Hence, the total flow energy associated with δM_1 may be obtained by addition of Equation (6.2) and (6.3).

$$\delta E_{inflow} = \delta M_1(u_1 + \frac{1}{2}C_1^2 + gZ_1 + p_1 v_1) \qquad \ldots \ldots (6.4)$$

Since the combination of $(u + pv)$ is defined as the enthalpy h, the above becomes

$$\delta E_{inflow} = \delta M_1(h_1 + \frac{1}{2}C_1^2 + gZ_1) \qquad \ldots \ldots (6.5)$$

Similarly for outflow element, we have

$$\delta E_{outflow} = \delta M_2(h_2 + \frac{1}{2}C_2^2 + gZ_2) \qquad \ldots \ldots (6.6)$$

For a time interval δt, δQ units of energy are transferred to the system as heat, and that δW units of energy are transferred to the surroundings as work. The non-flow energy no longer applies to the open system and it must be extended to include energy transfers associated with matter crossing the boundary of the system, ie.

$$\delta Q - \delta W = \delta E + \delta E_{(outflow)} - \delta E_{(inflow)} \qquad \ldots \ldots (6.7)$$

In the above, the open system possess a quantity of internal energy E which can be defined as

$$E = M(h + \frac{1}{2}C^2 + gZ) \qquad \ldots \ldots (6.8)$$

where h is the enthalpy. Substituting for Equations (6.5) and (6.6) in Equation (6.7) we have

$$\delta Q - \delta W + \delta M_1(h_1 + \frac{1}{2}C_1^2 + gZ_1)$$

$$- \delta M_2(h_2 + \frac{1}{2}C_2^2 + gZ_2) = \delta E \qquad \dots\dots (6.9)$$

Or

$$\frac{\delta Q}{\delta t} - \frac{\delta W}{\delta t} + \frac{\delta m_1}{\delta t}(h_1 + \frac{1}{2}C_1^2 + gZ_1)$$

$$- \frac{\delta m_2}{\delta t}(h_2 + \frac{1}{2}C_2^2 + gZ_2) = \frac{dE}{dt} \qquad \dots\dots (6.10)$$

When $\delta t \rightarrow 0$

$$H - W + m_1(h_1 + \frac{1}{2}C_1^2 + gZ_1)$$

$$- m_2(h_2 + \frac{1}{2}C_2^2 + gZ_2) = \frac{dE}{dt} \qquad \dots\dots (6.11)$$

where H is the heat flowrate transferred into the system, W the rate of work done to the surroundings and m_1, m_2 are the rates of mass flow.

6.7 Any particular length of pipe in a hydraulic system can be regarded as an open thermal system undergoing a thermodynamic process as shown in Fig. 6.3. The amount of work W transferred into the pipe section due to the power loss caused by the pressure loss in the pipe at each end of the pipe section will be converted into heat. The energy transfer taking place across the boundaries of the system is the heat energy H_1 which represents heat transferred from fluids to the pipe wall by the forced convection. The mass transfer occurs simultaneously with energy transfer, flow with rate of Q_1 and temperature T_{in} is entering the system while outlet flow has temperature of T_f and rate of Q_2. If an uniform fluid temperature is assumed within the open section of pipe, and the change in fluid kinetic energy and potential energy for a section of practical hydraulic pipeline are negligible, the thermodynamic flow process associated with the section of pipe can be studied by applying Equation (6.11) for open thermal system, ie.

$$W - H_1 + m_1 h_1 - m_2 h_2 = \frac{dE}{dt} \qquad \dots\dots (6.12)$$

Substituting Equation (6.8) into the above equation to define the system internal energy by ignoring its kinetic and potential energies, we write

$$W - H_1 + m_1 h_1 - m_2 h_2 = \frac{d(M_f h)}{dt} \qquad \dots\dots (6.13)$$

where M_f is the mass of fluid within the pipe section.

From the definition of specific heat, we know that the specific heat at constant volume (C_v) is defined as the heat required to raise the temperature of unit mass one degree during a reversible constant volume process, and the specific heat at constant pressure (C_p) as the heat required to raise unit mass one degree during a reversible constant pressure. These may be written as

$$C_v = (\frac{dh}{dt})_v$$

$$C_p = (\frac{dh}{dt})_p \qquad \qquad \dots\dots(6.14)$$

In our case, the effects of pressure on the internal energy is small and the heat exchange due to compression or expansion of the liquid will be ignored. Therefore a constant process is used to find the fluid enthalpy as

$$h = C_v T = C_p T \qquad \qquad \dots\dots(6.15)$$

Using the above equation in Equation (6.13), we obtain

$$W - H_1 + m_1 C_p T_{in} - m_2 C_p T_f = \frac{d(M_f C_p T_f)}{dt} \qquad \dots\dots(6.16)$$

where T_f is assumed to be the uniform fluid temperature within the pipe section. The above equation may be also written as

$$W - H_1 + m_1 C_p T_{in} - m_2 C_p T_f =$$
$$M_f C_p \frac{dT_f}{dt} + m_f C_p T_f \qquad \qquad \dots\dots(6.17)$$

In the equation above, the mass flowrate at any instant time is expressed as $m_f = m_1 - m_2$. In practice, the mass flowrate through a pipe section is generally assumed to remain as constant. Then the equation can be re-arranged as

$$M_f C_p \frac{dT_f}{dt} = W - H_1 + m_f C_p (T_{in} - T_f) \qquad \dots\dots(6.18)$$

The transient term of $M_f C_{pf} \dfrac{dT_f}{dt}$ was always ignored in the previous studies due to the only consideration of the steady state. This term, however, may be significant for the transient fluid temperature changes. Hence, the above equation is proposed

to analyse the transient fluid temperature conditions in an open section pipe of the hydraulic systems. In the above equation, the rate of heat flow H_1 transferred from fluid to the pipe wall may be defined through more intensive study.

6.8 **Heat Transfer** Heat transfer theory has been well established over years. For instance, Rogers and Mayhew (Ref. 6.8) and Adam (Ref.6.9) have given the excellent presentations regards to this subject. Here a brief summary is given for applying the theory to analyse the pipe wall temperature.

Heat is a form of energy which is transferred from one plate to another by a temperature difference. In general there are three ways in which heat may be transferred:

1. Conduction   is the transfer of heat from one part of a
substance to another part of the same substance without
appreciable displacement of the molecules forming the
substance.

2. Convection   is the transfer of heat within a fluid by the mixing
of one portion of the fluid with another. The movement of the
fluid may be entirely due to density gradients resulting from
the temperature gradients as in natural convection, or the
motion may be produced by mechanical means, as in forced
convection. The heat transfer between a fluid and a solid
boundary is partly by conduction and partly by convection, but
heat transfer by conduction can be neglected compared with heat
transfer by convection.

3. Radiation   All matter at a temperature above absolute zero emits
energy in the form of electromagnetic waves. Radiant energy
does not require the existence of an intervening medium for
its propagation, and will pass through a vacuum.

All three forms of heat transfer are involved to some extent in any practical case and it is generally possible to calculate the heat transfer by each mode separately and then sum up the results. In this way a complex problem can be resolved, and the relative importance of the various modes of heat transfer can be

assessed. With the calculations done by a digital computer, a study of unsteady state heat transfer flow H_1 in the open thermal system of the pipe section described in the Section 6.7 can be carried out.

In the work below two dimensional heat transfer, ie. heat transfer radially through the pipe wall material only is discussed, the effects of conduction along the pipe are ignored.

6.9   Forced Convection   The study of heat transfer by forced convection is usually concerned with the calculation of rates of heat exchange between fluid and solid boundaries. Because the liquid is flowing past the inside wall, a condition of forced convection applies to heat transfer across the wall as in Fig. 6.4, which shows an enlarged view of the open thermal system of a pipe section containing the heat transfer at any instant time. H_1 expresses the rate of heat transferred from moving fluid to the pipe wall due to the forced convection arising from the movement of the fluid. It is well known that the transfer of heat by forced convection can be written as

$$H_1 = h_f A_1 (T_f - T_1) \qquad\qquad \ldots\ldots(6.19)$$

where A_1 is the inside surface area of the pipe section. In the above, the forced convection heat transfer coefficient, h_f, depends on the Nusselt number $Nu = \dfrac{hL}{k}$, where L is the characteristic linear dimension, k thermal conductivity of fluid.

The value of Nusselt number for the forced convection in fully developed laminar flow through a tube is given in Ref. (6.8) as follows

(1). $Nu = 3.65$, for laminar flow in a tube at constant wall temperature boundary condition;

(2). $Nu = 4.36$, for laminar flow in a tube at constant heat flux which is equivalent to constant temperature gradient at the wall.

As the case being investigated is a tube which is heated by a hot flow passing

through it. case (2) applies in evaluating heat transfer coefficient by forced convection at inner surface of pipe wall.

When the flow is turbulent. Reynolds analogy and Dimensional analysis can be applied. The conclusions of these analysis may be summarised by introducing the Nusselt number, Nu, where

$$Nu = KF\left\{(Pr).(Re)\right\} \qquad \ldots \ldots (6.20)$$

In above the Prandtl number Pr and the Reynolds number Re are defined as Pr = $\frac{C\mu}{k}$ and Re = $\frac{\rho Cl}{\mu}$. (C the fluid velocity). Experiments can be performed in order to evaluate K and to determine the function F. From such experiments the Nusselt number for turbulent flow through tubes has been given in Ref. (6.8) as

$$Nu = 0.0243 \ Re^{0.8} \ Pr^{0.4}.$$

6.10 **Natural Convection and Radiation** The heat transfer from the outer pipe wall to atmosphere. H_2. involves both natural convection and radiation. The heat transferred by radiation can be determined by the Stefan-Boltzmann Law. It is found that the emissive power of a black body is directly proportional to the fourth power of its absolute temperature. i.e.

$$E_B = \sigma T^4 \qquad \ldots \ldots (6.21)$$

The energy emitted by a non-black body is given as

$$E = \epsilon\sigma T^4 \qquad \ldots \ldots (6.22)$$

where the Stefan-Boltzmann constant σ has the value of 56.7×10^{-9} in $W/m^2.K^4$ and ϵ is the emissivity of the body. Similarly, the energy emitted by the black surroundings is expressed as

$$E_B = \sigma T^4 \qquad\qquad\qquad \dots\dots (6.23)$$

Also it is noted that the energy emitting from one body like the wall of a pipe section is completely absorbed by the surroundings. Thus the heat transferred from the body to its surroundings is given as

$$H = \epsilon\sigma A_2(T_2^4 - T_a^4) \qquad\qquad \dots\dots (6.24)$$

where A_2 is the outside surface area of the pipe section.

Hence, the heat flow transferred from the pipe wall to its surrounding atmosphere by natural convection and radiation, H_2, can be determined from

$$H_2 = h_a A_2(T_2 - T_a) + \epsilon\sigma A_2(T_2^4 - T_a^4) \qquad \dots\dots (6.25)$$

where h_a is the heat transfer coefficient of natural convection, T_2 the uniform outside pipe wall temperature, T_a the atmospheric temperature surrounding to the pipe section and the value of ϵ for commonly used pipe wall material in hydraulics is given in Table 6.1 taken from Ref. (6.10). If the variation of Ta is assumed to be insignificant comparing to other factors, then T_a can be regarded as a constant value during the system operation. The heat transfer coefficient by natural convection, h_a, can be similarly found from experiment. Experimental values for h_a are to be found in various handbooks. For instance, Ref. (6.8) gives a relation for a natural convection for a horizontal pipe as

$$h_a = \begin{cases} 1.32(\dfrac{\theta}{d})^{0.25} & when \ 10^4 < Gr < 10^9 \\ 1.25\theta^{\frac{1}{3}} & when \ 10^9 < Gr < 10^{12} \end{cases} \qquad \dots \dots (6.26)$$

In the above equation, h_a is in W/m.K, θ is the temperature difference in K, and d is in m. The Grashof number Gr is defined as $Gr = \dfrac{gL^3\beta\theta}{\nu^2}$, where g the gravitational acceleration, L linear dimension, β the coefficient of cubical expansion and ν kinematic viscosity. Simplified formulae for natural convection for both the laminar and turbulent range in the different configurations are taken from Fig. 22.16 of Ref. (6.8) and summarised in Table 6.2.

6.11 Pipe Wall Temperature In the steady state, the heat flow transferred into the pipe wall, H_1, must be equal to the heat transferred out, H_2. Under the unsteady condition, the difference between H_1 and H_2 must be equal to the increment of the pipe wall internal energy. In other words, if the pipe wall is regarded as a closed thermal system, the heat flow supplied to the pipe wall must be equal to the gain in internal energy. Hence, we have

$$H_1 - H_2 = \frac{dE}{dt} \qquad \dots \dots (6.27)$$

From Equation (6.8) and (6.15), we obtain

$$\frac{dE}{dt} = \frac{d(M_p C_p T_2)}{dt}$$

where the inner and outside surface pipe wall temperatures, T_1 and T_2, are assumed to be uniform and both change at the same rate. Thus, Equation (6.27) becomes

$$M_p C_p \frac{dT_2}{dt} = H_1 - H_2 \qquad \dots \dots (6.28)$$

where the constant mass M_p and the specific heat C_p of the pipe wall material are

noted.

The values of C_p for usual pipe wall materials and oil used in hydraulics are listed in Table 6.3 quoted from Ref. (6.10).

If the rate of heat flow through the pipe wall is assumed to be transferred under one dimensional conduction, then the heat flows radially through the pipe wall can be expressed by   Fourier's Law, i.e.,

$$H = \frac{kA_m(T_1 - T_2)}{R_2 - R_1} \qquad \dots\dots(6.29)$$

where k is the thermal conductivity of the pipe wall in W/m.K, the values of k for often used pipe materials in hydraulics can be also obtained from Ref. (6.10) and a brief summary is given in Table 6.4. In the above equation, A_m is the logarithmic mean area and can be calculated from

$$A_m = \frac{2(R_2 - R_1)L}{\ln\dfrac{R_2}{R_1}} = \frac{A_2 - A_1}{\ln\dfrac{R_2}{R_1}} \qquad \dots\dots(6.30)$$

where R_1 and R_2 are the internal and external radiuses and L is the length of the pipe section respectively.

This rate of heat transferred through the pipe wall by conduction should be equal to the rate of heat transferred from fluid to the pipe wall by forced convection at the boundary of the inner surface of the pipe section. From Equation (6.19) and (6.29), we have

$$H_1 = h_f A_1(T_f - T_1) = \frac{kA_m(T_1 - T_2)}{R_2 - R_1} \qquad \dots\dots(6.31)$$

Re-arrange the above equation, the inner pipe wall temperature can be written as

$$T_1 = \frac{h_f A_1 T_f + \frac{kA_m}{R_2 - R_1} T_2}{h_f A_1 + \frac{kA_m}{R_2 - R_1}}$$

$$\dots\dots (6.32)$$

In summary, the fluid temperature and pipe wall temperature in a section of pipe at any instant time can be determined by resolving the following simultaneous equations,

$$h_a = 1.32 \left(\frac{\theta}{d}\right)^{0.25}$$

$$\dots\dots (6.33)$$

$$H_2 = h_a A_2 (T_2 - T_a) + \epsilon \sigma A_2 (T_2^4 - T_a^4)$$

$$\dots\dots (6.34)$$

$$H_1 = h_f A_1 (T_f - T_1)$$

$$\dots\dots (6.35)$$

$$T_1 = \frac{h_f A_1 T_f + \frac{kA_m}{R_2 - R_1} T_2}{h_f A_1 + \frac{kA_m}{R_2 - R_1}}$$

$$\dots\dots (6.36)$$

$$\frac{dT_2}{dt} = \frac{H_1 - H_2}{M_p C_{pp}}$$

$$\dots\dots (6.37)$$

$$\frac{dT_f}{dt} = \frac{W - H_1 + m_f C_{pf} (T_{in} - T_f)}{M_f C_{pf}}$$

$$\dots\dots (6.38)$$

where C_{pp} is the specific heat of pipe wall, C_{pf} the specific heat of fluid, ϵ the emissivity and k the thermal conductivity of pipe wall material. If the initial conditions are given, these equations can be used to calculate the fluid temperature, T_f, and the pipe wall temperature, T_2, by applying the numerical integration techniques which are widely used in computer simulation. Hence, the group of

equations (6.33) to (6.37) has been used to develop a HASP pipe temperature model PICH and a fluid temperature model FPGH of a pipe section is developed based upon Equation (6.38). The detailed descriptions of PICH and FPGH are given in Appendix II.

A Simple Theoretical Approach for Temperature Analysis in
an Unboosted Closed Hydraulic System

6.12 As introduced in Section 6.3 a simple approach for thermodynamic analysis in an unboosted closed hydraulic system has been suggested in this thesis. The temperature performance in the unboosted hydrostatic drive propeller system as shown Fig. 6.5 is of particular importance. This is because the decision, whether a cooler is needed or what size of the cooler is required, is critical because of space and power limitation. Since no mass flow exchanges occur within the system loop (not even with the reservoir under the steady state flow and pressure conditions), temperatures in such a system can be analysed by applying the simple approach in which the unboosted closed hydraulic system is considered as a closed thermal system with an uniform fluid and pipe wall temperatures. The power loss generated during the system operation due to inefficiencies of the system components and the losses of pressure and torque will inevitably be converted into heat energy which has to be entirely dissipated in the cooler if fitted or through the system pipelines to the surrounding atmosphere.

The thermal transient equations established before for an open thermal system of a pipe section can be applied to describe the thermal transients of a closed thermal system. The transient fluid temperature in a closed thermal system can be expressed by applying Equation (6.38) with the deletion of the flow energy term $m_f C_{pf} (T_{in} - T_f)$, and the transient inside and outside pipe wall temperatures of the system can be predicted using Equation (6.33) to (6.37). Because of the linkage requirements are now different, a further HASP model is needed to be developed. This is called FP3H and is also given in Appendix II.

An improvement may be made by considering the difference in the pipe wall temperatures of the closed thermal system due to the different pipe wall materials at various parts of the system pipelines. In such a case, Equation (6.38) becomes

$$\frac{dT_f}{dt} = \frac{W - \sum H_1}{M_f C_{pf}}$$

$$\dots\dots\ (6.39)$$

where $\sum H_1$ is the total heat flow losses from fluid to the different parts of the system pipelines. The above equation has been used to develop a fluid temperature model FPUH of a closed thermal system with an uniform fluid temperature. The detailed description of FPUH is documented in Appendix II. The same set of equations as Equation (6.33) to (6.37) in the pipe wall temperature model PICH can be used to calculate the transient pipe wall temperature in each section of pipeline of the system with the same type of material. Hence, the total heat flow losses $\sum H_1$ through the pipe wall to the system surrounding atmosphere can be found by using a lately developed power sum model POOH to add together the heat flow loss in each section of the pipeline with the same type of pipe wall material. In this way, the assumed uniform temperature of fluids in the system can be calculated using FPUH once the total power losses generated during the system operation has been found. In the models FPGH, FP3H, FPUH and PICH, the user is asked to supply the various heat transfer coefficients. The detail of these input parameters will be discussed in the later simulation sections.

6.13 The Calculation of Power losses in Hydraulic Systems

The power losses in hydraulic systems are usually generated by the mechanical and volumetric inefficiencies of the components such as pumps and motors. Losses are also originated from valves with pressure losses across the main flow paths. In addition, the power losses are also caused by pressure losses in the system pipelines due to pipe friction.

When the power loss generated by a pump is examined closely, the pump power loss can be divided into the flow slip loss, the pressure dependent and speed dependent torque losses. Values for these have been found by McCandlish and Dorey (Ref. 3.16). From an intensive study of the mathematical modelling of hydrostatic pumps and motors, their mathematical equations and corresponding coefficients proposed on the basis of test results have been converted into a HASP hydraulic pump-motor unit model, HUJT, in Ref. 6.11. This model was modified by the author to model gear pumps without external leakage. The modified gear pump model is named as PUAH and documented in Appendix II. When the pump power loss dissipation process is considered, it is difficult to estimate the accurate proportion of the pump power loss which is converted into heat energy of the fluid or dissipated directly through the pump body to the surrounding atmosphere.

Under the normal pump working conditions, from a wide range of results calculated in PUAH, it was found that the pump power loss caused by internal flow slip loss is a predominant factor compared to the loss caused by pressure dependent and speed dependent viscous losses. In the work discussed in this thesis it has been assumed that the mechanical losses caused by pressure dependent and speed dependent torque losses are dissipated directly through the pump body and the leakage loss converted into heat in the fluid. The same assumption applies to evaluate the power losses caused by the internal and external slip losses of hydraulic gear motors which are calculated by the equivalent model MOAH documented in Appendix II.

A similar assumption is applied to determine the power loss generated by the pressure losses across the various hydraulic valves. When a fluid with rate of Q passes through a valve with a pressure gradient Δp, the power loss caused by the fluid viscous loss is assumed to be dissipated through the valve body to atmosphere, while the power converted into fluid heat energy is given by

$$W = Q \, \Delta p \qquad\qquad \ldots\ldots (6.40)$$

For instance, the above equation can be used to calculate the power loss caused by the flow through an orifice restrictor valve. A orifice model with its power loss calculation OR3H is described and documented in Appendix II. In addition, the power losses in the hydraulic system pipelines caused by the pressure drops due to pipe frictions can be estimated by lumping the losses into the orifice model OR3H.

An Analytical Approach for Temperature Analysis in
a Hydraulic System with the Use of Reservoir

6.14   The simple approach described in Section 6.12 only deals with unboosted closed hydraulic systems. When a reservoir is used in a hydraulic system, as in the conventional open and closed or partially closed hydraulic systems, the system no longer can be regarded as a closed thermal system because of the flow energy transfer between the fluids in the loop and in the reservoir. The fluid in the loop is in general considered at a different temperature to the fluid in the reservoir. If the loop and reservoir fluid temperatures are assumed to be uniform, the hydraulic system may be considered as two open thermal systems: the loop and the reservoir.

For the open thermal system of the loop, the transient fluid temperature can be predicted by applying Equation (6.38), ie.

$$\frac{dT_f}{dt} = \frac{\sum W - \sum H_1 + m_f \, C_{pf} \, (T_{in} - T_f)}{M_f \, C_{pf}} \qquad \ldots \ldots (6.41)$$

In the above, $\sum W$ is the system total power losses, $\sum H_1$ the total heat flow transferred from fluid to the pipe walls, M_f the total the mass of fluid in the system loop, m_1 the mass flowrate exchanges between the loop and the reservoir, T_{in} the uniform reservoir transient fluid temperature and T_f the uniform loop transient fluid temperature. The above equation has been used to set up a HASP fluid temperature model FPOH of the hydraulic system loop and its detailed description is documented in Appendix II.

A particular example is given for temperature predictions of the partially closed hydrostatic drive propeller system in Fig. 6.6, the components power losses can be calculated separately using PUAH, MOAH and OR3H, then the system total power loss $\sum W$ can be found using a power sum model POOH. A similar procedure can be used to obtain $\sum H_1$, the total heat flow transferred from fluid to atmosphere through the system various pipelines. The heat flow transfer H_1 for each section of the pipe with the same wall material can be calculated using a pipe temperature model PICH, the next step is to sum up H_1 by using a POOH. The mass flowrate of

m_f can be given by ρQ_{net} where Q_{net} is the exchange flowrate between the reservoir and the loop. In order to find a appropriate theoretical value of the loop fluid temperature, a reservoir temperature model is necessitated to acquire the uniform fluid temperature in the reservoir.

6.15 Reservoir Temperatures   In practice, the fluid and wall temperatures in a reservoir are different from one specific point to another depending on its position related to the ports of the inlet and outlet pipelines, but these temperature differences are relatively small, so fluid temperature and the reservoir wall temperature may be assumed to be uniform. When the flow in the reservoir is considered to be an open thermal system as shown in Fig. 6.7, fluid temperature in the reservoir can be obtained from the calculations of the flow energy and heat flow transferred to the reservoir walls, i.e.

$$\frac{dT_f}{dt} = \frac{W + m_1 C_{pf} T_{in\,1} + m_2 C_{pf} T_{in\,2} - m_3 C_{pf} T_f - H_1 - H_2 - H_3}{M_f C_{pf}} \qquad \ldots \ldots (6.42)$$

In the above equation, W is the power loss caused by the external slip loss of the motor and also the pressure loss across the orifice A in the flow line to the reservoir. m_1 and m_2 are the mass flowrates of the fluid into the reservoir while m_3 is the mass flowrate of the fluid flow out the reservoir to the system loop. H_1 is the heat flow transferred from fluids to the four side vertical reservoir walls by one dimensional conduction. H_2 the heat flow conducted through the horizontal bottom of the reservoir wall and H_3 the heat flow transferred from the surface of fluids in the reservoir to atmosphere by free convection.

If the inner surface reservoir wall temperature is assumed to be equal to fluid temperature, then H_1 can be evaluated from

$$H_1 = \frac{2k}{x}(A_2 + A_3)(T_f - T_{wv}) \qquad \ldots \ldots (6.43)$$

where x is the tank wall thickness, k the thermal conductivity of the reservoir wall material, T_{wv} the outside vertical reservoir wall temperature, A_2 and A_3 the surface areas of the reservoir vertical side walls which are merging into fluid.

Similarly, H_2 can be expressed as

$$H_2 = \frac{k}{x}A_1(T_f - T_{wp})$$

$\ldots\ldots$ (6.44)

where T_{wp} is the outside wall temperature at reservoir bottom and A_1 is the area of the reservoir base.

If the radiation effect is assumed to be insignificant, the heat loss by natural convection from the four sides of the vertical reservoir wall to atmosphere H_v can be calculated from

$$H_v = 2h_{av}(A_2 + A_3)(T_{wv} - T_a)$$

$\ldots\ldots$ (6.45)

where h_{av} is the heat transfer coefficient caused by the natural convection along the reservoir vertical walls and the surrounding atmospheric temperature T_a is assumed to be constant. Also, the heat flow by natural convection along the reservoir bottom H_p is

$$H_p = h_{ap}A_1(T_{wp} - T_a)$$

$\ldots\ldots$ (6.46)

where h_{ap} is the heat transfer coefficient by natural convection along the reservoir bottom. In the above two equations, h_{av} and h_{ap} can be evaluated using the simplified equations provided in Table 6.2. For   simplicity, when the steady state processes of the heat flow transfer through the reservoir walls are considered, the heat flow conducted through the four side vertical reservoir walls must be equal to the heat flow transferred from the outside of the four vertical walls to the atmosphere, in other words H_1 in Equation (6.43) must be equal to H_v in Equation (6.45), hence the uniform outside vertical reservoir wall temperature T_{wv} can be expressed by

$$T_{wv} = \frac{\dfrac{k}{x}T_f + h_{av}T_a}{\dfrac{k}{x} + h_{av}}$$

$$\dots\dots (6.47)$$

In the similar way, the heat flow H_2 in Equation (6.44) must be equal to the heat flow H_p in Equation (6.46), hence the reservoir bottom wall temperature T_{wp} is calculated from

$$T_{wp} = \frac{\dfrac{k}{x}T_f + h_{ap}T_a}{\dfrac{k}{x} + h_{ap}}$$

$$\dots\dots (6.48)$$

The heat flow transferred from the surface of the fluid in the reservoir to atmosphere by natural convection can be obtained from

$$H_3 = h_{ap}A_1(T_f - T_t)$$

$$\dots\dots (6.49)$$

where T_t is the temperature of air inside the reservoir above the fluid surface. In the case being discussed, the top of reservoir is open to the surrounding atmosphere, hence the value of T_t can be assumed to be the same constant value of the surrounding atmospheric temperature T_a. In other practical cases, the air in the reservoir top is not directly open to its surrounding atmosphere but indirectly exchanges with outside air through an air breather. In those cases, the value of T_t would be slightly higher than that of T_a. Although the value of T_t can be carefully determined by considering the air inside the reservoir as an open thermal system, it is rather complex and unnecessary. A slight higher but constant value of T_t may be assumed in some cases to predict fluid temperature using Equation (6.42) without much loss of accuracy.

The group equations, Equation (6.42) to (6.49), which describe the thermodynamic process associated with a hydraulic reservoir, has been used to set up an equivalent HASP reservoir model FPTH for calculating fluid temperature and wall temperatures. The details of model FPTH is documented in HASP model

writing up form and given in Appendix II. Using the reservoir temperature model FPTH together with the open system temperature model FPOH, the uniform fluid temperatures in the loop and the reservoir of a hydraulic system can be theoretically predicted.

6.16   The fluid temperature changes in the hydraulic system will affect the fluid properties. The variation of fluid properties has great influence on the characteristics of hydraulic components. Fig. 6.8 taken from Fig. 2 of Ref. (6.12) shows the relationships of fluid dynamic viscosity against temperature changes for several types of commonly used hydraulic oil. An empirical relationship between the kinematic viscosity and fluid temperature was developed by McCoul (Ref. 6.13), under the atmospheric pressure it is expressed as

$$\nu = e^{10e^{10\left[A - B\log_{10}(T + 273)\right]}} + 0.6 \qquad \qquad \ldots \ldots (6.50)$$

where constant A and B depend on the type of fluid. The empirical values of constants A and B have been provided in HASP on the basis of experimental data obtained from Ref. (6.14).

The fluid density is assumed to be linear with temperature, the empirical expression recommended by Eirich (Ref. 6.15) as

$$\rho = D - C(T - 20) \qquad \qquad \ldots \ldots (6.51)$$

where D and C are empirical values for a specific fluid and can be evaluated once the type of fluid is chosen in HASP.

The fluid Bulk Modulus is also an empirical function of density and temperature as given by Hayward (Ref. 6.16) as follows

$$B = 10^4\left[1.78 + 7(\frac{\rho}{1000} - 0.86)\right]e^{10\left[25\times10^{-4}(20 - T)\right]} \qquad \ldots \ldots (6.52)$$

These relationships between temperature and fluid properties can be implemented into temperature FP*H series of models to calculate transient fluid properties after

every time step of model operation.

A Temperature Computational Technique

6.17 Temperature changes in hydraulic systems are extremely slow compared with other transients, typically taking several hours to reach steady state. If the temperature and fluid property models are used together with other HASP dynamic models, the transient fluid and pipe wall temperatures in the model PICH and the models of FP*H series have to be solved simultaneously with the differential equations of other flow and pressure models, resulting in a problem of high computational stiffness. This would generally require a long computational time. In order to overcome this problem, Tomlinson (Ref. 6.4) adopted a first order forward Euler integration process for calculating transient fluid temperature.

This technique for temperature calculations was developed based on the fact that temperature levels change relatively slowly in any a hydraulic system and the relevant fluid properties can be regarded as constant over a period of time (typically seconds) without significant loss of accuracy. The temperature transient equations are solved by using first order Euler integration: the temperatures are assumed to be constant for a fixed short period of time and then are updated. Meanwhile, the other differential equations are solved by Gear's Method as implemented in HASP.

The time step at which the temperatures are updated is provided as an user defined parameter. A typical value for this parameter is recommended between 1 to 3 seconds. A variable is introduced to monitor the time corresponding to the last temperature update. This variable is initially set to zero. If the simulation time exceeds the constant temperature period, the fluid and the pipe wall temperatures like in Equation (6.37) and (6.38) are updated by solving the equations as below

$$\Delta T_2 = \frac{dT_2}{dt} = \frac{H_1 - H_2}{M_p C_{pp}} \qquad \ldots \ldots (6.53)$$

$$T_2 = T_{2_o} + \Delta T_2 \delta t \qquad \ldots \ldots (6.54)$$

and

$$\Delta T_f = \frac{dT_f}{dt} = \frac{W - H_1 + m_f C_{pf} T_{in} - T_f}{M_f C_{pf}} \qquad \dots \dots (6.55)$$

$$T_f = T_{fo} + \Delta T_f \, \delta t \qquad \qquad \dots \dots (6.56)$$

where T_{fo} and T_{2o} are the initial fluid and pipe wall temperatures at t = 0, respectively, and the δt is the time increment.

With this background, all the fluid temperature and property models FP*H series and the pipe wall temperature model of PICH developed by the author have been incorporated with the first order Euler computational technique as to obtain a short computational time period. Computer simulations using HASP temperature models developed for thermodynamic analysis of hydraulic systems have been carried out to investigate the validity of the theoretical approaches proposed. The results of the simulations will be used to identify and analyse the experimental temperature results.

6.18   The simple theoretical approach proposed in Section 6.12 has been used to predict the transient fluid and pipe wall temperatures of the unboosted closed hydraulic system in Fig. 6.5. Fig. 6.9 shows a complete system simulation block diagram using the corresponding HASP models developed. Since the flow and pressure behaviours of the system have been closely examined in Chapter 5, the simulation will concentrate only on the temperature performance of the system.

6.19   **Simulation Block Diagram**   In the diagram, the engine model PM3H includes the engine speed droop characteristics. The engine model provides shaft speed ω from information obtained from the gear pump model PUAH for the torque T. The hydraulic gear pump model PUAH besides providing flow, given pressure information also provides power loss data through link 4 to model POOH(01) mentioned below. As discussed in Section 5.19, the characteristics of the four way three position directional control valve can be represented by two orifice restrictor models OR3H(01) and OR3H(02), with a two way two position direction control valve model DC1C acting as a by-pass valve. DC1C also represents the pressure loss across the directional control valve at its central position. This simplified representation is only valid   under the condition that two outlet ports of the directional control valve are linked to a hydraulic motor with two approximate equal length of pipelines. The model DC1C is operated by a duty cycle model DEDT to represent a sudden change in the operating position of the valve. The difference between the pressures in the return and suction pipelines is neglected, these two sections of pipeline are simulated by the frictionless pipe model PI05(04). Moreover, the dynamics in the suction line is not important for the temperature examination, hence the suction pressure is simply determined by the fluid head in this vertical suction pipe, the pressure loss in the suction pipe due to pipe friction is simulated in the standard orifice model OR00(01). The model of LROH describes the load characteristics of a propeller. This model provides a load to the hydraulic gear motor model MOAH which incorporates power losses caused by internal and external leakage losses. The standard orifice model OR00 in HASP has been modified and called OR3H to include the calculation of the power loss caused by the pressure drops across the directional control valve. The hydraulic reservoir is represented by a three-port tank model TK03.

The system main fluid path is in the clockwise direction. The pump delivery flow and pressure are given as the flow and effort variables on link 3. Before the system is loaded, the pump flow from link 3 delivers to the first part of the high pressure line model PIO5(01), then the flow is passed to link 6 and through DC1C01 to link 17 which links with another use of PIO5(04) of the return and suction pipelines model, and finally the flow is transmitted back to the pump inlet on link 2. The pump delivery flow will be passed to the motor inlet of link 8 through one side of the directional control valve OR3H(01) and the second part of the high pressure line of PIO5(02). The propeller speed and its required torque appear on link 10 in the forms of the flow and effort variables. The motor outlet flow on link 9 will be delivered through the first part of the return PIO5(03) to another flow pass of the directional control valve OR3H(02). Then the flow is transmitted to the return and suction lines PIO5(04) back to the inlet of the pump. In addition, the external flow leakage of the motor sends to the reservoir model TK03(01) from link 12.

If the flow exchanges between the system loop and the reservoir due to the motor external leakage flow is insignificant, the system can be regarded as a closed thermal system. If the fluid temperature variations in the different part of the system are ignored, an uniform temperature of the fluid in the system loop can be assumed. When the system is considered to use the same type of pipes, the temperature simulation method and the model of FP3H proposed in Section 6.12 can be used to predict the system fluid and pipe wall temperatures, after the total power loss $\sum W$ generated by the pump, motor and directional control valve during the system loading has been added by a power sum model POOH from each separate component.

6.20   **Data Acquisition for Simulations**   A number of simulations have been carried out to analyse the system temperature changes due to the thermodynamic and heat transfer processes in the system. On the basis of the experimental test rig described in Section 5.10 - 5.12, the user defined parameters for each model in the simulation block diagram in Fig. 6.9 have been obtained. The details of these parameters are listed in Table 6.6 - 6.22. The data determination and consideration for the system component models including the pump, motor, engine, propeller, directional control valve, the high pressure pipeline and the first part of the return line in Table 6.6 - 6.15 are identical with those given in Section 5.20 - 5.27. The

simulations were carried out for analysing 90 minute long experimental temperature test during the system loading, hence the operating period for the directional control valve is defined as 5400 seconds in its duty cycle model DEDT as shown in Table 6.20. The pipe length in Table 6.16 for the pipe model PI05(04) is the combined pipe length of the second part of the return and suction lines. The pressure drop in the orifice model OR00(01) in Table 6.17 is determined according to the experimental result to define the static suction pressure under the system steady conditions. The determination of the input data for temperature and fluid property model FP3H(01) in Table 6.22 is given as below.

In this simplified approach for the temperature simulation in a hydraulic system being regarded as a closed thermal system, the system is considered to be constructed by the same size of pipes and pipe wall material with an uniform fluid temperature throughout the whole system loop. On the basis close to the test rig, the pipes are taken as half inch (12.7 mm) internal bore single wired hydraulic hoses and the external diameter of the hose is measured as 21 mm. The total length of the pipes is taken as 7 m. The type of oil used in the simulation is BP-HLP 32. Using the data provided in Table 6.3 and 6.4, the specific heat and thermal conductivity for oil used in the system has been taken as being the same as for machine oil, ie 1909 J/kg.K and 0.143 W/m.K. Fig. 6.10 shows a typical single wire braid hydraulic hose constructed by synthetic rubber tube, single wire braid reinforcement and synthetic rubber cover. The specific heat and thermal conductivity of such hose have been taken as if it were made from pure rubber, ie 2010 J/kg.K and 0.15 W/m.K. The density of pure, rubber 1100 kg/m^3, has been obtained from the data provided Table 6.5 which gives the densities of often used pipe materials taken from Ref. (6.10). The emissivity of the hose is taken as the value of natural black rubber, ie 0.9. The data in Table 6.22 for initial fluid, pipe wall and surrounding air temperatures before the system loading have been evaluated from consideration of experimental test conditions.

6.21 **Simulation Results Discussion**   Using the input data defined above, the simulations using Fig. 6.9 have been carried out to predict the theoretical fluid and pipe wall temperatures in the system, and also to investigate the effects of various parameters on the system temperatures. In these simulations, the engine was running steadily at 1880 rpm. At the start of simulation the directional control valve was operated. As analysed in the mathematical modelling of the system

thermodynamic process, fluid and pipe wall temperatures of the system are affected by a number of parameters. A clear appreciation can be obtained from a close examination of a range of simulation results with its governing equations. The analysis of fluid and pipe wall temperatures in the unboosted closed hydraulic system is given as an example so similar analysis can be taken to examine fluid and pipe wall temperature results in the later system simulations.

The power loss of the components during the system loading is the only heat generation source to cause the increase of the fluid temperature in the unboosted closed hydraulic system. Fig. 6.11 shows the rise in the simulated fluid temperature as response to the increase of the total power loss in the system due to the increase in the engine supply speed or the slip losses of the pump and motor. In this specific case of the system simulation, when the power loss exceeds the value of 220 W, the fluid temperature in the loop will reach above the usual recommended maximum fluid temperature 60° C. In order to ensure an approporiate performance of the system, a cooler is needed to be incorporated in the system when the total system power loss is great than 220 W. These simulated results have shown that fluid temperatures have two distinct rates of increase: under the simulation conditions defined, a fast increase is shown within the first hour of the system loading, during the second hour of system loading, the increase rate of fluid temperature is much lower.

It has been pointed out that the fluid temperature is also a dependent of the fluid mass M_f and heat dissipated through the pipeline of the system, H_1. When the total pipe length of the system is changed, H_1 due to the corresponding change in the pipeline internal surface area and M_f will be affected and so the fluid temperature changes respectively. The simulation results in Fig. 6.12 shows the effects of the pipe length on fluid temperature. Similarly, when the inside diameter of pipe is changed, the fluid mass M_f in the pipe line is changed, hence the fluid temperature would be affected as suggested in the simulation results in Fig. 6.13. But the change in the pipe inside diameter has not found any influence on the outside pipe wall temperature. This is because the reduction in the internal pipe diameter not only reduces the pipe internal surface area but also increases the heat transfer coefficient by forced convection. Hence the combination effects cancel the diameter variation. On the contrary, the size of the pipe outside diameter has more significant influence on the pipe wall temperature as shown in Fig. 6.14. This is because the outside surface area of the pipe wall is a dominant factor in determining

the heat flow transferred from the outside pipe wall to atmosphere compared with the heat transfer coefficient by natural convection. The fluid temperature is not much affected by the variation of the outside pipe diameter, since the outside pipe diameter has little effects on the heat flow transferred from the fluid to the inside pipe wall, H_1.

Moreover, the type of the pipe wall material also plays an important role in determining the temperature distribution, since the values of pipe wall specific heat, density and thermal conductivity are depended by the pipe wall material. As expressed in Equation (6.31), the heat flow transferred within the pipe wall by conduction H_1 is affected by the thermal conductivity k of pipe wall. Fig. 6.15a plots a group of fluid temperatures against the variation of thermal conductivity of the pipe wall material. The results show that the reduction of the value of k will increase fluid temperature in the loop due to the corresponding reduction in H_1. But the value of pipe wall k has less influence on the outside pipe wall temperature as shown in the simulation results in Fig. 6.15b. The specific heat of pipe wall material affects the rate of increase in the pipe wall temperature as indicated in Equation (6.37). This effect is well reflected in the simulation results shown in Fig. 6.16a. Since fluid temperature distribution is affected by the pipe wall temperatures, Fig. 6.16b shows a similar change on fluid temperature with the variation of the pipe wall specific heat. For the same reason, the mass or density of the pipe wall has influence on the pipe wall temperature as shown in Fig. 6.17a and this influence is well reflected on the fluid temperature as shown in Fig. 6.17b. Above all, the temperature difference between the pipe wall outside and surrounding atmospheric temperatures is greatly affected by the effects of pipe wall heat radiation as expressed in Equation (6.34) by the emissivity of the pipe wall material ϵ. This is due to the heat flow transferred from outside pipe wall to its surrounding atmosphere is given by the natural convection and radiation. The radiation can be as important as the natural convection when the heat transfer coefficient by natural convection h_a is relative small. The effects of the emissivity of the pipe wall material on the pipe pipe wall and fluid temperatures are demonstrated in the simulation results shown in Fig. 6.18a and 6.18b.

If the pipeline of hydraulic hose in the system is replaced by the common used mild steel or copper pipes, the input simulation data for FP3H in Table 6.22 will be changed to the data in Table 6.23 or 6.24 respectively. A large difference between the outside pipe wall temperatures of steel (copper) and rubber hose is

shown in the simulation results in Fig. 6.19a, as it would be expected due to a big difference exists between the thermal conductivities of metallic and non-metallic materials as data suggested in Table 6.4 (for steel: k = 60.2 W/m.K; copper: k = 386 W/m.K; rubber: k = 0.15 W/m.K). An interesting phenomenon shown in the simulation fluid temperatures in Fig. 6.19b is that fluid temperature in the system with the steel or copper pipeline is higher than it in the system with the hydraulic hose. These simulation fluid temperatures have been resulted when the effects of radiation are taken into account. Although the thermal conductivities of steel and copper pipes are much higher than that of rubber hose, the emissivities of steel and copper are lower than that of rubber hose as data indicated in Table 6.1 (for mild steel: ϵ = 0.25; polished copper: ϵ = 0.023; rubber: ϵ = 0.9). This comparison of simulation fluid temperature results has challenged the widely accepted assumption in many text books, which ignores the radiation effects under 200° C. Moreover, common sense tells us that hot fluid in a steel (or copper) container cools faster than it in an identical rubber container.

In order to justify the simulation results in Fig. 6.19b, a number of simple experiments have been carried out. In a typical experiment, hot water with initial temperature of 50.4° C was simultaneously filled into a mild steel tube and a close sized rubber hose. The two tubes vertically held on a table with surrounding atmospheric temperature of 13.1° C. The geometric sizes of these tubes are listed in Table 6.25. The detailed recordings of the fluid and outside wall temperatures of both tubes, as the water in the pipes cools down, are provided in Table 6.26. The wall temperature of rubber hose is lower than that of steel in Fig. 6.20 as the trend of the simulation results in Fig. 6.19a suggested. A comparison of fluid temperatures in steel and rubber tubes in Fig. 6.21, obtained from the same experiment, has shown that the water temperature in the rubber hose is actually lower than it in the steel tube. This shows that   common sense is wrong and the radiation effects are far more significant than previously thought. Another group of experiments were also taken to confirm the effects of radiation from a different stand point of view. In these experiments, a polished copper tube, whose size is given in Table 6.27, was filled with hot water with different initial temperatures and held vertically on a table, then the water temperature was recorded within a time interval. Such experiments were repeated after the polished copper tube was painted black. Three typical experimental recordings are plotted in Fig. 6.22. As can be seen, the initial temperature has little effect on the rate of cooling, the emissivity surface condition of tube however has great influence on the decreasing rate of water. From these experiments, it can be concluded that metallic pipes on hydraulic machines should

be painted to dissipate more heat rather than being polished as in the present industrial practice.

6.22   A reservoir is required in the majority of the hydraulic systems. When it is
used, the hydraulic system no longer can be considered as a closed thermal system
because the exchange of the flow energies of the fluids in the loop and in the
reservoir. An analytical approach has been proposed in Section 6.14 and 6.15. The
principle of the approach is to consider the hydraulic system as two open thermal
systems: the loop and the reservoir. An assumption has been made to regard the
temperatures of the fluids in the loop and reservoir as two separate uniform values.
The equivalent HASP models developed for predicting these two fluid temperatures,
FPOH and FPTH, can be used for the simulation of the partially closed hydrostatic
drive propeller system in Fig. 6.6.

6.23   **System Block Diagram**   Fig. 6.23 shows the system block diagram using
the analytic approach proposed for simulating the system temperature behaviour. In
the diagram, two additional orifice models OR3H are used for the simulation of the
two orifice restrictor valves which control the proportion of the system flow
returning to the reservoir, and a four port tank model TK04 is used for the system
reservoir. The pressure and flow dynamics in the return and suction lines and also
in the suction pipe junction can be neglected in the system temperature simulations.
The model OR3H(03) separates the return line pipe PI05(04) and the pump entry
line PI05(05). The rest of the component models are the same with the previous
simulation diagram discussed in Section 6.20.

Again, the power sum model POOH(01) is used to find the total power loss
during the system loading and POOH(02) is for the addition of the total heat flow
transferred through pipelines in the loop. In the previous simple approach to
simulate temperature behaviour in the unboosted closed hydrostatic system, just
one type of the pipe wall material has been considered. In practice, pipelines in a
hydraulic system are constructed from pipes with different types of wall materials.
The simulations may be carried out to calculate wall temperatures for the different
types of pipe material in the system. The effects of the pipe wall material can be
estimated using the pipe wall temperature model PICH to calculate the heat flow

transferred from the system fluid to each part of the pipeline with the same type of the material. Once the loop uniform fluid temperature is solved in the open thermal temperature model of FPOH, it will be passed to the reservoir temperature model FPTH as the flow variable on link 33. The loop fluid temperature will be transmitted to all the models of PICH by a common block both in FPOH and PICH. The power loss in the motor caused by the external leakage is transmitted into FPTH by the flow variable on link 13. The rate of heat exchange flow between the loop and the reservoir is defined by the flowrate circulating in the reservoir. This flowrate is transmitted separately to FPOH and FPTH by the flow variables on line 31 and link 28. The solution of fluid temperature in FPTH will be transmitted to FPOH by the flow variable on link 34. The wall temperatures at the outside of the reservoir will be given on an internal link of FPTH.

6.24   Simulation Input Data   The simulation parameters for the system component models in Fig. 6.23 are essentially the same with the data provided in Table 6.6 - 6.21. The only difference is in the data defined in Table 6.28 for the operational time of the directional control valve in the duty cycle model DEDT01 as 7200 seconds. The simulation data for the thermodynamic pipe models of PICH are given in Table 6.29 - 6.38. Two types of pipe wall materials are classified: the natural rubber and mild steel. The thermodynamic properties of the natural rubber represent hydraulic hoses used in the system. While the thermodynamic properties of the mild steel are assumed to represent those of the pipe fittings, union blocks and some rigid pipes used in the system pipelines. The data for the natural rubber and mild steel are obtained from the data provided previously in Table 6.1, 6.3, 6.4 and 6.5. The input data for the loop fluid temperature model FPOH01 of an open thermal system are given in Table 6.39. The material of the reservoir is taken as cast iron. The thermodynamic properties of iron have been used for the input data of the reservoir temperature model FPTH as given in Table 6.40.

6.25   Simulation Results Discussions   The temperature behaviour of the partially closed hydrostatic drive propeller system can be simulated using a simplified analytic approach to consider an uniform temperature for the fluid in the system loop as in Fig. 6.23. Using the input data defined above, a number of simulations have been carried out to investigate the effects of reservoir and flowrate to reservoir on the loop fluid temperature.

The fluid height in the reservoir determines the vertical side areas of the reservoir (A_2 and A_3), as indicated in Equation (6.43) and (6.45), the amount of the heat flow dissipated through the reservoir side walls, H_1, is affected by these areas of the reservoir. This value of the heat dissipated through the side walls of the reservoir will affect fluid temperature inside the reservoir as as expressed in Equation (6.42). Moveover, the fluid temperatures inside the reservoir and in the system loop are dependent on each other, so the change in the fluid height in the reservoir will result a corresponding change in the fluid temperature in the system loop. A clear appreciation can be obtained from a collection of simulation results in Fig. 6.24 showing the effects of fluid height in the reservoir on the fluid temperature in the system loop. This suggests that any change of the fluid height in the reservoir will not only affect the mass of fluid in the reservoir, which is one of the factors to determine the change rate of the fluid temperature in the reservoir, but also change the amount of heat dissipated through the vertical side wall of the reservoir, as a consequence, the steady level of the fluid temperature in the reservoir is also affected by this change of the fluid height. For the same reason, the size of the reservoir base has its influence both on the fluid temperatures of the reservoir and the system loop. The simulation results in Fig. 6.25 and 6.26 predict the effects of the length and width of the reservoir on the fluid temperature in the system loop.

The fluid temperature in the system loop is also affected by the value of the flow returning to the reservoir as expressed Equation (6.41) in term of mass flowrate m_f. As already stated in the temperature analytic approach for a hydraulic system using a reservoir, the whole hydraulic system can be considered as a combination of two open thermal systems: the loop and the reservoir. The energy transfer between the loop and reservoir thermal systems is expressed in Equation (6.41) in terms of $m_f C_{pf} (T_{in} - T_f)$, where the mass flowrate m_1 is given by $m_f = \rho Q$. T_{in} is the uniform fluid temperature in the reservoir. The first term $\rho Q C_{pf} T_{in}$ represents the flow energy received by the loop thermal system while the second term $\rho Q C_{pf} T_f$ indicates the flow energy exit the loop to the reservoir. The effects of the rate of the flow between the loop and reservoir Q on the loop temperature are demonstrated in the simulation results in Fig. 6.27. As can be seen, when no flow returns to the reservoir, the increase of fluid temperature in the system loop during the system loading is identical with the fluid temperature of the unboosted closed hydrostatic drive propeller system discussed in Section 6.21. As this flowrate rises, the flow energy transferred from the system loop to the reservoir increases and so the loop temperature will reduce. Meanwhile, the loop fluid temperature will be affected by the rise of the reservoir temperature due to this increase of the flow

energy transferred from the loop.

Another feature of these temperature results is that when the flowrate returning to reservoir exceeds 0.3 L/min, the reduction of the loop temperature with the increase of the system flowrate to the reservoir gradually becomes insignificant. For instance, only a small temperature difference is shown between fluid temperature of the partially closed system loop (with its half system flowrate 4.7 L/min circulating in the reservoir) and that of the open system loop (with full system flowrate 9.4 L/min through the reservoir). This phenomenon may be explained in the following way. When the flowrate circulating in the reservoir Q exceeds a value at which an equilibrium of heat dissipation process is established, the value of the heat dissipated through the pipes of the system loop and the value of flow energy transferred to the reservoir will become constant. In this case, any further increase of the flowrate will not affect the final value of the flow energy in terms of $\rho Q C_{pf} (T_{in} - T_f)$ but introduce a small reduction in the fluid temperature difference between the loop and the reservoir, $T_{in} - T_f$. Hence, once the equilibrium of the heat proportion dissipated through the pipes of the loop and the reservoir is established, the loop temperature will not affected by any further change in the system flowrate returning to the reservoir as indicated in Fig. 6.27.

From another stand point of view, the fluid temperature in the reservoir is greatly affected by the small value of the flowrate circulating in the reservoir. When this flowrate exceeds a value at which the equilibrium of heat dissipation process is established, a further increase of the flowrate will only cause a small rise in fluid temperature in the reservoir as a group simulation results shown in Fig. 6.28. As expressed in Equation (6.42), fluid temperature in the reservoir is determined by the parameters which include the power loss, mass flowrate and heat dissipated through the walls of the reservoir. When no flow returns to the reservoir, the power loss and the flow energy transferred from the loop are zero so the fluid temperature in the reservoir remains constant. In the case of the partially closed hydrostatic drive propeller system, when 50 percent of the system flow with the rate of 4.7 L/min returns to the reservoir, the power loss converted into heat in the reservoir has been calculated as 29 watts which is caused by the external motor slip loss (21 watts) and the pressure loss across the orifice A (8 watts). The rate of the heat dissipated through the walls of the reservoir and calculated in the reservoir temperature model FPTH with the defined parameters of the reservoir size, together with the power loss and flow energy transferred from the loop, $\rho Q C_{pf} (T_{in} - T_f)$,

have resulted the gradual fluid temperature increase shown in Fig. 6.28. When all the system flow returns to the reservoir as in the open hydraulic system, since the values of the flow energy and the heat dissipation are the same with the above case, the rise of the power loss (36.8 watts) due to the increase of flowrate across the orifice A has led a small increase in the reservoir fluid temperature.

Meanwhile, the proportion of heat dissipated through the loop pipes is expressed by $\sum H_1$ in Equation (6.41) and calculated in the simulation by the pipe temperature models PICH. For instance, in the case of the partially closed hydrostatic drive propeller system, the simulation result of the heat dissipated through the pipes is shown in Fig. 6.29. The rest of the loop heat dissipated in the reservoir has led a small difference between the fluid temperature of the loop and that of the reservoir as shown in a comparison of these two temperatures in Fig. 6.30. A further investigation into the temperature performance during the system loading may be carried out by considering a big increase in the power loss to the value of 1000 W. As shown in the comparison of the simulation results for the fluid temperatures in the loop and the reservoir in Fig. 6.31, although the increase in the power loss has increased the rate of change and steady value of the fluid temperatures of the loop and the reservoir, nevertheless the difference between these two fluid temperatures is not as big as it otherwise might have been expected. In order to investigate these temperature results obtained by simulation, a range of experimental two hour run tests has been carried out in a partially closed test rig to measure both the fluid temperatures of the loop and the reservoir. The experimental temperature recordings and their comparisons to the simulation results will be discussed in the next section.

From the analysis of the above simulation results, it has been found that the heat dissipation through the pipes of a hydraulic system plays an important part in determining the temperature distributions in the loop and the reservoir. The assumption to ignore this vital thermodynamic process during the loading of a hydraulic system in Ref. (6.3) and (6.4) may lead to greater errors in predicting both the fluid temperature in the loop and that in the reservoir than had been previously thought.

6.26   Experimental Test Rig and Measurements   In order to investigate the validity of these theoretical approaches, a number of tests were undertaken to determine experimentally the fluid and pipe wall temperatures in a practical system. The experimental test rig being used in the investigation is the same test rig described in Chapter 5. The detailed descriptions about the test rig with its instruments for monitoring the flow and pressure conditions have been given in Section 5.10 to 5.13. The pipe wall temperatures were measured by thermocouples with a digital output. These five thermocouples were firmly stuck onto the surface of the mild steel pipes at the locations in the test rig hydraulic circuit shown in Fig. 6.32. In corresponding locations except for the suction line, four Platinum Resistance Probe (PRT) were carefully inserted into the pipes to monitor fluid temperature differences at the different parts of the test rig. These PRTs were linked with a carrier amplifier to give the digital outputs.

6.27   Experimental Test Procedure   First step was to set up the test circuit by the control of opening areas of two orifice restrictors in the return line as shown in Fig. 6.32. A conventional open circuit can be tested with fully opening of the orifice A and closing orifice B. Similarly, the unboosted closed circuit can be obtained with fully opening orifice B and closing orifice A. Any a combination of opening areas of these two orifices can be set to examine the temperature performances of the partially closed unboosted closed hydraulic circuit.

The procedure for operating the test rig is identical with those described in Section 5.14. The system was run for two hours under load in leading towards the steady thermal conditions. Changes of fluid temperatures and pipe wall temperatures were rapid initially and the temperature readings were therefore recorded every one minute for the first ten minutes, every two for the following half an hour and then every five minutes towards the end of tests. An extensive test programme was carried out and the experimental temperature results will be described below.

6.28 **Temperature Tests in a Partially Closed Hydraulic Circuit** The first group of tests was under taken setting the equal opening areas of two orifice restrictors in the return line. A typical set of temperature recordings from these tests is presented in Fig. 6.33. These temperature values were obtained from the experimental recordings at each time interval, but for the convenience of temperature analysis, every two data of these temperature recordings have been simply joined together with a straight line. Some scatter is inevitably shown in Fig. 6.33 and the other curves of the experimental temperature results. Nevertheless these experimental curves can indicate the trends of temperature rise with sufficient accuracy. The constant temperature values of steady state have not been achieved in the fluid temperatures in Fig. 6.33. A possible reason is the gradual increase in the atmospheric temperature surrounding to the test rig during the tests of the system loading. Moreover, fluid temperature at the motor inlet in the second part of the high pressure line is approximately $2°C$ higher than that recorded at the pump outlet in the first part of the high pressure line. On the basis of the well known temperature-pressure drop coefficient $5.9°C/100$ bar in a pipe line, it can be seen that the $2°C$ difference value in the experimentally measured fluid temperatures in the parts of the high pressure line is only partly caused by 2.5 bar pressure loss across the directional control valve, but mainly caused by the errors in the experimental fluid temperature measurements.

When the method of the experimental fluid temperature measurements are closely examined, a heat conduction problem will be related to a hollow rod of a thermometer pocket such as PRT immersed in a fluid stream as shown in Fig. 6.34. The hollow rod is fixed at one end to an inside pipe wall of temperature T_1 and the other projecting into the fluid of temperature T_f. The problem is that the thermometer evidently will indicate a temperature T_t some where between T_1 and T_f. Hence the order of error may be involved when using this method of fluid temperature measurement. In addition, the inaccuracy of locating the thermometer into fluid at the axis of the pipe will inevitably cause errors in the fluid temperature readings. These errors have introduced a bigger difference in fluid temperatures at the different parts of the system pipelines.

Similarly, a bigger temperature difference is shown in the corresponding pipe wall temperatures in Fig. 6.35. For the practical purposes, these small temperature differences can be ignored, so the fluid temperature as well as pipe wall temperature can be regarded as having an uniform value over the pipeline. However, the

- 140 -

temperature results experimentally obtained from the different parts of the system show a significant difference between fluid and pipe wall temperatures, a typical example is shown in Fig. 6.36 where the motor outlet is considered. These temperature differences between the fluid and pipe wall can not be ignored even if the experimental measurement errors have been taken into account.

In this test, the maximum fluid temperature is well below the usual recommended working value of 60° C, in spite of the steady state thermodynamic conditions of the system have not been achieved in the two hours run tests. Hence no cooler is needed in this particular case of test rig.

6.29 **Temperature Tests in the Conventional Open Circuit** In order to investigate temperature performances in the conventional open circuit as a comparison to the partially closed circuit proposed, a temperature test was under taken on the test rig by fully opening the orifice A and closing orifice B in Fig. 6.32.

In the conventional open circuit, as discussed in Section 5.16, the pump static suction pressure is determined by the fluid height and pipe friction in the suction line. Since the pump takes all the system flow through the suction line from the reservoir, the pressure at the pump suction flange was found to be - 0.2 bar gauge. As a result, a large percentage of air bubbles floating in the oil surface can be clearly observed in the reservoir and the loud noises were generated by showing that extensive cavitation was occurring. Under these conditions, the test was only conducted for 24 minutes and the engine was cut off to prevent any possible damage to the pump.

Again, the fluid temperature is different from the pipe wall temperature at the motor outlet as shown by Fig. 6.37. Fig. 6.38 plots fluid temperatures in the different parts of the system. The maximum difference between the measured fluid temperatures in the different parts of the pipelines is up to 5° C. But the corresponding maximum calculated temperature difference is less than 1.2° C, which is identical to 5.9° C/100 bar temperature-pressure drop coefficient, under the conditions that the maximum pressure loss in the system is 21 bar (the pressure drop across the outlet to the inlet of the pump). Hence, the errors in the

temperature measurements have introduced a bigger difference value in the measured temperature results. A similar bigger difference is also shown in the experimentally obtained pipe wall temperatures in Fig. 6.39. In comparisons of the measured and simulated temperatures given in Section 6.31, average fluid and pipe wall measured temperatures will be quoted to avoid inaccuracy in the temperature analysis.

In comparison of temperature distributions in two types of the systems, Fig. 6.40a and 6.40b show that not much difference exists in measured fluid and pipe wall average temperature values obtained from the open and partially closed hydrostatic drive propeller systems. This validates the simulated results given in Fig. 6.27 and 6.28, where the effects of flowrate circulating in the reservoir on the loop fluid temperature is investigated. Since a large reservoir is usually required and a low suction pressure occurs in the open circuit, it can be concluded that the conventional open circuit with the pipe line sizes considered is not suitable for this hydrostatic boat drive application.

6.30   **Temperature Tests in the Unboosted Closed Circuit**   When orifice A is completely closed with fully opening of orifice B, the test rig becomes an unboosted closed circuit. In this unboosted closed circuit, flow recirculates in the system loop all the time and so the system temperatures are expected to be higher than those in the other two circuits as the results shown in Fig. 6.41 and 6.42. These differences in the average temperatures of the unboosted and partially closed hydrostatic drive propeller systems show the function of reservoir heat dissipation.

A conclusion can be drawn from the above comparisons of the test results that the partially closed circuit is the best circuit design for the hydrostatic drive propeller system.

6.31   The Unboosted Closed Hydrostatic Drive Propeller System   The system total power loss shown on link 24 in Fig. 6.9 has been taken as 97.5 W according to the test conditions, the remainder of the input data given in Table 6.6 - 6.22 closes to the parameters measured from the test rig. The simulated fluid temperature in loop against the mean experimental fluid temperature is shown in Fig. 6.43, where the measured fluid temperature appears to be rising due to the gradual increase of atmospheric temperature surrounding the test rig and this increase has not been taken into account in the simulations. As stated in Equation (6.50) - (6.52), fluid property is the function of the fluid temperature so its value will be updated after every simulation time step. The simulation result of Fig. 6.44 shows the fluid density change as a result of fluid temperature variation during the system operation. Meanwhile, a variation can be found both in fluid viscosity and effective fluid Bulk Modulus as shown in Fig. 6.45 and 6.46. These transient fluid properties are provided to other models relevant to the system loop. The simulated pipe wall temperature of hydraulic hose against the mean experimental temperature distribution on steel pipes is shown in Fig. 6.47. The difference between the calculated and measured pipe wall temperature values demonstrates a great effect of the pipe wall material on the wall temperature distribution.

6.32   Improved Simulations to Consider Wall Temperatures of Different Pipe Material   In the simulation using the simple approach, just one type of the pipe wall material is considered. In practice, the pipelines on the test rig are constructed from the pipes with different types of materials. For instance, the system high pressure line consists five different lengths of pipes. The first section connected with the outlet flange of the pump is a small mild steel pipe, which is linked with a 1 m long hydraulic hose. This hose is used to connect another short length of steel pipe fixed at each end of the direction control valve. The other end of the steel pipe at the valve outlet in the high pressure line is joined with one side of a 1.15 m long hydraulic hose, the other side of hose is linked together with a steel pipe fixed to the inlet flange of the motor. When the simulation is carried out for analysing the temperature performance in the unboosted hydrostatic drive propeller system, the effects of these pipe wall materials on the results of the simulation temperatures, particularly on the pipe wall temperatures in the different parts of

the system, should be taken into account.

Using the system block diagram shown in Fig. 6.48, the temperature results of the pipe wall at the different parts of the system pipelines will be calculated by the corresponding pipe wall temperature models PICH. The system block diagram is essentially the same with the descriptions given for that of Fig. 6.9. The effects of the pipe wall material can be estimated using the pipe wall temperature model PICH to calculate the heat flow transferred from the system fluid to each part of the pipeline with the same type of the material. In the diagram, the sum of the heat flow transferred to the five sections of the high pressure pipes is calculated by the power sum model POOH(03). Similarly, the model POOH(04) is used to calculate the sum of the heat energy losses to the return line pipes, and POOH02 is used to find the total heat dissipation through the system pipelines. The result of the heat dissipation is provided to the closed thermal hydraulic system fluid temperature model FPUH(01) for the calculation of the uniform fluid temperature. The results of the fluid and pipe wall temperatures will separately show on the model internal links of FPUH(01) and PICHs. The fluid temperature calculated in FPUH will be transmitted to all the models of PICH by a common block both in FPUH and PICH.

The input data for the system component models are the same as those given in Table 6.6 - 6.21. The input parameters for the fluid temperature and property model FPUH of the closed thermal system are the same as the data given in Table 6.39 for FPOH. The total volume of fluid in the system is the calculated result of the total volume of the pipelines on test rig. This value can be obtained by adding the pipe volume in each pipe model PICH and then transmitted to FPUH through an external link. For the simplicity of the model linking of PICH, the value has been designed to be input by the model user. All the data for the models of PICH to calculate the pipe wall temperature and heat dissipation in each section of pipe with the same material are identical with those provided in Table 6.29 - 6.38. The errors for these simplified data acquisitions will be analysed in discussions of the simulation results as follows.

The simulation result in Fig. 6.49 has shown a difference between the calculated temperatures of the mild steel pipe and hydraulic hose in the different pipelines of the system. A closer agreement can be found in Fig. 6.50 between the calculated and measured pipe wall temperatures at the outside of the mild steel

pipes. The calculated pipe wall temperature is rather lower than the mean wall temperature of the system mild steel pipes towards the endings of the temperature values. This difference of these two temperature distributions is raised from the various assumptions being made for the unboosted closed hydraulic system temperature simulation. It has been found from a range of simulation results that this difference is partly caused by the errors in defining the input data for the emissivity for the mild steel pipes. The emissivity of the steel pipes had been taken the maximum value recommended for the polished mild steel as 0.32 in Table 6.1. In practice, the surface conditions of one section of the steel pipe in the system is arbitrarily varying during the system loading due to the change of the outside pipe wall temperature. When an uniform constant value of 0.2 for ϵ is assumed to represent the surface radiation conditions of all the steel pipes in Table 6.29 - 6.38, a reasonably close agreement has been achieved shown in Fig. 6.51. Again the higher measured pipe wall temperature resulted from the increase of the atmospheric temperature surrounding the test rig.

Up to this stage, it can be seen that the combination of errors in defining parameters for the simulation input data has resulted the difference between simulation and experimental fluid temperatures shown in Fig. 6.43. Since the difference of the heat transfer within two types of the pipes has been taken into account, the fluid temperature obtained in such a simulation with modified input data has been found a closer agreement to the measured fluid temperature in the system as shown in Fig. 6.52. However, the pipe wall temperature difference in the same type of pipe but in the different part of the system still cannot be identified due to the uniform fluid temperature has been assumed throughout the system loop in this type of theoretical approach.

6.33   The Partially Closed Hydrostatic Drive Propeller System   The experimental temperature measurements on the test rig for the partially closed system can be analysed using the simplified analytic approach to consider an uniform temperature for the fluid in the system loop in Section 6.15 with the simulation block diagram in Fig. 6.23.

When the fluid height in the reservoir is defined to be the value of 0.11 m to represent the measured 5 litres oil in the reservoir, an agreement has been found in

Fig. 6.53 between the simulated and measured temperature distributions. It is also shown in these results that the rise rate of calculated temperature values is lower than the experimentally obtained average loop temperature. From a range of the system temperature simulation, this error in the loop temperature simulation has been found to be caused by the inaccuracy in predicting the fluid temperature in the reservoir. This inaccuracy is due to ignoring the effect of the radiation at the outside walls of the reservoir in the temperature model of FPTH. This means the calculated values of heat flow dissipated through the walls of the reservoir are greater than those of practical values. When a higher degree of accuracy is required for predicting the loop fluid temperature, the radiation effect may be included in the simulation by assuming that the values of the effective heat transfer coefficients in Equation (6.45) and (6.46) are 30 percent greater as in order to avoid difficulties in mathematical modelling for the reservoir temperatures. In this way, a more accurate correlation of the measured and calculated loop fluid temperatures has been obtained as in Fig. 6.54. But the measured temperature values at the end of the test are higher than those simulated due to the rise of the atmospheric temperature surrounding to the test rig.

The pipe wall temperatures of the two different types of pipe materials and the outside wall temperatures of the reservoir can be identified. After the simulation input data for the pipe temperature models PICH have been modified in the way as described in the above section on the basis of the test conditions, Fig. 6.55 shows the calculated loop pipe wall temperatures as compared to the mean experimentally obtained wall temperature of the mild steel pipes. In the simulation, the rise in the outside pipe wall temperature due to the increase of surrounding atmospheric temperature has not been taken into account, hence a small error is resulted in the simulated outside steel pipe wall temperature of the system. Fig. 6.56 shows the simulated outside vertical and bottom wall temperatures of the reservoir. The small difference between these wall temperatures results from the difference in the heat transfer coefficients at the outside outside vertical and bottom of the reservoir by natural convection. These heat transfer coefficients have been calculated using the relations provided in Table 6.2.

6.34   A Suggested Theoretical Approach   The essence of the previous theoretical approach discussed is to assume an uniform hydraulic system loop temperature so that the system loop can be considered as an open thermal system. In a practical hydraulic system, however, the difference exists between the loop fluid temperatures in the different part of the system pipelines. This fluid temperature difference in the loop can be significant, since the heat generation in one part of the system differs from another part of the system, particularly in a hydraulic system with a large value of power loss or the use of a cooler. In these cases, an analytic theoretical approach has been proposed in this thesis to regard the system loop as a series of open thermal systems with a constant fluid temperature in each section of the system. In this way, the established theoretical presentation of an open thermal system of a pipe section can be applied for theoretical solutions of fluid temperatures at the different part of the system. The principle of this suggested approach is to develop a series of fluid temperature models for the different sections of pipe in the system, then fluid temperature in each particular section of the pipe can be estimated separately. The simulations of temperature distribution in the partially closed hydrostatic drive propeller system is again given as a comprehensive example to demonstrate this more accurate theoretical approach proposed.

6.35   Fluid Temperature Modelling   It is a feature of an open thermal system mentioned in Section 6.5 that the boundary of the system is arbitrary, but that the fluid and wall temperatures within it will be considered constant. The determination of the system boundary depends on fluid temperature at one particular part of the system, which is considered to be significantly different to the others.

For instance, in the system being considered, if the fluid temperatures at the outlet of the pump and the inlet of the motor are considered to have different values due to power loss caused by the pressure drop across the directional control valve, then the system high pressure line can be regarded as two open thermal

systems in parallel. In the first part of the high pressure line from the suction flange of the pump up to inlet of the directional control valve, there is an energy transformation process in which the mechanical energy of the engine shaft driving the pump is converted into hydraulic energy in the form of pressurized fluid. This process is accompanied by a fluid power loss resulting from leakage and mechanical torque losses from speed dependent viscous and pressure dependent friction. An assumption has been made in Section 6.13 that the mechanical losses caused by pressure and speed dependents torque losses are dissipated directly through the pump body and the leakage loss converted into heat in the fluid. Hence, the pump energy loss associated with internal flow slip loss is assumed to be the power loss which causes the variation of fluid temperature in this pipe section. If the pressure losses caused by the pipe friction are lumped into the direction control valve model, no other power loss is converted into heat in this first part of high pressure line. The fluid temperature in this pipe section can be expressed by Equation (6.38), where W is the power loss caused by the pump internal slip loss. Such an equation has been used to set up a fluid temperature model of an open pipe section FPCH, which is essentially the same with FPOH but has a different model linking in order to connect with other pipe fluid temperature models. The details of FPCH is given in Appendix II. A proportion of the fluid power loss in the pipe section, H_1, is transferred to the pipe wall to cause a simultaneous increase in the pipe wall temperature. H_1 can be calculated using the pipe wall temperature model PICH. The effects of the different pipe wall material, in this first part of the system high pressure line, on fluid and pipe wall temperatures can be estimated using several models of PICH and each PICH represents to one part of pipeline with the same type of pipe wall material.

In the same way, thermodynamic processes in the second part of the high pressure line (another open thermal system) can be studied, and the temperature distribution in the part of the pipeline can be simulated by using a pipe fluid temperature model FPCH with one (or several) model of PICH. The only difference between the two parts of the high pressure pipeline is that the power loss in the second part differs from that of the first part and is caused by the pressure loss across. In addition, the power loss caused by the pressure drop across the direction control valve can be calculated by an orifice model OR3H.

A similar pipe fluid temperature model FPGH, using Equation (6.38) with two fluid temperature outputs has been set up to simulate the fluid temperature in

the outlet of the motor to inlet of the directional control valve in the return line. In this part of pipeline, there are two flow outputs. One goes to the reservoir through the motor external leakage drain line and the other flows to the second part of the return line. In the same way, the fluid temperature in the second part of the return line can be predicted by using another FPGH to consider two fluid outputs (one goes to the pump entry line and another to the return line to reservoir).

In the system suction pipe junction, the flow energies from the suction line and the return line through the orifice B are the heat source for this section of the pipe as shown in Fig. 6.57. Equation (6.38) can be appropriately modified to express the fluid temperature in this part of the system, ie.

$$\frac{dT_f}{dt} = \frac{m_1 C_{pf} T_1 + m_2 C_{pf} T_2 - m_3 C_{pf} T_f - \sum H_1}{M_f C_{pf}} \qquad \ldots\ldots (6.57)$$

The above equation has been used to set up an equivalent HASP fluid temperature model FPDH, as given in the model library in Appendix II.

6.36 **Temperature Simulation Using the Suggested Approach**   When the above developed fluid temperature models FPCH, FPGH and FPDH are linked together, a complete system simulation block diagram in Fig. 6.58 can be obtained to predict fluid and pipe wall temperatures at each part of pipelines in the partially closed hydrostatic drive propeller system during the system loading.

In the diagram, the system component models are the same with those given in the above two approaches. The model FPCH(01) is used to simulate fluid temperature at the inlet flange of the pump up to the inlet direction control valve in the high pressure line. The power loss caused by the pump internal slip loss is delivered to FPCH(01) by the flow variable on link 4. The flow energy in this section of the pipe is estimated in FPCH(01) by receiving the flowrate on link 49 and the temperature of the fluid from in the suction line obtained on link 12. Two types of the wall material in the pipe section are used. As a length of hydraulic hose is sandwiched between two short mild steel pipes, the wall temperature and the heat flow dissipated from the fluid H_1 in each type of pipe are estimated in a lately

- 149 -

developed pipe temperature model PIGH. PIGH uses the same group of mathematical equations as PICH but it is linked with FPCH by an external link. This is because several fluid temperature models are used in the simulation, hence the fluid temperature in each pipe section no longer can be transferred to PICH through a common block. Therefore, the fluid temperature calculated in FPCH(01) is transferred to the two PICH in the form of flow variables on two external link 60 and 61 while the efforts on these links are the calculated results of heat flow dissipated from the fluid to the pipes. If the thermodynamic conditions, in the second section of the high pressure line from the outlet of the directional control valve to the inlet of the motor, is considered to be different to those in the first section, then the fluid temperature in the second section will be calculated in FPCH(02).

The power loss caused by the internal flow slip loss of the motor is transmitted from the motor model MOAH(01) to FPGH(01) by the flow variable on link 22. The temperature value calculated in FPCH(02) for the fluid temperature in the second part of the high pressure line is transmitted by the flow variable on link 17 to FPGH(01). The heat flow dissipated through the first sections of the return line are calculated in PICH(05) and PICH(06). The fluid temperature in this section is transmitted both to FPGH(02) for the fluid temperature calculation in the second section of the return line and to the reservoir temperature model FPTH(01) as to define the flow energy of the motor external drain. The model FPDH(01) calculates the fluid temperature in the suction pipe junction of the system.

The updated fluid properties after every step of model operation will be passed to its relevant models through a common block in the model calculation subroutine. In other words, since the fluid temperature is not considered as uniform throughout the whole system loop, then fluid properties no longer can be calculated in a single common fluid property model, FLPROP. The transient fluid properties have to be evaluated in each separate fluid temperature and properties model. As a result, the other pressure and flow models associated with the fluid properties have to be identified in the common block of calculation subroutine in order to make specific reference to the updated fluid properties in the region. This is only needed in modelling the steady hydraulic system performance, when the effects of fluid property variations on the system flow and pressure characteristics are considered to be important.

If the input parameters for the system component models in Fig. 6.58 are entirely identical to those in Fig. 6.23, since the difference of the power loss generated in the different parts of the system loop is small, the accurate features of the theoretical approach suggested cannot be demonstrated. However, when the system is subjected to a big power loss load conditions under which a cooler has to be used, the difference between the fluid temperatures in the different parts of the loop will increase to a significantly big value. In these cases, if a simplified system simulation block diagram in Fig. 6.59 is used, the suggested approach can be applied to examine the effects of loading conditions on fluid loop temperature in each section of the loop

In the diagram, the fluid temperature and property models FPCH, FPDH and FPGH as well as the pipe wall temperature models PICH are identical with those in Fig. 6.58 but a number of duty cycle models DFDT has been used to define the system loading conditions separately. DFDT(01) in the diagram gives the flowrate through the first part of the high pressure line while DFDT(02) defines the power loss in the first section of the system high pressure line. Similarly, DFDT(03) and DEDT(04) give the power loss and flowrate in the second section of the high pressure pipeline. In the same way, the arrangement has been made to use DFDT(05) to DEDT(08) in defining the power losses and flowrates in the two sections of the return line pipes. For simulating the fluid temperature in the reservoir using FPTH(01), DFDT(09) and DEDT(10) input the power losses caused by the motor external slip loss and the flow across the orifice A in Fig. 6.32, while DEDT(11) and DFDT(12) give the flowrate in the flow line to the reservoir and also the external motor leakage flowrate. In the simulation of the fluid temperature in the suction line using FPDH(01), DFDT(13) defines the power loss across the orifice B in Fig. 6.32 and DFDT(14) and DEDT(15) give the flowrate through the orifice B and from the reservoir to the suction pipeline. In this way, the power losses and flowrates in each section of the pipe in the loop can be easily changed without the change of any other parameters, in order to investigate each individual effect on the loop fluid temperature. This simplified simulation block diagram only concerns with the system temperature behaviour during the loading of the system.

6.37   **Simulation Results**   The input data for the reservoir fluid temperature in FPTH(01) are the same with the data given in Table 6.40, and the input parameters for all pipe temperature models PICH are identical with those provided in Table

6.29 - 6.38. The input simulation data for FPCH. FPDH and FPGH in Fig. 6.59 are given in Table 6.41 - 6.45. Again, these data are based upon the initial test conditions and the recommended thermodynamic data for various materials provided in Table 6.1, 6.3, 6.4 and 6.5. If the system flowrate is the same with that in the simulation shown in Fig. 6.23, while the power losses caused by the internal flow slip losses of the pump and motor are assumed to be 1 kw, which is defined in DFDT(01) and DEDT(05), and also a cooler with capacity of 2 kw is incorporated in the system and its heat dissipation is defined in DFDT(07).

Under these system loading conditions defined, a difference shows in Fig. 6.60 for the simulated fluid temperatures at the inlet and outlet of the pump due to the power loss generated by the pump internal slip loss. But the calculated fluid temperature at the motor outlet is almost the same with that at the motor inlet as shown in Fig. 6.61. This is because fluid temperature at the motor outlet is associated both with the motor inlet slip loss and the fluid temperature in the reservoir. In the simulated results in Fig. 6.62, the fluid temperature in the reservoir is compared with that at the motor outlet. Fig. 6.63 shows a fluid temperature difference in the inlet and outlet of the cooler due to the power dissipation by the cooler.

The fluid temperature difference between the inlet and outlet of an open thermal system is defined by the flow energy $\rho Q C_{pf} (T_{in} - T_f)$. In the case of a pipe section considered, a proportion of the power loss generated in the pipe section is directly dissipated through the pipe wall to surrounding atmosphere, the remainder of the power loss is converted into the heat flow energy, which causes the increase in fluid temperature within the pipe section. As examined in the simulation analysis given in Section 6.21, the heat flow dissipated through pipe wall, H_1, depends very much on the geometrical size and pipe wall material. In many practical hydraulic system, the difference of the power losses generated by the losses in the pumps, motors and valves (relief valves as particular) in the different pipe sections of the system loop can be much bigger than those defined in the last run of simulation. Hence, the fluid temperature differences in the loop could be much greater than those shown in Fig. 6.60 to 6.63. Moreover, if the system flowrate is 10 times smaller than that defined before, as 0.94 L/min, while the assumed power losses generated by the pump and motor and the power dissipation by the cooler remain unchanged, a greater temperature difference will result in the simulated fluid temperatures as shown in Fig. 6.64 to 6.67.

When the fluid temperature in one part of the loop significantly differs from another part in a hydraulic system, the assumption of an uniform loop fluid temperature in the previous two theoretical approaches can no longer be applied. In this case, the suggested more accurate theoretical approach can be used with a higher degree in accuracy to predict the temperature distribution in the different sections of the loop during the system loading. Although the simulated temperature results in this theoretical approach have been well reflected by the measured temperatures in a high power hydrostatic transmission system, which is currently under investigation in the University of Bath, more experimental temperature investigations in other hydraulic systems are required to be taken to validate this theoretical approach proposed.

It can be seen from the above examination of temperature simulations and corresponding experimental results that the theoretical approaches with different degree in accuracy have been implemented into the computer HASP software package and hence they can be improved to cover temperature modelling in other more complex hydraulic systems.

Normal Total Emissivity of Various Surfaces		
Surface	T, deg. C	Emissivity, ϵ
Copper		
Polished	100	0.023
Polished	117	0.052
Plate, heated long time, covered with thick oxide layer	25	0.78
Iron		
Polished	427-627	0.14-0.38
Cast iron, newly turned	22	0.44
Paints		
Black gloss	20	0.90
Black lacquer	20	0.80-0.93
White paint	20	0.89-0.97
White lacquer	20	0.80-0.95
Various oil paints	20	0.92-0.96
Rubber, hard, glossy plate	25	0.9
Steel		
Mild steel	45-1065	0.18-0.32
Water	0-100	0.95-0.963

Table 6.1 Normal Total Emissivity Data for Often Used Materials in Hydraulics Taken from Table C-7 of Ref. (6.10)

1, d in m	average h $W/m^{2o} K$	
	laminar or transition	turbulent
Vertical plate, or cylinder of large diameter, of height 1	$10^4 < Gr < 10^9$ $1.42(\frac{\theta}{l})^{\frac{1}{4}}$	$10^9 < Gr < 10^{12}$ $1.31\,\theta^{\frac{1}{3}}$
Horizontal cylinder of diameter d	$10^4 < Gr < 10^9$ $1.32(\frac{\theta}{l})^{\frac{1}{4}}$	$10^9 < Gr < 10^{12}$ $1.25\,\theta^{\frac{1}{3}}$
Square plate 1 x 1: heated plate facing up or cooled plate facing down	$10^5 < Gr < 2 \times 10^7$ $1.32(\frac{\theta}{l})^{\frac{1}{4}}$	$2 \times 10^7 < Gr < 3 \times 10^{10}$ $1.52\,\theta^{\frac{1}{3}}$
Square plate 1 x 1: cooled plate facing up or heated plate facing down	$3 \times 10^5 < Gr < 3 \times 10^{10}$ $0.59\,(\frac{\theta}{l})^{\frac{1}{4}}$	

Table 6.2   Simplified Equations for Free Convection Heat
Transfer Coefficients in Air at Atmospheric Pressure
(Taken from Fig. 22.17 of Ref. (6.8))

Specific Heat of Various Materials		
Substance	T, deg. C	Specific Heat. (J/kg.K)
Copper Pure	20 300	383 —
Iron Pure	20 300	447 —
Mild steel	50	486
Machine Oil	47	1909
Rubber	25	2010
Water	40	4179

Table 6.3   Specific Heat for Commonly Used Materials in Hydraulics
Taken from Table C-1 and C-2 of Ref. (6.10)

Thermal Conductivity of Various Surfaces		
Substance	T, deg. C	Thermal Conductivity, K (W/m.K)
Copper Pure	20 300	386 369
Iron Pure	20 300	80.2 55
Mild steel	50	60.2
Machine Oil	47	0.143
Rubber	25	0.15
Water	0-100	0.95-0.963

Table 6.4   Thermal Conductivity for Commonly Used Materials in
Hydraulics Taken from Table C-1 and C-2 of Ref. (6.10)

Thermal Conductivity of Various Surfaces	
Substance	Density ρ (kg/m^3)
Copper Pure	8900
Iron Pure	7800
Mild steel	7700
Machine Oil	870
Rubber	1100
Water	1000

Table 6.5   Density for Commonly Used Materials in Hydraulics
Taken from Table C-1 and C-2 of Ref. (6.10)

Fluid Properties Section Model FLPROP			
No.	Parameters	Data	Unit
1	oil temperature	15	deg. C
2	oil type	BP HLP 32	
3	fluid density	872.5	$\frac{kg}{m^3}$
4	fluid Bulk Modulus	18400	bar
5	fluid kinematic viscosity	94.50	cSt
6	fluid absolute viscosity	82.45	cP

Table 6.6   parametric Data Used in Simulation for Fluid Properties

Component No. 1: Speed Droop Engine Model PM3H (No. 1)			
No.	Input Parameters	Data	Unit
1	initial engine speed	2300	rev/min
2	speed/torque gradient	91	(rev/min)/Nm
3	governor set speed	2400	rev/min
4	engine inertia	0.008	$kg.m^2$

Table 6.7   parametric Data Used in Simulation for Engine

Component No. 2:   Hydraulic Pump Model PUAH (No. 1)
No.	Input Parameters	Data	Unit
1	maximum pump displacement	5	cc/rev
2	slip loss coefficiency at low speed	2.91×10^{-9}	
3	low speed at which slip is quoted	1000	rev/min
4	slip loss coefficiency at high speed	3.76×10^{-9}	
5	high speed at which slip is quoted	2500	rev/min
6	speed dependent torque loss coefficient	3×10^5	
7	pressure dependent torque loss coefficient at low speed condition	0.029	
8	pressure dependent torque loss coefficient at high speed condition	0.043	
9	reference viscosity in centipoise at which volumetric efficiency is quoted	74	cSt

Table 6.8   parametric Data Used in Simulation for Hydraulic Pump

Component No. 3: Frictionless Pipe Model PI05 (No. 1)			
No.	Input Parameters	Data	Unit
1	pipe internal diameter	12.7	mm
2	pipe length	1.32	m
3	pipe volume	0.1672	Litres
4	fluid/pipe Bulk Modulus	11261	bar
5	air saturation pressure	0	bar
6	proportion of dissolved air	0.1	
7	initial pressure	2.5	bar

Table 6.9   Parametric Data Used in Simulation for High Pressure
Pipeline Before Directional Control Valve

Component No. 4: Orifice Restrictor Model OR3H (No. 1)			
No.	Input Parameters	Data	Unit
1	steady state flowrate	0.145	L/sec
2	corresponding pressure drop	2.5	bar
3	laminar boundary in bar	0.1	bar

Table 6.10   Parametric Data Used in Simulation for Orifice Model
to Represent Pressure Loss Across Directional
Control Valve in High Pressure Line

Component No. 5: Frictionless Pipe Model PI05 (No. 2)			
No.	Input Parameters	Data	Unit
1	pipe internal diameter	12.7	mm
2	pipe length	1.53	m
3	pipe volume	0.1938	Litres
4	fluid/pipe Bulk Modulus	11261	bar
5	air saturation pressure	0	bar
6	proportion of dissolved air	0.1	
7	initial pressure	0	bar

Table 6.11   Parametric Data Used in Simulation for High Pressure Pipeline After Directional Control Valve

Component No. 6:	Hydraulic Motor Model MOAH (No. 1)		
Stage	Spool Displacement	Time (second)	Valve Position
1	maximum motor displacement	5	cc/rev
2	slip loss coefficiency at low speed	2.91×10^{-9}	
3	low speed at which slip is quoted	1000	rev/min
4	slip loss coefficiency at high speed	3.76×10^{-9}	
5	high speed at which slip is quoted	2500	rev/min
6	fraction of slip loss coefficient for drain leakage	0.08	
7	speed dependent torque loss coefficient	3×10^5	
8	pressure dependent torque loss coefficient at low speed condition	0.029	
9	pressure dependent torque loss coefficient at high speed condition	0.043	
10	ratio of gearbox between motor and propeller	3.5	
11	reference viscosity in centipoise at which volumetric efficiency is quoted	94	cSt

Table 6.12   Parametric Data Used in Simulation for Hydraulic Motor

Component No. 7: Propeller Load Model LR0H (No. 1)			
No.	Input Parameters	Data	Unit
1	effective inertia of propeller	0.02	$kg.m^2$
2	non-dimensional torque coefficient	0.101	
3	diameter of propeller	230	mm
4	initial angular velocity	0	rev/min
5	density of fluid surrounding propeller	1000	kg/m^3

Table 6.13   Parametric Data Used in Simulation for Propeller Load

Component No. 8: Frictionless Pipe Model PI05 (No. 3)			
No.	Input Parameters	Data	Unit
1	pipe internal diameter	12.7	mm
2	pipe length	2.257	m
3	pipe volume	0.28591	Litres
4	fluid/pipe Bulk Modulus	11261	bar
5	air saturation pressure	0	bar
6	proportion of dissolved air	0.1	
7	initial pressure	0	bar

Table 6.14   parametric Data Used in Simulation for Motor Outlet Pipeline

Component No. 9: Orifice Restrictor Model OR3H (No. 2)			
No.	Input Parameters	Data	Unit
1	steady state flowrate	0.145	L/sec
2	corresponding pressure drop	2	bar
3	laminar boundary in bar	0.1	bar

Table 6.15   parametric Data Used in Simulation for Orifice
Restrictor to Represent Pressure Loss Across
Directional Control Valve in Return Line

Component No. 10: Frictionless Pipe Model PI05 (No. 4)			
No.	Input Parameters	Data	Unit
1	pipe internal diameter	12.7	mm
2	pipe length	3.1	m
3	pipe volume	0.2446	Litres
4	fluid/pipe Bulk Modulus	13116	bar
5	air saturation pressure	0	bar
6	proportion of dissolved air	0.1	
7	initial pressure	0.05	bar

Table 6.16   parametric Data Used in Simulation for the Return
and Suction Pipelines

Component No. 11: Orifice Restrictor Model OR00 (No. 1)			
No.	Input Parameters	Data	Unit
1	steady state flowrate	0.01405	L/sec
2	corresponding pressure drop	0.05	bar
3	laminar boundary in bar	0.1	bar

Table 6.17   parametric Data Used in Simulation for the Pressure
            in the Suction Line

Component No. 12:	3 Link Fixed Level Tank Model TK03 (No. 1)		
No.	Input Parameters	Data	Unit
1	first link to suction line	0.1	bar
2	second link from return line	0	bar
3	third link from motor drain line	0	bar
4	fourth link from relief valve	0	bar

Table 6.18   parametric Data Used in Simulation for Reservoir

Component No. 13:	2 Way 2 Position DCV Model DC1C (No. 1)		
No.	Input Parameters	Input Data	Unit
1	defined flowrate	0.145	L/min
2	corresponding pressure drop	5	bar
3	linear region limit	0.0256	bar

Table 6.19   parametric Data Used in Simulation for 2 Way 2 Position Directional Control Valve

Component No. 14: Movement of DCV Model DEDT (No. 1)			
Stage	Spool Displacement	Time (second)	Valve Position
1	0	0	open
2	1	0.02	close
3	1	5400	close

Table 6.20   parametric Data Used in Simulation for Different Time
Relate Slip of Directional Control Valve

Component No. 15: Relief Valve Model PC01 (No. 1)			
No.	Input Parameters	Data	Unit
1	Relief Valve Cracking Pressure	40	bar
2	Relief Valve Constant	0.05	(L/sec)/bar

Table 6.21   parametric Data Used in Simulation for a Single
Stage Relief Valve

Component No. 16:	Closed System Temperature Model FP3H (No. 1)		
No.	Input Parameters	Data	Unit
1	inside pipe diameter	12.7	mm
2	outside pipe diameter	21	mm
3	length of pipe section	7	m
4	fluid specific heat	1909	J/(kg.deg.K)
5	pipe wall specific heat	2010	J/(kg.deg.K)
6	density of pipe wall material	1100	kg/m^3
7	conductivity of pipe wall material	0.15	W/m.K
8	conductivity of fluid	0.143	W/m.K
9	emissivity of pipe section	0.9	
9	initial fluid temperature	289	deg.K
10	initial outside pipe wall temperature	287	deg.K
11	initial surrounding atmosphere temperature	285	deg.K
12	type of oil used	32 BP HLP	

Table 6.22   parametric Data Used in Simulation for Temperature and Fluid Property Calculation in the Unboosted Closed Hydrostatic Drive Propeller System with Hydraulic Hoses

Component No. 16:	Closed System Temperature Model FP3H (No. 1)		
No.	Input Parameters	Data	Unit
1	inside pipe diameter	12.7	mm
2	outside pipe diameter	17	mm
3	length of pipe section	7	m
4	fluid specific heat	1909	J/(kg.deg.K)
5	pipe wall specific heat	486	J/(kg.deg.K)
6	density of pipe wall material	7700	kg/m^3
7	conductivity of pipe wall material	60.2	W/m.K
8	conductivity of fluid	0.143	W/m.K
9	emissivity of pipe section	0.32	
9	initial fluid temperature	289	deg.K
10	initial outside pipe wall temperature	287	deg.K
11	initial surrounding atmosphere temperature	285	deg.K
12	type of oil used	32 BP HLP	

Table 6.23   parametric Data Used in Simulation for Temperature and Fluid
Property Calculation in the Unboosted Closed Hydrostatic Drive
Propeller System with Steel Pipes

Component No. 16:	Closed System Temperature Model FP3H (No. 1)		
No.	Input Parameters	Data	Unit
1	inside pipe diameter	12.7	mm
2	outside pipe diameter	17	mm
3	length of pipe section	7	m
4	fluid specific heat	1909	J/(kg.deg.K)
5	pipe wall specific heat	383	J/(kg.deg.K)
6	density of pipe wall material	8900	kg/m^3
7	conductivity of pipe wall material	386	W/m.K
8	conductivity of fluid	0.143	W/m.K
9	emissivity of pipe section	0.023	
9	initial fluid temperature	289	deg.K
10	initial outside pipe wall temperature	287	deg.K
11	initial surrounding atmosphere temperature	285	deg.K
12	type of oil used	32 BP HLP	

Table 6.24   parametric Data Used in Simulation for Temperature and Fluid Property Calculation in the Unboosted Closed Hydrostatic Drive Propeller System with Copper Pipes

Pipe Type	Pipe Volume (ml)	Pipe Length (cm)	External Diameter (mm)	Internal Diameter (mm)
Rubber Hose	260	53.5	39.7	24.9
Steel Tube	300	52	33.9	27

Table 6.25   Pipe Dimensional Sizes for Comparison Tests of Steel + Rubber

Surrounding atmospheric temperature: 16 deg. C				
Cooling Time in minutes	Fluid Temp. in Steel Tube in deg. C	Fluid Temp. in Rubber Hose in deg. C	Outside Steel Tube Temp. in deg. C	Outside Rubber Hose Temp. in deg. C
0	53.3	53.3	18.3	17.9
1.5	45.3	40.8	38.6	28.7
5	42.8	38	36.5	32.8
15	37.9	33.4	32	29.8
20	35.8	31.2	30.8	28
25	33.7	29.6	29.1	26.4
30	32	28.2	28.1	25.3
35	30.4	26.6	26.2	24.6
40	29.3	25.9	25.4	23.6
45	27.8	24.4	24.9	22.4
50	26.7	23.6	24	21.9
55	25.5	22.5	22.6	21
60	24.5	21.8	22	20.5

Table 6.26   Experimental Temperature Recordings

Pipe Type	Pipe Volume (ml)	Pipe Length (cm)	External Diameter (mm)	Internal Diameter (mm)
Copper Tube	617	68	38	34

Table 6.27　　Pipe Dimensional Sizes for Comparison Tests of Copper + Rubber

Component No. 19:	Movement of DCV Model DEDT (No. 1)		
Stage	Spool Displacement	Time (second)	Valve Position
1	0	0	open
2	1	0.02	close
3	1	7200	close

Table 6.28　　parametric Simulation Data Used for Operating Time
Related to the Slip of the Directional Control Valve

Component No. 16: Pipe Wall Temperature Model PICH (No. 1)			
No.	Input Parameters	Data	Unit
1	inside pipe diameter	12.7	mm
2	outside pipe diameter	17	mm
3	length of pipe section	0.23	m
4	pipe wall specific heat	486	J/(kg.deg.K)
5	density of pipe wall material	7700	kg/m^3
6	conductivity of pipe wall material	60.2	W/m.K
7	conductivity of fluid	0.143	W/m.K
8	emissivity of pipe section	0.32	
9	initial outside pipe wall temperature	287	deg.K
10	initial surrounding atmosphere temperature	285	deg.K

Table 6.29   parametric Simulation Data Used for the Steel Pipe at
the Pump Outlet in the Unboosted Closed Hydrostatic Drive
Propeller System

Component No. 17:	Pipe Wall Temperature Model PICH (No. 2)		
No.	Input Parameters	Data	Unit
1	inside pipe diameter	12.7	mm
2	outside pipe diameter	21	mm
3	length of pipe section	1	m
4	pipe wall specific heat	2010	J/(kg.deg.K)
5	density of pipe wall material	1100	kg/m^3
6	conductivity of pipe wall material	0.15	W/m.K
7	conductivity of fluid	0.143	W/m.K
8	emissivity of pipe section	0.9	
9	initial outside pipe wall temperature	287	deg.K
10	initial surrounding atmosphere temperature	285	deg.K

Table 6.30   parametric Simulation Data Used for the Single Wired
Hydraulic Hose in the High Pressure Pipeline Before the
Directional Control Valve

Component No. 18:	Pipe Wall Temperature Model PICH (No. 3)		
No.	Input Parameters	Data	Unit
1	inside pipe diameter	12.7	mm
2	outside pipe diameter	17	mm
3	length of pipe section	0.21	m
4	pipe wall specific heat	486	J/(kg.deg.K)
5	density of pipe wall material	7700	kg/m^3
6	conductivity of pipe wall material	60.2	W/m.K
7	conductivity of fluid	0.143	W/m.K
8	emissivity of pipe section	0.32	
9	initial outside pipe wall temperature	287	deg.K
10	initial surrounding atmosphere temperature	285	deg.K

Table 6.31   parametric Simulation Data Used for the Steel Pipe at
the Inlet and Outlet of the Directional Control Valve

Component No. 19: Pipe Wall Temperature Model PICH (No. 4)			
No.	Input Parameters	Data	Unit
1	inside pipe diameter	12.7	mm
2	outside pipe diameter	21	mm
3	length of pipe section	1.9	m
4	pipe wall specific heat	2010	J/(kg.deg.K)
5	density of pipe wall material	1100	kg/m^3
6	conductivity of pipe wall material	0.15	W/m.K
7	conductivity of fluid	0.143	W/m.K
8	emissivity of pipe section	0.9	
9	initial outside pipe wall temperature	287	deg.K
10	initial surrounding atmosphere temperature	285	deg.K

Table 6.32 parametric Simulation Data Used for the Single Wired Hydraulic Hose in the High Pressure Pipeline After the Directional Control Valve

Component No. 20: Pipe Wall Temperature Model PICH (No. 5)			
No.	Input Parameters	Data	Unit
1	inside pipe diameter	12.7	mm
2	outside pipe diameter	17	mm
3	length of pipe section	0.23	m
4	pipe wall specific heat	486	J/(kg.deg.K)
5	density of pipe wall material	7700	kg/m^3
6	conductivity of pipe wall material	60.2	W/m.K
7	conductivity of fluid	0.143	W/m.K
8	emissivity of pipe section	0.32	
9	initial outside pipe wall temperature	287	deg.K
10	initial surrounding atmosphere temperature	285	deg.K

Table 6.33   parametric Simulation Data Used for the Steel Pipe at the Inlet of the Motor

Component No. 21: Pipe Wall Temperature Model PICH (No. 6)			
No.	Input Parameters	Data	Unit
1	inside pipe diameter	12.7	mm
2	outside pipe diameter	17	mm
3	length of pipe section	0.18	m
4	pipe wall specific heat	486	J/(kg.deg.K)
5	density of pipe wall material	7700	kg/m^3
6	conductivity of pipe wall material	60.2	W/m.K
7	conductivity of fluid	0.143	W/m.K
8	emissivity of pipe section	0.32	
9	initial outside pipe wall temperature	287	deg.K
10	initial surrounding atmosphere temperature	285	deg.K

Table 6.34   parametric Simulation Data Used for the Steel Pipe at
the Outlet of the Motor

Component No. 22: Pipe Wall Temperature Model PICH (No. 7)			
No.	Input Parameters	Data	Unit
1	inside pipe diameter	12.7	mm
2	outside pipe diameter	21	mm
3	length of pipe section	1.15	m
4	pipe wall specific heat	2010	J/(kg.deg.K)
5	density of pipe wall material	1100	kg/m^3
6	conductivity of pipe wall material	0.15	W/m.K
7	conductivity of fluid	0.143	W/m.K
8	emissivity of pipe section	0.9	
9	initial outside pipe wall temperature	287	deg.K
10	initial surrounding atmosphere temperature	285	deg.K

Table 6.35   parametric Simulation Data Used for the Single Wired
Hydraulic Hose in the Return line Before the
Directional Control Valve

Component No. 23:	Pipe Wall Temperature Model PICH (No. 8)		
No.	Input Parameters	Data	Unit
1	inside pipe diameter	12.7	mm
2	outside pipe diameter	17	mm
3	length of pipe section	0.21	m
4	pipe wall specific heat	486	J/(kg.deg.K)
5	density of pipe wall material	7700	kg/m^3
6	conductivity of pipe wall material	60.2	W/m.K
7	conductivity of fluid	0.143	W/m.K
8	emissivity of pipe section	0.32	
9	initial outside pipe wall temperature	287	deg.K
10	initial surrounding atmosphere temperature	285	deg.K

Table 6.36   parametric Simulation Data Used for the Steel Pipe at
the Inlet and Outlet of the Directional Control Valve
in the Return Line

Component No. 24: Pipe Wall Temperature Model PICH (No. 9)			
No.	Input Parameters	Data	Unit
1	inside pipe diameter	9.5	mm
2	outside pipe diameter	17	mm
3	length of pipe section	2.9	m
4	pipe wall specific heat	2010	J/(kg.deg.K)
5	density of pipe wall material	1100	kg/m^3
6	conductivity of pipe wall material	0.15	W/m.K
7	conductivity of fluid	0.143	W/m.K
8	emissivity of pipe section	0.9	
9	initial outside pipe wall temperature	287	deg.K
10	initial surrounding atmosphere temperature	285	deg.K

Table 6.37   parametric Simulation Data Used for the Single Wired
Hydraulic Hose in the Return Line After the Directional
Control Valve

Component No. 25: Pipe Wall Temperature Model PICH (No. 10)			
No.	Input Parameters	Data	Unit
1	inside pipe diameter	12.7	mm
2	outside pipe diameter	17	mm
3	length of pipe section	0.44	m
4	pipe wall specific heat	486	J/(kg.deg.K)
5	density of pipe wall material	7700	kg/m^3
6	conductivity of pipe wall material	60.2	W/m.K
7	conductivity of fluid	0.143	W/m.K
8	emissivity of pipe section	0.32	
9	initial outside pipe wall temperature	287	deg.K
10	initial surrounding atmosphere temperature	285	deg.K

Table 6.38   parametric Simulation Data Used for the Steel Pipe in
the Interconnecting and Suction Pipelines

Component No. 26: Closed System Fluid Temperature Model FPOH (No. 1)			
No.	Input Parameters	Data	Unit
1	inside pipe diameter	12.7	mm
2	outside pipe diameter	21	mm
3	length of pipe section	7	m
4	fluid specific heat	1909	J/(kg.deg.K)
5	initial fluid temperature	289	deg.K
6	type of oil used	32 BP HLP	

Table 6.39   parametric Data Used in Simulation for Fluid Temperature and
Property Calculation in the Unboosted Closed Hydrostatic Drive
Propeller System Using the Improved Theoretical Approach

Component No. 27: Tank Fluid Temperature Model FPTH (No. 1)			
No.	Input Parameters	Data	Unit
1	width of tank base	0.19	m
2	length of tank base	0.25	m
3	fluid height in tank	0.11	m
4	fluid specific heat	1909	J/(kg.deg.K)
5	conductivity of tank wall material	80	W/m.K
6	thickness of tank wall	8	mm
7	initial fluid temperature	289	deg.K
8	initial outside tank vertical wall temperature	287	deg.K
9	initial outside tank bottom wall temperature	287.3	deg.K
10	initial surrounding atmosphere temperature	285	deg.K
11	type of oil used	32 BP HLP	

Table 6.40   parametric Simulation Data Used for Fluid Temperature
             Calculation in the Reservoir of the Partially Closed
             Hydrostatic Drive Propeller System

Component No. 26:	Pipe Fluid Temperature Model FPCH (No. 1)		
No.	Input Parameters	Data	Unit
1	inside pipe diameter	12.7	mm
2	outside pipe diameter	21	mm
3	length of pipe section	1.29	m
4	fluid specific heat	1909	J/(kg.deg.K)
5	initial fluid temperature	289	deg.K
6	type of oil used	32 BP HLP	

Table 6.41   parametric Simulation Data Used for Fluid Temperature and
Property Model in the First Part of the High Pressure
Line Using More Accurate Theoretical Approach

Component No. 27:	Pipe Fluid Temperature Model FPCH (No. 2)		
No.	Input Parameters	Data	Unit
1	inside pipe diameter	12.7	mm
2	outside pipe diameter	21	mm
3	length of pipe section	2.26	m
4	fluid specific heat	1909	J/(kg.deg.K)
5	initial fluid temperature	289	deg.K
6	type of oil used	32 BP HLP	

Table 6.42   parametric Simulation Data Used for Fluid Temperature and
Property Model in the Second Section of the High Pressure Line

Component No. 28:	Pipe Fluid Temperature Model FPGH (No. 1)		
No.	Input Parameters	Data	Unit
1	inside pipe diameter	12.7	mm
2	outside pipe diameter	21	mm
3	length of pipe section	1.41	m
4	fluid specific heat	1909	J/(kg.deg.K)
5	initial fluid temperature	289	deg.K
6	type of oil used	32 BP HLP	

Table 6.43   parametric Simulation Data Used for Fluid Temperature and
Property Model in the First Section of the Return Line

Component No. 29:	Pipe Fluid Temperature Model FPGH (No. 2)		
No.	Input Parameters	Data	Unit
1	inside pipe diameter	12.7	mm
2	outside pipe diameter	21	mm
3	length of pipe section	3.13	m
4	fluid specific heat	1909	J/(kg.deg.K)
5	initial fluid temperature	289	deg.K
6	type of oil used	32 BP HLP	

Table 6.44   parametric Simulation Data Used for Fluid Temperature
and Property Model in the Second Section of the
Return Line

Component No. 30: Pipe Fluid Temperature Model FPDH (No. 1)			
No.	Input Parameters	Data	Unit
1	inside pipe diameter	12.7	mm
2	outside pipe diameter	21	mm
3	length of pipe section	0.44	m
4	fluid specific heat	1909	J/(kg.deg.K)
5	initial fluid temperature	289	deg.K
6	type of oil used	32 BP HLP	

Table 6.45   parametric Simulation Data Used for Fluid Temperature and
Property Calculation in the Interconnecting and Suction Pipes

Surroundings   Boundary (not necessarily fixed)

Heat transfer

System

(usually variable mass)

Work transfer

Entering mass $\int M_{in}$

leaving mass $\int M_{out}$
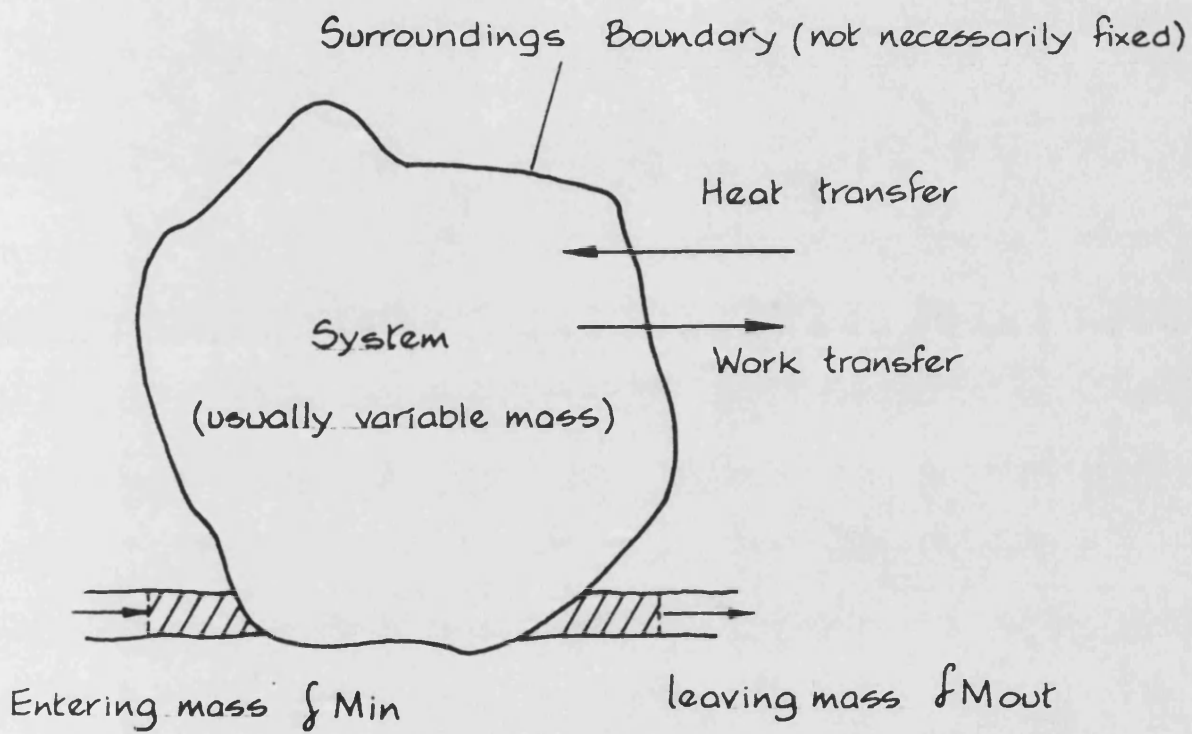
FIG. 6.1 OPEN THERMAL SYSTEM UNDERGOING
AN IMAGINARY NON-FLOW PROCESS
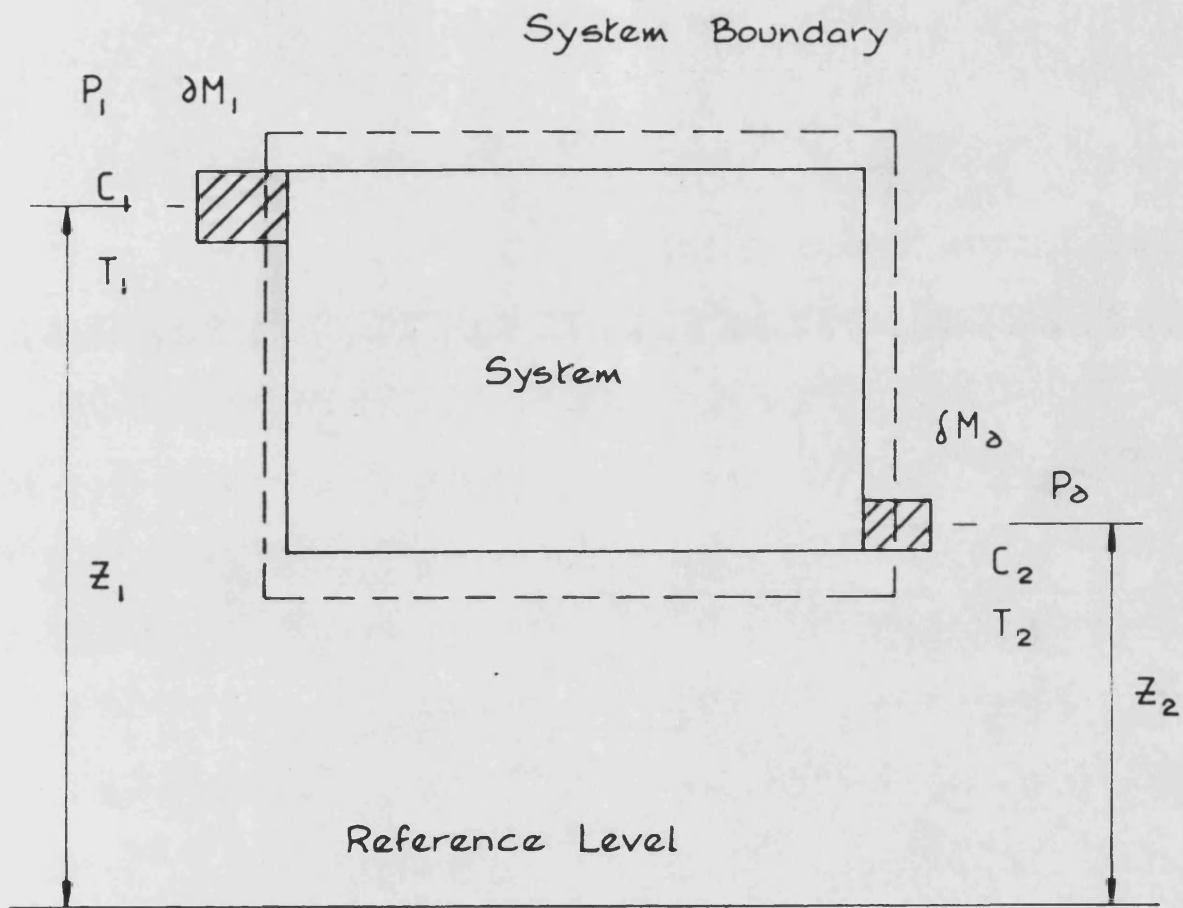
FIG. 6.2   OPEN   SYSTEM

SUM OF HEAT LOSSES IN PIPE WALL

$$H_1$$

$$Q_1 = Q_2$$

$$Q_2$$

$$Q_1$$

$$T_f$$

$$T_f$$

$$T_{IN}$$

W

POWER LOSS

CONVERTED INTO HEAT

$$H_1$$
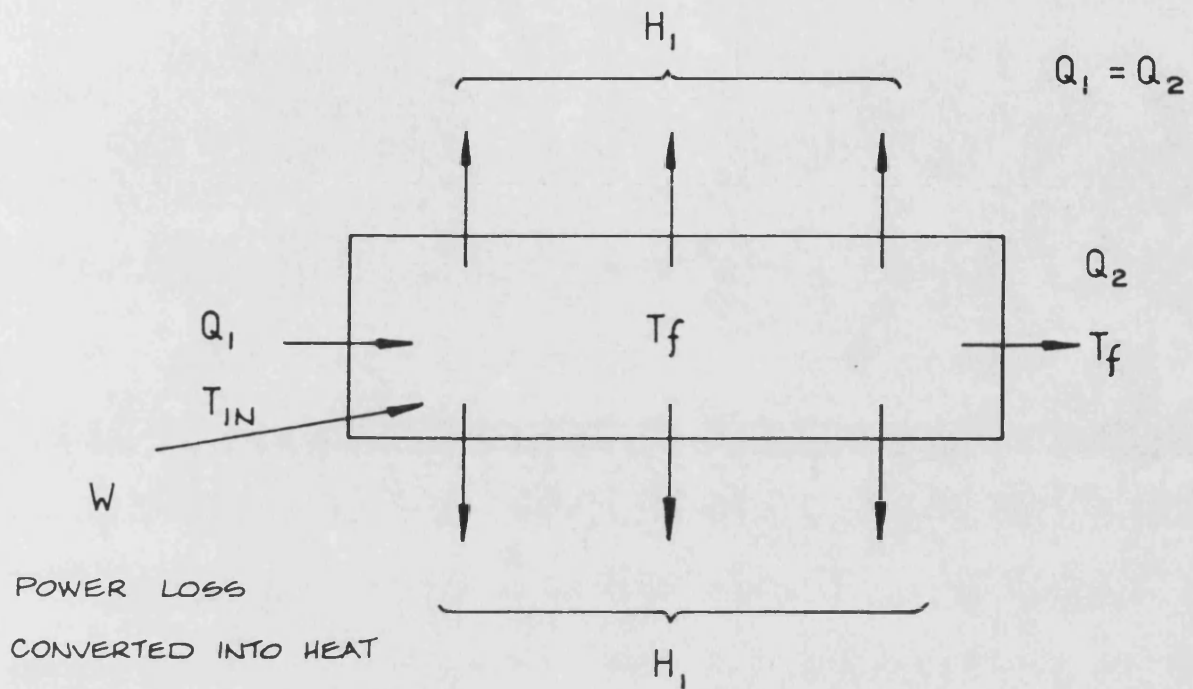
SUM OF HEAT LOSSES IN PIPE WALL

FIG. 6.3   OPEN THERMAL SYSTEM OF FLUIDS
IN A PIPE SECTION

Inside Pipe

outsider pipe wall

T_f

Natural Convection + Radiation

H

Fluid

T_1

H_2

atmosphere

Forced Convection

T_2

T_a

$R_2 - R_1$

T_1

$M_P C_{PP} \dfrac{dT_2}{dt}$

Pipe wall absorbs Heat energy

Heat flow transferred from fluid to pipe wall

H_1

H_2

Heat flow transferred from pipe wall to atmosphere

T_2
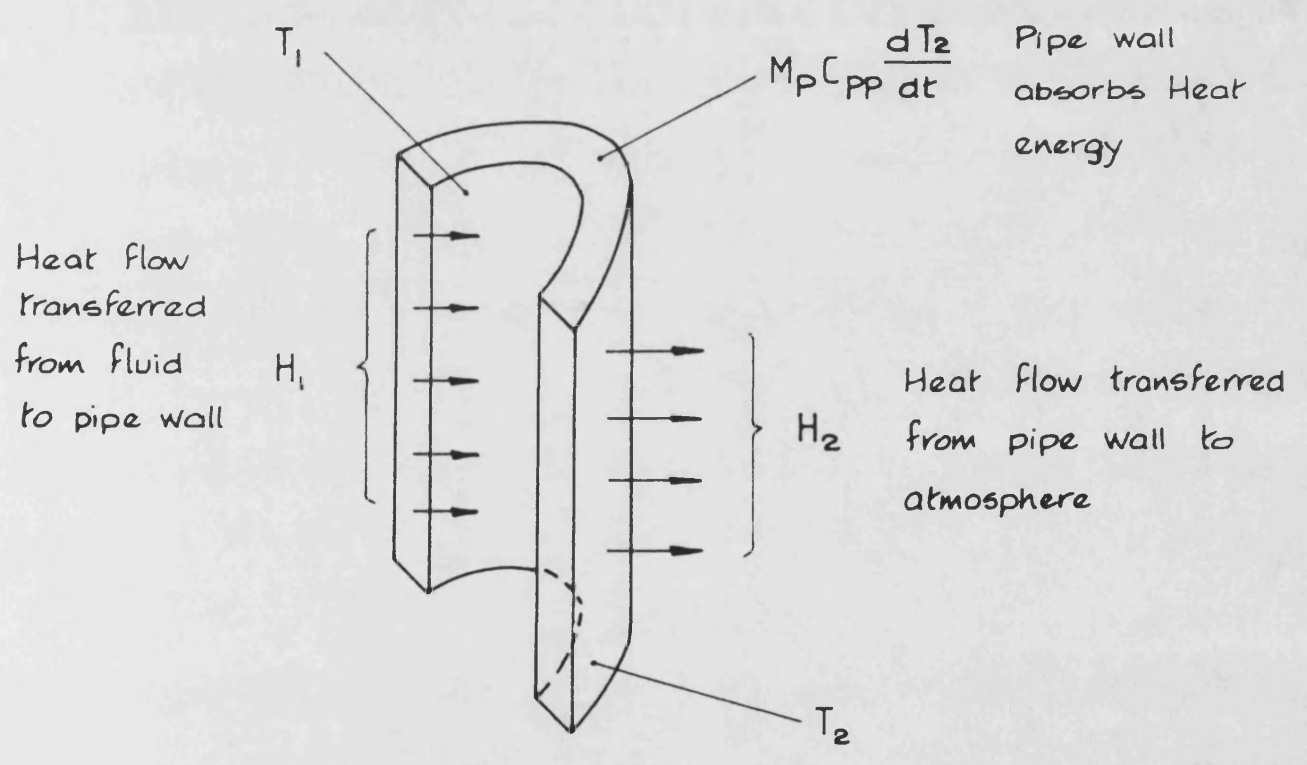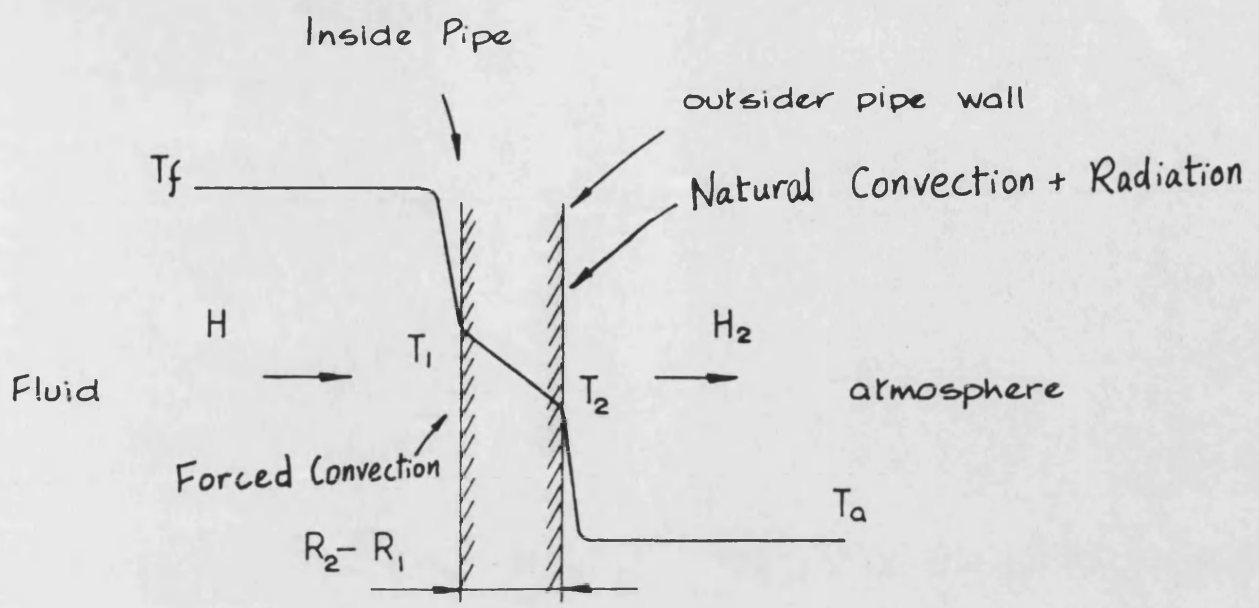
FIG. 6.4   HEAT FLOW LOSS THROUGH THE PIPE WALL
IN SURROUNDING ATMOSPHERE
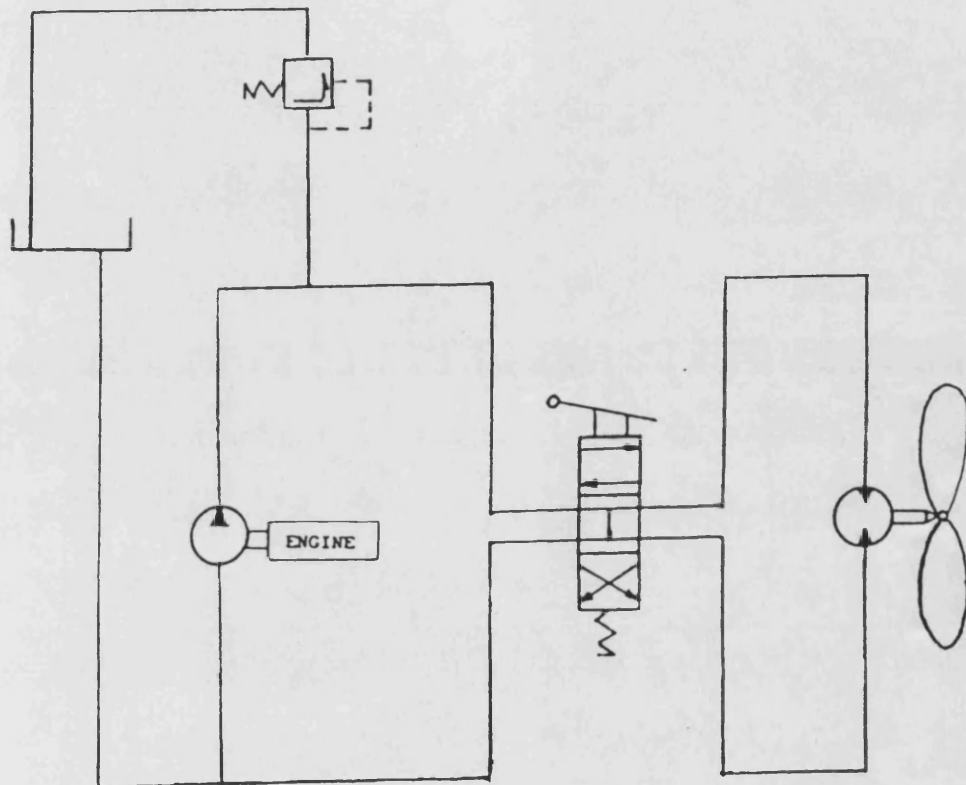
Fig. 6.5   An Unboosted Hydrostatically Driven Boat Propeller System
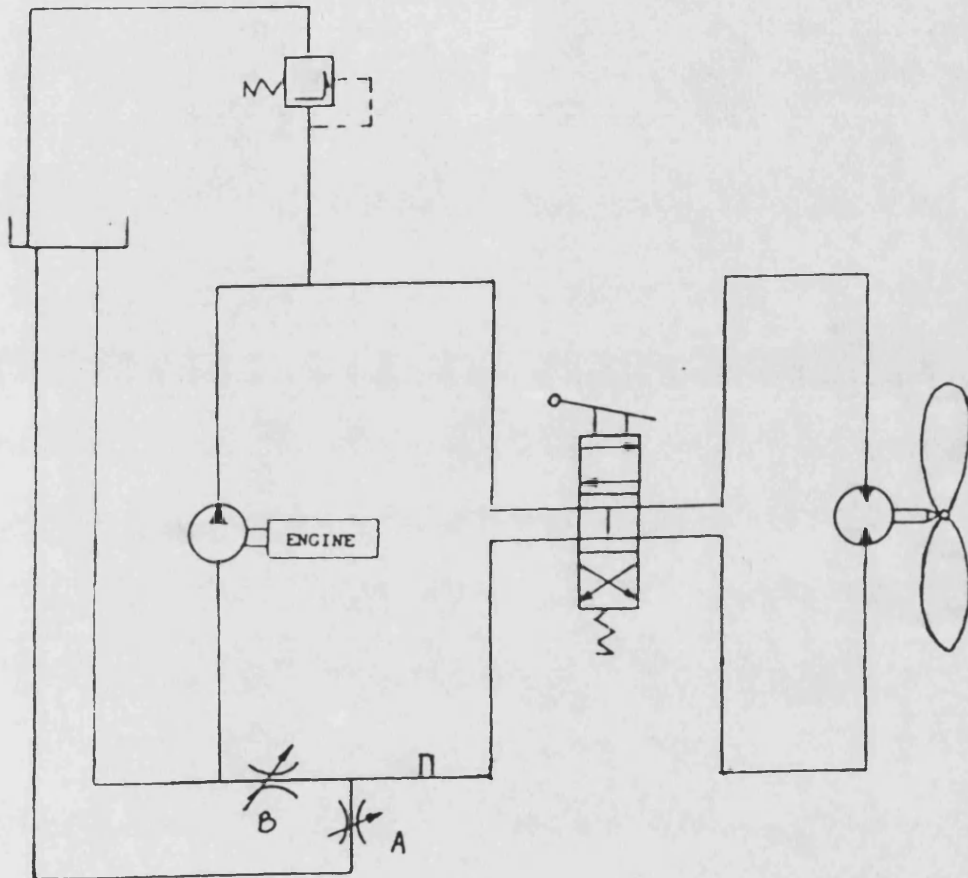
Fig. 6.6   A Partially Closed Hydrostatically Driven Boat Propeller System
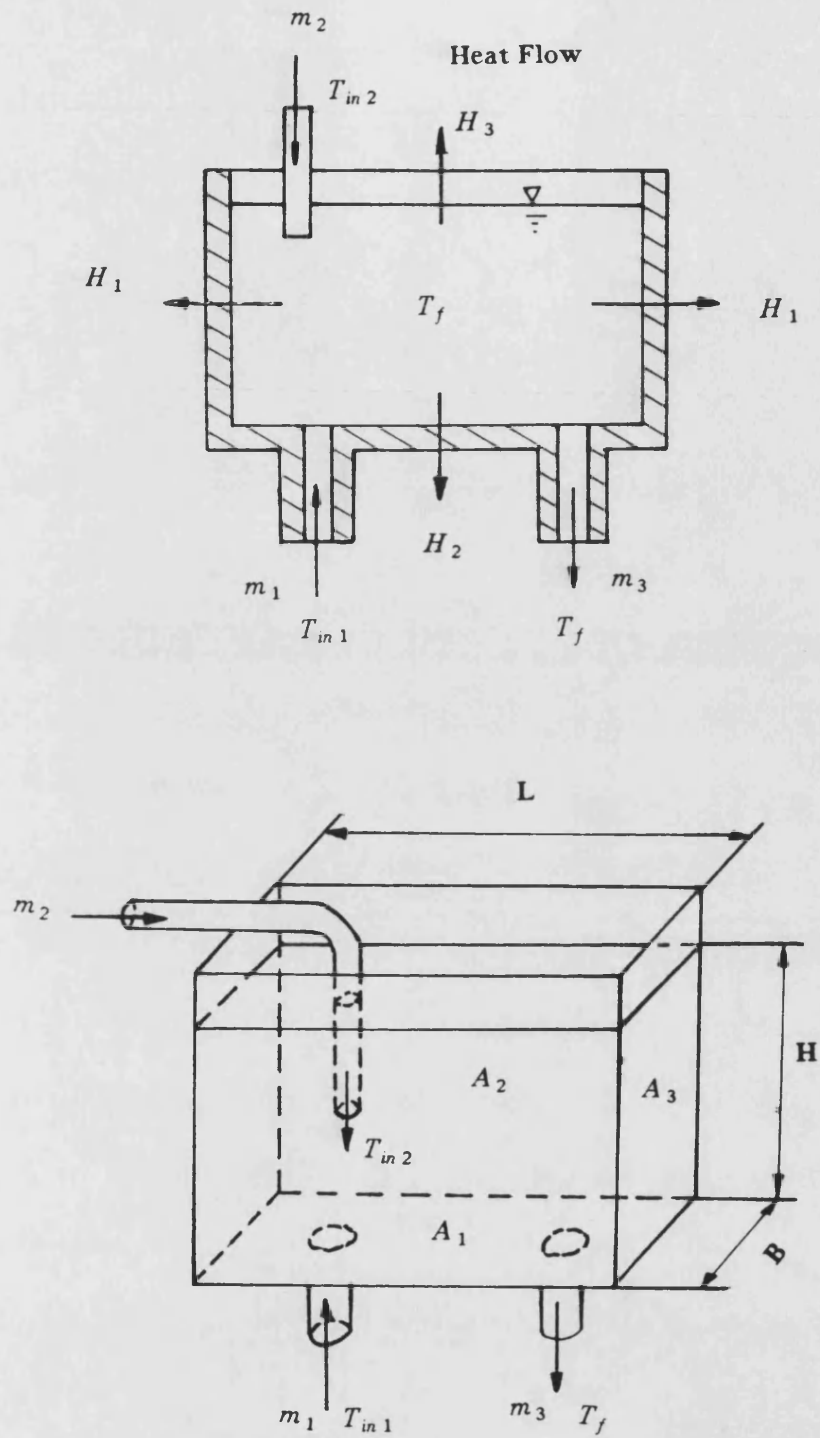
Fig. 6.7   A Hydraulic Reservoir Regarded as an Open Thermal System
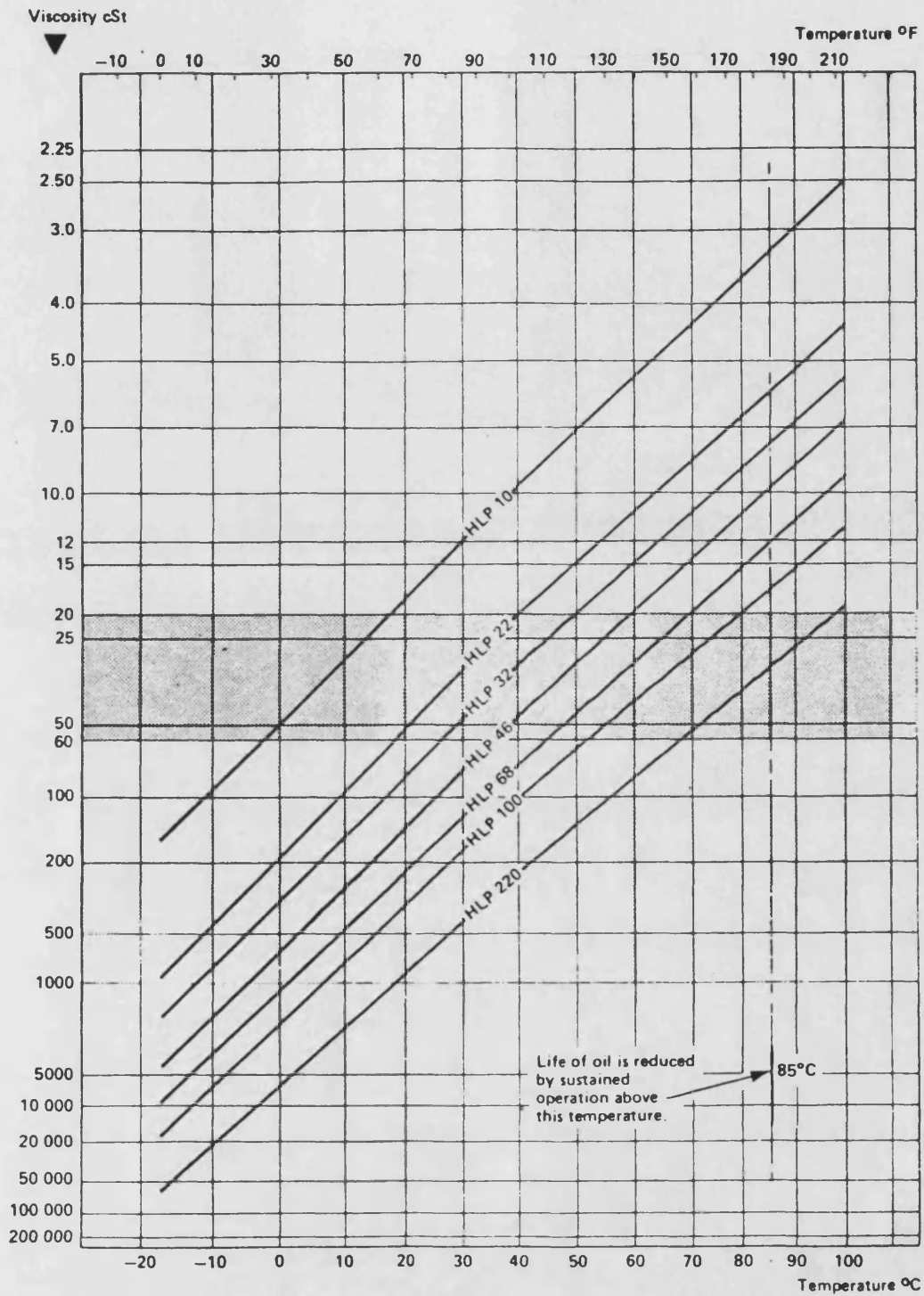
Fig. 6.8   Variation of Viscosity in Several Types of Commonly Used
                Mineral Oils with Temperature Change
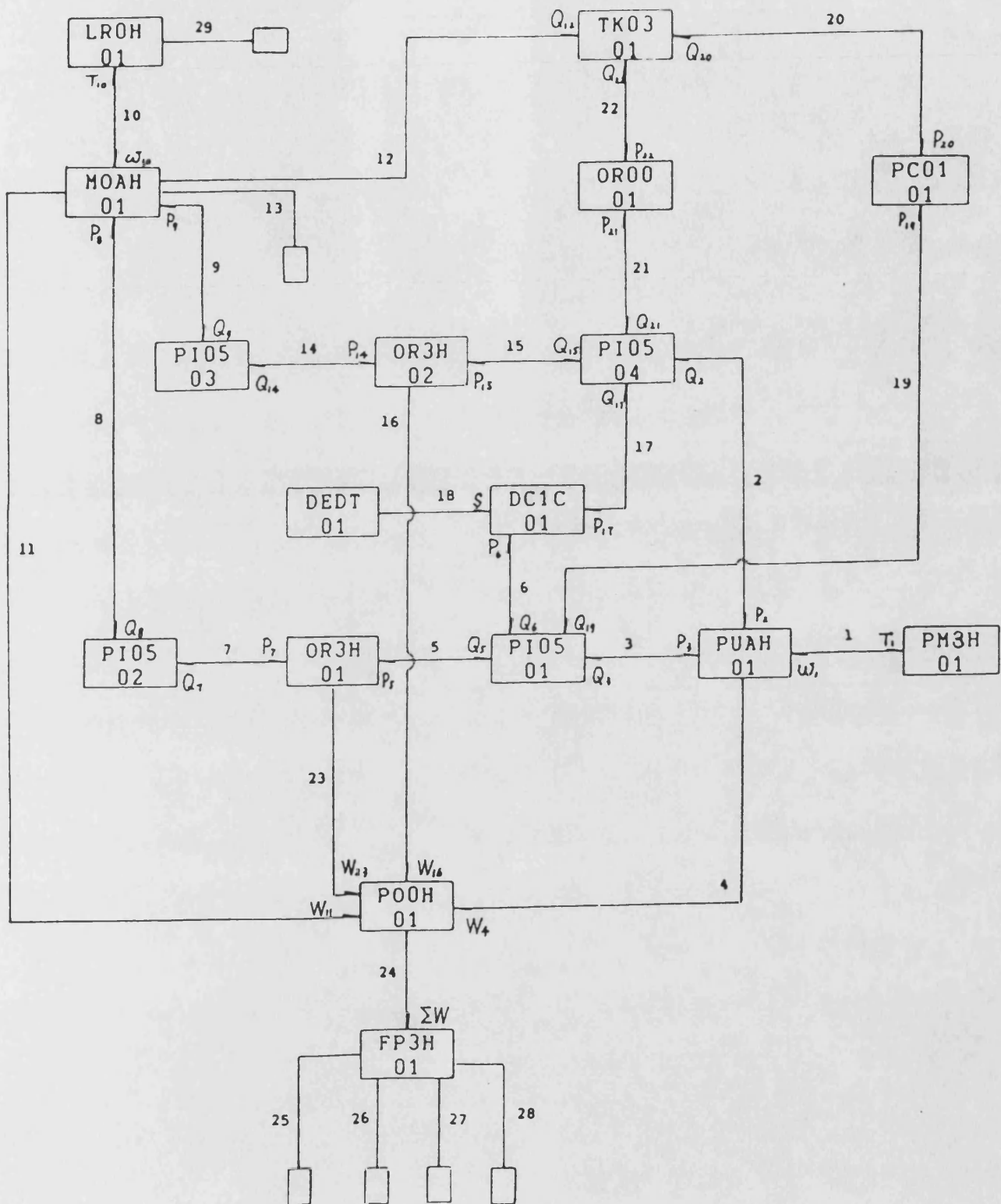
Fig. 6.9   Block Diagram for Simulating the Unboosted Hydrostatic Drive
Propelelr System with a Simple Approach to Assume an
Uniform Loop Fluid Temperature

single wire braid reinforcement

synthetic rubber

Fig. 6.10   Structure of A Typical Single Wire Braid Hydraulic Hose

Power Loss:

P = 300 W

P = 220 W

P = 170 W

P = 97.5 W
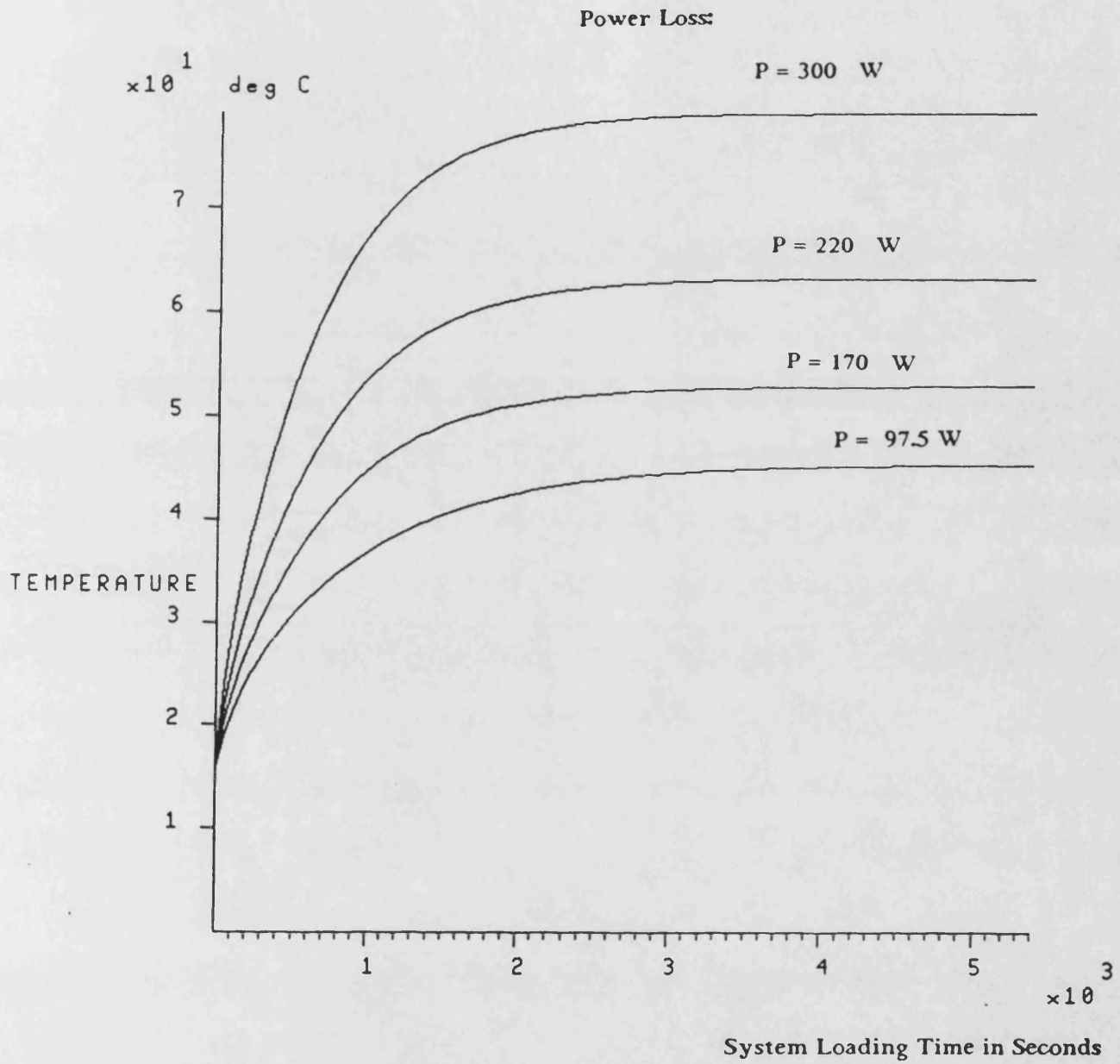
Fig. 6.11   The Effects of Power Loss on the Fluid Temperature in the
                 Unboosted Closed Hydrostatic Drive Propeller System
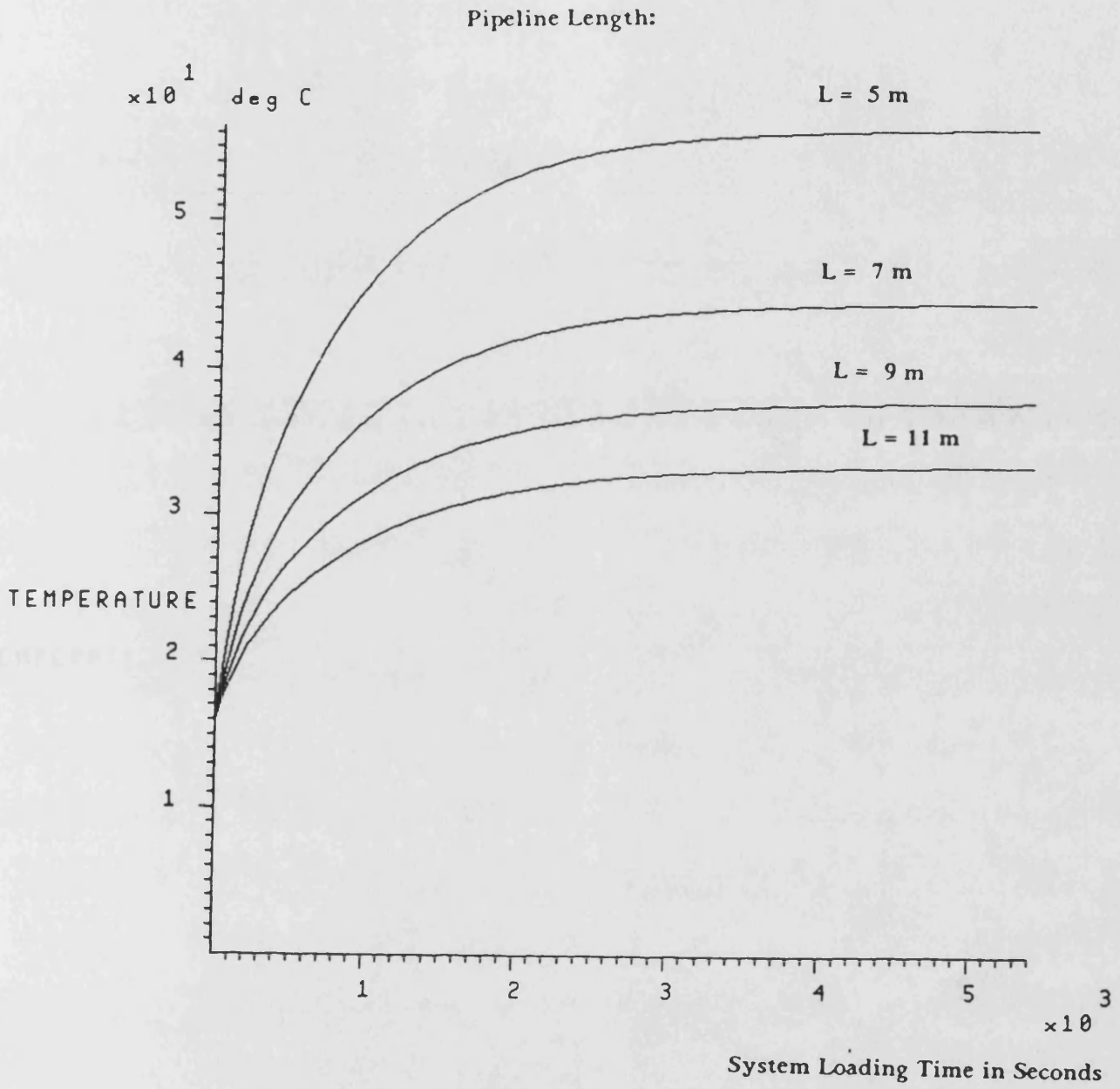
Fig. 6.12   The Effects of Pipelength on the Fluid Temperature in the
Unboosted Closed Hydrostatic Drive Propeller System
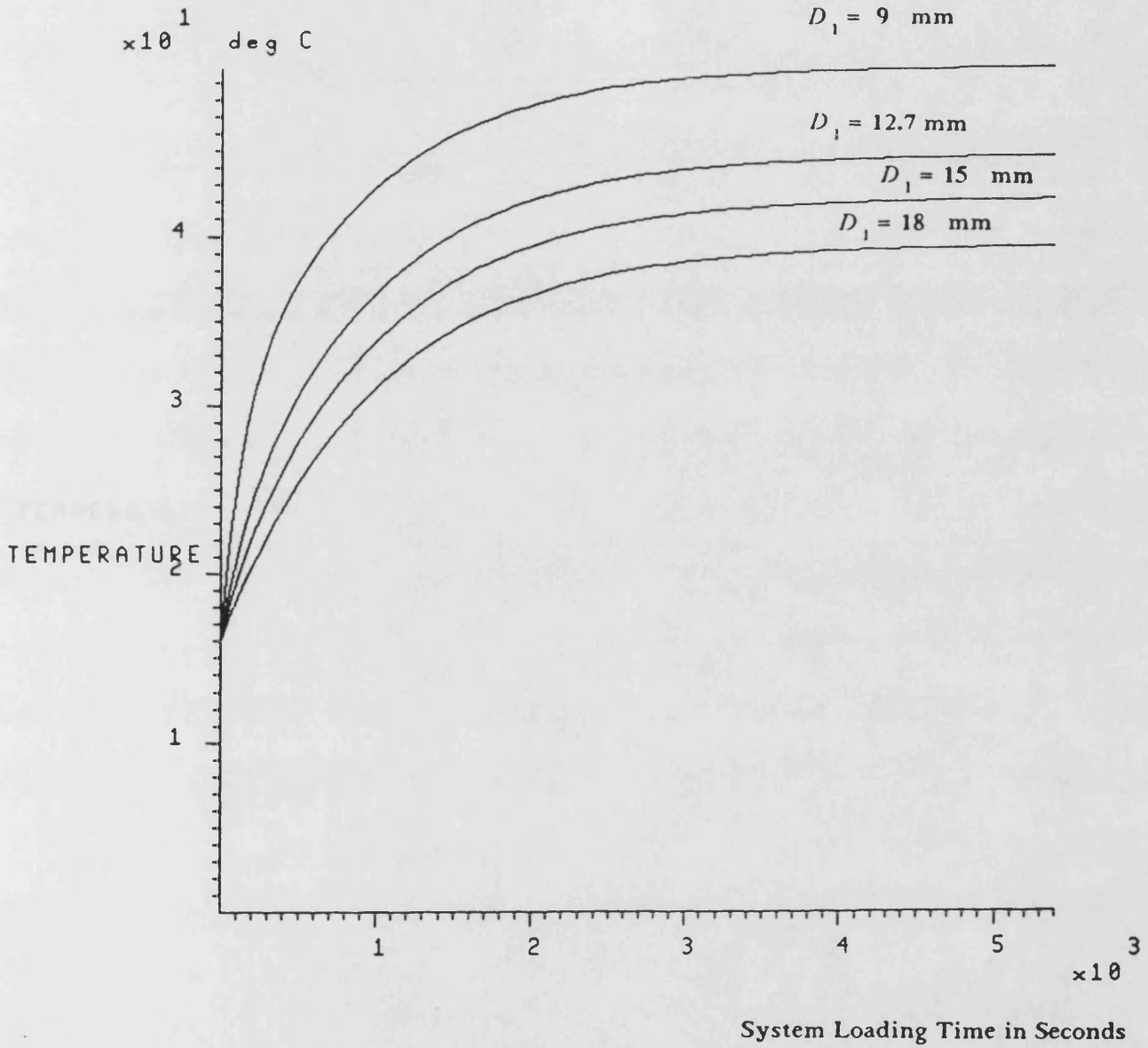
Fig. 6.13   The Effects of Internal Pipe Diameter on the Fluid Temperature
in the Unboosted Closed Hydrostatic Drive Propeller System
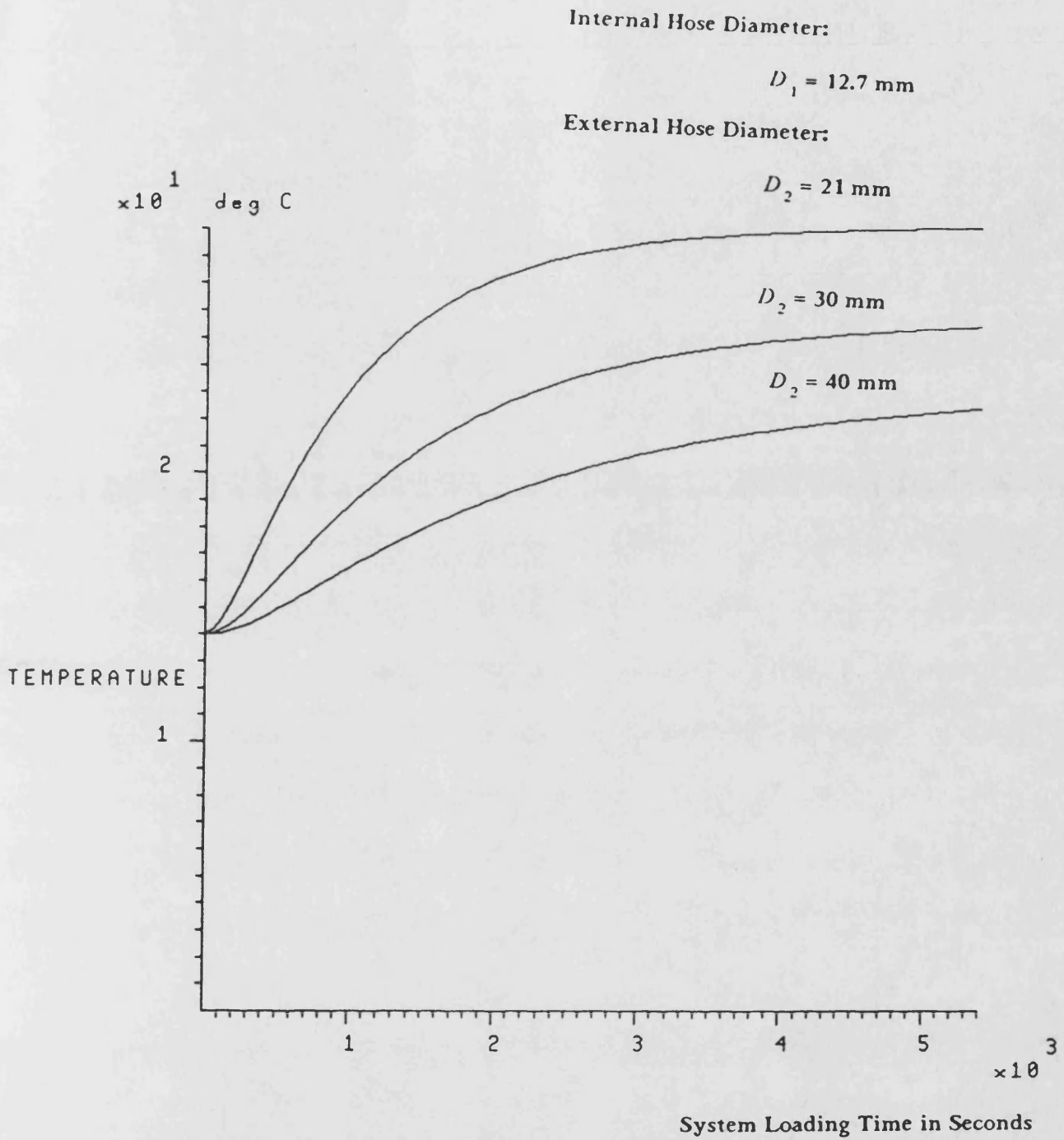
Fig. 6.14   The Effects of External Hose Diameter on the Outside Hose Wall
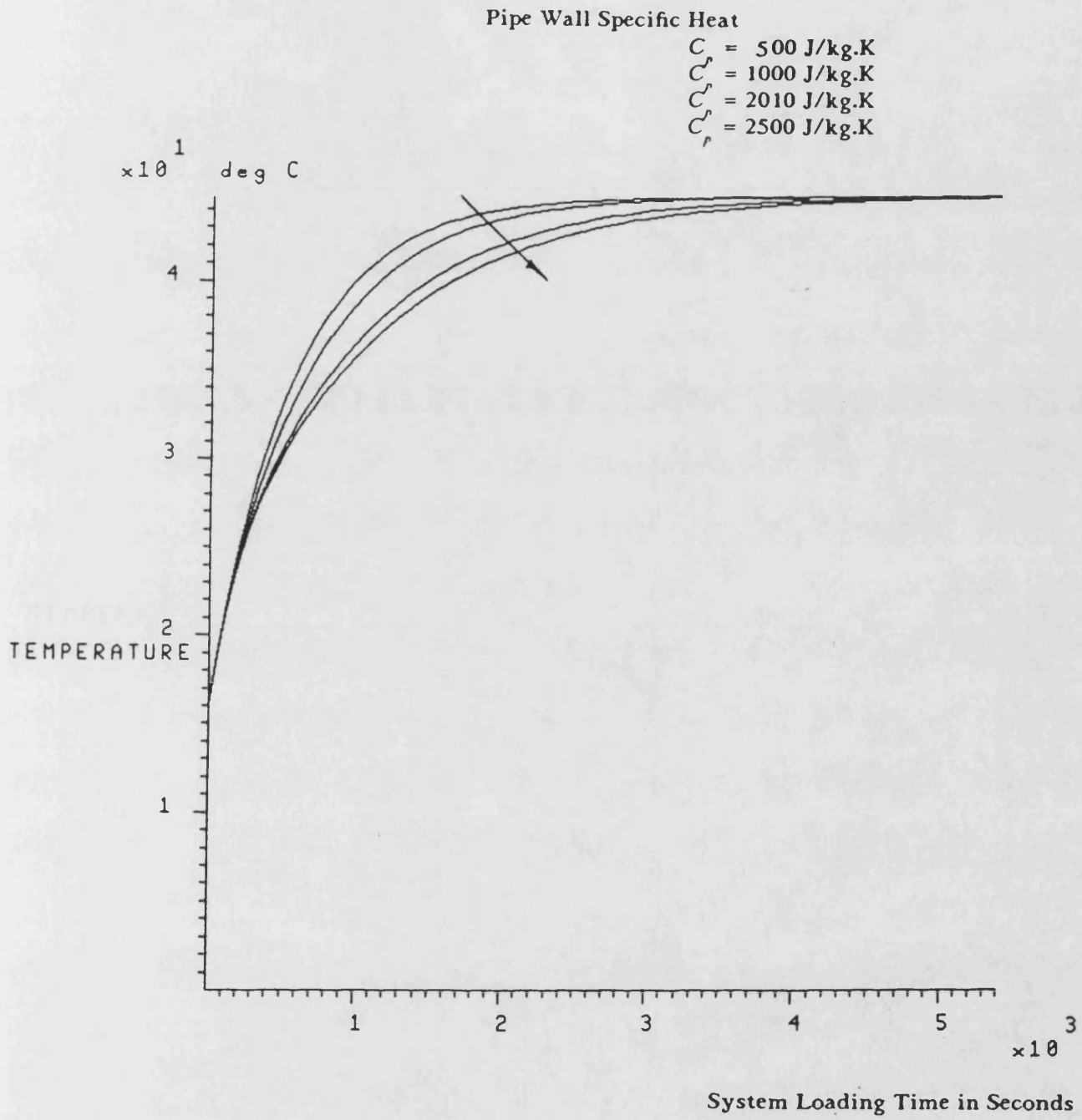Temperature in the Unboosted Closed Hydrostatic Drive
Propeller System

Thermal Conductivity
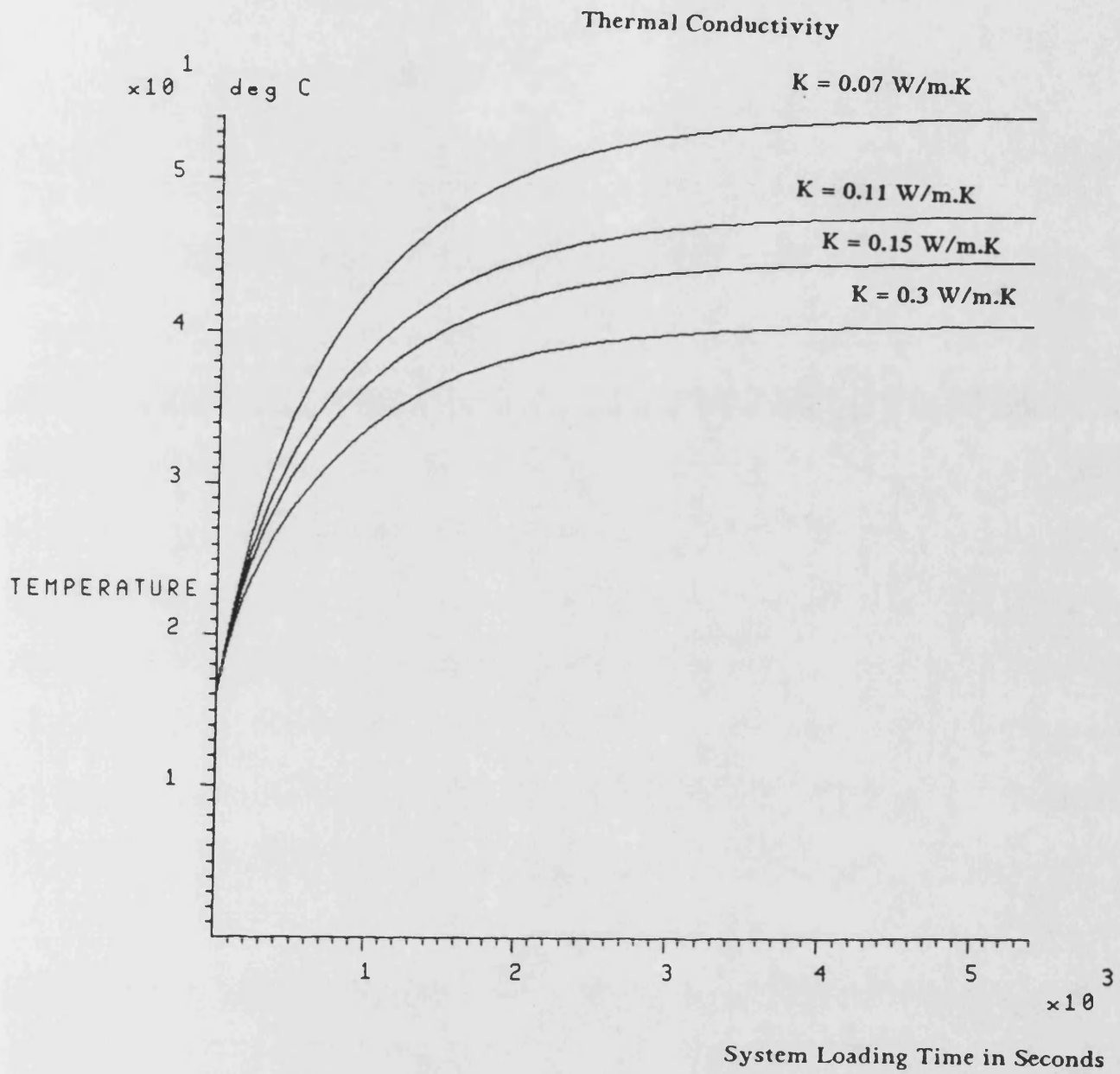
Fig. 6.15 a   The Effects of Thermal Conductivity of Pipe Wall Material on the Fluid Temperature in the Unboosted Closed Hydrostatic Drive Propeller System
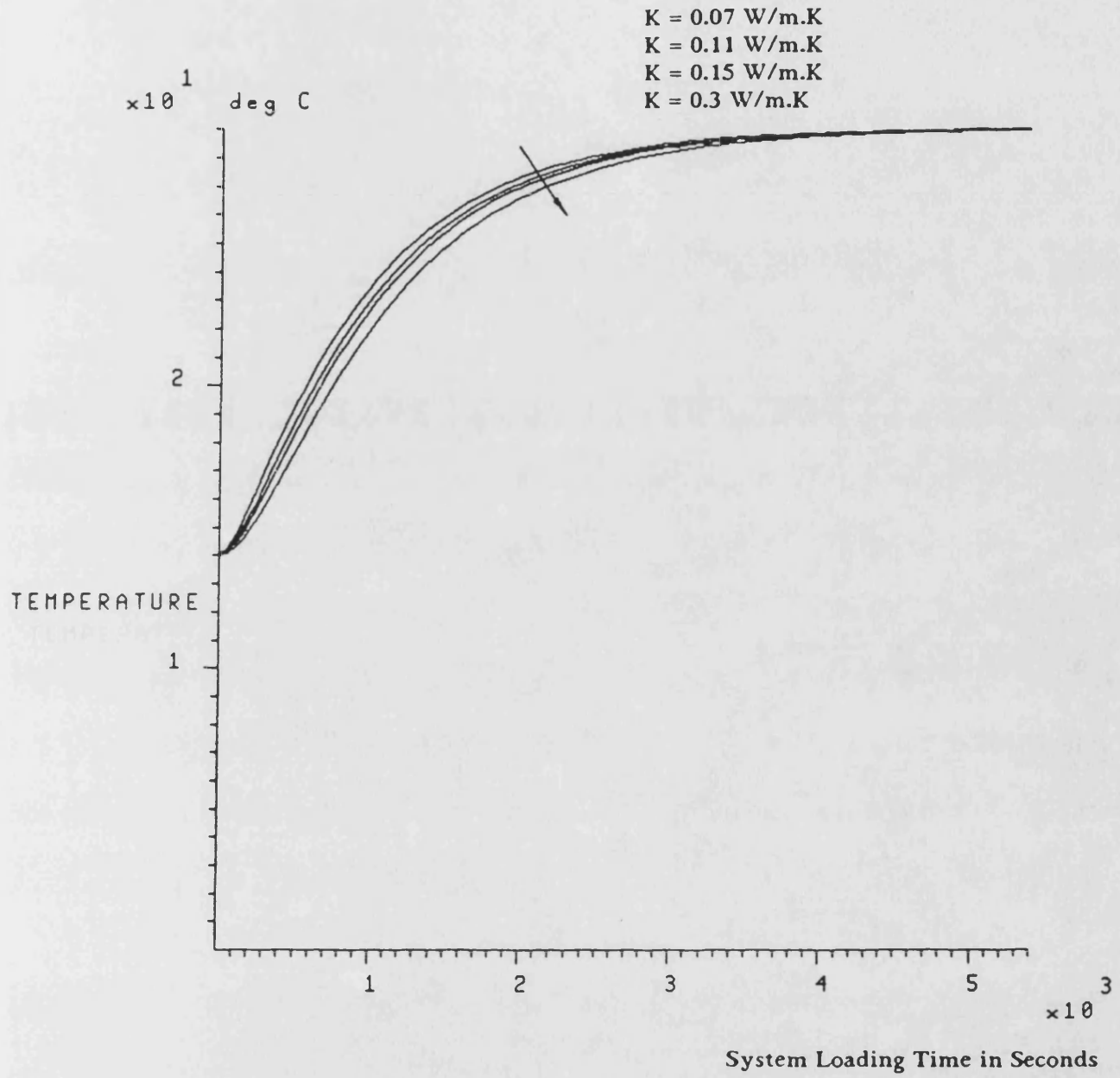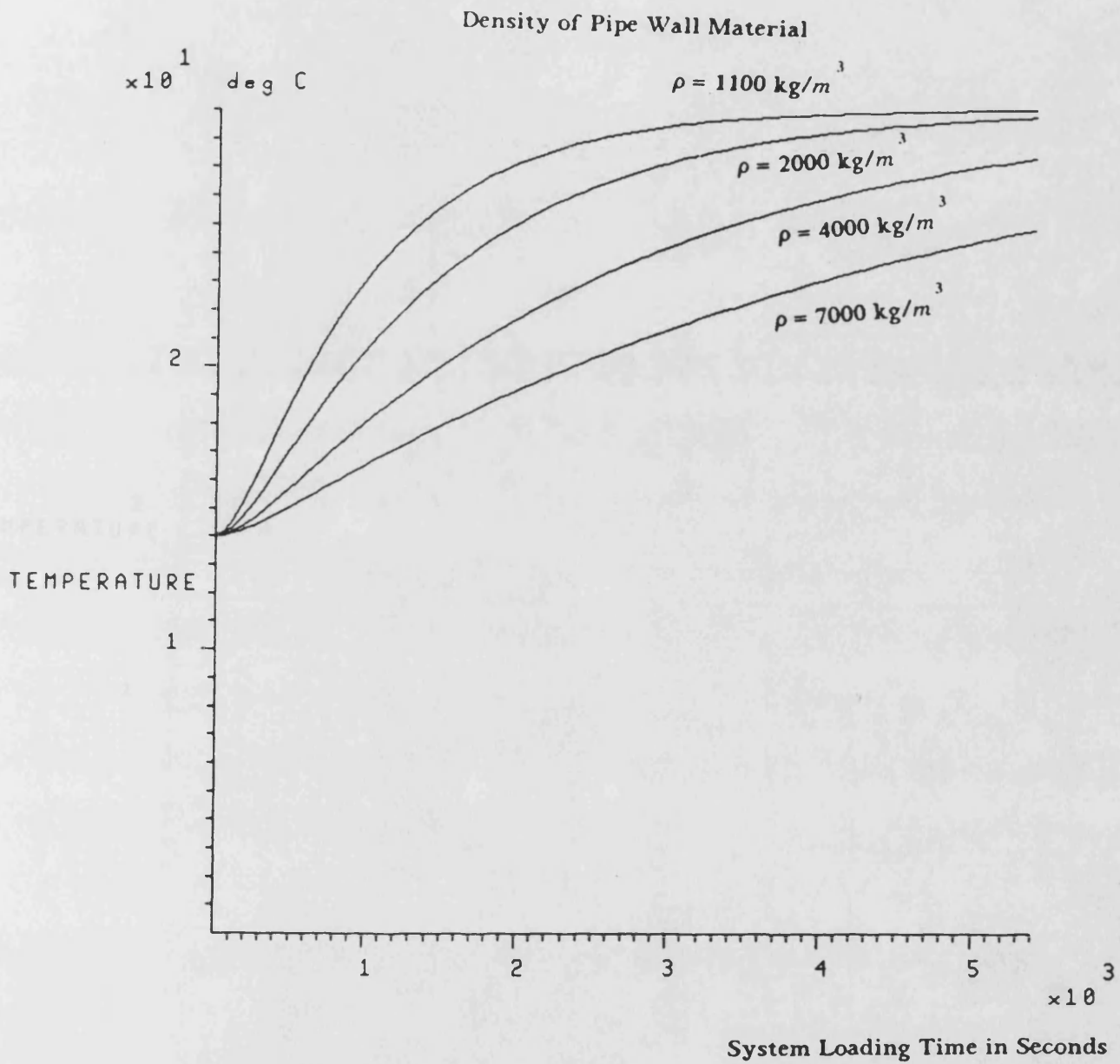
Fig. 6.15b   The Effects of Thermal Conductivity of Pipe Wall Material on
the Outside Pipe Wall Temperature in the Unboosted Closed
Hydrostatic Drive Propeller System

Pipe Wall Specific Heat
C_p = 500 J/kg.K
C_p = 1000 J/kg.K
C_p = 2010 J/kg.K
C_p = 2500 J/kg.K
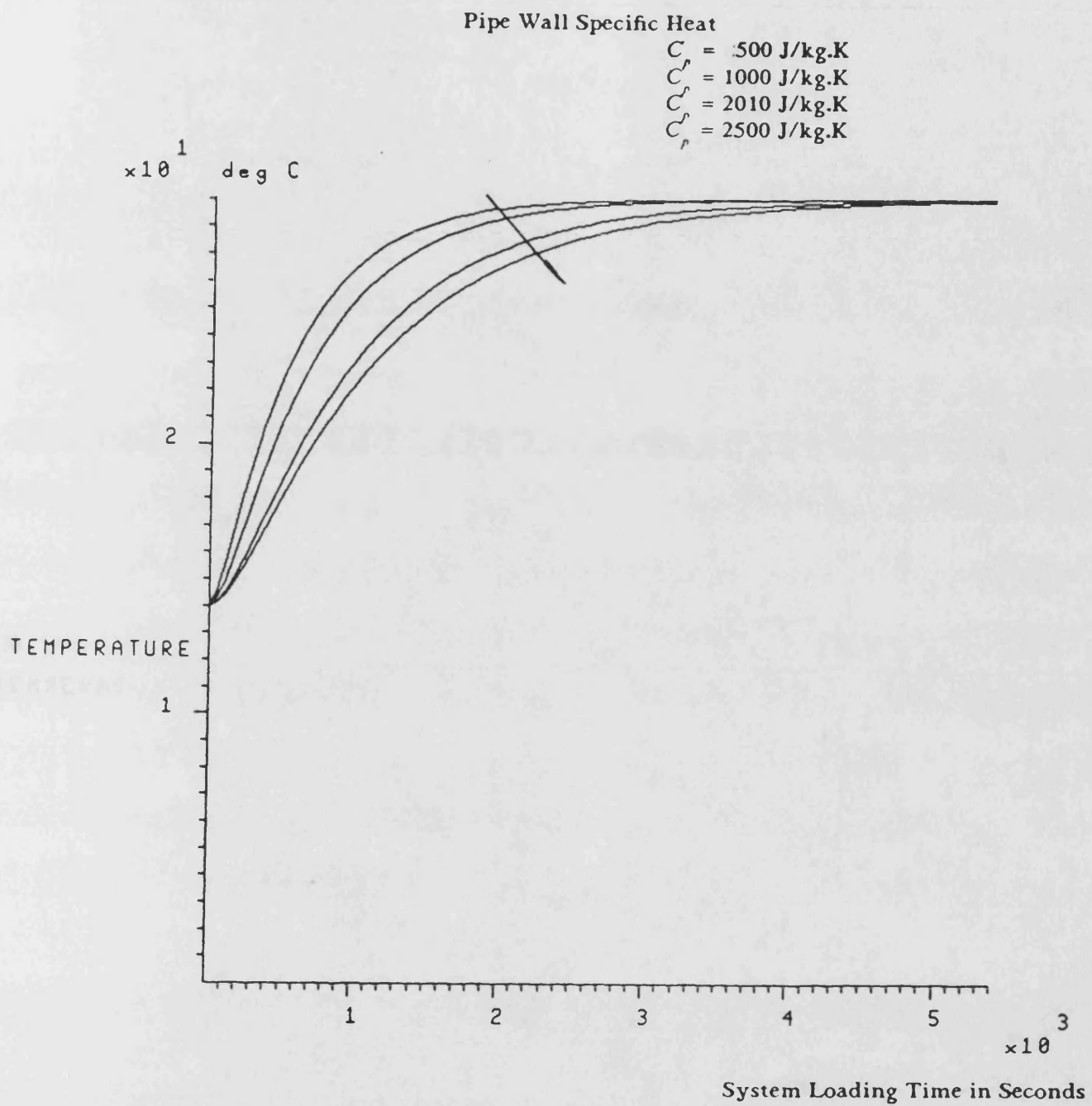
Fig. 6.16 a   The Effects of Specific Heat of Pipe Wall Material on
the Outside Pipe Wall Temperature in the Unboosted Closed
Hydrostatic Drive Propeller System

Fig. 6.16 b   The Effects of Specific Heat of Pipe Wall Material on
the Fluid Temperature in the Unboosted Closed Hydrostatic
Drive Propeller System

Density of Pipe Wall Material

Fig. 6.17a   The Effects of Density of Pipe Wall Material on
the Outside Pipe Wall Temperature in the Unboosted
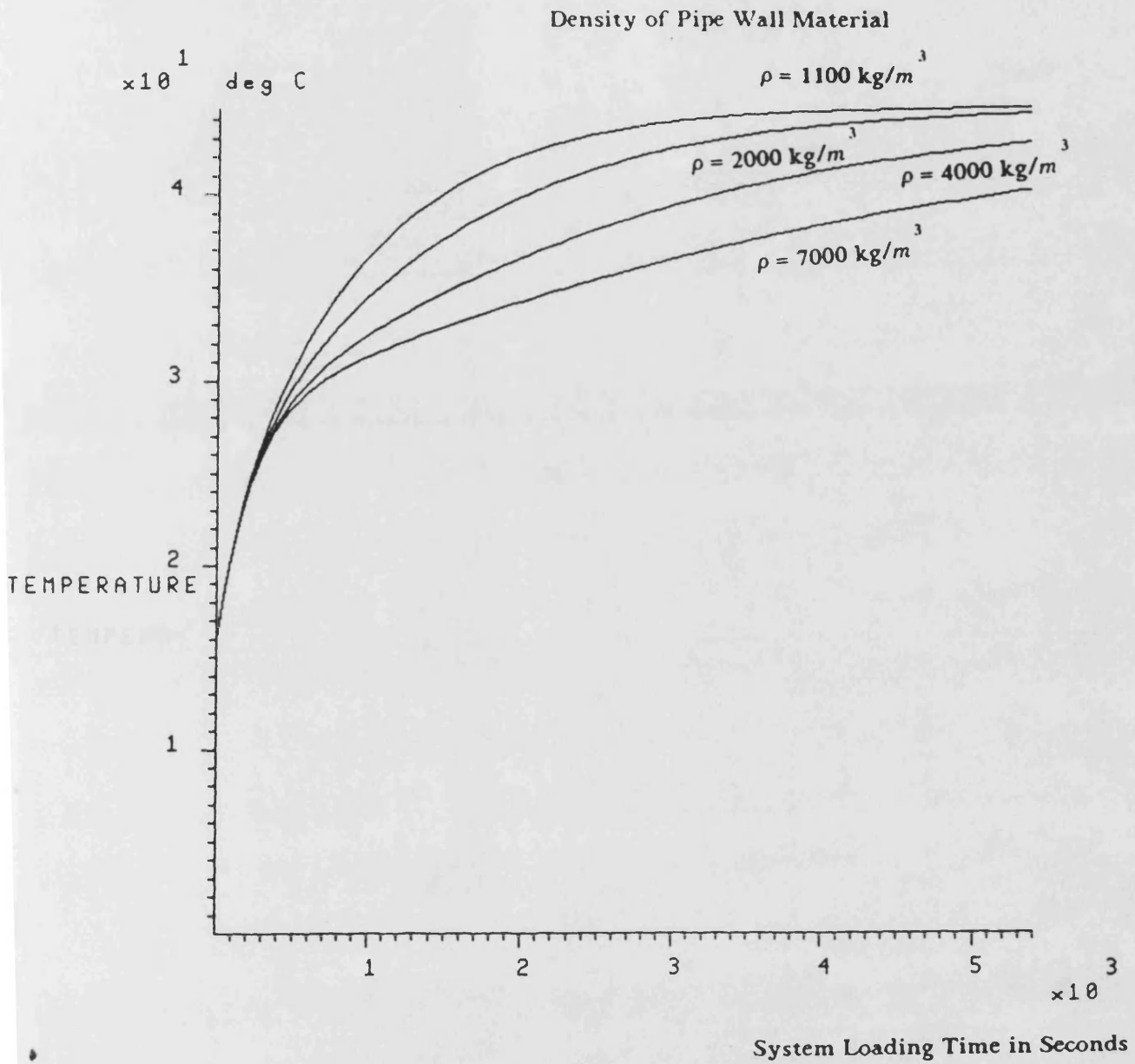Closed Hydrostatic Drive Propeller System

Fig. 6.17 b   The Effects of Density of Pipe Wall Material on
the Fluid Temperature in the Unboosted Closed
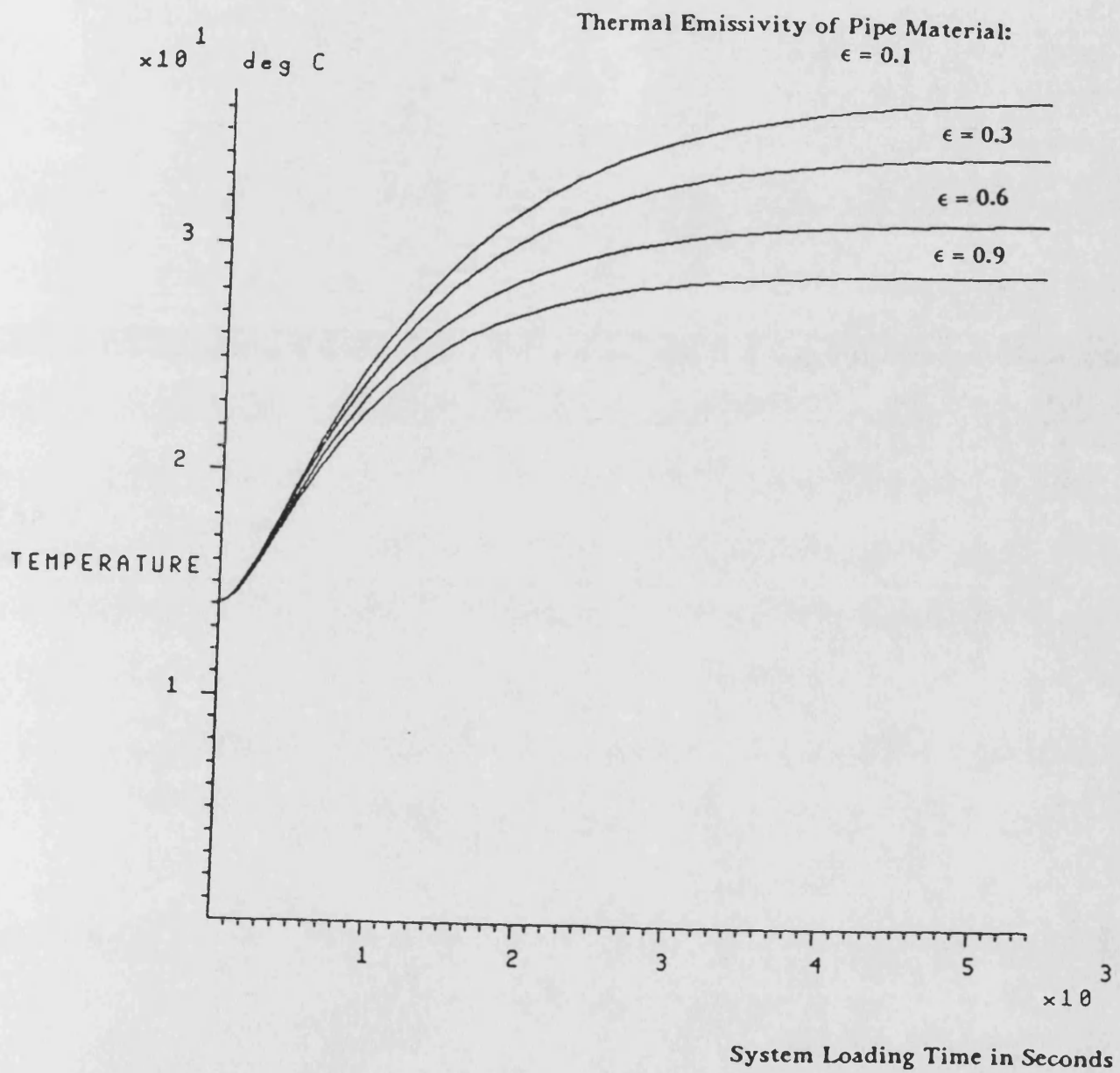Hydrostatic Drive Propeller System

Fig. 6.18 a   The Effects of Emissivity of Pipe Material on Outside
Pipe Wall Temperature in the Unboosted Closed Hydrostatic
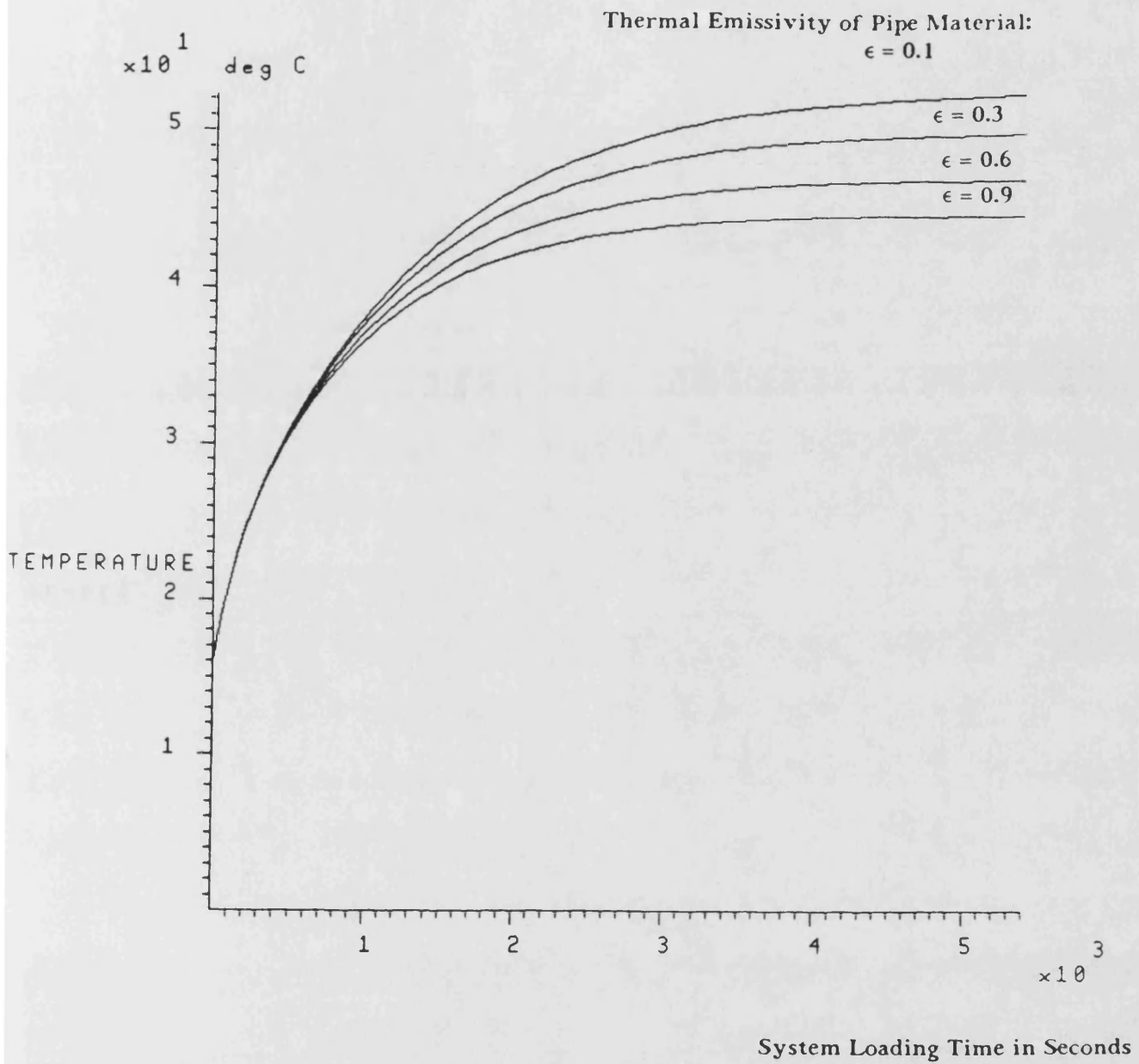Drive Propeller System

Fig. 6.18b   The Effects of Emissivity of Pipe Material on Fluid Temperature in the Unboosted Closed Hydrostatic Drive Propeller System
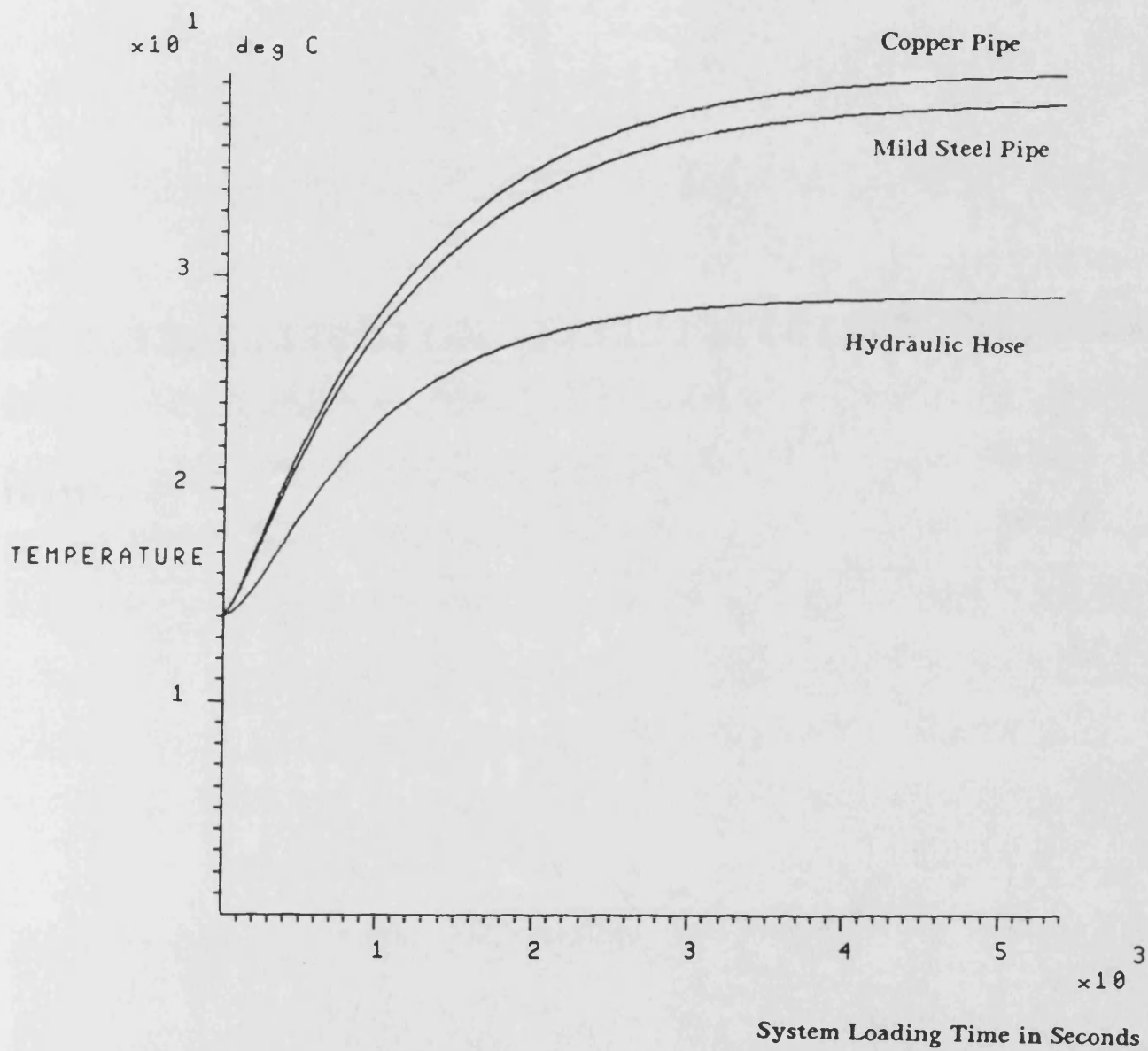
Fig. 6.19a   The Effects of Type of Pipe Material on Outside
Pipe Wall Temperature in the Unboosted Closed
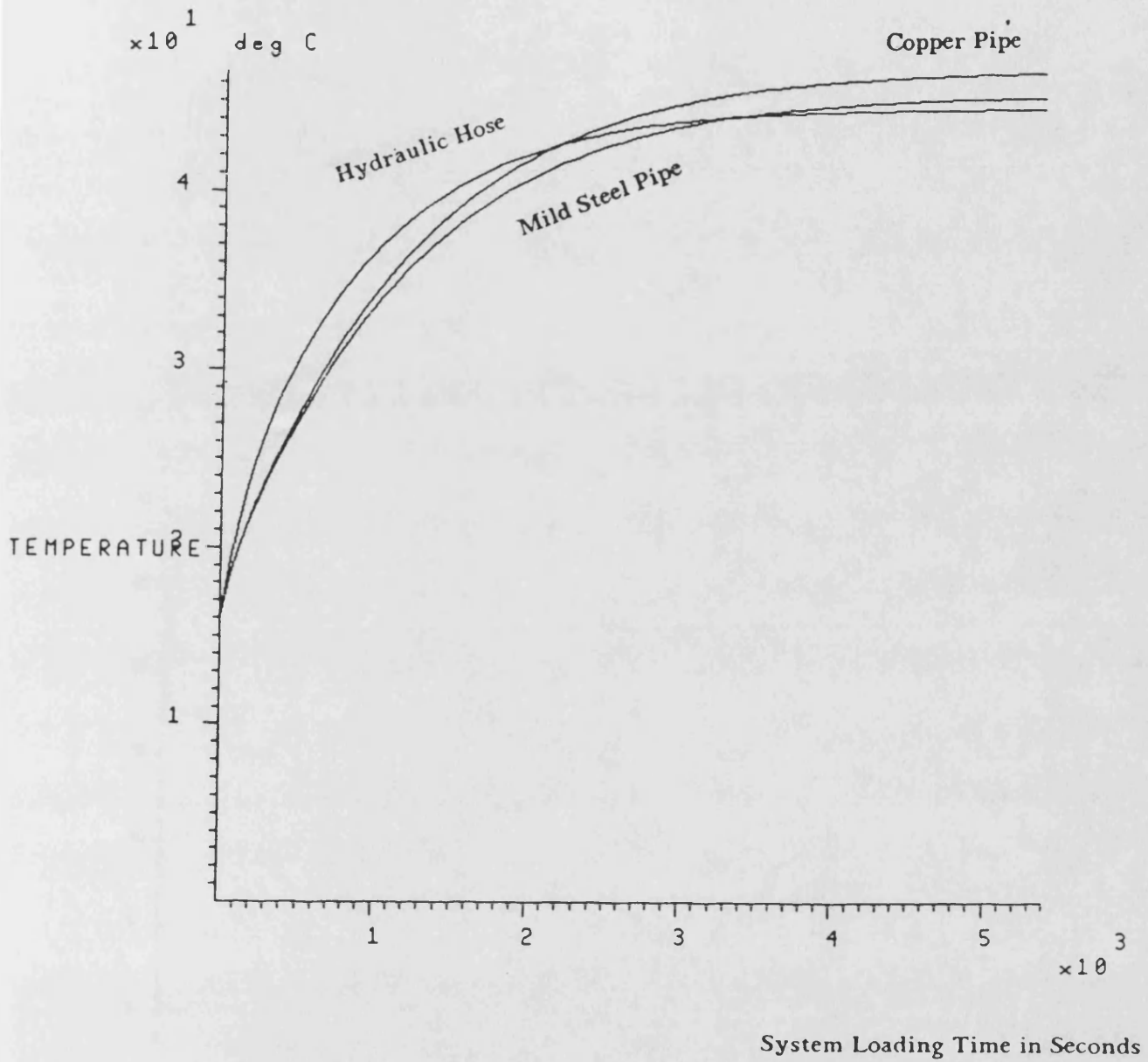Hydrostatic Drive Propeller System

Fig. 6.19 b   The Effects of Type of Pipe Material on Fluid
Temperature in the Unboosted Closed Hydrostatic
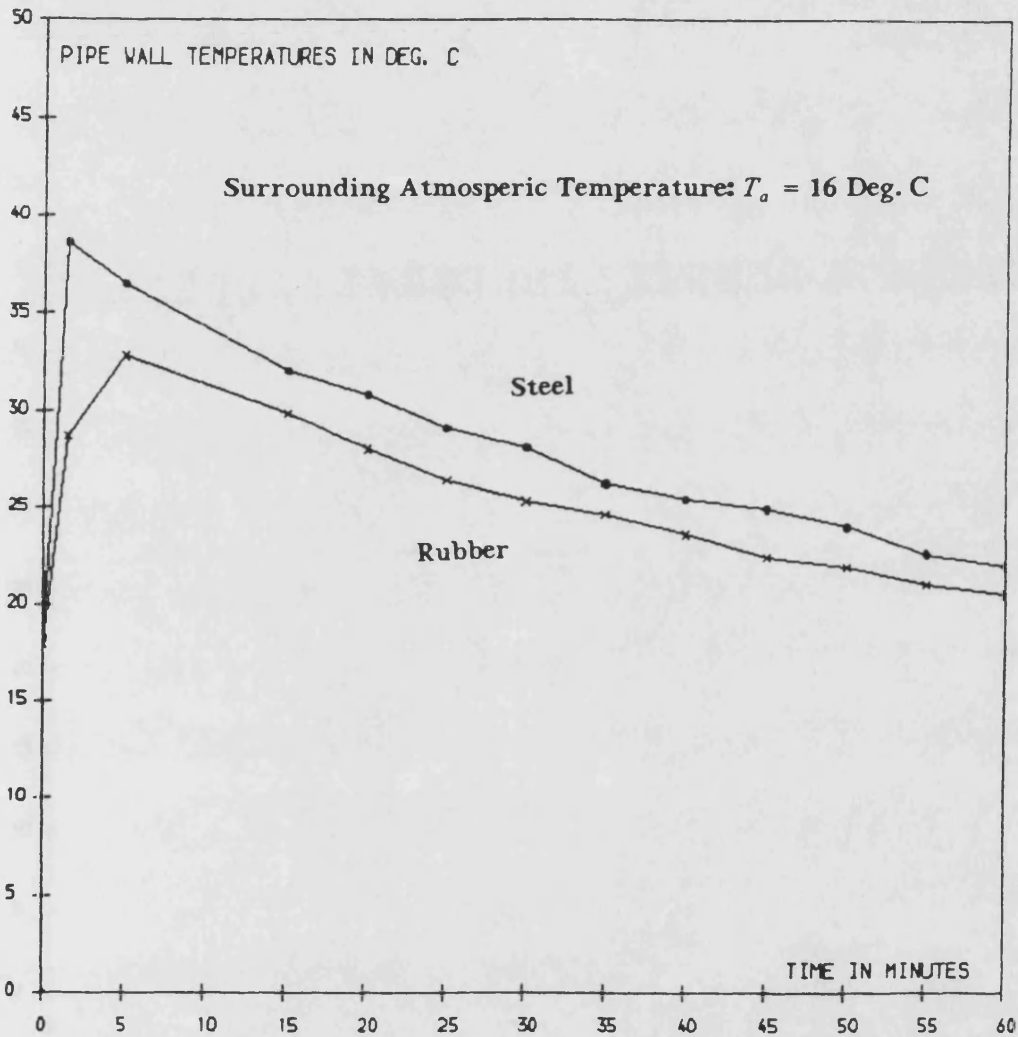Drive Propeller System

Fig. 6.20   Comparison of Measured Outside Wall Temperatures of a
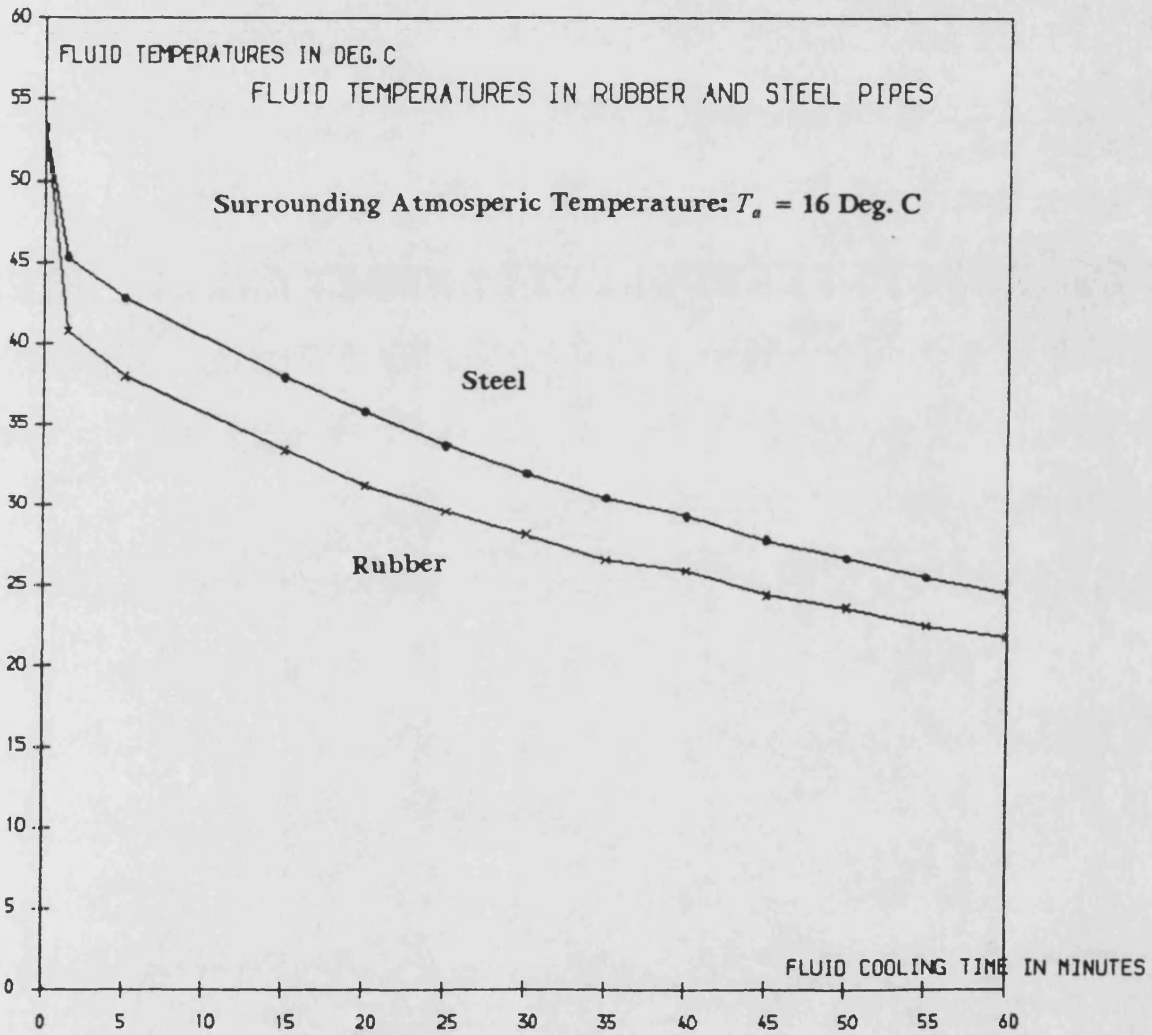Mild Steel Tube and a Rubber Hose

Fig. 6.21   Comparison of Measured Fluid Temperatures inside a Mild Steel Tube and a Rubber Hose
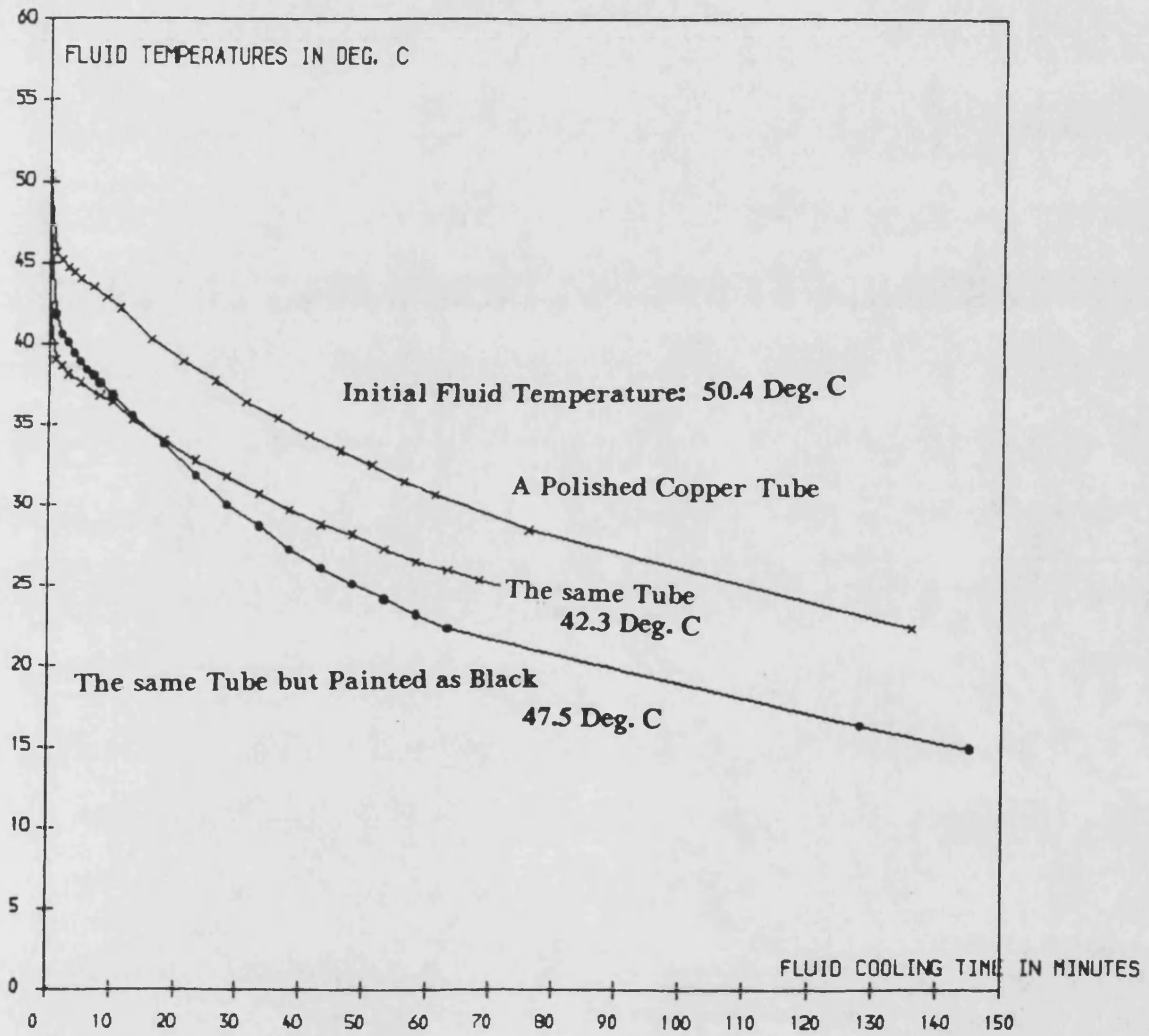
Fig. 6.22   Comparisons of Measured Fluid Temperatures Obtained from a Copper Tube Under Different Conditions
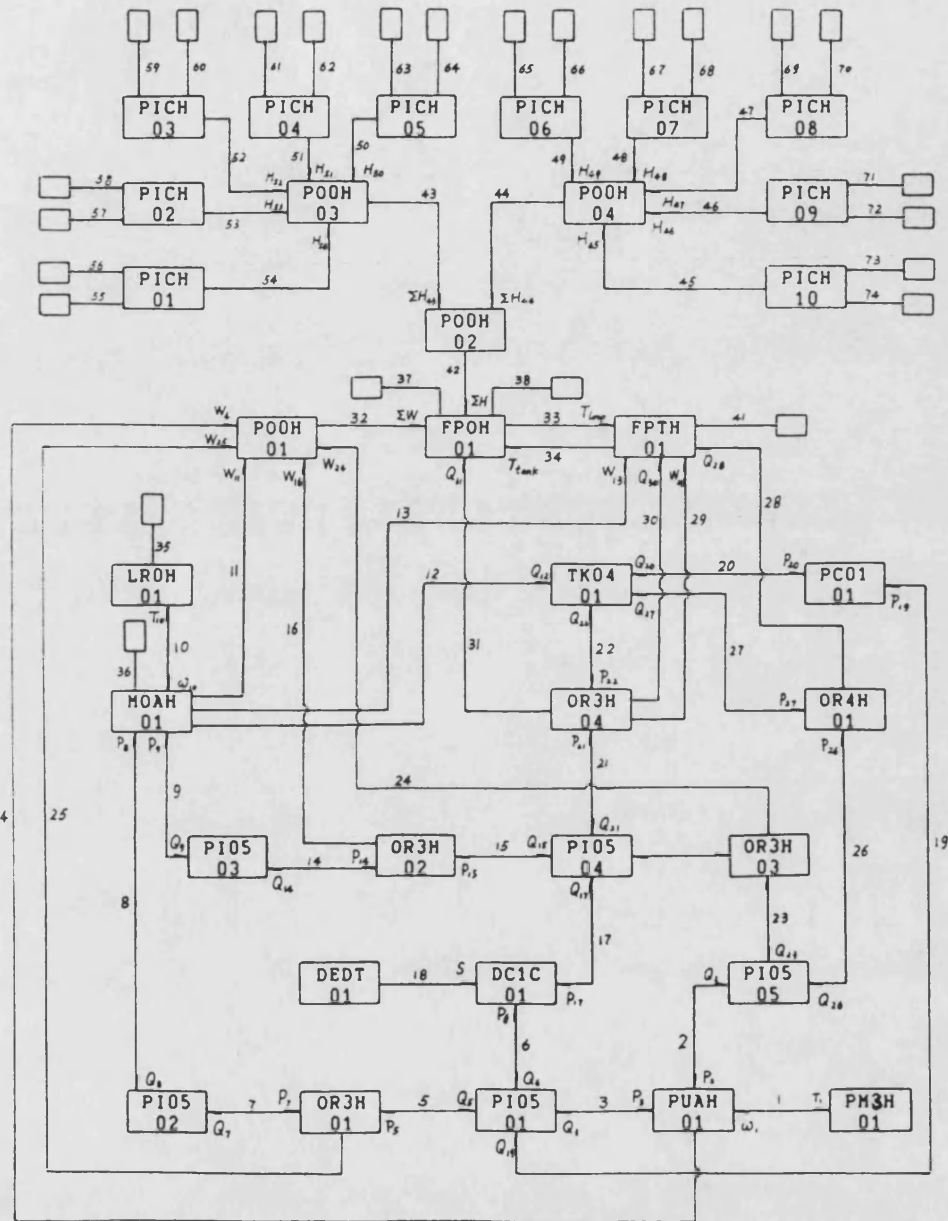
Fig. 6.23   Block Diagram for the Simulation of the Partially Closed
Hydrostatic Drive Propeller System with an Approach to Assume
an Uniform Loop Fluid Temperature and to Consider the Effects
of the Different Types of Pipe Wall Materials
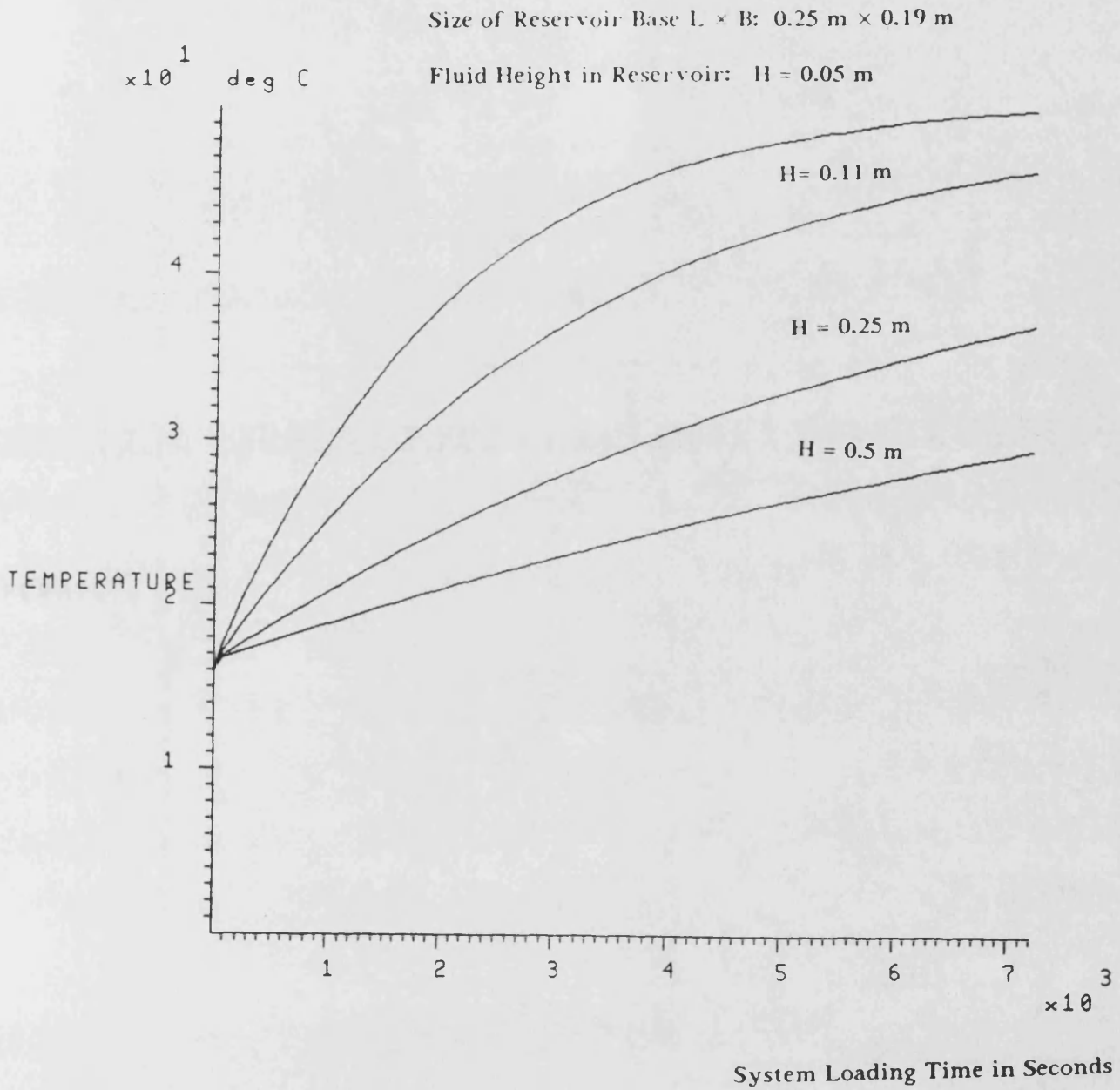
Fig. 6.24   The Effects of Fluid Height in the Reservoir on Fluid
Temperature in the System Loop

Width of Reservoir Base B: B = 0.19 m

Fluid Height in Reservoir: H = 0.11 m

Length of Reservoir Base L: L = 0.05 m
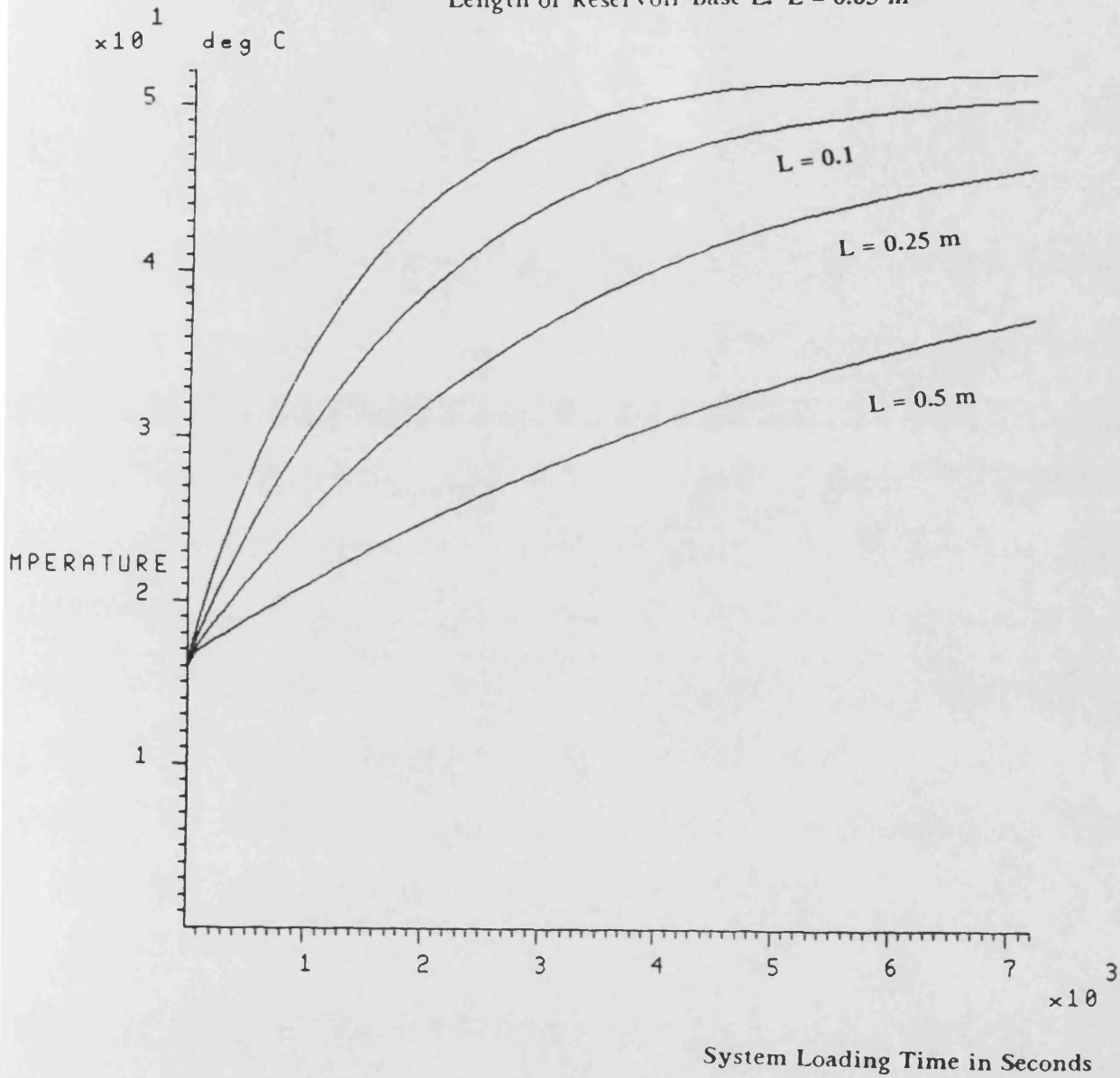
Fig. 6.25   The Effects of the Length of Reservoir Base on Fluid
Temperature in the System Loop

Length of Reservoir Base L: L = 0.25 m

Fluid Height in Reservoir: H = 0.11 m

Width of Reservoir Base B: B = 0.05 m

B = 0.1 m

B = 0.19 m

B = 0.5 m

System Loading Time in Seconds
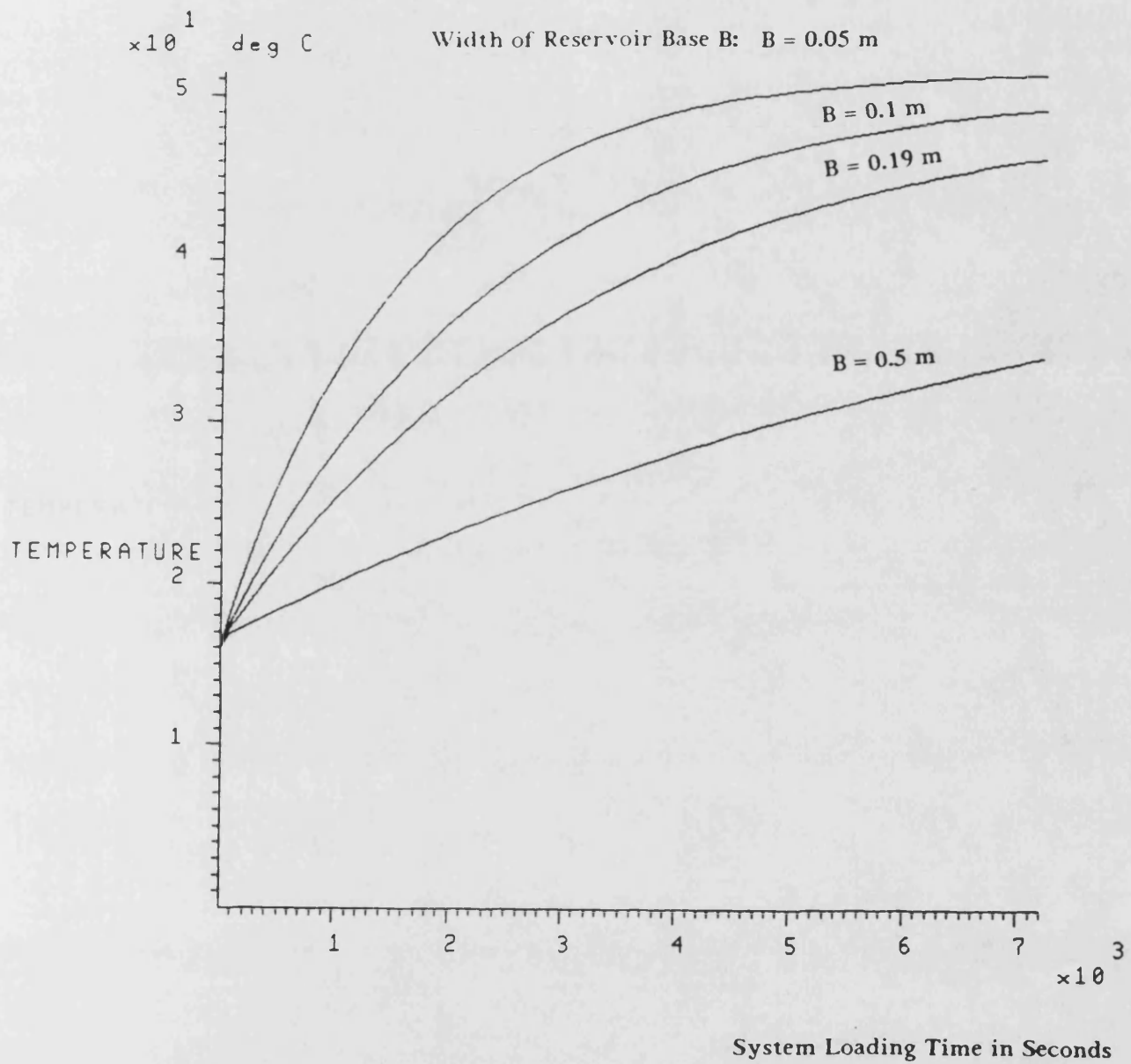
Fig. 6.26   The Effects of the Width of Reservoir Base on Fluid
Temperature in the System Loop

Exchange Flowrate between Loop and Reservoir:
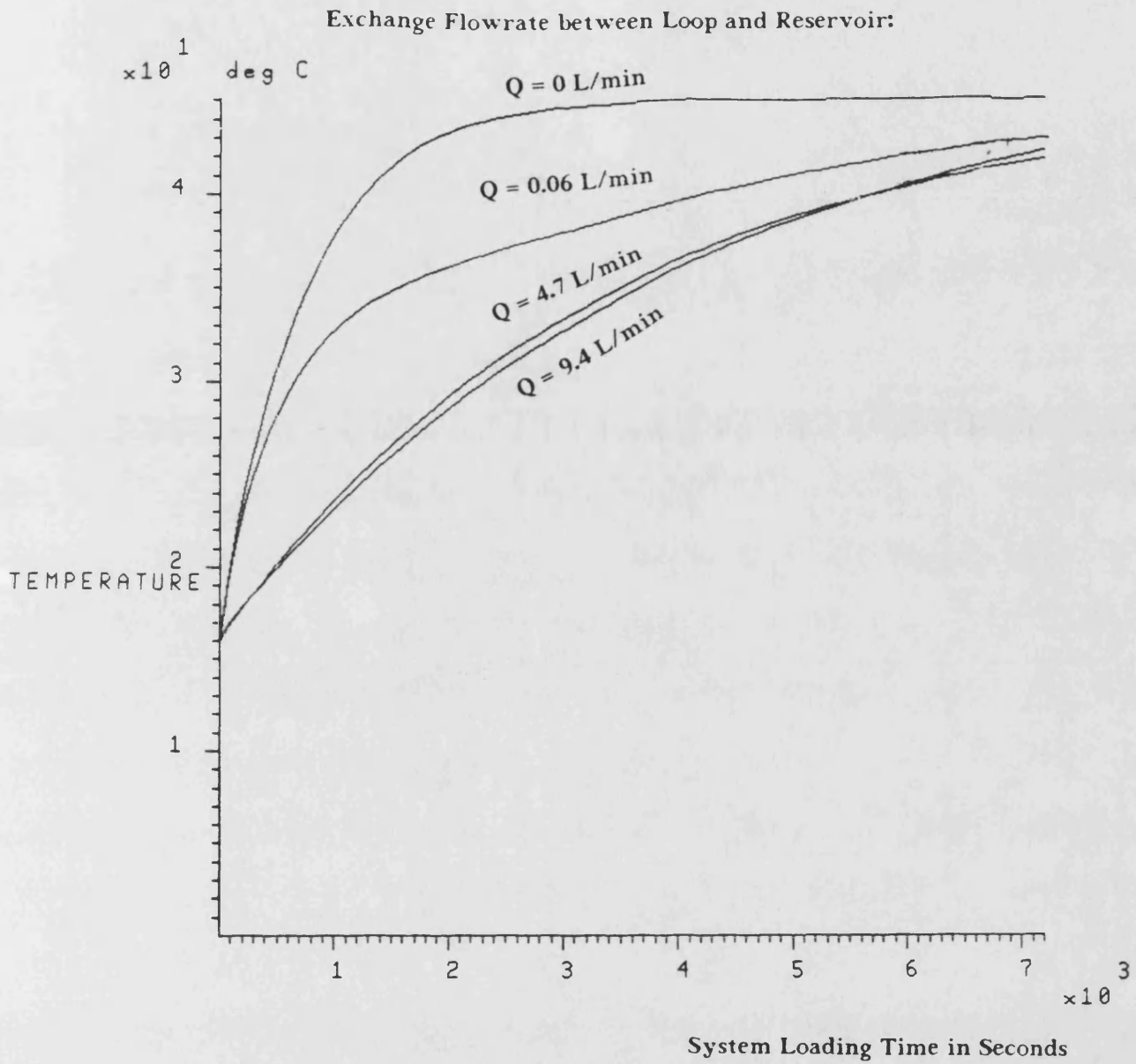
Fig. 6.27   The Effects of Exchange Flowrate Between Loop and Reservoir on Loop Fluid Temperature
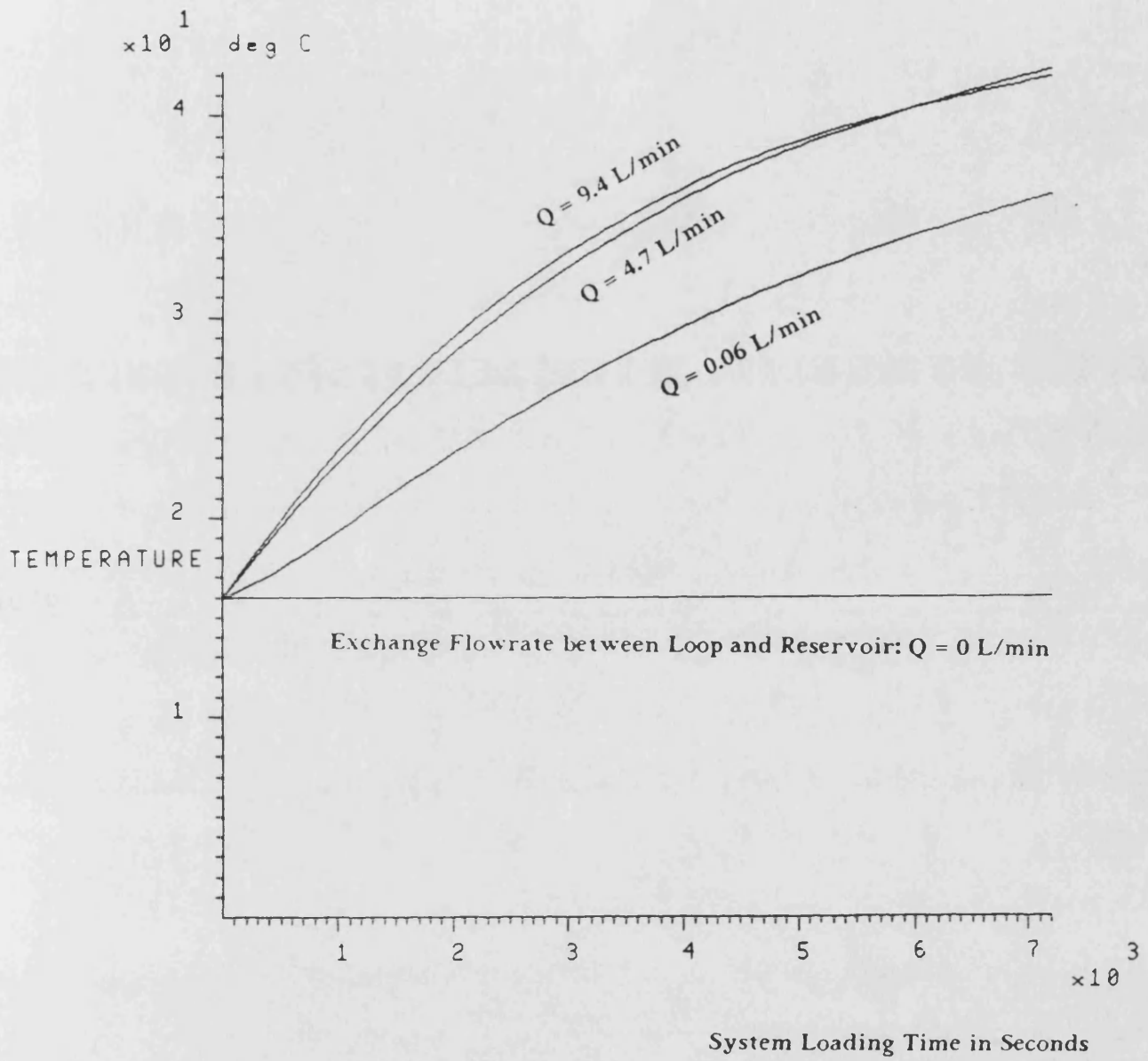
Fig. 6.28   The Effects of Flowrate Returning to Reservoir on Reservoir
                   Fluid Temperature

Power Loss Generated During the System Loading: P = 97.5 W

Exchange Flowrate between Loop and Reservoir: Q = 4.7 L/min
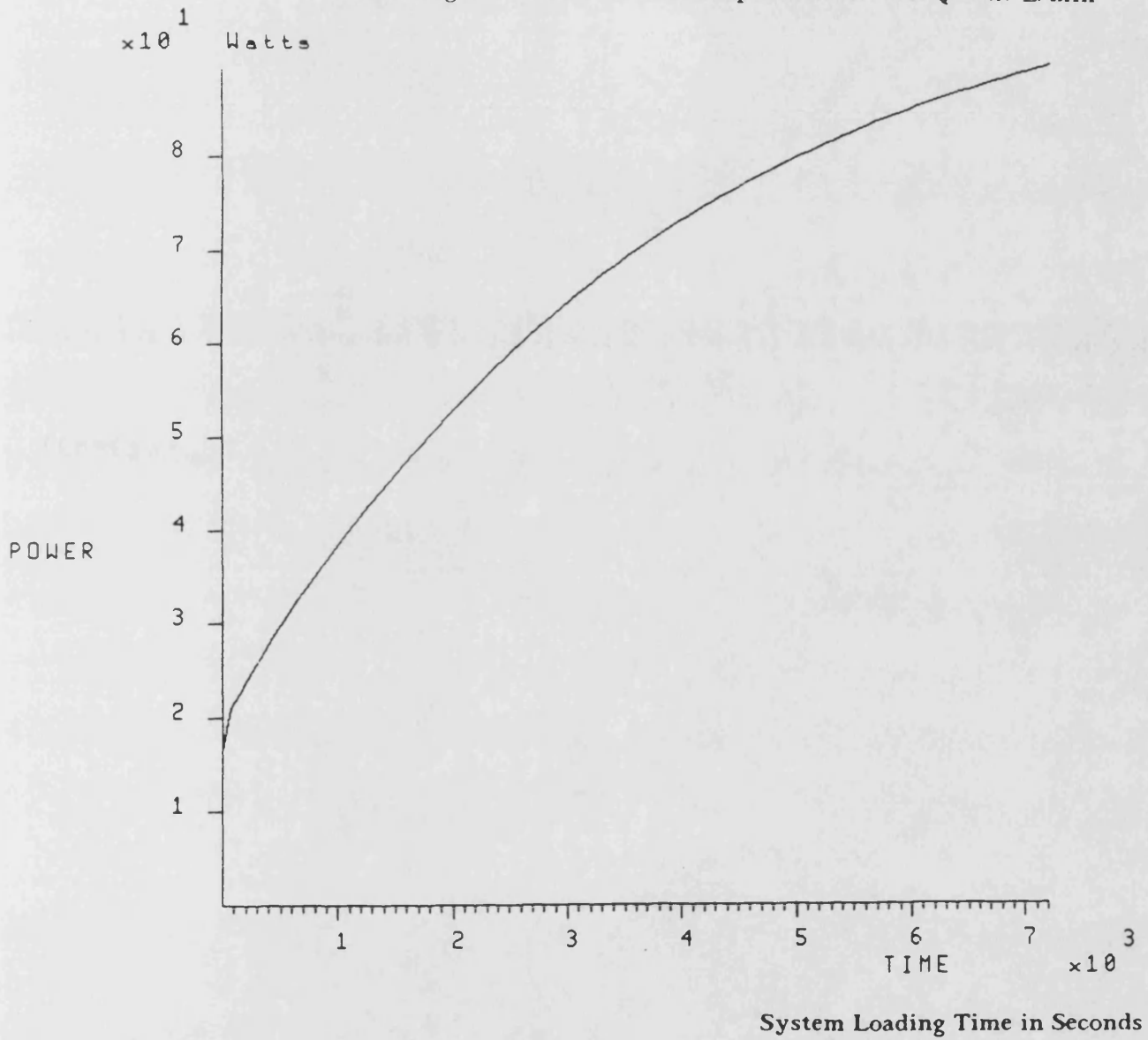
Fig. 6.29   Heat Flow Being Dissipated Through the Pipes of the System Loop in the Partially Closed Hydrostatic Drive Propeller System
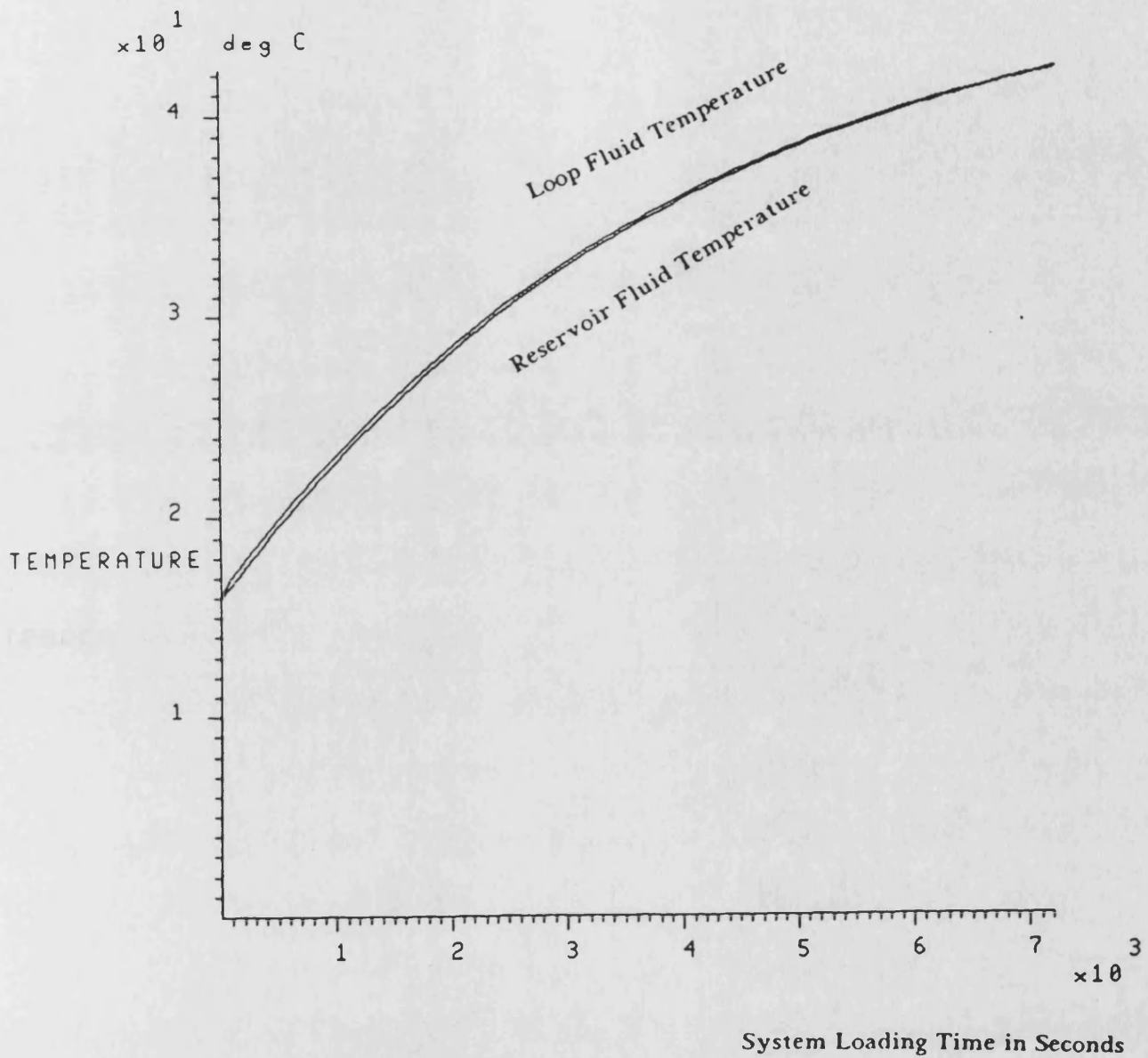
Fig. 6.30   Comparison of Calculated Loop and Reservoir Fluid Temperatures
in the Partially Closed Hydrostatic Drive Propeller System

Power Loss Generated During the System Loading: P = 1000 W
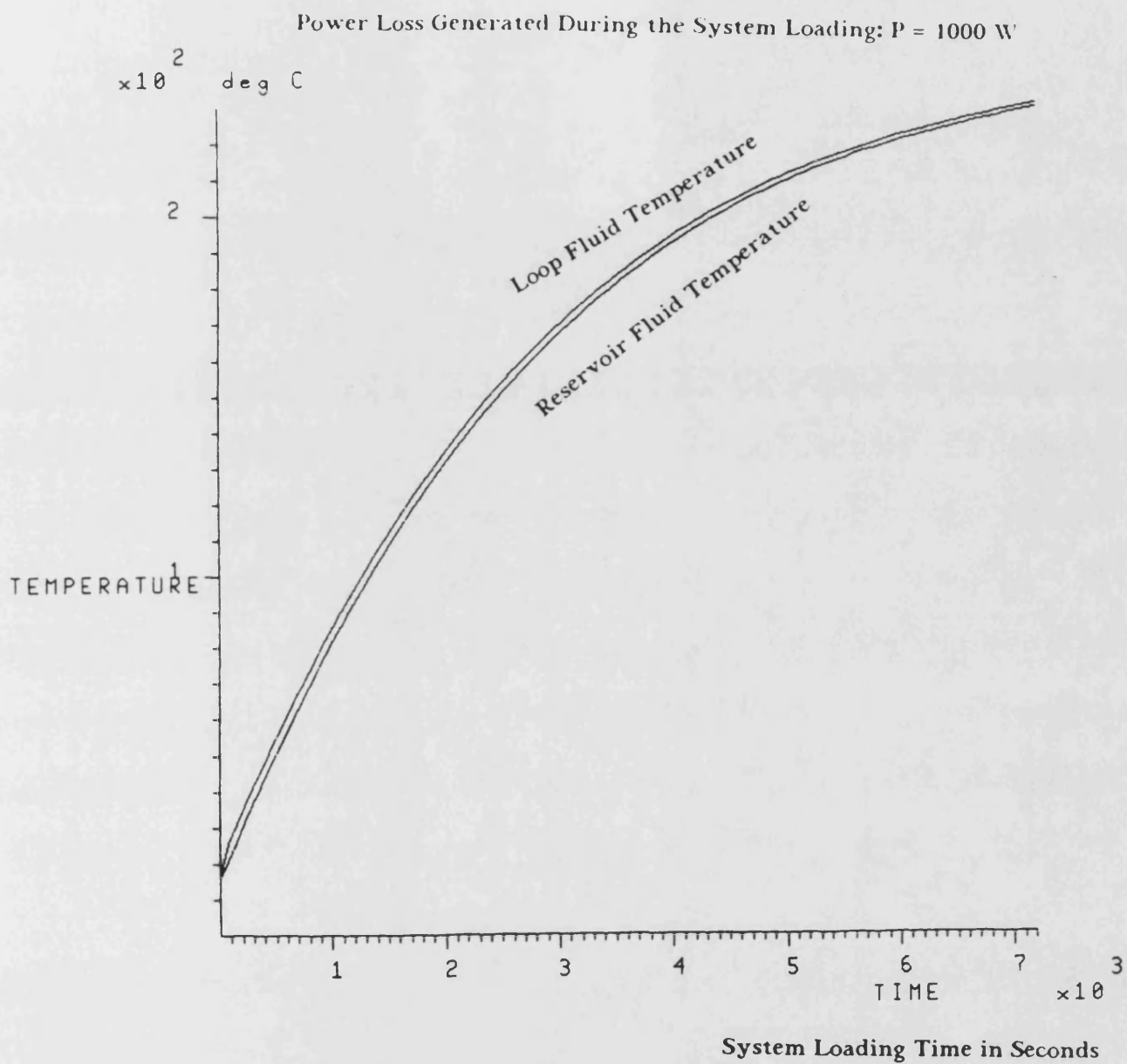
Fig. 6.31   Comparison of Calculated Loop and Reservoir Fluid Temperatures
                 With a Big Increase of the System Power Loss in the Partially
                 Closed Hydrostatic Drive Propeller System
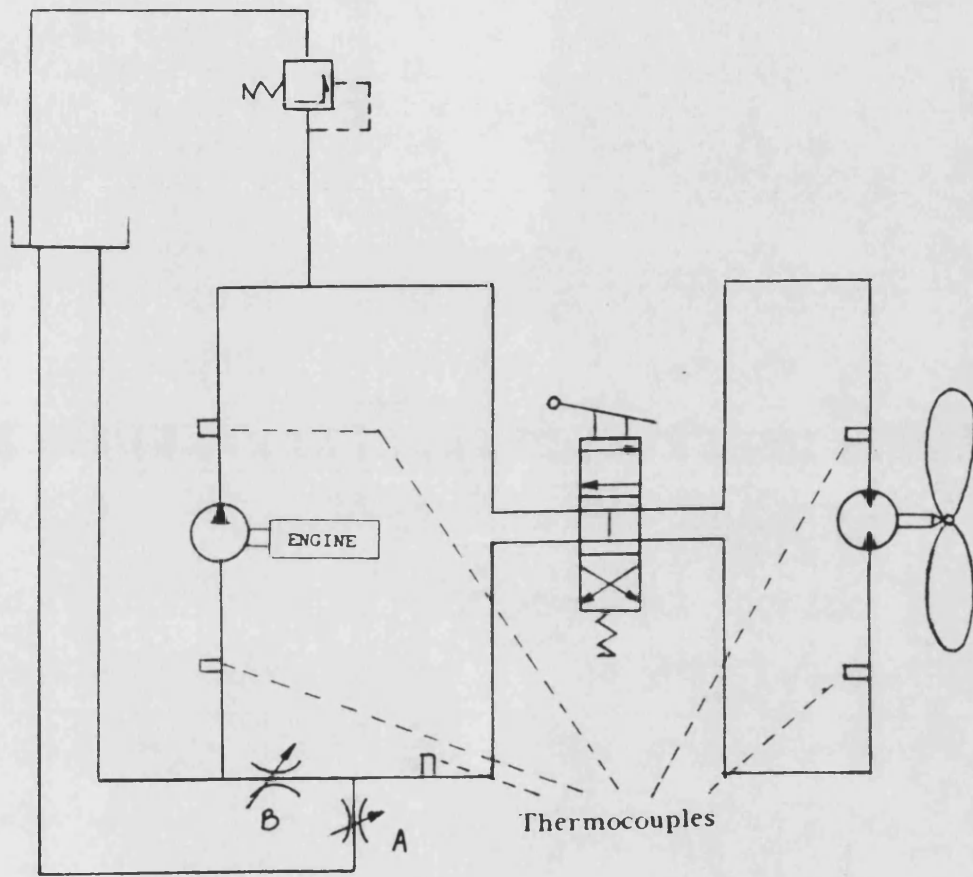
Fig. 6.32   The Positions of Thermocouples on the Test Rig
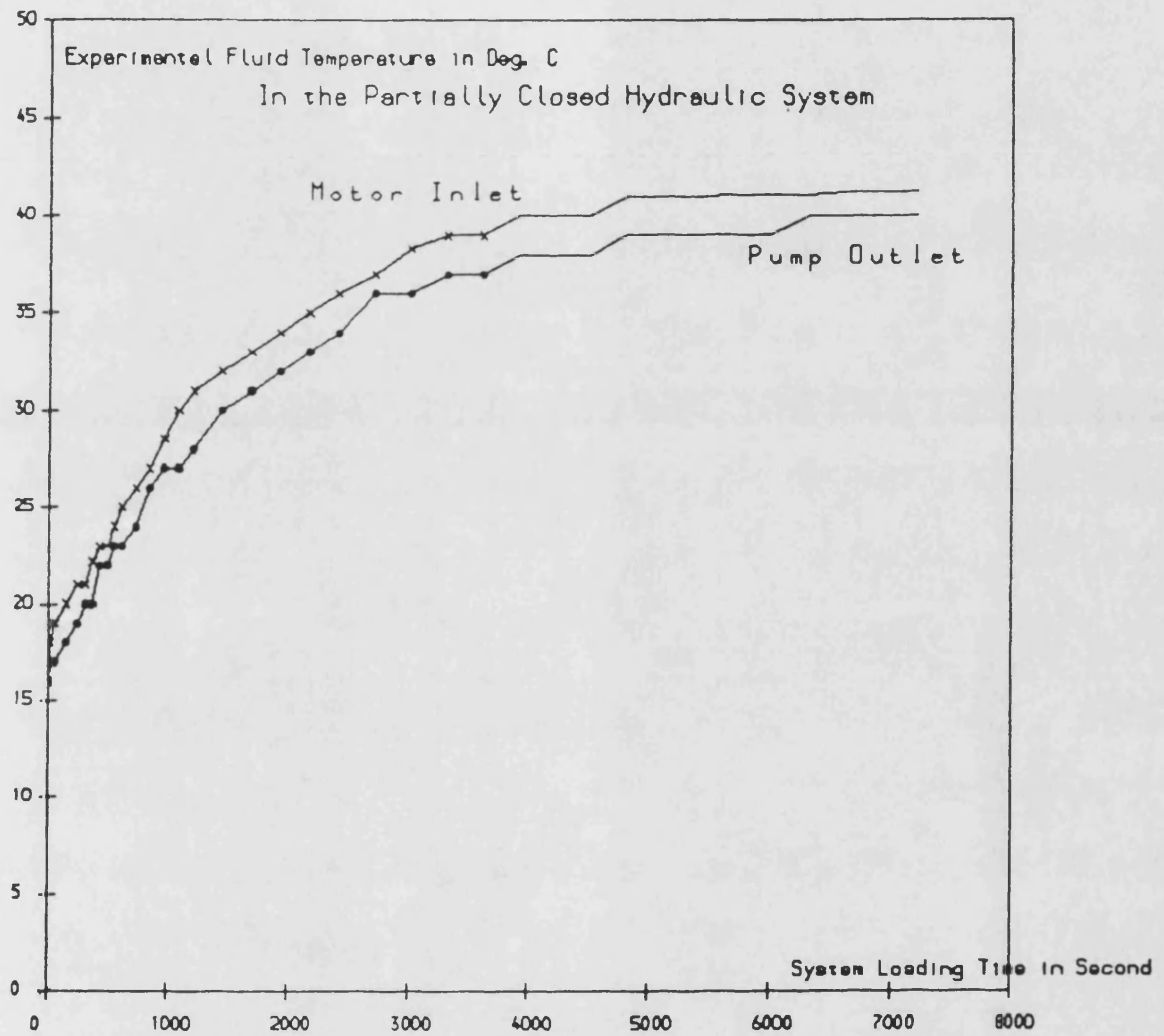
Fig. 6.33   Comparison of Fluid Temperatures During a Two Hour Run Test
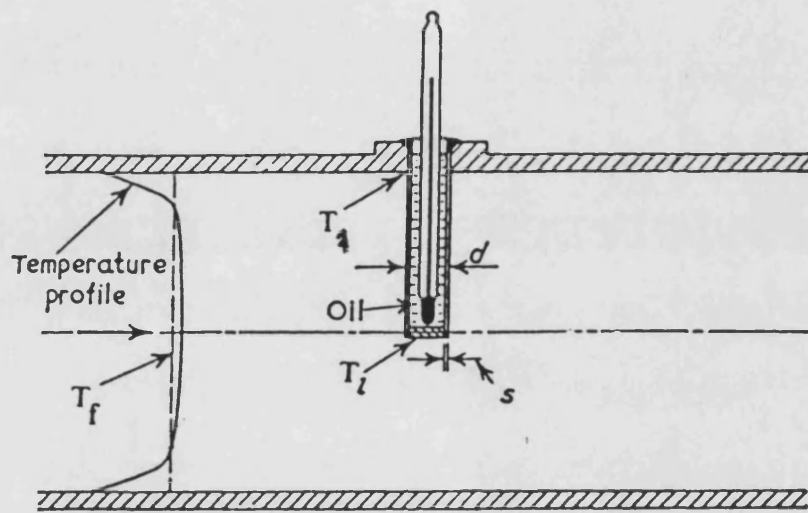
Fig. 6.34   The Thermometer Pocket
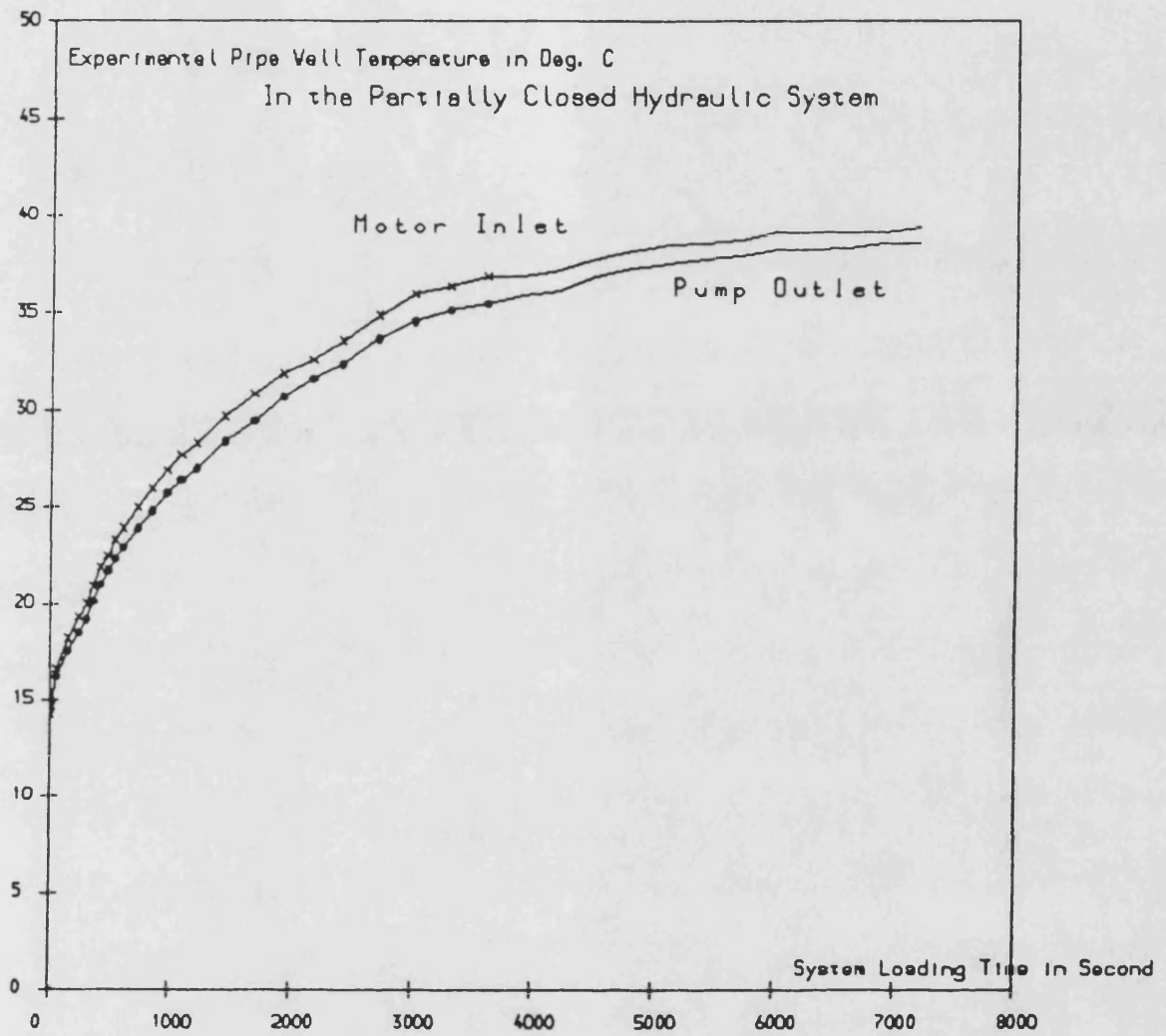
Fig. 6.35   Comparison of Pipe Wall Temperatures in the System High
                   Pressure Pipeline
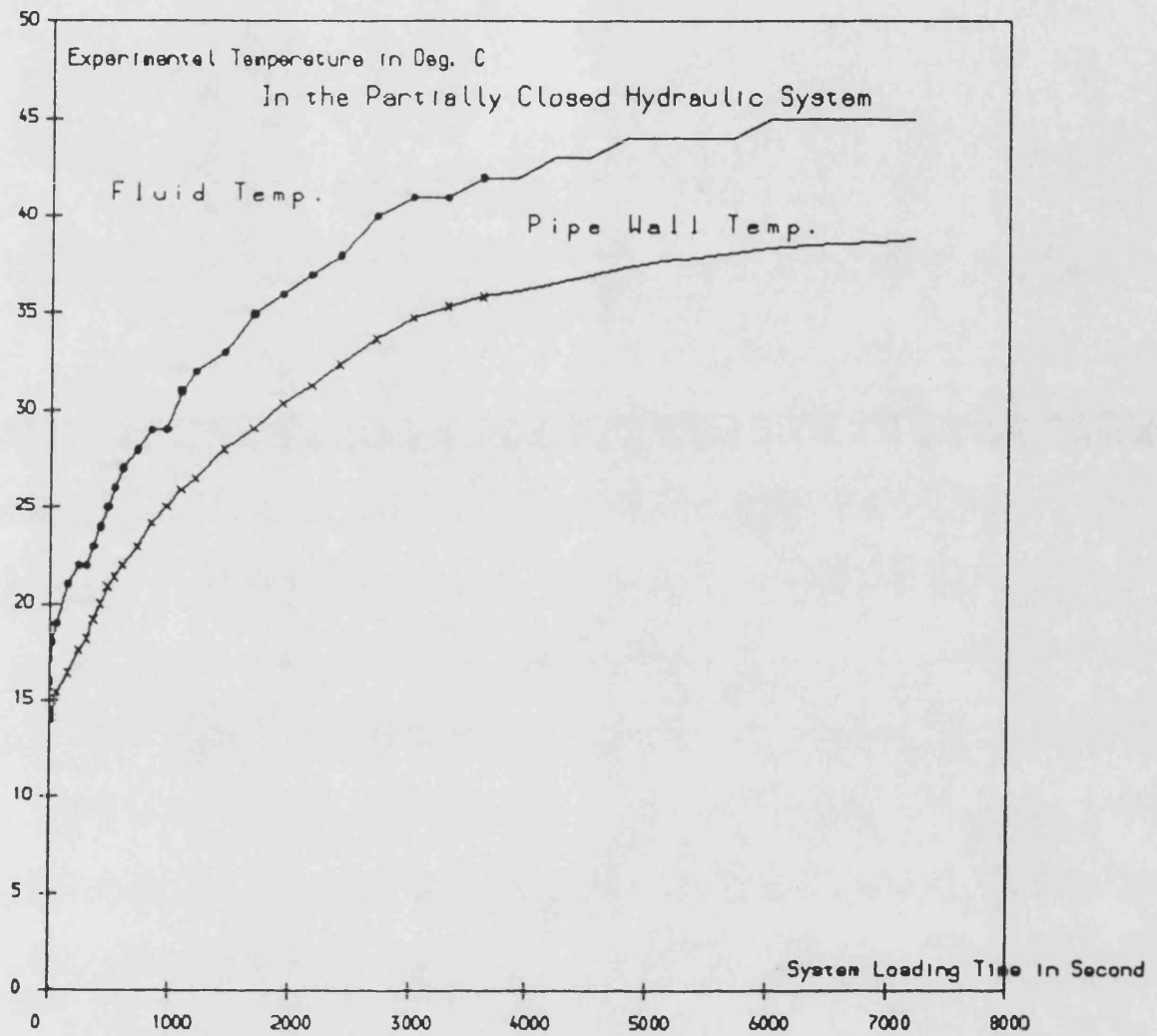
Fig. 6.36   Comparison of Fluid and Pipe Wall Temperatures at the
Motor Outlet
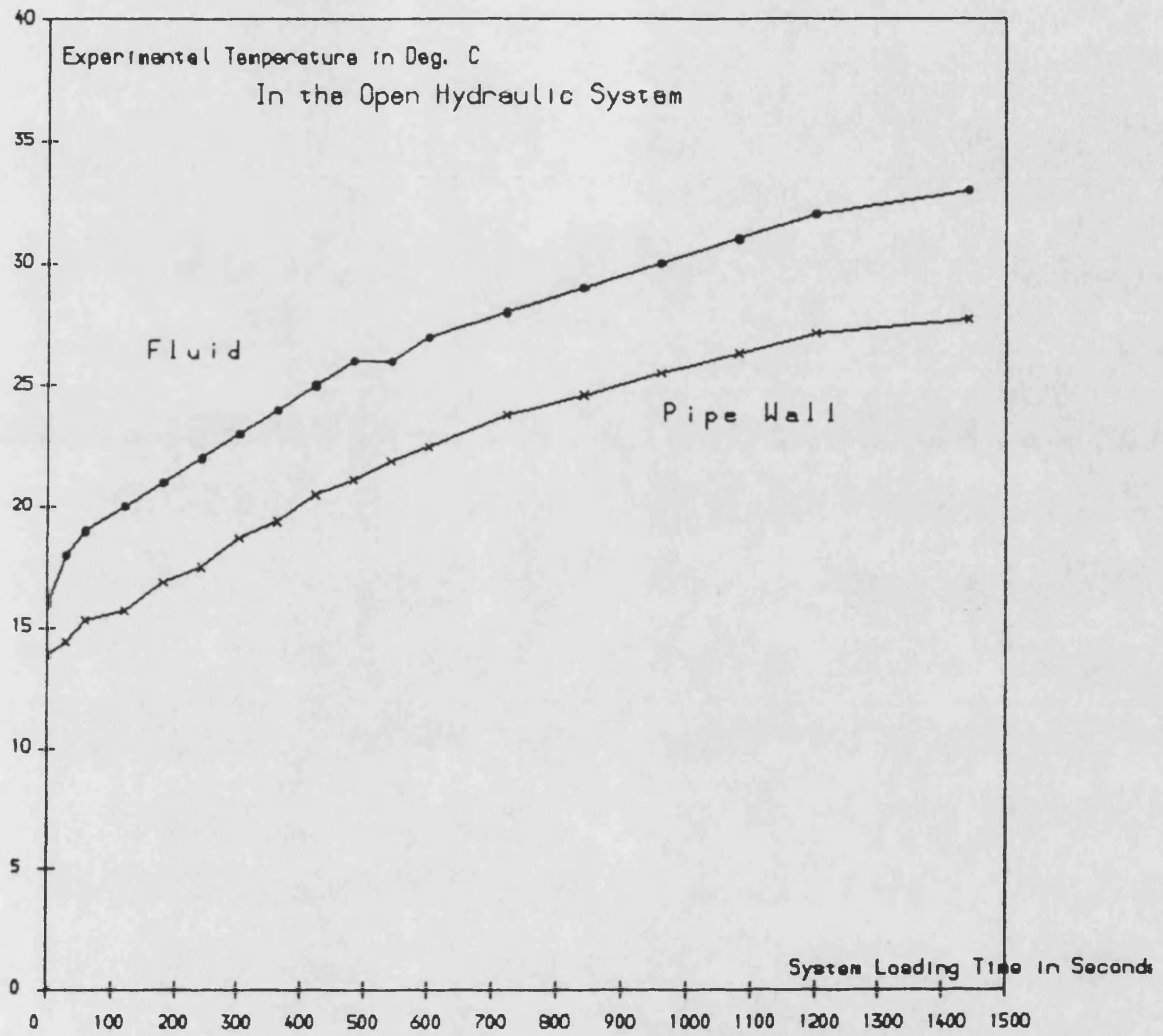
Fig. 6.37   Comparison of Fluid and Pipe Wall Temperatures at the
                   Motor Outlet
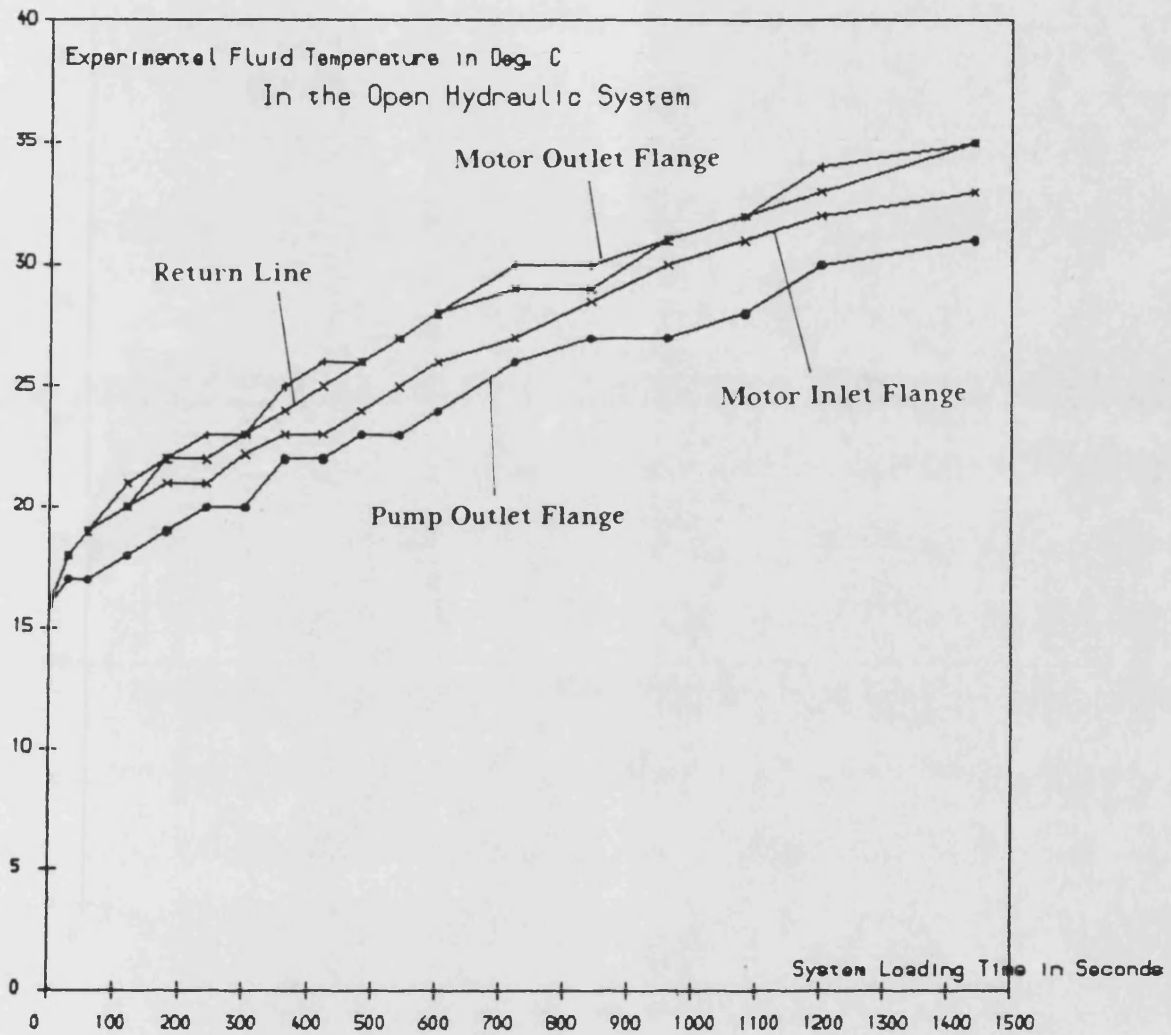
Fig. 6.38   Experimentally Obtained Fluid Temperatures in the Open Hydraulic System
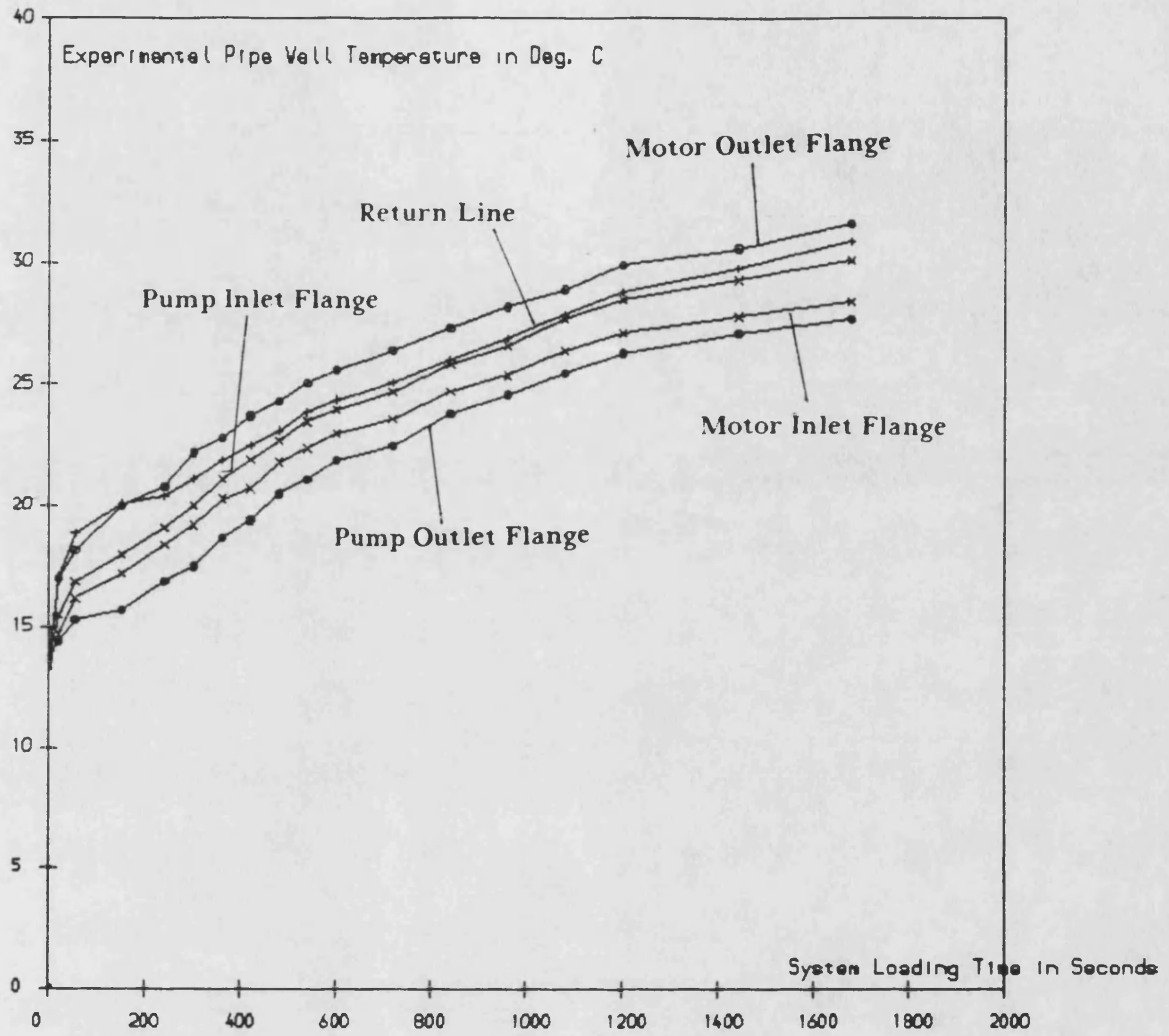
Fig. 6.39   Experimentally Obtained   Pipe Wall Temperatures in the
                 Open Hydraulic System
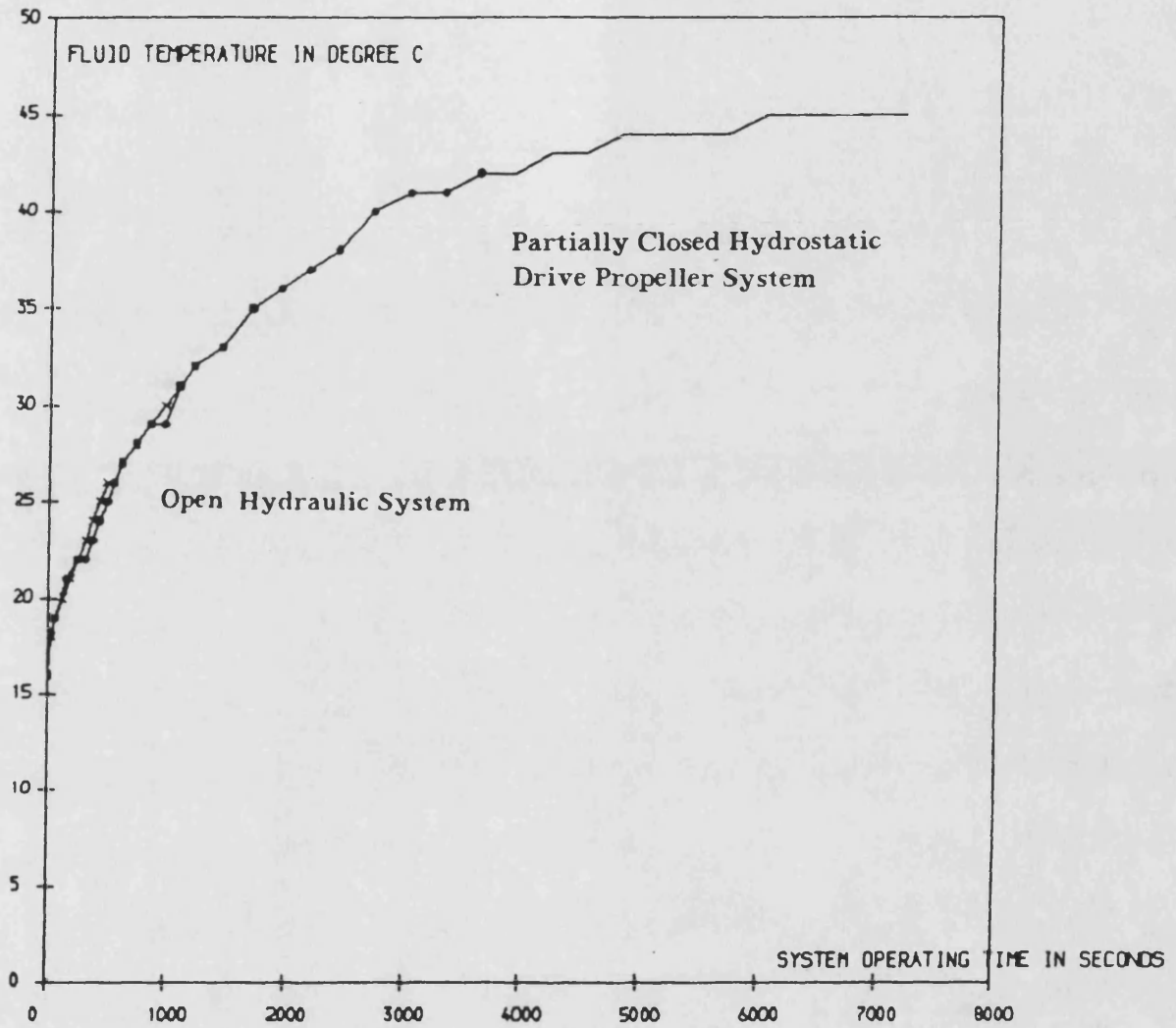
Fig. 6.40a Comparison of Average Fluid Temperatures of the Open and Partially Closed Systems
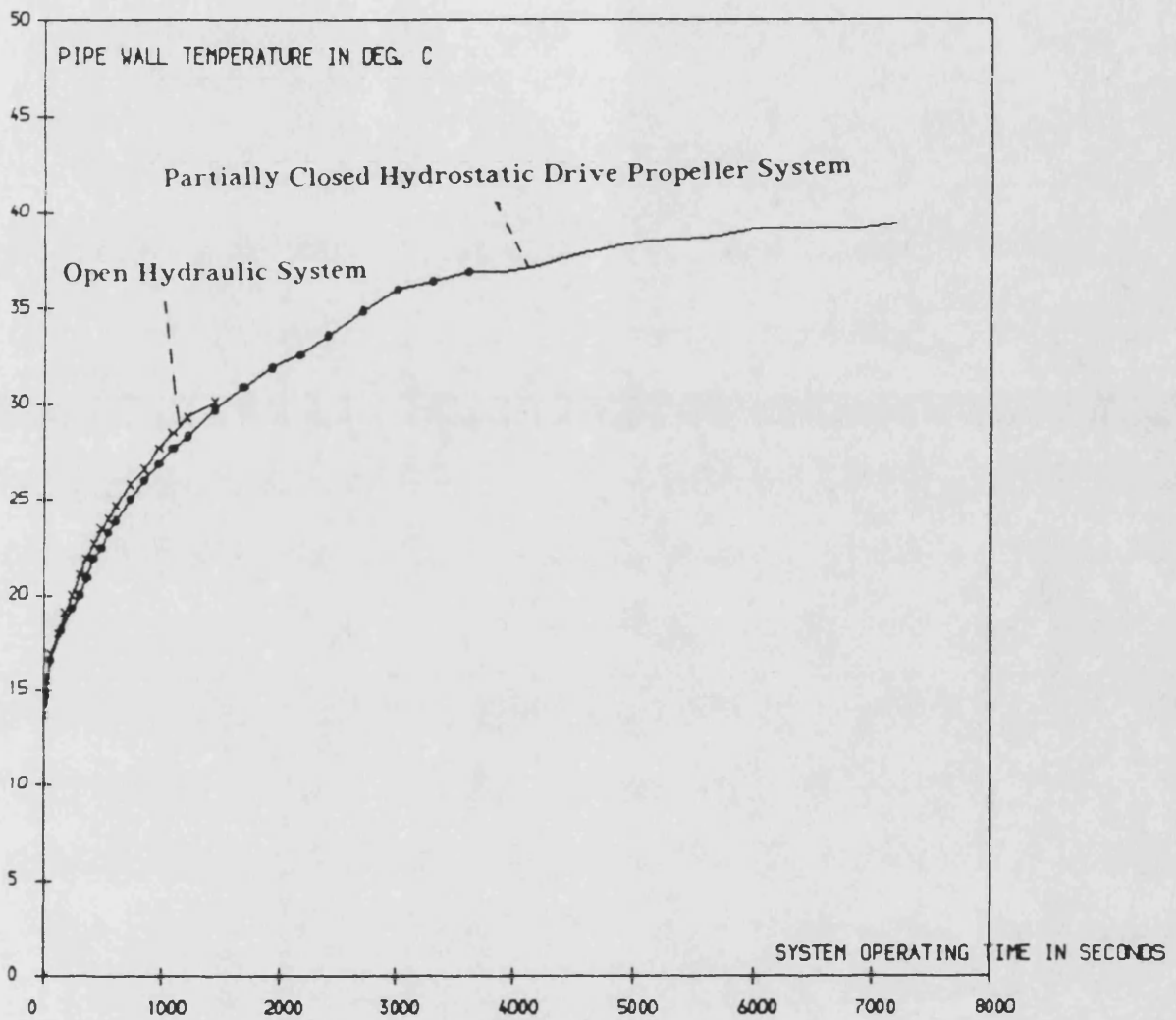
Fig. 6.40b   Comparison of Average Pipe Wall Temperatures of the Open and Partially Closed Systems
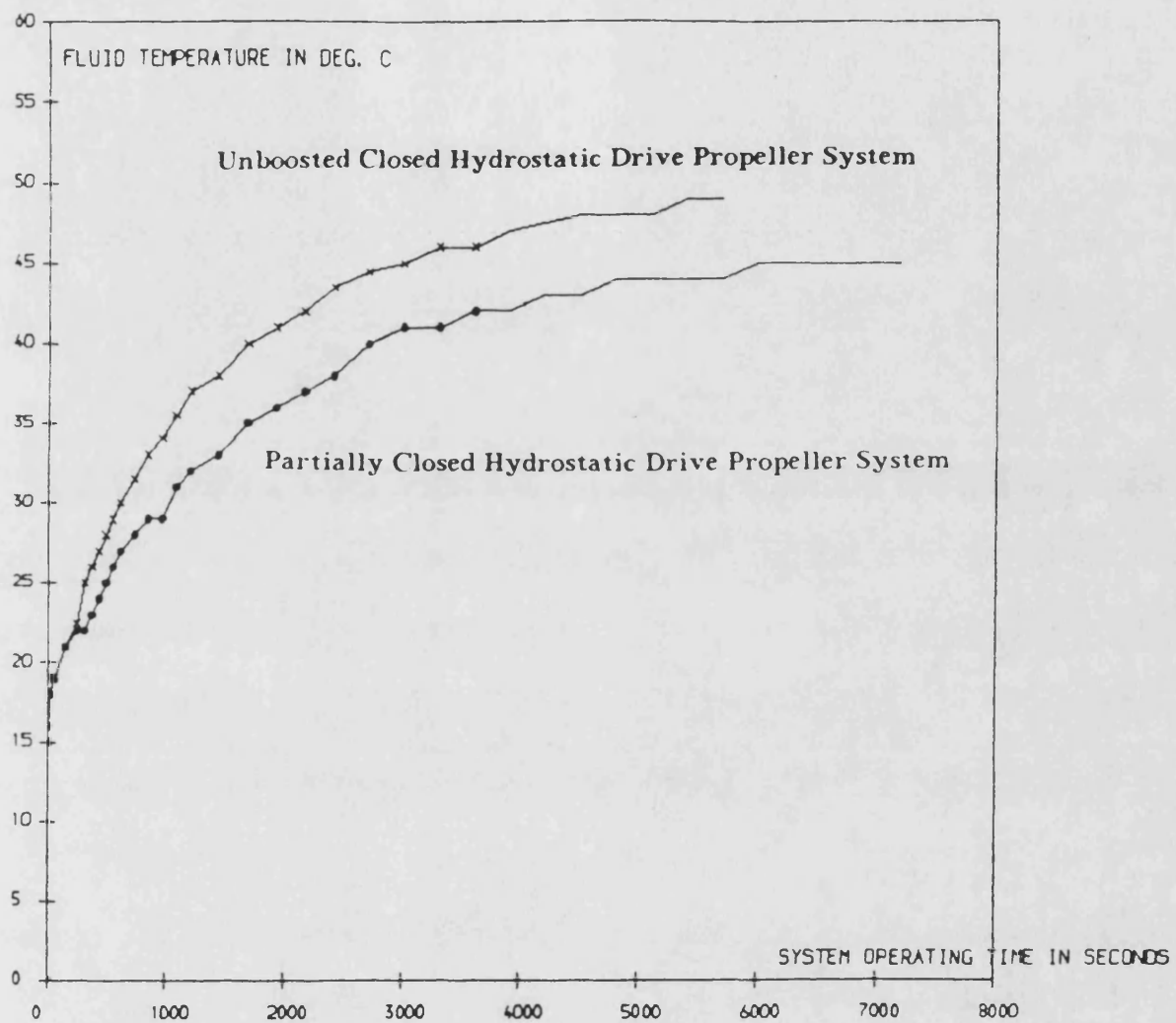
Fig. 6.41   Comparison of Average Fluid Temperatures of the Unboosted
and Partially Closed Systems
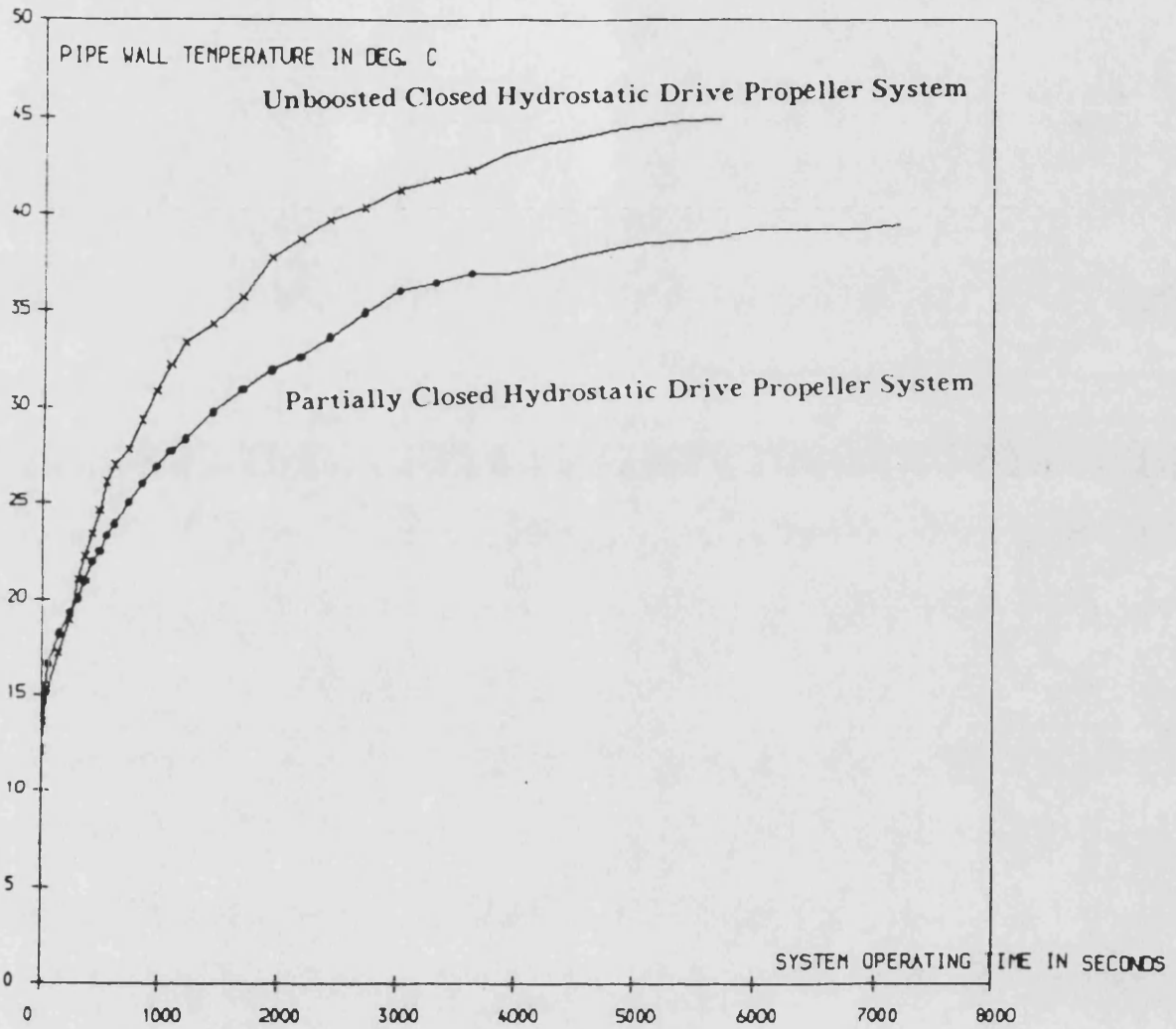
Fig. 6.42   Comparison of Average Pipe Wall Temperatures of the Unboosted and Partially Closed Systems
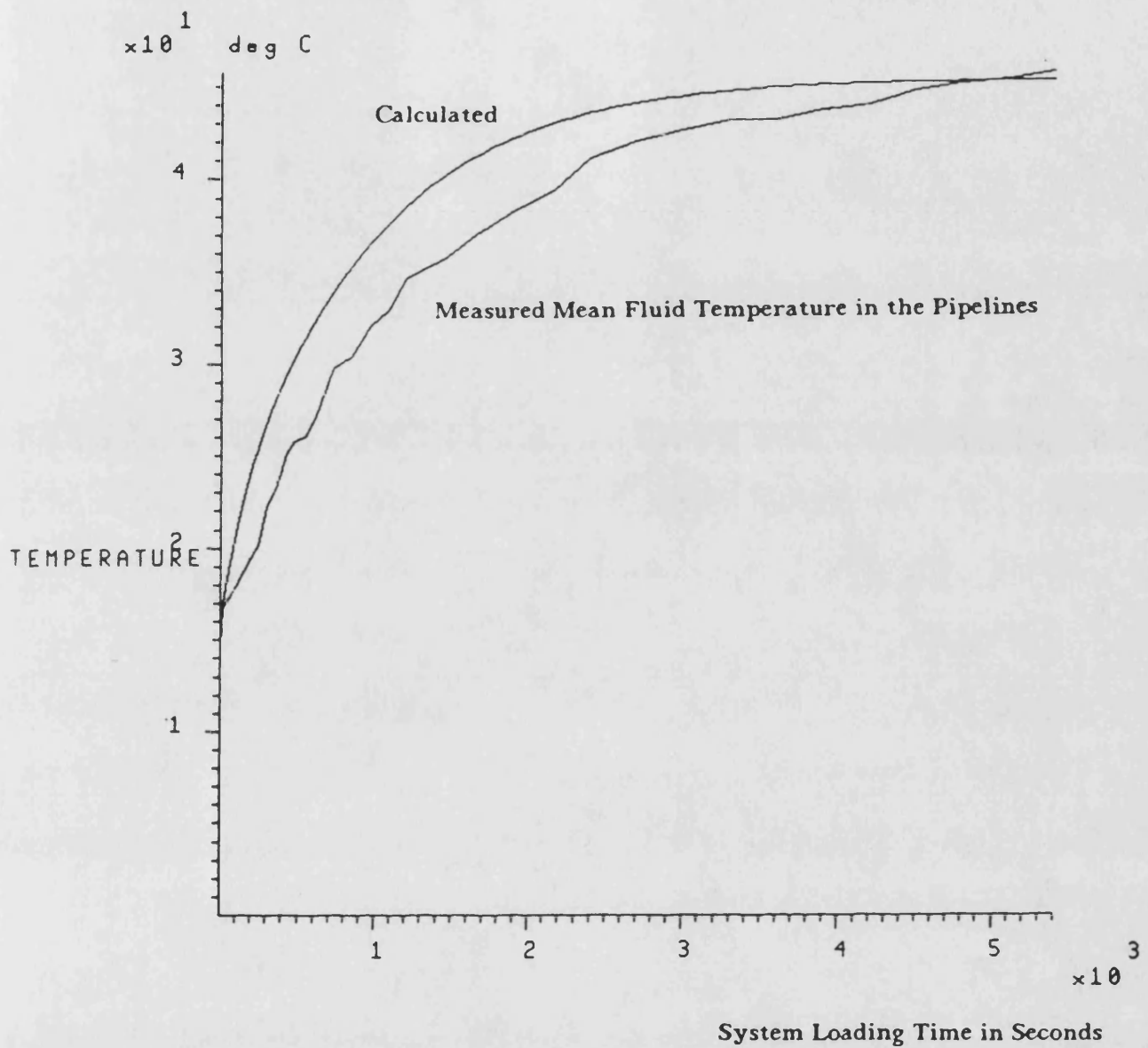
Fig. 6.43   Comparison of the Calculated and Measured Fluid Temperatures
in the Unboosted Closed Hydrostatic Drive Propeller System

×10² Kg/m*3

8

7

6

5

4

DENSITY

3

2

1

1   2   3   4   5   3

TIME   ×10

System Loading Time in Seconds
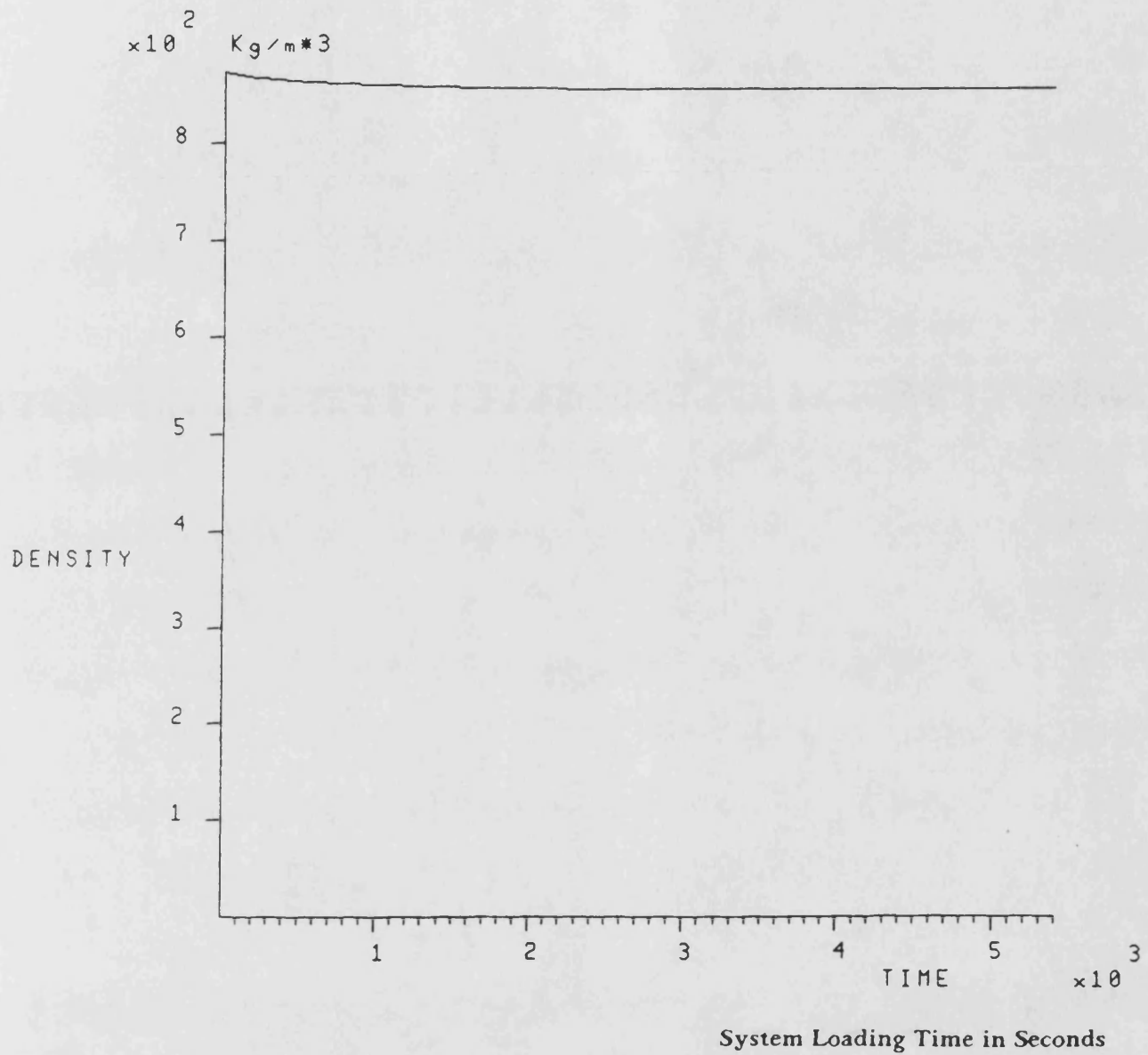
Fig. 6.44   The Updated Fluid Density in the Unboosted Closed Hydrostatic
Drive Propeller System
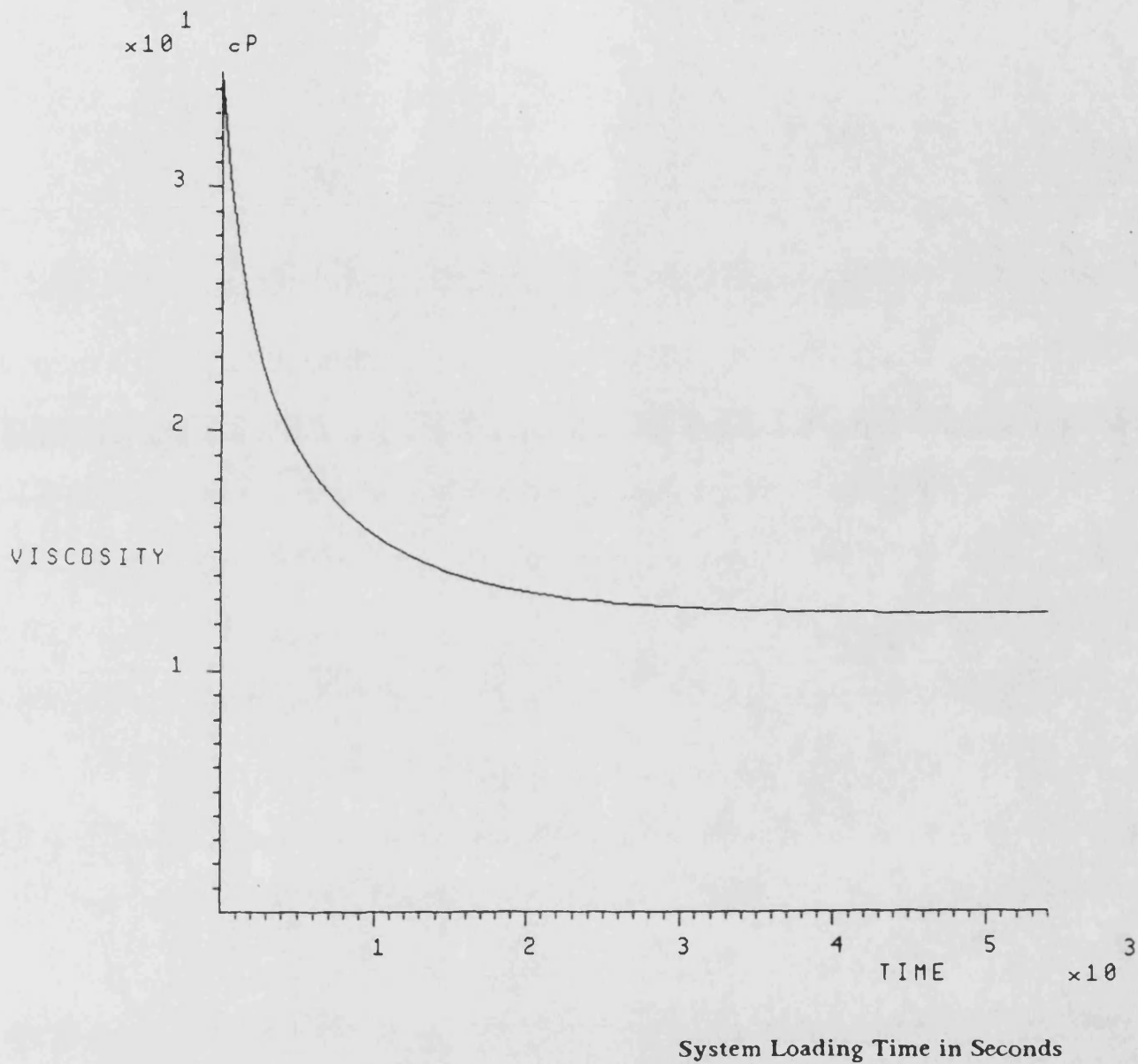
Fig. 6.45   The Updated Fluid Viscosity in the Unboosted Closed Hydrostatic Drive Propeller System
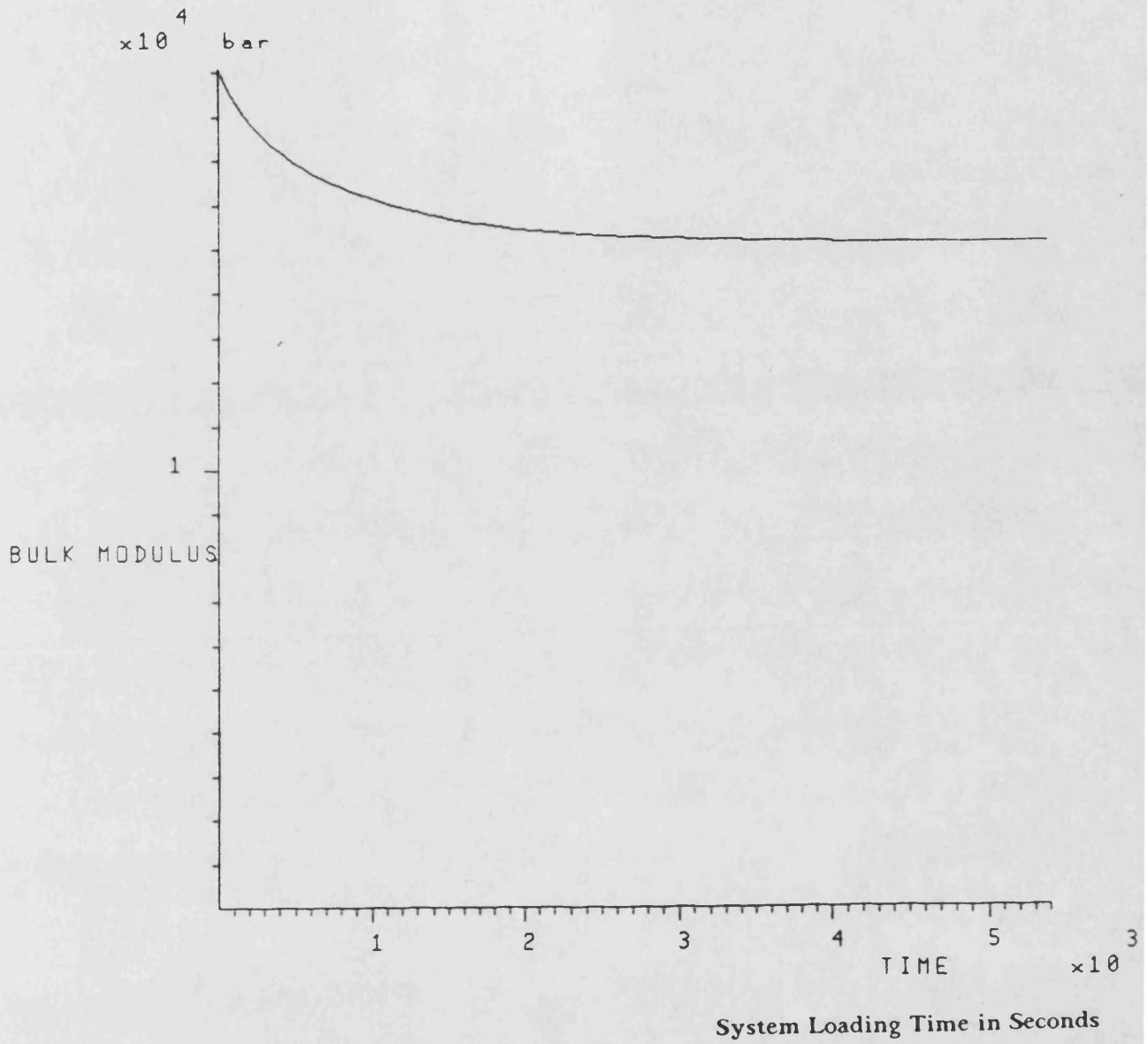
Fig. 6.46   The Updated Fluid Bulk Modulus in the Unboosted Closed
Hydrostatic Drive Propeller System
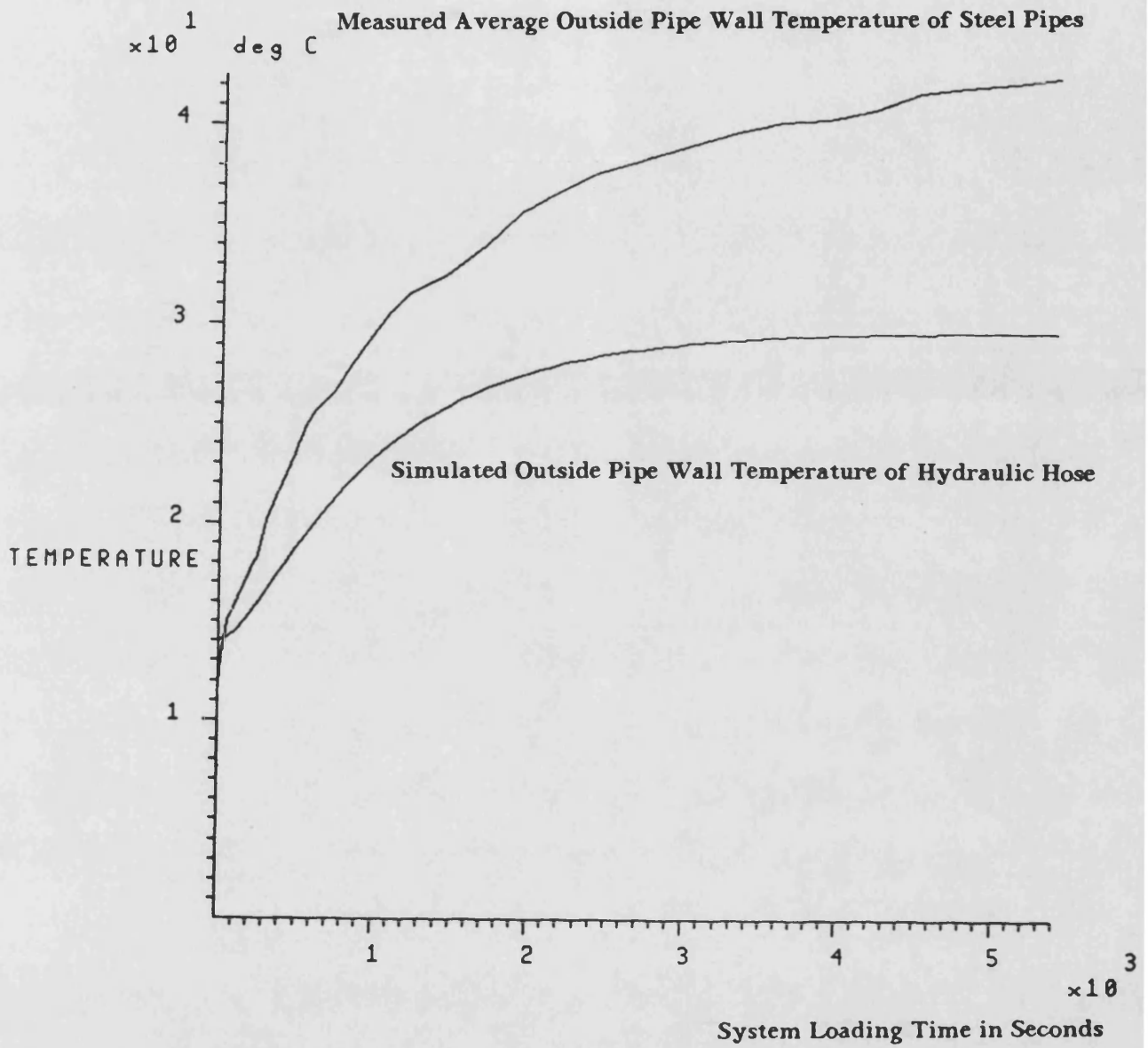
Fig. 6.47   Comparison of the Simulated and Measured Pipe Wall Temperatures
of the Unboosted Closed Hydrostatic Drive Propeller System
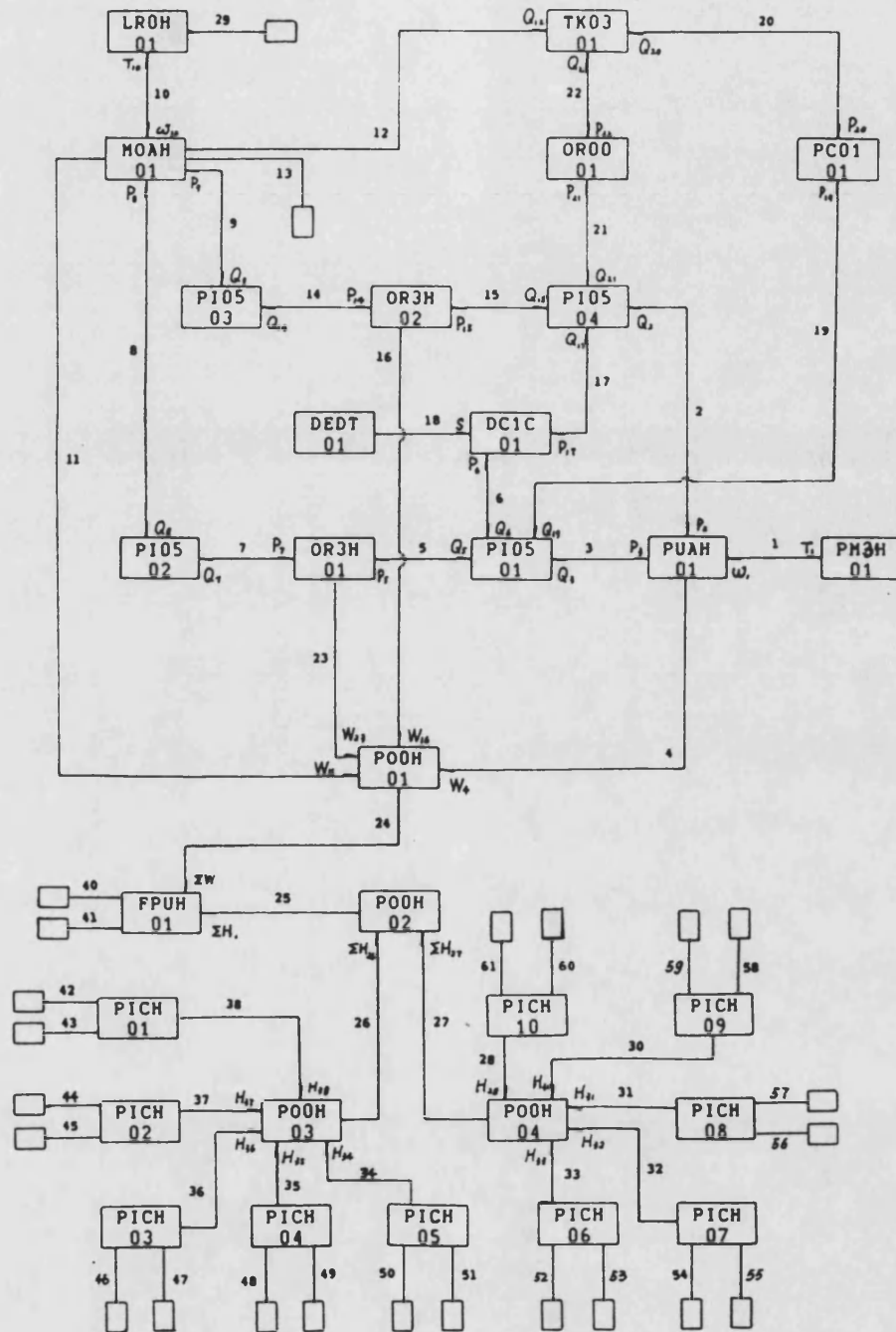
Fig. 6.48
Block Diagram for the Simulation of the Unboosted Closed
Hydrostatic Drive Propeller System with an Approach to Assume
an Uniform Loop Fluid Temperature and to Consider the Effects
of the Different Types of Pipe Wall Materials

Calculated Pipe Wall Temperature of
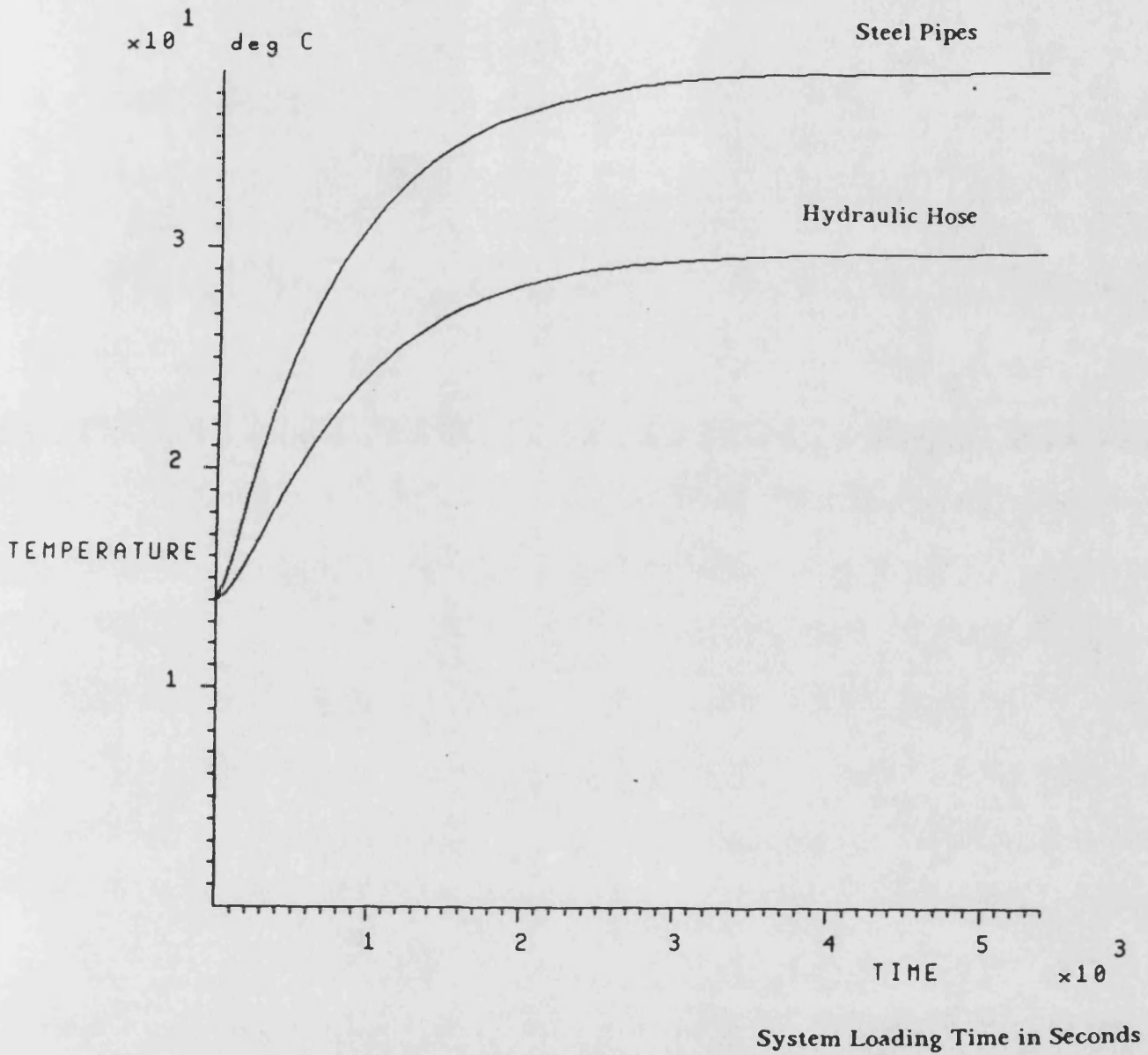
Fig. 6.49   Comparison of Pipe Wall Temperatures of Hydraulic Hoses and Mild Steel Pipes in the Unboosted Closed Hydrostatic Drive Propeller System
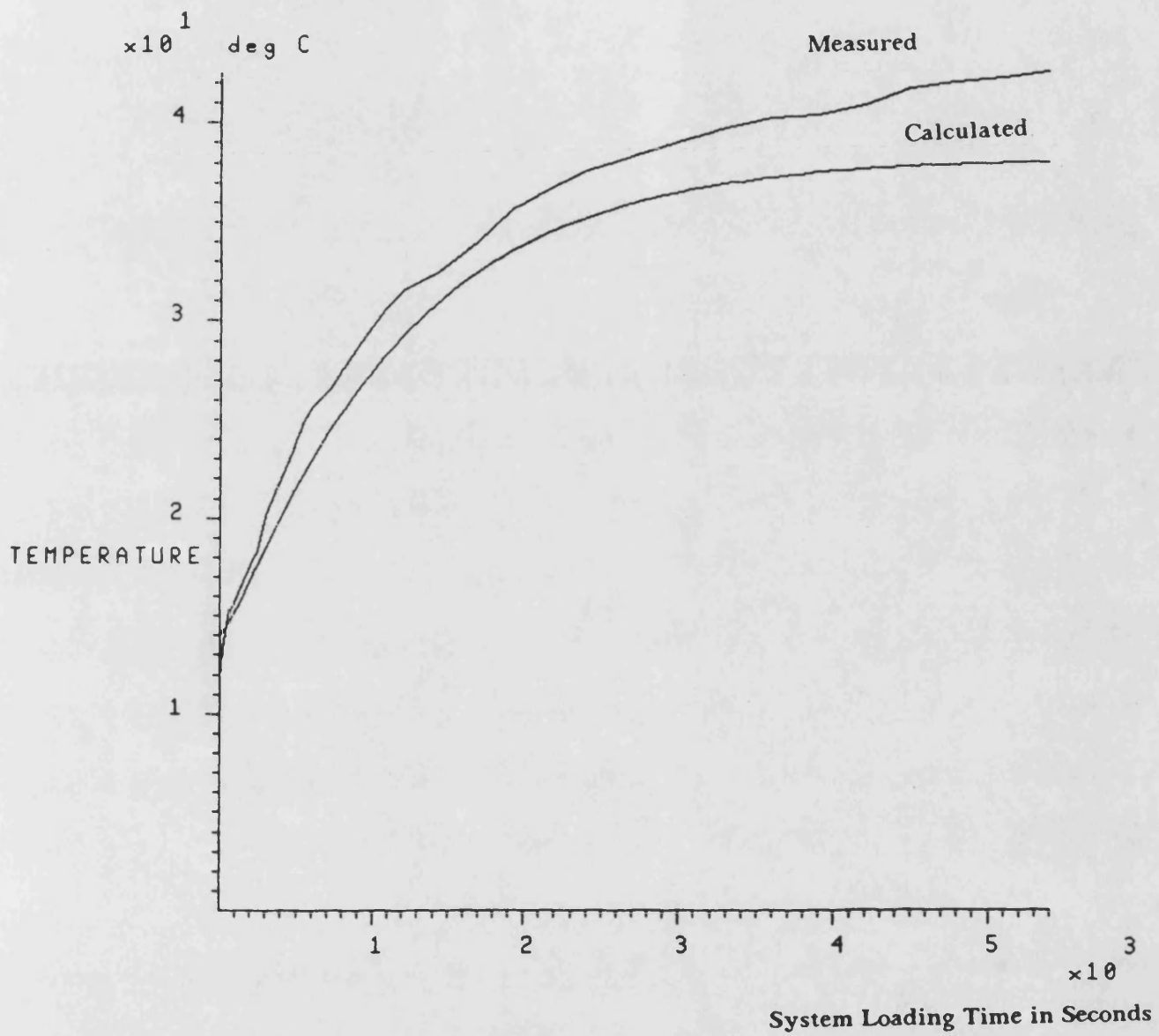
Fig. 6.50   Comparison of Calculated and Measured Pipe Wall Temperatures
at Outside of Mild Steel Pipes in the Unboosted Closed
Hydrostatic Drive Propeller System
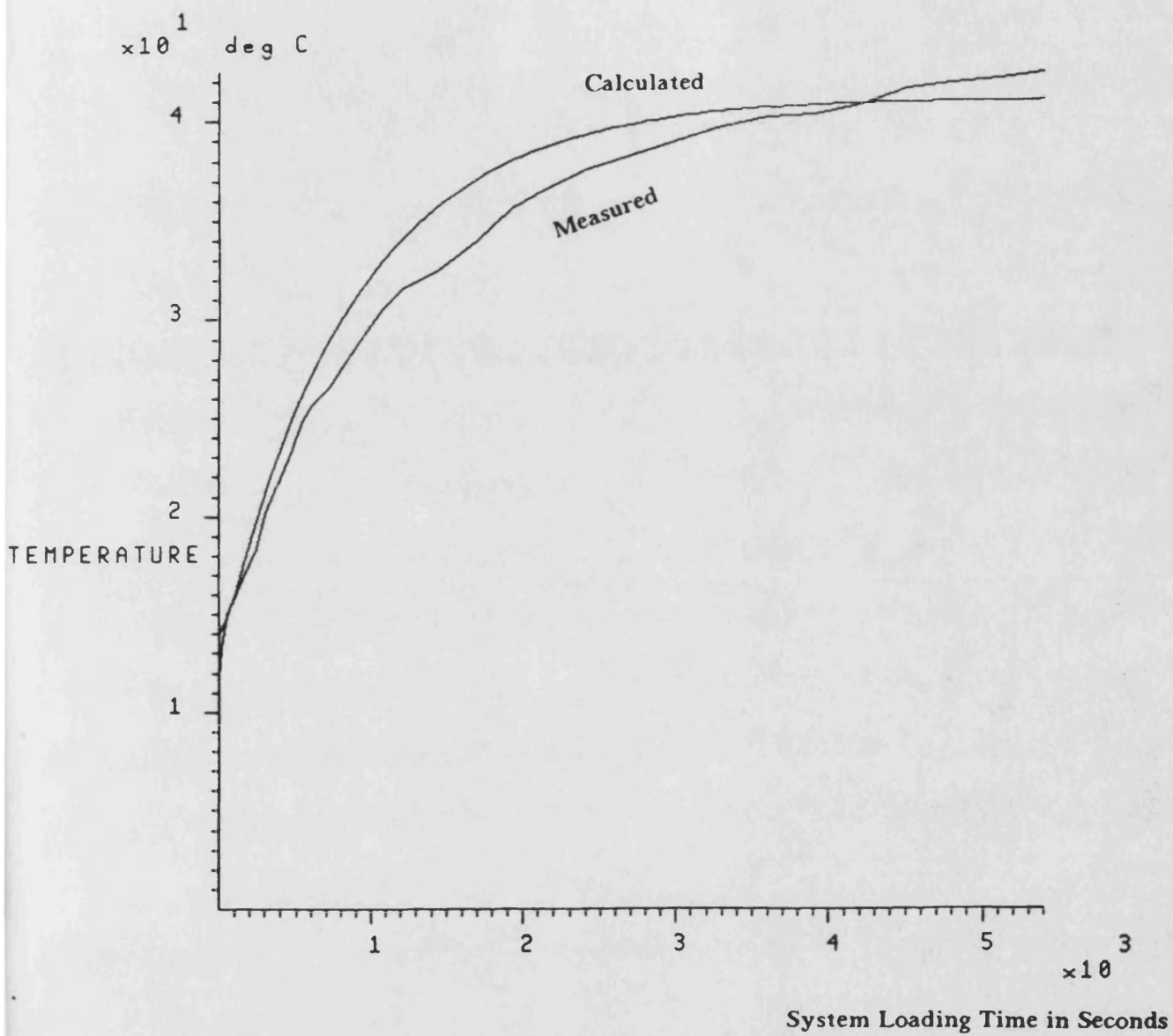
Fig. 6.51   Comparison of Calculated and Measured Pipe Wall Temperatures
at Outside of Mild Steel Pipes in the Unboosted Closed
Hydrostatic Drive Propeller System After the Simulation
Data Being Justified According to Test Conditions
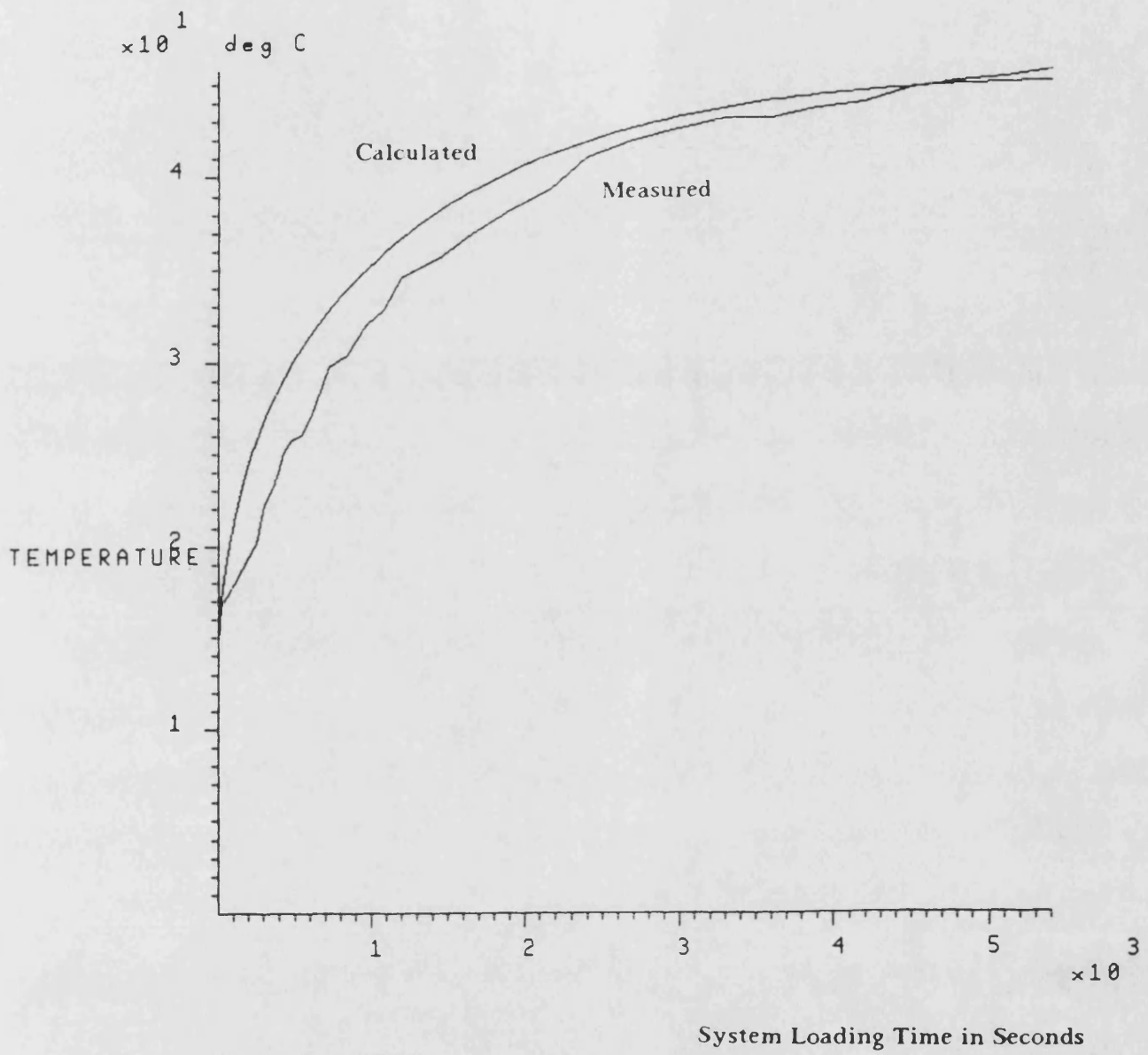
Fig. 6.52   Comparison of Calculated and Measured Fluid Temperatures
in the Unboosted Closed Hydrostatic Drive Propeller System
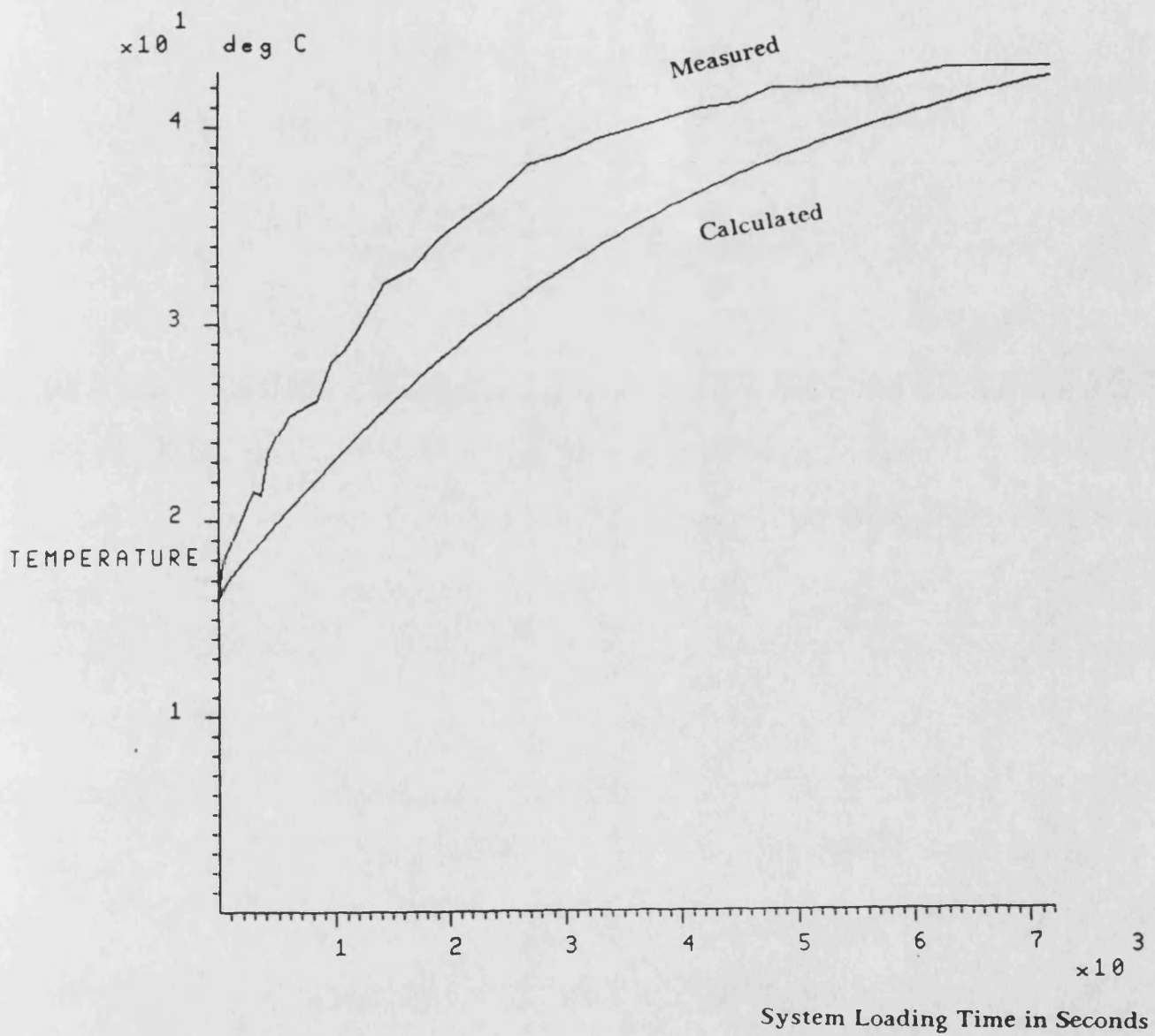
Fig. 6.53   Comparison of Calculated and Measured Fluid Temperatures
in the Partially Closed Hydrostatic Drive Propeller System
After the Input Data for the Fluid Height in the Reservoir
Being Justified
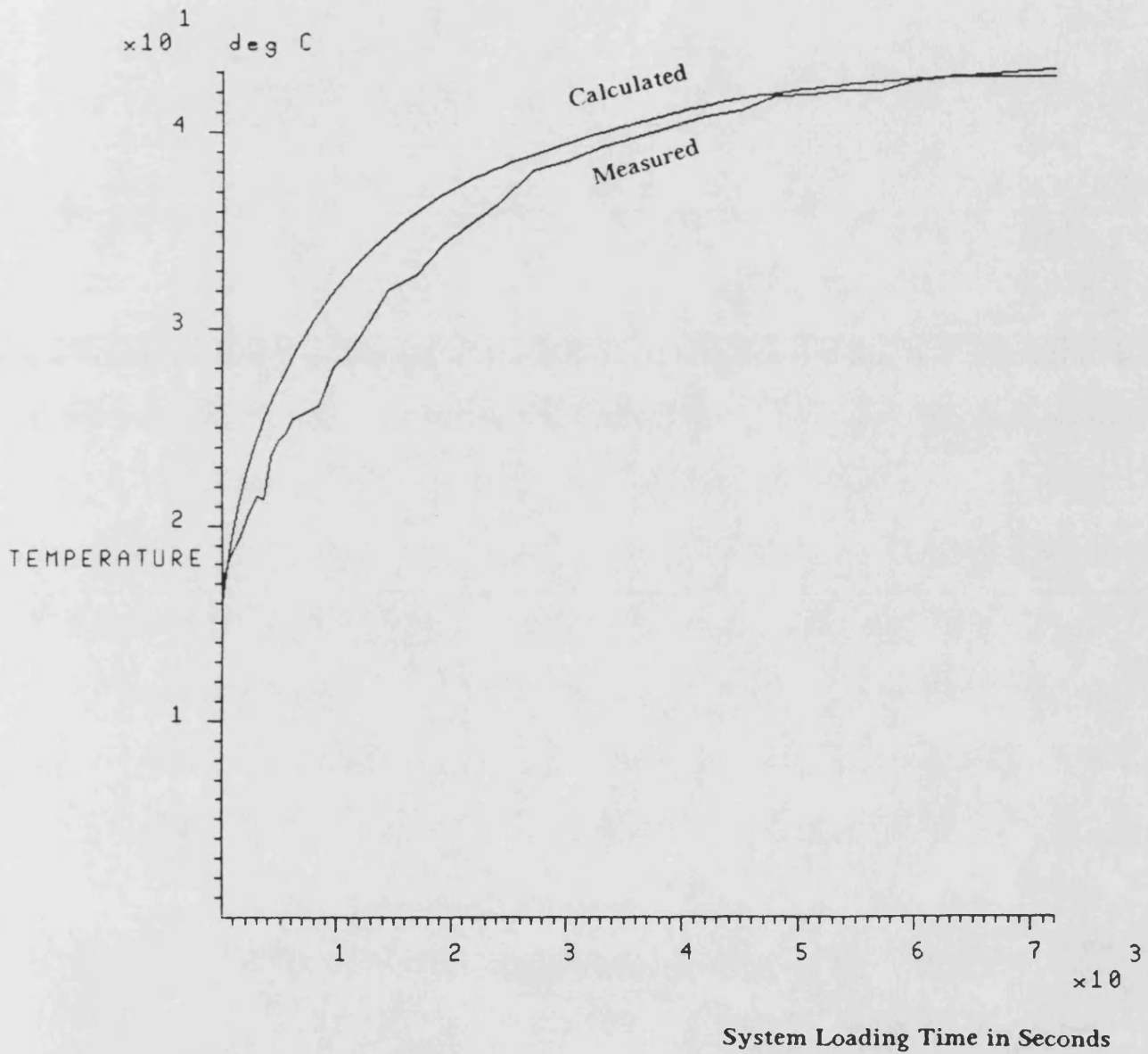
Fig. 6.54   Comparison of Calculated and Measured Loop Fluid Temperatures
in the Partially Closed Hydrostatic Drive Propeller System
When the Calculated Fluid Temperature in the Reservoir
is Justified to Include the Radiation Effect at the
Outside Walls of the Reservoir
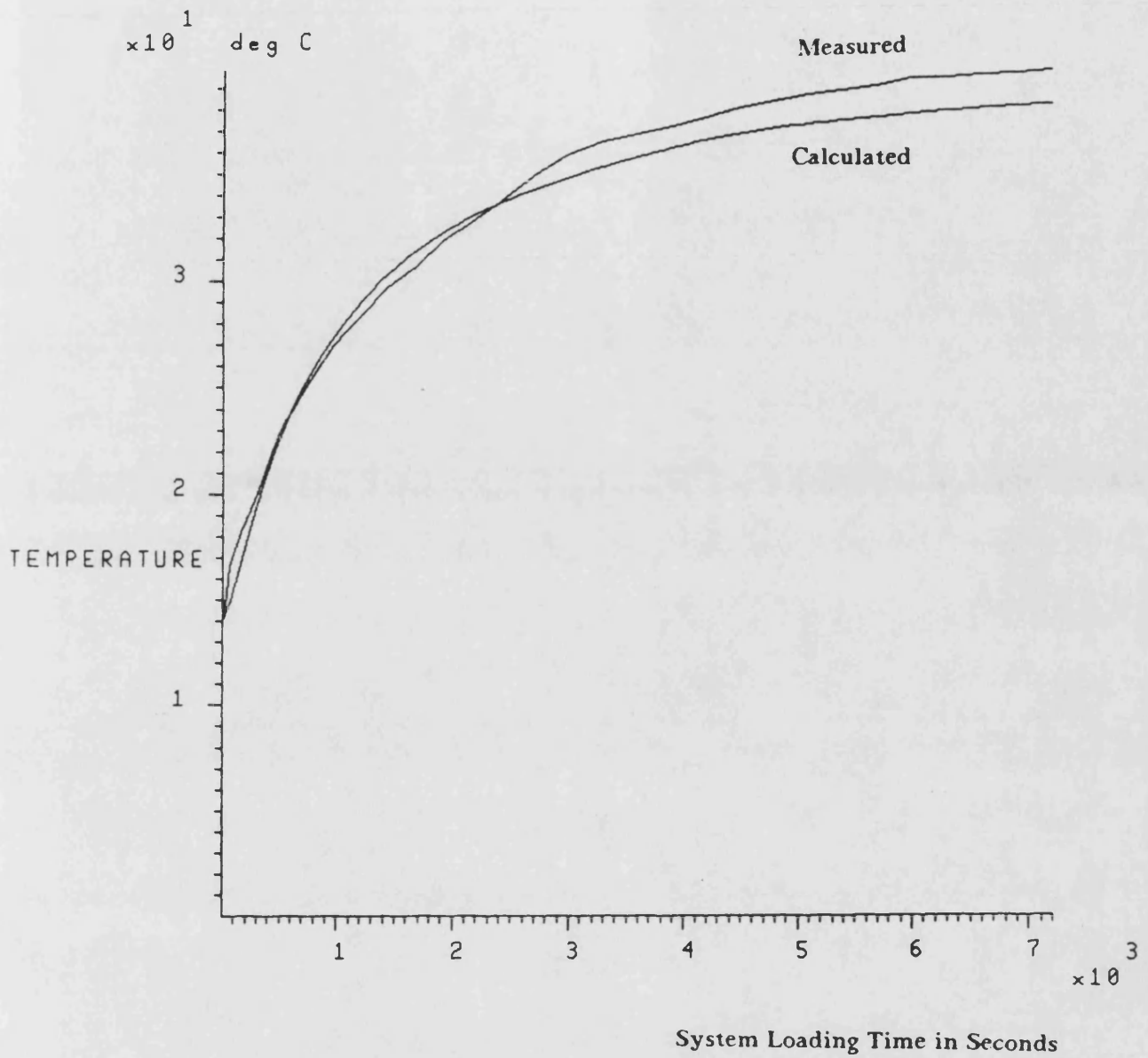
Fig. 6.55   Comparison of Calculated and Measured Wall Temperatures at the Outside of the Mild Steel Pipes in the Partially Closed Hydrostatic Drive Propeller System
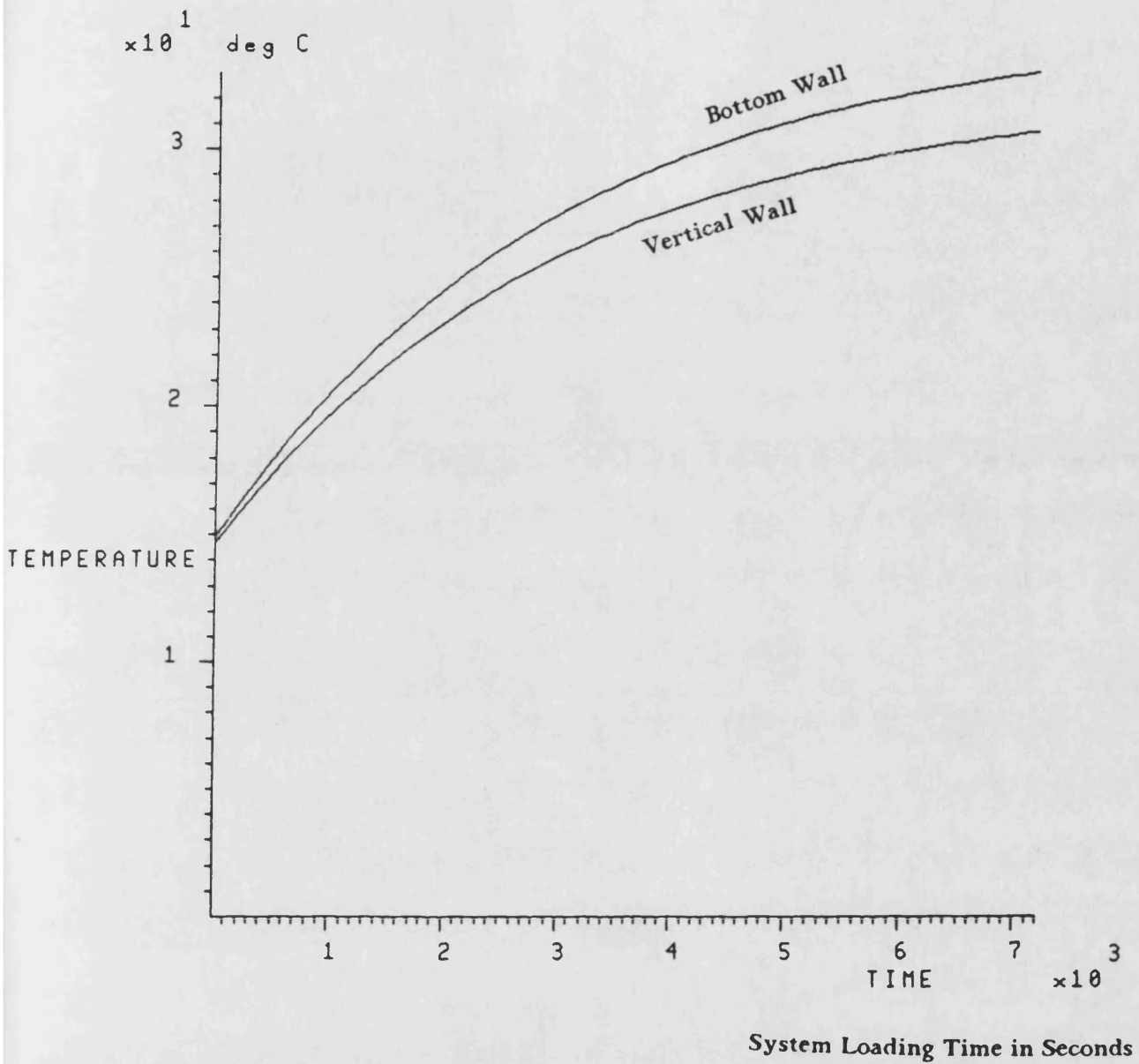
Fig. 6.56   Comparison of Simulated Outside Temperatures of the
Vertical and Bottom Walls of the Reservoir
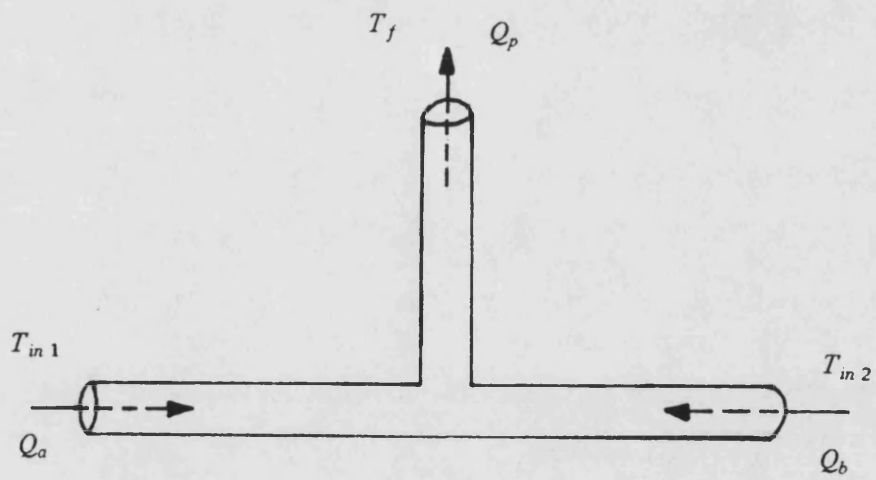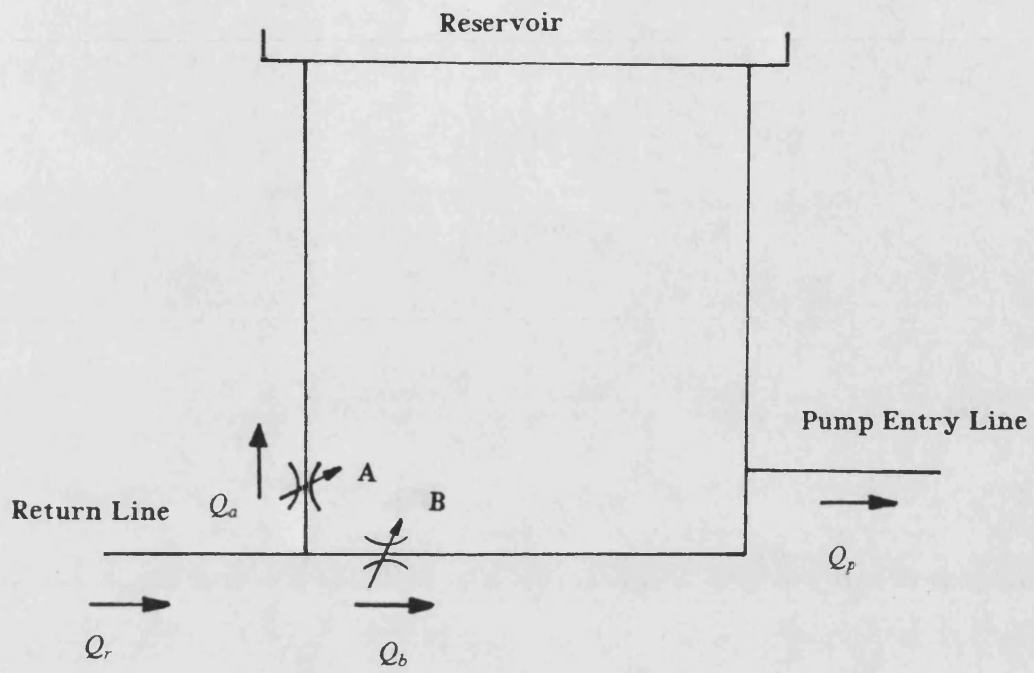
Fig. 6.57   System Y-junction Suction Pipe
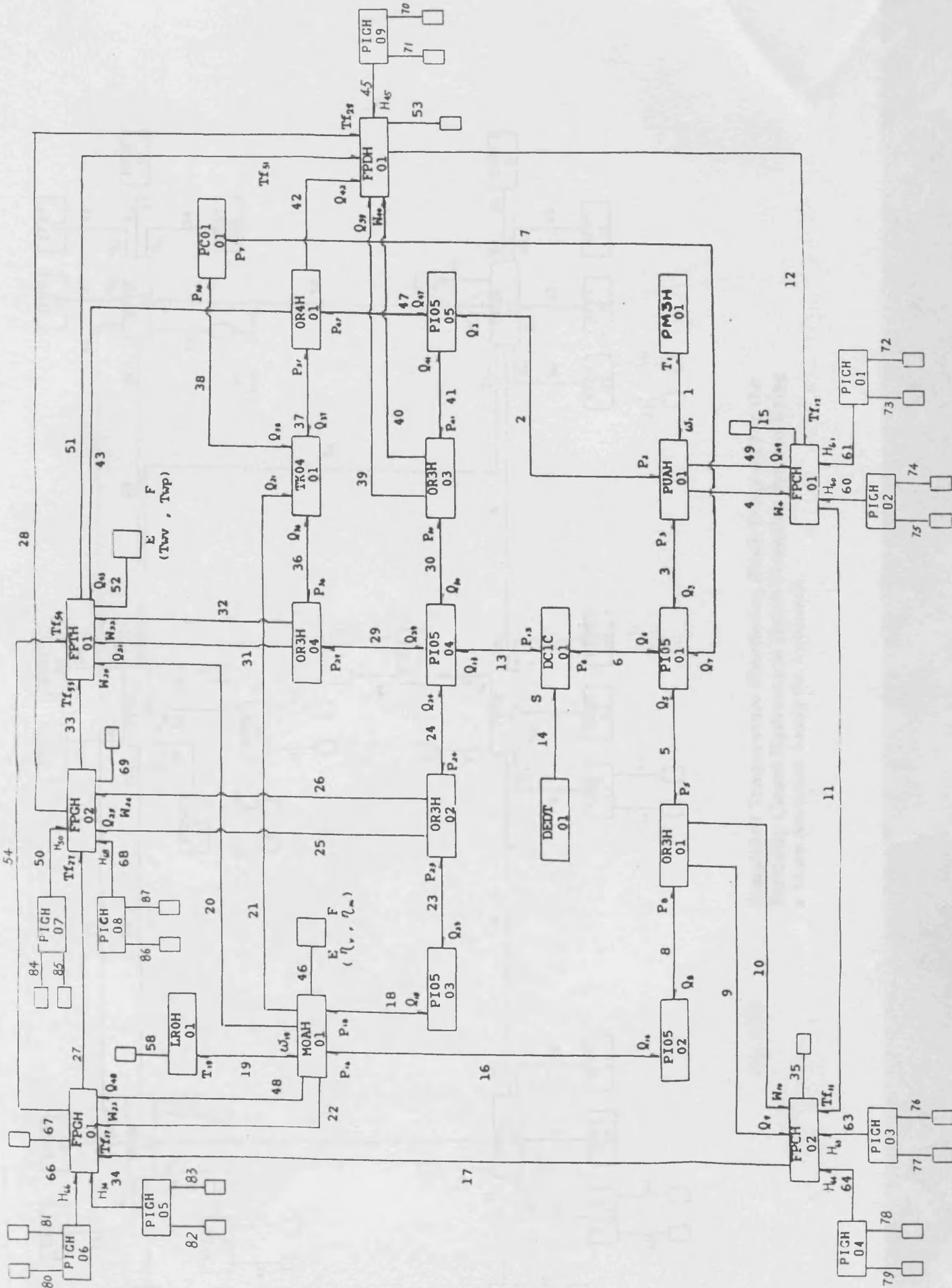
Fig. 6.58   Block Diagram for the Simulation of the Partially Closed
Hydrostatic Drive Propeller System with an Approach to Predict
Fluid and Pipe Wall Temperatures at the Different Sections of
the System Pipelines
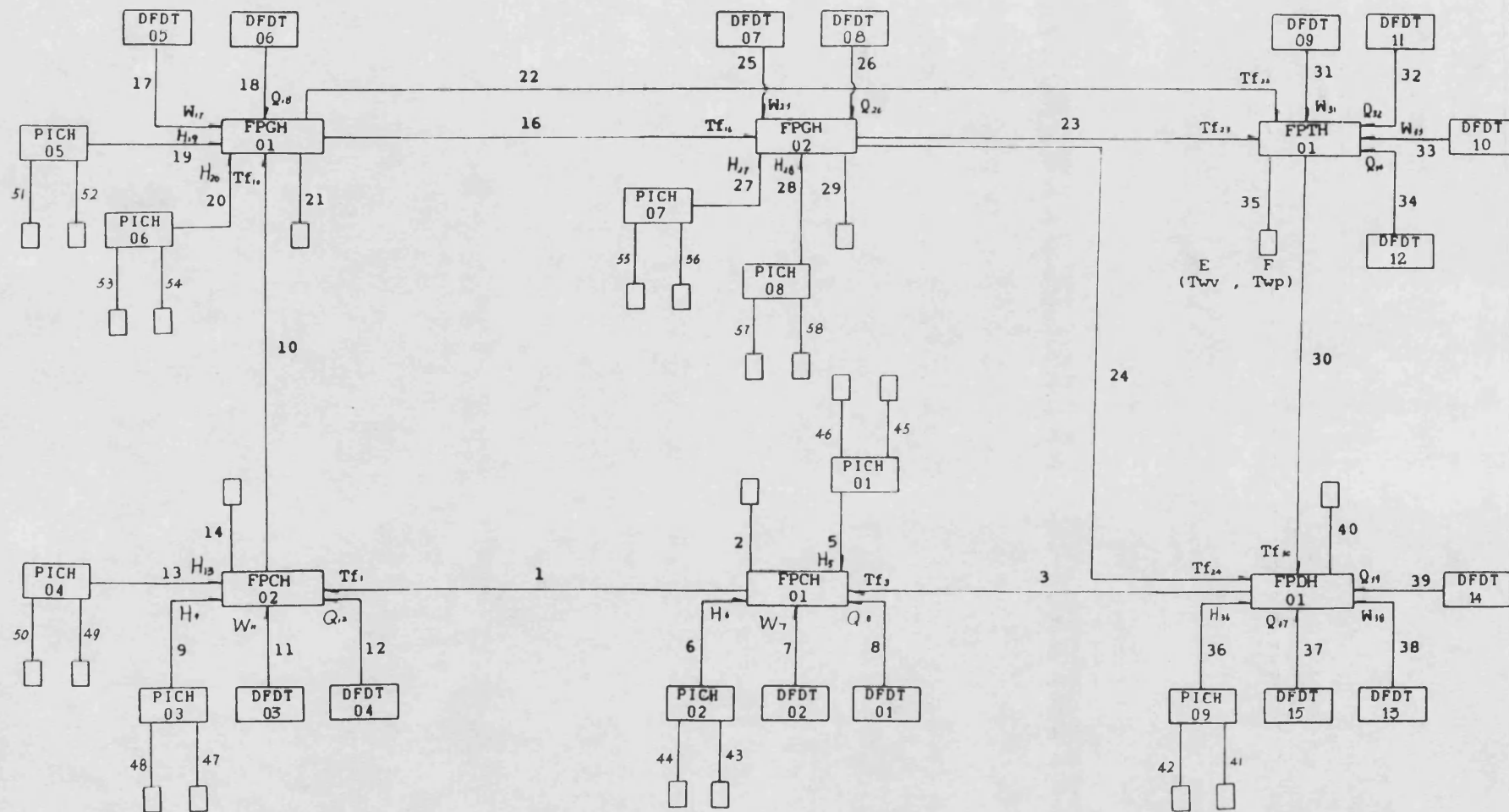
Fig. 6.59 Simplified Temperature Simulation Block Diagram for the
Partially Closed Hydrostatic Drive Propeller System Using
a More Accurate Analytic Approach
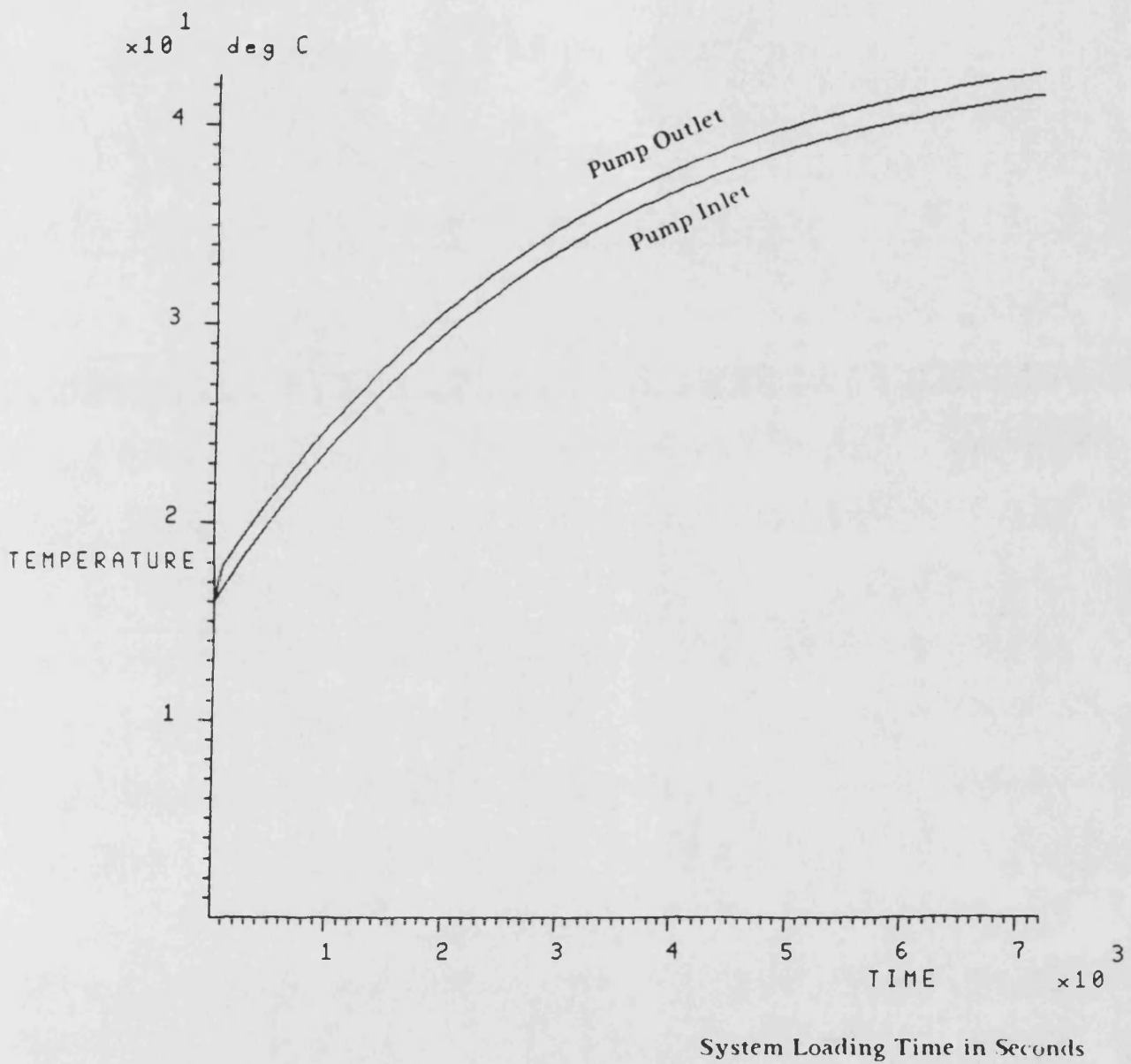
Fig. 6.60   Comparison of Calculated Fluid Temperatures at the Inlet and Outlet of the Pump When a Cooler is Used in the Partially Closed Hydrostatic Drive Propeller System
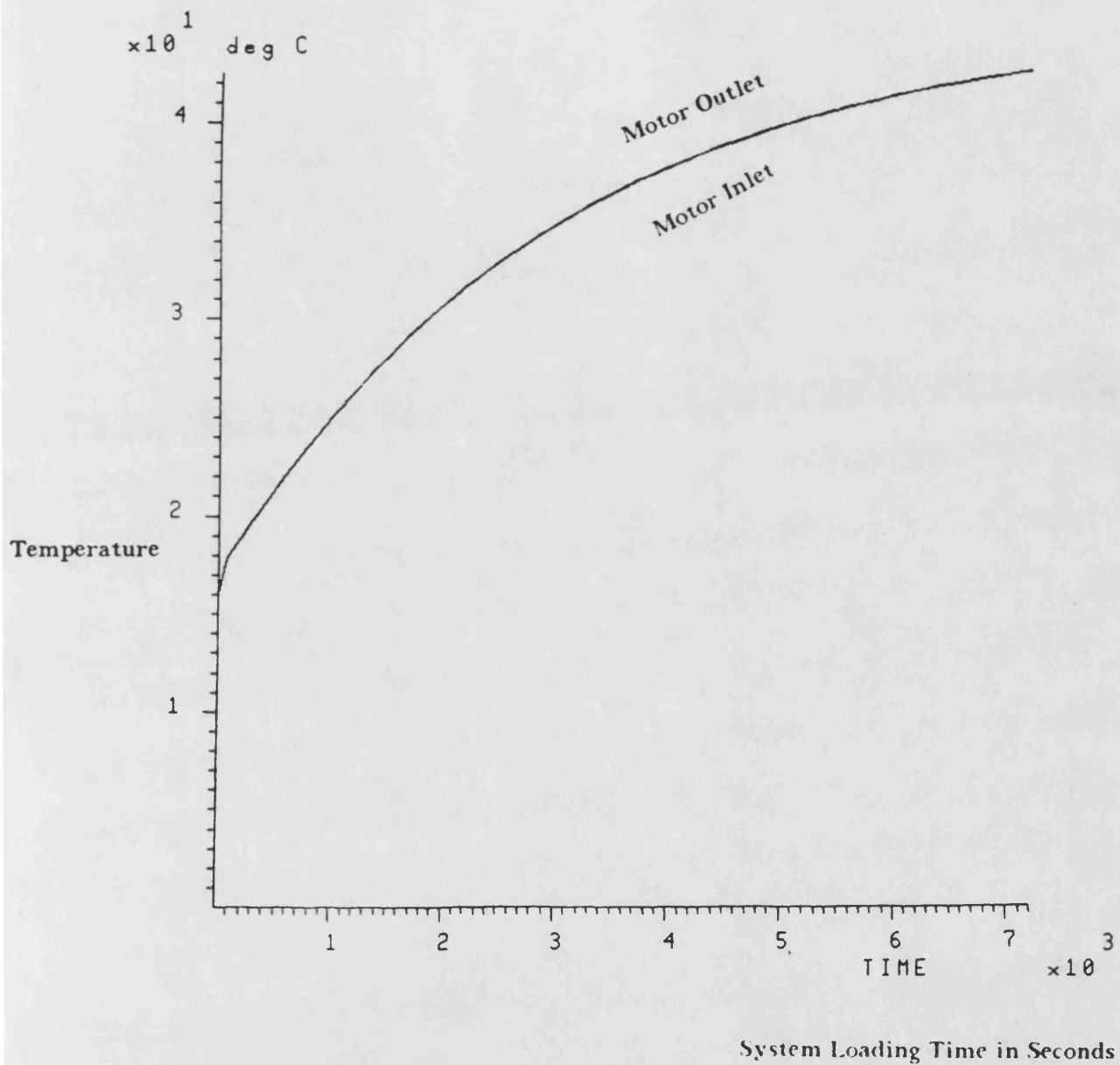
Fig. 6.61   Comparison of Simulated Fluid Temperatures at the Inlet and
              Outlet of the Motor When a Cooler is Used in the Partially
              Closed Hydrostatic Drive Propeller System
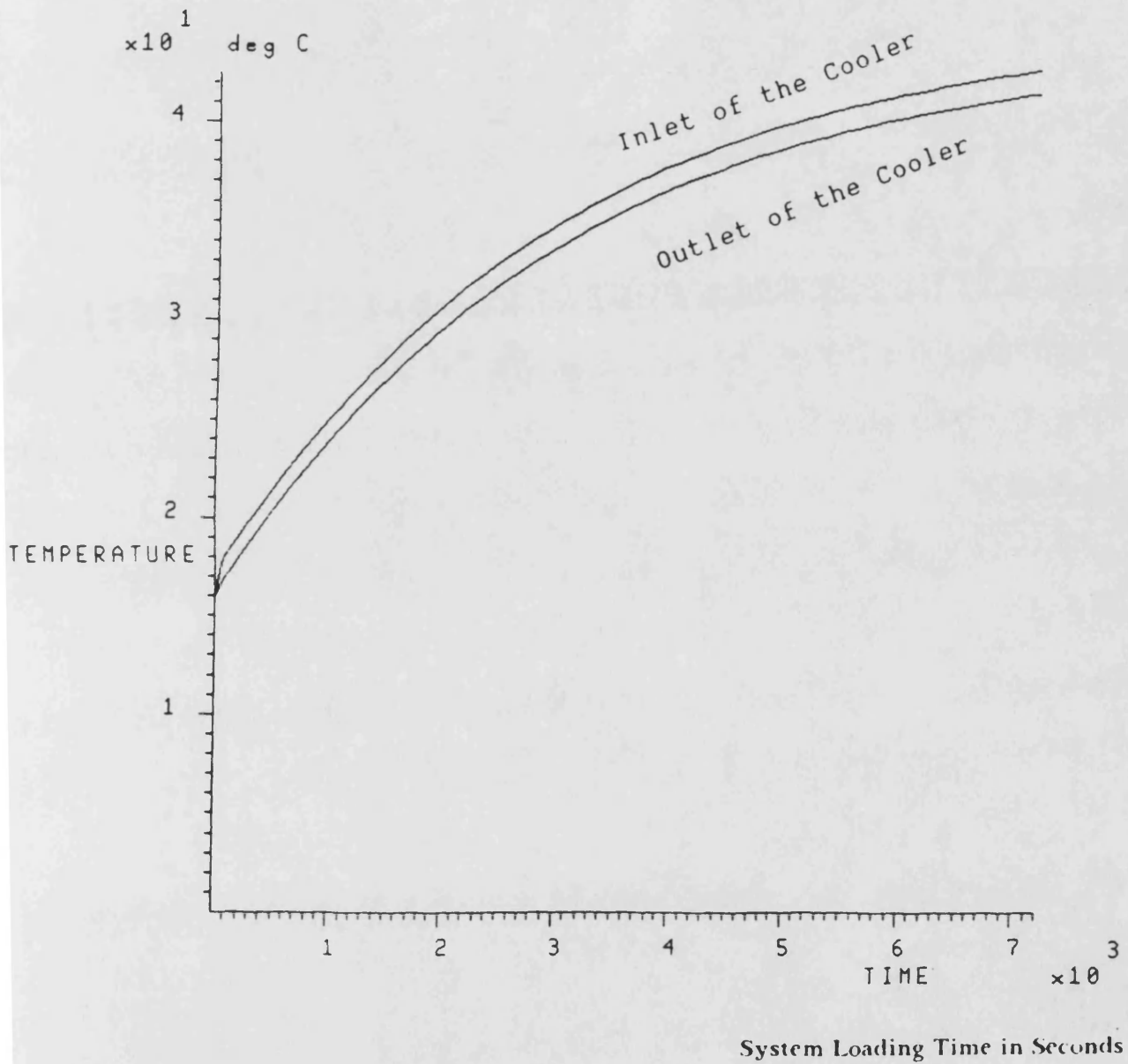
Fig. 6.62   Comparison of Simulated Fluid Temperatures at the Inlet and
Outlet of the Cooler Incorporated in the Partially Closed
Hydrostatic Drive Propeller System
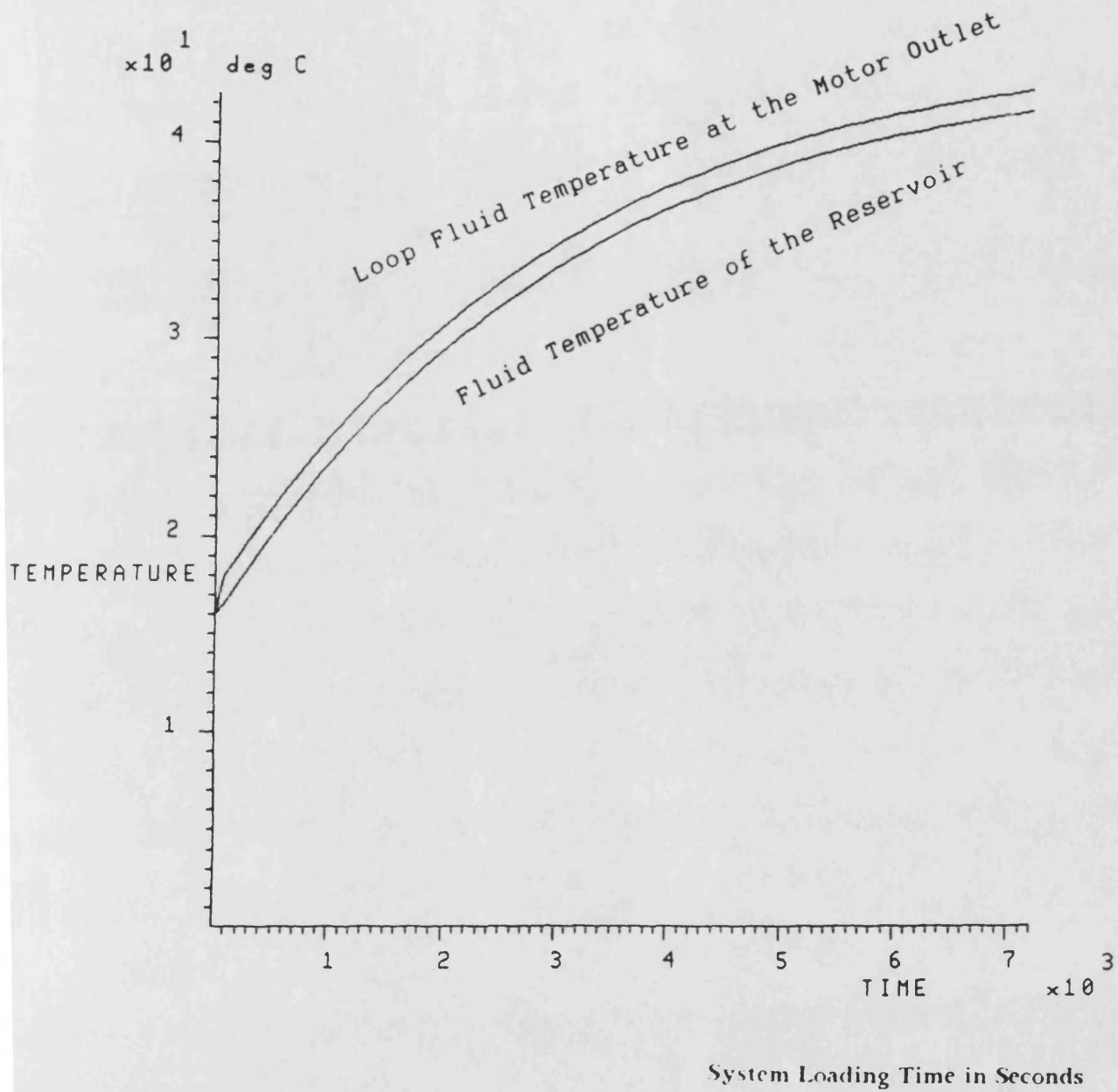
Fig. 6.63   Comparison of Simulated Fluid Temperatures in the Reservoir
                 and Outlet of the Motor When a Cooler is Used in the Partially
                 Closed Hydrostatic Drive Propeller System
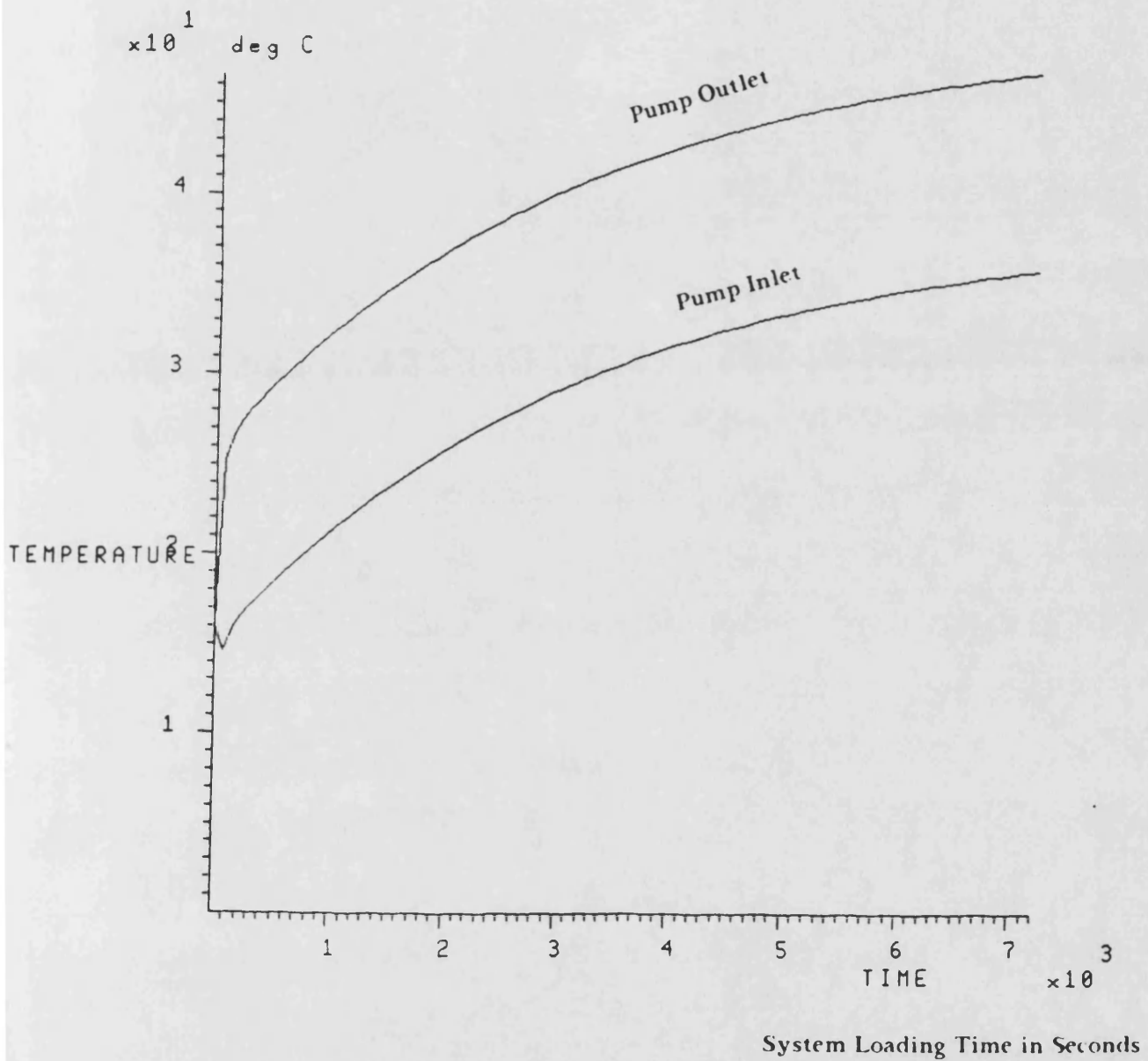
Fig. 6.64   Comparison of Simulated Fluid Temperatures at the Inlet and
Outlet of the Pump with a Small Flowrate in the Partially
Closed Hydrostatic Drive Propeller System
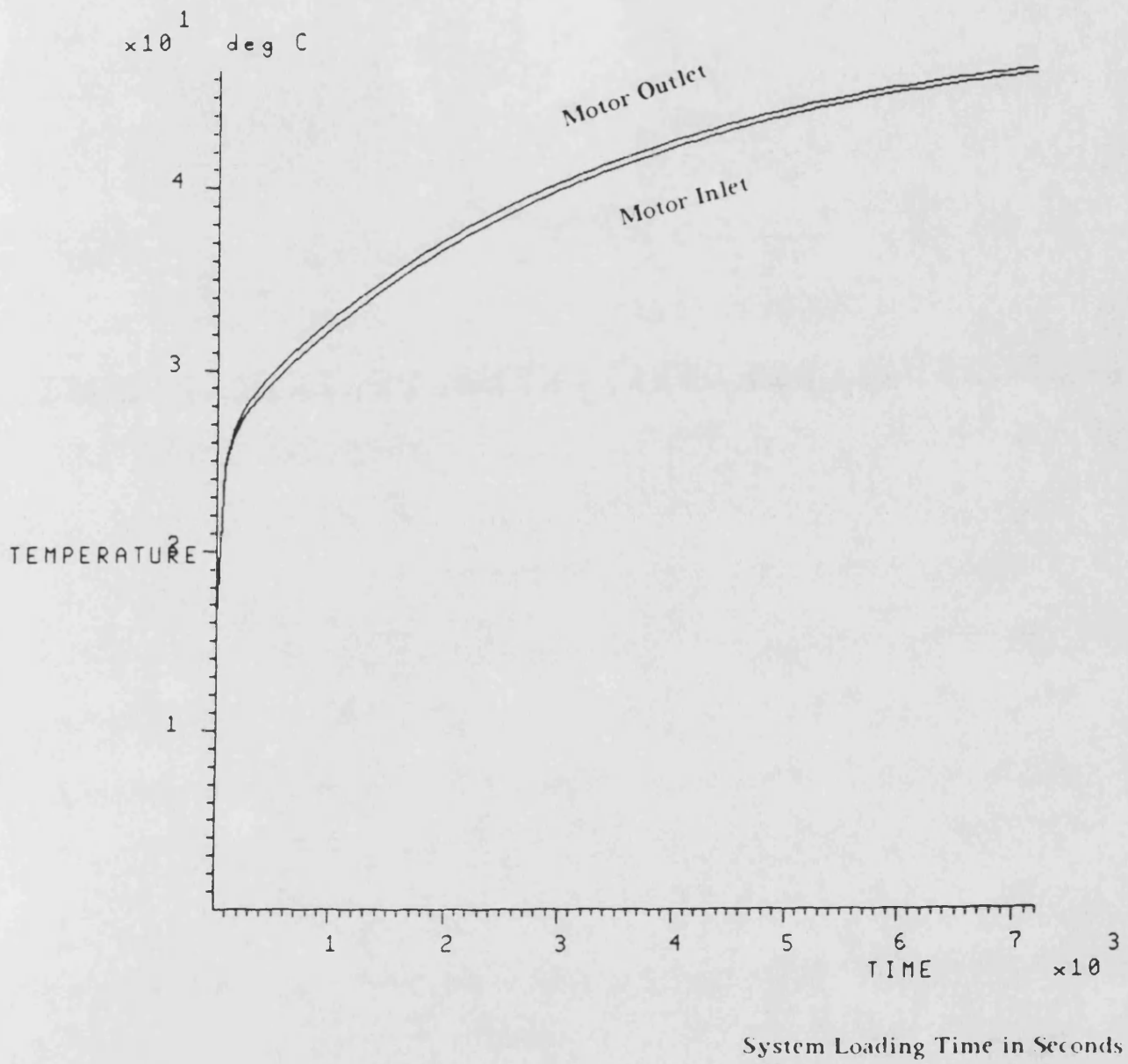
Fig. 6.65   Comparison of Simulated Fluid Temperatures at the Inlet and Outlet of the Motor with a Small Flowrate in the Partially Closed Hydrostatic Drive Propeller System
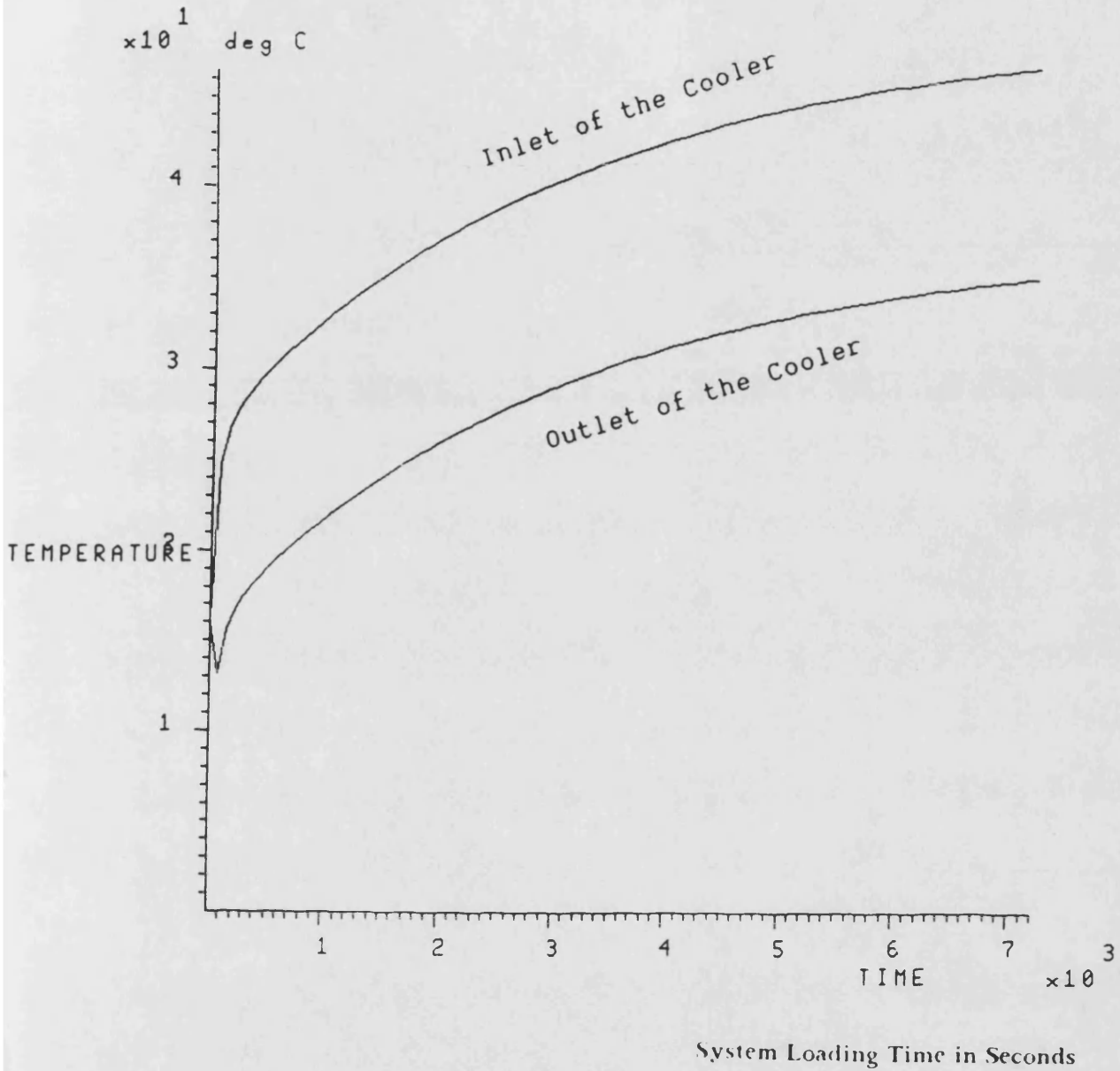
Fig. 6.66   Comparison of Simulated Fluid Temperatures at the Inlet and Outlet of the Cooler Incorporated in the Partially Closed Hydrostatic Drive Propeller System with a Small System Flowrate
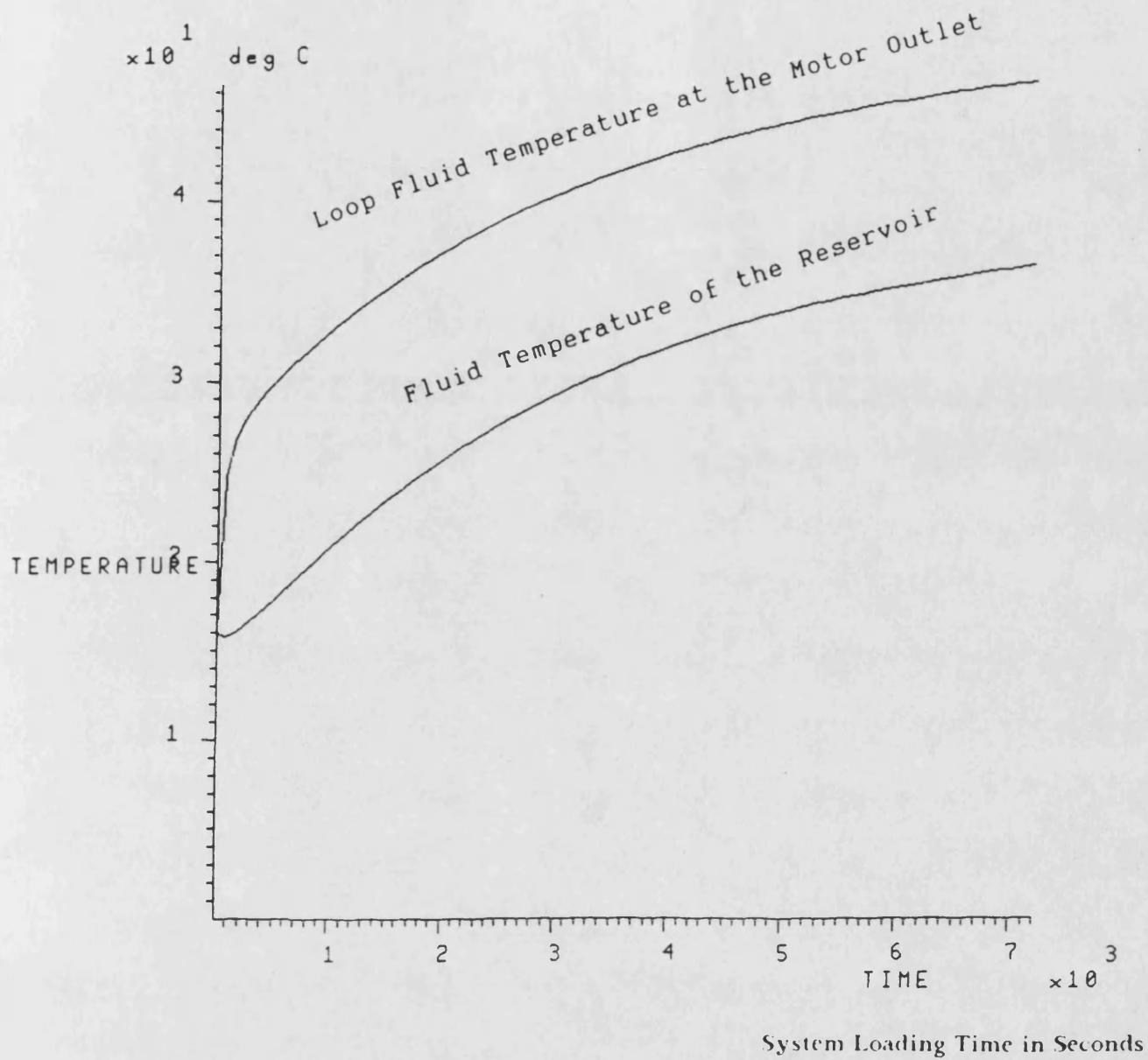
Fig. 6.67   Comparison of Simulated Fluid Temperatures in the Reservoir
and Outlet of the Motor with a Small Flowrate in the Partially
Closed Hydrostatic Drive Propeller System

CHAPTER 7

CONCLUSIONS

7.1   In this thesis the middle ground between open and closed hydraulic circuits has been explored. Using this approach unboosted closed and partially closed hydraulic circuits have been introduced as alternative circuit designs. An experimental investigation into the performance of the unboosted closed circuit has shown that, with no external leakage and with equal area actuators, the reservoir can be removed from the circuit, the only problem likely to occur is the diminution of air from the circuit. An extreme case was tested in which the reservoir was completely removed from the system. In order to obtain a reasonably accurate simulation of the system behaviour, more complex models have been necessary for the electric motor, orifice and suction line. It has been concluded from these studies that the fluid jet at downstream of the orifice plays in an important role in determining the dynamic characteristics of the system. The effects of the suction pipe length on the pump suction pressure and the necessity of considering flowrate difference across a pressure control valve caused by fluid expansion downstream have also been revealed.

7.2   The experimental study for the performance of the partially closed hydraulic circuit has shown its advantages in air release and cooling and flexibility of circuit design. It has been suggested that 10 - 15 % of the system flow should be returned to reservoir for optimal system performance. The theoretical prediction for the system behaviour has resulted the development of dynamic reservoir and pipe junction models. It has been pointed out that fluid momentum is a predominant factor in the transient modelling of vertical pipes in low pressure region. Moreover, two alternative approaches for avoiding implicit relationships in the linking of components have been proposed as a result of the theoretical study.

7.3 A small boat hydrostatic drive propeller system has been shown as being ideally suited to exploit the potential of the partially closed circuit. For the simulation of the system behaviour a simplified engine model and a propeller load model have been developed, and the simulation has been used to determine the setting pressure of the system relief valve. With 10 % system flow being returned to reservoir and remainder being directly fed to the pump inlet, a considerable reduction in reservoir size compared with conventional systems is permissible. The suction pipe diameter can also be reduced. These attributes can be applied to many open hydraulic systems to reduce the cost of the systems.

7.4 A study of thermodynamic behaviour of the hydrostatic drive propeller system has led the way to develop three simulation approaches with different degrees of accuracy for temperature prediction in hydraulic systems. In these approaches the heat transfer between the fluid and pipe walls have been taken into account. These approaches could be applied to simulate thermodynamic behaviour of other hydraulic systems. A particularly interesting development of the work has been the simulation and experimental investigations of radiation effects under room temperature region. On the basis of the work it has been concluded that the radiation effects in the region considered are far more significant than previously thought. This has challenged the widely accepted assumption in many text books, which ignores the radiation effects under 200° C.

7.5 The simulations described in this thesis have been given sufficient close agreement with the experiments to validate the theoretical approaches. They have been used to give full explanation of the behaviour of the systems considered. They can be also used to be an effective design tool for the system components including suction pipe, cooler, filter and reservoir sizing.

7.6 It is proposed that a most promising development would be to carry out a test programme on a practical boat in the hope of this will lead to the integration of the partially closed hydraulic circuit design with a potential large number of hydraulic systems in the boat industry. This it is suggested would enable savings in size, cost and energy supply of the hydraulic systems. A most interesting possibility is to

apply the partially closed circuit on to open pump-actuator systems and this is strongly recommended as the basis of further investigation.

REFERENCES

Chapter 2

2.1   Bowns, D. E. and Rolfe, A. C.. The Digital Computation of
       Pressures and Flows in Interconnected Fluid Volumes, Using
       Lumped Parameter Theory. 4th International Fluid Power
       Symposium, U. K., 1975.

2.2   Bowns, D. E., Tomlinson, S. P. and Dugdale, S. K.. Progress
       towards a General Purpose Hydraulic Simulation Language. 6th
       International Fluid Power Symposium, Cambridge, U. K.,
       April, 1981.

2.3   Bowns, D. E., Tomlinson, S. P. and Dorey, R. E.. Computer
       Simulation Techniques for the Dynamic Performance Assessment
       of Fluid Power Systems. 7th International Fluid Power
       Symposium, Bath, U. K., September, 1986.

2.4   Bowns, D. E. and Tomlinsion, S. P.. Prediction of Thermal
       Transient Effects Using the Hydraulic Automatic Simulation
       Package, 2nd Royal Navy Hydraulic Engineering Conference,
       Manadon, April, 1986.

2.5   Gear, C. W.. Numerical Initial Value Problems in Ordinary
       Differential Equations. Prentice-Hall, Englewood Ciffs.
       New Jersey, 1971.

2.6   Oldenburger, R. and Goodson, R. E.. Simplification of
       Hydraulic Line Dynamics by Use of Infinite Products. ASME
       Journal of Basic Engineering, Vol. 86, pp. 1-10 January,
       1964.

2.7   Skarbek-Wazynski, C. M.. Wave Propagation by the Method of

Characteristics. Ph. D. Thesis, University of Bath, 1981.

2.8   Tomlinson, S. P.. HASP Component Model Library Manual. Vol 1,
       Report No. 556, School of Engineering, University of Bath,
       August, 1981.

Chapter 3

3.1   Foster, K. and Parker, G. A.. Transmission of Power by
       Sinusoidal Wave Motion through Hydraulic Oil in An Uniform
       Pipe. Proc Inst Mech Engrs, 179 pt 1, (19), 1964-65.

3.2   Magnussen, P. C.. Transmission Lines and Wave Propagation.
       Allyn and Bacon, 1965.

3.3   Bowns, D. E. and McCandlish, D.. Quieter Oil Hydraulics
       Seminar, I. Mech. E., November 1977.

3.4   D'S ouza, A. F. and Oldenburger, R.. Dynamic Response of
       Fluid Lines. ASME Journal of Basic Engineering, September,
       1964.

3.5   Johnansen, F. C.. Flow through Pipe Orifices at Low Reynolds
       Numbers. ARC Reports and Memoranda, 1252, 1929.

3.6   Ward-Smith, A. J.. Pressure Losses in Ducted Flow.
       Butterworths, London, 1971.

3.7   -   . Flow of Liquids, Pressure Losses Across Orifice
       Plates, Perforated Plates and Thick Orifice Plates in Ducts.
       Engineering Science Data Item Number 81039. London,
       November, 1981.

3.8   Mills, R. D.. Numerical Solution of Viscous Flow through a
       Pipe Orifice at Low Reynolds Numbers. J. Mech. Engng. Sci.,
       10(2), 133-40, 1968.

3.9   Hall, W. B. and Orme, E. M.. Flow of a Compressible Fluid
        through a Sudden Enlargement in a Pipe. Proceedings,
        I.Mech.E, Vol. 169, 1007, 1955.

3.10   Yang, H.. A Study of an Unboosted Closed Loop Hydraulic
        System. Report for the Transfer from the Degree of MSc. to
        the Degree of Ph. D., School of Engineering, University of
        Bath, February, 1986.

3.11   Rouse, H. and Abul-Fetouh, A.. Characteristics of
        Irrotational Flow through Axially Symmethic Orifice.
        J. Appl. Mech, Vol 17N4, pp. 421-426, 1950.

3.12   Wuest, W.. Stromung durch Schlitz-und Lochblenden bei
        Kleinen Reynolds-Zahlen, Ingenieur Archiv. Nr. 22,
        pp. 357-367, 1954.

3.13   Zalmonzon and Semikova. Investigation of Pneumatic Jet-Tube
        Elements. Pneumatic and Hydraulic Control Systems,
        Pergamon Press, 1968.

3.14   Blasius, H.. Das Aehnlichkeitsgesetz bei Reibungsvorgangen
        in Flussigkeiten. VDI-Forschungsheft, Vol 131, 1913.

3.15   Whitaker, s.. Fundamental Principles of Heat Transfer,
        Pergamon Press Inc., New York, 1977.

3.16   McCandlish, D. and Dorey, R. E.. The Mathematical Modelling
        of Hydrostatic Pumps and Motors. pp. 165-174, Proc I.Mech.E
        Vol 198B No 10, 1984.

3.17   Edge, K. A. and Freitas, F. J. T. de. A Study of Pressure
        Fluctuation in the Suction Lines of Positive Displacement
        Pumps. Proc Instn Mech Engr Vol 199 No B4, U. K., May, 1985.

3.18   Edge, K. A. and Freitas, F. J. T. de. Fluid Borne Pressure
        Ripple in Positive Displacement Pump Suction Lines. 6th
        International Fluid Power Symposium, Cambridge, U. K.,
        April, 1981.

3.19 Bowns, D. E. and McCandlish, D.. Pressure Ripple Propagation.
     I.Mech.E. - Quiet Oil Hydraulics, London, November, 1977.

Chapter 4

4.1 - . Pressure Losses in Three-Leg Pipe Junctions: Combining
     Flows. Engineering Science Data Item No 73023, London, 1973.

Chapter 5

5.1 Bowns, D. E.. The Dynamic Characteristics of Reciprocating
    Engines. Ph.D. Thesis, School of Engineering, University
    of Bath, 1972.

5.2 Hargreaves, M. R. O.. The Transient Response of Diesel Engine
    and Turbo-machinery Combinations. Ph.D. Thesis, School of
    Engineering, University of Bath, 1975.

5.3 Huckvale, S. A.. The Simulation of Heavy Vehicle Transmission
    System Incorporating Epicyclic Gear Trans & Hydrostatic
    Elements. Ph.D. Thesis, School of Engineering, University of
    Bath, 1978.

5.4 Streeter, V. L.. Handbook of Fluid Dynamics. McGraw-Hill,
    London, 1961.

5.5 Duncan, W. J., Thom, A. S. and Young, A. D.. Mechanics of
    Fluids. Edward Arnold Ltd., London, 1970.

Chapter 6

6.1   Frankenfield, T. C.. Using Industrial Hydraulics. Rexroth,
        Hydraulics & Pneumatics Magazine, Ohio, 1984.

6.2   Warring, R. H.. Hydraulic Handbook. 8th Edition, Trade &
        Technical Press Ltd, Surrey, 1983.

6.3   Buckingham, J.. Thermodynamic Analysis of Hydraulic Systems.
        MSc. Thesis, School of Engineering, University of Bath, 1985.

6.4   Tomlinson, S. P.. Applications of the Hydraulic Automatic
        Simulation Package to Analyse Thermal Transient Effects.
        Chapter 4, Ph.D. Thesis, School of Engineering, University
        of Bath, 1986.

6.5   Gillespie, L. J. and Coe, J. R.. The Heat Expansion of a Gas
        of Varying Mass. J. chem. Phys. 1, 103-13, 1933.

6.6   Wallace, F. J. and Linning, W. A.. Basic Engineering
        Thermodynamics. P61-65, Pitman Publishing, London, 1970.

6.7   Look, R. C. and Sauer, C. W.. Engineering Thermodynamics.
        McGraw-Hill, 1986.

6.8   Rogers, G. F. C. and Mayhew, Y. R.. Engineering
        Thermodynamics Work and Heat Transfer. Longman House, London,
        1980.

6.9   Adam, W. H.. Heat Transmission. 3rd Edition, McGraw-Hill,
        New York, 1954.

6.10   Reynolds, W. C. and Perkins, H. C.. Engineering
        Thermodynamics. McGraw-Hill, New York, 1977.

6.11   Tomlinson, S. P.. HASP Component Model Library Manual. Vol 2,
        Report No. 602, School of Engineering, University of Bath,
        August, 1985.

6.12   - . Hydraulic Fluids. BP booklet, mp55, England, 1975.

6.13   McCoull and Walther, Eirich. Rheology Volume 1. Academic
        Press, New York, 1953.

6.14   - . Fuels, Lubricants, and Associated Products. Defence
        Standard DEF STAN 01-5/4-HMSO, MoD, U.K., 1981.

6.15   Eirich, F. R.. Rheology Theory and Applications. Vol 1,
        Academic Press, New York, 1956.

6.16   Hayward, A. T.. How To Estimate the Bulk Modulus of Hydraulic
        Fluids. Hydraulic & Pneumatic Power, January, 1970.

APPENDIX I

AN APPROACH TO SOLVE NONLINEAR ALGEBRAIC AND DIFFERENTIAL EQUATIONS IN A SINGLE HASP MODEL USING LINEAR INTERPOLATION METHOD

Introduction

A1.1 **Backgrounds** The problem of 'implicit relationship of model linking' has been discussed in Section 4.6. A false transient technique has been proposed in Section 4.7 to replace the conventional way of combining algebraic models into a single model. Such a technique for model building may be applied to solve a majority simple cases of implicit relationship on model linking as an example given in the development of dynamic reservoir model. In the mathematical modelling of the vertical pipe junction for combining flows in the suction line of the partially closed system, three algebraic and two differential equations in Equation (4.17) - (4.20) have been resulted. The false transient method is not applicable to build these five equations into a single model since a long computational time could be required. In such cases, a new approach to resolve this type of the implicit problem for solving algebraic and differential equations in a single HASP model is required.

A1.2 **An Approach Proposed** A new approach has been developed to deal with this type of special cases. The essence of the approach is to use a separate computational program, which is implemented outside of HASP, to solve the nonlinear algebraic equations, then the numerical results will be transferred into a normal HASP model which carrys out the calculations of differential equations. A number of numerical methods for solving a set of nonlinear algebraic equations are available in the literature. The method being chosen is the Linear Interpolation Method.

A1.3   In this appendix, the fundamental principle of Linear Interpolation Method will be discussed. Then the computational theorem is obtained for the solution of group equations. The computational program of the linear interpolation method has been written for the solution of a group of nonlinear algebraic equations. In order to solve both nonlinear algebraic and differential equations in a single model without generating the problem of implicit relationship on model linking, this program developed is merged into a standard HASP model. The detailed coding of the HASP pipe junction model PITH is given to demonstrate its program structure.

A1.4 Fundamental Concept

If the function is assumed to be linear over the interval (x_1, x_2), where $f(x_1)$ and $f(x_2)$ are of opposite sign. Based upon the similarity of triangles shown in Fig. A1.1, the following equations can be written:

$$\frac{x_2 - x_3}{x_2 - x_1} = \frac{f(x_2)}{f(x_2) - f(x_1)} \qquad \ldots \ldots (A1.1)$$

and

$$x_3 = x_2 - \frac{f(x_2)}{f(x_2) - f(x_1)} x_2 - x_1 \qquad \ldots \ldots (A1.2)$$

The new value $f(x_3)$ then can be computed and again interpolated linearly between the values at which the function changes sign, giving a new value for x_3. When this numerical procedure is repeated, the estimates of the root should be improved. For example, consider the cubic

$$f(x) = x^3 + x^2 - 3x - 3 = 0 \qquad \ldots \ldots (A1.3)$$

At x = 1, the value of f is -4, while at x = 2 f has the value +3. The change in sign of the function between x = 1 and x = 2 results at least one root on the interval (1,2) since the function is continuous as shown in Fig. A1.2. Suppose the function is revaluated at x = 1.5 and compared with the function values at x = 1 and x = 2. Since the function changes sign between x = 1.5 and x = 2, a root must lie between these values. This linear interpolation procedure can continue to determine a smaller and smaller interval within which a root must lie. The process is illustrated in Fig. A1.3. Applying the method to $f(x) = x^3 + x^2 - 3x - 3 = 0$, the results are obtained and listed in Table A1.1.

The method of interpolation requires that starting values must be obtained before the method can begin. A knowledge of the physical problem will often suggest a reasonable starting values. When this is not available, the starting values

can be obtained by making a rough graph, or by trial calculations.

However, if the approach to the root is one-sided, particularly when f(x) has significant curvature between x_1 and x_2, then the convergence of the iterative scheme can be severely affected as shown in Fig. A1.4. A remedy for this is the Modified Linear Interpolation Method where the value of f(x) is replaced at the stagnant end position with $\dfrac{f(x)}{2}$. This helps, as Fig. A1.5 shows.

A1.5   Mathematical Discussion for Group Equations   When this method is used to solve group equations under the defined initial values, the Linear Interpolation equations are used to search the roots of equations using successive approximate iteration. The problem we are interested in is to find the solutions of the system of equations

$$F_i(x_1,x_2,\ldots,x_n) = 0 \qquad (i=1,2,\ldots,n) \qquad\qquad \ldots\ldots(A1.4)$$

The principal of the Linear Interpolation method is to solve the above equation for x_i by using a Theorem with a set of initial defined parameters of x_i under going an iterative procedure. A brief description of the process can be given as follows.

If a group of parameters known as $(x_1,x_2,\ldots,x_{r-1},x_r{}^0,\ldots,x_n{}^0)$ satisfies the criterion

$$\begin{vmatrix} F_i(x_1,x_2,\ldots,x_{r-1},x_r{}^0,\ldots,x_n{}^0) \end{vmatrix} \leqslant EP \qquad\qquad \ldots\ldots(A1.5)$$
$$\scriptstyle (i\,=\,1,2,\ldots,r-1)$$

where EP is the tolerance error of the function, then a new set of $(x_1,x_2,\ldots,x_r,x_{r+1}^0,\ldots,x_n{}^0)$ can be found by using the Theorem

$$x_i{}^{(k+1)} = x_i{}^{(k-1)} - (x_i{}^{(k)} - x_i{}^{(k-1)})\dfrac{\epsilon_r{}^{(k-1)}}{(\epsilon_r{}^{(k)} - \epsilon_r{}^{(k-1)})} \qquad\qquad \ldots\ldots(A1.6)$$

$$(i = 1,2,\ldots,r, \ \ 1 \leqslant r \leqslant n)$$

where ϵ_r is the tolerance error of roots. The above Theorem has been well proved in the Gauss-Seidel method and one version of the proof can be found in Ref. (A1.1)*.

If the solution satisfies

$$|F_i(x_1, x_2, \ldots, x_r, x_{r+1}^0, \ldots, x_n^0)| \leqslant EP \qquad (i = 1, 2, \ldots, r) \qquad \ldots\ldots (A1.7)$$

then x_{r+1} will be obtained as follows. However, if it does not satisfy this equation, the above procedure will be repeated from r-1 until it does. Carry out the same procedure continuously, a group of real roots of Equation (A1.4), which is entirely satisfactory to Equation (A1.7), will be obtained in the end.

---

* Ref. (A1.1)   Ortega, J. M. and Rheinboldt, W. G.. Iterative Solution of Nonlinear Equations in Several Variables. Academic Press, New York, 1970.

A1.6   In order to show the program structure. the program was tested with a set of nonlinear equations, ie.

$$F_1 = x_1 - 5x_2 + 7x_3 + 12 = 0$$
$$F_2 = 3x_1x_2 + x_1x_2 - 11x_1 = 0$$
$$F_1 = 2x_2x_3 + 40x_1 = 0$$

The program given below was run with input data as follows:

$x_{10} = 0.1$

$x_{20} = 0.5$

$x_{30} = -0.4$ (set as initial values)

EP $= 10^{-4}$ (tolerance error)

H $= 10^{-9}$ (initial length of interpolation step)

```
PROGRAM MAIN
DIMENSION X(3),Y(3),DEL(3),X₁(3), X₂(6),M(4)
X(1) = 0.1
X(2) = 0.5
X(3) = -0.4
CALL YANG(X,Y,DEL,X₁,X₂,M,3,6,4,10⁻⁹,10⁻⁴)
WRITE(5,1)X,Y
1       FORMAT(3E20.10)
STOP
END
```

```
SUBROUTINE YANG(X,Y,DEL,X₁,X₂,M,N,J,J₁,H,EP)
************************************************************************
C       X   - one dimensional real input or output data of N variables
C       Y   - one dimensional real output data for storing the values
C              of function
C       DEL- one dimensional real data of N variables, working element
```

```
C       X₁  - one dimensional real data of N variables, working element
C       X₂  - one dimensional real data of J variables, working element
C       M   - one dimensional integral data of J₁ variables, working element
C       N   - input integral parameter, number of equations
C       J   - input integral parameter, J = N(N+1)/2
C       J₁  - input integral parameter, J₁ = N+1
C       H   - input integral parameter, initial length of interpolation,
C             normal value between 10⁻⁷ to 10⁻⁹
C       EP  - input integral parameter, tolerable value for Fᵢ
*******************************************************************************
        DIMENSION X(N),Y(N),DEL(N),X₁(N),X₂(N),M(J₁)
        IR=N
        M(N+1)=3
01      M(IR)=1
02      IF(IR.NE.1)GOTO 08
        CALL F(X,Y)
05      DEL(IR)=Y(IR)
        IP=IR*(IR-1)/2
        DO 10 I=1,IR
          K=IP+I
10        X2(K)=X(I)
        X(IR)=X(IR)+H
03      IF(IR.NE.1)GOTO 09
        CALL F(X,Y)
06      Q=Y(IR)-DEL(IR)
        IF(ABS(Q).LT.1.D-25)GOTO 04
        Q=DEL(IR)/Q
        DEL(IR)=Y(IR)
        IP=IR*(IR-1)/2
        DO 11 I=1,IR
          K=IP+I
          X1(I)=X2(K)-(X(I)-X2(K))*Q
          X2(K)=X(I)
11        X(I)=X1(I)
        CALL F(X,Y)
        DO 12 I=1,IR
          IF(ABS(Y(1)).GT.EP)GOTO 03
12      CONTINUE
04      IR=IR+1
```

```
        L=M(IR)
        GOTO(05,06,07),L
07      RETURN
08      IR=IR-1
        GOTO 01
09      M(IR)=2
        GOTO 02
        END



        SUBROUTINE F(X,Y)
        DIMENSION X(3),Y(3)
        Y(1)=X(1)-5.D0*X(2)**2+7.D0*X(3)**2+12.D0
        Y(2)=3.D0*X(1)*X(2)+X(1)*X(3)-11.D0*X(1)
        Y(3)=2.D0*X(2)*X(3)+40.D0*X(1)
        RETURN
        END
```

The exact roots are

$$x_1 = 0, \qquad\qquad x_2 = 2.4, \qquad\qquad x_3 = 0$$

and the program finds them with excellent precision

$$x_1 = -0.4215 \times 10^{-7}, \qquad x_2 = 1.549, \qquad x_3 = 0.5442 \times 10^{-6}$$

and

$$F_1 = 0.8784 \times 10^{-5}, \qquad x_2 = 0.2677 \times 10^{-6}, \qquad x_3 = 0.1857 \times 10^{-9}$$

During the execution of the program, if iterations are not converging, the following steps can be taken:

1). change the initial values;
2). reduce the value of initial length of interpolation H;
3). increase the value of tolerance EP;
4). change the order of equations.

```
      SUBROUTINE PITH(PT,P2,P3,P1,QT,Q2,Q3,Q1,
   +  T,LIMIT,CON,ICON,QTDOT,P1DOT)
      IMPLICIT DOUBLE PRECISION(A-H,O-Z)
      COMMON /FLUPRO/THETA,RHO,BF,RNU,RMU,IOIL
      DIMENSION CON(20),ICON(1)
      PARAMETER (PI=3.1415926D0,G=9.81D0)
C **********************************************************************
C     MODEL OF PIPE Y-JUNCTION CONTAINING A VERTICAL
C     PIPE OF CONSTANT FLUID HEIGHT WITH CONSIDERATION
C     OF FLUID INERTIA, PIPE FRICTION AND FLUID
C     COMPRESSIBILITY
C **********************************************************************
C INPUT INFORMATION:
C **********************************************************************
C     CON(1)- PIPE DIAMETER IN MM
C     CON(2)- PIPE CROSS-SECTIONAL AREA IN M**2
C     CON(3)- GRAVITATIONAL ACCELERATION IN M/S**2
C     CON(4)- FLUID DENSITY IN KG/M**3
C     CON(5)- PRESSURE/VELOCITY CONSTANT (LARMINAR FLOW)
C     CON(6)- LENGTH OF PIPE IN M
C     CON(7)- FLUID BULK MODULUS IN BAR
C     CON(8)- COEFFICIENCY OF FLOWRATE/PRESSURE IN BAR/(L/S)**2
C     CON(9)- COEFFICIENCY OF PRESSURE LOSS OF VERTICAL BRANCH
C             PIPE
C     CON(10)-COEFFICIENCY OF PRESSURE LOSS OF RETURN LINE
C             BRANCH PIPE
C     QT-    VERTICAL PIPE INLET FLOWRATE IN L/S
C     Q2-    RETURN LINE FLOWRATE IN L/S
C     Q3-    SUCTION LINE FLOWRATE IN L/S
C     PT-    VERTICAL PIPE INLET PRESSURE (TANK PRESSURE) IN BAR
C     P2-    RETURN LINE PRESSURE IN BAR
C     P3-    SUCTION LINE PRESSURE IN BAR
C **********************************************************************
C OUTPUT INFORMATION:
C **********************************************************************
```

```
C       QT    -VERTICAL PIPE INLET FLOWRATE IN L/S
C       Q2    -RETURN LINE FLOWRATE IN L/S
C       Q3    -SUCTION LINE FLOWRATE IN L/S
C ************************************************************************
        DP=PT-P1
        DP1=P1-P3
        DP2=P2-P3
        CALL YONG(DP1,DP2,Q1,Q2,Q3)
        QTDOT=(DP*CON(2)*1.D5/(CON(4)*CON(6))
   +    -CON(5)*QT+CON(3)*CON(2))*1.D3
        RETURN
        END



        SUBROUTINE YONG(DP1,DP2,Q1,Q2,Q3)
        IMPLICIT REAL*8(A-H,O-Z)
        DIMENSION X(3),Y(3),DEL(3),X1(3),X2(6),M(4)
        X(1)=-0.04D0
        X(2)=-0.1D0
        X(3)=0.14D0
        CALL GUI(X,Y,DP1,DP2,DEL,X1,X2,M,3,6,4,1.D-8,1.D-4)
        Q1=X(1)
        Q2=X(2)
        Q3=X(3)
        RETURN
        END



        SUBROUTINE GUI(X,Y,DP1,DP2,DEL,X1,X2,M,N,J,J1,H,EP)
        DIMENSION X(3),Y(3),DEL(3),X1(3),X2(6),M(4)
        IR=N
        M(N+1)=3
01      M(IR)=1
02      IF(IR.NE.1)GOTO 08
        CALL F(X,Y,DP1,DP2)
05      DEL(IR)=Y(IR)
        IP=IR*(IR-1)/2
        DO 10 I=1,IR
        K=IP+I
```

- 172 -

```
10      X2(K)=X(I)
        X(IR)=X(IR)+H
03      IF(IR.NE.1)GOTO 09
        CALL F(X,Y,DP1,DP2)
06      Q=Y(IR)-DEL(IR)
        IF(ABS(Q).LT.1.D-25)GOTO 04
        Q=DEL(IR)/Q
        DEL(IR)=Y(IR)
        IP=IR*(IR-1)/2
        DO 11 I=1,IR
        K=IP+I
        X1(I)=X2(K)-(X(I)-X2(K))*Q
        X2(K)=X(I)
11      X(I)=X1(I)
        CALL F(X,Y,DP1,DP2)
        DO 12 I=1,IR
        IF(ABS(Y(1)).GT.EP)GOTO 03
12      CONTINUE
04      IR=IR+1
        L=M(IR)
        GOTO(05,06,07),L
07      RETURN
08      IR=IR-1
        GOTO 01
09      M(IR)=2
        GOTO 02
        END


        SUBROUTINE F(X,Y,DP1,DP2)
        DIMENSION X(3),Y(3)
        Y(1)=1.65D0*X(3)**2-X(1)**2-2.92D0*DP1
        Y(2)=1.57D0*X(3)**2-X(2)**2-2.92D0*DP2
        Y(3)=X(3)+X(2)+X(1)
        RETURN
        END
```

A1.7 When PITH is used with other standard models, one control file of CAD.ODL in PDP11 HASP needs to be altered so that the subroutines of Yong and GUI will be admitted into AUX.FOR to link with other models during the task building. For instance, the CAD.ODL for the above test circuit should be added in the way shown below:

```
        .ROOT MAIN-*(INPUT,CALCS)


    CGEAR:      .FCTRGEAR4-GEAR5-F01DFF
    CPERM:      .FCTRAUX-OUT-CGEAR-PTC-YONG-GUI


    C1:   .FCTR TS5T-PITH
    CALCS:      .FCTRCPERM-C1


    IPERM:      .FCTRCONTROL-FPROP-MESAGE-PTI
    IA:   .FCTR TS5TIN-PITHIN
    INPUT:      .FCTRIPERM-(IA)


        .END
```

The theoretical predictions of the transient suction pressure have already been carried out in Chapter 4 using PITH. Such a model has been validated by the agreement of the calculated and experimental suction pressure transients. Hence, the extension of this approach may be used in other HASP models in order to solve algebraic and differential equations together within a single model.

Iteration number	x_1	x_2	x_3	$f(x_1)$	$f(x_2)$	$f(x_3)$
1	1.0	2.0	1.57142	-4.0	3.0	-1.36449
2	1.57142	2.0	1.70540	-1.36449	3.0	-0.24784
3	1.70540	2.0	1.72788	-0.24784	3.0	-0.03936
4	1.70540	2.0	1.73140	-0.03936	3.0	-0.00615
5	1.73140	2.0	1.7314*			

* Error in x_3 after 5 iterations is 0.00011.

Table A1.1   Method of Linear Interpolation for $f(x) = x^3 + x^2 - 3x - 3 = 0$
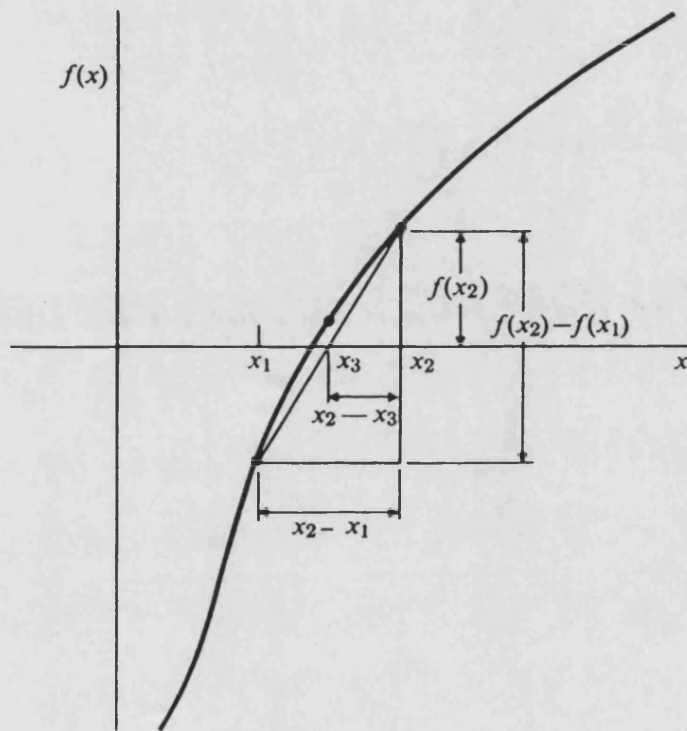
Fig. A1.1
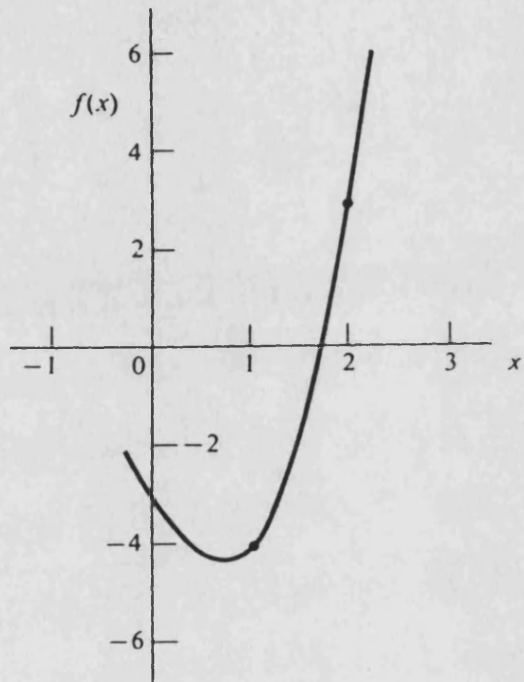
Fig. A1.2
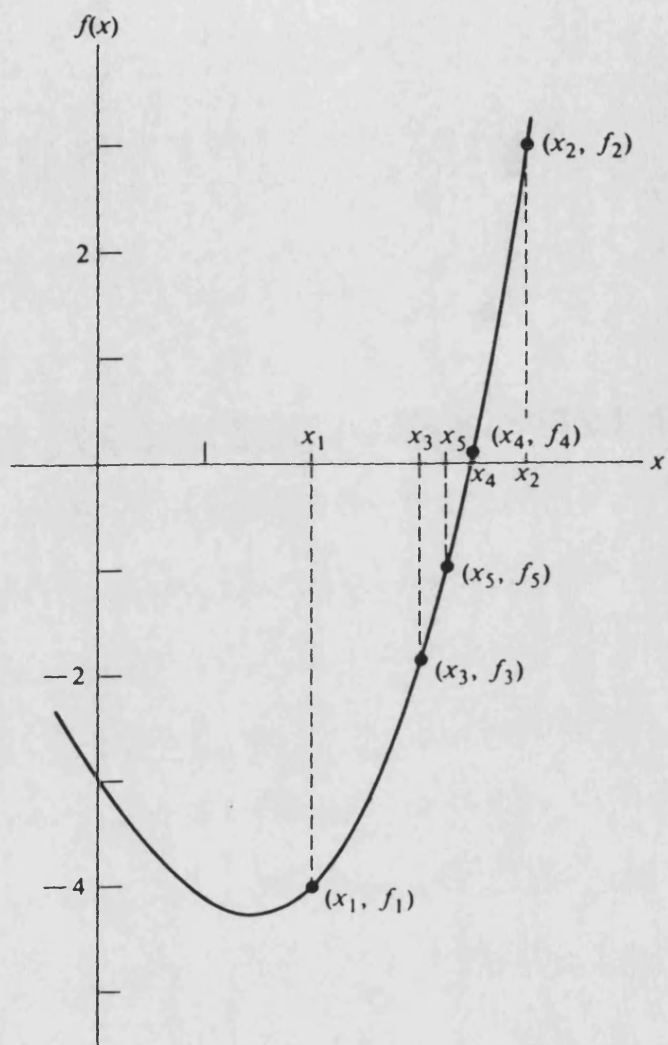
Fig. A1.3
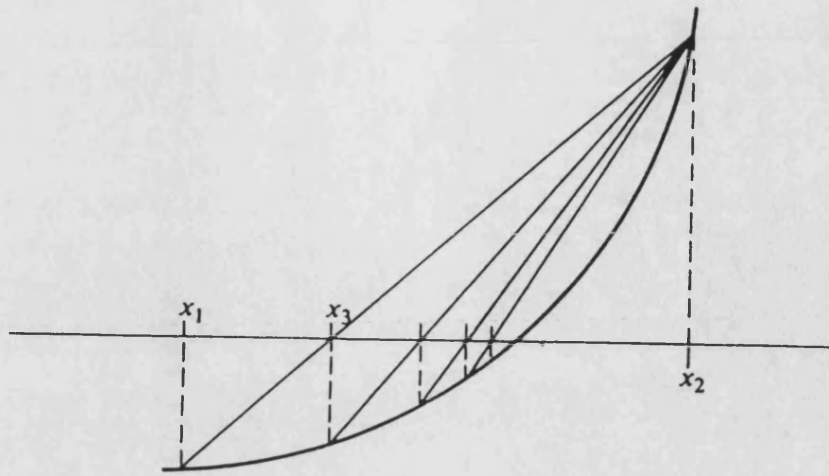
Fig. A1.4
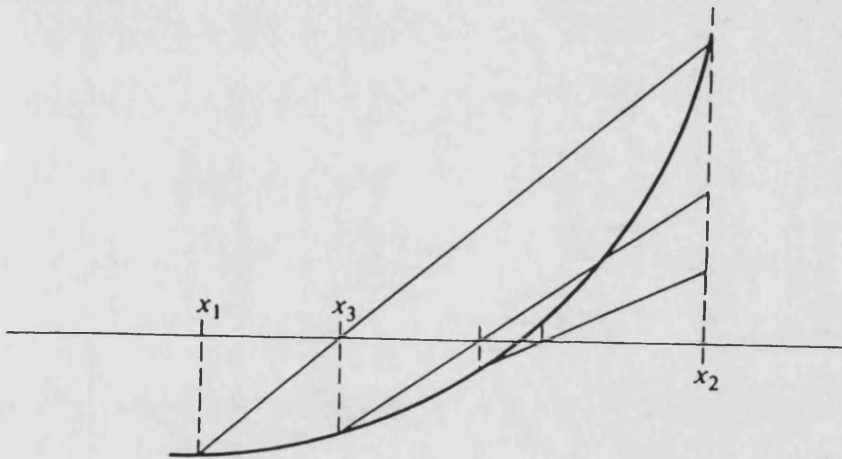
Fig. A1.5

APPENDIX II

DESCRIPTION OF NEW HASP COMPUTER MODELS DEVELOPED

CONTENTS

A2.1 FP3H Temperature and Fluid Property Model
of an Unboosted Closed Hydraulic System

1   Introduction   FP3H models the temperature behaviour of an unboosted closed hydraulic system which has no flow exchange with the reservoir under steady state and can be regarded as a closed thermal system. The model considers the dynamic and steady state behaviour of fluid and pipe wall temperatures during the system loading. The model takes into account the difference between fluid and pipe wall temperatures as a result of basic thermodynamic processes taking place in a closed thermal system. The changes in fluid properties caused by fluid temperature variation are also calculated in the model.

2   Assumptions

(i).   The model assumes that the total power loss will be provided as input data, and calculated in a power sum model POOH.

(ii).   The model assumes that the system is constructed by one type of pipe and uniform fluid and pipe wall temperatures can be found the system.

(iii).   The model assumes that the heat transfer within the pipe wall is one dimensional conduction.

3   Nomenclature

A_m	logarithmic mean surface area of pipe
A_2	outside surface area of pipe
A_1	inside surface area of pipe
B	fluid bulk modulus
C_{pf}	fluid specific heat
C_{pp}	pipe wall specific heat
d	pipe diameter
g	gravitational acceleration

h_f	heat transfer coefficient by forced convection
h_a	heat transfer coefficient by natural convection
k	thermal conductivity of pipe wall material
L	pipe length
M_f	fluid mass in the system
M_p	mass of pipe wall material
H_1	rate of heat flow transferred from fluid to pipe wall by forced convection
H_2	rate of heat flow transferred from pipe wall to atmosphere by natural convection
R_1	pipe inside radius
R_2	pipe outside radius
T_1	wall temperature at internal pipe surface
T_2	wall temperature at external pipe surface
T_a	constant atmospheric temperature
T_f	fluid temperature
W	rate of power loss converted into heat energy

DIMENSIONLESS GROUPS

Nu	Nusselt number
Re	Reynolds number

GREEK SYMBOLS

ϵ	emissivity
ν	kinematic viscosity
ρ	density
σ	Stefan-Boltzman constant; surface tension

4   User Defined Parameters

(i). C_{pf}, fluid specific heat (typically 1909) in J/(kg.K);

(ii). C_{pp}, pipe specific heat (hose: 2010) in J/(kg.K);

(iii). D_o, outside diameter of pipe in mm;

(iv). D_i, inside diameter of pipe in mm;

(v).   L, length of pipe in m;

(vi). ρ_p, density of pipe wall material in $\frac{kg}{m^3}$;

(vii). ϵ, emissivity of pipe material (black hose: 0.9):

(viii).   k, conductivity of pipe material (hose: 0.15) in W/m.K:

(ix). T_{fo}, initial fluid temperature in K:

(x). T_{2o}, initial outside pipe wall temperature in K:

(xi). T_a, atmospheric temperature in K:

(xii).   type of oil used.

5   **Model Equations**   The heat flow transferred from pipe wall to its surrounding atmosphere by natural convection can be determined from:

$$H_2 = h_a A_2 (T_2 - T_a) + \epsilon\sigma A_2 (T_2^4 - T_a^4) \qquad \ldots\ldots (2.1)$$

Under laminar flow conditions, the heat transfer by natural convection h_a is calculated from

$$h_a = \begin{cases} 1.32(\dfrac{T_2 - T_a}{d})^{0.25} & when\ 10^4 < Gr < 10^9 \\ 1.25(T_2 - T_a)^{\frac{1}{3}} & when\ 10^9 < Gr < 10^{12} \end{cases} \qquad \ldots\ldots (2.2)$$

In the above equation, h_a is in W/m.K and d is in m.

The heat flow transferred from fluid to pipe wall by forced convection can be given from:

$$H_1 = h_f A_1 (T_f - T_1) \qquad \ldots\ldots (2.3)$$

where the heat transfer coefficient h_f by forced convection can be evaluated from Nusselt number Nu $= \dfrac{hl}{k}$, where l is the characteristic linear dimension, k thermal conductivity of fluid. The value of Nusselt number for the forced convection in fully developed laminar flow through a tube is given in as follows

(1).   Nu = 3.65, for laminar flow in a tube at constant wall temperature

boundary condition;

.

(2). Nu = 4.36, for laminar flow in a tube at constant heat flux which is equivalent to constant temperature gradient at the wall.

If the rate of heat flow through the pipe wall is assumed to be transferred under one dimensional conduction, then the heat flows radially through the pipe wall can be expressed by the Fourier's Law, i.e.,

$$H = \frac{kA_m(T_1 - T_2)}{R_2 - R_1} \qquad \qquad \ldots\ldots(2.4)$$

In the above equation, k is the thermal conductivity of the pipe wall in W/M.k. A_m is the logarithmic mean area and can be calculated from

$$A_m = \frac{2(R_2 - R_1)L}{\ln\dfrac{R_2}{R_1}} = \frac{A_2 - A_1}{\ln\dfrac{R_2}{R_1}} \qquad \qquad \ldots\ldots(2.5)$$

where R_1 and R_2 are the internal and external radiuses and L is the length of the pipe section respectively.

This rate of heat transferred through the pipe wall by conduction should be equal to the rate of heat transferred from fluid to the pipe wall by forced convection at the boundary of the inner surface of the pipe section. From Equation (2.3) and (2.4), we have

$$H_1 = h_f A_1(T_f - T_1) = \frac{kA_m(T_1 - T_2)}{R_2 - R_1} \qquad \qquad \ldots\ldots(2.6)$$

Re-arrange the above equation, the inner pipe wall temperature T_1 can be determined from

$$T_1 = \frac{h_f A_1 T_f + \frac{kA_m}{R_2 - R_1} T_2}{h_f A_1 + \frac{kA_m}{R_2 - R_1}}$$

$$\dots \dots (2.7)$$

In the steady state, the heat flow transferred into the pipe wall, H_1, must be equal to the heat transferred out, H_2. Under the unsteady condition, the difference between H_1 and H_2 must be equal to the increment of the pipe wall internal energy. In other words, if the pipe wall is regarded as a closed thermal system, the heat flow supplied to the pipe wall must be equal to the gain in internal energy. From this concept, the following equation can be established to express the pipe wall temperature at any instant time, ie.

$$\frac{dT_2}{dt} = \frac{H_1 - H_2}{M_p C_p}$$

$$\dots \dots (2.8)$$

Similarly, the fluid temperature in the closed thermal system, T_f, can be expressed from:

$$\frac{dT_f}{dt} = \frac{W - H_1}{M_f C_{pf}}$$

$$\dots \dots (2.9)$$

The above two temperature transient equations will be solved by using first order Euler integration in order to achieve a short computational time. The temperatures are assumed to be constant for a fixed short period of time. This time step at which the temperatures are increased is provided as an user defined parameter. A typical value for this parameter is recommended between 1 to 5 seconds (3 seconds as a default). A variable is introduced to monitor the time corresponding to the last temperature update. This variable is initially set to zero. If the simulation time exceeds the constant temperature period, the fluid temperature and the pipe wall temperature are updated by solving the equations as below

$$\Delta T_2 = \frac{dT_2}{dt} = \frac{H_1 - H_2}{M_p C_p} \qquad \dots \dots (2.10)$$

$$T_2 = T_{2_0} + \Delta T_2 \Delta t \qquad \dots \dots (2.11)$$

and

$$\Delta T_f = \frac{dT_f}{dt} = \frac{W - H_1}{M_f C_{pf}} \qquad \dots \dots (2.12)$$

$$T_f = T_{f_0} + \Delta T_f \Delta t \qquad \dots \dots (2.13)$$

where T_{f_0} and T_{2_0} are the initial fluid and pipe wall temperatures at $t = 0$, respectively, and the Δt is the constant time increment.

The empirical relationship between the kinematic viscosity and fluid temperature, under the atmospheric pressure, is expressed as

$$\nu = e^{10e^{10\left[A - B \log_{10}(T_f + 273)\right]}} + 0.6 \qquad \dots \dots (2.14)$$

The fluid density is assumed to be linear with temperature and calculated from

$$\rho = D - C(T_f - 20) \qquad \dots \dots (2.15)$$

In the above two equations, the constants A, B, C and D are empirical values, and can be evaluated once the type of fluid is chosen in HASP.

The fluid Bulk Modulus is an empirical function of density and temperature and given by

$$B = 10^4 \left[1.78 + 7\left(\frac{\rho}{1000} - 0.86\right) \right] e^{10 \left[25 \times 10^{-4}(20 - T_f) \right]} \qquad \ldots \ldots (2.16)$$

6 Model Testing The model has been verified by applying power loss. The block diagram for the test circuit is shown in Fig. A2.1.

7 Model Linking The model has one external and 4 internal links. The external link connected to port 1 supplies the total power loss during the system loading. The link diagram for model FP3H is shown in Figure A2.2.

model inputs:

(a). W, power losses in W;

model outputs:

(a). fluid temperature in deg.C;

(b). outside pipe wall temperature in deg.C;

(c). heat flow from fluid to pipe wall in W;

(d). heat flow from pipe wall to atmosphere in W;

(e). updated fluid viscosity in cSt;

(f). updated fluid density in kg/m^3;

(g). updated fluid bulk modulus in bar.

The link ordering during program generation must correspond to the port ordering shown in Fig. A2.2. The only acceptable input to the program generator for the sub-circuit shown in Figure A2.1 is:

FP3H01 01 02 03 04 05

1 <u>Introduction</u>   FPCH models the thermodynamic behaviour of a pipe with
fluid property changes. The model considers the dynamic and steady state
behaviour of fluid temperature for any a specific length of pipe in a fluid power
system. The model takes into account the difference between fluid and pipe wall
temperatures as a result of basic thermodynamic processes taking place in an open
thermal section of the pipe. The changes in fluid properties caused by fluid
temperature variation are also calculated in the model.

2   <u>Assumptions</u>

(i).   The model assumes that the power loss input to the
pipe will be provided as input data, and calculated
in other models.

(ii).   The model assumes that the heat flow transferred to
the wall of the pipe section will be provided as
input data, and calculated in the pipe wall
temperature model of PICH.

(iii).   The model assumes that the pipe inlet fluid temperature
is provided and has been calculated in another pipe
fluid temperature model.

(iv).   The model assumes an uniform fluid temperature in the
pipe section.

3   <u>Nomenclature</u>

B	fluid bulk modulus
C_{pf}	fluid specific heat
d	pipe internal diameter
L	length of pipe section

m_f	mass flow rate of fluid
M_f	fluid mass in the pipe section
H_1	rate of heat flow transferred from fluid to pipe wall by forced convection
T_{in}	fluid temperature at the inlet of the pipe section
T_f	fluid temperature
W	rate of power loss converted into heat energy

GREEK SYMBOLS

ν	kinematic viscosity
ρ	density

4   User Defined Parameters

(i). C_{pf} , fluid specific heat (typically 1909) in J/(kg.K);

(ii). D_i , inside diameter of pipe in mm;

(iii).   L, length of pipe in m;

(iv). T_{fo} , initial fluid temperature in K;

(v).   type of oil used.

5   Model Equations

When the First Law applied to the open thermal system of a pipe section, the temperature of the fluid in the pipe, T_f , can be expressed from:

$$\frac{dT_f}{dt} = \frac{W - H_1 + m_f C_{pf} (T_{in} - T_f)}{M_f C_{pf}} \qquad \ldots\ldots (2.17)$$

where the mass flowrate through the pipe can be found as $m_f = \rho Q$, and W, H_1 and T_{in} will be provided as input data.

The above transient temperature equation can be solved by using first order Euler integration in order to achieve a short computational time. The fluid temperature is assumed to be constant for a fixed short period of time. This time step at which the fluid temperature is increased is provided as an user defined parameter. A typical value for this data is recommended between 1 to 5 seconds. A

variable is introduced to monitor the time corresponding to the last temperature update. This variable is initially set to zero. If the simulation time exceeds the constant temperature period, the fluid temperature can be updated by solving the equations as below

$$\Delta T_f = \frac{dT_f}{dt} = \frac{W - H_1 + m_f\, C_{pf}\, (T_{in} - T_f)}{M_f\, C_{pf}} \qquad \ldots\ldots(2.18)$$

$$T_f = T_{fo} + \Delta T_f\, \Delta t \qquad \ldots\ldots(2.19)$$

where T_{fo} is the initial fluid temperature at t = 0, respectively, and the Δt is the constant time increment.

The empirical relationship between the kinematic viscosity and fluid temperature, under the atmospheric pressure, is expressed as

$$\nu = e^{10e^{10\left[A\, -\, B\log_{10}(T_f\, +\, 273)\right]}} + 0.6 \qquad \ldots\ldots(2.20)$$

The fluid density is assumed to be linear with temperature and calculated from

$$\rho = D - C(T_f - 20) \qquad \ldots\ldots(2.21)$$

In the above two equations, the constants A, B, C and D are empirical values, and can be evaluated once the type of fluid is chosen in HASP.

The fluid Bulk Modulus is an empirical function of density and temperature and given by

$$B = 10^4\left[1.78 + 7(\frac{\rho}{1000} - 0.86)\right]e^{10\left[25\times10^{-4}(20\, -\, T_f)\right]} \qquad \ldots\ldots(2.22)$$

6   Model Testing   The model has been verified by applying power loss, flowrate and input fluid temperature. The block diagram for the test circuit is shown in Fig. A2.3.

7   Model Linking   The model has 5 external and 2 internal links. The external link connected on port 2 provides the power loss. The link diagram for model FPCH is shown in Figure A2.4.

model inputs:

        (a). W, power losses in W;

        (b). T_{in} , inlet fluid temperature in K;

        (c). Q, flowrate in the pipe in l/s;

        (d). heat flow loss to   pipe wall material in W;

model outputs:

        (a). fluid temperature in deg.C;

        (b). fluid viscosity in cSt;

        (c). fluid density in kg/m^3;

        (d). fluid bulk modulus in bar.

The link ordering during program generation must correspond to the port ordering shown in Fig. A2.4. The only acceptable input to the program generator for the test circuit shown in Figure A2.3 is:

FPCH01 01 02 03 04 05 06 07

A2.3 FPDH Fluid Temperature and Property Model
of a Pipe Y-Junction

1   **Introduction**   FPDH models the temperature behaviour of a pipe Y-junction with fluid property changes. The model considers the dynamic/steady state behaviour of fluid temperature in a pipe Y-junction in a fluid power system. The changes in fluid properties caused by fluid temperature variation are also calculated in the model.

2   **Assumptions**

    (i). The model assumes that the power loss input to the pipe will be provided as input data, and calculated in other models.

    (ii). The model assumes that the heat flow transferred to the wall of the pipe section will be provided as input data, and calculated in the pipe wall temperature model of PICH.

    (iii). The model assumes that the pipe inlet fluid temperatures are provided and have been calculated in another fluid temperature models.

    (iv). The model assumes an uniform fluid temperature in the pipe section.

3   **Nomenclature**

B	fluid bulk modulus
C_{pf}	fluid specific heat
d	pipe internal diameter
L	length of pipe section

m_1	inlet mass flow rate of fluid at port 1
m_2	inlet mass flow rate of fluid at port 2
m_3	outlet mass flow rate of fluid at port 3
M_f	fluid mass in the pipe section
H_1	rate of heat flow transferred from fluid to pipe wall by forced convection
T_1	inlet fluid temperature at port 1
T_2	inlet fluid temperature at port 2
T_f	fluid temperature in the pipe section
W	rate of power loss converted into heat energy

GREEK SYMBOLS

ν	kinematic viscosity
ρ	density

4   User Defined Parameters

(i). C_{pf} . fluid specific heat (typically 1909) in J/(kg.K):

(ii). D_i . inside diameter of pipe in mm:

(iii). L. length of pipe in m:

(iv). T_{fo} . initial fluid temperature in K:

(v).   type of oil used.

5   Model Equations

When the First Law applied to this open thermal system of the pipe junction. the temperature of the fluid in the pipe. T_f . can be expressed from:

$$\frac{dT_f}{dt} = \frac{W + m_1 C_{pf} T_1 + m_2 C_{pf} T_2 - m_3 C_{pf} T_f - H_1}{M_f C_{pf}} \qquad \dots \dots (2.23)$$

where $m_1 C_{pf} T_1$ represents heat flow energy at inlet pipe line 1 and $m_2 C_{pf} T_2$ at inlet pipeline 2. and m_3 is mass flowrate at outlet.

The above transient temperature equation can be solved by using first order

Euler integration in order to achieve a short computational time. The fluid temperature is assumed to be constant for a fixed short period of time. This time step at which the fluid temperature is increased is provided as an user defined parameter. A typical value for this data is recommended between 1 to 5 seconds. A variable is introduced to monitor the time corresponding to the last temperature update. This variable is initially set to zero. If the simulation time exceeds the constant temperature period, the fluid temperature can be updated by solving the equations as below

$$
\Delta T_f = \frac{dT_f}{dt}
$$
$$
= \frac{W + m_1 C_{pf} T_1 + m_2 C_{pf} T_2 - m_3 C_{pf} T_f - H_1}{M_f C_{pf}} \qquad \ldots\ldots (2.24)
$$

$$
T_f = T_{fo} + \Delta T_f \Delta t \qquad \ldots\ldots (2.25)
$$

where T_{fo} is the initial fluid and pipe wall temperatures at t = 0, respectively, and the Δt is the time increment.

The empirical relationship between the kinematic viscosity and fluid temperature, under the atmospheric pressure, is expressed as

$$
\nu = e^{10e^{10\left[A - B\log_{10}(T_f + 273)\right]}} + 0.6 \qquad \ldots\ldots (2.26)
$$

The fluid density is assumed to be linear with temperature and calculated from

$$
\rho = D - C(T_f - 20) \qquad \ldots\ldots (2.27)
$$

In the above two equations, the constants A, B, C and D are empirical values, and can be evaluated once the type of fluid is chosen in HASP.

The fluid Bulk Modulus is an empirical function of density and temperature and

given by

$$B = 10^4 \left[1.78 + 7(\frac{\rho}{1000} - 0.86) \right] e^{10 \left[25 \times 10^{-4}(20 - T_f) \right]} \qquad \ldots \ldots (2.28)$$

6   Model Testing   The model has been verified by applying power loss, flowrate, fluid pressure and input fluid temperatures. The block diagram for the test circuit is shown in Fig. A2.5.

7   Model Linking   The model has 7 external and one internal links. The external link connected to port 1 supplies fluid temperature. The link diagram for model FPDH is shown in Fig. A2.6.

model inputs:

(a). W, power losses in W;

(b). T_1, inlet fluid temperature at entrance 1 in K;

(c). T_2, inlet fluid temperature at entrance 2 in K;

(d). heat flow loss to the pipe wall in W;

(e). Q_1, inlet flowrate from entrance 1 in l/s;

(f). Q_2, inlet flowrate from entrance 2 in l/s.

model outputs:

(a). fluid temperature in deg.C;

(b). fluid viscosity in cSt;

(c). fluid density in kg/m^3;

(d). fluid bulk modulus in bar.

The link ordering during program generation must correspond to the port ordering shown in Fig. A2.6. The only acceptable input to the program generator for the sub-circuit shown in Figure A2.5 is:

A2.4 FPGH Pipe Temperature and Fluid Property Model
of a Pipe Section with Two Flow Outputs

1
Introduction

FPGH models the thermodynamic behaviour
of a pipe with fluid property changes.
The model considers the dynamic and steady state behaviour of fluid
temperature for any a specific length of pipe with two flow outputs in
a fluid power system. The model takes into account the difference between
fluid and pipe wall temperatures as a result of basic thermodynamic processes
taking place in an open thermal section of the pipe.
The changes in fluid properties caused by fluid temperature
variation are also calculated in the model.

2
Assumptions

(i). The model assumes that the power loss input to the
pipe will be provided as input data, and calculated
in other models.

(ii). The model assumes that the heat flow transferred to
the wall of the pipe section will be provided as
input data, and calculated in the pipe wall
temperature model of PICH.

(iii). The model assumes that the pipe inlet fluid temperature
is provided and has been calculated in another pipe
fluid temperature model.

(iv). The model assumes an uniform fluid temperature in the
pipe section.

3 Nomenclature

B	fluid bulk modulus
C_{pf}	fluid specific heat
d	pipe internal diameter
L	length of pipe section
m_f	mass flow rate of fluid
M_f	fluid mass in the pipe section
H_1	rate of heat flow transferred from fluid to pipe wall by forced convection
T_{in}	fluid temperature at the inlet of the pipe section
T_f	fluid temperature
W	rate of power loss converted into heat energy

GREEK SYMBOLS

ν	kinematic viscosity
ρ	density

4 User Defined Parameters

(i). C_{pf} , fluid specific heat (typically 1909) in J/(kg.K);

(ii). D_i , inside diameter of pipe in mm;

(iii).   L, length of pipe in m;

(iv). T_{fo} , initial fluid temperature in K;

(v).   type of oil used.

5 Model Equations

When the First Law applied to the open thermal system of a pipe section, the temperature of the fluid in the pipe, T_f , can be expressed from:

$$\frac{dT_f}{dt} = \frac{W - H_1 + m_f C_{pf} (T_{in} - T_f)}{M_f C_{pf}} \qquad \ldots \ldots (2.29)$$

where the mass flowrate through the pipe can be found as $m_f = \rho Q$, and W, H_1 and T_{in} will be provided as input data.

The above transient temperature equation can be solved by using first order Euler integration in order to achieve a short computational time. The fluid temperature is assumed to be constant for a fixed short period of time. This time step at which the fluid temperature is increased is provided as an user defined parameter. A typical value for this data is recommended between 1 to 5 seconds. A variable is introduced to monitor the time corresponding to the last temperature update. This variable is initially set to zero. If the simulation time exceeds the constant temperature period, the fluid temperature is updated by solving the equations as below

$$\Delta T_f \ = \ \frac{dT_f}{dt} \ = \ \frac{W - H_1 + m_f \, C_{pf} \, (T_{in} - T_f)}{M_f \, C_{pf}} \qquad \ldots \ldots (2.30)$$

$$T_f \ = \ T_{fo} + \Delta T_f \, \Delta t \qquad \ldots \ldots (2.31)$$

where T_{fo} is the initial fluid temperature at $t = 0$, respectively, and the Δt is the constant time increment.

The empirical relationship between the kinematic viscosity and fluid temperature, under the atmospheric pressure, is expressed as

$$\nu \ = \ e^{10e^{10\left[A \, - \, B \log_{10}(T_f \, + \, 273)\right]}} + 0.6 \qquad \ldots \ldots (2.32)$$

The fluid density is assumed to be linear with temperature and calculated from

$$\rho = D - C(T_f - 20) \qquad \ldots \ldots (2.33)$$

In the above two equations, the constants A, B, C and D are empirical values, and can be evaluated once the type of fluid is chosen in HASP.

The fluid Bulk Modulus is an empirical function of density and temperature and given by

$$B = 10^4 \left[1.78 + 7 \left(\frac{\rho}{1000} - 0.86 \right) \right] e^{10 \left[25 \times 10^{-4} (20 - T_f) \right]} \qquad \dots \dots (2.34)$$

6   Model Testing   The model has been verified by applying power loss, flowrate and input fluid temperature. The block diagram for the test circuit is shown in Fig. A2.7.

7   Model Linking   The model has 7 external and one internal links. The external link connected on port 1 provides the power loss. The link diagram for model FPGH is shown in Figure A2.8.

model inputs:

        (a). W, power losses in W:

        (b). T_{in} , inlet fluid temperature in K:

        (c). Q, flowrate in the pipe in l/s:

        (d). heat flow loss to one type of pipe wall material in W:

        (e). heat flow loss to another type of pipe wall material in W.

model outputs:

        (a). fluid temperature at port 1 in deg.C:

        (b). fluid temperature at port 2 in deg.C:

        (c). fluid viscosity in cSt:

        (d). fluid density in kg/m^3:

        (e). fluid bulk modulus in bar.

The link ordering during program generation must correspond to the port ordering shown in Fig. A2.8. The only acceptable input to the program generator for the test circuit shown in Figure A2.7 is:

FPGH01 01 02 03 04 05 06 07 08

A2.5 FPOH Loop Fluid Temperature and Property Model
of a Hydraulic System with the use of a Tank

1   **Introduction**   FPOH models the thermodynamic behaviour of a hydraulic loop with fluid property changes. The model considers the dynamic and steady state behaviour of loop fluid temperature for a hydraulic system with the use of a tank. The model takes into account the difference between fluid and pipe wall temperatures as a result of basic thermodynamic processes taking place in an open thermal system. The changes in fluid properties caused by fluid temperature variation are also calculated in the model.

2   **Assumptions**

(i).   The model assumes that the power loss input to the
       system loop will be provided as input data, and
       calculated in other models.

(ii). The model assumes that the total heat flow transferred
       to the pipelines of the loop will be provided as an
       input data, and calculated in the power sum model POOH.

(iii). The model assumes that the tank fluid temperature
       is provided and has been calculated in the tank
       temperature model FPTH.

(iv). The model assumes an uniform fluid temperature throughout
       the system loop.

3   **Nomenclature**

B	fluid bulk modulus
C_{pf}	fluid specific heat
d	pipe internal diameter
L	length of pipe section
m_f	mass flow rate of fluid

M_f	fluid mass in the system loop
H_1	rate of heat flow transferred from fluid to pipe wall by forced convection
T_{in}	fluid temperature at the inlet of the pipe section
T_f	fluid temperature
W	rate of power loss converted into heat energy

GREEK SYMBOLS

ν	kinematic viscosity
ρ	density

4   User Defined Parameters

(i). C_{pf} , fluid specific heat (typically 1909) in J/(kg.K):

(ii). D_i , inside diameter of pipe in mm:

(iii).   L, total pipe length of loop in m:

(iv). T_{fo} , initial fluid temperature in K:

(v).   type of oil used.

5   Model Equations   When the First Law applied to the open thermal system of a system loop, the fluid temperature in the loop, T_f , can be expressed from:

$$\frac{dT_f}{dt} = \frac{W - H_1 + m_f C_{pf} (T_{in} - T_f)}{M_f C_{pf}} \qquad \ldots \ldots (2.35)$$

where the mass flow exchange between the loop and tank is given as $m_f = \rho Q$, and W, H_1 and T_{in} will be provided as input data.

The above transient temperature equation can be solved by using first order Euler integration in order to achieve a short computational time. The fluid temperature is assumed to be constant for a fixed short period of time. This time step at which the fluid temperature is increased is provided as an user defined parameter. A typical value for this data is recommended between 1 to 5 seconds. A variable is introduced to monitor the time corresponding to the last temperature

update. This variable is initially set to zero. If the simulation time exceeds the constant temperature period, the fluid temperature is updated by solving the equations as below

$$\Delta T_f = \frac{dT_f}{dt} = \frac{W - H_1 + m_f C_{pf} (T_{in} - T_f)}{M_f C_{pf}} \qquad \ldots \ldots (2.36)$$

$$T_f = T_{fo} + \Delta T_f \, \Delta t \qquad \ldots \ldots (2.37)$$

where T_{fo} is the initial fluid temperature at $t = 0$, respectively, and the Δt is the constant time increment.

The empirical relationship between the kinematic viscosity and fluid temperature, under the atmospheric pressure, is expressed as

$$\nu = e^{10e^{10\left[A - B \log_{10}(T_f + 273)\right]}} + 0.6 \qquad \ldots \ldots (2.38)$$

The fluid density is assumed to be linear with temperature and calculated from

$$\rho = D - C (T_f - 20) \qquad \ldots \ldots (2.39)$$

In the above two equations, the constants A, B, C and D are empirical values, and can be evaluated once the type of fluid is chosen in HASP.

The fluid Bulk Modulus is an empirical function of density and temperature and given by

$$B = 10^4 \left[1.78 + 7(\frac{\rho}{1000} - 0.86)\right] e^{10\left[25 \times 10^{-4}(20 - T_f)\right]} \qquad \ldots \ldots (2.40)$$

6   **Model Testing**   The model has been verified by applying power loss, flowrate and input fluid temperature. The block diagram for the test circuit is shown in Fig.

A2.9.

7 Model Linking The model has 5 external and 2 internal links. The external link connected on port 1 provides the loop total power loss. The link diagram for model FPOH is shown in Figure A2.10.

model inputs:

(a). W, the total power loss in the loop in W;

(b). T_{in} , tank fluid temperature in K;

(c). Q, flowrate in the loop in 1/s;

(d). the total heat flow loss to pipe walls in W.

model outputs:

(a). loop fluid temperature in deg.C;

(b). fluid viscosity in cSt;

(c). fluid density in kg/m^3;

(d). fluid bulk modulus in bar.

The link ordering during program generation must correspond to the port ordering shown in Fig. A2.10. The only acceptable input to the program generator for the test circuit shown in Figure A2.9 is:

FPOH01 01 02 03 04 05 06 07

A2.6 FPTH Tank Temperature and Fluid Property Model

1 Introduction FPTH models the temperature behaviour of a tank. The model considers the dynamic/steady state behaviour of fluid and pipe wall temperatures within a tank opening to atmosphere. The changes in fluid properties caused by fluid temperature variation are also calculated in the model.

2 Assumptions

(i). The model assumes that the power loss input to the
tank will be provided as input data, and calculated
in other models.

(ii). The model assumes that the inlet fluid temperatures
will be provided as input data and calculated in
other fluid property models.

(iii). The model assumes an uniform fluid temperature in the
tank and its extending pipelines.

(iv). The model assumes that the inside wall temperature
is equal to fluid temperature and heat radiation from
tank wall atmosphere is ignored.

(v). The model assumes that the heat transferred within the
tank wall is one dimensional conduction.

3 Nomenclature

A_1	tank base area
A_2	one side of fluid vertical area in the tank
A_3	another side of fluid vertical area in the tank
B	fluid bulk modulus
C_{pf}	fluid specific heat
C_{pp}	pipe wall specific heat

g	gravitational acceleration
h_{av}	heat transfer coefficient by natural convection for tank vertical plate
h_{ap}	heat transfer coefficient by natural convection for tank horizontal plate at bottom
k	thermal conductivity of pipe wall material
L	length of pipe section
m_1	mass flowrate of fluid into tank at line 1
m_2	mass flowrate of fluid into tank at line 2
m_3	mass flowrate of fluid at outlet of tank
M_f	fluid mass in the tank
M_p	mass of tank wall material
Q_1	rate of heat flow conducted from fluid to four sides of vertical tank wall
Q_2	rate of heat flow conducted from fluid to the tank wall at bottom
Q_3	rate of heat flow transferred from fluid to atmosphere by natural convection
T_a	constant surrounding atmospheric temperature
T_f	fluid temperature and inside tank wall temperature
T_{wp}	outside tank bottom wall temperature
T_{wv}	outside tank vertical wall temperature
W	rate of power loss converted into heat energy
x	thickness of tank wall

DIMENSIONLESS GROUPS

Nu	Nusselt number
Re	Reynolds number

GREEK SYMBOLS

ϵ	emissivity
θ	temperature difference (relative to wall)
μ	dynamic viscosity
ρ	density
σ	Stefan-Boltzman constant; surface tension

4   User Defined Parameters

(i). C_{pf}, fluid specific heat (typically 1909) in J/(kg.K);

(ii). C_{pp}, pipe specific heat (hose: 2100) in J/(kg.K);

(iii).   L, length of tank in m;

(iv).   D, width of tank in m;

(v).   h, fluid height in tank in m;

(vi). ρ, density of tank wall material in $\frac{kg}{m^3}$;

(vii).   k, conductivity of tank wall (iron: 80.2) in W/m.K;

(viii). T_{wvo}, initial outside vertical tank wall temperature in K;

(ix). T_{fo}, initial fluid temperature in K;

(x). T_{wpo}, initial tank bottom wall temperature in K;

(xi). T_a, atmospheric temperature in K;

(xii).   x, thickness of tank wall in mm;

(xiii).   type of oil used.

5   Model Equations

The heat flow transferred from vertical tank wall to its surrounding atmosphere by natural convection is given by

$$Q_1 = 2h_{av}(A_2 + A_3)(T_{wv} - T_a) \qquad \dots\dots(2.41)$$

In the above h_{av} is calculated from

$$h_{av} = \begin{cases} 1.42\left(\dfrac{\theta}{l}\right)^{0.25} & \text{when } 10^4 < Gr < 10^9 \\ 1.31\theta^{\frac{1}{3}} & \text{when } 10^9 < Gr < 10^{12} \end{cases} \qquad \dots\dots(2.42)$$

In the above equation, h_a is in W/m.K, θ is the temperature difference in K, and l is in m and Gr is defined as

$$Gr = \frac{gL^3\beta\rho^2\theta}{\mu^2} = \frac{gL^3\beta\theta}{\nu^2} \qquad \dots\dots(2.43)$$

The heat flow transferred from fluid to atmosphere by natural convection at horizontal wall of tank bottom can be expressed from:

$$Q_2 = h_{ap}A_1(T_{wp} - T_a)$$ ......(2.44)

Similarly, the heat flow transferred from the surface of fluids in the tank to atmosphere by free convection can be obtained from

$$Q_3 = h_{ap}A_1(T_f - T_a)$$ ......(2.45)

The heat flow convected from vertical tank wall to atmosphere must be equal to the value of heat conduction. The heat flow conducted through vertical tank walls is expressed from

$$Q_1 = \frac{2k}{x}(A_2 + A_3)(T_f - T_{wv})$$ ......(2.46)

where x is the tank wall thickness and T_{wv} is the outside vertical tank wall temperature.

Hence, Twv can be resolved from

$$T_{wv} = \frac{h_{av}T_a + \frac{k}{x}T_f}{h_{av} + \frac{k}{x}}$$ ......(2.47)

Similarly, from the heat flow conducted through the horizontal bottom of tank tank

$$Q_2 = \frac{k}{x}A_1(T_f - T_{wp})$$ ......(2.48)

where T_{wp} is the outside tank wall temperature at bottom.

Hence, Twp can be calculated from

- 204 -

$$T_{wp} = \frac{h_{ap} T_a + \frac{k}{x} T_f}{h_{ap} + \frac{k}{x}}$$

$$\dots\dots (2.49)$$

Therefore, fluid temperature in the tank can be obtained from

$$\frac{dT_f}{dt} = \frac{m_1 C_{pf} T_{in1} + m_2 C_{pf} T_{in2} - m_3 C_{pf} T_f - Q_1 - Q_2 - Q_3}{M_f C_{pf}} \quad \dots\dots (2.50)$$

The above temperature transient equation will be solved by using first order Euler integration in order to achieve a short computational time. The temperature is assumed to be constant for a fixed short period of time. This time step at which the temperatures are increased is provided as an user defined parameter. A typical value for this parameter is recommended between 1 to 5 seconds. A variable is introduced to monitor the time corresponding to the last temperature update. This variable is initially set to zero. If the simulation time exceeds the constant temperature period, the fluid temperature and the pipe wall temperature are updated by solving the equations as below

$$\Delta T_f = \frac{dT_f}{dt}$$
$$= \frac{m_1 C_{pf} T_{in1} + m_2 C_{pf} T_{in2} - m_3 C_{pf} T_f - Q_1 - Q_2 - Q_3}{M_f C_{pf}} \quad \dots\dots (2.51)$$

$$T_f = T_{fo} + \Delta T_f \Delta t \qquad \dots\dots (2.52)$$

where T_{fo} is the initial fluid temperature at t = 0, respectively, and the Δt is the time increment.

The empirical relationship between the kinematic viscosity and fluid temperature, under the atmospheric pressure, is expressed as

$$v = e^{10e^{10\left[A - B \log_{10}(T_f + 273)\right]}} + 0.6 \qquad \dots\dots(2.53)$$

The fluid density is assumed to be linear with temperature and calculated from

$$\rho = D - C(T_f - 20) \qquad \dots\dots(2.54)$$

In the above two equations, the constants A, B, C and D are empirical values, and can be evaluated once the type of fluid is chosen in HASP.

The fluid Bulk Modulus is an empirical function of density and temperature and given by

$$B = 10^4\left[1.78 + 7(\frac{\rho}{1000} - 0.86)\right]e^{10\left[25\times10^{-4}(20 - T_f)\right]} \qquad \dots\dots(2.55)$$

6 **Model Testing**   The model has been verified by applying power loss, flowrate and input fluid temperature. The block diagram for the test circuit is shown in Fig. A2.11.

7 **Model Linking**   The model has 7 external and one internal links. The external link connected to port 1 supplies fluid temperature. The link diagram for model FPTH is shown in Fig. A2.12.

model inputs:

(a). W_1, power loss at port 1 in W;

(b). W_2, power loss at port 2 in W;

(c). $T_{in\,1}$, inlet fluid temperature at port 1 in K;

(d). $T_{in\,2}$, inlet fluid temperature at port 2 in K;

(e). Q_1, inlet flowrate in port 1 in l/s;

(f). Q_2, inlet flowrate in port 2 in l/s.

model outputs:

> (a). fluid temperature in K;
>
> (b). vertical tank wall temperature in K;
>
> (c). horizontal tank wall temperature in K.

The link ordering during program generation must correspond to the port ordering shown in Fig. A2.12. The only acceptable input to the program generator for the sub-circuit shown in Fig. A2.11 is:

FPTH01 01 02 03 04 05 06 07 08

A2.7 FPUH Loop Fluid Temperature and Property Model
of an Unboosted Closed Hydraulic System

1 Introduction FPOH models the loop fluid temperature of an unboosted closed hydraulic system with fluid property changes. The model takes into account the difference between fluid and pipe wall temperatures as a result of basic thermodynamic processes taking place in an open thermal system. The changes in fluid properties caused by fluid temperature variation are also calculated in the model.

2 Assumptions

(i). The model assumes that the power loss input to the
system loop will be provided as input data, and
calculated in other models.

(ii). The model assumes that the total heat flow transferred
to the pipelines of the loop will be provided as an
input data, and calculated in the power sum model POOH.

(iii). The model assumes an uniform fluid temperature throughout
the system loop.

3 Nomenclature

B	fluid bulk modulus
C_{pf}	fluid specific heat
d	pipe internal diameter
L	length of pipe section
M_f	fluid mass in the system loop
H_1	rate of heat flow transferred from fluid to pipe wall by forced convection
T_f	fluid temperature
W	rate of power loss converted into heat energy

GREEK SYMBOLS

ν kinematic viscosity

ρ density

4 Underlined Parameters

(i). C_{pf} , fluid specific heat (typically 1909) in J/(kg.K);

(ii). D_i , inside diameter of pipe in mm;

(iii).   L, total pipe length of loop in m;

(iv). T_{fo} , initial fluid temperature in K;

(v).   type of oil used.

5 Model Equations
When the First Law applied to the closed thermal system of an unboosted closed system loop, the fluid temperature in the loop, T_f , can be expressed from:

$$\frac{dT_f}{dt} = \frac{W - H_1}{M_f \, C_{pf}} \qquad\qquad \ldots\ldots(2.56)$$

where W, H_1 will be provided as input data.

The above transient temperature equation can be solved by using first order Euler integration in order to achieve a short computational time. The fluid temperature is assumed to be constant for a fixed short period of time. This time step at which the fluid temperature is increased is provided as an user defined parameter. A typical value for this data is recommended between 1 to 5 seconds. A variable is introduced to monitor the time corresponding to the last temperature update. This variable is initially set to zero. If the simulation time exceeds the constant temperature period, the fluid temperature is updated by solving the equations as below

$$\Delta T_f \; = \; \frac{dT_f}{dt} \; = \; \frac{W - H_1}{M_f \, C_{pf}} \qquad \ldots\ldots(2.57)$$

$$T_f \; = \; T_{fo} \; + \; \Delta T_f \, \Delta t \qquad \ldots\ldots(2.58)$$

where T_{fo} is the initial fluid temperature at $t = 0$, respectively, and the Δt is the constant time increment.

The empirical relationship between the kinematic viscosity and fluid temperature, under the atmospheric pressure, is expressed as

$$\nu \; = \; e^{10e^{10\left[A \, - \, B \, \log_{10}(T_f \, + \, 273)\right]}} + 0.6 \qquad \ldots\ldots(2.59)$$

The fluid density is assumed to be linear with temperature and calculated from

$$\rho = D - C(T_f - 20) \qquad \ldots\ldots(2.60)$$

In the above two equations, the constants A, B, C and D are empirical values, and can be evaluated once the type of fluid is chosen in HASP.

The fluid Bulk Modulus is an empirical function of density and temperature and given by

$$B \; = \; 10^4 \left[1.78 + 7(\frac{\rho}{1000} - 0.86) \right] e^{10 \left[25 \times 10^{-4}(20 - T_f) \right]} \qquad \ldots\ldots(2.61)$$

6 **Model Testing** The model has been verified by applying power loss, flowrate and input fluid temperature. The block diagram for the test circuit is shown in Fig. A2.13.

7   Model Linking   The model has 2 external and 2 internal links. The external link connected on port 1 provides the loop total power loss. The link diagram for model FPUH is shown in Figure A2.14.

model inputs:

> (a). W. the total power loss in the loop in W;
> (b). the total heat flow loss to pipe walls in W.

model outputs:

> (a). loop fluid temperature in deg.C;
> (b). fluid viscosity in cSt;
> (c). fluid density in kg/m^3;
> (d). fluid bulk modulus in bar.

The link ordering during program generation must correspond to the port ordering shown in Fig. A2.14. The only acceptable input to the program generator for the test circuit shown in Figure A2.13 is:

FPUH01 01 02 03 04

A2.8 LR0H A Propeller Load Model

1 **Introduction**   LR0H models the characteristics of a marine propeller, rotating in still water, without moving forward or reverse as shown in Fig. A2.15. The model simulates the dynamic angular speeds of the propeller and motor, and also the propeller load torque. The effects of the gear box in the speed reduction, and also the density of fluid surrounding to the propeller are taken into account. The model allows a modification to the propeller torque coefficient to be carried out in considering the particular propeller shape and operation conditions.

2 **Assumptions**

(i). The model assumes that the torque supplied from hydraulic motor will be provided as input data and calculated in another model;

(ii). The model assumes that the coefficients of the propeller closely follow the standard marine propeller curves taken from Ref. (5.4). When the model is applied to a particular system simulation, alterations to the propeller coefficients are necessary since the propeller does not make any advance movement and the particular propeller shape has to be taken · into account.

3 **Nomenclature**

D	diameter of propeller
K_t	propeller torque coefficient
J	effective inertia of propeller/motor
R_e	ratio of gear box between motor and propeller
T_m	hydraulic torque supplied from motor
T_p	propeller load torque

GREEK SYMBOLS

ρ density of fluid surrounding to the propeller

ω_m angular speed of motor shaft

ω_p angular speed of propeller shaft

4   User Defined Parameters

(i).   J, effective inertia of propeller/motor in $kg.m^2$;

(ii).   non-dimensional torque coefficient;

(iii).   D, diameter of propeller in m;

(iv). R_e, ratio of gear box between motor and propeller;

(v). ρ, density of fluid surrounding to propeller in kg/m^3;

(vi). ω_{mo}, initial angular speed of motor in rev/min.

5   Model Equations   The dynamic speed of the motor shaft is given by

$$\frac{d\,\omega_m}{dt} = \frac{T_m - \dfrac{T_p}{R_e}}{J} \qquad \ldots \ldots (2.62)$$

In the above, the propeller load torque T_p can be determined from

$$T_p = K_t \rho \frac{\omega_p^2}{4\pi^2} D^5 \qquad \ldots \ldots (2.63)$$

where the propeller speed $\omega_p = 2\pi n_p$ is noted. When this model is applied to a particular system simulation, the non-dimensional torque coefficient K_t is supplied by the user in order to consider the particular propeller shape and working conditions. The angular speed of the propeller can be obtained from

$$\omega_p = \frac{\omega_m}{R_e} \qquad \ldots \ldots (2.64)$$

6   **Model Testing**   The model has been verified by applying a simple test circuit. The block diagram for the test circuit is shown in Fig. A2.16.

7   **Model Linking**   The model has one external and 2 internal links. The external link connected on port 1 provides the hydraulic torque from motor. The link diagram for model LROH is shown in Figure A2.17.

model inputs:

        (a). torque supplied from hydraulic motor;

model outputs:

        (a). angular speed of motor in rev/min;
        (b). angular speed of propeller in rev/min;
        (c). propeller torque.

The link ordering during program generation must correspond to the port ordering shown in Fig. A2.17. The only acceptable input to the program generator for the test circuit shown in Figure A2.16 is:

LROH01 01 02 03

A2.9 MOAH A Hydraulic Gear Motor Model with Power Loss Calculation

1 **Introduction** MOAH models the characteristics of a hydraulic gear motor with an external leakage path. The motor displacement is defined by the user. The model takes into account of compressibility flow loss, viscous and pressure dependent torque losses and computes the power losses. The model receives inlet and outlet pressure, shaft speed from adjoining models, and supplies torque, inlet and outlet flows to adjoining models. The model uses the technique given by McCandlish and Dorey (Ref. 3.16) for the estimation of the motor loss coefficients. The slip loss coefficient is assumed to vary linearly with speed. The torque loss coefficient is divided into two parts, a pressure dependent loss which is assumed to vary linearly with speed and a speed dependent loss. Pressure and torque characteristics must be available for the motor to be modelled.

2 **Assumptions**

(i) The slip flow loss coefficient is assumed to vary linearly with speed. The overall slip loss coefficient for this model must be known at two extreme speeds. The loss coefficient can then be obtained by interpolation at intermediate speeds. The coefficient is assumed to be independent of differential pressure across the motor.

(ii) The slip flow loss is assumed to vary inversely as the fluid viscosity: no account is taken of the effect of temperature on internal clearances of the motor.

(iii) The pressure dependent mechanical loss coefficient is assumed to vary linearly with speed. This loss coefficient must be known at two extreme speeds. The loss coefficient can then be obtained at intermediate speeds by interpolation. The coefficient is assumed to be independent of differential pressure across the motor.

(iv) The speed dependent mechanical loss term used is viscosity

- 215 -

and hence temperature dependent.

(v)   The slip flow in a hydraulic motor with an external leakage
        drain caused a heating effect both in the outlet pipeline
        (internal slip loss) and in the case drain return line to the
        reservoir (external slip loss). These internal and external
        fractions are difficult to determine and are likely to vary
        considerably from one particular motor to another. This
        model allows the user to select the fraction of both
        these loss terms affecting the outlet pipeline and reservoir,
        thus enabling the importance of the factors to be determined.

(vi)   The model takes into account volumetric losses due to
        compressibility.

(vii)   In the model it is assumed that the power loss associated
        with mechanical friction loss are dissipated through the
        motor casing. They are therefore not taken into account
        in the heat transfer computation.

3   Nomenclature

a	coefficient used for fraction slip flow power loss transmitted to fluid in the loop
C_f	pressure dependent torque loss coefficient
C_{f1}	pressure dependent torque loss coefficient at low speed condition
C_{f2}	pressure dependent torque loss coefficient at high speed condition
C_s	slip loss coefficient
C_{s1}	slip loss coefficient at low speed condition
C_{s2}	slip loss coefficient at high speed condition
C_{se}	external slip loss coefficient
C_{si}	internal slip loss coefficient
C_v	speed dependent torque loss coefficient
C_{v1}	speed dependent torque loss coefficient at low speed condition
C_{v2}	speed dependent torque loss coefficient at

high speed condition

D	displacement of pump
P_{dr}	drain line pressure of motor in bar
P_{in}	inlet pressure of motor in bar
P_{out}	outlet pressure of motor in bar
Q_{in}	inlet flow rate of motor in L/s
Q_{out}	outlet flow rate of motor in L/s
Q_s	total leakage flow rate in L/s
Q_{si}	internal leakage flow rate in L/s
Q_{thM}	maximum theoretical flow rate of motor in L/s
T_n	net torque in Nm
T_{th}	theoretical torque in Nm
T_{loss}	mechanical torque loss in Nm
T_l	torque referred to load in Nm
W_{in}	internal power loss to outlet pipeline in watts
W_{ext}	external power loss to drain in watts
B	bulk modulus of fluid in bar
μ	viscosity of fluid in Ns/(m*m)
η_{vol}	volumetric efficiency of unit
η_{mec}	mechanical efficiency of unit
ρ	density of hydraulic fluid in kg/cm^3
ω	angular velocity of motor in rev/min
ω_1	low angular speed of motor at which loss coefficients are quoted in rev/min
ω_2	high angular speed of motor at which loss coefficients are quoted in rev/min

4   <u>User defined parameters</u>

(i).   motor displacement in cc/rev;

(ii).   slip loss coefficient at low speed condition;

(iii).   low speed in rev/min at which loss coefficients is quoted;

(iv).   slip loss coefficient at high speed condition;

(v).   high speed in rev/min at which loss coefficient is quoted;

(vi).   fraction of slip loss coefficient for drain (external) leakage;

(vii). pressure dependent torque loss coefficient at low speed condition;

(viii). pressure dependent torque loss coefficient at high speed condition;

(ix).   reference viscosity in centipoise at which volumetric

efficiency is quoted(not used).

(x).   speed dependent torque loss coefficient at low speed condition.

5   Model equations   The net flow rate delivered is given by:

$$Q_{out} = Q_{th} - Q_{si} - Q_{se} - Q_c$$
$$= \omega D - C_{si}\frac{(p_{in} - p_{out})}{\mu} - C_{se}\frac{(p_{out} - p_{tank})}{\mu}$$
$$- \frac{p_{out} - p_{in}}{B}\omega D \qquad \qquad \dots\dots\dots (2.65)$$

and the net inflow by

$$Q_{in} = Q_{th} - Q_{si} \qquad\qquad \dots\dots\dots (2.66)$$

The overall slip loss coefficient C_s is assumed to vary according to the linear relationship:

$$C_s = C_{s1} + (C_{s2} - C_{s1})\frac{(\omega - \omega_1)}{(\omega_2 - \omega_1)} \qquad\qquad \dots\dots\dots (2.67)$$

This represents the total slip flow lost by the motor, which is the sum of the internal (outlet to inlet) and external (outlet to tank) loss coefficients. The actual fractions of the overall slip loss which are internal and external are ill-defined quantities and probably vary considerably between (i) various proprietary makes of motor as well as (ii) a given motor in new and worn conditions. For this reason, a fraction 'a' is defined enabling a user to study the effects of variations in this quantity between 0 and 1. The internal slip loss coefficient is given by:

$$C_{si} = aC_s$$

and the external slip loss coefficient by:

$$C_{si} = (1 - a)C_s$$

The torque delivered by a motor is given by:

$$T_{net} = T_{th} - T_v - T_f \qquad \cdots\cdots (2.68)$$

The speed dependent torque loss is given by:

$$T_v = C_v \mu \omega D \qquad \cdots\cdots (2.69)$$

The pressure dependent mechanical loss coefficient C_f is assumed to vary linearly with speed and is given by:

$$C_f = C_{f1} + (C_{f2} - C_{f1})\frac{(\omega - \omega_1)}{(\omega_2 - \omega_1)} \qquad \cdots\cdots (2.70)$$

and the pressure dependent torque loss is given by:

$$T_f = C_f (p_{out} - p_{in})D \qquad \cdots\cdots (2.71)$$

Hence the total torque loss T_l is

$$T_l = T_f + T_v \qquad \cdots\cdots (2.72)$$

The net power loss associated with fluid flow in the outlet of a hydraulic motor is given by

$$W_{in} = Q_{si}(p_{in} - p_{out}) \qquad \cdots\cdots (2.73)$$

The net power loss dissipated to the drain by

$$W_{ext} = Q_{se}(p_{out} - p_{dr}) \qquad \cdots\cdots (2.74)$$

6 Model linking   Model MOAH has seven external and one internal links. The

links connected to ports 1 and 2 supply inlet and outlet pressures. In return they give inlet and outlet flow rates respectively. The link at port 3 is connected to a rotational load and supplies torque and receives angular speed. The link connected to port 4 displays the drain flow. The link connected to port 5 supplies the outlet pipeline power loss (internal) and that connected to port 6 the external (case drain to reservoir) power loss. Both of these losses are supplied to a temperature and fluid properties subroutine (eg. FPGH, FPTH). The link connected to port 7 supplies the flowrate at outlet to calculate mass flowrate. Neither ports 4, 5, 6 or 7 receive information from other models. The internal link connected to port 8 displays volumetric and mechanical efficiencies. The link diagram for model MOAH is shown in Fig. A2.18.

model inputs:

        (a). inlet pressure in bar.

        (b). outlet pressure in bar.

        (c). angular speed in rev/min.

model outputs:

        (a). inlet flow rate in L/s.

        (b). outet flow rate in L/s.

        (c). torque in Nm.

        (d). power loss to case drain in W.

        (e). power loss to outlet pipeline in W.

        (f). external leakage flowrate in L/s.

        (g). volumetric efficiency.

        (h). mechanical efficiency.

A typical sub-circuit containing model MOAH, together with its block diagram is shown in Fig. A2.19. The link ordering during program generation must correspond to the port ordering shown in Fig. A2.18. The only acceptable input to the program generator for the sub-circuit shown in Fig. A2.19 is:

A2.10 PIOH A Vertical Open-Ended Pipe Model

1 Introduction PIOH models the dynamic behaviour of a vertical open ended pipe in the unboosted closed hydraulic system. From the pressure provided by other models, the model determines the respective transient flowrate of the open ended pipe by taking into account of the pipe friction and fluid effective inertia in the pipe. The model receives pressure and supplies the dynamic flowrate to adjoining pump model.

2 Assumptions

(i). the input pressure p_1 will be provided as an input data and calculated in another model;

(ii). since the value of p_1 is comparatively low, the effects of fluid compressibility is not taken into account;

(iii). the fluid height is normally a positive value, the air release will only become significant under extreme conditions so its effects can be ignored.

3 Nomenclature

A	pipe across sectional area
d	diameter of pipe section
g	gravitation
h	fluid height in the pipe
m	fluid mass
p_1	pressure at the pipe bottom
p_f	friction pressure loss
v	transient fluid velocity in the pipe
V	fluid volume in the pipe
ρ	fluid density
μ	fluid viscosity

λ   friction factor

4   User defined parameters

(i). p_1. pressure at pipe bottom in bar:

(ii).   initial height of fluids in the pipe in m:

(iii).   initial fluid velocity in the pipe in m/s.

5   Model equations

In the vertical open ended pipe being simulated is shown in Fig. A2.19. The force balance equation for the flow in the open ended pipe is

inertia force + friction force + static pressure head =
transient pressure force at the bottom of the pipe

ie.

$$\frac{d\,(mv)}{dt} + p_f\,A + A\,\rho g h = p_1 A \qquad\qquad \ldots\ldots (2.75)$$

In the above equation, the pressure loss to friction is defined by the flow conditions as

$$p_f = \begin{cases} \dfrac{32\mu h v}{d} & \textit{Laminar Condition } \mathrm{Re} \leqslant 2000 \\[2mm] \lambda\dfrac{h\,\rho v^2}{d} & \textit{Turbulent Condition } \mathrm{Re} > 2000 \end{cases}$$

$$\ldots\ldots (2.76)$$

For the smooth circular pipes under turbulent condition, the friction factor λ can be obtained from the empirical relations

$$\lambda = \begin{cases} \dfrac{0.3164}{Re^{0.25}} & 10^4 < Re < 10^5 \\[2mm] 0.0032 + \dfrac{0.221}{Re^{0.237}} & 10^5 < Re < 3 \times 10^6 \end{cases}$$

$$\dots\dots (2.77)$$

In Equation (A2.75), m = ρAh, and

$$\frac{d(mv)}{dt} = m\,\frac{dv}{dt} + v\,\frac{dm}{dt} \qquad \dots\dots (2.78)$$

where for any flow in the pipe changes in the volume, oil density and mass with time are related according to the following equation

$$\frac{dm}{dt} = \rho\,\frac{dV}{dt} + V\,\frac{d\rho}{dt} = \rho A\,\frac{dh}{dt} + Ah\,\frac{d\rho}{dt} \qquad \dots\dots (2.79)$$

substitute Equation (A2.78) and (A2.79) into (A2.75), then re-arrange as

$$\rho h\,\frac{dv}{dt} + \rho v\,\frac{dh}{dt} + vh\,\frac{d\rho}{dt} + p_f + \rho gh = p_1 \qquad \dots\dots (2.80)$$

The variation of the density of mineral oil in the open ended pipe is not considered to be sufficiently significant to include in the theoretical analysis. If the column of the flow in the open ended pipe is assumed to move as a whole, the fluid velocity in the pipe is expressed from $v = \dfrac{dh}{dt}$. Hence, Equation (A2.80) becomes

$$p_1 = \rho h\,\frac{dv}{dt} + \rho v^2 + p_f + \rho gh \qquad \dots\dots (2.81)$$

As can be observed, there are considerable difficulties in any attempt to solve this equation as being a non-homogeneous differential equation. However, a clearer view can be obtained by putting the time derivation on the left hand side

$$\frac{dv}{dt} = \frac{p_1 - p_f}{\rho h} - \frac{v^2}{h} - g \qquad\qquad \dots\dots(2.82)$$

Therefore, the transient flowrate of Q in the open ended pipe can be calculated from

$$Q = -Av \qquad\qquad \dots\dots(2.83)$$

where the sign '-' indicates the directions of fluid velocity and outlet flowrate are conventionally opposite as shown in Fig. A2.20.

6   **Model linking**   The model has one external link and one internal link. The external link connected to port 1 receives pressure and supplies dynamic flowrate. The internal link connected to port 2 indicates the fluid velocity and fluid height. The link diagram for model PIOH is shown in Fig. A2.21.

model inputs:

> (a). pressure at pipe bottom in bar;
> (b). initial fluid height in m;
> (c). initial fluid velocity in m/s.

model outputs:

> (a). pipe outlet flowrate in L/min;
> (b). fluid velocity in the pipe in m/s;
> (c). fluid height in the pipe in m.

A typical sub-circuit containing model PIOH, together with its block diagram is shown in Fig. A2.22. The link ordering during program generation must correspond to the port ordering shown in Fig. A2.21. The only acceptable input to the program generator for the sub-circuit shown in Fig. A2.22 is:

PIOH01 01 02

A2.11 PI3H A Vertical Return Line Pipe Model

1 **Introduction**   PI3H models the dynamic behaviour of a vertical return pipe to reservoir in the partially closed hydraulic system. From the pressure provided by other models, the model determines the respective flowrate of the return line by taking into account of the pipe friction and fluid effective inertia in the pipe. The model receives pressure and supplies the flowrate to adjoining pump model.

2 **Assumptions**

   (i).   the pressures at the pipe each end will be provided as
          input data and calculated in other models;

   (ii). since the pipe is in low pressure region, the
          effects of fluid compressibility is ignored;

3 **Nomenclature**

   A   pipe across sectional area
   d   diameter of pipe section
   g   gravitation
   l   pipe length
   m   fluid mass in the pipe
   p_b pressure at the pipe bottom
   p_f friction pressure loss
   p_t pressure at the pipe top to tank
   v   transient fluid velocity in the pipe
   V   fluid volume in the pipe
   ρ fluid density
   μ fluid viscosity
   λ friction factor

4 **User defined parameters**

- 226 -

(i). p_b, pressure at pipe bottom in bar:

(ii). p_t, pressure at pipe top in bar;

(iii).   initial fluid velocity in the pipe in m/s.

5   **Model equations**   In the vertical return line pipe being simulated is shown in Fig. A2.22. The equation describing the fluid forces on the vertical return line pipe may be written as

inertia force + friction force - static pressure head = transient pressure force across the pipe

ie.

$$\frac{d\,(mv\,)}{dt} + p_f\,A\, - A\,\rho g h\, = (p_b\, - p_t\,)A \qquad\qquad \ldots\ldots(2.84)$$

In the above equation, the pressure loss to friction is defined by the flow conditions as

$$p_f = \begin{cases} \dfrac{32\mu l v}{d} & \textit{Laminar Condition } Re \leqslant 2000 \\ \lambda\dfrac{l\rho v^2}{d} & \textit{Turbulent Condition } Re > 2000 \end{cases} \qquad \ldots\ldots(2.85)$$

For the smooth circular pipes under turbulent condition, the friction factor λ can be obtained from the empirical relations

$$\lambda = \begin{cases} \dfrac{0.3164}{Re^{0.25}} & 10^4 < Re < 10^5 \\ 0.0032 + \dfrac{0.221}{Re^{0.237}} & 10^5 < Re < 3\times10^6 \end{cases} \qquad \ldots\ldots(2.86)$$

It is noted that in Equation (A2.84), m = $\rho A l$ = constant. Following closely the derivation given in the above section for model PIOH, Equation (A2.84) becomes

$$\frac{dv}{dt} = \frac{p_b - p_t - p_f}{\rho h} + g \qquad \qquad \ldots \ldots (2.87)$$

Therefore, the flowrate Q in the return line pipe to reservoir can be calculated from

$$Q = Av \qquad \qquad \ldots \ldots (2.88)$$

6   **Model linking**   The model has two external links. The external link connected to port 1 receives pressure and supplies flowrate. The link diagram for model PI3H is shown in Fig. A2.23.

model inputs:

(a). pressure at pipe bottom in bar:

(b). pressure at pipe top in bar:

(c). initial fluid velocity in m/s.

model outputs:

(a). pipe inlet flowrate in L/min:

(b). pipe outlet flowrate in L/min:

A typical sub-circuit containing model PI0H, together with its block diagram is shown in Fig. A2.24. The link ordering during program generation must correspond to the port ordering shown in Fig. A2.23. The only acceptable input to the program generator for the sub-circuit shown in Fig. A2.24 is:

PI3H01 01 02

A2.12 PICH Pipe Wall Temperature Model
of a Pipe Section

1 Introduction PICH models the dynamic and steady state pipe wall temperatures of any a pipe section in hydraulic system. The model takes into account the difference between fluid and pipe wall temperatures as a result of basic thermodynamic processes taking place in a closed thermal system.

2 Assumptions

(i). The model assumes that the fluid temperature in the pipe will be provided as input data. and calculated in another fluid temperature model.

(ii). The model assumes the uniform inside and outside pipe wall temperatures of the pipe section.

(iii). The model assumes that the heat transfer within the pipe wall is one dimensional conduction.

3 Nomenclature

A_m	logarithmic mean surface area of pipe
A_2	outside surface area of pipe
A_1	inside surface area of pipe
C_{pp}	pipe wall specific heat
d	pipe inlet diameter
g	gravitational acceleration
h_f	heat transfer coefficient by forced convection
h_a	heat transfer coefficient by natural convection
k	thermal conductivity of pipe wall material
L	pipe length
M_p	mass of pipe wall material
H_1	rate of heat flow transferred from fluid to pipe wall by forced convection

H_2	rate of heat flow transferred from pipe wall to atmosphere by natural convection
R_1	pipe inside radius
R_2	pipe outside radius
T_1	wall temperature at internal pipe surface
T_2	wall temperature at external pipe surface
T_a	constant atmospheric temperature
W	rate of power loss converted into heat energy

DIMENSIONLESS GROUPS

Nu	Nusselt number
Re	Reynolds number

GREEK SYMBOLS

ϵ	emissivity
σ	Stefan-Boltzman constant; surface tension

4   User Defined Parameters

(i). C_{pp}, pipe specific heat (hose: 2010) in J/(kg.K);

(ii). D_o, outside diameter of pipe in mm;

(iii). D_i, inside diameter of pipe in mm;

(iv).   L, length of pipe in m;

(v). ρ_p, density of pipe wall material in $\frac{kg}{m^3}$;

(vi). ϵ, emissivity of pipe material (black hose: 0.9);

(vii). k, conductivity of pipe material (hose: 0.15) in W/m.K;

(viii). T_{2o}, initial outside pipe wall temperature in K;

(ix). T_a, atmospheric temperature in K.

5   Model Equations

The heat flow transferred from pipe wall to its surrounding atmosphere by natural convection can be determined from:

$$H_2 = h_a A_2(T_2 - T_a) + \epsilon\sigma A_2(T_2^4 - T_a^4) \qquad \dots\dots(2.89)$$

Under laminar flow conditions, the heat transfer by natural convection h_a is calculated from

$$h_a = \begin{cases} 1.32(\dfrac{T_2 - T_a}{d})^{0.25} & \text{when } 10^4 < Gr < 10^9 \\ 1.25(T_2 - T_a)^{\frac{1}{3}} & \text{when } 10^9 < Gr < 10^{12} \end{cases} \qquad \dots\dots(2.90)$$

In the above equation, h_a is in W/m.K and d is in m.

The heat flow transferred from fluid to pipe wall by forced convection can be given from:

$$H_1 = h_f A_1(T_f - T_1) \qquad \dots\dots(2.91)$$

In the above equation, the inside pipe wall temperature T_1 can be determined from

$$T_1 = \frac{h_f A_1 T_f + \dfrac{kA_m}{R_2 - R_1}T_2}{h_f A_1 + \dfrac{kA_m}{R_2 - R_1}} \qquad \dots\dots(2.92)$$

where A_m is the logarithmic mean area and can be calculated from

$$A_m = \frac{2(R_2 - R_1)L}{\ln\dfrac{R_2}{R_1}} = \frac{A_2 - A_1}{\ln\dfrac{R_2}{R_1}} \qquad \dots\dots(2.93)$$

where R_1 and R_2 are the internal and external radiuses and L is the length of the pipe section respectively.

The outside pipe wall temperature at any instant time can be obtained from

$$\frac{dT_2}{dt} = \frac{H_1 - H_2}{M_p C_p} \qquad \ldots \ldots (2.94)$$

The above equation will be solved by using first order Euler integration in order to achieve a short computational time. The temperatures are assumed to be constant for a fixed short period of time. This time step at which the temperatures are increased is provided as an user defined parameter. A typical value for this parameter is recommended between 1 to 5 seconds (3 seconds as a default). A variable is introduced to monitor the time corresponding to the last temperature update. This variable is initially set to zero. If the simulation time exceeds the constant temperature period, the pipe wall temperature is updated by solving the equations as below

$$\Delta T_2 = \frac{dT_2}{dt} = \frac{H_1 - H_2}{M_p C_p} \qquad \ldots \ldots (2.95)$$

$$T_2 = T_{2_o} + \Delta T_2 \Delta t \qquad \ldots \ldots (2.96)$$

where T_{2_o} is the initial pipe wall temperature at t = 0, respectively, and the Δt is the constant time increment.

6   Model Testing   The model has been verified by applying power loss. The block diagram for the test circuit is shown in Fig. A2.25.

7   Model Linking   The model has one external and 2 internal links. The external link connected to port 1 supplies the fluid temperature in the pipe section. The link diagram for model PICH is shown in Figure A2.26.

model inputs:

(a). T_f , fluid temperature in deg.C:

model outputs:

(a). outside pipe wall temperature in deg.C;

(b). heat flow from fluid to pipe wall in W;

(c). heat flow from pipe wall to atmosphere in W;

The link ordering during program generation must correspond to the port ordering shown in Fig. A2.26. The only acceptable input to the program generator for the sub-circuit shown in Figure A2.25 is:

PICH01 01 02 03

A2.13 PM2H A Dynamic Model of An Induction Motor

1   **Introduction**   PM2H models the dynamic behaviour of an induction motor. From the shaft load torque provided, the model determines the respective dynamic and steady state shaft speed of the motor by taking into account of the effective inertia which includes the motor and connected components. The model receives load torque and supplies the shaft speed to adjoining model.

2   **Assumptions**

   (i)   the output torque of induction motor is a linear function of the shaft speed under the normal operating conditions;

   (ii)   the shaft torque T_L will be provided as an input data and calculated in the appropriate component model.

3   **Nomenclature**

   K_1 damping coefficient due to eddy currents
   K_e electric motor torque/speed coefficient
   J effective inertia
   T_e electric developed torque
   ω angular shaft speed
   ω_s maximum angular shaft speed

4   **User defined parameters**

   (i). K_1, damping coefficient in Nm/rev/min;
   (ii). K_e, motor torque/speed coefficient in Nm/(rev/min);
   (iii).   J, effective inertia of pump/motor in kg.m^2;
   (iv).   initial speed of motor in rev/min.

5   **Model equations**   It is noticed, under the normal operating conditions of

- 234 -

electric motor in hydraulic systems, that the change in the speed is relatively small. The torque must be a linear function of speed, so the developed electric torque at ω can be described as

$$T_e = K_e (\omega_s - \omega) \qquad \qquad \dots\dots (2.97)$$

In the above equation, the coefficient K_e can be obtained from

$$K_e = \tan\alpha = \frac{T_2 - T_1}{\omega_1 - \omega_2} \qquad \qquad \dots\dots (2.98)$$

where T_1 and T_2 can be determined by giving two practical measurements of the motor load conditions.

In the general equation for torque, the dynamic electrically developed torque with the motor on load for induction motor can be evaluated as follows

$$T_e = T_L + J\frac{d\omega}{dt} + K_1\omega \qquad \qquad \dots\dots (2.99)$$

where J is the effective inertia and K_1 is the damping torque due to eddy currents. Substituting Equation (A2.97) to the above equation and re-arranging enables the dynamic speed to be expressed

$$\frac{d\omega}{dt} = \frac{K_e\omega_s - (K_e + K_1)\omega - T_L}{J} \qquad \qquad \dots\dots (2.100)$$

6 **Model linking** The model has one external link. The external link connected to port 1 receives torque and supplies dynamic shaft angular speed. The link diagram for model PM2H is shown in Fig. A2.27.

model inputs:

        (a). shaft torque required in Nm;
        (b). initial motor speed in rev/min.

model outputs:

       (a). shaft speed of motor in rev/min.

A typical sub-circuit containing model PM2H, together with its block diagram is shown in Fig. A2.28. The link ordering during program generation must correspond to the port ordering shown in Fig. A2.27. The only acceptable input to the program generator for the sub-circuit shown in Fig. A2.28 is:

PM2H01 01

A2.14 PM3H A Dynamic Model of A Governed Internal Combustion Engine

1   Introduction   PM3H models the dynamic behaviour of a governed engine. From the shaft torque provided. the model determines the respective dynamic and steady state shaft speed of the engine/pump by taking into account of the engine effective inertia. The model receives hydraulic load torque and supplies the shaft speed to adjoining model.

2   Assumptions

(i)   the output torque of engine is a linear function of
       the difference between the governor set speed and
       the engine working speed.

(ii)   all the dynamic characteristics of the engine internal
       components are unimportant compared with the overall
       engine characteristics. so the engine meets all changes
       in load conditions instantaneously.

(iii) the shaft torque T_L will be provided as an input
       data and calculated in the appropriate model.

3   Nomenclature

C_e constant speed/torque gradient coefficient
J effective inertia of engine/pump
T_e torque supplied from engine
ω angular shaft speed
ω_g governor set shaft speed

4   User defined parameters

(i). C_e . speed/torque gradient coefficient in rev/min/Nm:

- 237 -

(iii).   governor set speed in rev/min;

(iv).   initial speed of motor in rev/min.

5   Model equations

When the above assumptions are applied, the torque produced by a governed engine T_e may be expressed from

$$T_e = F(\omega_g - \omega) \qquad \dots\dots (2.101)$$

A constant speed/torque gradient coefficient may be introduced and defined as C_e, which gives the relation

$$T_e = \frac{\omega_g - \omega}{C_e} \qquad \dots\dots (2.102)$$

The above relation can be only used under the condition where, for all ω,

$$T_{brake} \leqslant T_e \leqslant T_{max} \qquad \dots\dots (2.103)$$

If the total effective engine inertia is denoted by J_e, T_h the torque required by the hydraulic pump, then the engine acceleration can be found in

$$\frac{d\omega}{dt} = \frac{T_e - T_h}{J_e} \qquad \dots\dots (2.104)$$

6   Model linking

The model has one external link. The external link connected to port 1 receives torque and supplies dynamic shaft angular speed. The link diagram for model PM3H is shown in Fig. A2.29.

model inputs:

(a). torque required by a hydraulic pump in Nm;

(b). initial engine speed in rev/min.

- 238 -

model outputs:

(a). shaft speed of engine in rev/min.

A typical sub-circuit containing model PM3H, together with its block diagram is shown in Fig. A2.30. The link ordering during program generation must correspond to the port ordering shown in Fig. A2.29. The only acceptable input to the program generator for the sub-circuit shown in Fig. A2.30 is:

PM3H01 01

A2.15 PUAH A Hydraulic Gear Pump Model with Power Loss Calculation

1 **Introduction**   PUAH models the characteristics of a hydraulic gear pump with an internal leakage path. The pump displacement is defined by the user. The model takes into account of compressibility flow loss, viscous and pressure dependent torque losses and computers the power dissipation. The model receives inlet and outlet pressure and shaft speed from adjoining models, and supplies inlet and outlet flow and torque to adjoining models. The slip loss coefficient is assumed to vary linearly with speed. The torque loss coefficient is divided into two parts, a pressure dependent loss which is assumed to vary linearly with speed and a speed dependent loss. Pressure and torque characteristics must be available for the pump to be modelled.

2 **Assumptions**

(i) The slip flow loss coefficient is assumed to vary linearly with speed. The overall slip loss coefficient for this model must be known at two extreme speeds. The loss coefficient can then be obtained by interpolation at intermediate speeds. The coefficient is assumed to be independent of differential pressure across the pump.

(ii) The slip flow loss is assumed to vary inversely with the fluid viscosity and no account is taken of the effect of temperature on internal clearances of the pump.

(iii) The pressure dependent mechanical loss coefficient is assumed to vary linearly with speed. This loss coefficient must be known at two extreme speeds. The loss coefficient will then be obtained at intermediate speeds by interpolation. The coefficient is assumed to be independent of differential pressure across the pump.

(iv) The speed dependent mechanical loss term used is viscosity and hence temperature dependent.

(v) The model takes into account volumetric losses due to compressibility.

(vi) In the model it is assumed that the power loss associated with mechanical friction loss are dissipated through the pump casing. They are therefore not taken into account in the heat transfer computation.

3 Nomenclature

C_f pressure dependent torque loss coefficient

C_{f1} pressure dependent torque loss coefficient at low speed condition

C_{f2} pressure dependent torque loss coefficient at high speed condition

C_s slip loss coefficient

C_{s1} slip loss coefficient at low speed condition

C_{s2} slip loss coefficient at high speed condition

C_{si} internal slip loss coefficient

C_v speed dependent torque loss coefficient

C_{v1} speed dependent torque loss coefficient at low speed condition

C_{v2} speed dependent torque loss coefficient at high speed condition

D displacement of pump

P_{in} inlet pressure of unit in bar

P_{out} outlet pressure of unit in bar

Q_{in} inlet flow rate of unit in L/s

Q_{out} outlet flow rate of unit in L/s

Q_{si} internal leakage flow rate in L/s

Q_{thM} maximum theoretical flow rate of pump in L/s

T_n net torque in Nm

T_{th} theoretical torque in Nm

T_{loss} mechanical torque loss in Nm

T_l torque referred to load in Nm

W_{in} internal power loss to pump entrance in watts

B – bulk modulus of fluid in bar

μ - viscosity of fluid in Ns/(m*m)

η_{vol} - volumetric efficiency of unit

η_{mec} - mechanical efficiency of unit

ρ - density of hydraulic fluid in kg/cm^3

ω - angular velocity of unit in rev/min

ω_1 - low angular velocity of unit at which loss coefficients are quoted in rev/min

ω_2 - high angular velocity of unit at which loss coefficients are quoted in rev/min

4   User defined parameters

(i). pump displacement in cc/rev;

(ii). slip loss coefficient at low speed condition;

(iii). low speed in rev/min at which loss coefficients are quoted;

(iv). slip loss coefficient at high speed condition;

(v). high speed in rev/min at which loss coefficient are quoted;

(vi). pressure dependent torque loss coefficient at low speed condition;

(vii). pressure dependent torque loss coefficient at high speed condition;

(viii). reference viscosity in centipoise at which volumetric efficiency is quoted(not used).

5   Model equations   The net flow rate delivered is given by:

$$Q_{out} = Q_{th} - Q_{si} - Q_c$$
$$= \omega D - C_{si} \frac{(p_{out} - p_{in})}{\mu} - \frac{p_{out} - p_{in}}{B} \omega D \qquad \dots \dots (2.105)$$

and the net inflow by

$$Q_{in} = Q_{th} - Q_{si} \qquad \dots \dots (2.106)$$

The torque required by the pump is the sum of the theoretical torque and the torque loss, ie.

$$T_{net} = T_{th} + T_v + T_f \qquad\qquad \dots\dots (2.107)$$

The speed dependent torque loss is given by:

$$T_v = C_v \mu \omega D \qquad\qquad \dots\dots (2.108)$$

The pressure dependent mechanical loss coefficient C_f is assumed to vary linearly with speed and is given by:

$$C_f = C_{f\,1} + (C_{f\,2} - C_{f\,1}) \frac{(\omega - \omega_1)}{(\omega_2 - \omega_1)} \qquad\qquad \dots\dots (2.109)$$

and the pressure dependent torque loss is given by:

$$T_f = C_f (p_{out} - p_{in}) D \qquad\qquad \dots\dots (2.110)$$

The power loss associated with fluid flow in the inlet of a hydraulic pump is given by

$$W = Q_{si} (p_{out} - p_{in}) \qquad\qquad \dots\dots (2.111)$$

6   **Model linking**   Model PUAH has 5 external links. The links connected to ports 1 and 2 supply inlet and outlet pressures, and in return they give inlet and outlet flow rates respectively. The link at port 3 is connected to a prime mover and supplies torque and receives angular speed. The link connected to port 4 gives the pump power loss due to the pump internal slip loss. The link connected to port 5 supplies the pump delivery flowrate to a fluid temperature model (eg. FPCH) for the computation of mass flowrate in the system. The link diagram for model PUAH is shown in Fig. A2.31.

model inputs:

(a). inlet pressure in bar.

(b). outlet pressure in bar.

(c). angular speed in rev/min.

model outputs:

(a). inlet flow rate in L/s.

(b). outet flow rate in L/s.

(c). outet flow rate at port 4 in L/s.

(d). shaft torque in Nm.

(e). power dissipation in W.

A typical sub-circuit containing model PUAH, together with its block diagram is shown in Fig. A2.32. The link ordering during program generation must correspond to the port ordering shown in Fig. A2.31. The only acceptable input to the program generator for the sub-circuit shown in Fig. A2.32 is:

PUAH01 01 02 03 04 05

A2.16 OR2H Dynamic Model of A Sharp Edged Orifice

1 **Introduction** OR2H models the dynamic behaviour of a sharp edged orifice. From the pressure drop data provided by other models, the model determines the respective dynamic and steady state flowrates. The model receives inlet and outlet pressure and supplies inlet and outlet flows to adjoining models. Account is taken of fluid expansion in calculating outlet flow.

2 **Assumptions**

(i) the orifice inlet and outlet pressures, p_{in} and p_{out} will be provided as input data will have been calculated in other models;

(ii) the formation of fluid jet at the orifice downstream is very significant to affect the dynamic response of a sharp edged orifice;

(iii) the inlet and outlet flowrates are different due to fluid expansion across the orifice inlet and outlet ports;

(iv) the length of fluid jet is independent of time and is assumed as 6 times the diameter of pipe duct.

3 **Nomenclature**

A area of pipe across section in mm^2

A_o opening area of orifice in mm^2

B bulk modulus in bar

C_c coefficient of contraction

C_d coefficient of discharge

D orifice diameter in mm

L equivalent fluid jet length in m

L_1 fluid jet length in m

p_{in} inlet pressure in bar

p_{out} outlet pressure in bar

Q_{in} inlet flow in l/sec

Q_{out} outlet flow in l/sec

ρ fluid density in Kg/m^3

ϕ coefficient of area ratio

Re   Reynolds Number

4   User defined parameters

Either

(i).   D, an orifice diameter in mm;

(ii). C_d, a coefficient of discharge;

or

(iii).   a flow in L/sec;

(iv).   a corresponding pressure difference in bar to allow
the orifice diameter to be calculated;

both

(v).   equivalent fluid jet length of orifice in m;

(vi).   initial downstream flowrate in L/sec;

(vii).   either effective Bulk Modulus of fluid/pipe in bar,
or pipe bore and wall thickness in mm and also pipe
wall material (steel, tungum, cupro-nickel and
flexible hose) to allow the value to be calculated.

5   Model equations   Generally, the absolute pressure difference across the orifice is written as

$$\Delta p = p_{in} - p_{out}$$ ......(2.112)

Following the derivation given in Chapter 3, the downstream flowrate of a sharp edged orifice is proposed to be expressed

$$\frac{dQ_{out}}{dt} = \frac{A}{\rho L}(\Delta p - \frac{\rho}{2C_d^2A^2}Q_{out}^2)$$ ......(2.113)

- 246 -

In the above equation, the equivalent length of downstream fluid jet, L, can be determined from

$$L = \frac{L_1}{2}(C_c + \frac{1}{\phi C_c})$$

...... (2.114)

where C_c is the coefficient of contraction and ϕ is defined as $\phi = \frac{A_o}{A}$, and the length of fluid jet L_1 is taken as 6D of the downstream pipe duct for in line sharp edged orifice. Hence, Equation (A2.113) can be re-written more simply as

$$\frac{dQ_{out}}{dt} = R (\Delta p - C Q_{out} \, sign(Q_{out}))$$

...... (2.115)

where R and C are constants which may be evaluated from the user defined parameters.

When the cavitation occurs at the orifice downstream, the flowrate through the orifice becomes maximum and is given by

$$Q_{out} = C_d A_o (\frac{2p_{in}}{\rho})^{\frac{1}{2}}$$

...... (2.116)

In considering the variation of fluid density with pressure, the relation of the orifice inlet and outlet flowrates can be obtained from

$$Q_{in} = -(1 - \frac{\Delta p}{B})Q_{out}$$

...... (2.117)

By convention the inlet flow is taken to be opposite in sign to the outlet flow.

6   Model linking   The model has 2 external links. The external link connected to port 1 receives inlet pressure and supplies inlet flow. The external link connected to port 2 receives outlet pressure and supplies outlet flow. The link diagram for model OR2H is shown in Fig. A2.33.

model inputs:

      (a). inlet pressure in bar;

      (b). outlet pressure in bar.

model outputs:

      (a). inlet flow in L/sec;

      (b). outlet flow in L/sec.

A typical sub-circuit containing model OR2H, together with its block diagram is shown in Fig. A2.34. The link ordering during program generation must correspond to the port ordering shown in Fig. A2.33. The only acceptable input to the program generator for the sub-circuit shown in Fig. A2.34 is:

OR2H01 01 02

A2.17 OR3H An Orifice Model with Calculation of Power Loss

1 **Introduction** OR3H models the behaviour of an orifice, used for the control of fluid flow. The model receives inlet and outlet pressure and supplies inlet and outlet flow to adjoining models. Account is taken of fluid expansion at the orifice downstream in calculating inlet flow. The model is similar in most respects to the standard HASP orifice model OR3Z but the power loss is added into the model computation.

2 **Assumptions**

(i). For pressure differences above 0.1 bar, a parabolic flow-differential pressure law is assumed.

(ii). For pressure differences below 0.1 bar, a linear flow-differential pressure law is assumed. This is necessary to overcome computational difficulties associated with modelling a parabolic law at the origin where an infinite gradient is encountered. This is considered to be a realistic representation of the laminar flow condition which occurs at low flows.

(iii). Fluid expansion at the orifice downstream is taken into account.

3 **Nomenclature**

B bulk modulus
C_d coefficient of discharge
d orifice diameter
Q_{in} inlet flow
Q_{out} outlet flow
p_{in} inlet pressure
p_{out} outlet pressure
W power loss
ρ fluid density

- 249 -

4   User defined parameters

Either

(i).   D, an orifice diameter in mm:

(ii). C_d, a coefficient of discharge:

or

(iii).   a flow in L/sec:

(iv).   a corresponding pressure difference in bar to allow
the orifice diameter to be calculated:

both

(v).   either effective Bulk Modulus of fluid/pipe in bar,
or pipe bore and wall thickness in mm and also pipe
wall material (steel, tungum, cupro-nickel and
flexible hose) to allow the value to be calculated.

5   Model equations   Generally, the absolute pressure difference across the orifice is written as

$$\Delta p = p_{in} - p_{out} \qquad \qquad \text{......(2.118)}$$

For an orifice differential pressure greater than 0.1 bar, the standard orifice law is assumed. The flow can be estimated from

$$Q_{out} = C_d \left(\frac{\pi d^2}{4}\right)\left(\frac{2\Delta p}{\rho}\right)^{\frac{1}{2}} \qquad \qquad \text{......(2.119)}$$

When the differential pressure across the orifice is less than 0.1 bar, a linear relationship is assumed.

$$Q_{out} = K \Delta p \qquad \qquad \text{......(2.120)}$$

where K is selected to give a continuous flow-differential pressure relationship. The use of the linear relationship prevents numerical instability at the origin when the

parabolic law has infinite gradient.

The inlet flow to the orifice is calculated taking into account the effects of fluid expansion at the orifice downstream due to the pressure change at the sides of the orifice. By convention the inlet flow to the valve is taken to be opposite in sign to the outlet flow:

$$Q_{in} = -(1 - \frac{\Delta p}{B})Q_{out}$$

$$\dots\dots (2.121)$$

The power loss caused by the orifice is calculated from

$$W = p_{in} Q_{in} - p_{out} Q_{out}$$

$$\dots\dots (2.122)$$

6   Model linking   The model has 4 external links. The external link connected to port 1 receives inlet pressure and supplies inlet flow. The external link connected to port 2 receives outlet pressure and supplies outlet flow. The external link connected to port 3 supplies the power loss and the external link connected to port 4 gives the orifice outlet flowrate for the thermodynamic calculations using temperature and fluid property models (eg. FP*H series models). The link diagram for model OR3H is shown in Fig. A2.35.

model inputs:

> (a). inlet pressure in bar;
> (b). outlet pressure in bar.

model outputs:

> (a). inlet flow in L/sec;
> (b). outlet flow in L/sec;
> (c). power loss in W.

A typical sub-circuit containing model OR3H, together with its block diagram is shown in Fig. A2.36. The link ordering during program generation must correspond to the port ordering shown in Fig. A2.35. The only acceptable input to the program generator for the sub-circuit shown in Fig. A2.36 is:

A2.18 TKSH A Tank Model with Varying Fluid Level

1   **Introduction**   TKSH models the dynamic behaviour of a tank with Varying fluid level. In the hydraulic system with the use of a small tank, such as in the case of the partially closed hydraulic circuit, the variation of fluid height in the tank may be significant in determining the transient pressure of flow provided from tank. The model receives inlet and outlet flow and supplies inlet and outlet pressure to adjoining models. Account is taken of the variation of fluid height in the tank and the difference between the static and mean pressures.

2   **Assumptions**

  (i).   The tank inlet and outlet flowrates will be provided as input data and calculated in other models.

  (ii).   Tank is of constant across-sectional area.

  (iii).   The error introduced by the 'false transient technique' is tolerable.

3   **Nomenclature**

  A area of inlet and outlet pipe across section
  A_t area of tank base
  C_i coefficient of pressure loss at inlet
  C_o coefficient of pressure loss at outlet
  G coefficient of the first order lag
  H fluid height in the tank
  Q_i inlet flow
  Q_o outlet flow
  p_i inlet pressure
  p_{is} inlet piezometric pressure
  p_o outlet pressure
  p_{os} outlet piezometric pressure
  W power loss in watts

ρ fluid density

4 User defined parameters

(i). A_t, area of tank base in m^2;

(ii).   d, diameter of extending pipe in mm;

(iii).   initial fluid height in tank in m;

(iv).   initial inlet pressure in bar;

(v).   initial outlet pressure in bar;

(vi).   reciprocal time constant of the first order
        lag (typically above 1000).

5 Model equations   The variation of fluid height in the tank can be estimated from

$$\frac{dH}{dt} = \frac{Q_o - Q_i}{A_t} \qquad \cdots\cdots (2.123)$$

When the 'false transient technique' is applied, the transient inlet pressure p_i can be obtained by solving the following equations, ie.

$$\frac{dp_i}{dt} = G(p_{is} - p_i) \qquad \cdots\cdots (2.124)$$

where p_{is} is defined by

$$p_i = \rho g H - \frac{\rho}{2A^2}(1 + C_i)Q_i^2 \qquad \cdots\cdots (2.125)$$

Similarly, the transient outlet pressure p_o can be determined from

$$\frac{dp_o}{dt} = G(p_{os} - p_o) \qquad \cdots\cdots (2.126)$$

where p_{os} is given by

$$p_o = \rho g H - \frac{\rho}{2A^2}(1 + C_o)Q_o^2 \qquad \ldots\ldots(A2.22)$$

where C_i and C_o are the pressure loss coefficients at the reservoir entrance and exit due to flow enlarge and contraction.

6 Model linking The model has 2 external links. The external link connected to port 1 receives inlet flow and supplies inlet pressure. The external link connected to port 2 receives outlet flow and supplies outlet pressure. The link diagram for model TKSH is shown in Fig. A2.37.

model inputs:

   (a). inlet flowrate in L/sec;
   (b). outlet flowrate in L/sec.

model outputs:

   (a). inlet pressure in
   (b). outlet pressure in bar.

A typical sub-circuit containing model TKSH. together with its block diagram is shown in Fig. A2.38. The link ordering during program generation must correspond to the port ordering shown in Fig. A2.37. The only acceptable input to the program generator for the sub-circuit shown in Fig. A2.38 is:

TKSH01 01 02
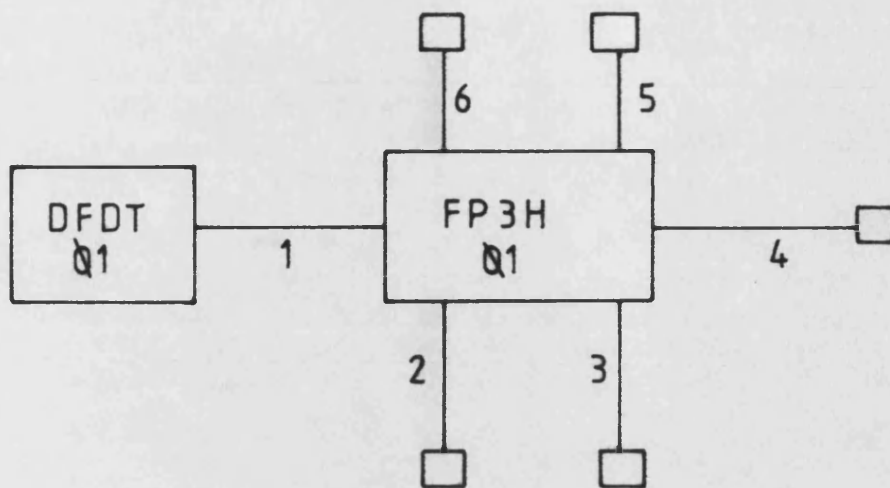
FIG. A2.1   BLOCK   DIAGRAM   FOR   VERIFICATION   TEST
SIMULATION   OF   MODEL   FP3H
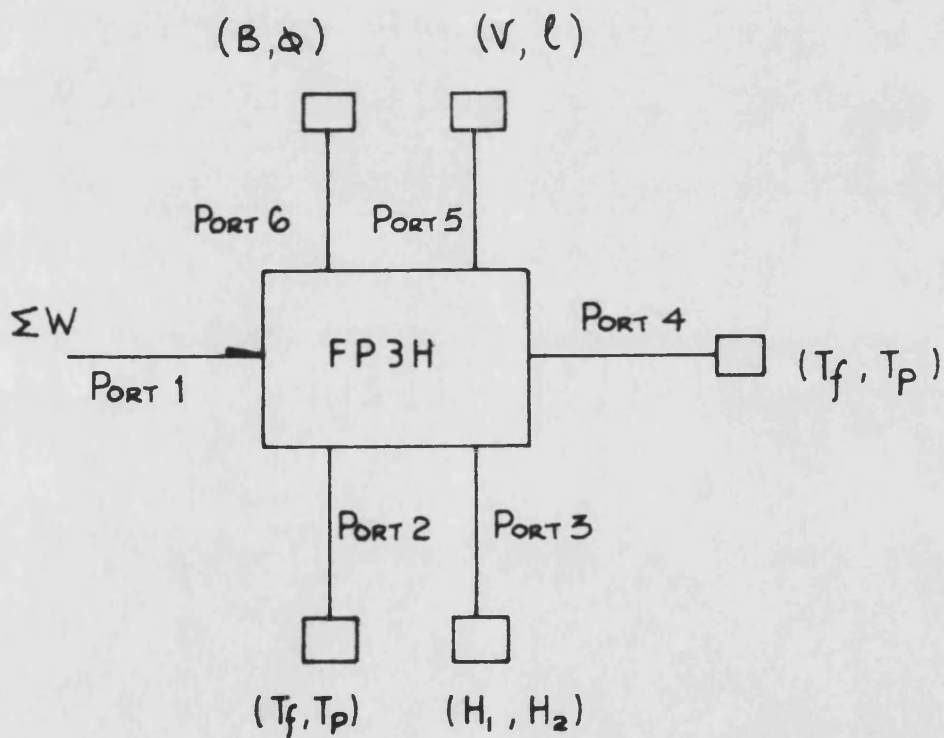
EFFORTS: T_f, H_1, T_f, V, B

FLOWS : T_p, H_2, T_p, ℓ

FIG. A2.2   LINK   DIAGRAM   FOR   TEMPERATURE   AND
FLUID   PROPERTY   MODEL   FP3H
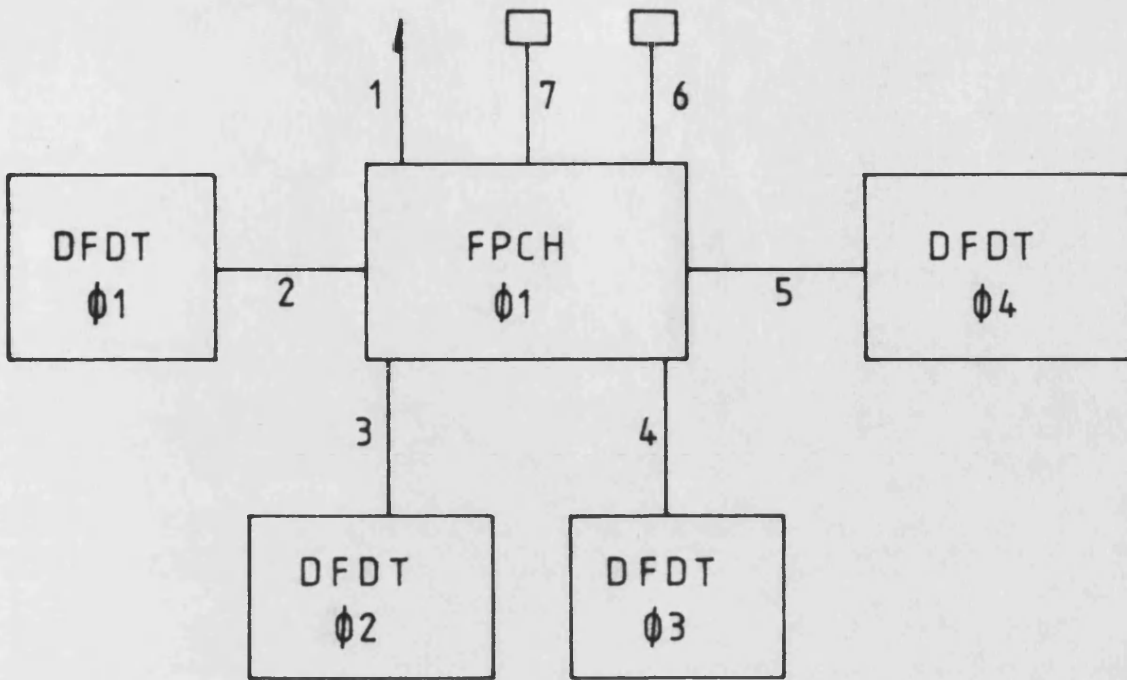
FIG. A2.3 BLOCK DIAGRAM FOR VERIFICATION TEST
         SIMULATION OF MODEL FPCH

EFFORTS : V , B

FLOWS : T_f , ΣW , T_{IN} , ΣH_1 , Q , l
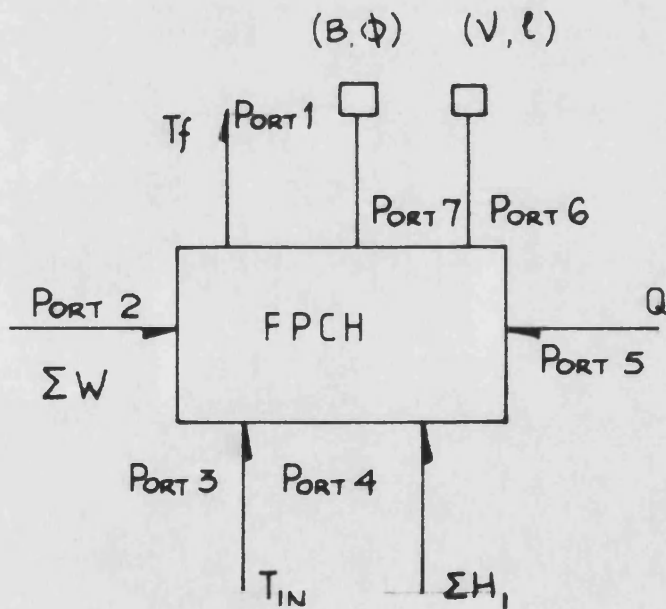
FIG. A2.4 LINK DIAGRAM FOR TEMPERATURE AND FLUID
         PROPERTY MODEL FPCH
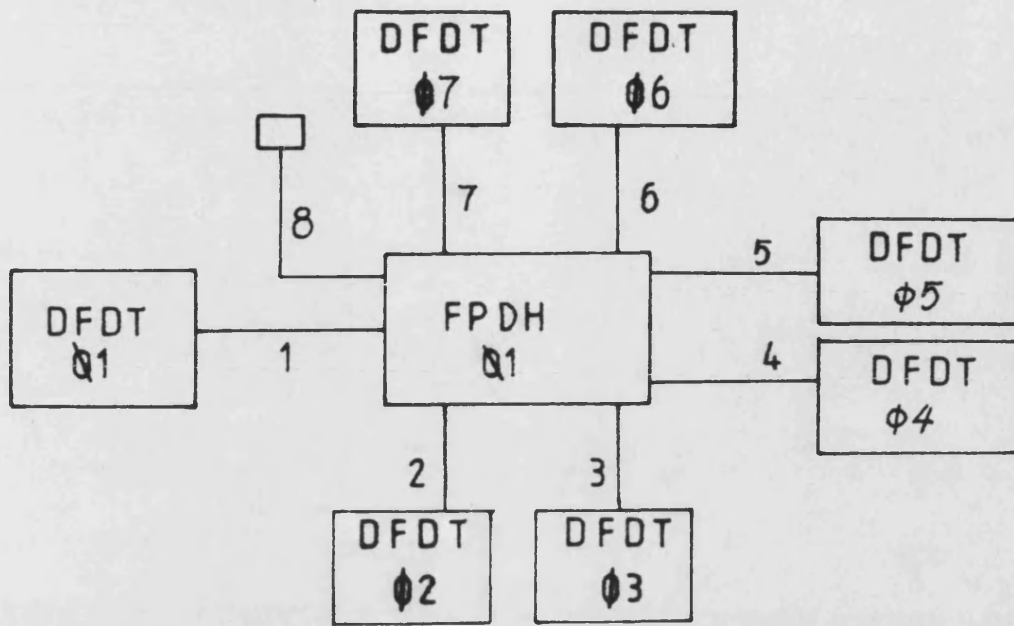
FIG. A2.5 BLOCK DIAGRAM FOR VERIFICATION TEST
SIMULATION OF MODEL FPDH

EFFORTS: ν

FLOWS : $\Sigma W, T_1, T_2, \Sigma H_1$
Q_1, Q_2, T_f, ρ
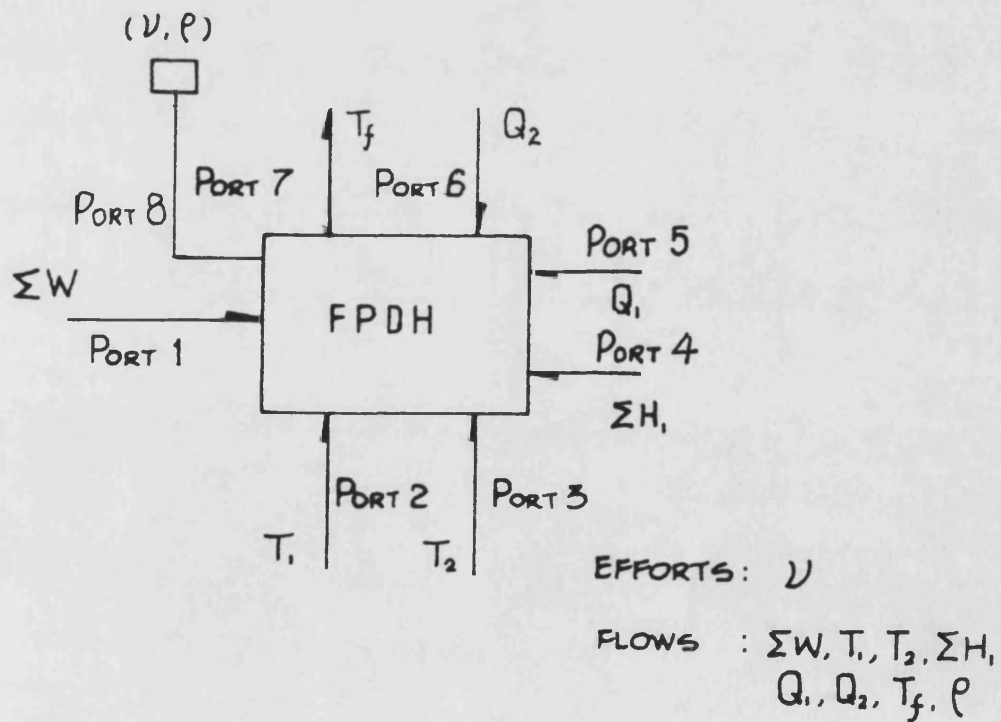
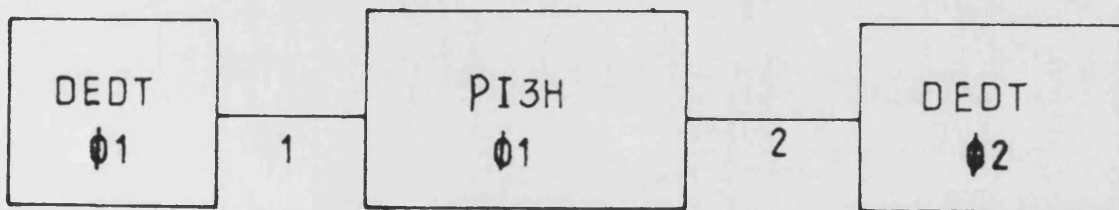FIG. A2.6 LINK DIAGRAM FOR TEMPERATURE AND
FLUID PROPERTY MODEL FPDH
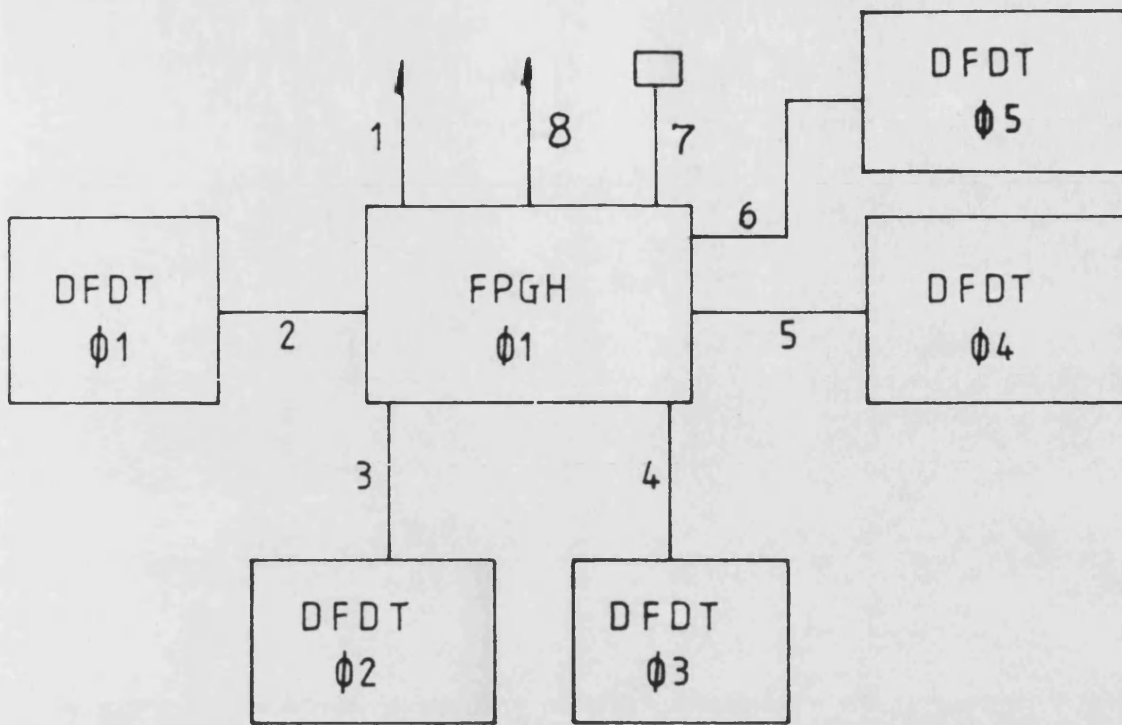
FIG. A2.7 BLOCK DIAGRAM FOR VERIFICATION TEST
SIMULATION OF MODEL FPGH
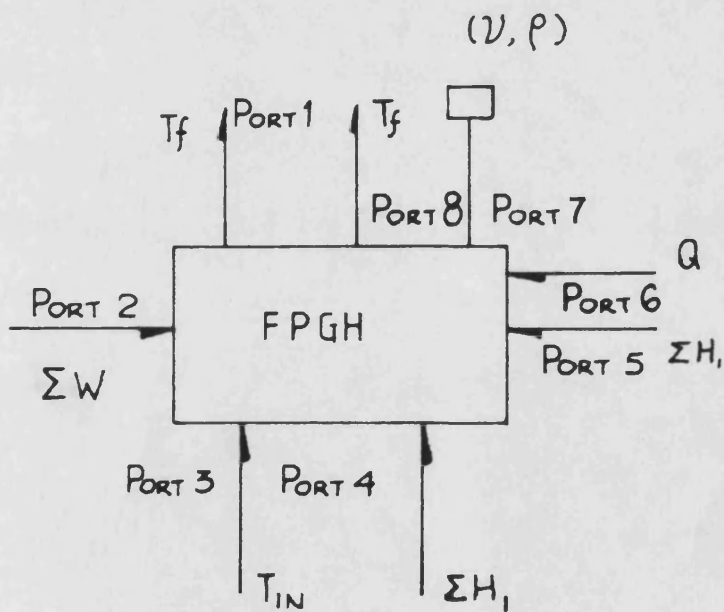
EFFORTS : V

FLOWS : T_f, ΣW, T_{IN}, ΣH_1, Q, ℓ

FIG. A2.8 LINK DIAGRAM FOR TEMPERATURE AND FLUID
PROPERTY MODEL FPGH
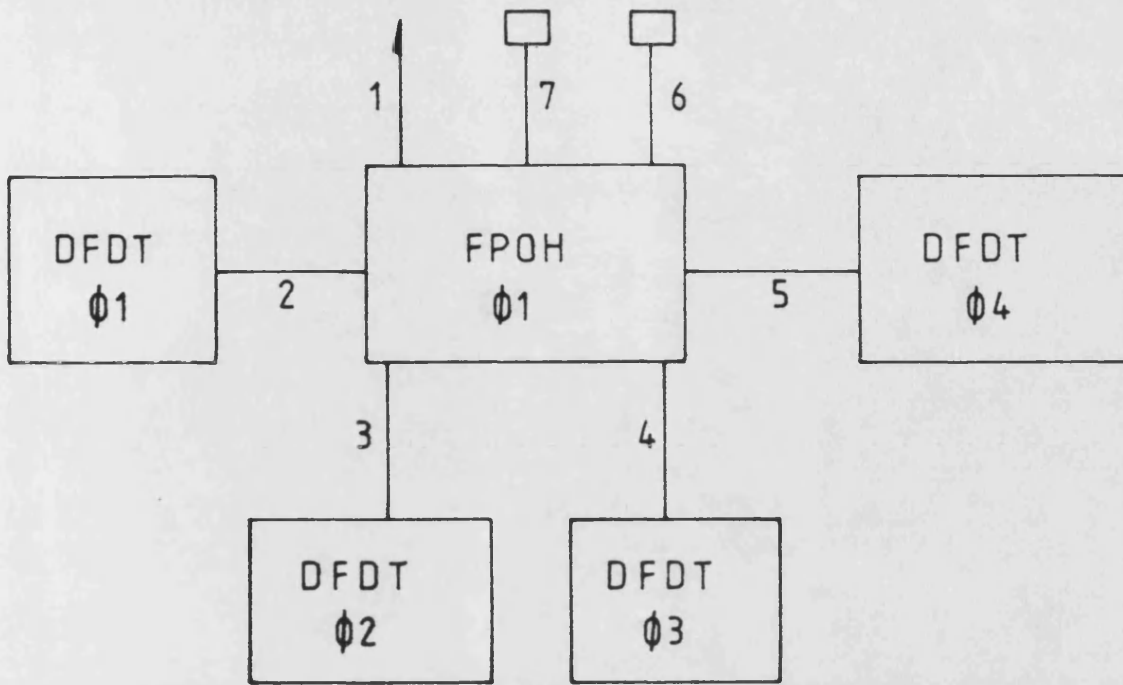
FIG. A2.9 BLOCK DIAGRAM FOR VERIFICATION TEST
SIMULATION OF MODEL FPOH

EFFORTS : V , B

FLOWS : T_f, ΣW, T_{IN}, ΣH_1, Q, ℓ
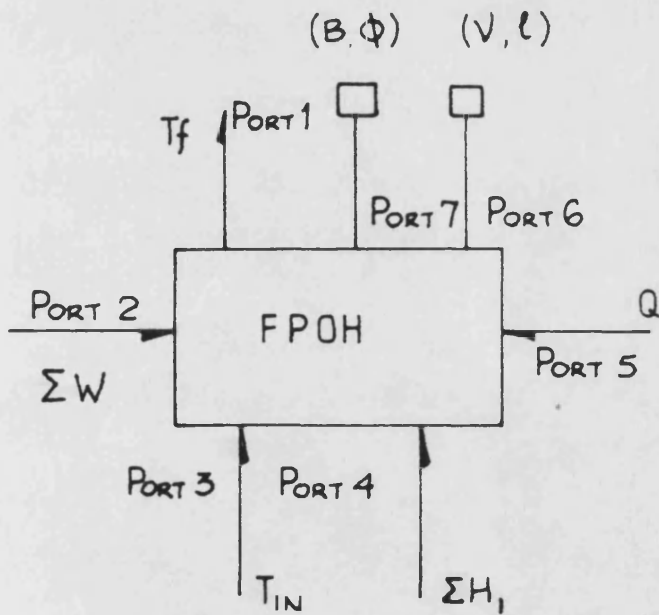
FIG. A2.10 LINK DIAGRAM FOR TEMPERATURE AND FLUID
PROPERTY MODEL FPOH
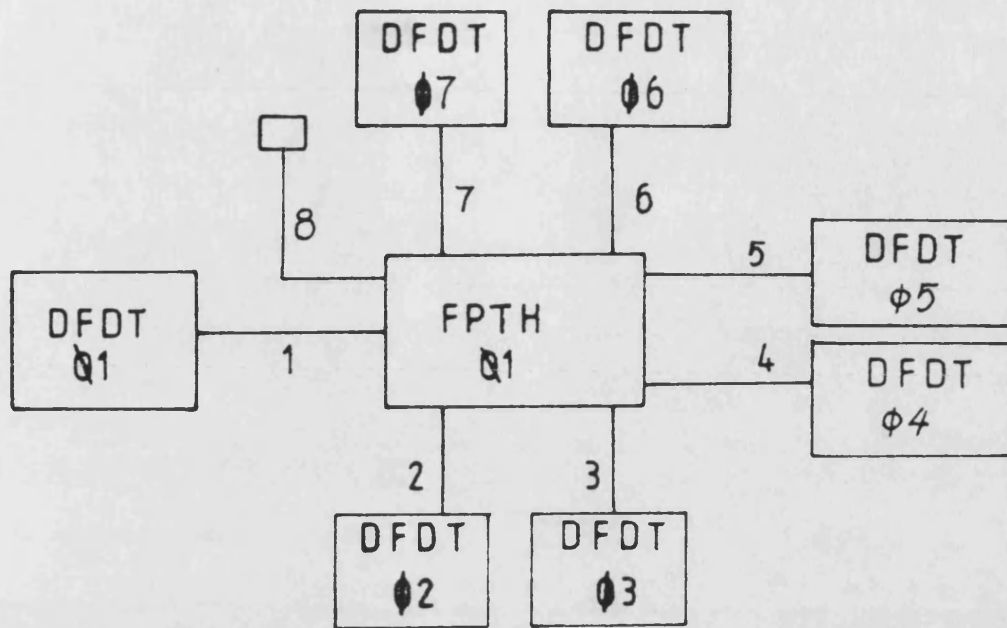
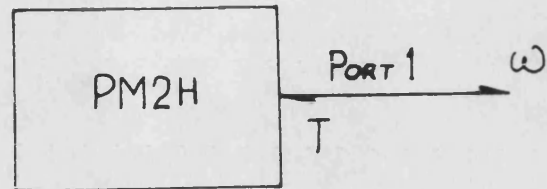FIG. A2.11 BLOCK DIAGRAM FOR VERIFICATION TEST
SIMULATION OF MODEL FPTH

EFFORTS : T_v

FLOWS : $W_1, W_2, T_{in1}, T_{in2}$
Q_1, Q_2, T_f, T_B
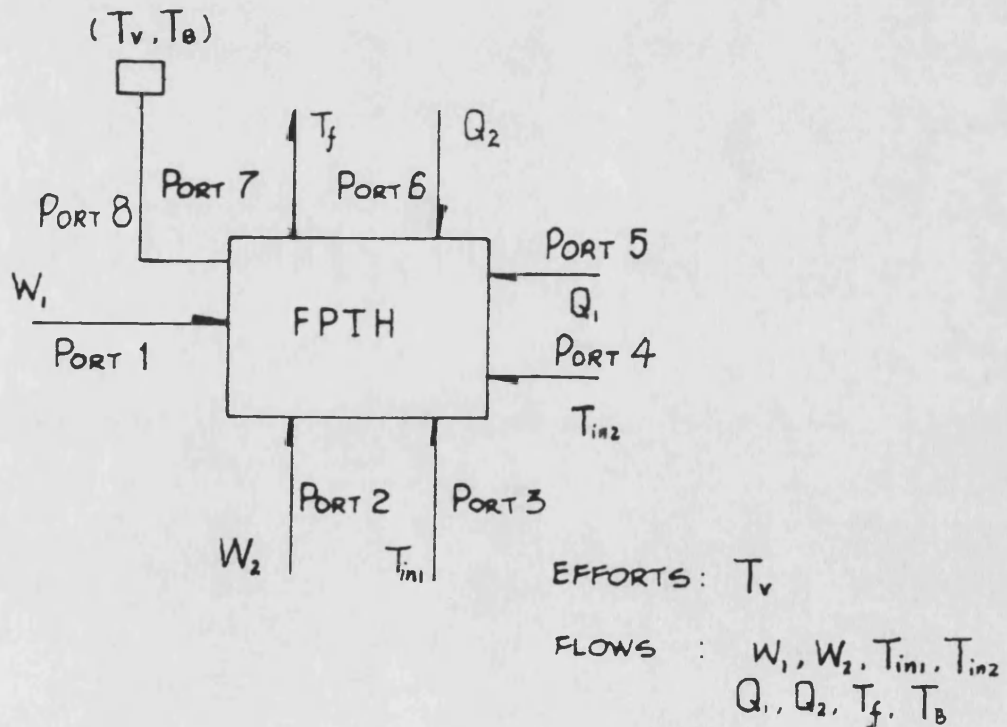
FIG. A2.12 LINK DIAGRAM FOR TEMPERATURE AND
FLUID PROPERTY MODEL FPTH
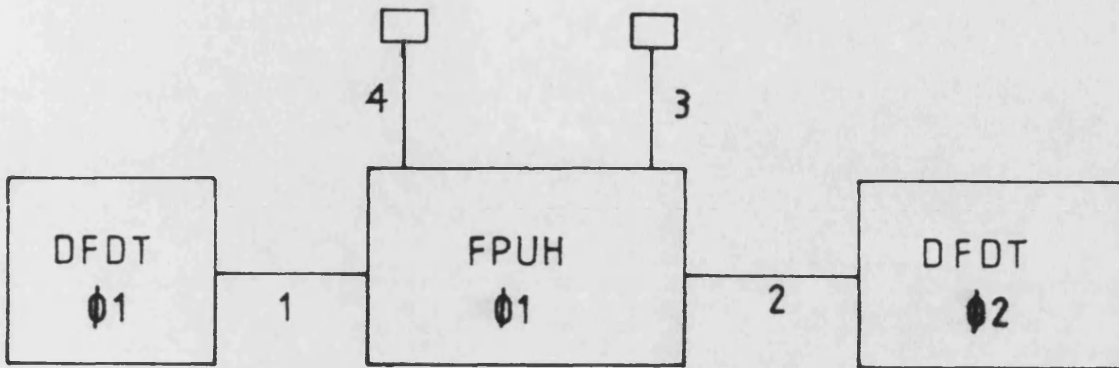
FIG. A2.13 BLOCK DIAGRAM FOR VERIFICATION TEST
SIMULATION OF MODEL FPUH
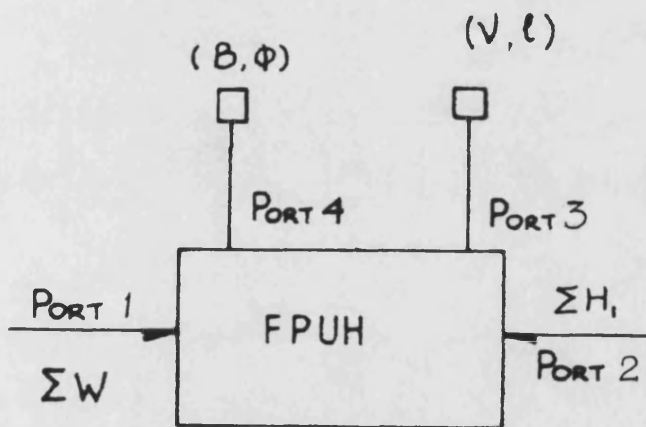
EFFORTS : V , B

FLOWS : $\Sigma W, \Sigma H_1, \rho$

FIG. A2.14 LINK DIAGRAM FOR TEMPERATURE AND FLUID
PROPERTY MODEL FPUH
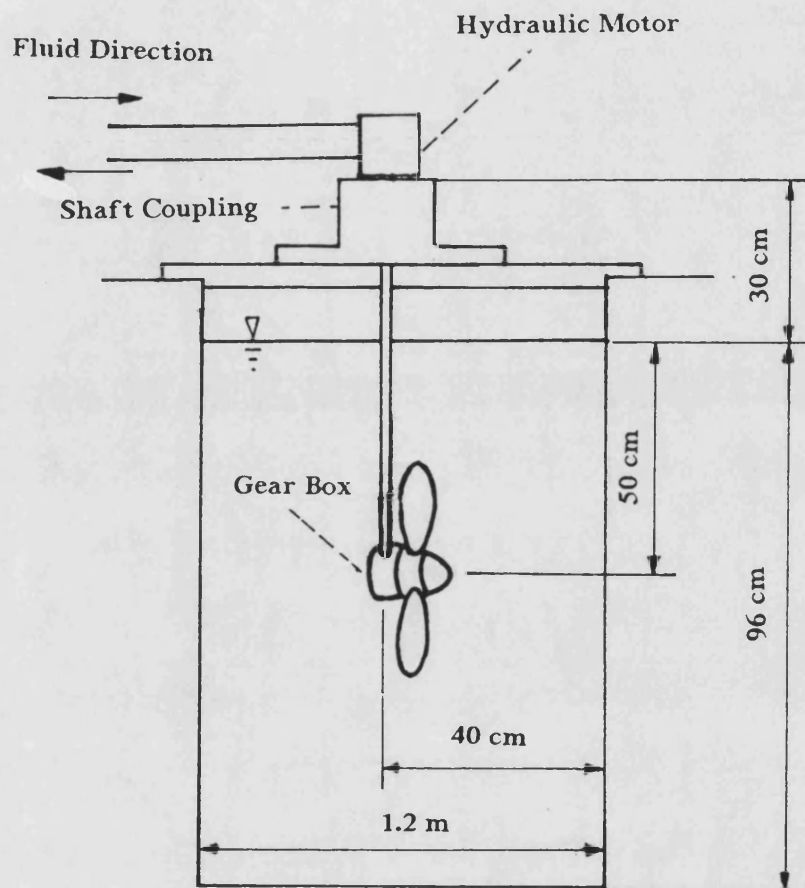
Fig. A2.15   The Location of the Propeller Inside A Water Pool
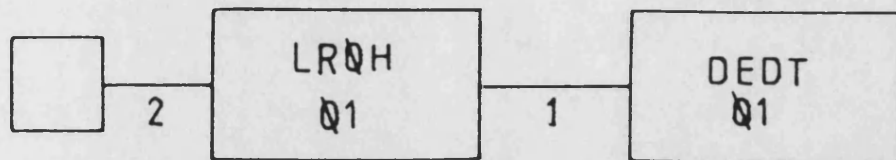
FIG. A2.16 BLOCK DIAGRAM FOR VERIFICATION TEST
SIMULATION OF MODEL LROH
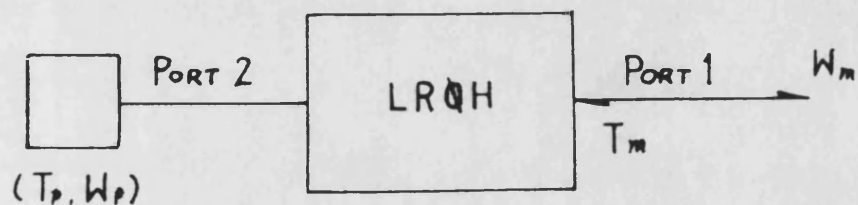
EFFORTS: T_m, T_p

FLOWS : W_m, W_p

FIG. A2.17 LINK DIAGRAM FOR PROPELLER MODEL LPOH
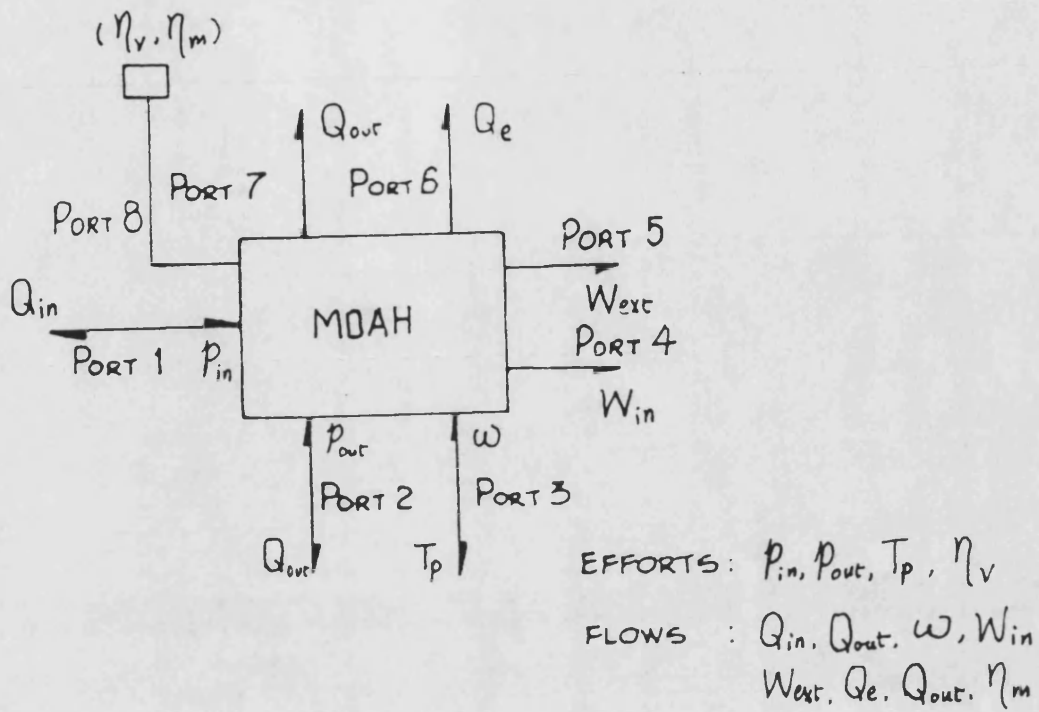
FIG. A2.18 LINK DIAGRAM FOR HYDRAULIC MOTOR

MODEL MOAH
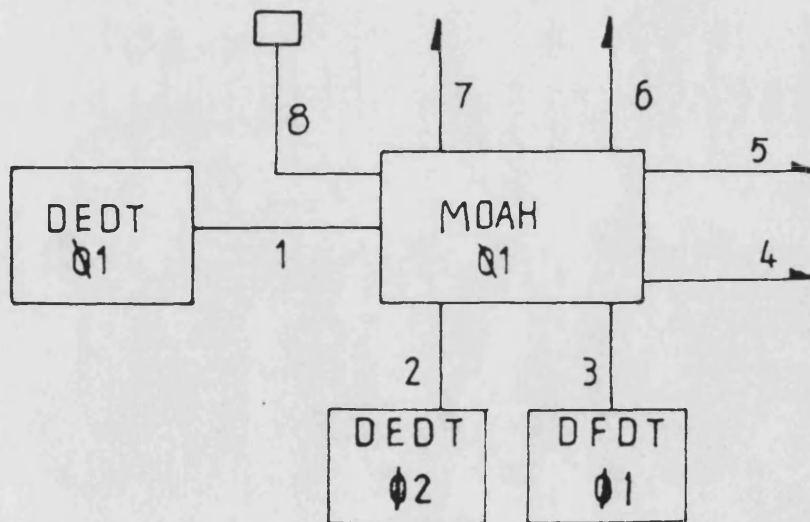
FIG. A2.19 BLOCK DIAGRAM FOR VERIFICATION TEST

SIMULATION OF MODEL MOAH
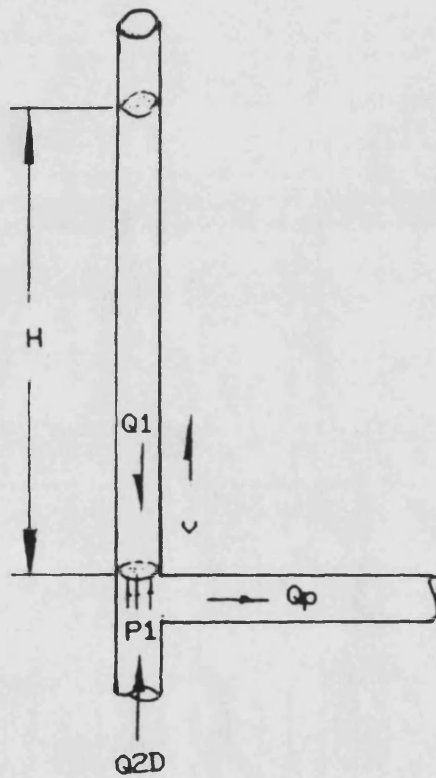
Fig.A2.20   Transient Flow Demanding from the Open-Ended Pipe

When the Pump is   loaded
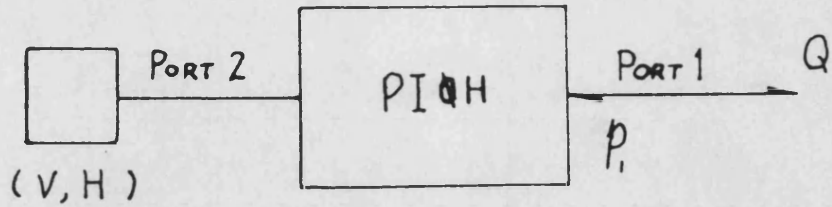
EFFORTS: P_1, V
FLOWS : Q, H

FIG. A2.21 LINK DIAGRAM FOR OPEN—ENDED PIPE
MODEL PIQH
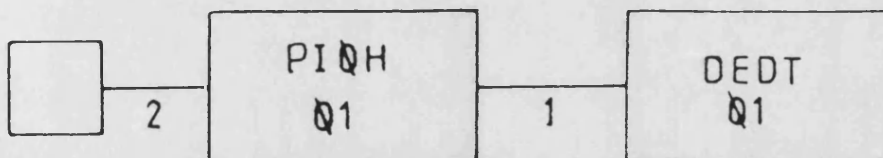
FIG. A2.22 BLOCK DIAGRAM FOR VERIFICATION TEST
SIMULATION OF MODEL PIQH
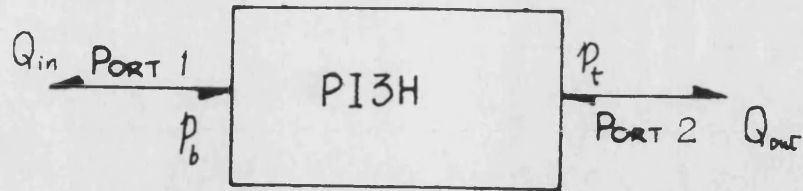
EFFORTS : P_b, P_t

FLOWS : Q_{in}, Q_{out}

FIG. A2.23 LINK DIAGRAM FOR VERTICAL RETURN LINE
MODEL PI3H

FIG. A2.24 BLOCK DIAGRAM FOR VERIFICATION TEST
SIMULATION OF MODEL PI3H
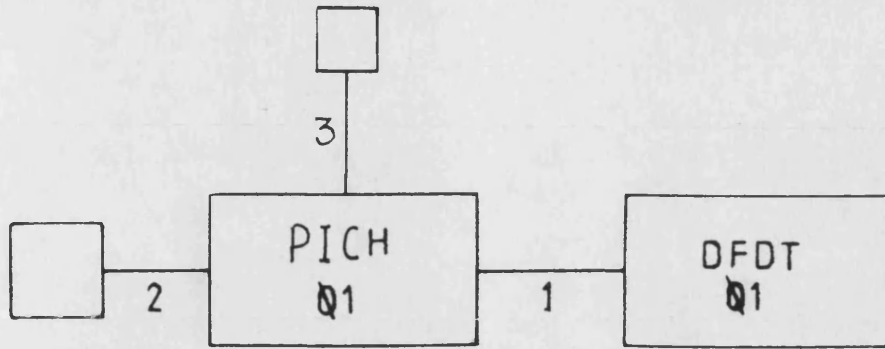
FIG. A2.25 BLOCK DIAGRAM FOR VERIFICATION TEST
SIMULATION OF MODEL PICH
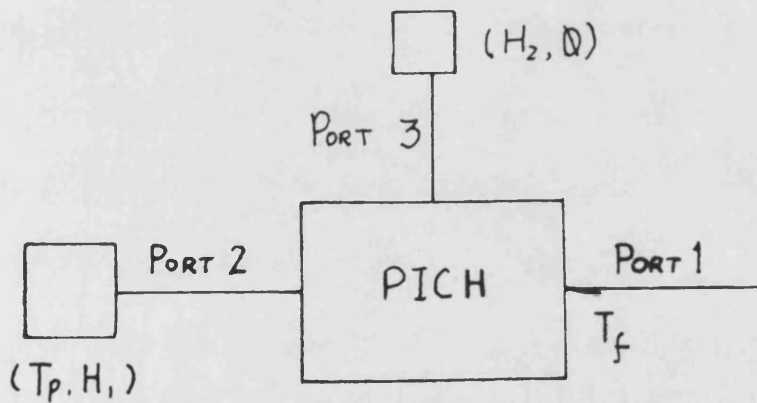
EFFORTS: T_f, T_p, H_2

FLOWS: H_1

FIG. A2.26 LINK DIAGRAM FOR PIPE TEMPERATURE MODEL PICH

EFFORTS: T

FLOWS : ω

FIG. A2.27 LINK DIAGRAM FOR ELECTRIC MOTOR MODEL PM2H
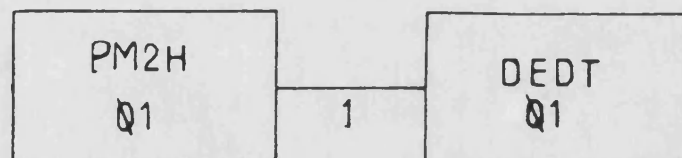
FIG. A2.28 BLOCK DIAGRAM FOR VERIFICATION TEST
SIMULATION OF MODEL PM2H
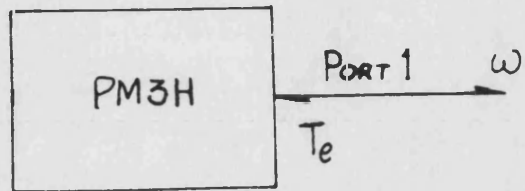
EFFORTS: T_e

FLOWS : ω

FIG. A2.29 LINK DIAGRAM FOR ENGINE MODEL PM3H
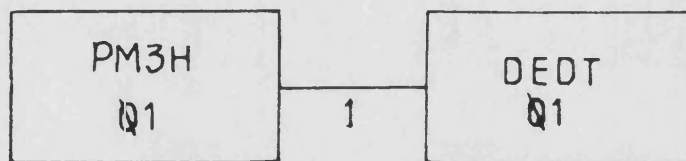
FIG. A2.30 BLOCK DIAGRAM FOR VERIFICATION TEST

SIMULATION OF MODEL PM3H
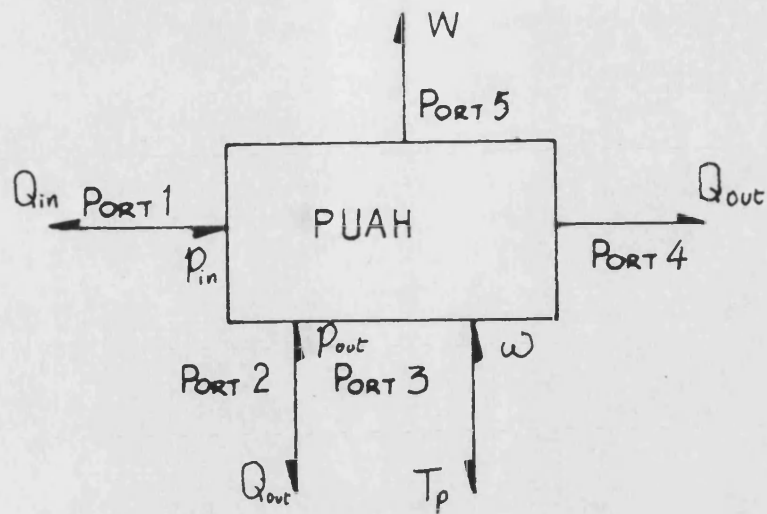
EFFORTS : P_{in}, P_{out}, T_p

FLOWS : $Q_{in}, Q_{out}, \omega, Q_{out}, W$
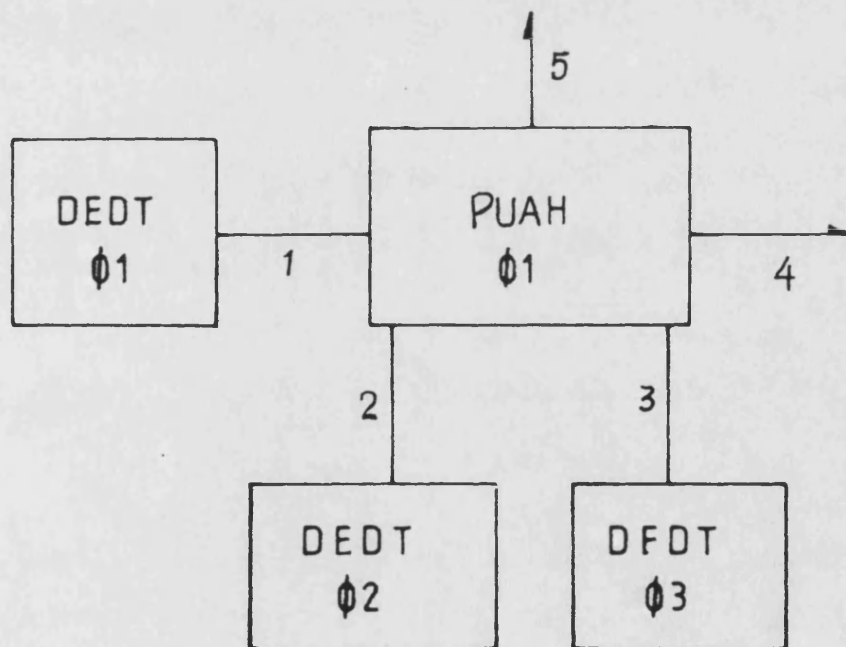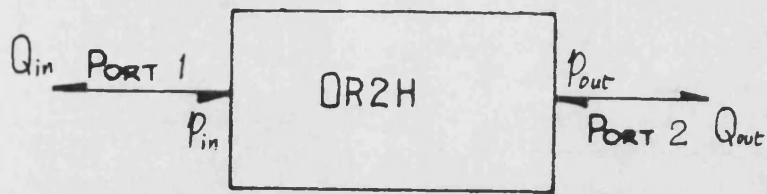
FIG. A2.31 LINK DIAGRAM FOR PUMP MODEL PUAH

FIG. A2.32 BLOCK DIAGRAM FOR VERIFICATION TEST
SIMULATION OF MODEL PUAH

EFFORTS : P_{in}, P_{out}

FLOWS : Q_{in}, Q_{out}
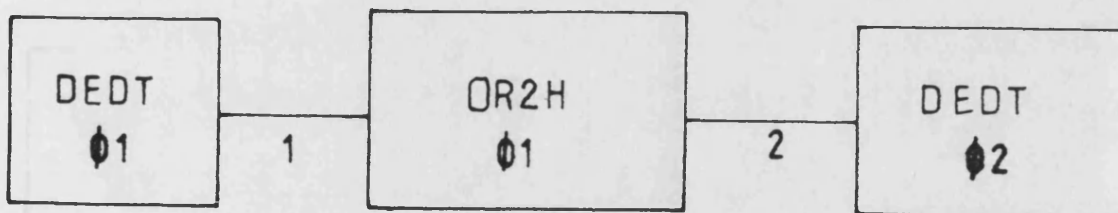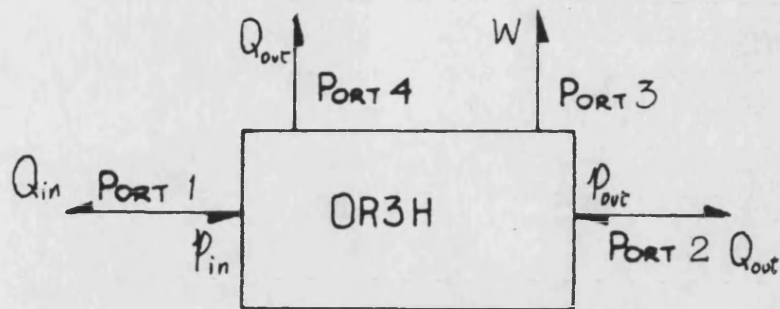
FIG. A2.33 LINK DIAGRAM FOR ORIFICE MODEL OR2H

FIG. A2.34 BLOCK DIAGRAM FOR VERIFICATION TEST
SIMULATION OF MODEL OR2H

EFFORTS : P_{in}, P_{out}

FLOWS : Q_{in}, Q_{out}, W, Q_{out}

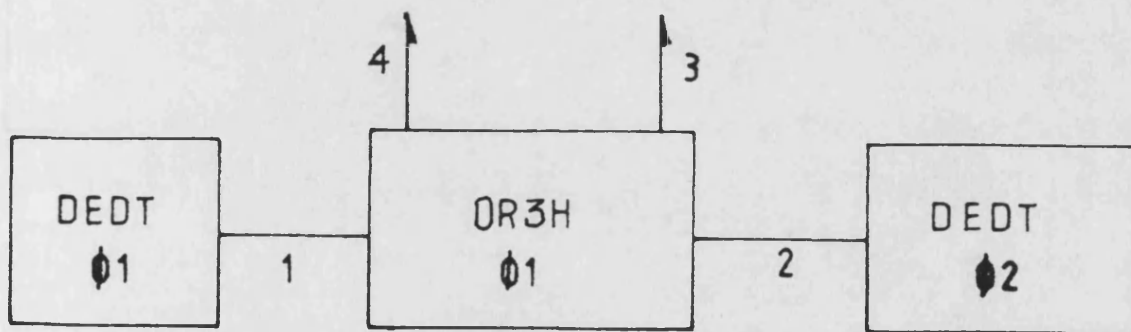## FIG. A2.35 LINK DIAGRAM FOR ORIFICE MODEL OR3H

FIG. A2.36 BLOCK DIAGRAM FOR VERIFICATION TEST
SIMULATION OF MODEL OR3H

FIG. A2.37 LINK DIAGRAM FOR TANK MODEL TKSH
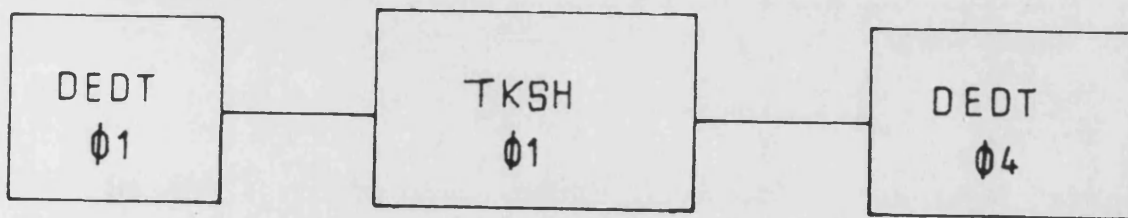
FIG. A2.38 BLOCK DIAGRAM FOR VERIFICATION TEST SIMULATION OF MODEL TKSH

SOME THOUGHTS ON HYDRAULIC CIRCUIT DESIGN

D E Bowns and H Yang

Fluid Power Centre, University of Bath, U. K.

SUMMARY

This paper shows that it is possible to obtain savings in size and cost in many hydraulic circuits by using closed or partially closed circuits in place of the normal open circuit designs usually employed. It also shows how simulation can be used to give accurate prediction of system performance in conditions where normal deductive or mathematical techniques would fail.

INTRODUCTION

In the minds of most hydraulic engineers, circuits can be classified as open or closed. In the former, fluid is taken direct from the reservoir and returned to it, whilst in the latter the main pump is in a closed loop, with a boost pump providing the make-up flow necessitated by leakage losses together with transient losses due to compressibility when the load is changed. The closed circuit applications are generally found in hydrostatic systems with piston type pumps and motors. However, the vast majority of systems are of the open circuit variety using fixed displacement pumps.

The object of this paper is to explore the middle ground between open and closed circuits and to suggest that the closed circuit concept

can be used more widely. The paper provides experimental data from two distinct circuits and considers the physical behaviour of each in detail. It goes on to check this behaviour with careful computer simulations both of the system dynamics and of the thermal characteristics of the systems considered.

SUCTION PIPE SIZING

The function of a hydraulic circuit is to provide flow to operate actuators and motors at a pressure determined by the load. It must perform this function without causing damage to the circuit components directly or indirectly by physical or chemical changes of the fluid properties.

One of the difficulties for the open circuit system designer is to specify the diameter of the suction line. The mininum suction pressure is usually specified by the pump manufacturer, and the pressure loss in the suction line, the suction strainer and the head in the reservoir (when it is at its lowest level) must be taken into account. Since the fluid flow regime will most probably be viscous, the losses will critically depend on the fluid temperature and in some installations the reservoir oil may have to be heated in order to give acceptable start-up conditions. Very often large and expensive suction lines have to be installed.

It may be pertinent at this stage to state that physical factors determining limiting suction conditions are not particularly well established. Edge and de Freitas [1][2] have shown that it is a dynamic rather than steady state phenomenon. The flow ripple due to the pumping mechanism in positive displacement pumps gives rise to pressure waves in the suction line. If cavitation did not occur, the peaks of these pressure ripples would be well below absolute zero pressure since the theoretical amplitude of the pressure ripple can often be as high as 5 bar. The implication of this is that incipient cavitation and air release can occur in the suction pipe of even well behaved pumps. Although this does not usually show as a reduction of volumetric efficiency, it is important to recognise that its presence makes the conditions at the suction port of a pump extremely complex.

CLOSED LOOP CIRCUITS WITHOUT BOOST

In the circuit of Fig. 1, the whole of the flow from the system is returned to the pump inlet. Thus the suction pipe has to provide fluid to compensate for leakage and other losses together with the flow required when unequal area actuators are extending. With this type of system, the suction line can be relatively small in diameter. It is a corollary that, since large flows are not being transferred to and from the reservoir, the reservoir itself can be drastically reduced in size.
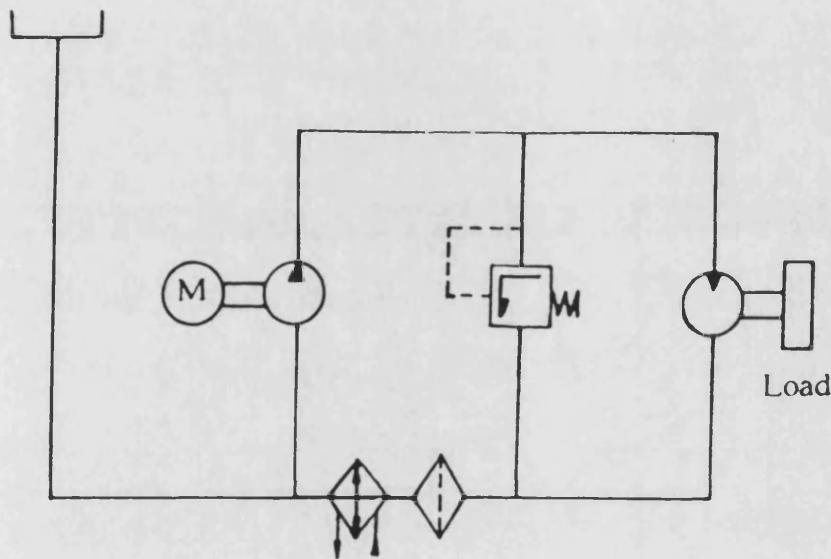

FIGURE 1   An Unboosted Closed Hydraulic Circuit

The functions which need to be considered before using such a system can be listed as follows:

      1) effects on pump suction behaviour;
      2) air release and its elimination;
      3) fluid contamination;
      4) leakage.

An experimental set up is described below and the detailed test results obtained will go some way towards understanding the above problems. Indeed, in an ideal situation, with no leakage and equal area actuators, a closed loop system of this type would not need a reservoir at all. Some interesting results have been obtained by removing the reservoir from the experimental set up.

The partially closed system in Fig. 2 is a modification which allows some proportion of the fluid to return to the reservoir but ensures that majority is passed directly to the pump inlet. The idea of this system is to allow the thermal inertia of the fluid in the reservoir to be used to reduce the need for a cooler during periods of high loading. Also it allows more flexibility in installation of the cooler. Air bubbles in the fluid can rise to the surface of the reservoir and thus control the amount of free air in the fluid. Another advantage is that the return line filter can be reduced in size since the flow of fluid is relatively low, with a significant saving in cost.
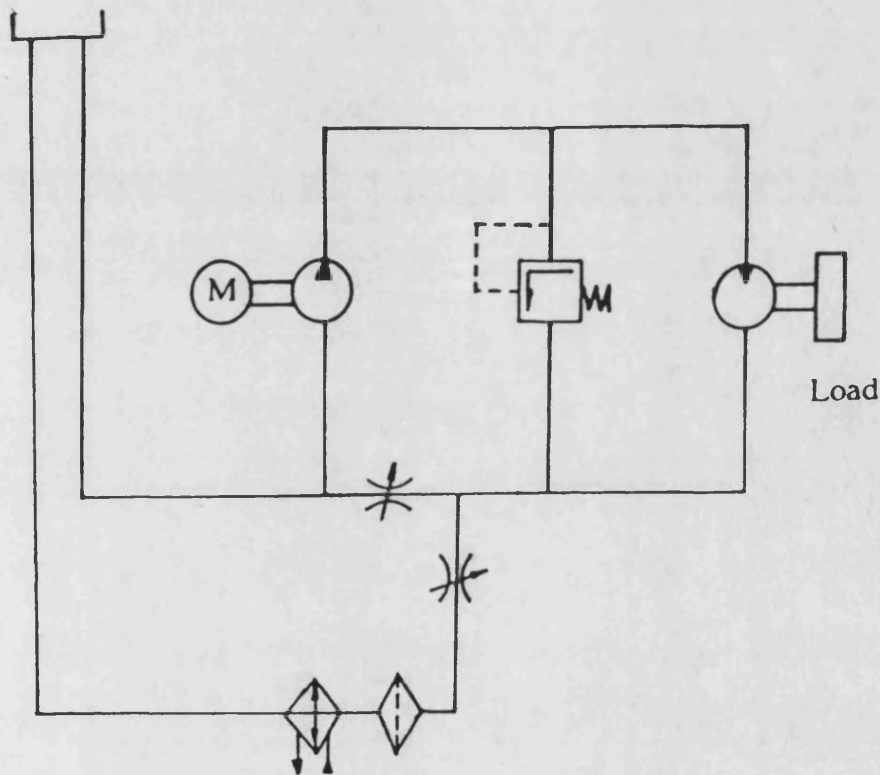

FIGURE 2   An Partially CLosed Hydraulic Circuit

Simulation

The circuits have been investigated both experimentally and by simulation. The simulation has been carried out using the hydraulic system simulation program HASP developed at Bath University and reported in (3)(4)(5). The models used for most of the components existed in the model library, but because of the particular interest in

the suction line condition, additional models including fluid inertia effects have been developed and have now been added to the model library.

Experimental Circuit

The circuit shown in Fig. 3 consists of a gear pump delivering to a fixed restrictor with a loading valve in parallel. The fluid from the restrictor and/or loading valve is returned to the inlet flange of the gear pump. It is considered that this simple system would be a good test of an unboosted closed loop system since closure of the loading valve will compress fluid in the delivery line from the pump and thus transiently starve the pump inlet. Correspondingly, sudden opening of the loading valve will release the compressed fluid, resulting in a sudden increase of flow to the pump inlet, which can in extreme cases cause an instantaneous reversal of flow in the suction line. The relief valve is fitted only as a safety device.
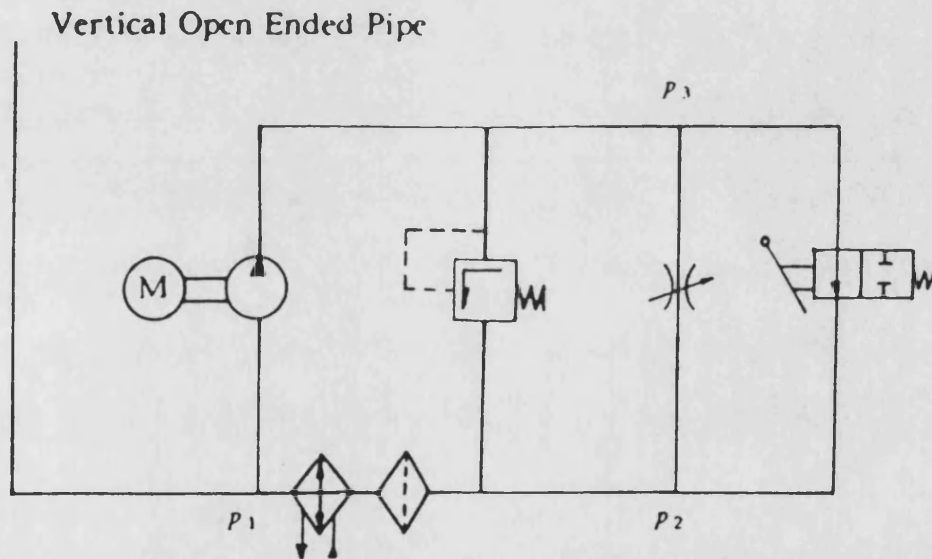

Vertical Open Ended Pipe

FIGURE 3   Experimental Circuit Tested - Unboosted Closed Circuit

A gear pump of nominal capacity 57.3 cc/rev is driven by an induction motor at a nominal speed of 1500 rev/min. On the delivery side of the pump there is a 1 metre length of steel pipe followed by a 2.6 metre length of hose. The flow from the loading circuit is returned

to the pump inlet via a filter and cooler. Since the gear pump is internally drained, there is negligible leakage flow in the circuit. Hence, an extreme case could be tested in which the reservoir is removed and the suction line held vertically above the pump inlet, with its upper end open to atmospere.

Transients During Loading

Many tests were carried out, but the results given below were for the extreme case in which the reservoir was removed and the suction line held vertically, the level in the pipe being about 1.5 m above the pump inlet. The rapid closure of the two way valve caused the delivery pressure to rise to about 100 bar, and, because of the increase of the pump slip loss and the compressibility a temporary reduction of flow occurred which entailed some fluid being drawn from the inlet line. Pressure oscillations consequent on valve closure are shown in Fig. 4. It will be seen that the delivery pressure rose to 100 bar, in about 0.2 second, and some oscillation occurred with a slight dip in pressure at about .70 ms after the valve was closed. The suction pressure dropped from its static head of 0.15 bar to – 0.3 bar but then oscillated with a peak of 0.5 bar at about 0.06 second. The pressure at the junction P_2 between the restrictor and the two way loading valve was also reduced.

Long Term Effects

The test rig was operated for 5 periods each of 7 hours duration under load. The only problem found was that of air release. In the system air is released as the fluid is passed through the loading valve or orifice restrictor and does not redissolve readily. Because there is no flow back to tank the majority of the air remains as bubbles in the system. This caused a 5% drop in delivery pressure in the 7 hours of operation.

Simulation of Transients

A simple theoretical approach, taking into account the compressibility of the fluid, the orifice steady state characteristics and the pump leakage could not explain the significant oscillation which
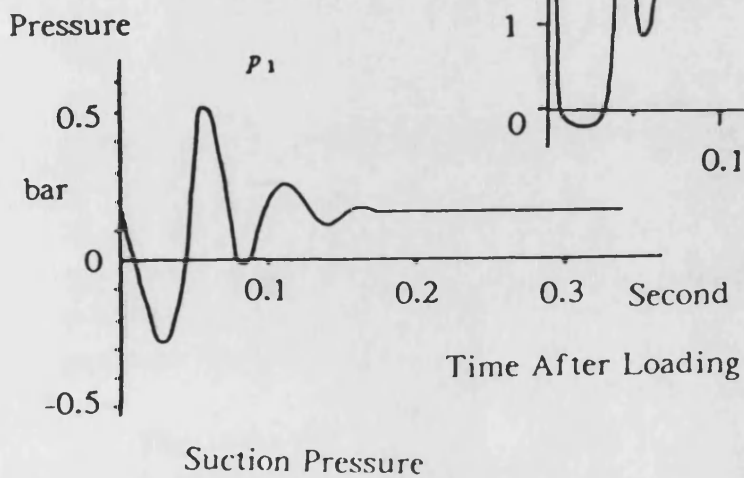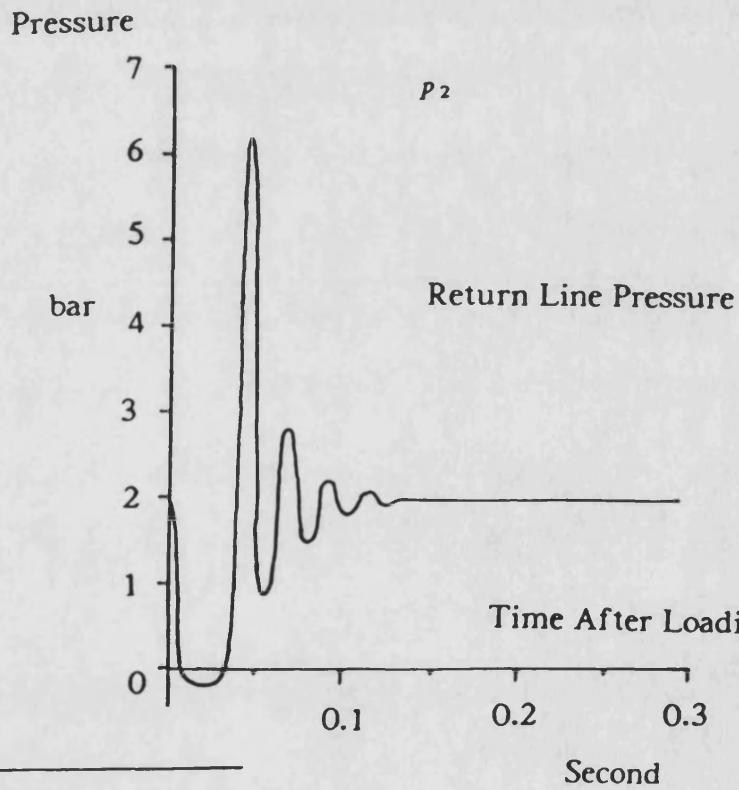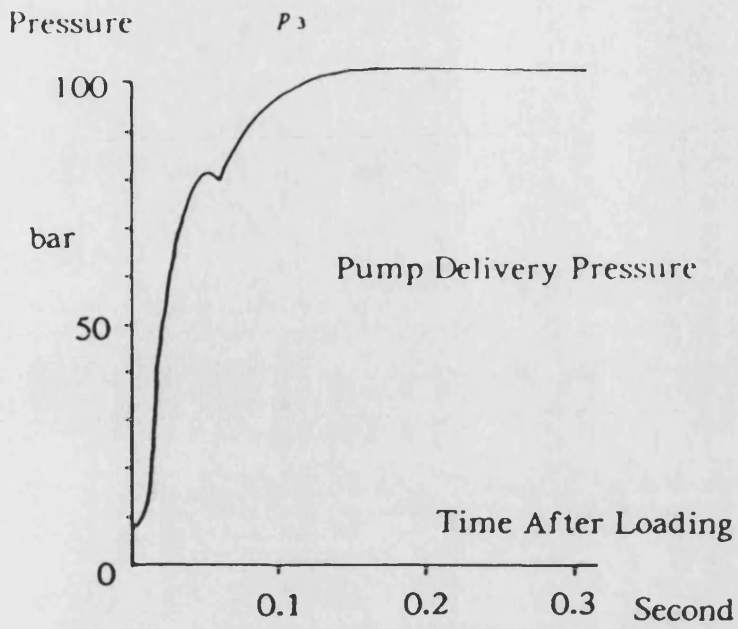
FIGURE 4   Typical Experimental Transient Pressures Recorded

occurred. Thus it was necessary to incorporate other factors. The factors included were

1) variation in motor speed during transients;
2) acceleration of the fluid in the suction line;
3) acceleration of fluid in the return line;
4) the dynamic behaviour of the fluid jet in the restrictor used to load the system.

HASP models were developed to take into account each of these effects and the whole system then simulated. Each of these models will now be described.

Electric Motor   The slip in an induction motor is to a first approximation proportional to the load torque, during steady state operation. During transients the inertia of the motor and the pump need to be taken into account and the dynamic equation is as follows

$$K_e(\omega_s - \omega) - T_p = J\frac{d\omega}{dt} + K_1\omega \qquad \dots\dots(1)$$

In the above equation

J is the combined inertia of pump and electric motor;

T_p is the torque supplied to the pump;

$K_e(\omega_s - \omega)$ is the electric motor torque developed;

$K_1\omega$ is the damping torque due to eddy currents.

A model has been developed incorporating these factors and allotted the mnemonic PM2H.

Pipe Line Modelling   The flow in pipes due to transient changes in pressure, is modified by the compressibility of the fluid and the compliance of the pipeline. Acceleration of   the fluid gives rise to fluid inertia terms and a complete dynamic model necessitates the use of the transmission line equation (6)(7). For most practical purposes, the effects of compressibility only are significant, except in the case of extremely long pipelines or when it is required to examine noise or pressure ripple at pumping frequence and its harmonics.

This simplified approach has been used for the pump delivery and return lines, but the suction line has been treated as a special case and

is described below.

Suction Line   The pressure variations are not of sufficient magnitude to make compressibility a significant factor, but fluid acceleration is, and in the case of open ended suction line the height of the fluid column, h will have a significant effect on the pressure at the junction between the return and suction lines.

Applying simple momentum theory

$$\frac{d(mv)}{dt} + p_f A + A \rho g h = p_1 A \qquad \ldots \ldots (2)$$

where m, v, A are the mass, velocity, and cross section area of the suction line, h its height, p_f its frictional return resistance and p_1 the pressure at the junction. Appropriate manipulation of the above equation yields

$$p_1 = \rho h \frac{dv}{dt} + \rho v^2 + p_f + \rho g h \qquad \ldots \ldots (3)$$

In the above equation, the pressure loss to friction is generally defined by the flow conditions as

$$P_f = \begin{cases} \dfrac{32\mu h v}{d_1} & \textit{Laminar Condition } Re \leqslant 2000 \\ \lambda \dfrac{l \rho v^2}{d} & \textit{Turbulent Condition } Re > 2000 \end{cases} \qquad \ldots \ldots (4)$$

The corresponding model is given the mnemonic PIOH.

Loading Orifice   In many cases orifice can be modelled by simply considering their static characteristics. For instance, a square law pressure-flow characteristic with some modification to take account laminar flow when the pressure drop is low is usually adequate. However, during transients the velocities at the vena contracta are very high and the momentum term in the jet $\rho A L \frac{dv}{dt}$ may be significant. The difficulty is obviously that the fluid momentum gradually diminishes as the distance from the orifice increases. In this

-263-

work, a rather arbitrary value of 6 pipe diameters has been taken, using, as area, the area of the jet in the orifice at its vena contracta. This figure has some justification in the literature, and certainly is justified by the present experimental results. The mnemonic OR2H was given to this model.

Pressure loss and compressibility were also taken into account in the pipe line downstream of the orifice. The filter and cooler were simulated by two orifices, to give their pressure drops, and a pipe, to simulate their combined compliance. Although the pressures are small, the volumes in these units were relatively large and their compliance significant.

Synthesis of Circuit

The power bond diagram in the form used for HASP is shown on Fig. 5. The electric motor model PM2H, obtained the motor speed which is transferred to the pump model PUOH. This is supplied with pressure from the delivery pipe model PI05(01) and suction pipe model PI05(04). The supply is taken via the delivery pipe to the orifice model OR2H and the directional control valve model DC1C (both in parallel). The change in loading valve position is given by duty cycle model DEDT. The combined flow is passed into the return line [PI05(02)], through the orifice-pipe combination representing the cooler and filter. As stated above, model PIOH represents the pipe from the tank.

Theory and Experimental Compared

Fig. 5 shows simulation and experimental results. They show remarkable agreement. It is apparent that the more complex modelling for the electric motor, orifice and suction line is very necessary if this level of agreement is to be achieved. Further the computer yielded other values which would be impossible to determine otherwise. The flow through the filter was shown to oscillate sharply and thus some reduction to filter performance could be implied. It is pointed out that such oscillatory behaviour is due to the nature of the transients involved, not the type of system.
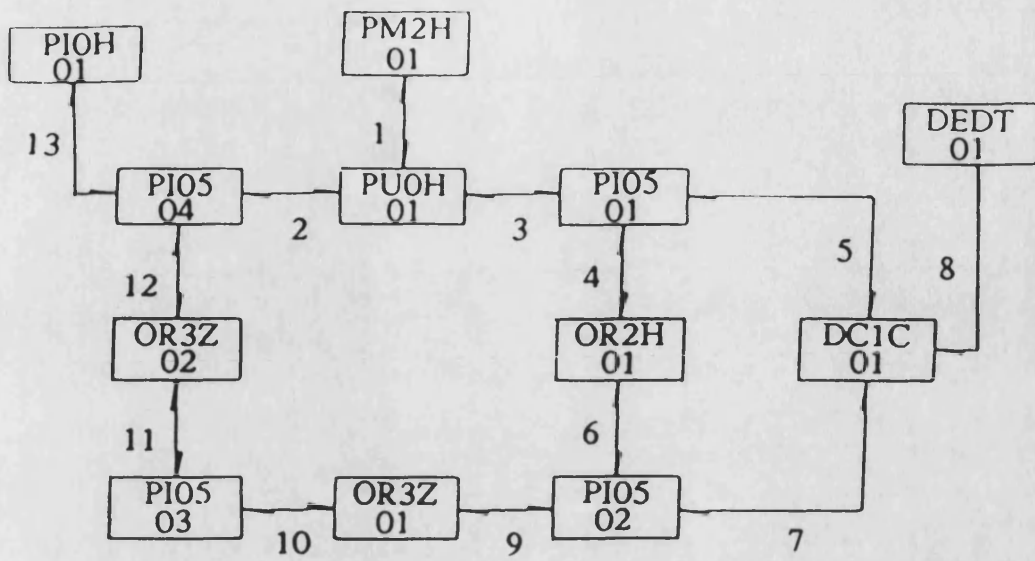
Power Bond Diagram

Pressure

p_3

Pressure

p_2
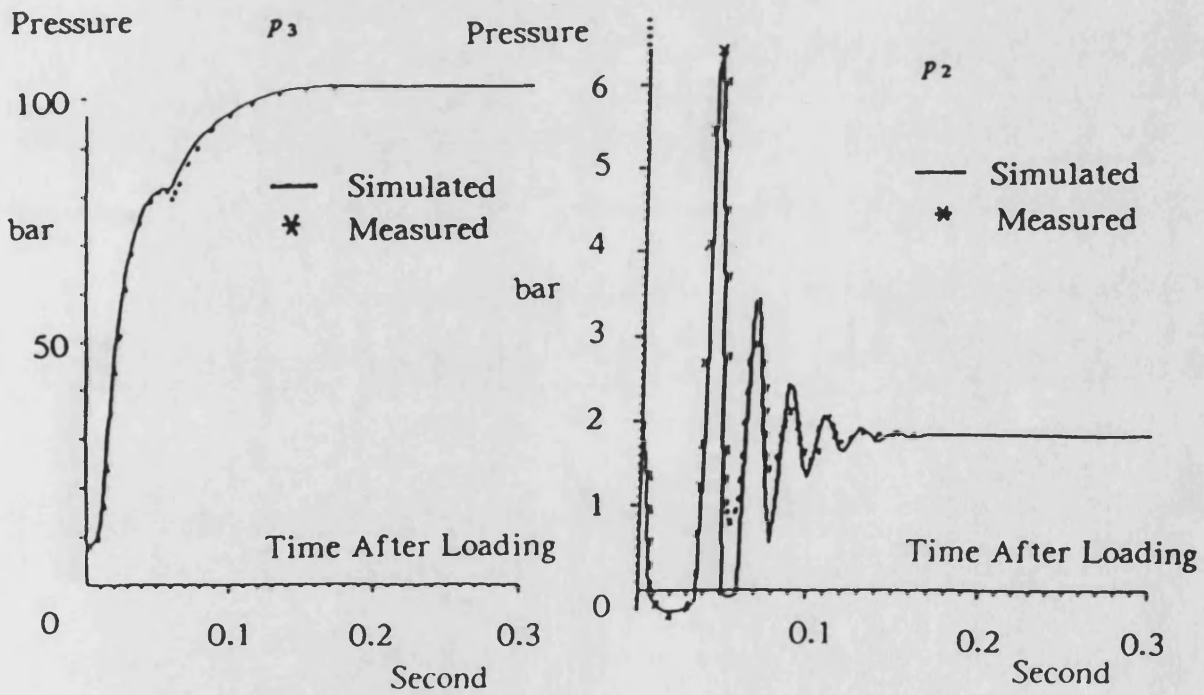
Pump Delivery Pressure After
Sudden Increase in Load

Corresponding Return Line Pressure

FIGURE 5   Simulation of Unboosted Circuit
(Results Compared With Experiment)

PARTIALLY CLOSED SYSTEMS

As stated above the disadvantage of a completely closed system can be avoided by allowing a controlled amount of fluid to return to tank as in Fig. 6. Two adjustable restrictors were fitted to alter the proportion of fluid returning to tank. The remainder of the system was loaded in the same manner as before.
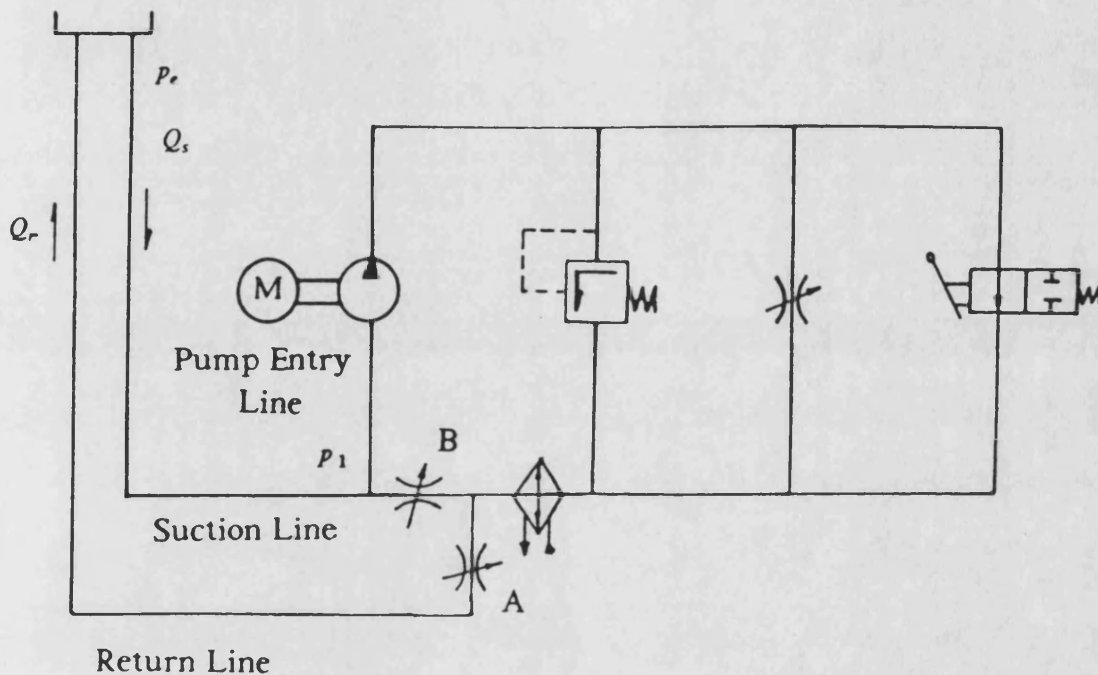

FIGURE 6   Experimental Circuit Tested - Partially Closed Circuit

Effect of Orifice Size   By changing the relative sizes of the orifices A and B the proportion of fluid returned to the reservoir could be altered. Fig. 7 shows these effects. Complete closure of orifice B caused all the fluid to be returned to tank. The suction pressure was then steady at -0.2 bar but with the pipe line used, cavitation occurred at the pump inlet, with a consequent fall off in pump discharge. At the other extreme, orifice A is closed, the closed loop situation described above occurred, and the suction pressure oscillated, the magnitude and frequency of oscillation depending on the valve operating time. As the flow to the reservoir increased the oscillations were damped but the mean suction port pressure was reduced.

The ideal compromise seemed to be to allow some flow to return to tank, for cooling and air release purposes but to limit this to a relatively small value. It is suggested, based on these results, and also on the established values used in conventional hydrostatic transmission that between 10 - 15 % of the flow should be returned to tank for optimal results.
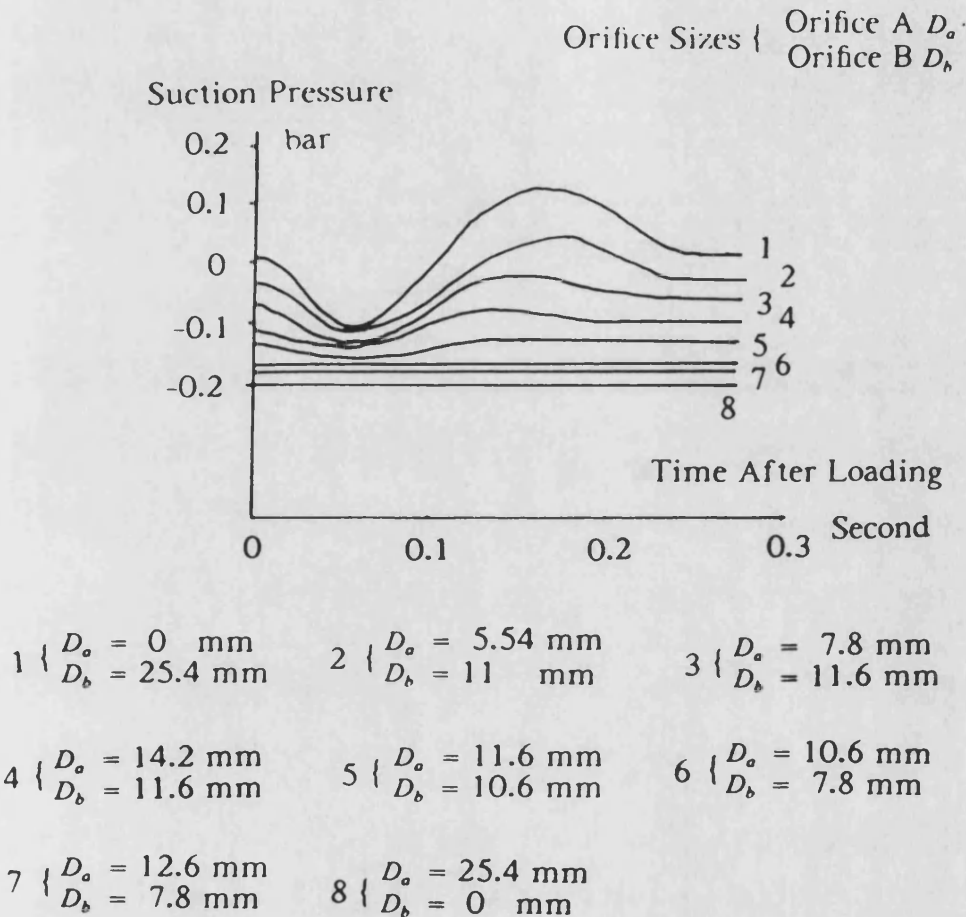
Orifice Sizes { Orifice A D_a
                 Orifice B D_b

$$1 \left\{ \begin{array}{l} D_a = 0 \ \text{mm} \\ D_b = 25.4 \ \text{mm} \end{array} \right. \quad 2 \left\{ \begin{array}{l} D_a = 5.54 \ \text{mm} \\ D_b = 11 \ \text{mm} \end{array} \right. \quad 3 \left\{ \begin{array}{l} D_a = 7.8 \ \text{mm} \\ D_b = 11.6 \ \text{mm} \end{array} \right.$$

$$4 \left\{ \begin{array}{l} D_a = 14.2 \ \text{mm} \\ D_b = 11.6 \ \text{mm} \end{array} \right. \quad 5 \left\{ \begin{array}{l} D_a = 11.6 \ \text{mm} \\ D_b = 10.6 \ \text{mm} \end{array} \right. \quad 6 \left\{ \begin{array}{l} D_a = 10.6 \ \text{mm} \\ D_b = 7.8 \ \text{mm} \end{array} \right.$$

$$7 \left\{ \begin{array}{l} D_a = 12.6 \ \text{mm} \\ D_b = 7.8 \ \text{mm} \end{array} \right. \quad 8 \left\{ \begin{array}{l} D_a = 25.4 \ \text{mm} \\ D_b = 0 \ \text{mm} \end{array} \right.$$

FIGURE 7   The Effects of the Sizes of Orifices A and B on the Experimental Transient Suction Pressure

Simulation

Certain new models were needed in order to simulate the system. For example, the reservoir used was small, and changes in inlet and outlet flow could affect the head in the reservoir and thus would have an effect on the inlet and return line pressure.

If h is the depth of fluid in the reservoir

$$\frac{dh}{dt} = \frac{Q_r - Q_s}{A_r} \qquad \ldots \ldots (5)$$

where Q_r, Q_s are return and suction flows respectively and A_r the cross sectional area of the reservoir.

Suction Line   Allowance for the fluid dynamic pressure in the pipes yields the equation

$$p_e = \rho g h - \frac{1}{2}\rho(1 + C_s)(\frac{Q_s}{A_s})^2 \qquad \ldots \ldots (6)$$

where p_e is the pressure at entry to the suction line, and Q_s, A_s, C_s are the flow, area and entry loss coefficient for the line. Fluid inertia and friction are important but compressibility effects can be ignored. Unlike Equation (3) the mass being accelerated in the line is constant and the following equation can be derived

$$\frac{dQ_s}{dt} = \frac{A}{\rho h}(p_e - p_1 - p_f) - Ag \qquad \ldots \ldots (7)$$

where p_1 is the pressure at the junction with the pump entry, suction and return lines, and p_f is defined in Equation (4).

Pipe Junction   The pipe junction between the return and the suction lines adds significantly to the computational difficulties as there is a continuous flow from both the tank and the return line. Pressure loss coefficients have to be assumed and these were taken from Engineering Science Data Ref.(8). A further HASP model was written to take this into account.

Simulation Block Diagram   The block diagram resulting for the system is shown in Fig. 8, and it was found that the additional complication was essential to give an adequate simulation. Subsequent computer runs showed complete agreement between simulation and experiment. It was very easy with the computer runs to adjust the sizes of the orifice to ensure suitable proportions of return line flow.

Further the computer simulation would be used with other loads, and synthesed with unequal area actuators to determine suitable tank and orifice sizes.
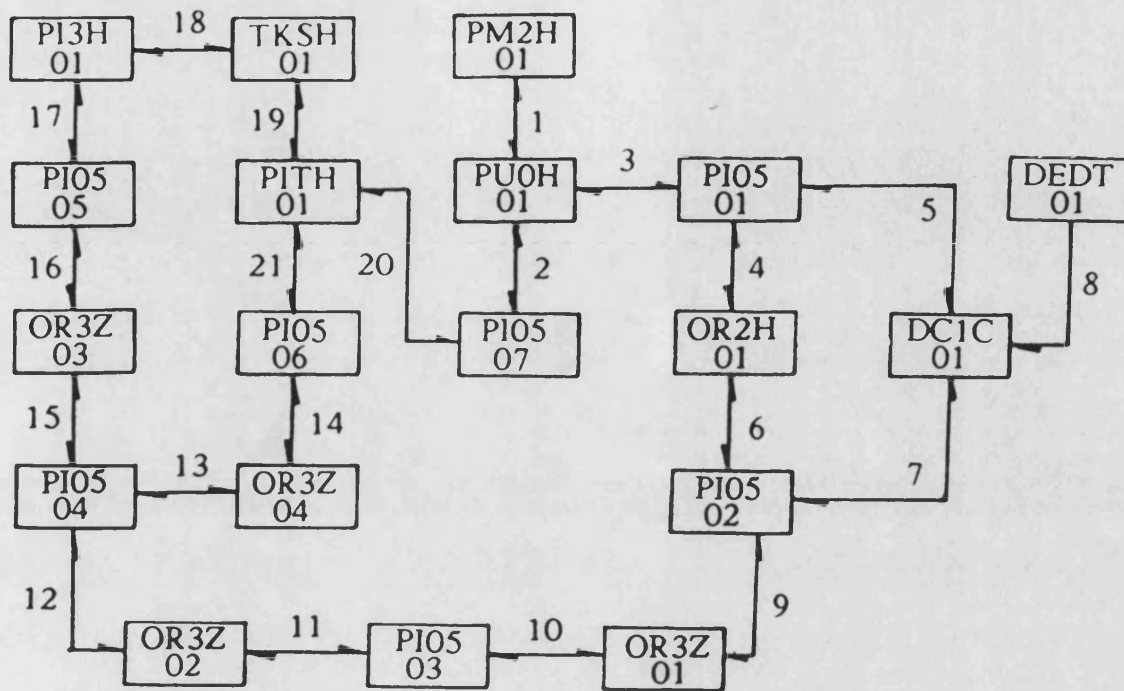

FIGURE 8   Block Diagram for the Simulation of the Partially
            Closed Hydraulic Circuit

EXAMPLE – A SMALL BOAT PROPELLER SYSTEM

One possible application of a hydrostatic transmission system is in the propulsion of small boats. The system proposed is to replace an outboard engine by an inboard engine and at the same time provide a hydraulic power take off, for use in powering the boat trailer up to beaches or for other uses. Such a system must be of low cost and for that reason the hydraulic design must be extremely simple.

The outboard engine was replaced by a hydraulic gear motor which was vertically mounted. Hoses connected the motor to the gear pump and directional control valve. In a boat the hydraulic power pack could be mounted amidships or wherever convenient. With this circuit, the boat could be reversed very simply by movement of the

directional control valve. The system used is shown in Fig. 9. The amount of fluid circulating back to the reservoir could be adjusted on the test rig by adjusting restrictors A and B. Loading the system was affected by simply moving the directional control valve from its centre position to forward, or reverse as required.
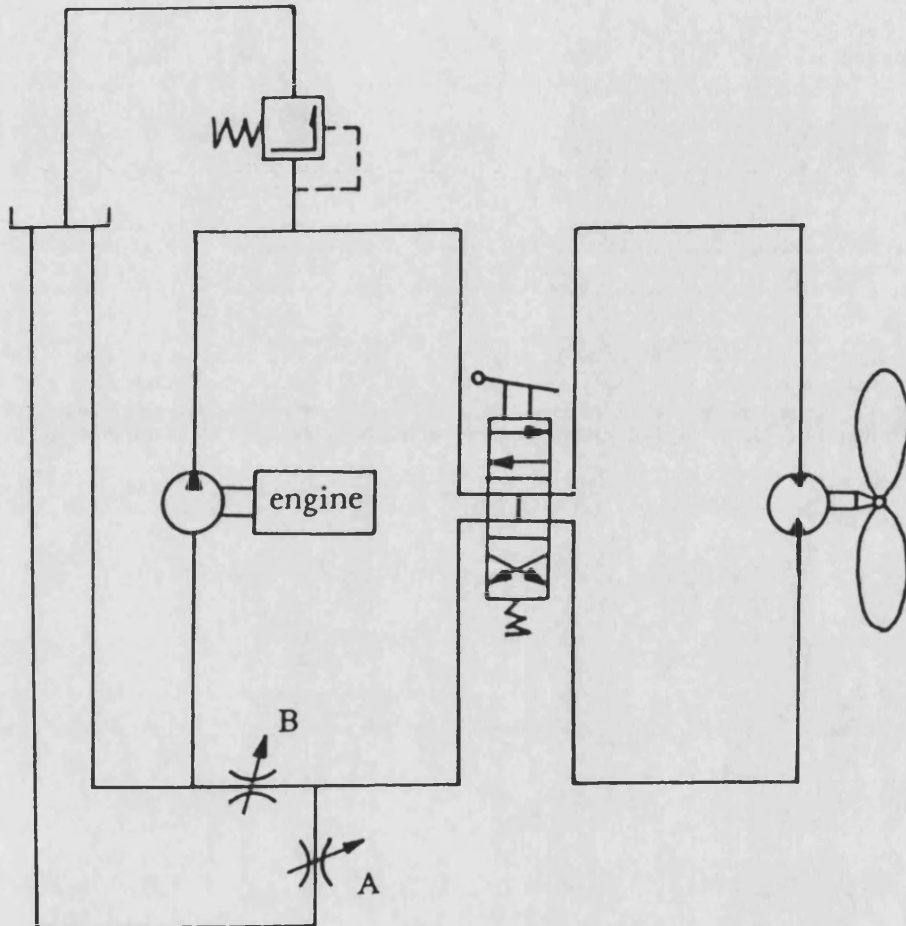

FIGURE 9   A Small Boat Hydrostatic System

In the experimental set up a 1 kw petrol engine was used as prime mover. The hydraulic motor and the pump were somewhat oversized for the propeller load due to unit availability and hence the pressures in the pipe lines were low. However the results obtained can be seen to show the feasibility of the system from an engineering standpoint.

Tests Carried Out

The results of the tests were as would be expected. The pump delivery pressure rose to 26 bar and after 40 ms fell off to 22 bar, due to inertia effects of the propeller. In the next 10 minutes of running, the pressure fell to 21 bar and then remained constant during the remainder of the 2 hours test. This small fall off in pressure was attributed to the reduction of friction loss in the hydraulic motor as the oil heated up and also the reduction in friction in the right angled gear box in the drive to the propeller. In the tests, the return flow to tank was adjusted to approximately 10 % of the pump discharge flow.

Simulation

The simulation of this system was carried out in the way described above. A hydraulic gear motor model existed in the library as did a directional control valve model. A model had to be developed for the propeller load and was developed according to established propeller theory. The torque T_p can be established from the relation

$$T_p = C_t \rho N^2 D^4 \qquad \ldots \ldots (8)$$

where C_t is a torque coefficient, N the speed and D the propeller diameter and ρ the density of water. The torque coefficient C_t is a function of the advance ratio $J = \dfrac{V}{ND}$, where V is boat forward speed in the water. It depends also on the design of the propeller and also a propeller hull interaction. A model for the propeller was set up, using standard propeller curves obtained from the literature. However, values had to be amended because of the particular propeller shape and the fact that in the test rig the propeller was not attached to a boat. The adjustment was made by measuring the hydraulic torque applied to the motor at one particular operating condition, allowing for motor and gearbox friction and then adjusting the coefficient C_t on a proportional basis.

Experimental Results Compared with Simulation

Fig. 10 shows the initial transient pressure in the high pressure line consequent on selecting forward gear. The pressure rose from its

initial value of about 5 bar to a peak of 26 bar in about 20 ms and then fell rapidly. The equilibrium value of 21 bar was not reached for some time. This was due to the fall off of the motor torque as the oil is heated up and also due to reduction in gear box losses for the same reason. Some slight reduction in suction pressure occurred during the initial transient but did not amount to a negative pressure of less than 0.12 bar.
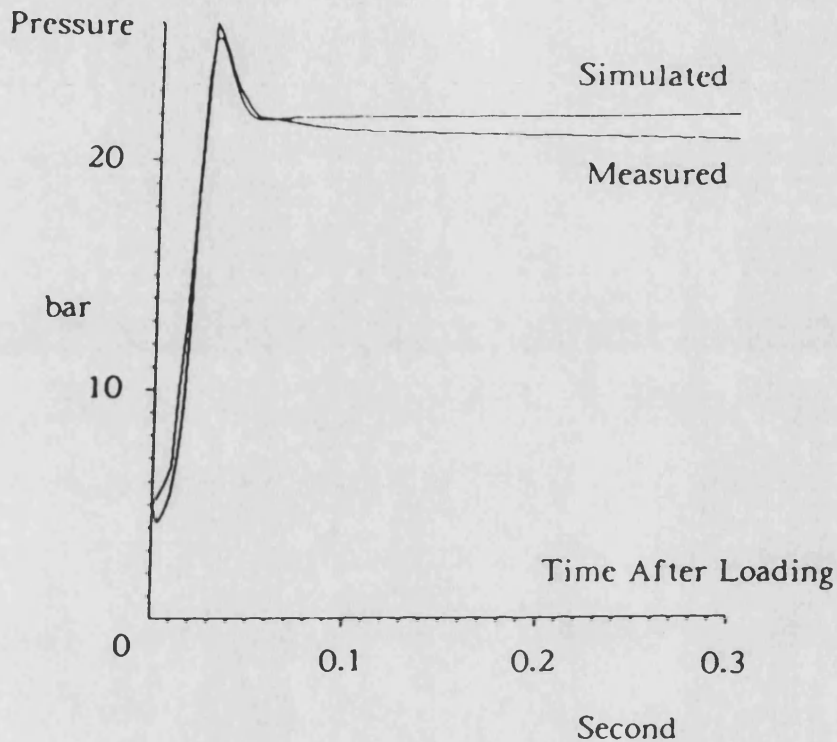

FIGURE 10 Comparison of the Simulated and Experimental Transient High Pressures

The efficiency of HASP as a method of simulation can also be seen from Fig. 10. The fall off of pressure due to heating was not predicted as oil viscosity was assumed to remain constant. This change of viscosity during a run is often important and a version of HASP is now available to simulate such effects. This version was described in (9) and has now been extended to include heat transfer from the pipe walls. Careful comparisons between simulation and experimental results have been carried out using measurements of both fluid and pipe wall temperatures. Radiation effects were found to be particularly important and will be discussed in a later paper.

CONCLUSION

The tests showed that closed and partially closed hydraulic circuits could be used for many applications. The cost of such systems would be lower due to a reduction in reservoir size, suction line size, and, in most cases, the size of the filter necessary for the installation.

The simulation work described above gave very good agreement with the experiment, and it allowed many points of the system behaviour to be satisfactorily explained. It has been shown to be an effective design tool for suction pipe, cooler, filter and reservoir sizing.

REFERENCES

1.   Edge, K. A. and Freitas, F. J. T. de, A Study of Pressure Fluctuation in the Suction Lines of Positive Displacement Pumps. Proc Instn Mech Engr Vol 199 No B4, U. K., May, 1985.

2.   Edge, K. A. and Freitas, F. J. T. de, Fluid Borne Pressure Ripple in Positive Displacement Pump Suction Lines. 6th International Fluid Power Symposium, Cambridge, U. K., April, 1981.

3.   Bowns, D. E. and Rolfe, A. C., The Digital Computation of Pressures and Flows in Interconnected Fluid Volumes, Using Lumped Parameter Theory. 4th International Fluid Power Symposium, U. K., 1975.

4.   Bowns, D. E., Tomlinson, S. P. and Dugdale, S. K., Progress towards a General Purpose Hydraulic Simulation Language. 6th International Fluid Power Symposium, Cambridge, U. K., April, 1981.

5.   Bowns, D. E., Tomlinson, S. P. and Dorey, R. E., Computer Simulation Techniques for the Dynamic Performance Assessment of Fluid Power Systems. 7th International Fluid Power Symposium, Bath, U. K., September, 1986.

6.   D'S ouza, A. F. and Oldenburger, R. E., Dynamic Response of

Fluid Lines. ASME Journal of Basic Engineering, September, 1964.

7. Bowns, D. E. and McCandlish, D., Quieter Oil Hydraulics Seminar, I. Mech. E., November 1977.

8. Pressure Losses in Three-Leg Pipe Junctions: Combining Flows. Engineering Science Data Item No 73023, 1973.

9. Bowns, D. E. and Tomlinsion, S. P., Prediction of Thermal Transient Effects Using the Hydraulic Automatic Simulation Package, 2nd Royal Navy Hydraulic Engineering Conference, Manadon, April, 1986.